NASA Contractor Report 165630

INTEGRATED APPLICATION OF ACTIVE CONTROLS (IAAC) TECHNOLOGY TO AN ADVANCED SUBSONIC TRANSPORT PROJECT—

WING PLANFORM STUDY AND FINAL CONFIGURATION SELECTION

FINAL REPORT

BOEING COMMERCIAL AIRPLANE COMPANY
P.O. BOX 3707, SEATTLE, WASHINGTON 98124

FOR EARLY DOMESTIC DISSEMINATION

NASA
National Aeronautics and
Space Administration

Langley Research Center
Hampton, Virginia 23665

FOREWORD

This document constitutes the final report of the Wing Planform Study Configuration Design that was completed under Contract NAS1-15325.

NASA Technical Monitors for this task were D. B. Middleton and R. V. Hood of the Energy Efficient Transport Project Office at Langley Research Center.

The work was accomplished within the Preliminary Design Department of the Vice President-Engineering organization of the Boeing Commercial Airplane Company. Key contractor personnel who contributed were:

G. W. Hanks	Program Manager
H. A. Shomber	IAAC Project Manager
H. A. Dethman	Design Integration
L. B. Gratzer	Technology Integration
J. D. Vachal	Task Manager (Wing Planform Study)
C. C. Flora	Flight Controls Technology
R. J. Fraser	Flight Controls Technology
R. L. Sullivan	Aerodynamics Technology
G. E. Seidel	Configurations
A. Maeshiro	Flight Controls Technology
C. E. Roth	Flight Controls Technology
E. Heineman	Structures Design
M. T. McIntosh	Structures Technology
M. J. Omoth	Systems Technology
J. D. Brown	Weight Technology

During this study, principal measurements and calculations were made in customary units and were converted to Standard International units for this document. The Wing Planform Study Configurations model numbers (768-102, -103, -104, -105, -106, and -107) appear as applicable, in the lower right-hand corner of each illustration for ease in identification.

i

Page intentionally left blank

CONTENTS

CONTENTS (Continued)

CONTENTS (Continued)

CONTENTS (Continued)

CONTENTS (Concluded)

FIGURES

FIGURES (Continued)

FIGURES (Continued)

FIGURES (Concluded)

TABLES

TABLES (Concluded)

1.0 SUMMARY

This report documents results of the final airframe configuration task of the "Integrated Application of Active Controls (IAAC) Technology to an Advanced Subsonic Transport" Project. Analysis of the performance of three airplane configurations with differing wing sweeps and spans, using Active Controls Technology (ACT), led to the selection and definition of a Final ACT Configuration. To determine the benefits of ACT in combination with wing planform variations, the active controls configurations were compared to the Conventional Baseline Configuration, a state-of-the-art transport selected and defined in a previous task (see NASA CR-159248). It was assumed that all beneficial ACT functions could be implemented with appropriate reliability and availability. Non-ACT technology levels were held constant for all configurations.

The aspect ratio (AR) 12 Configuration (768-104), with the largest span of those considered, had the best fuel efficiency and was therefore selected as the best candidate for the Final ACT Configuration. A detailed analysis was focused on this configuration, and trade and sensitivity studies were made to support its selection. The work concluded with sizing the Final ACT Configuration to the range of the Baseline Configuration. Relative to the Baseline, the Final ACT Configuration (768-107) required 10% less block fuel at the design range. This is shown in Figure 1.

The major ACT benefit resulted from making the airplane depend upon the pitch-augmented stability (PAS) and angle-of-attack limiting (AAL) functions, which resulted in a smaller horizontal stabilizer and less trim drag. PAS/AAL accounted for over 90% of the ACT fuel savings; the remainder was from wing-load alleviation (maneuver-load control). Reducing the criticality of the PAS/AAL system may provide a beneficial cost/performance trade and should be investigated further.

Increasing wing span resulted in approximately 3.5% better fuel efficiency. The large wing root chords, required for landing gear integration with the more aft center-of-gravity locations of the ACT Configuration, resulted in a structurally efficient inboard wing box, which allowed the wing span to be increased for only a modest weight penalty due to flutter and dynamic gust conditions. Although flutter-mode control
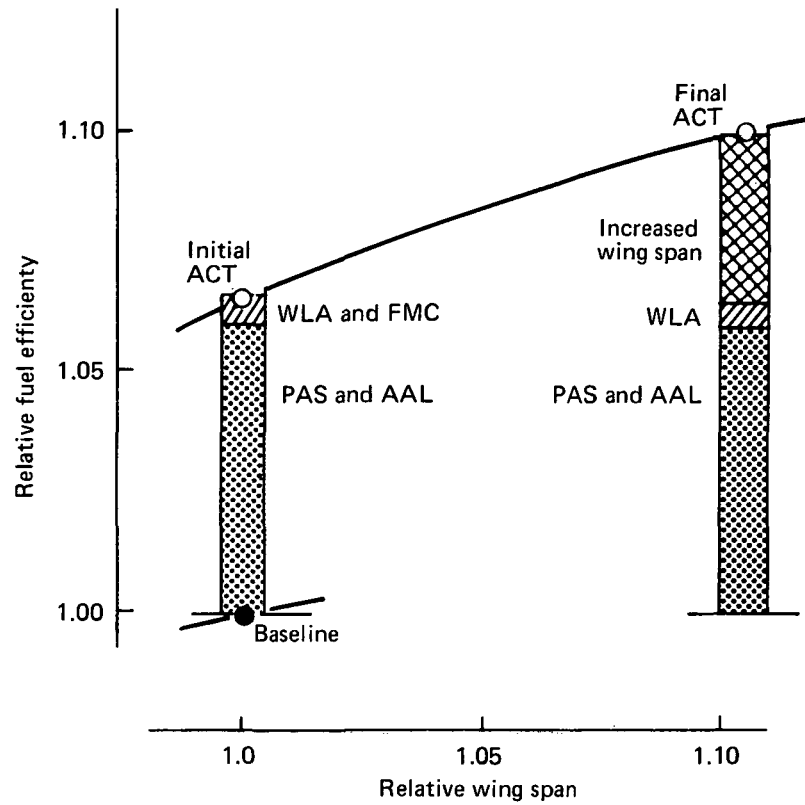
Figure 1. ACT and Planform Effects on Fuel Efficiency

(FMC) and gust-load alleviation (GLA) systems were synthesized, the surface rates required were judged too high for practical implementation, and neither system was included on the Final ACT Configuration.

2

2.0 INTRODUCTION

The main objective of the Integrated Application of Active Controls (IAAC) Technology to an Advanced Subsonic Transport Project is to assess the benefits associated with a major application of Active Controls Technology (ACT) to the design of a modern, subsonic, commercial transport. This project, initially entitled "Maximum Benefit of ACT," is one of several under the NASA Energy Efficient Transport (EET) Program. The IAAC Project has three major elements: the design of an airplane configuration and a related current technology ACT system, an examination of advanced technology implementation of ACT functions, and the testing and evaluation of selected elements of the proposed ACT system. A detailed discussion of the IAAC Project Plan is presented in Reference 1.

Figure 2 shows the makeup of the Configuration/ACT System Design and Evaluation Element. After the selection of a Conventional Baseline Configuration, described in Reference 2, the configuration design activity proceeded to the Initial ACT Configuration, which was a constrained application of ACT. This work is described in
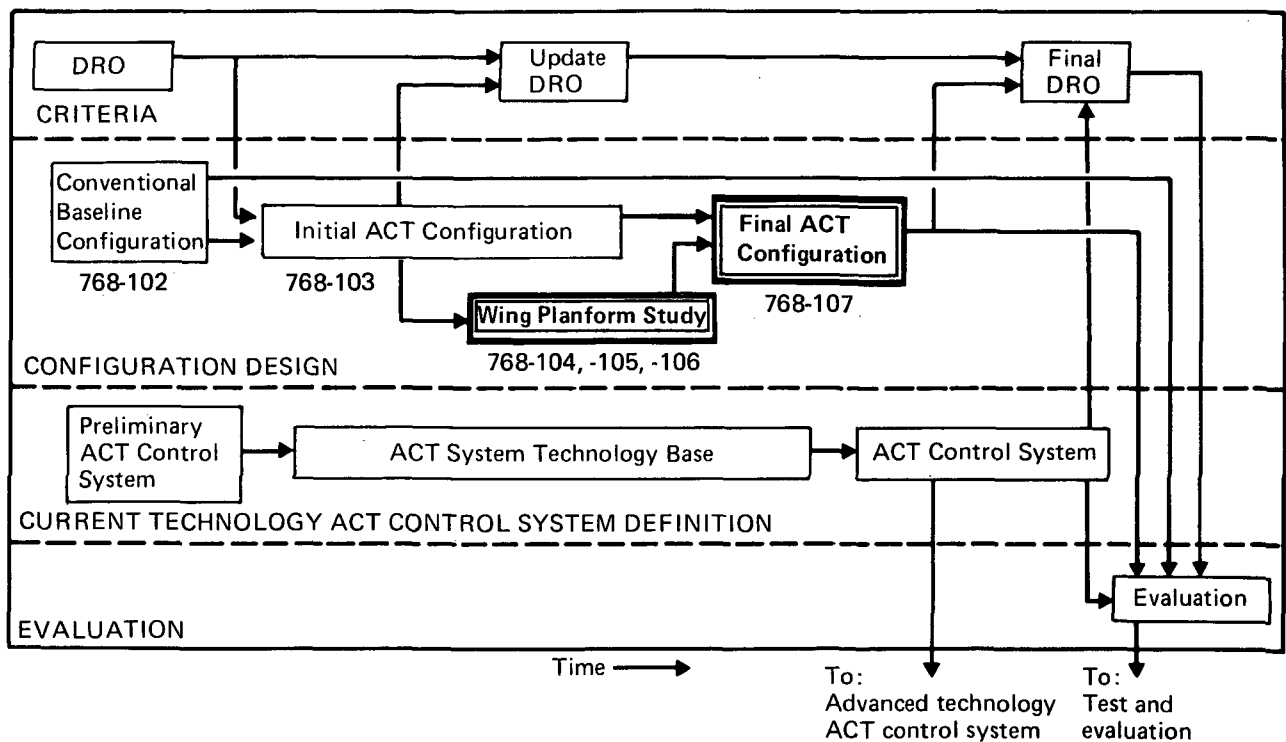
Figure 2. Configuration/ACT System Design and Evaluation Element

3

Reference 3. The first part of the next stage, which is described herein, was an examination of various wing planforms resulting in three airplane configurations. The second part consisted of the selection and definition of a Final ACT Configuration based on the results of the Wing Planform Study. The configuration evolution is shown in Figure 3. To facilitate discussion, model numbers are assigned to each configuration, as shown at the bottom of Figure 3.

| Baseline Configuration Model 768-102 | Initial ACT Configuration Model 768-103 | Wing Planform Studies—Models 768-104, -105, -106 | Final ACT Configuration Model 768-107 | Final ACT |
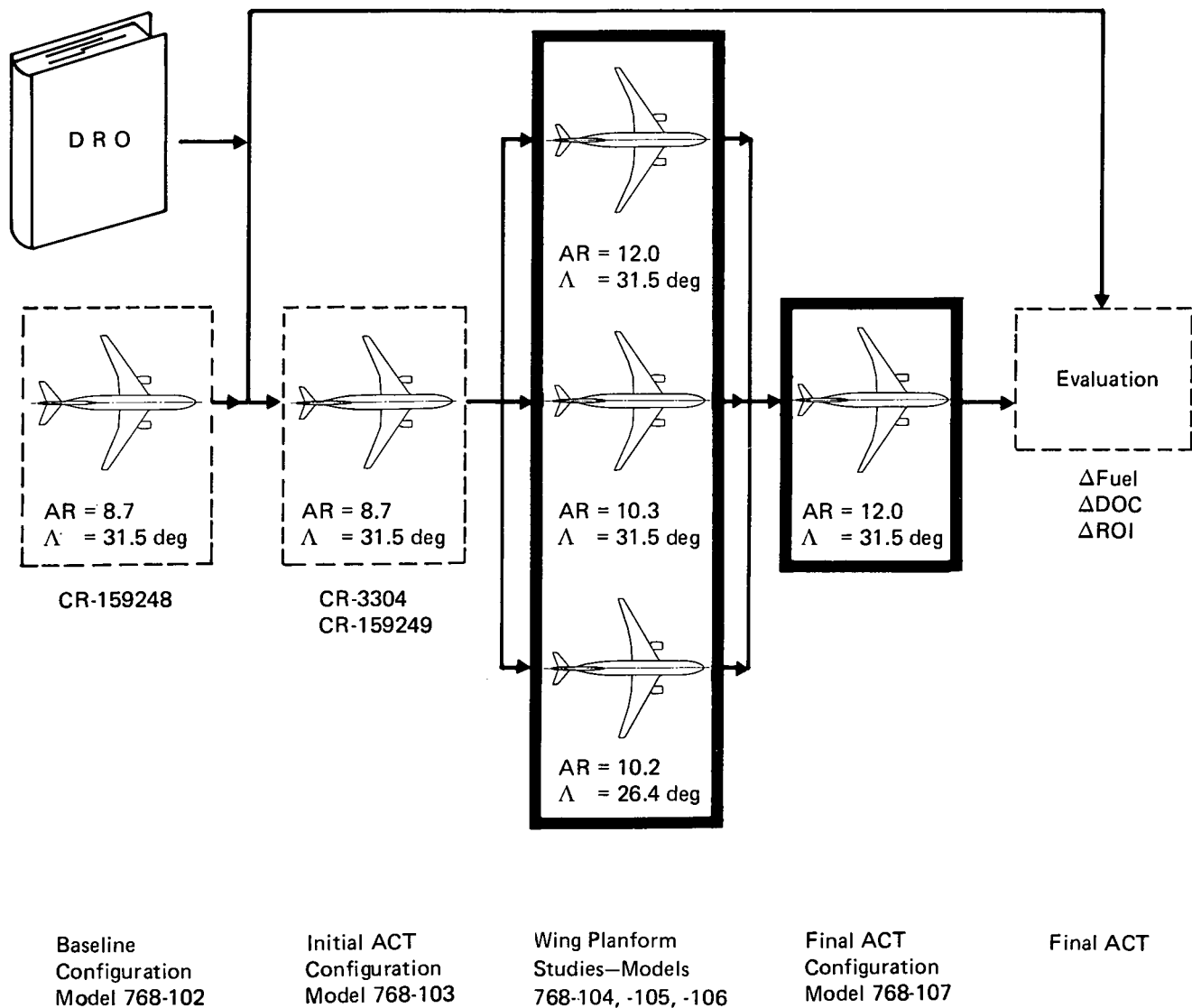
Figure 3. ACT Configuration Evolution

4

2.1 OBJECTIVES

The objectives of the Wing Planform Study task were to:

- Determine the effect of changes to the wing geometry (sweep [Λ], aspect ratio [AR], and thickness to chord ratio [t/c]) on overall airplane performance for an ACT Configuration

- Use these results, together with Initial ACT Configuration data, to recommend wing geometry for the Final ACT Configuration

- Determine sensitivity of study results to key assumptions

- Define the Final ACT Configuration

2.2 APPROACH

The IAAC Project began with a contemporary airplane configuration for which Boeing had accumulated substantial preliminary design background. The choice, data collection, and validation of this starting point constituted the Conventional Baseline Configuration Study. The Initial ACT Configuration evolved from the Baseline Configuration with the constraints that both the wing planform and the airplane size (i.e., the maximum takeoff weight, wing area, and engine) be unchanged. The fuel consumption per passenger mile was taken as the measure of improved performance. This approach allowed a reasonably thorough analysis without re-estimating aerodynamic characteristics for wing planform changes, or sizing to the design mission. Within these constraints, pitch-augmented stability (PAS) and angle-of-attack limiting (AAL) were used to rebalance the airplane and reduce the horizontal tail size to the minimum required for controllability. Wing trailing-edge surfaces and surface controls were reconfigured to accommodate ACT functions. The purpose of these functions is to alleviate wing loads and to control flutter and thus permit the removal of structural weight from the wing.

It was assumed that all required ACT functions would be available and could be mechanized. This assumption, which underlies the configuration development reported

5

herein, cannot be accepted casually. The increased dependence of the airplane on active systems for controlled flight and structural integrity demands careful consideration of the system's suitability, reliability, and interrelationship with the flight crew. A preliminary development effort in this area is the subject of the ACT System Technology Base Task (fig. 2), which will be detailed in a separate report (ref 4).

Previous studies have shown that wing planform changes, such as increased aspect ratio and reduced sweep, reduce cruise drag. In conventional designs, this has been counteracted by the effect of increased structural weight; however, ACT functions were expected to reduce the structural weight penalty associated with these planform changes. The next phase of the IAAC Project, therefore, was the Wing Planform Study and definition of a Final ACT Configuration.

2.3 SCOPE OF DOCUMENT

This document contains six major sections: 4.0 through 9.0. As described in Section 4, the planform study configurations were derived from the Conventional Baseline and the Initial ACT Configurations, with changes to the wing geometry.

Section 5.0 includes drawings showing the major components and payload capabilities of the three Wing Planform Study Configurations. The illustrations show general arrangement, inboard profile, body cross section, seating arrangement, cargo capability of the lower and upper lobes, and principal characteristics. Mission rules, performance, design weight, and center-of-gravity management also are shown.

Detailed data on the design of the airframe, propulsion, and flight control systems constitute Section 6.0. The major structures, components, and systems that will affect or are affected by an active controls system are described.

Section 7.0 describes a unified and substantially detailed program of structural, handling qualities, control system, and dynamic modeling development. This program established the feasibility of the three airplane configurations and the performance benefits relative to the Baseline and the Initial ACT Configurations. Most of the detailed analysis focused on the highest aspect ratio, highest sweep airplane configuration (768-104) due to its better fuel efficiency characteristics.

6

Section 8.0 summarizes the results of trade and sensitivity studies based primarily on the 768-104 Configuration. The purpose of the studies was to evaluate the effect of configuration variations on performance and substantiate the selection of a Final ACT Configuration.

Section 9.0 describes the selection of the Final ACT Configuration and defines the characteristic data.

Figure 4 compares the plan view, side view, and characteristic data of the Baseline Configuration and the Final ACT Configuration.

	Baseline Configuration	Final ACT Configuration
Passengers Mixed class All tourist	197 207	
Containers LD-2 or LD-3	22 or 11	
Engines	(2) CF6-6D2	
Wing area, m^2 (ft^2)	256.3[a] (2759)	226.8[b] (2441)
Maximum takeoff gross weight, kg (lb)	122 470 (270 000)	121 580 (268 040)
Operating empty weight, kg (lb)	78 300 (172 610)	79 890 (176 120)
Design range, km (nmi)	3590 (1938)	
Cruise Mach	0.8	

[a] Trapezoid geometry quoted, aero reference area—275.1 m^2 (2961 ft^2)

[b] Trapezoid geometry quoted, aero reference area—275.8 m^2 (2969 ft^2)

Wing shift 1.7m (5.5 ft)

5 cargo containers

Baseline

Final ACT

47.2m (155 ft) span   52.2m (171.3 ft) span

Baseline   Final ACT

8.6m (28.3 ft)

768-102, -107
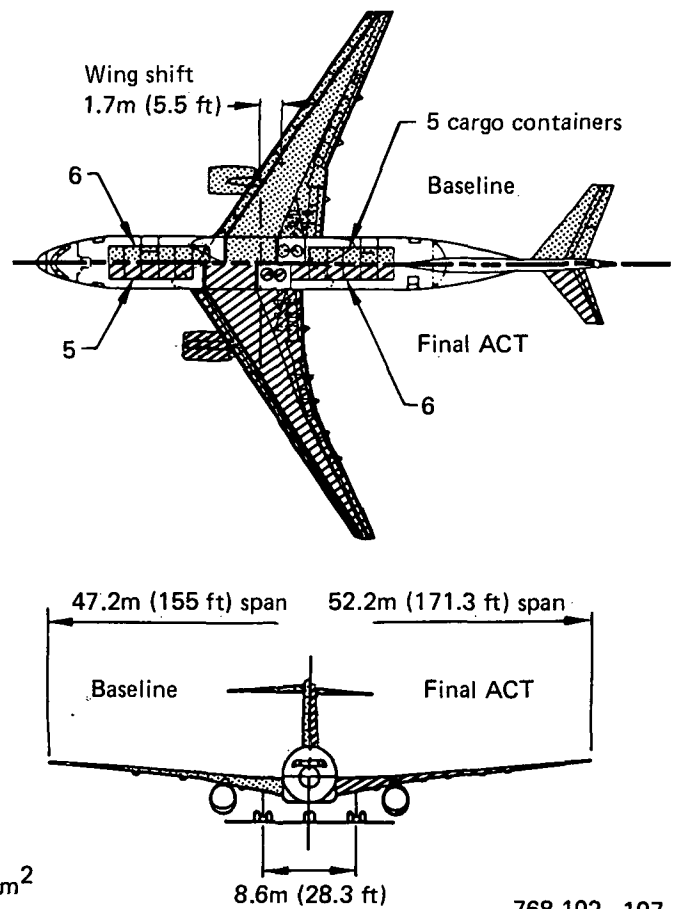
Figure 4. Final ACT and Conventional Baseline Configuration Comparison

7

3.0 SYMBOLS AND
ABBREVIATIONS

3.0 SYMBOLS AND ABBREVIATIONS

This section contains five subsections: Configuration Model Numbers, General Abbreviations, Subscripts, Symbols, and Axes and Sign Nomenclature. Each subsection is arranged in alphabetical order. For ease of reference, Subsection 3.3 is further divided into three parts—coefficient subscripts (3.3.1), velocity and Mach number subscripts (3.3.2), and general subscripts (3.3.3). Axes and sign nomenclature are illustrated in Figure 5.

3.1 AIRPLANE MODEL NUMBERS

768-102 Conventional Baseline Configuration
768-103 Initial ACT Configuration
768-104 AR 12.0, Λ 31.5, Configuration
768-105 AR 10.3, Λ 31.5, Configuration
768-106 AR 10.2, Λ 26.4, Configuration
768-107 Final ACT Configuration

3.2 GENERAL ABBREVIATIONS

a	aerodynamic lag constant; lift curve slope
ac	aerodynamic center; alternating current
ac^{WB}	wing-body aerodynamic center
accel	accelerometer
alt	altitude (same as h)
app	appendix
A	ampere
AAL	angle-of-attack limiter
ACT	Active Controls Technology
AFCS	automatic flight control system
Ah	ampere-hour
AIL	aileron

AP	autopilot
APB	auxiliary power breaker
APL	airplane
APU	auxiliary power unit
AR	aspect ratio (trapezoid)
ARCS	Airborne Advanced Reconfigurable Computer System
ARINC	Aeronautical Radio Incorporated
ASYM	antisymmetric
ATDP	air-turbine-driven pump
$\bar{A}$	gust response factor; ratio of root-mean-square incremental load to root-mean-square gust velocity
b	aerodynamic lag constant; wing span (airplane coordinates)
b_R	reference length
BBL	body buttock line
BL	buttock line
BLKF	block fuel
BM	bending moment
BS	body station
BHD	bulkhead
BTB	bus tie breaker
BWL	body water line
c	chord
cg	center of gravity
cm^3	cubic centimeter
$\bar{c}$	mean aerodynamic chord (same as MAC)
C	Celsius; flight condition
CPU	central processing unit

CR	contractor report
d	differential quantity
dB	decibel
dc	direct current
deg	degree
$\dfrac{d\delta_E}{dn}$	elevator deflection per unit load factor
D	drag
DADC	digital air data computer
DATCOM	U.S. Air Force Stability and Control Data Compendium
DMF	dynamic magnification factor
DOC	direct operating cost
DRO	design requirements and objectives
ext	extension
ECS	environmental control system
EDP	engine-driven pump
EET	Energy Efficient Transport Program
EI	bending stiffness
ELEV	elevator
EMP	electric-motor-driven pump
EOALT	engine-out altitude
EPC	external power contactor
f	applied stress; fuel; function
fig.	figure
ft	feet
fwd	forward
F	allowable stress; Fahrenheit; force

FAR	Federal Aviation Regulations
FMC	flutter-mode control
FS	front spar
g	acceleration due to gravity; structural damping coefficient for neutral stability
gal	gallon
gen	generator
GAF	generalized aerodynamic force
GCB	generator contactor breaker
GJ	torsional stiffness
GLA	gust-load alleviation
GPM	gallons per minute
GSE	ground service equipment
GW	gross weight
h	altitude (same as alt)
horiz	horizontal
hr	hour
H	height
HAA	high angle of attack
Hz	hertz
i	imaginary number $(\sqrt{-1})$
in	inch
IAAC	Integrated Application of Active Controls Technology to an Advanced Subsonic Transport Project
ICAC	initial cruise altitude capability
IDG	integrated drive generator
INBD	inboard
I/O	input/output

IRS	inertial reference system
k	gain; reduced frequency
kg	kilogram
km	kilometer
kn	knot
kPa	kilopascal
kVA	kilovoltampere
K	thousand
KE	wing-load alleviation elevator gain
KEAS	knots equivalent airspeed
KF	flutter-mode control gain
KG	gust-load alleviation aileron gain
KGW	gust-load alleviation wing-tip sensor gain
KGCG	gust-load alleviation center-of-gravity sensor gain
KMA	maneuver-load control aileron gain
KME	maneuver-load control elevator gain
KMN	maneuver-load control center-of-gravity sensor gain
KP	pilot command gain
KQ	pitch-augmented stability pitch-rate gain
KTAS	knots true airspeed
KU	pitch-augmented stability speed gain
Kθ	pitch-augmented stability pitch-attitude gain
lb	pound
lb-in	pound inch
lb/in	pounds per inch
lb/in^2	pounds per square inch
ℓ	lift loading; liter; rolling moment; tail arm

ℓ (L/b)	nondimensional loading
L	lag constant; lift
LAS	lateral/directional-augmented stability
LAT	lateral
LD- (2,3,4,8)	lower deck containers (various sizes)
L/D	lift/drag
LE	leading edge
LRU	line replaceable unit
LVDT	linear variable differential transformer
m	meter
max	maximum
min	minute
mm	millimeter
ms	millisecond
M	Mach number; mass; moment
MAC	mean aerodynamic chord (same as $\bar{c}$)
MCU	modular control unit
MLC	maneuver-load control
MLG	main landing gear
MLW	maximum design landing weight
MTBF	mean time between failure
MTOW	maximum design takeoff weight or maximum takeoff weight
MTW	maximum design taxi weight
MZFW	maximum design zero fuel weight
n	acceleration; normal load factor
nmi	nautical mile
nom	nominal

n/α	normal acceleration per unit of angle of attack
n_z	vertical acceleration in g or load factor
N	newton; ultimate normal load factor
N·m	newton meter
N/m	newton per meter
N/m^2	newton per square meter
NLG	nose landing gear
No.	number
OEW	operational empty weight
OUTBD	outboard
p	incremental roll rate
psi	pounds per square inch
P	roll rate
$\hat{p}$	nondimensional roll rate
PAS	pitch-augmented stability
PCU	power control unit
PSD	power spectral density
q	dynamic pressure; incremental pitch rate
$\hat{q}$	nondimensional pitch rate
Q	pitch rate
QSAE	quasi-static aeroelastic
r	incremental yaw rate
$\hat{r}$	nondimensional yaw rate
rad	radian
ref	reference
rms	root mean square
R	yaw rate

RAM	random access memory
RAT	ram-air turbine
ROI	return on investment
ROM	read-only memory
RS	rear spar
s	Laplace variable; second (same as sec)
sec	second (same as s)
S	surface planform area
SAR	still air range
SL	sea level
SLST	sea level static thrust
SOB	side of body
SSFD	signal selection and failure detection
STA	station
STAB	stabilizer
S_w	wing aerodynamic reference area
SW	switch
SYM	symmetric
sync	syncronous
t	surface gage; time
t/c	thickness to chord ratio
$\bar{t}$	equivalent total gage
t_{2X}	time to double amplitude
t_ϕ	time to bank angle
T	torque or torsion moment
TBD	to be determined
TE	trailing edge

TOFL	takeoff field length
TOGW	takeoff gross weight
TP	tangent point
TR	taper ratio
T-R	transformer-rectifier
TRAP	trapezoid
TX/RCV	transmitter/receiver
u	forward center-of-gravity velocity; incremental value of forward-speed component
util	utility
U	forward-speed component
U_σ	true vertical gust velocity
v	incremental value of lateral speed component
V	shear; velocity; volt
VA	volt-ampere
VOR	very high frequency omnidirectional radio range
V_1	takeoff decision speed
V_2	takeoff climb speed
$\bar{V}_H$	horizontal tail volume coefficient = $\dfrac{S_H}{S_W} \times \dfrac{\ell_H}{c_W}$
$\bar{V}_V$	vertical tail volume coefficient = $\dfrac{S_V}{S_W} \times \dfrac{\ell_V}{b_W}$
V_∞	flight path
W	pitch frequency; watt; width
WB	wing body
WBL	wing buttock line
WL	water line

WLA	wing-load alleviation
x	longitudinal center-of-gravity displacement
y	lateral center-of-gravity displacement
z	vertical center-of-gravity displacement
X, Y, Z	airplane reference axes as defined in Figure 5
$\ddot{Z}$	vertical acceleration

3.3 SUBSCRIPTS

3.3.1 Subscripts Related to Coefficient C

c	compressibility correction factor
D	drag
D_i	induced drag
D_P	polar shape or residual drag
D_M	compressibility drag
D_T	trim drag
D_0	profile drag
ℓ	rolling moment
ℓ_β	change in rolling moment with sideslip
L	lift
L_0	lift at zero angle of attack
$L\alpha^{WB}$	wing-body lift due to angle of attack
m	pitching moment
m_α	change in pitching moment due to angle of attack
m_δ	change in pitching moment due to control deflection
m_0	pitching moment at zero lift
n	section normal force; yawing moment

18

n_α	normal force slope
n_β	change in yawing moment due to sideslip
N	normal force
R	rudder
T	thrust
Y	side force

3.3.2 Subscripts Related to Velocity V or Mach Number M

APP	approach
B	gust penetration
C	cruise
D	dive
e	equivalent airspeed
g	gust
INC	incompressible
LO	lift-off
MCA	minimum control air
MCG	minimum control ground
MO	maximum operating
R	takeoff rotation speed
S	stall
∞	infinity; free-stream value

3.3.3 General Subscripts

A	aileron; antisymmetric
APP	approach
B	body; wing box

c	control airforce
com	command
COL	column command
COM	pilot command
D	Dutch roll
E	elevator
EQV	equivalent
F	flap
g	gust
H	high frequency; horizontal tail; mechanical mistrim
INST	instantaneous
max	maximum
n	natural
0	zero angle of attack
OA	outboard aileron
OAI	outboard aileron (inboard section); outboard aileron intersect
OAO	outboard aileron (outboard section)
P	phugoid
R	control rudder roll; root (trapezoid); rudder
REF	reference
s	shear
scr	plate shear (buckling)
ss	steady state
S	symmetric
SP	short period; spoiler
t	time
T	horizontal tail; tip

trap	trapezoidal
vol	volume
V	vertical tail
w	control wheel; vertical gust velocity; wing
W	wing

3.4 SYMBOLS

$\mathcal{C_L}$	centerline
α	angle of attack
$\hat{\alpha}$	nondimensional rate of change of angle of attack
β	sideslip angle
γ	flight path angle with horizon
δ	control deflection angle
$\dot{\delta}$	flutter-mode control rate
Δ	change in quantity
ϵ	downwash angle
ζ	damping ratio
η	fraction of semispan
θ	jig twist; pitch attitude
$\dot{\theta}$	rate of change of pitch attitude (equivalent to Q for zero bank angle)
$\ddot{\theta}$	pitch acceleration
λ	failure rate
λ'	taper ratio of chord at $\eta = 0.55$/chord at side-of-body
Λ	sweep
ρ	air density
σ	density ratio; real part; root mean square gust velocity; vertical tail sidewash angle
τ	time constant

21

τ_{GLA}		time constant of gust load alleviation system feedback filter
ϕ		roll attitude
$\ddot{\phi}$		roll acceleration
ψ		yaw attitude
$\ddot{\psi}$		yaw acceleration
ω		frequency
$\mathcal{L}$		Laplace transform
∂		partial differential
$[A + iA']$		box aerodynamic influence coefficients
$[A_0], [A_1], [A_2]$		approximating function coefficients
$[\bar{A}_0], [\bar{A}_1], [\bar{A}_2]$		approximating function coefficients for body axis airforces
$[B_1], [B_2]$		approximating function coefficients
$[\bar{B}_1], [\bar{B}_2]$		approximating function coefficients for body axis airforces
$[\hat{H}_1], [\hat{H}_2], [\hat{H}_3]$		mode shapes at aerodynamic boxes
$[k]$		nodal stiffness
$[K]$		stiffness
$[M]$		mass
$[\bar{M}_1]$		load coefficients
$[Q + iQ']$		generalized aerodynamic force
$[Q + iQ]$		generalized aerodynamic force in body axis
$[S_0, S_1, S_2]$		coefficients of S^0, S^1, S^2 in Laplace equations of motion
$[\Sigma]$		load-summing matrix
$[\phi]$		mode shapes at structural nodes
$\{F\}$		nodal forces and moments
$\{L\}$		load
$\{R\}$		body and control surface variables

$\{q\}$	variables in equations of motion
$\{\xi\}$	elastic generalized coordinates
$\lfloor PSF \rfloor$	pressure scale factors
$\lfloor S \rfloor$	box areas

3.5 AXES AND SIGN NOMENCLATURE

$$C_D \quad C_Y \quad C_L \quad C_\ell \quad C_m \quad C_n \quad \text{—nondimensional}$$

Hinge moment sign convention:

    Positive hinge moment produces positive surface deflection

Roll control:
$$+\delta_W = f \left(+\delta_A \, +\delta_{SP} \right)$$
$$\delta_A = \frac{\delta_{left} - \delta_{right}}{2}$$

768-102, -103, -104, -105, -106, -107

Figure 5. Axes and Sign Nomenclature

24

4.0 WING PLANFORM STUDY

4.0 WING PLANFORM STUDY

Definition of the Baseline Configuration (ref 2) and Initial ACT Configuration (ref 3) preceded development of the three Wing Planform Study Configurations (Models 768 -104, -105, and -106). Overall fuselage dimensions were retained, as were control surface types. The main landing gear (MLG) type common to the Initial ACT Configuration was also used. The wing geometry, empennage size, structure, and systems were tailored to realize advantages of ACT for each of the three wing planforms. This section identifies study constraints, defines the design criteria and objectives that were influenced by ACT, and describes the resulting three planform study configurations.

4.1 STUDY GROUND RULES AND CONSTRAINTS

Key ground rules and constraints adopted for this study are described in the following subsections.

4.1.1 ACT FUNCTIONS

ACT functions were applied to improve the airplane performance through reduced drag and/or weight. These objectives were achieved by: (1) relying upon pitch augmentation and rebalancing the airplane with the center-of-gravity (cg) range farther aft, and (2) reducing structural design loads and/or airframe structural stiffness requirements. The ACT functions that make these changes possible are:

- Pitch-augmented stability (PAS)—The PAS function augments the airplane longitudinal stability to provide acceptable flying qualities. Both long-period (static stability) and short-period augmentation are included.

- Lateral/directional-augmented stability (LAS)—The LAS function is a conventional yaw damper identical to that of the Baseline Configuration. In the Baseline, the yaw damper is implemented in the analog control systems electronics unit, which is retained in the selected configurations. Therefore, the LAS function is not considered part of the ACT system added in these configurations.

- Angle-of-attack limiter (AAL)—The AAL function prevents the airplane from exceeding a limiting angle of attack, which is a small margin beyond that for maximum lift and allows a reduction in the horizontal tail size required to provide nose-down control margin for stall recovery.

- Wing-load alleviation (WLA)—The WLA function has two submodes composed of:

  - Maneuver-load control (MLC)—MLC reduces the wing vertical bending moment in longitudinal maneuvers and low-frequency gusts by deflecting the outboard ailerons to redistribute the wing loads.

  - Gust-load alleviation (GLA)—GLA reduces the wing loads due to atmospheric disturbances by deflecting outboard ailerons to reduce and redistribute the induced loads.

- Flutter-mode control (FMC)—FMC stabilizes the critical wing flutter mode by sensing wing motion and commanding deflection of a small wing trailing-edge surface. It may be used to provide the required flutter-mode stability to $1.2V_D/M_D$; however, at and below V_D/M_D stability is required without dependence on FMC.

The safety impact of failure of any ACT function depends on its necessity for continued safe flight or its function criticality levels, defined as follows:

- Flight crucial—Complete loss of function results in an immediate, unconditional hazard to safe and continued flight

- Flight critical—Complete loss of function results in a potential hazard to safe, continued flight; i.e., appropriate flight crew action can avert the hazard

- Flight noncritical—Complete loss of function may result in increased crew workload or passenger discomfort but does not result in hazard to safe, continued flight.

26

Table 1 relates criticality levels to reliability levels required for the ACT systems. The PAS short-period system was designed to be flight crucial; other ACT functions are flight critical.

Table 1. Relationship of Reliability to
Criticality Levels

Criticality level	Failure probability requirement, per flight hour
Crucial	$< 1 \times 10^{-9}$
Critical	$< 1 \times 10^{-5}$
Noncritical	$< 1 \times 10^{-3}$

768-103, -104, -105, -106, -107

4.1.2 CONFIGURATION CONSTRAINTS

To ensure close correlation between data base and performance of the Baseline and Wing Planform Study Configurations, the Wing Planform Study Configurations were defined by the following framework of constraints:

● Fuselage—The same payload and cargo capacity as the Baseline and Initial ACT Configurations were used on all three Wing Planform Study Configurations. Structural arrangements were varied to suit wing, empennage, and landing gear for each configuration.

● Wing—The three wing planform geometries were developed for the same wing aerodynamic reference area as the Baseline and Initial ACT Configurations, approximately 275 m^2 (2960 ft^2). Because the required trailing-edge extension (yehudi) varies considerably with wing geometry, the aerodynamic reference areas rather than trapezoid areas were held constant. Figure 6 illustrates the procedure for wing reference area calculation. The trailing-edge extension could be modified to accommodate the landing gear. The quantity, type, and location of control surfaces could change within the geometric constraints. Wing location, relative to the body, was constrained to increments of approximately 1.68m (66 in), consistent with fuselage frame spacing and the requirement to

27

accommodate 22 LD-2 containers. For balance, the wings were located on the fuselage with the 0.35 mean aerodynamic chord (MAC) of each trapezoidal planform at the same point; 0.35 MAC is the approximate cruise cg location.

- Main landing gear—The swing arm double-post main landing gear configuration was developed for the Initial ACT Configuration. Being consistent with the desired balance and ground-handling features of these airplanes, it was retained for the Wing Planform Study. It was located at a constant distance behind the wing 0.35 MAC.

- Empennage—The T-tail arrangement of the Baseline and Initial ACT Configurations was retained; however, the sizes of the vertical and horizontal tails and of the control surfaces could be varied. Horizontal tail sizing assumes the use of PAS and AAL.

- Propulsion—Two CF6-6D2 engines, located with the pylon centerline intersecting the wing reference plane leading edge at wing buttock line (WBL) 7.87m (310 in), were the same as for the Baseline and Initial ACT Configurations. Fuel containment and fuel systems were to be defined.

- Systems—Electric, electronic, hydraulic, and mechanical systems were modified as required to accommodate the ACT functions and systems.

4.1.3 STUDY GROUND RULES

4.1.3.1 Operational Characteristics

Maximum and minimum operating characteristics, consistent with safe ground and flight operations provided by the Baseline Configuration, were maintained. Examples include cabin pressurization, structural limits on speed, and payload capacity. Gate space limitations for higher span wings have not been a restriction in the planform study.

The 122 470 kg (270 000 lb) maximum takeoff weight (MTOW) and design payload of 17 870 kg (39 400 lb) of the Baseline Configuration were held constant.

$$S_w = S_T + S_{Y1a} + S_{Y2a} + S_{Ga} + \left(S_{Y1b}\right)\frac{\left(b_{Y1}\right)}{\left(b_T\right)} + \left(S_{Y2b}\right)\frac{\left(b_{Y2}\right)}{\left(b_T\right)} + \left(S_{Gb}\right)\frac{\left(b_G\right)}{\left(b_T\right)}$$

S_w = wing aerodynamic reference area

S_T = wing basic trapezoid area (includes area covered by body)

S_{Y1a} = exposed area of first trailing-edge extension

S_{Y1b} = hidden area of first trailing-edge extension (area covered by body)

S_{Y2a} = exposed area of second trailing-edge extension

S_{Y2b} = hidden area of second trailing-edge extension (area covered by body)

S_{Ga} = exposed area of glove

S_{Gb} = hidden area of glove (area covered by body)

Y = wing trailing-edge extension

G = glove (wing leading edge extension)

$b_{subscript}$ = exposed span of element

$c_{subscript}$ = chord of element at $\mathcal{C}_L$ airplane except:

c_R = root chord of basic trapezoid wing

c_T = tip chord

Note: Abbreviations apply only to this figure except: S, S_w, c_R, and c_T
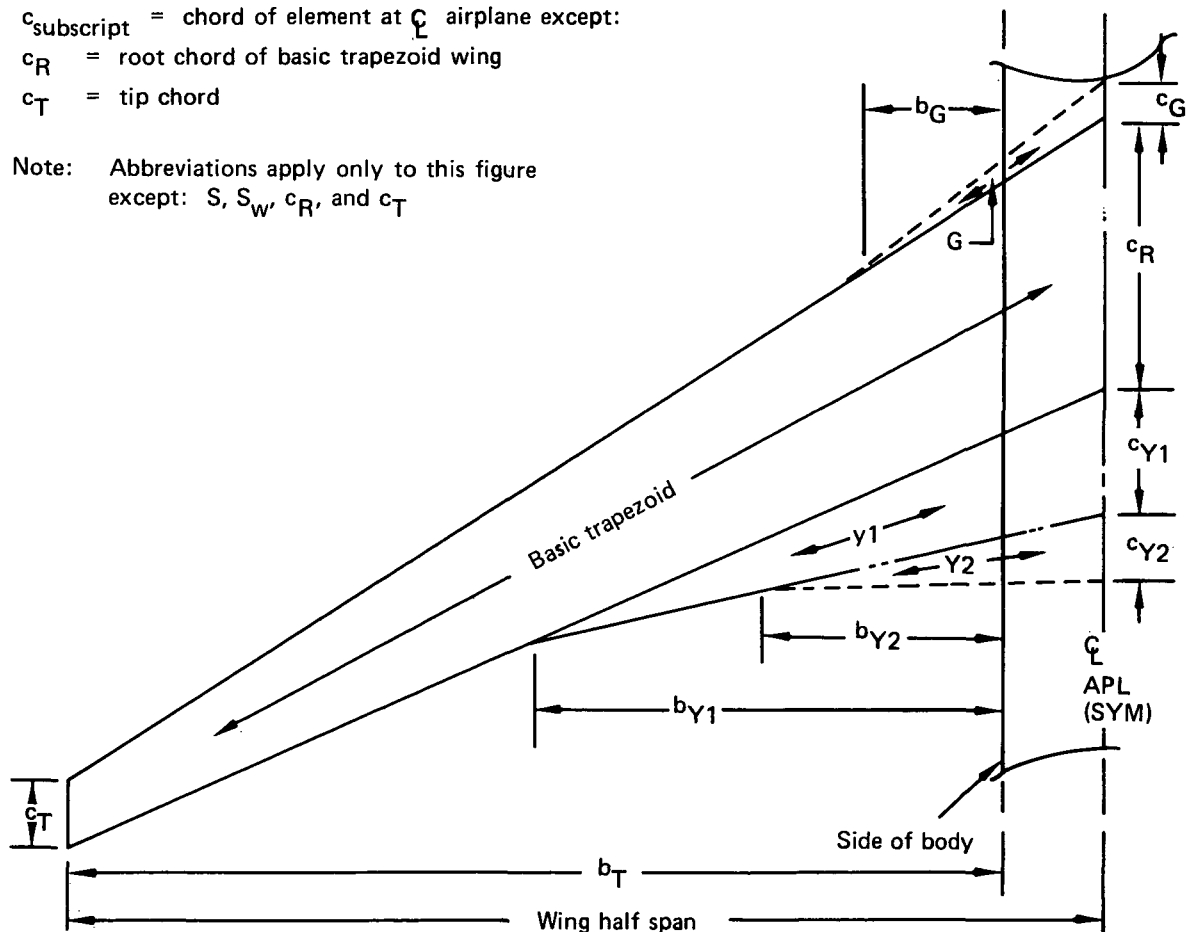
768-102, -103, -104, -105, -106, -107

Figure 6. Wing Aerodynamic Reference Area

29

4.1.3.2 Technology Application

Except for the control system, state-of-the-art technologies applied to the Baseline Configuration were maintained. Structural materials included advanced aluminum alloys and limited use of composites in secondary structure. Wing aerodynamics technologies (i.e., type of airfoil, sweep, and thickness-to-chord ratio) were maintained. Wing thickness and twist could be locally tailored to accommodate ACT.

4.2 DESIGN REQUIREMENTS AND OBJECTIVES

The design requirements and objectives (DRO) developed for the Initial ACT Configuration (ref 3) are applicable for the Wing Planform Study Configurations.

4.3 PREVIOUS IAAC CONFIGURATIONS

4.3.1 CONVENTIONAL BASELINE CONFIGURATION

As the first task on the IAAC Project, a comprehensive data base was established for a modern Mach 0.8 transport design. The following paragraphs are excerpts from the Conventional Baseline Configuration Study document (ref 2).

Characteristics of the U.S. domestic fleet were evaluated to determine the mission characteristics that would have the most impact on future U.S. transport fuel use. Selection of a 197-passenger (plus cargo) configuration with a mission of about 3590 km (1938 nmi) allowed Boeing to apply considerable analytical and test data that had been derived during earlier preliminary design efforts.

The existing data base was reviewed, and additional analyses were conducted to complete the technical descriptions. Significant characteristics of the resulting Baseline Configuration are shown in Figure 7. The configuration has a double-lobe, but nearly circular, body with seven-abreast seating. Externally, it has an 8.71 aspect ratio, 31.5 deg sweep wing, a T-tail empennage, and a dual CF6-6D2, wing-mounted engine arrangement. The lower lobe can accommodate 22 LD-2 or 11 LD-3 containers plus bulk cargo. Passenger/cargo loading, servicing, taxi/takeoff speeds, and field length characteristics are compatible with accepted airline operations and regulations.

30

Configuration	
Passengers	197 mixed class, 207 all tourist
Containers	22 LD-2, or 11 LD-3
Engines	2 (CF6-6D2)
Design mission	
Cruise Mach	0.8
Range	3590 km (1938 nmi)
Takeoff field length	2210m (7250 ft)
Approach speed	70 m/s (136 kn)
Noise	FAR 36, Stage 3
Flying qualities	Current commercial transport practice
Airplane technology	Current commercial transport practice (aerodynamics, structure, propulsion, etc.)

768-102
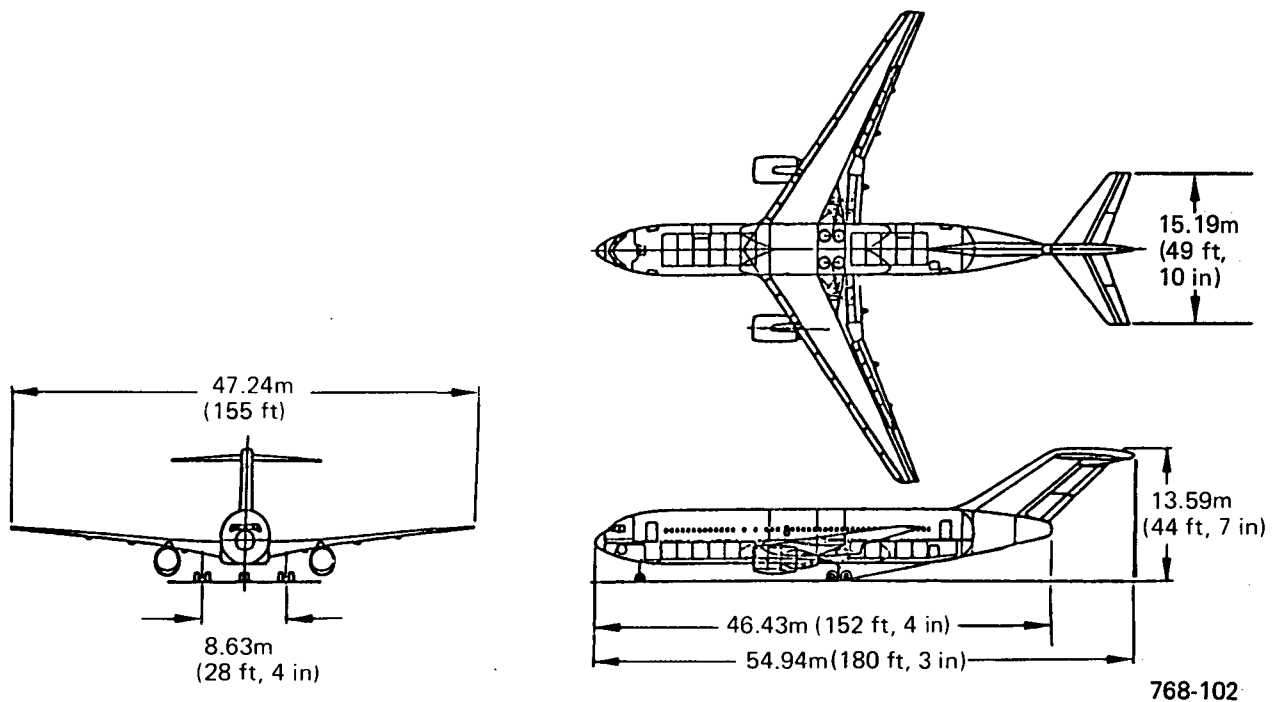
Figure 7. Baseline Configuration

The Baseline Configuration construction is conventional aluminum structure except for use of advanced alumimum alloys and a limited amount of graphite-epoxy secondary structure. It uses advanced guidance, navigation, and controls systems, which emphasize application of digital electronics and advanced displays.

The initial task of the IAAC Project resulted in a well-defined Baseline Configuration that provided a firm base for definition and evaluation of the benefits offered by configurations that use ACT.

4.3.2 INITIAL ACT CONFIGURATION DEVELOPMENT

In the second task on the IAAC Project, a constrained application of active controls was made to the Baseline Configuration, resulting in the Initial ACT Configuration. The following paragraphs are excerpts from the Initial ACT Configuration Design Study document (ref 3).

The performance and economic benefits of a constrained application of ACT were identified, and the approach to airplane design was established for subsequent steps leading to the development of a less constrained Final ACT Configuration. The active controls configurations were measured against the Baseline Configuration to determine whether the performance and economic changes resulting from ACT merit proceeding with the project. The technology established by the Baseline Configuration was held constant except for the addition of ACT. The wing, with the same planform, was moved forward on the Initial ACT Configuration to. move the loading range aft relative to the wing MAC. Wing trailing-edge surfaces and surface controls also were reconfigured for load alleviation and structural stabilization.

The PAS active controls function together with a double-hinged elevator to allow the cruise cg to be moved aft 10% and the horizontal tail size to be reduced 45%. The fuel system and tank arrangement were revised to preclude flutter, yet the overall wing structure became lighter because of WLA. The net effect of these changes was a 930 kg (2050 lb) reduction in airplane operational empty weight (OEW) and a 3.6% improvement in cruise aerodynamic efficiency.

The Initial ACT Configuration was not resized to the Baseline mission. Consequently, there was a 13% increase in range at the same takeoff gross weight and payload as the Baseline Configuration. Adjusted to the 3590 km (1938 nmi) Baseline mission range, this becomes approximately a 6% reduction in block fuel and a 15.7% incremental return on investment (ΔROI); i.e., the incremental capital costs (based on factored cost data) for design, development, and installation of the equipment and configuration

32

differences between the Initial ACT and Baseline Configurations. This 15.7% ΔROI corresponds to a $0.1057/ℓ ($0.40/gal) fuel cost, in 1978 dollars. Much larger return on investment may be expected if recent high fuel inflation rates continue.

The encouraging results of the Initial ACT Configuration design task clearly indicated that the IAAC Project should proceed to determine what further benefits may be achieved through wing planform changes and advanced ACT systems.

Significant characteristics of the Initial ACT Configuration are shown in Figure 8.

4.4 PLANFORM MATRIX

Prior to the development of the Wing Planform Study, planforms with aspect ratios from conventional values to as high as 20 and various sweeps were given a preliminary examination.

As constraints were established, a matrix of 11 wing planform geometries plus the Baseline/Initial ACT wing was assembled. Trapezoidal aspect ratios ranged from 8.7 (Baseline value) to 14, and quarter chord sweeps ranged from 26.4 to 36.5 deg. A computer-drawn plot of the 12 wings is shown in Figure 9. It was judged that these 12 wings cover the extremes of airplanes that could be configured for study in relation to the Baseline Configuration without introducing unconventional features that might seriously distort the study results. The lower chart in Figure 10 indicates the trend of one such feature, landing gear complexity.

4.5 WING PLANFORM SELECTION

4.5.1 SELECTION PROCESS

The 11 wings in the geometry matrix described in Subsection 4.4 were the candidates for the study that, with the Initial ACT wing, would serve as the data base for selection of the Final ACT Configuration. As indicated in Figure 10, the several parameters to be considered in the selection process tend to bias the selection in different directions. Therefore, to some extent, selection of planforms for indepth study must be a subjective process, based on the experience and judgment of the

Configuration	
Passengers	197 mixed class, 207 all tourist
Containers	22 LD-2 or 11 LD-3
Engines	2 (CF6-6D2)
Design mission	
Cruise Mach	0.8
Range	4061 km (2193 nmi)
Takeoff field length	2118m (6950 ft)
Approach speed	68.6 m/s (133.4 kn)
Noise	FAR 36, Stage 3
Flying qualities	Current commercial transport practice
Airplane technology	Current commercial transport practice (aerodynamics, structural, propulsion, etc. with the addition of active control functions)
Active controls functions	
Pitch-augmented stability	(PAS)
Maneuver-load alleviation	(MLA) } Wing-load alleviation (WLA)
Gust-load alleviation	(GLA)
Flutter-mode control	(FMC)
Angle-of-attack limiting	(AAL)

47.24m
(155 ft)

11.30m
(37 ft, 1 in)

13.46m
(44 ft, 2 in)

Static ground line

8.63m
(28 ft, 4 in)

46.43m (152 ft, 4 in)

54.18m (177 ft, 9 in)
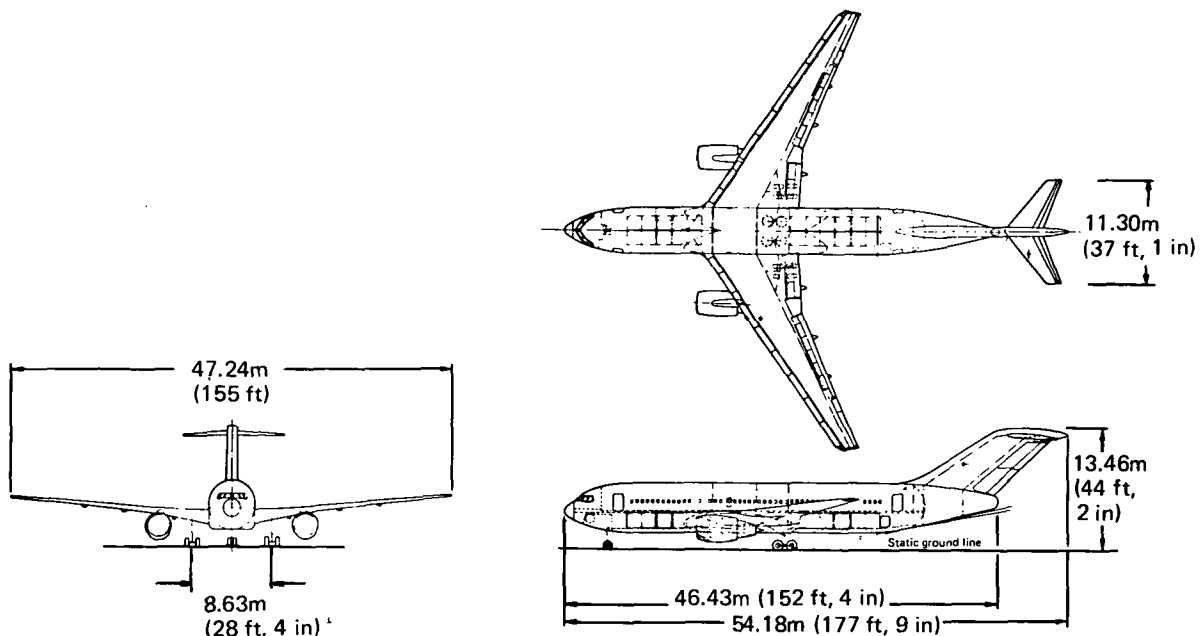
768-103

Figure 8. Initial ACT Configuration
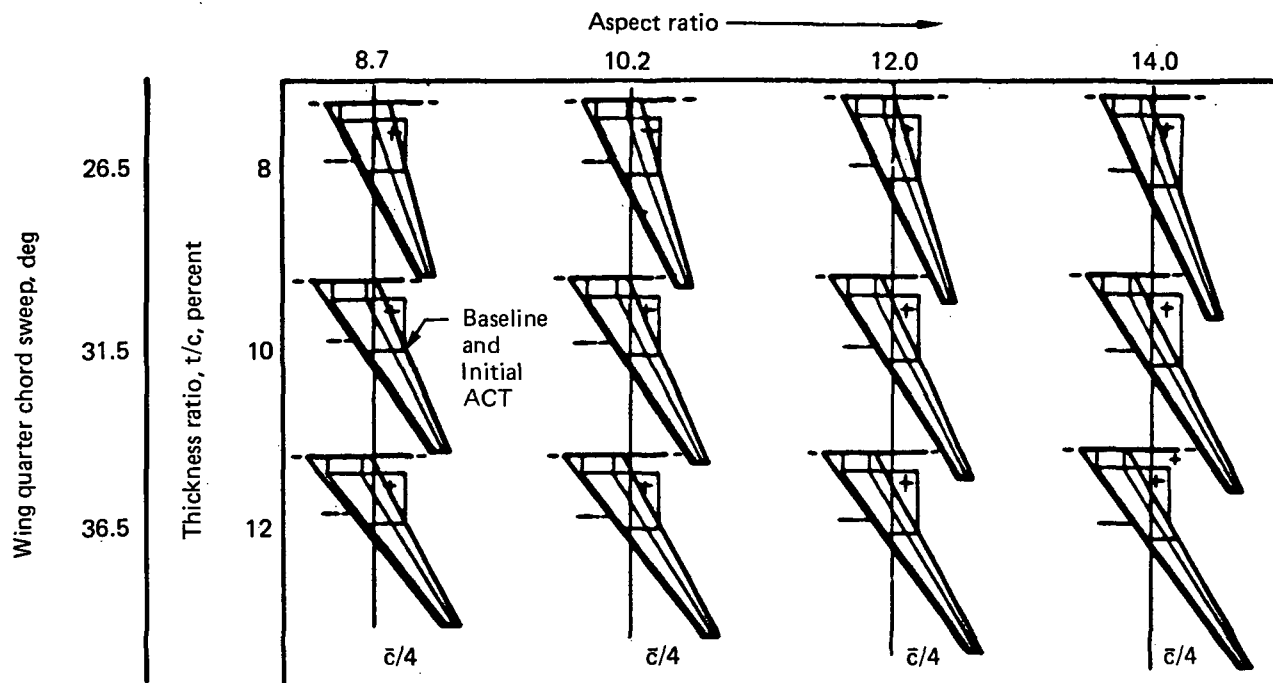
Figure 9. Wing Planform Study, Matrix of Candidates

selectors, to cover the range of reasonable configurations needed to guide the Final ACT selection.

4.5.2 SELECTED PLANFORMS

The selected wing planforms are highlighted in Figure 11, the reprinted geometry matrix. Two wings were selected with higher aspect ratios at the Baseline and Initial ACT wing sweep; i.e., 31.5 deg. These aspect ratios are 10.3 and 12. A wing with 5 deg less sweep was also selected at an intermediate aspect ratio of 10.2.

Detailed development of the selected planforms and integration into complete airplane configurations resulted in small changes to the geometry, the most conspicuous difference being the addition of a second trailing-edge break.

The resulting wing planform configurations are shown in Figure 12.

35
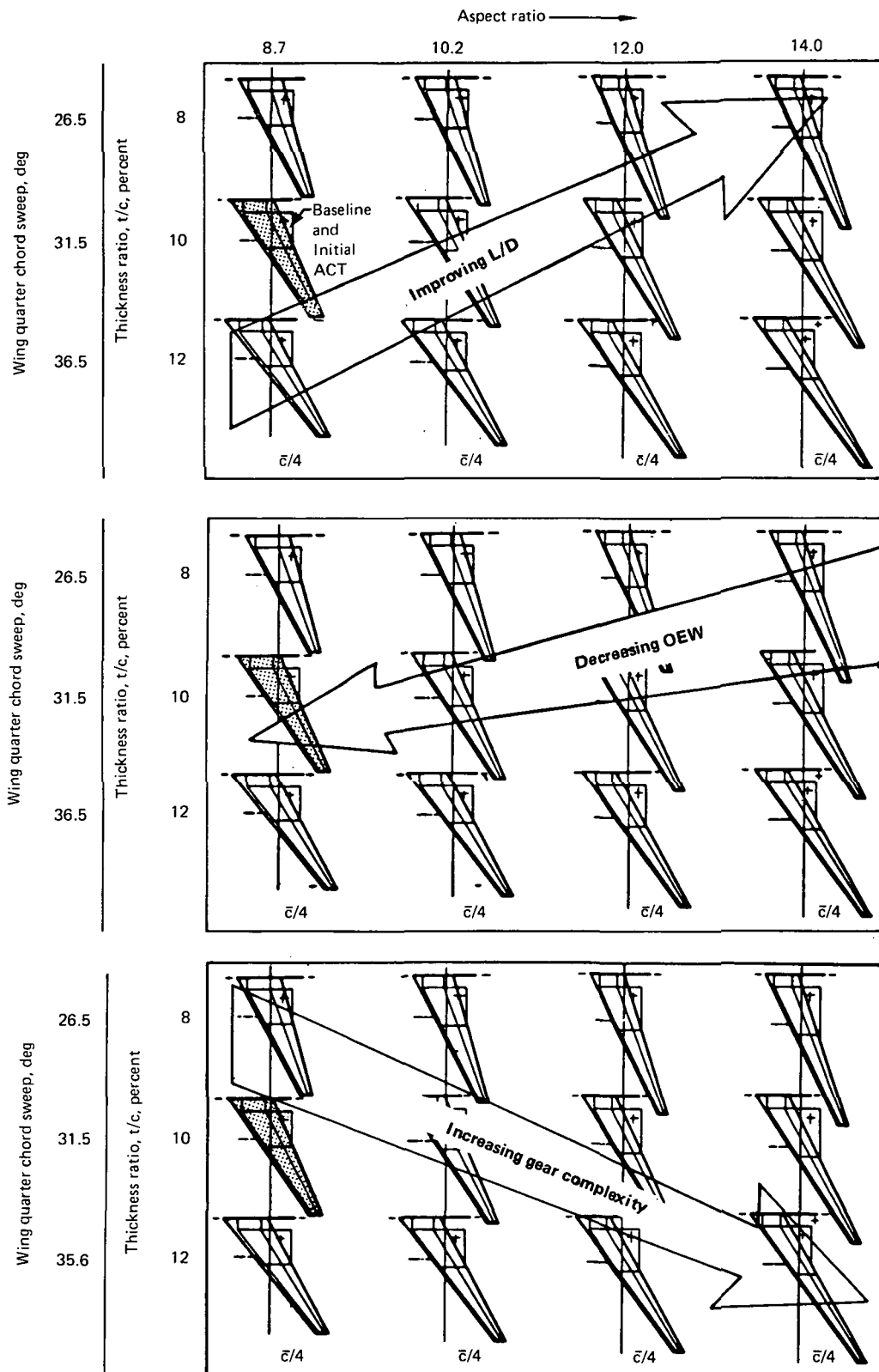
Figure 10. Matrix of Candidate Planforms
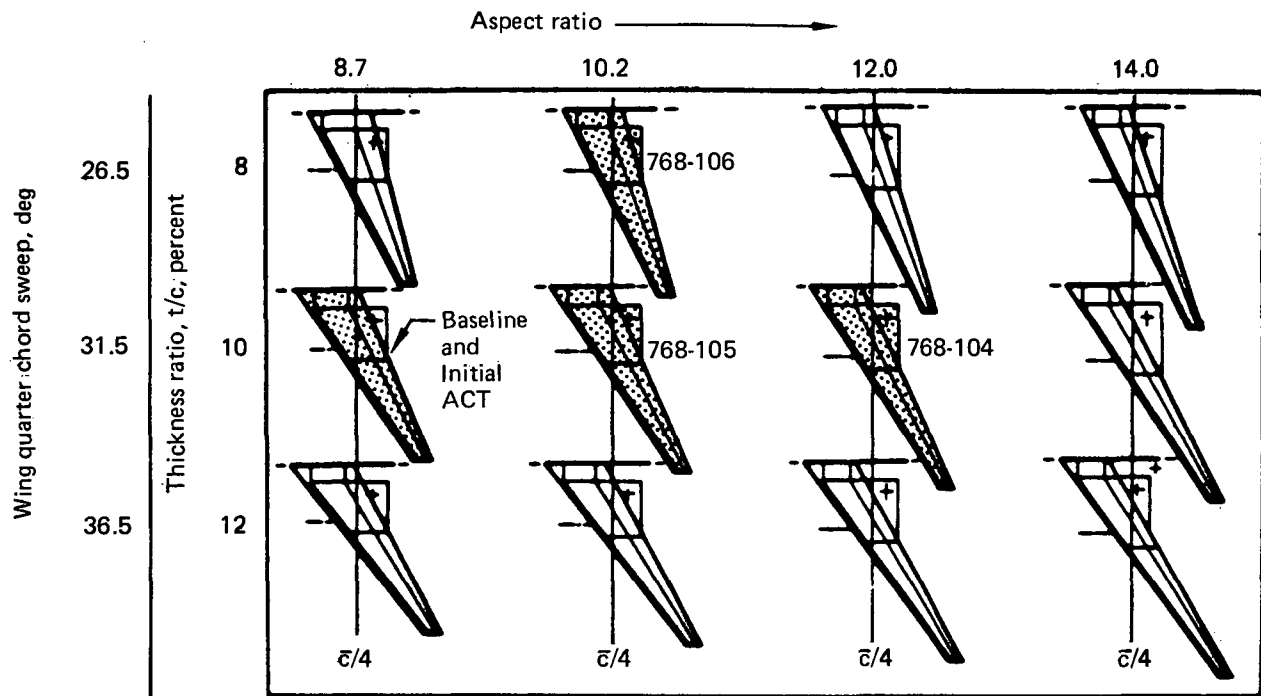
Figure 11. Selected Wing Planform Geometries
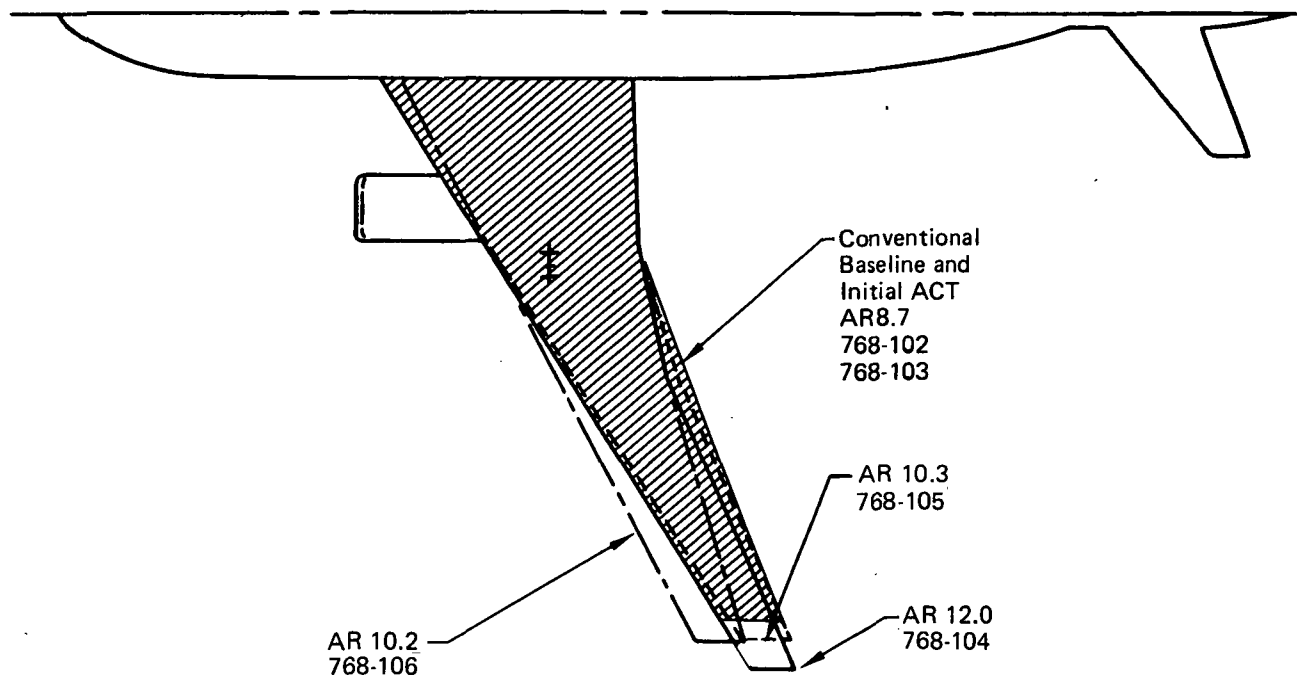
Figure 12. Wing Planform Comparison

Page intentionally left blank

Page intentionally left blank

5.0 CONFIGURATION DESCRIPTION

This section briefly describes the evolution of the Wing Planform Study Configurations. Illustrations of the general arrangements and payload capabilities are supplemented by descriptions of principal configuration characteristics. Also presented are the mission rules, performance and noise characteristics, design weights, and center-of-gravity (cg) management.

5.1 CONFIGURATION EVOLUTION

Two major decision stages were involved in developing the planform study configurations:

- Selection of three wing planforms that would become a data base for the Final ACT Configuration selection

- Design of realistic airplanes, combining the ACT functions with a feasible general arrangement, structure, systems, and constant payload provisions

The Initial ACT Configuration (ref 3) served as a baseline for configuration development. Wing, main landing gear, empennage, and systems were revised as required for each new configuration.

The most significant configuration changes were:

- The new wing geometries
- New cg locations
- Revised empennage size

5.1.1 ACT FUNCTIONS

All the active controls functions shown in Subsection 4.1 were considered in the planform study, but the gust-load alleviation (GLA) and flutter-mode control (FMC) functions were not judged beneficial (see subsecs 7.2 and 7.3). The control surfaces

39

used by the remaining functions are shown in Figure 13. The lateral/directional-augmented stability (LAS) system function is common to the Initial ACT Configuration.

Single-surface,
dual-hinged elevator
(PAS, MLC, AAL via column)

Horizontal
stabilizer
(PAS)

Dual rudder
(LAS)

Stick pusher
(AAL)

Outboard aileron—
(WLA and existing
lateral control)

ACT function		Control
PAS (short period)		Elevator
PAS (speed)		Elevator and stabilizer
LAS		Rudder
AAL		Column/elevator
WLA	MLC	Outbd aileron and elevator (through PAS command)

768-104, -105, -106
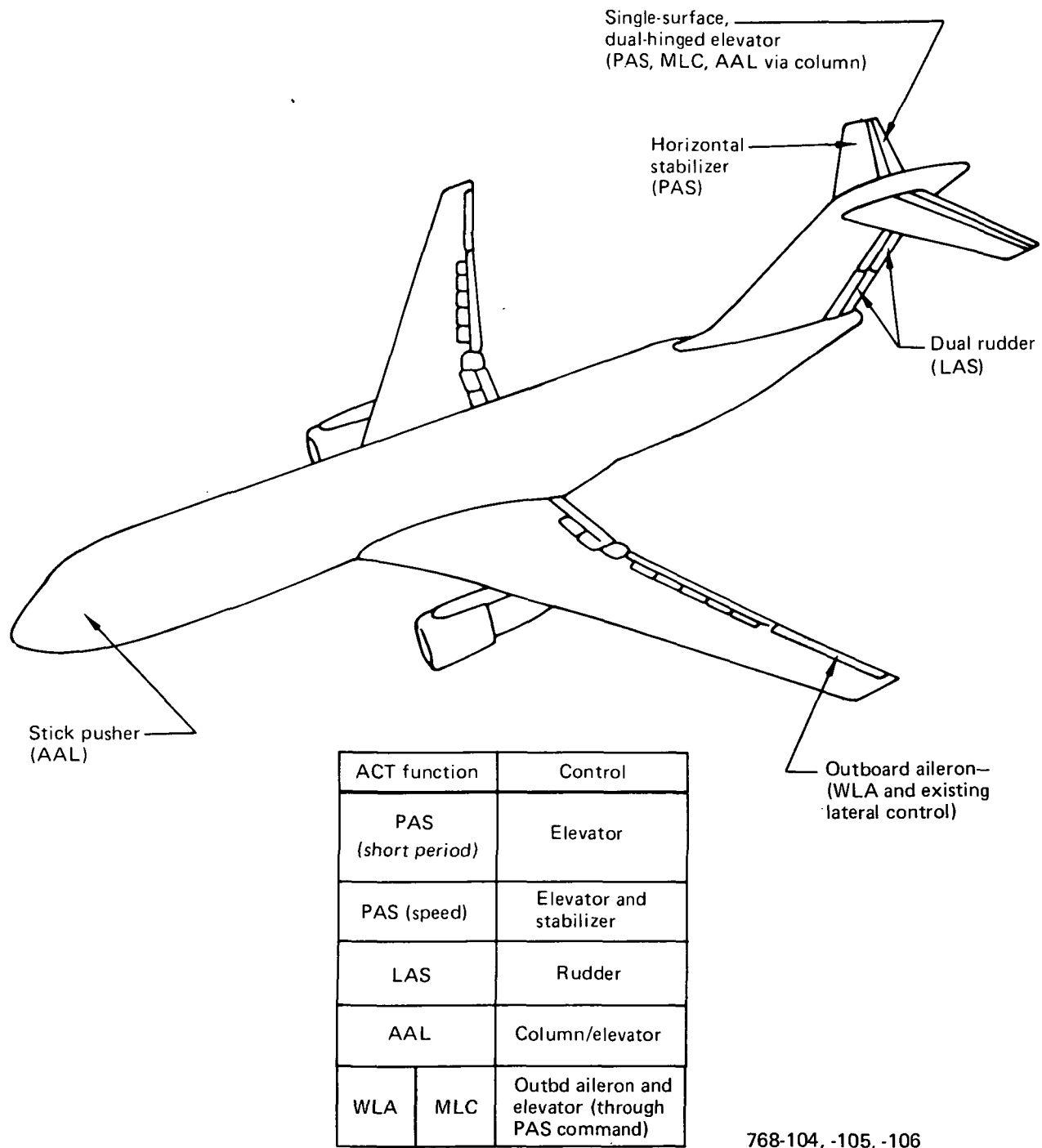
Figure 13. ACT Control System Surfaces

40

5.1.2 INTERNAL ARRANGEMENT AND LANDING GEAR

The constraints discussed in Subsection 4.1.2 dictated the placement of each of the three wings at approximately the same location relative to the body as that of the Initial ACT Configuration (see subsec 5.2.1). Doors, cargo provisions, and seating arrangement are therefore the same as those of the Initial ACT. Balance and cg limits for each configuration are similar but not identical to each other and to the Initial ACT.

The main landing gear configuration selected for the Initial ACT proved, with very minor geometry changes, to meet the requirements of each of the three planform study configurations. It is described in Subsection 6.1.5. The landing gear support beam concept of the previous configurations was used on Models 768-104 and 768-105. The 768-106 Configuration with its different wing structural arrangement and thinner, smaller-chord inboard wing, could not use the gear beam support concept. A cantilever support extending from the rear of the wing box was used for this configuration.

5.2 CONFIGURATIONS

5.2 CONFIGURATIONS

This section describes physical configuration data. The external shape of the airplane and the major internal views (systems, passengers, and cargo) are shown. The geometric data are supplemented by pertinent characteristics of engine, fuel capacity, and flight crew. The descriptions focus on Model 768-104, and distinctions are made for Models 768-105 and -106.

5.2.1 GENERAL ARRANGEMENT

The principal dimensions and general arrangement of all Wing Planform Study Configurations are shown in Figures 14, 15, and 16. These twin-engine, low-wing, land-based commercial transport airplanes are sized for a payload of 197 passengers in mixed-class accommodations, and 22 LD-2 containers or other types up to 2.44m (96 in) wide. General Electric CF6-6D2 engines in wing-pylon-mounted nacelles power the airplanes. Structural materials and design are conventional.

The aerodynamic reference areas of the three planform study wings were held approximately constant and similar to the Initial ACT Configuration (ref 3). A dual break in the trailing edge provides a smooth transition and separates the outboard flaps into two parts for convenient manufacturing. All wings have five outboard spoilers on each side. The 35% mean aerodynamic chords (MAC) of the three wings are located at the same body station (BS 24.039m [946.43 in]) as on the Initial ACT Configuration. The three wings' rear- and front-spar intersections are similarly located, except for Model 768-106, where the narrower wing box moves the front spar intersection back by 0.56m (22 in).

The area and planforms of the Models 768-104 and -105 horizontal tails are identical to those of the Initial ACT Configuration; the area on the Model 768-106 is about 9% larger. These are all trimmable surfaces with elevators.

The vertical tail areas vary within +5% from the Initial ACT Configuration. A two-segment, double-hinged rudder was used on all three configurations.

43

Geometry:

Body cross section, m (in)	
Shape	Vertical double lobe
Maximum width m (in)	5.029 (198.0)
Maximum height, m (in)	5.410 (213.0)

Landing gear	Nose	Main
Type	Dual	Truck
Location, m (in)	BS 6.896 (271.50)	72.4% MAC
Spacing, m (in)	0.610 (24)	1.143 x 1.422 (45 x 56)
Tire size, m (in)	0.940 x 0.330-0.406 (37 x 13-16)	1.092 x 0.394-0.508 (43 x 15.5-20)
Oleo stroke, m (in)	0.381 (15)	0.508 (20)

Aerodynamic surfaces	Wing	Vertical tail	Horizontal tail
Area, m2 (ft2)	226.8 (2441)a	56.6 (609)	32.0 (344)
Aspect ratio	12.03a	0.67	4.00
Taper ratio	0.267a	0.700	0.400
Sweep at c/4, deg	31.5a	55.0	35.0
Incidence, SOB, deg	3.8a		
Dihedral, deg	6.0a	–	-3.0
Root t/c, percent	15.1	12.0	11.0
Tip t/c, percent	10.3	12.0	9.0
Root chord, m (in)	6.855 (269.89)a	10.811 (425.64)	4.038 (158.98)
Tip chord, m (in)	1.830 (72.06)	7.568 (297.94)	1.615 (63.59)
MAC m(in)	4.827 (190.05)a	9.285 (365.57)	3.000 (118.10)
Span, m (in)	52.222 (2056)	6.157 (242.40)	11.291 (444.53)
Tail arm, m (in)	–	21.534 (847.78)	28.709 (1130.27)
Tail volume coefficientb	–	0.085	0.689

Engine toe-in angle = 1 deg to a BBL
Nacelle incidence = 2.625 deg to a BWL
Wing upper surface at SOB rib at BWL 4.953m (195 in)

aTrapezoid geometry quoted: aero reference area = 275.8 m2 (2969 ft2)
bBased on aero reference area

Passenger accommodations	Passengers	Abreast	Pitch
First class:	18	6	0.965m (38 in)
Tourist:	179	7	0.864m (34 in)

Cargo and baggage, m3 (ft3):

Containers	22 LD-2	or	11 LD-3	or	11 LD-4
Forward	33.98 (1200)		22.37 (790)		27.61 (975)
Aft	40.78 (1440)		26.85 (948)		33.13 (1170)
Bulk cargo (aft only)	11.33 (400)		11.33 (400)		11.33 (400)
Total	86.09 (3040)		60.55 (2138)		72.07 (2545)

Weights, kg (lb):
TOGW: 122 470 (270 000)
OEW: 79 960 (176 280)
MLW: 114 230 (251 830)

Propulsion: Two CF6-6D2
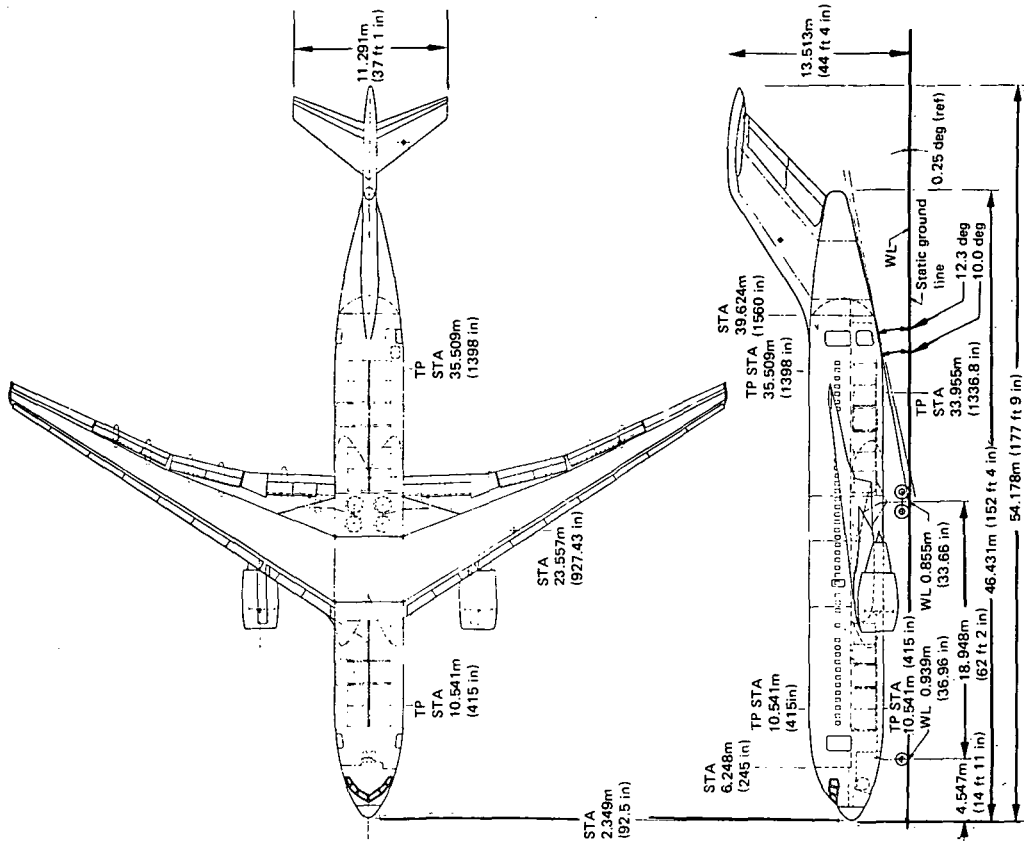
Figure 14. Model 768-104 General Arrangement

Weights, kg (lb):

TOGW: 122 470 (270 000)
OEW: 78 834 (173 800)
MLW: 113 100 (249 350)

Propulsion: Two CF6-6D2

Passenger accommodations:

	Passengers	Abreast	Pitch
First class:	18	6	0.965m (38 in)
Tourist:	179	7	0.864m (34 in)

Cargo and baggage, m³ (ft³):

Containers	22 LD-2 or	11 LD-3 or	11 LD-4
Forward	33.98 (1200)	22.37 (790)	27.61 (975)
Aft	40.78 (1440)	26.85 (948)	33.13 (1170)
Bulk cargo (aft only)	11.33 (400)	11.33 (400)	11.33 (400)
Total	86.09 (3040)	60.55 (2138)	72.07 (2545)

Geometry:

Body cross section, m (in)

Shape	Vertical double lobe
Maximum width, m (in)	5.029 (198.0)
Maximum height, m (in)	5.410 (213.0)

Landing gear

	Nose	Main
Type	Dual	Truck
Location, m (in)	85.6.896 (271.50)	68.6% MAC
Spacing, m (in)	0.610 (24)	1.143 × 1.422 (45 × 56)
Tire size, m (in)	0.940 × 0.330-0.406	1.092 × 0.394-0.508
	(37 × 13-16)	(43 × 15.5-20)
Oleo stroke, m (in)	0.381 (15)	0.508 (20)

Aerodynamic surfaces

	Wing	Vertical tail	Horizontal tail
Area, m² (ft²)	241.5 (2599)ᵃ	55.3 (595)	32.0 (344)
Aspect ratio	10.3ᵃ	0.67	4.00
Taper ratio	0.266ᵃ	0.700	0.400
Sweep at c/4, deg	31.5ᵃ	55.0	35.0
Incidence, SOB, deg	3.8ᵃ	—	—
Dihedral, deg	6.0ᵃ	—	-3.0
Root t/c, percent	15.1	12.0	11.0
Tip t/c, percent	10.3	12.0	9.0
Root chord, m (in)	7.642 (300.85)ᵃ	10.686 (420.72)	4.038 (158.98)
Tip chord, m (in)	2.035 (80.1)	7.480 (294.50)	1.615 (63.59)
MAC,m (in)	5.379 (211.79)ᵃ	9.178 (361.32)	3.000 (118.10)
Span, m (in)	49.898 (1964.48)	6.086 (239.59)	11.291 (444.53)
Tail arm, m (in)	—	21.597 (850.28)	28.654 (1128.10)
Tail volume coefficientᵇ	—	0.087	0.618

Engine toe-in angle = 1 deg to a BBL
Nacelle incidence = 2.625 deg to a BWL
Wing upper surface at SOB rib at BWL 4.953m (195 in)

ᵃTrapezoid geometry quoted: aero reference area = 275.6m² (2966 ft²)
ᵇBased on aero reference area

Figure 15. Model 768-105 General Arrangement

45

Geometry:

Body cross section, m (in)
- Shape: Vertical double lobe
- Maximum width, m (in): 5.029 (198.0)
- Maximum height, m (in): 5.410 (213.0)

Landing gear

	Nose	Main
Type	Dual	Truck
Location, m (in)	BS 6.896 (271.50)	67.9% MAC
Spacing, m (in)	0.610 (24)	1.143 x 1.422 (45 x 56)
Tire size, m (in)	0.940 x 0.330-0.406 (37 x 13-16)	1.092 x 0.394-0.508 (43 x 15.5-20)
Oleo stroke, m (in)	0.381 (15)	0.508 (20)

Aerodynamic surfaces

	Wing	Vertical tail	Horizontal tail
Area, m2 (ft2)	246.8 (2656)a	55.83 (601)	34.932 (376)
Aspect ratio	10.15a	0.67	4.00
Taper ratio	0.262a	0.700	0.400
Sweep at c/4, deg	26.43a	55.0	35.0
Incidence, SOB, deg	3.8a	—	-3.0
Dihedral, deg	6.0a	—	11.0
Root t/c, percent	13.1	12.0	11.0
Tip t/c, percent	8.3	12.0	9.0
Root chord, m (in)	7.815 (307.69)a	10.470 (422.84)	4.222 (166.21)
Tip chord, m (in)	2.047 (80.58)	7.518 (295.98)	1.689 (66.48)
MAC, m (in)	5.494 (216.28)a	9.224 (363.14)	3.136 (123.47)
Span, m (in)	50.032 (1969.76)	6.116 (240.80)	11.820 (465.361)
Tail arm, m (in)	—	21.605 (850.59)	28.655 (1128.16)
Tail volume coefficient b	—	0.088	0.662

Engine toe-in angle = 1 deg to a BBL
Nacelle incidence = 2.625 deg to a BWL
Wing upper surface at SOB rib at BWL 4.775m (188 in)

aTrapezoid geometry quoted: aero reference area = 275.1m² (2961 ft²)
bBased on aero reference area

Weights, kg (lb):
TOGW: 122 470 (270 000)
OEW: 81 020 (178 620)
MLW: 115 290 (254 170)

Propulsion: Two CF6-6D2

Passenger accommodations:

	Passengers	Abreast	Pitch
First class:	18	6	0.965m (38 in)
Tourist:	179	7	0.864m (34 in)

Cargo and baggage, m3 (ft3):

Containers	22 LD-2 or	11 LD-3 or	11 LD-4
Forward	33.98 (1200)	22.37 (790)	27.61 (975)
Aft	40.78 (1440)	26.85 (948)	33.13 (1170)
Bulk cargo (aft only)	11.33 (400)	11.33 (400)	11.33 (400)
Total	86.09 (3040)	60.55 (2138)	72.07 (2545)
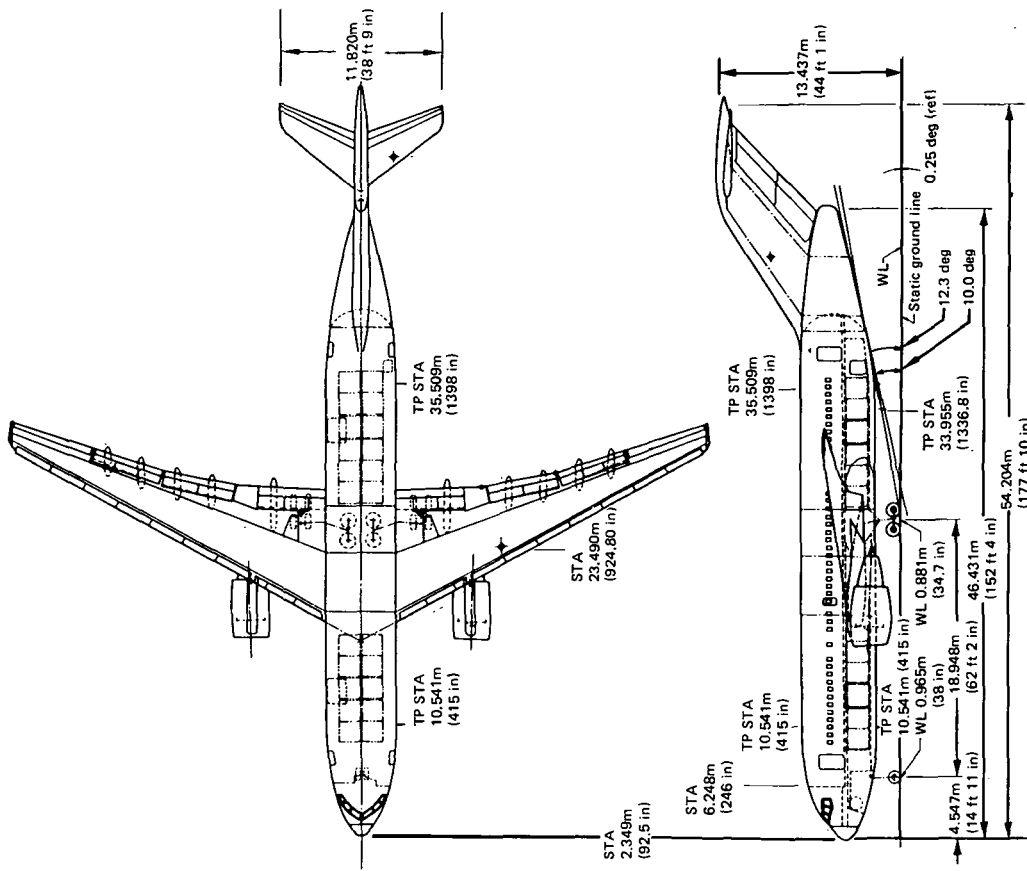
Figure 16. Model 768-106 General Arrangement

46

5.2.2 EQUIPMENT

The locations of the major body components including passenger seats, cargo containers, electric and electronic bays, environmental control packs and mixing bays, and landing gear for all three configurations are identical to the Initial ACT Configuration. Doors for passenger entry, galley, emergency escape, and cargo are also the same.

5.2.3 BODY CROSS SECTION

The body cross section for all three configurations is identical to the Initial ACT Configuration. The upper-lobe diameter measures 5.03m (198 in) and provides 4.67m (184 in) seating width. The lower lobe, sized for containers with bases 2.44m (96 in) wide, has a diameter of 4.92m (193.6 in). The total section height is 5.41m (213 in).

5.2.4 SEATING ARRANGEMENT

Seating arrangements for the basic two-class 197-passenger version, including the locations of galleys, lavatories, cabin attendants' seats, and cabin doors for all three configurations are identical to the Initial ACT Configuration. The all-tourist version accommodates 207 passengers sitting seven-abreast. There are two aisles, and seats are spaced at 0.86m (34 in) pitch.

5.2.5 CARGO CAPABILITY (LOWER LOBE)

Lower-lobe cargo capability for all three configurations is identical to the Initial ACT Configuration. In the lower lobe, two compartments for containerized and bulk cargo accommodate a dual row of LD-2 containers or a single row of LD-3 containers. The aft cargo compartment also accommodates three pallets, each with a base 2.44m (96 in) wide and 3.18m (125 in) long, plus bulk cargo.

5.2.6 CARGO CAPABILITY (UPPER LOBE)

Upper-lobe cargo capability for all three configurations is also identical to the Initial ACT. In all-cargo or in passenger/cargo combination versions, the upper lobe of the

body accommodates cargo containers that are 2.44m (8 ft) wide by 2.44m (8 ft) high by 3.05m (10 ft) long. Cargo pallets on a 2.44m (96 in) wide by 3.18m (125 in) long base also can be carried. A large forward cargo door, 2.57m (101 in) high by 3.40m (134 in) long, enables these cargo containers and/or pallets to be loaded. Although this feature is optional, space for installing this door was provided in the Initial ACT Configuration.

5.2.7 PRIMARY FLIGHT CONTROL SYSTEM

The primary flight control system, as described in Subsection 6.2.2, is identical to the Initial ACT Configuration system except for very minor configuration-related changes.

5.2.8 PRINCIPAL CHARACTERISTICS

Principal characteristics of the Wing Planform Study Configurations are listed in Table 2.

Table 2. Wing Planform Studies, Principal Configuration Characteristics

Geometric characteristics			
Airplane size	Model 768-104	Model 768-105[a]	Model 768-106[a]
Maximum takeoff weight, kg (lb)	122 470 (270 000)		
Wing: Aspect ratio[b]/sweep, deg	12.03[b]/31.5[b]	10.30[b]/31.5[b]	10.15[b]/26.43[b]
Area[b]/area[c], m^2 (ft²)	226.8[b]/275.8[c] (2441[b]/2969[c])	241.5[b]/275.6[c] (2599[b]/2966[c])	246.8[b]/275.1[c] (2656[b]/2961[c])
Span, m (ft)	52.222 (171.33)	49.898 (163.71)	50.032 (164.15)
Location on body, percent body length	45.7	42.7	
Location—engine pod on wing, percent b/2	30.4		
Trailing-edge flaps	Single slot		
Leading-edge devices	Slats		
Horizontal tail area/$\bar{V}_H$, m^2 (ft²)	31.96/0.689[c] (344/0.689[c])	31.96/0.618[c] (344/0.618[c])	34.932/0.662[c] (376/0.662[c])
Sweep, deg	35		
AR/taper ratio	4.0/0.40		
Vertical tail area/$\bar{V}_V$, m^2 (ft²)	56.58/0.085[c] (609/0.085[c])	55.28/0.087[c] (595/0.087[c])	55.835/0.088[c] (601/0.088[c])
Sweep, deg	55		
AR/taper ratio	0.67/0.70		
Body, m (in)			
Cross section	5.03W/5.410H (198.0W/213.0H)		
Length/overall length, m (ft-in)	46.43/54.18 (152-4/177-9)		46.43/54.20 (152-4/177-10)
Cabin length	33.38 (1314)		
Doors, number, type, size	4, type A, 1.07 x 1.83 (42 x 72)		
	2, type III, 0.51 x 0.97 (20 x 38)		
Systems			
Engine: number/type	2/CF6-6D2		
Engine thrust (SLST), N (lb)	182 377 (41 000)		
Nacelle and acoustic treatment	FAR 36, Stage 3		
Fuel capacity, m^3 (gal)			
Wing tanks	42.550 (11 240)		
Center tanks	Dry		
Total	42.550 (11 240)		
Landing gear, m (in)			
Main gear wheelbase/track	1.42/1.14 (56.0/45.0)		
Location, percent MAC	72.4	68.6	67.9
Stroke/extended length	0.51/3.18 (20/125)		
Tire size: wheel size	1.09 x 0.39 − 0.51 (43 x 15.5 − 20)		
Nose gear type/tire spacing	Dual/0.61 (Dual/24)		
Stroke/extended length	0.38/2.18 (15/86.0)		
Tire size: wheel size	0.94 x 0.33 − 0.41 (37 x 13 − 16)		
Payload			
Flight crew/attendants	3/6		
Mixed class passengers/split	197/9% first class/91% tourist		
All tourist passengers	207		
Containers: number/type	22 LD-2 or 11 LD-3		
Cargo, m^3 (ft³)			
Containerized	74.76 (2640) 49.22 (1738)		
Bulk	11.33 (400) 11.33 (400)		
Total	86.09 (3040) 60.55 (2138)		
Center-of-gravity location			
Forward, percent MAC	17.5	19.3	18.1
Average cruise, percent MAC	30.6	—	—

[a]Blank areas same as Model 768-104
[b]Trapezoid geometry
[c]Aero reference geometry

49

5.3 PERFORMANCE

5.3 PERFORMANCE

Estimated performance data for the Initial ACT and Wing Planform Study Configurations are discussed in this section, with comparisons to the Baseline Configuration.

5.3.1 PERFORMANCE OBJECTIVES

The objective of the planform study was to maintain performance equal to or better than the Baseline Configuration while keeping takeoff gross weight (TOGW), engine, payload, and wing area fixed. The major performance objectives are:

- Still air range (SAR) $\geq$ 3589 km (1938 nmi)
- Takeoff field length (TOFL), at sea level at 29°C (84°F) $\leq$ 2210m (7250 ft)
- Landing approach velocity (V_{APP}) at maximum design landing weight (MLW) $\leq$ 70.0 m/s (136.1 KEAS)
- Initial cruise altitude capability (ICAC) $\geq$ 10.7 km (35 000 ft)
- Cruise Mach = 0.80

Selection criteria for further analysis were based on fuel efficiency and off-design performance after the minimum Baseline Configuration performance levels had been met.

5.3.2 MISSION RULES

The design mission is flown with a step-cruise procedure beginning at 10.7 km (35 000 ft) altitude, a cruise Mach of 0.8, and standard day atmosphere conditions. When maximum TOGW airplane ICAC is equal to or greater than 11.9 km (39 000 ft), a constant cruise altitude is flown at 11.9 km (39 000 ft). Air Transport Association 1967 domestic reserves with a 370 km (200 nmi) alternate are used for determining range capability, which is quoted for a typical U.S. domestic mission profile (fig. 17) with full passenger payload and nominal performance.

51

Mission

Taxi out, 0.15 hr (9 min)
Takeoff to 10.7m (35 ft)
Climb to 457m (1500 ft)
Accelerate to 129 m/s (250 kn)
Climb to 3048m (10 000 ft) at 129 m/s (250 kn)
Accelerate to climb speed
Climb
Cruise
Descend to 3048m (10 000 ft)
Decelerate to 129 m/s (250 kn)
Descend to 457m (1500 ft)
Approach and land
Taxi in, 0.083 hr (5 min) from reserves

Still air range

Block time, fuel

Domestic Reserves

1.0 hr at long-range cruise Mach at final altitude and weight
Missed approach V_APP at 10.7m (35 ft) to 129 m/s (250 kn) at 457m (1500 ft)
Climb
Long-range cruise
Descend to sea level

370 km (200 nmi)

Domestic reserves

768-102, -103, -104, -106

Figure 17. *Typical Mission Profile*

52

5.3.3 PERFORMANCE CHARACTERISTICS

All the airplanes discussed in this section have the same design gross weight, engine size, wing area, and payload. The effects of wing planform changes (higher wing span and reduced sweep) on airplane performance capabilities were assessed.

Figure 18 shows the effects of span and sweep on the cruise aerodynamic lift-drag (L/D) ratio. The highest span shows an improvement of 10% relative to the Baseline and about 4% relative to the Initial ACT Configuration, primarily due to the span increase. The reduced sweep wing at intermediate span had about the same L/D as the comparable higher sweep wing.

Figure 19 shows the effects of span and sweep on operational empty weight (OEW). The highest span increases the OEW about 3.5% relative to the Initial ACT
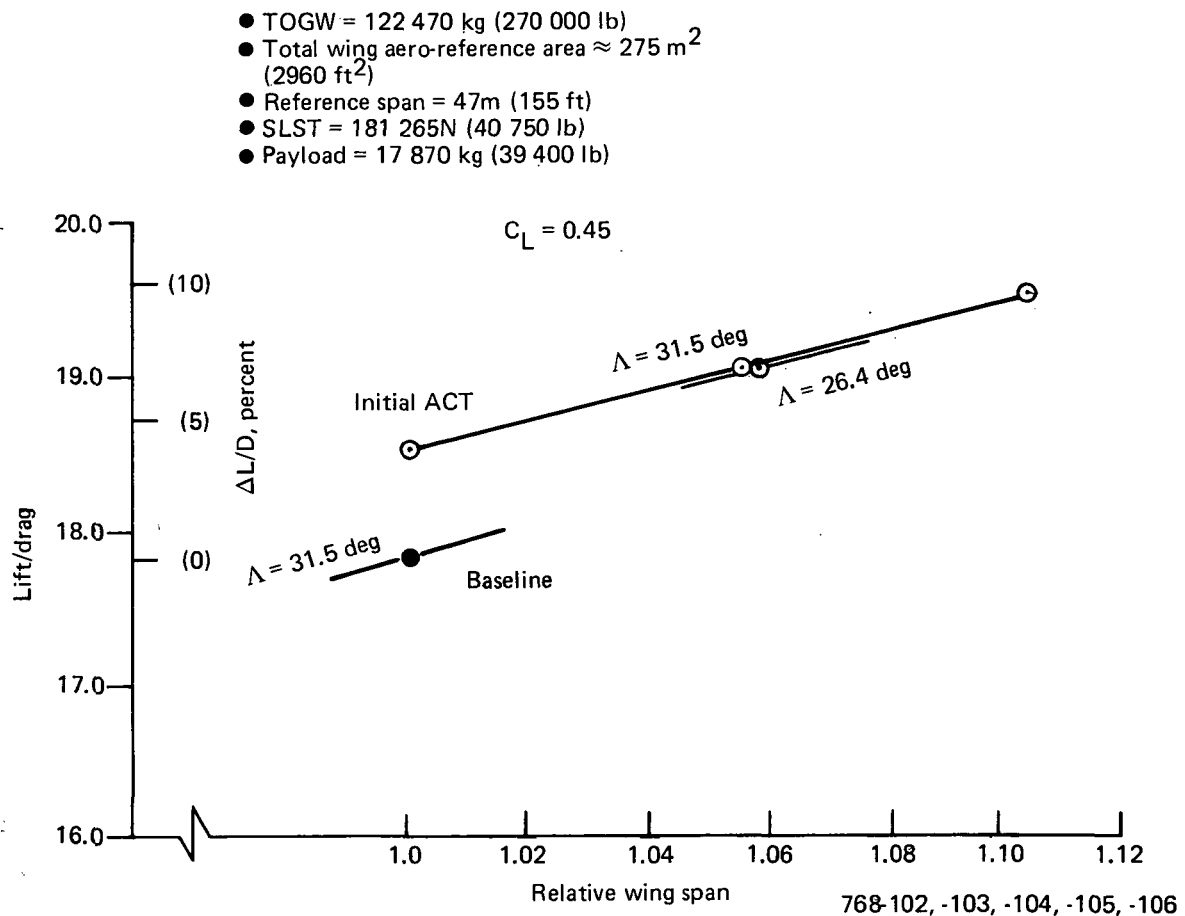
Figure 18. Effect of Wing Span on Cruise Drag

53
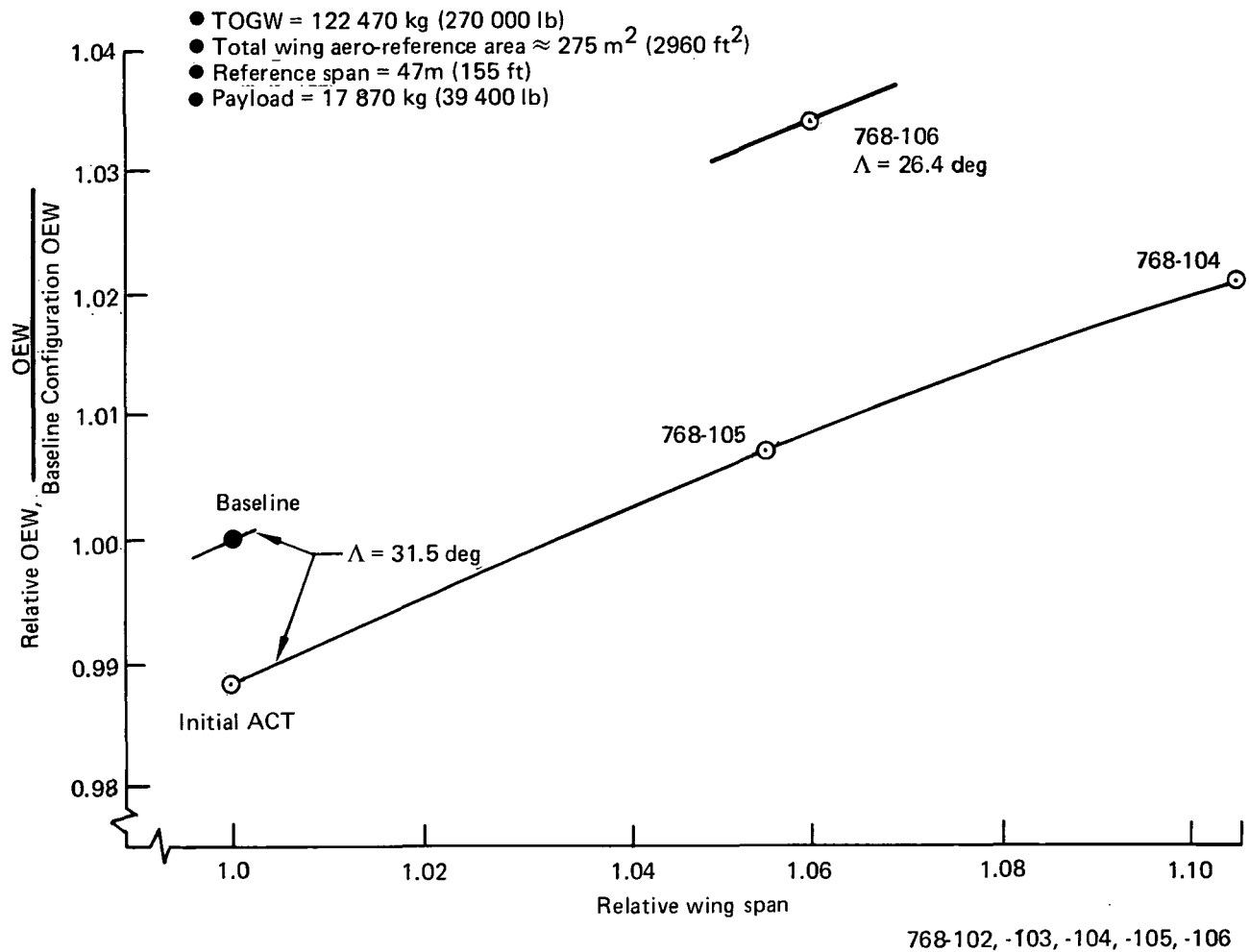
Figure 19. Relative Weights

Configuration and about 2.2% relative to the Baseline Configuration. The reduced sweep wing at intermediate span had an OEW about 2.5% higher than the comparable higher sweep wing.

The net result of these trends in L/D and OEW on airplane fuel efficiency is shown in Figure 20. These data clearly show the Model 768-104 with the highest span to have the best fuel efficiency and that reducing wing sweep degraded fuel efficiency.

The substantial improvements in TOFL, ICAC, and engine-out altitude (EOALT) capability of all the ACT configurations relative to the Baseline are shown in Figure 21. The Model 768-104 with the highest span has the best performance capabilities with respect to TOFL, ICAC, and EOALT. Relative range capability is

54

- TOGW = 122 470 kg (270 000 lb)
- Total wing aero-reference area ≈ 275 m^2 (2960 ft^2)
- Reference span = 47m (155 ft)
- SLST = 181 265N (40 750 lb)
- Payload = 17 870 kg (39 400 lb), including 197 passengers

768-102, -103, -104, -105, -106
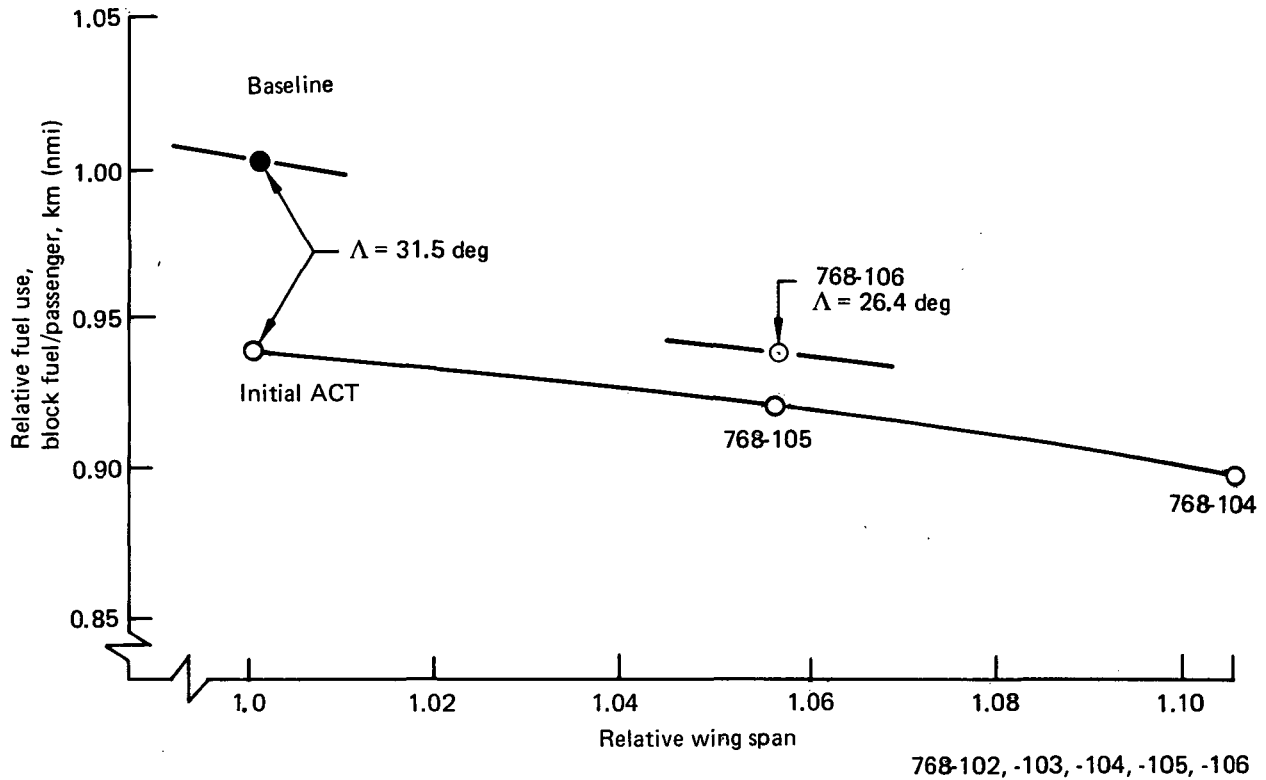
Figure 20. Relative Fuel Usage

also shown in Figure 21. Only the reduced sweep Model 768-106 had less range than the Baseline, due primarily to its OEW being the highest of the wing planforms investigated.

The most fuel efficient airplane, the Model 768-104, is compared to the Baseline in Table 3. For a fixed TOGW, payload, engine size, and wing area, it has more range—174 km (95 nmi)—and a lower landing approach speed—1.0 m/s (1.9 kn). This extra performance capability may produce benefits when resizing to the same range as the Baseline. This is discussed in Subsection 9.1.

In summary, the ACT Configurations with the same maximum takeoff gross weight, payload, engine, wing area, and sweep as the Baseline Configuration offered these performance benefits:

55

- TOGW = 122 470 kg (270 000 lb)
- Total wing aero-reference area ≈ 275 m^2 (2960 ft^2)
- Reference span = 47m (155 ft)
- SLST = 181 265N (40 750 lb)
- Payload = 17 870 kg (39 400 lb)

Symbol	Λ
●	31.5 Baseline
☉	31.5
□	26.4

768-102, -103, -104, -105, -106
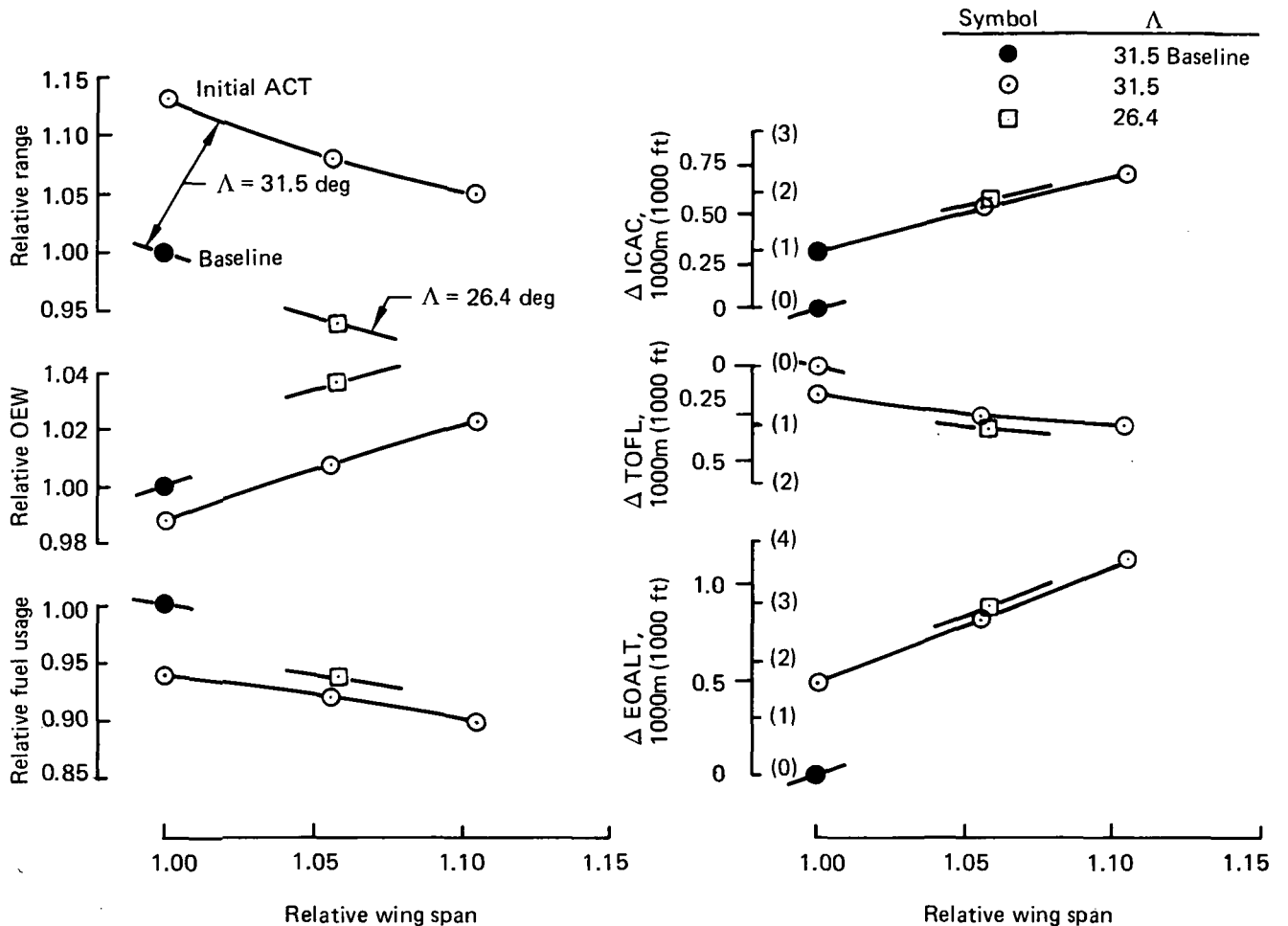
Figure 21. Performance Relative to Baseline

- Increased range = 5 to 13%
- Reduced block fuel = 6 to 10% (at Baseline range limit)
- Reduced TOFL = 4 to 14% (sea level)
- Reduced landing approach speed = 1.5 to 2%

Further performance benefits may be realized for missions where payload is limited by takeoff performance. For example, at Denver on a hot day, payload may be increased due to a higher TOGW that satisfies both TOFL and climb gradient requirements. Model 768-104 has full payload-range capability from Denver. This added effect of

56

Table 3. Conventional Baseline and Model 768-104 (AR = 12.0) Performance Comparison

	Baseline	Model 768-104	Δ
MTW, kg (lb)	122 920 (271 000)	122 920 (271 000)	− −
TOGW, kg (lb)	122 470 (270 000)	122 470 (270 000)	− −
MZFW, kg (lb)	104 400 (230 160)	106 060 (233 830)	+1660 (+3670)
MLW, kg (lb)	112 570 (248 160)	114 230 (251 830)	+1660 (+3670)
OEW, kg (lb)	78 300 (172 610)	79 960 (176 280)	+1660 (+3670)
Forward center of gravity, percent MAC	10.0	17.5	+7.5
Average cruise center of gravity, percent MAC	20.5	30.6	+10.1
Cruise L/D, (M = 0.8, C_L = 0.45)	17.8	19.6	+1.8
SAR, km (nmi)	3 589 (1 938)	3 763 (2 032)	+174 (+94)
TOFL, (SL 29°C (84°F) m (ft)	2 210 (7 250)	1 902 (6 240)	-308 (-1010)
V_{APP} at maximum landing weight, m/s (kn)	70.0 (136.1)	69.0 (134.2)	-1.0 (-1.9)
Landing field length, sea level, dry, at maximum landing weight, m (ft)	1 443 (4 735)	1 411 (4 630)	-32 (-105)
Relative fuel use, block fuel per passenger—km (nmi)	1.00	0.90	-10%

768-102, -104

increasing payload or range on some route segments could increase the profitability of the airplane for some operators.

5.3.4 NOISE

Because the propulsion system and the low-speed performance characteristics of the ACT Configurations are so little changed from the Baseline, a specific noise analysis was not undertaken. Because the changes are all expected to be small improvements, the ACT Configurations noise characteristics are conservatively considered to be better than the Baseline Configuration. Model 768-104, which has the largest wing span and best low-speed lift/drags should have better noise characteristics at a given payload range than the Baseline or Initial ACT Configurations.

5.4   WEIGHT, BALANCE, AND INERTIA

5.4 WEIGHT, BALANCE, AND INERTIA

5.4.1 DESIGN WEIGHTS

Table 4 lists design weights used for structural loads and performance analysis.

Table 4. Design Weights

Item	Weight					
	Model 768-104		Model 768-105		Model 768-106	
	kg	(lb)	kg	(lb)	kg	(lb)
Operational empty weight (OEW)	79 960	176 280	78 830	173 800	81 020	178 620
Maximum zero fuel weight (MZFW)	106 060	233 830	104 940	231 350	107 130	236 170
Maximum landing weight (MLW)	114 230	251 830	113 100	249 350	115 290	254 170
Maximum takeoff weight (MTOW)	122 470	270 000	122 470	270 000	122 470	270 000
Maximum taxi weight (MTW)	122 920	271 000	122 920	271 000	122 920	271 000

768-104, -105, -106

5.4.2 AIRPLANE MOMENTS OF INERTIA

Airplane moments of inertia for the Wing Planform Study Configurations were derived from the Initial ACT Configuration, Reference 3, Subsection 5.4.3. Inertias were increased for increases in wing span and empennage area.

5.4.3 CENTER-OF-GRAVITY MANAGEMENT

A detailed cg analysis was performed on the Model 768-104 Configuration, consistent with the level of detail available from the weight analysis. Models 768-105 and -106 were not analyzed in as much detail.

Figure 22 diagrams cg management (loadability) for the Model 768-104 Configuration. In determining the cg loading range requirements, a tolerance (+3% to -4% MAC) was applied to the nominal OEW cg of 35% MAC to account for manufacturing variations and airline options, such as increased cargo accommodations and engine substitution. The aft payload envelope is critical for 197 mixed-class passengers (18/179), establishing the aft cg limit for payload. The forward envelope is critical for 207

59

Wing Planform Study
Wing, Model 768-104

- $\frac{\bar{c}}{4}$ balance arm = 23.56m (927.4 in)
- MAC = 4.83m (190.0 in)
- Main landing gear location = 72.4% MAC

Gross weight 1000 kg (1000 lb)

120 (265)
110 (243)
100 (220)
90 (198)
80 (176)

Aft required flight limit 48.8% MAC

197 mixed class

MZFW 106 060 kg (233 830 lb)

MLW 114 230 kg (251 830 lb)

OEW — Typical payload (mixed)

OEW cg tolerance

Passenger + baggage

207 all tourist

Fuel tanks No. 1 and 3

Forward required flight limit 17.5% MAC

[a]⊳ In-flight movement
[b]⊳ Typical cruise center of gravity = 30.6% MAC
[c]⊳ Bulk cargo 11.33 m³ (400 ft³) located aft of containerized cargo
[d]⊳ Forward cargo containers, 12 LD-2s
[e]⊳ Aft cargo containers, 10 LD-2s

MTOW 122 920 kg (271 000 lb)

768-104

Figure 22. Center-of-Gravity Management

tourist-class passengers and establishes the forward required cg limit. The "typical payload (mixed)" line is a prediction of passenger loading obtained from many airline surveys conducted throughout the airline industry.

The forward and aft cargo compartment cargo-moment vectors were based on 22 LD-2s at 105 kg/m³ (6.58 lb/ft³) density. Adding vectors for the bulk cargo compartment completed the loading envelope for the zero fuel weight airplane. Maximum design zero fuel weight (MZFW) established the maximum allowable payload.

The forward and aft required operating cg limits must accommodate loading full containerized cargo, with or without bulk, with any passenger load (assuming seating order is window, aisle, remaining seats). The aft flight limit was established aft of the aft operating limit by a moment margin that covers in-flight movements of passengers

60

and crew, control surface deflections, landing gear movements, and fuel vector moment difference. The forward operating limit was established by the cg range required for payload loadability. The 17.5% MAC forward required flight limit then clears the forward operating limit by a similar margin for in-flight movement (fig. 22, footnote a).

The typical cruise cg was based on a definition consistent with the performance analysis ground rules used for a typical airline customer.

As configured, the Model 768-104 will not meet the 48.8% MAC aft required flight limit criteria. To be within the design cg envelope, the configuration would require 340 kg (750 lb) of ballast in the nose-gear wheel well, or a wing shift aft of approximately 0.1m (4 in) with minor weight changes. Resources were not used to recycle the configuration. To maintain compatibility with the Initial ACT Configuration, Model 768-103, and the Baseline Configuration, Model 768-102, the ballast weight was not included in the OEW.

6.0 DESIGN DATA

The design details for the three configurations considered in the Wing Planform Study (described in sec 5.0) are discussed in this section. A structures description of the major airplane components is presented in Subsection 6.1; Subsection 6.2 describes the major airplane systems affecting, or affected by, ACT systems. Structural and system details of the Model 768-104 (aspect ratio [AR] 12.0, sweep [Λ] 31.5 deg) Configuration described in Section 5.0 are presented here. Except for wing definition, horizontal and vertical stabilizer sizes, and minor body and systems differences, details of the Model 768-105 (AR 10.3, Λ 31.5 deg) and 768-106 (AR 10.2, Λ 26.4 deg) Configurations are identical to those of the Model 768-104. These configurations are presented in the text and figures only where such differences exist.

6.1 AIRPLANE STRUCTURE

The airplane structure is presented in five major elements that are described in the following subsections:

- Wing (6.1.1)
- Body (6.1.2)
- Horizontal stabilizer (6.1.3)
- Vertical stabilizer (6.1.4)
- Main landing gear (6.1.5)

Although these elements are similar to those of the Initial ACT Configuration (ref 3), some details differ. Elements identical to the Initial ACT are not discussed in this section.

Conventional materials and construction are used in the design and fabrication of the airframe, except for the same degree of graphite-epoxy composite secondary structure as used in the Initial ACT Configuration. The airframe consists primarily of aluminum alloys.

6.1.1 WING

The wing structure basically duplicates that of the Initial ACT Configuration (ref 3, sec 6.1). It consists of left and right main outboard sections joined to a wing center section through the body (figs. 23, 24, and 25). The outboard sections include the wing box, the fixed leading- and trailing-edge structures, leading-edge slats and trailing-edge flaps, ailerons, spoilers, and wing tip. The wing-box structure is of conventional two-spar construction. High-lift and control surfaces consist of three-position leading-edge slats, single-slotted trailing-edge flaps, spoilers, and inboard and outboard ailerons.

6.1.2 BODY

The body consists of permanently joined major subsection assemblies. The basic body structure, of aluminum alloy, is of semimonocoque construction with formed hat section longitudinal stiffeners attached to the skin panels. A centerline diagram of the body structure is shown in Figure 26.

6.1.3 HORIZONTAL STABILIZER

The horizontal stabilizer is adjustable for airplane pitch trim and is actuated by a fail-safe jack-screw actuator. The horizontal stabilizer primary structure consists of a torque box from the side-of-fairing rib to the tip rib. The torque box is constructed of stiffened panels supported by built-up ribs and spars. The center section consists of the front and rear spars. The leading edge is a removable assembly of skin and closely spaced sheet-metal ribs. The double-hinged elevator, controlled by hydraulic actuators, is removable at the actuators and hinges. The horizontal stabilizer tapers in thickness and width. Space for logo lights is provided. A centerline diagram of the horizontal tail structure is shown in Figure 27.

6.1.4 VERTICAL STABILIZER

The vertical stabilizer supports the horizontal stabilizer. The rudder-hinge ribs are attached to its rear spar. The rudder consists of upper and lower double-hinged segments controlled by hydraulic actuators. The rudders are removable at the
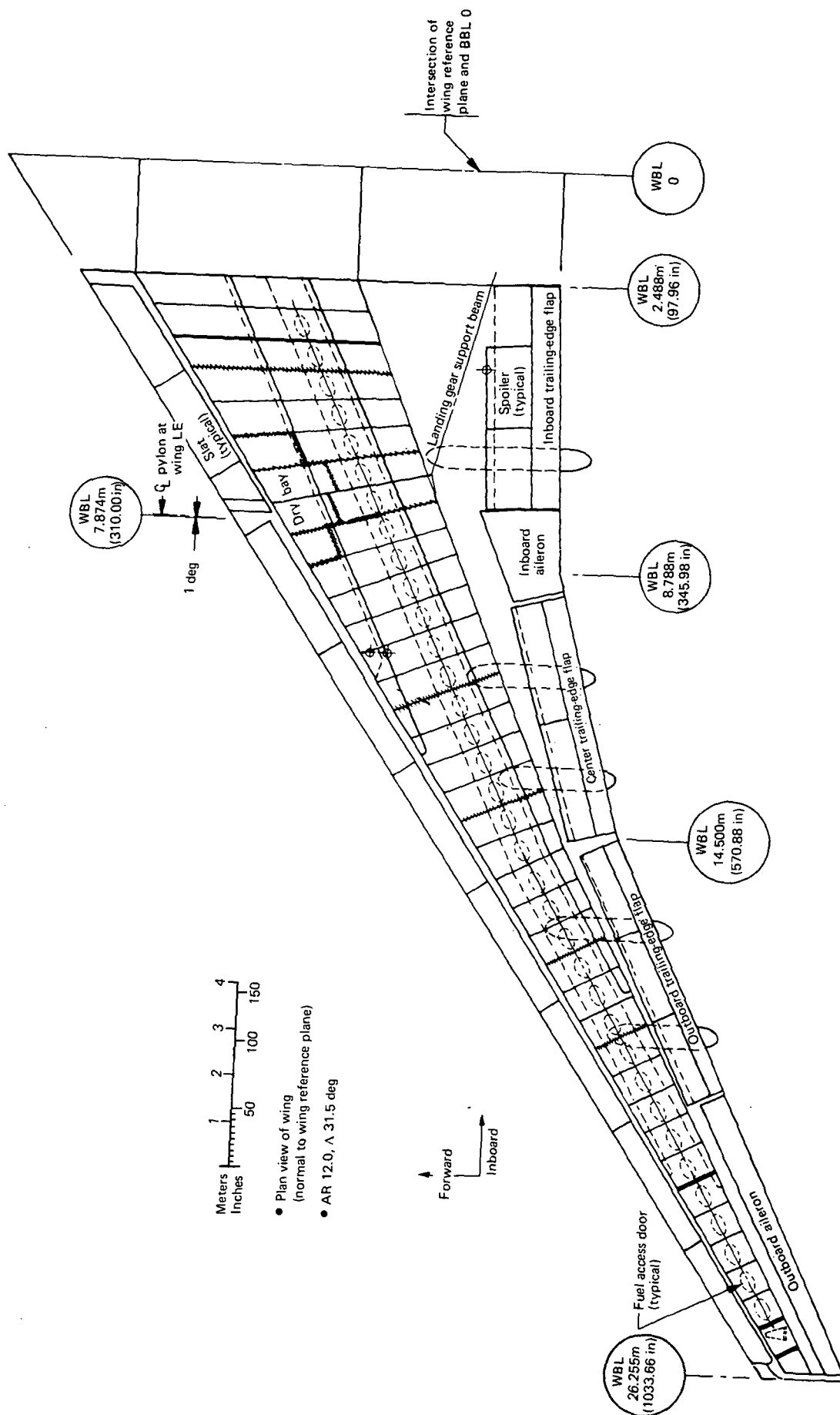
Figure 23. Wing Structure Diagram, Model 768-104

65
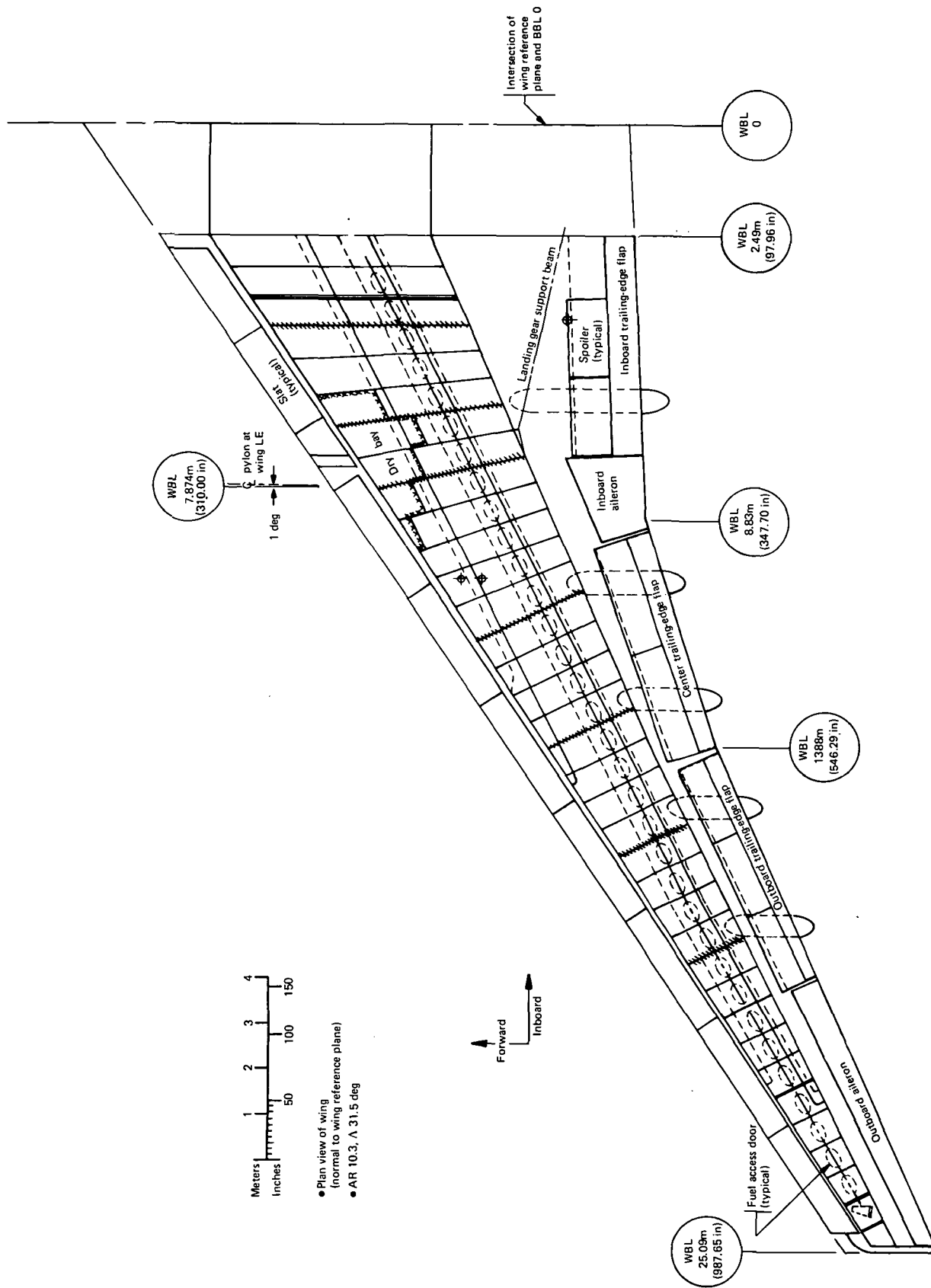
Figure 24. Wing Structure Diagram, Model 768-105
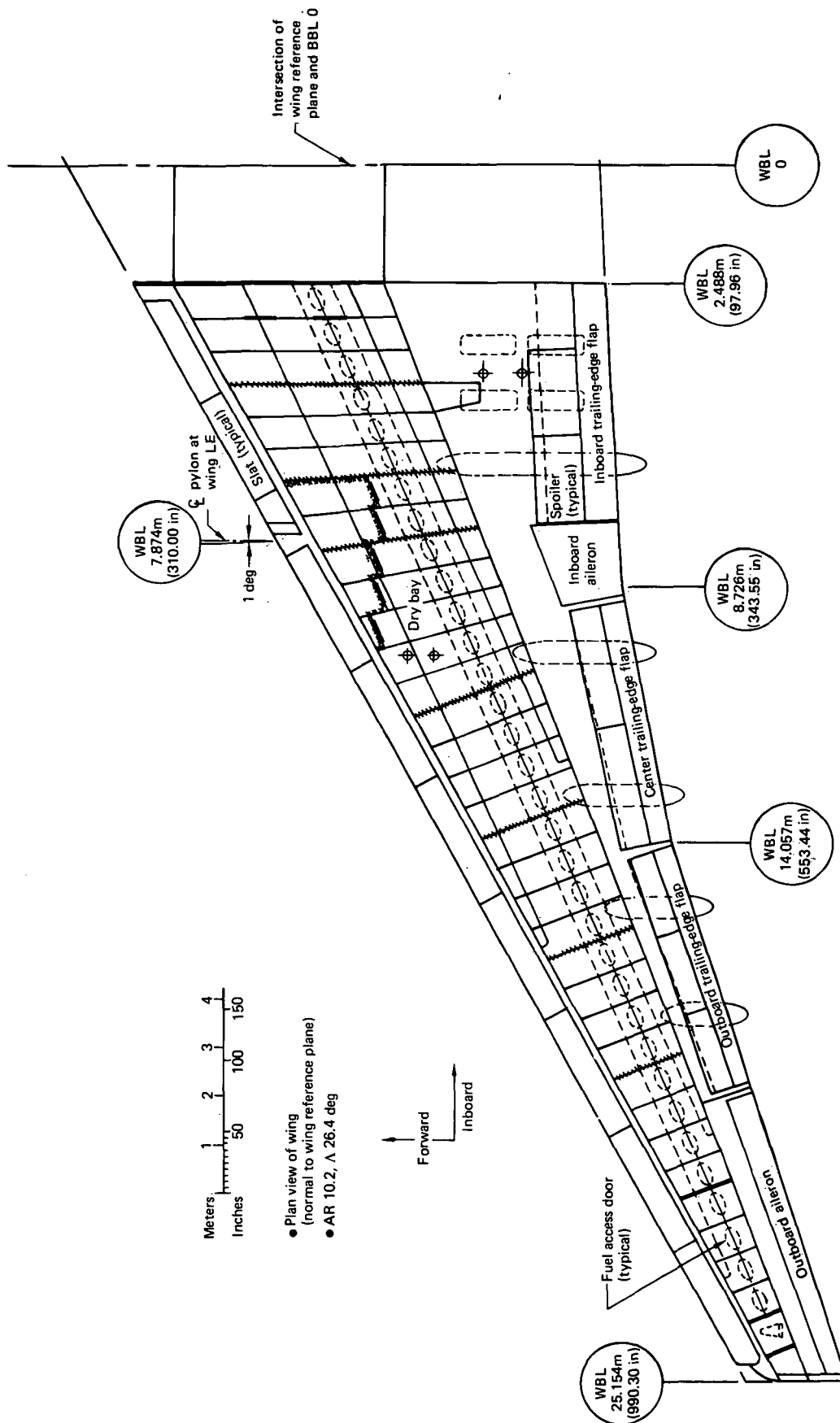
Figure 25. Wing Structure Diagram, Model 768-106

67

Constant Area Cross Section
Rear View

WL 8.121m
(319.73 in)

0.192m
(7.50 in)

WL 3.161m
(124.43 in)

0.127m
(5 in)

WL 5.080m
(200 in)

WL 2.711m
(106.73 in)

Model 768-106 Only
(identical except as shown)

STA 23.012m (906 in)

STA 26.340m (1037 in)

wheel well BHD

RS BHD

FS BHD

STA 18.745m (738 in)

Main gear wheel well

ECS packs

STA 39.624m (1560 in)

Type A entry door right and left side

Bulk cargo door (left side only)

Cargo net

Cargo door right side (two places)

wheel well BHD

STA 26.340m (1037 in)

RS BHD

STA 23.012m (906 in)

Main gear wheel well

Wing center section

ECS packs

Type III exit right and left side

STA 18.186m (716 in)

FS BHD

Models 768-104, -105, and -106 are identical, except as shown above.

Cargo door left side (space provision)

ECS duct two places right side four places left side

Type A entry door right and left side

Electric/ electronics access hatch

STA 2.349m (92.50 in)

Figure 26. Body Centerline Diagram, Models 768-104, -105, and -106

68
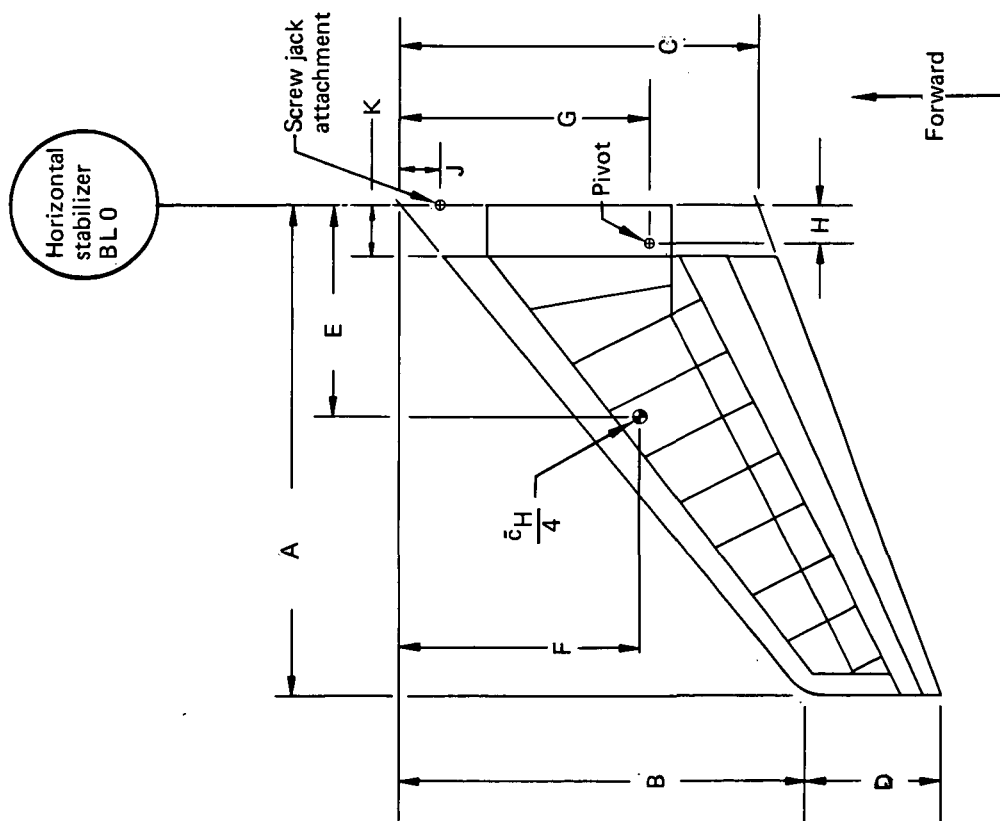
Characteristics		Models 768-104, -105	Model 768-106
Area	m² (ft²)	31.960 (344.00)	34.931 (376.00)
AR		4.00	4.00
TR		0.40	0.40
Λ (0.25c), deg		35	35
t/c		0.11 (root), 0.09 (tip)	0.11 (root), 0.09 (tip)
MAC	m (in)	3.000 (118.10)	3.136 (123.47)
Anhedral, deg		3	3
Trim limits		4 deg up, 14 deg down	4 deg up, 14 deg down
Elevator travel		28 deg up, 20 deg down	28 deg up, 20 deg down
Tab travel		28 deg up, 20 deg down	28 deg up, 20 deg down
A	m (in)	5.653 (222.57)	5.918 (233.00)
B	m (in)	4.564 (179.69)	4.777 (188.08)
C	m (in)	4.038 (158.98)	4.222 (166.21)
D	m (in)	1.615 (63.59)	1.689 (66.48)
E	m (in)	2.423 (95.39)	2.536 (99.86)
F	m (in)	2.706 (106.53)	2.832 (111.48)
G	m (in)	2.827 (111.28)	2.999 (118.06)
H	m (in)	0.386 (15.20)	0.419 (16.50)
J	m (in)	0.457 (18.00)	0.622 (24.50)
K	m (in)	0.577 (22.70)	0.577 (22.70)

768-104, -105, -106

Figure 27. Horizontal Stabilizer Geometry, Plan View of Surface

69

actuators and hinges. The vertical stabilizer tapers in thickness and width. Space for a very high frequency omnidirectional radio range (VOR) antenna is provided.

The vertical stabilizer primary structure is a full-span torque box of stiffened panels supported by built-up ribs and spars, with fixed attachments to the aft body. The leading edge consists of a forward removable assembly supported by closely spaced sheet-metal ribs. A centerline diagram of the vertical stabilizer structure is shown in Figure 28.

6.1.5 MAIN LANDING GEAR

The swing-arm, double-post main-landing-gear (MLG) arrangement is shown in Figure 29. The gear is stowed in the wing and body. On Models 768-104 and -105, the gear is mounted from the rear spars and from auxiliary beams attached to the rear spars and body frames. The beams are pin-jointed at the rear-spar attachments. At the body end, the beams are pin-jointed to hinged support fittings suspended between extensions of two upper-lobe body frames. On Model 768-106, the gear is supported by torque-box extensions of the wing-box structure.
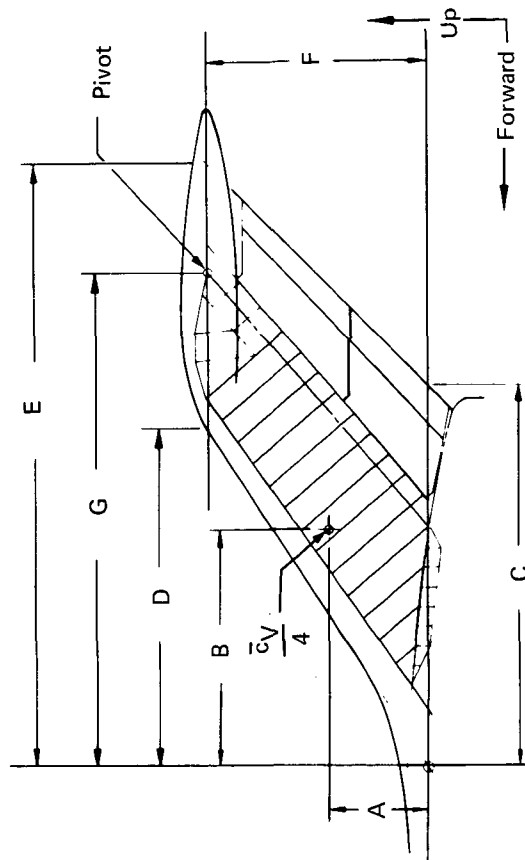
Characteristics		Model 768-104	Model 768-105	Model 768-106
Area	m² (ft²)	56.578 (609.00)	55.277 (595.00)	55.835 (601.00)
AR		0.67	0.67	0.67
TR		0.70	0.70	0.70
Λ (0.25c), deg		55	55	55
t/c		0.12	0.12	0.12
MAC	m (in)	9.285 (365.54)	9.178 (361.32)	9.224 (363.14)
A	m (in)	2.897 (114.07)	2.864 (112.75)	2.878 (113.32)
B	m (in)	6.841 (269.32)	6.762 (266.20)	6.796 (267.54)
C	m (in)	10.811 (425.63)	10.686 (420.72)	10.740 (422.84)
D	m (in)	9.604 (378.11)	9.493 (373.72)	9.541 (375.61)
E	m (in)	17.172 (676.05)	16.973 (668.22)	17.058 (671.59)
F	m (in)	6.157 (242.40)	6.086 (239.59)	6.116 (240.80)
G	m (in)	14.111 (555.56)	13.939 (548.77)	14.013 (551.69)

768-104, -105, -106

Figure 28. Vertical Stabilizer Geometry, Left-Hand Side View

Cantilever
(torque-box)
support (b)

Forward

Outboard

$\mathrel{C}$ RS (b)

$\mathrel{C}$ RS (a)

$\mathrel{C}$ beam support (a)

Plan view

Forward

(b)

(a)

Outboard

1.092 x 0.394m
(43 x 15.5 in)

0.064m
(2.50 in)

Compressed

Static

Extended

1.422m
(56 in)

0.445m
(17.50 in)

Side view

1.143m
(45 in)

Rear view

(a) Model 768-104, -105 only
(b) Model 768-106 only
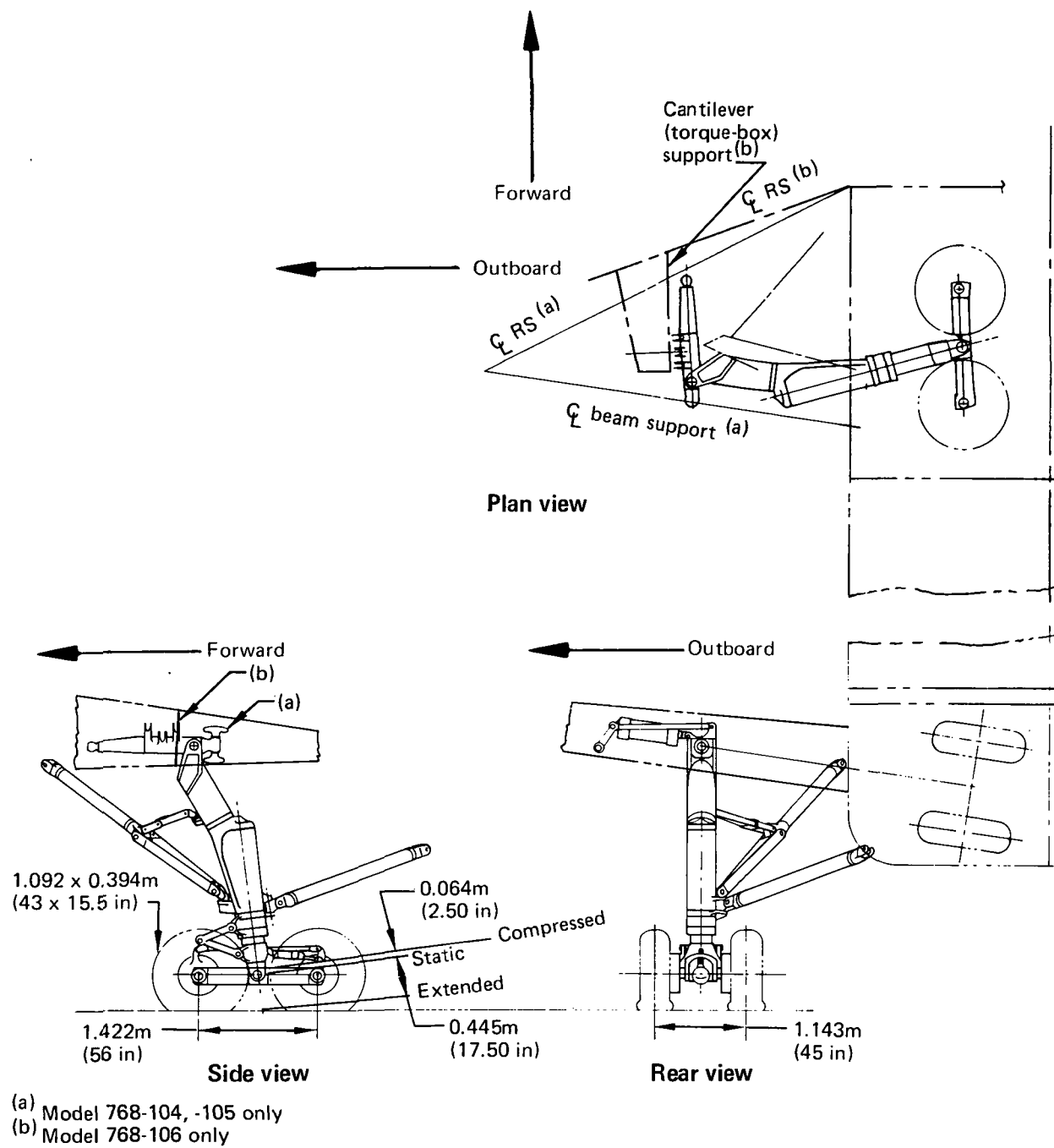
Figure 29. Typical Main-Landing Gear Assembly, Models 768-104, -105, and -106

6.2   AIRPLANE SYSTEMS

6.2 AIRPLANE SYSTEMS

This section describes the systems of the planform study configurations, including propulsion (subsec 6.2.1), flight controls (subsec 6.2.2), hydraulic power (subsec 6.2.3), and electric power (subsec 6.2.4). Proven state-of-the-art concepts are used in defining and evaluating the systems for the ACT Configurations.

6.2.1   PROPULSION SYSTEM

The propulsion system is identical to that of the Initial ACT Configuration (ref 3).

6.2.2   FLIGHT CONTROL SYSTEM

The flight control surfaces of these airplanes are similar to those of the Initial ACT Configuration. Operation of the primary controls is unchanged; changes in surface size and some features of surface design are described in the following subsections. Mechanical features of the secondary flight control system are the same as the Initial ACT Configuration; some stabilizer trim commands originate in the ACT system.

Figure 30 shows the location of all control surfaces. Only those control surfaces associated with the active controls are described in detail.

6.2.2.1 Elevator Control Surface

Two single-segment, double-hinged elevators are used for longitudinal control. Each elevator is powered by three side-by-side primary actuators, as shown in Figures 31 and 32. The ACT electric signals command the secondary actuators that are·series-summed with the pilot's mechanical input. To meet the pitch-augmented stability (PAS) redundancy requirement, three side-by-side force-summed secondary actuators provide dual fail-operational capability. In the improbable event that one secondary actuator jams, the combined force of the other two secondary actuators would open the jammed actuator's disconnect assembly, and the system would be fail operational. Figure 32 shows a jam/disconnect assembly.

73
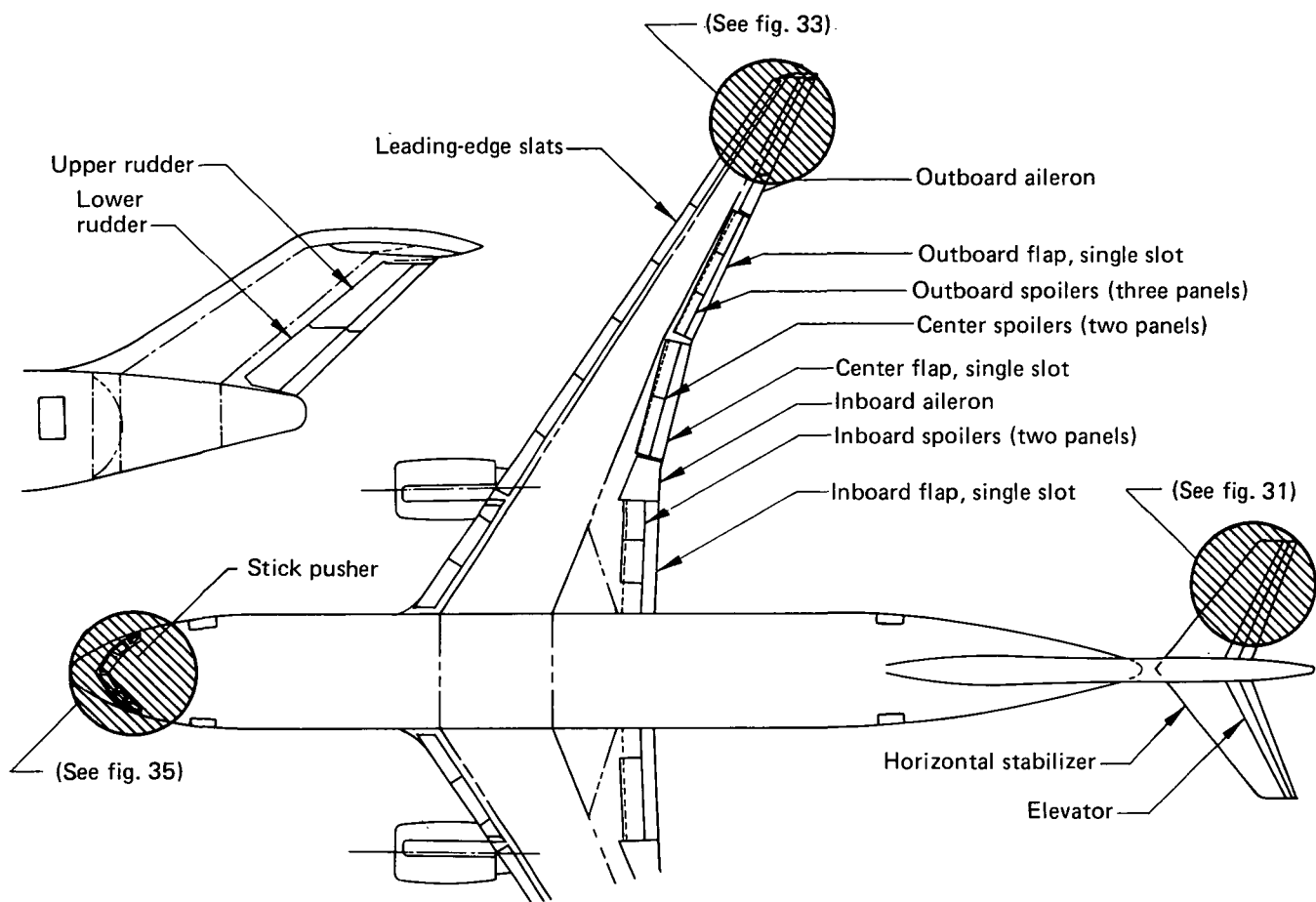
Figure 30. Flight Control Surfaces

768-104, -105, -106

74

Section views are shown in
Figure 32

PCU (typical six places)

Summation link (typical two places)

Secondary actuator (typical three places)

Jam disconnect
(typical three places)

768-104, -105, -106

Forward
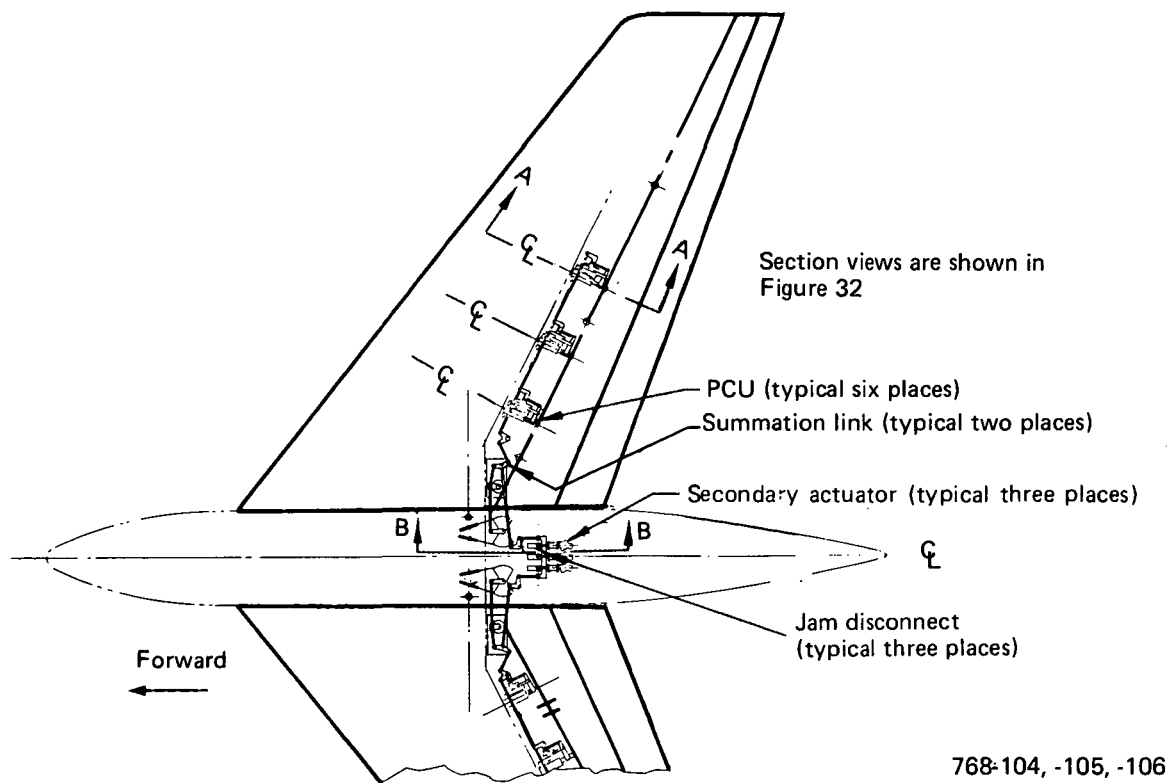
Plan View of Horizontal Stabilizer and Elevator

Figure 31. Flight Control Surfaces—Elevator Actuation Installation

Section A-A. Primary Actuator
(typical six places)

Secondary actuator (three places)

1739N (391 lb) maximum output force per actuator

Disconnects when jam drag in actuator
reaches 2890 ± 200N (650 ± 45 lb)
(typical three places)

Section B-B. Secondary Actuator and Jam Disconnect Assembly
768-104,-105, -106
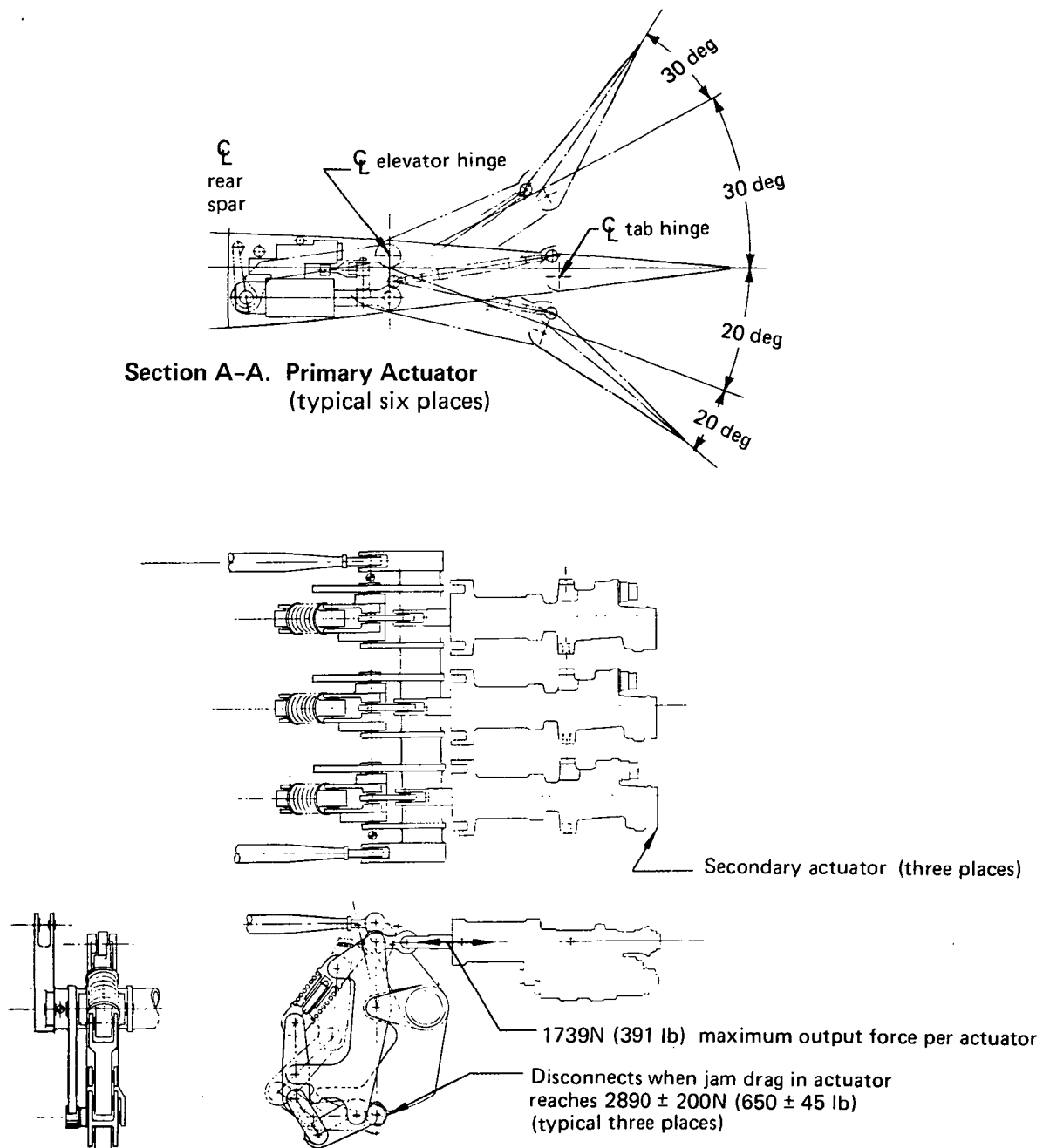
Figure 32. Flight Control Surfaces and Actuator Details—Elevator

76

6.2.2.2 Outboard Aileron Control Surface

The outboard aileron is used for low-speed roll control as well as wing-load alleviation (WLA). ACT control signals are fed through two force-summed secondary actuators and are series-summed with the pilot's mechanical input.

The side-by-side single-point, end-mounted actuators of previous configurations are replaced by trunnion-mounted, side-by-side actuators because the higher-aspect-ratio wings allow less space for installation of outboard aileron actuators. Although no cost or detailed weight analysis was made, the trunnion-mounted actuators are expected to cost and weigh slightly more than the other types. See Figures 33 and 34.

6.2.2.3 Pilot's Control Column (Stick-Pusher)

A dual-tandem pneumatic floating actuator on the pilot's control column provides an angle-of-attack limiter (AAL) function, which is fail operational. When pressurized on either end or both ends, the actuator will exert the same amount of forward force to the control column, and that force will continuously decrease as the column travels forward (fig. 35).

6.2.3 HYDRAULIC POWER SYSTEMS

The hydraulic power and distribution systems (figs. 36 and 37) are the same as for the Initial ACT Configuration, except for minor configuration differences, as shown in Figure 37.

6.2.4 ELECTRIC POWER SYSTEM

The electric power system for all three configurations is the same as used in the Initial ACT Configuration. Reference 3 contains a detailed description of this system.

6.2.4.1 Modifications to the Baseline Electric Power System Required for ACT

In all three configurations, the electric system is modified to provide quadruple-redundant power for the quadruple-redundant ACT channels, with two power sources to each channel. This was also done on the Initial ACT Configuration.

Section B-B

Section C-C

31.5 deg
30.0 deg
16.5 deg
15.0 deg

2.75R

Section A-A

Rear spar

Aileron hinge $\mathcal{C}_L$

0.305m
(12.00 in) (ref)

Actuator locations
Outboard aileron

Forward

Inboard
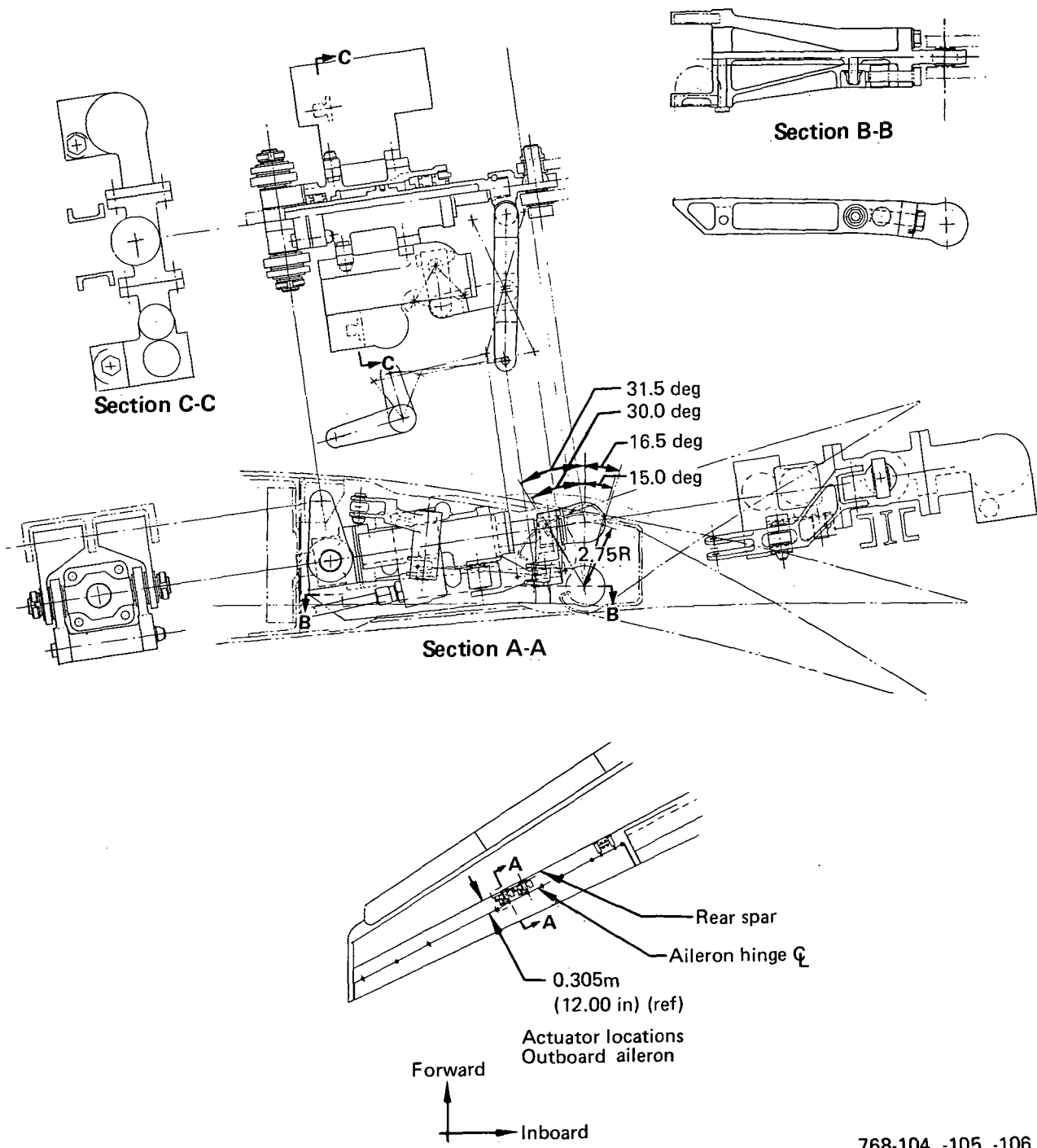
768-104, -105, -106

Figure 33. Outboard Aileron Actuator

Outboard aileron actuator
Two side-by-side units, Model 768-104
Two side-by-side units, Model 768-103
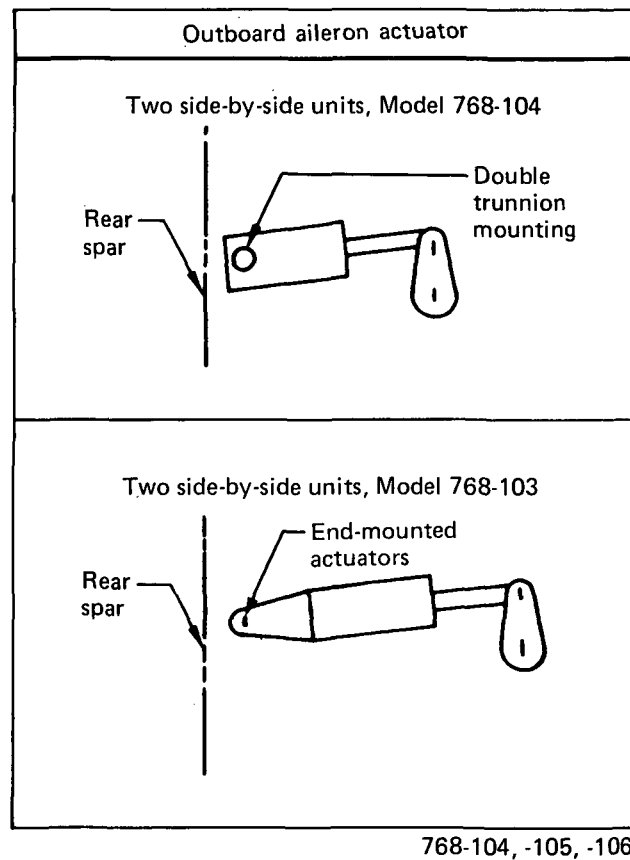
768-104, -105, -106

Figure 34. Actuator Configuration Comparison

Force at
control wheel   300 (67.5)
level, from   200 (45.0)
pusher, N (lb)   100 (22.5)

Forward   Aft
control column position

Floor

20 deg
minimum

0.076m
(3.0 in)

0.165m
(6.5 in)

Dual tandem
pneumatic actuator

Typical for Baseline Configuration

A

Forward   Up

Extended

Retracted

Stroke

Stop

Section A-A

Dual Tandem Floating Pneumatic Actuator—Retracting Type
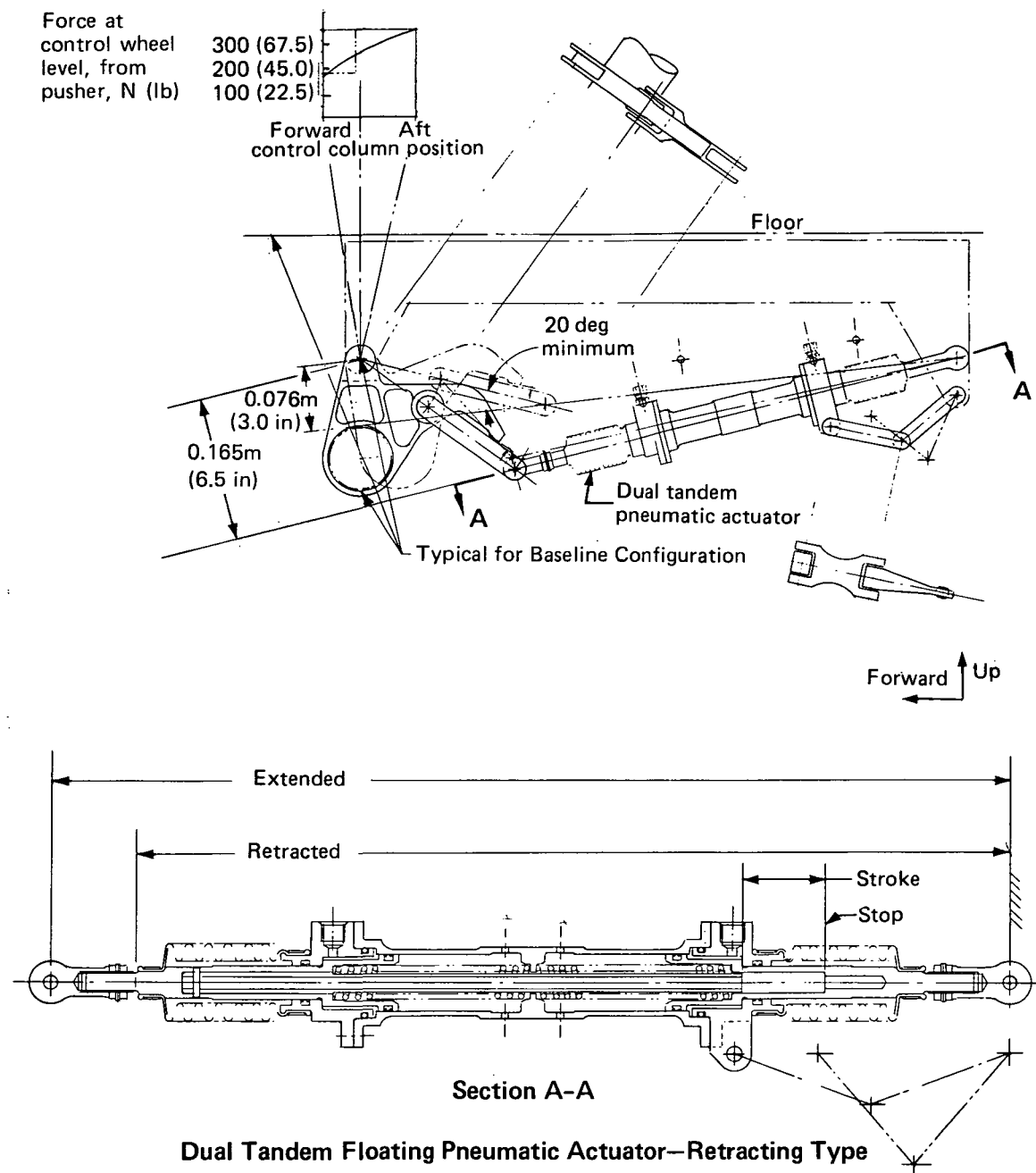
Figure 35.   Stick-Pusher Actuation Installation

768-103

80
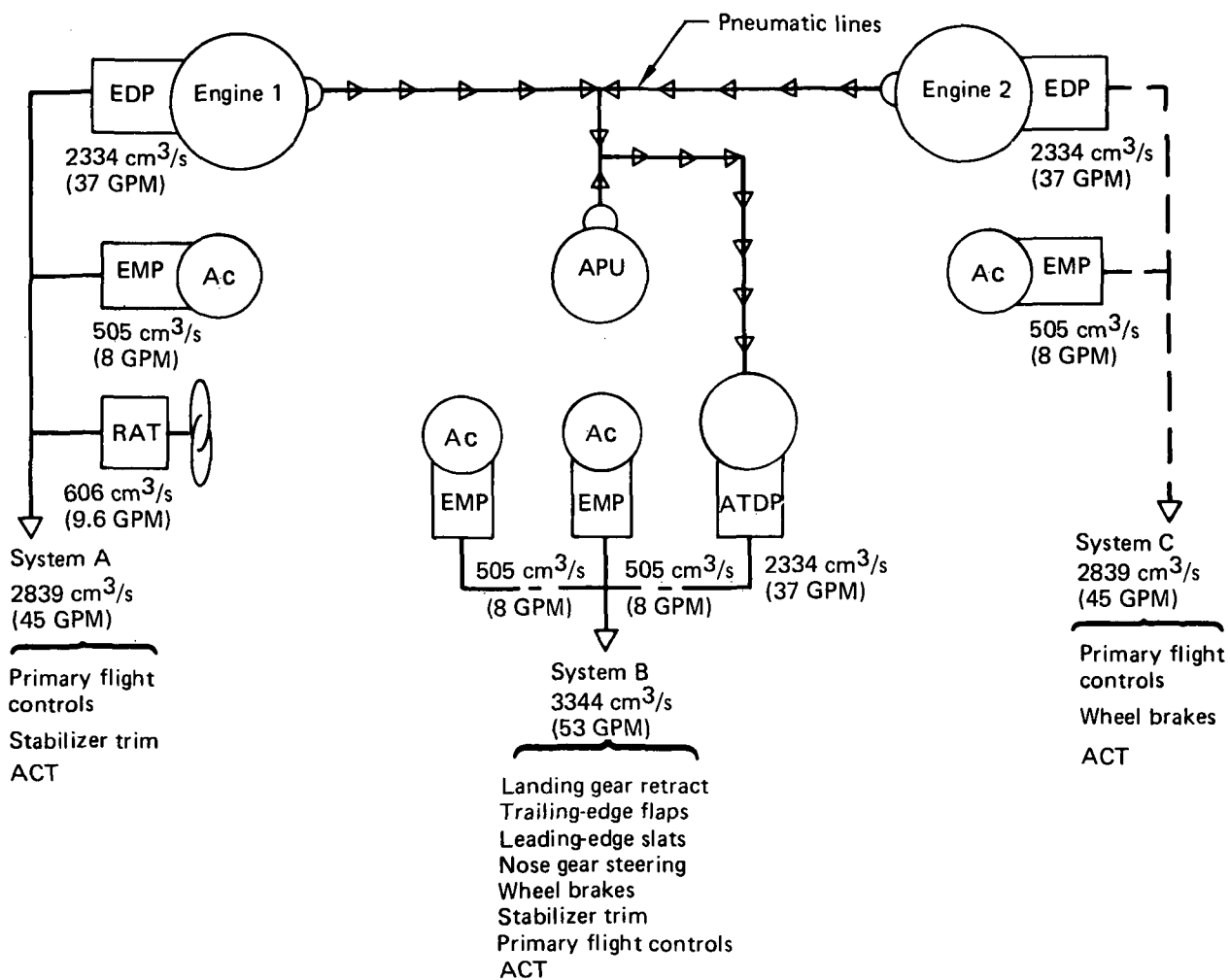
Figure 36. Hydraulic Power System
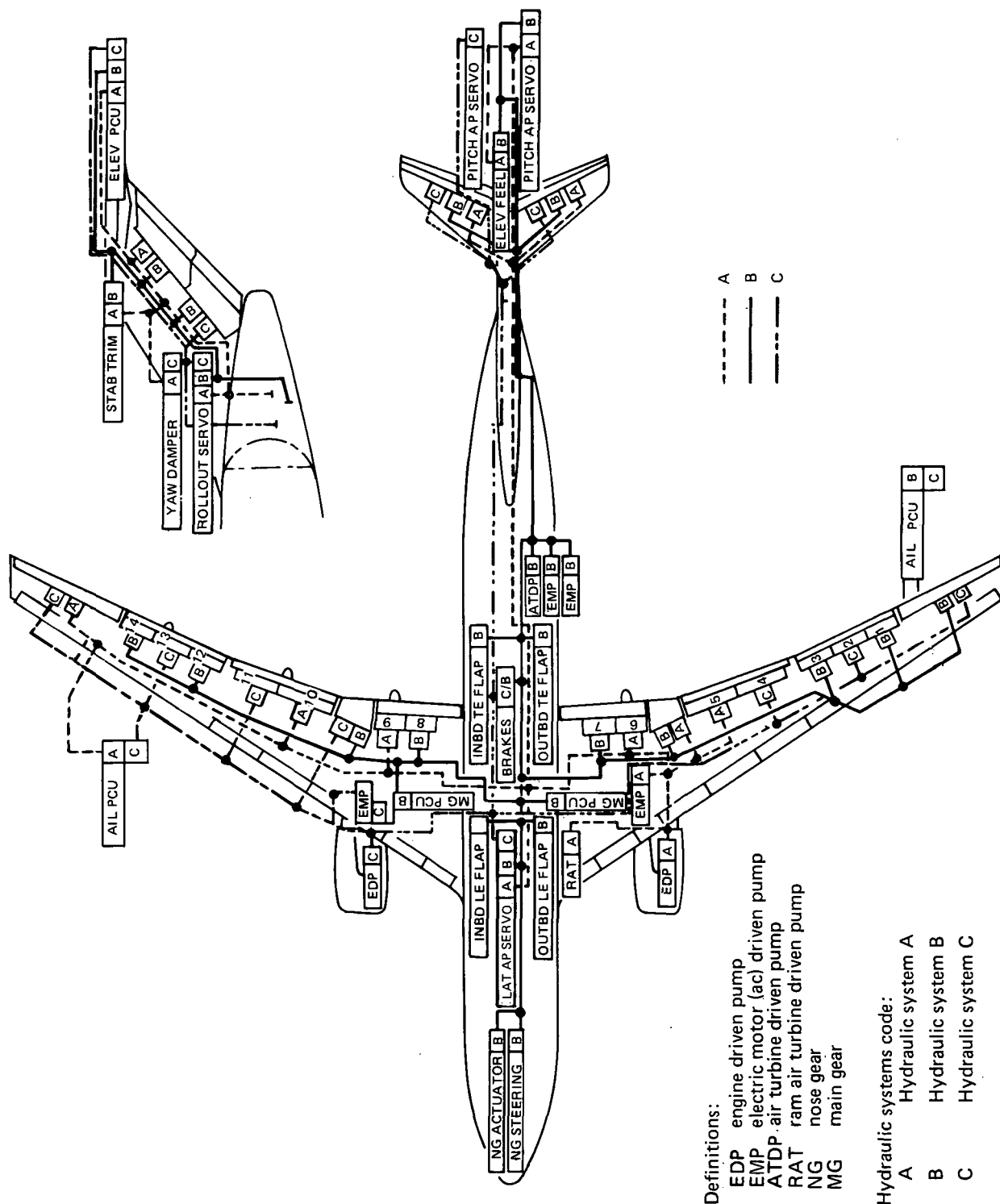
768-104, -105, -106

Figure 37. Hydraulic System Distribution

768-104, -105, -106

Definitions:
EDP   engine driven pump
EMP   electric motor (ac) driven pump
ATDP   air turbine driven pump
RAT   ram air turbine driven pump
NG   nose gear
MG   main gear

Hydraulic systems code:
A   Hydraulic system A
B   Hydraulic system B
C   Hydraulic system C

82

7.0 ANALYSIS

This section provides the analyses used in studying the three planform study configurations. It includes comparisons of these three configurations and the Initial ACT Configuration and highlights reasons for the selection of the Final ACT Configuration.

7.1 FLYING QUALITIES

This subsection describes the methods used to determine the flying-quality parameters. Tail sizing, trim, control, and stability characteristics are described in Subsections 7.1.2, 7.1.3, 7.1.4, and 7.1.5, respectively. Each subsection is organized with the longitudinal axis followed by the lateral/directional axes data and emphasizes the critical flight characteristics. The data are presented for the Model 768-104 Configuration; however, data are shown for the other configurations when significant differences occur.

Figure 38 shows the flight envelope for the planform study configurations, which is the same as that for the Initial ACT and Baseline Configurations. The operational flight envelope is designated, and good flying qualities are required within this boundary. The design envelope for emergency flight extends to dive, flap placard, and stall speeds; minimum safe flying qualities are required to these limits.

Flying qualities were determined for the most demanding conditions considering weight, center of gravity (cg), inertia, and loading possibilities. Failures such as engine-out, hydraulic failure, and mistrim were also included.

7.1.1 AEROPARAMETER ESTIMATION (METHODS)

As with the Initial ACT and Baseline Configurations, the Wing Planform Study Configurations required aerodynamic data representing the particular airplane with which analysis could be made. The Baseline Configuration was modeled with wind tunnel data. The Initial ACT Configuration, which has essentially the same wing-body geometry as the Baseline, required only changes to the tail data. The planform study wings, which have new wing geometry, required revised aerodynamic data for analysis

83
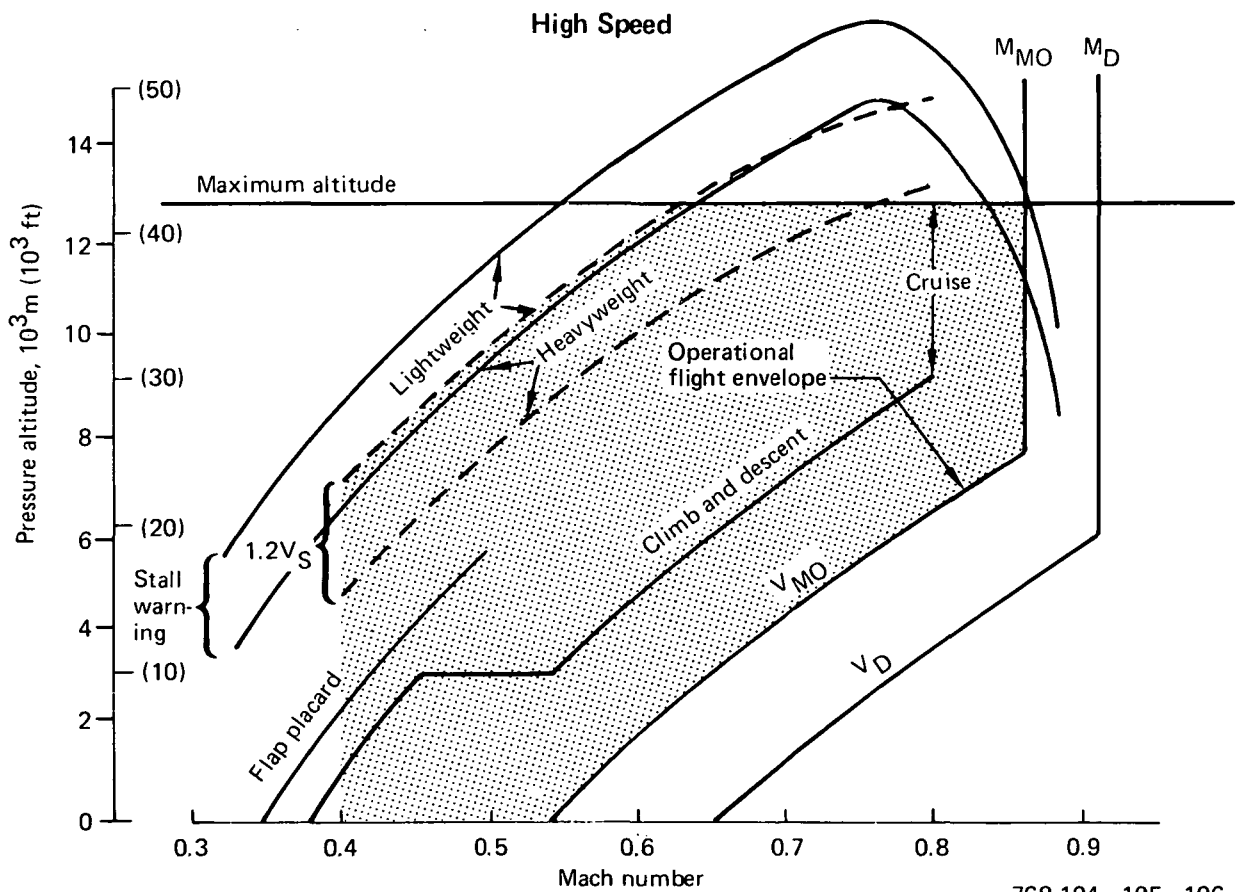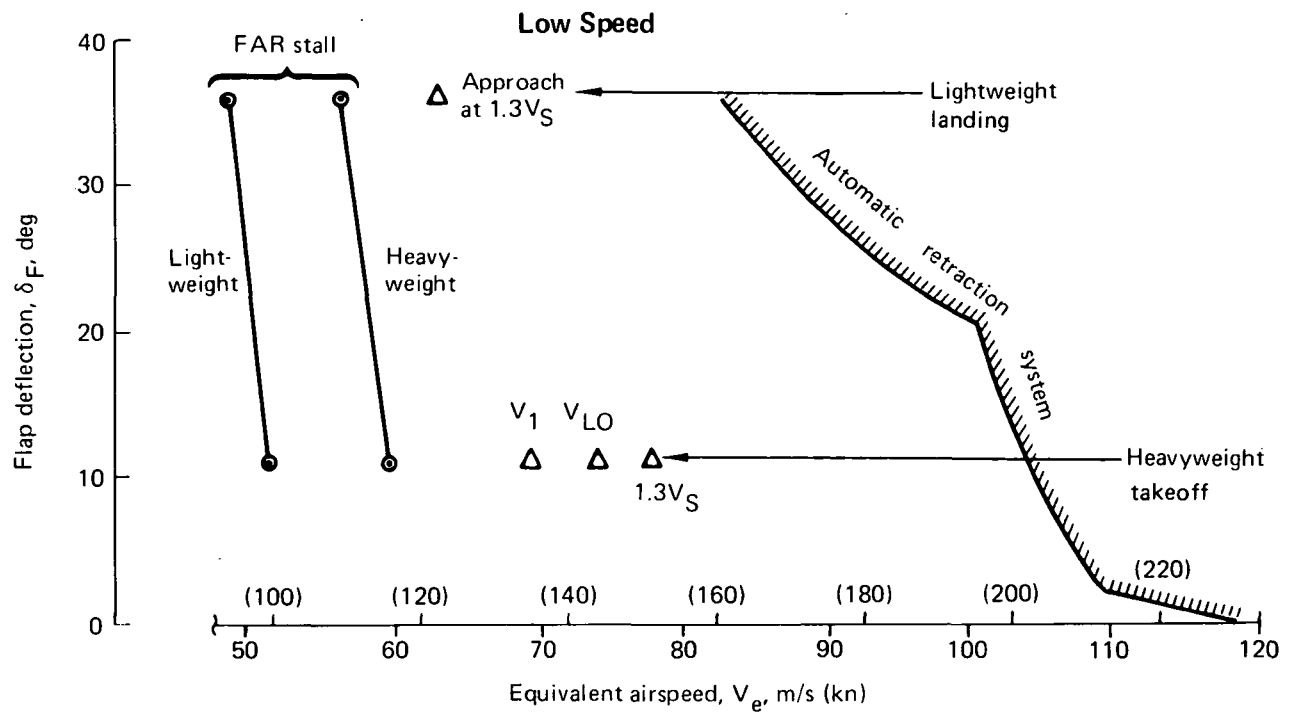
Figure 38. Speed and Altitude Flight Envelopes

768-104, -105, -106

of performance and flying-quality characteristics. Because new wind tunnel testing was not within the scope of the task, theoretical increments were calculated and applied to the wind tunnel data in the most appropriate manner for consistent comparison of the planform study and Initial ACT Configurations.

All the configuration changes of the planform study wings and their effects, including fuselage and landing-gear relocation, wing aspect ratio, and sweep, were considered. Effects on the wing-body lift curve slope, aerodynamic center, and tail downwash were considered important. Minor changes such as wing lift at zero alpha and pitching moment at zero lift were not included.

U.S. Air Force Stability and Control Data Compendium (DATCOM), Reference 5, was used to estimate $\Delta C_{L\alpha}^{WB}$, Δac^{WB} and $\Delta \varepsilon_{\alpha}$ increments. For each pertinent Mach number, data estimates were made for the Initial ACT and Wing Planform Study wings; the increments were obtained by taking the difference between the two cases. These increments were then applied to the Initial ACT quasi-static aeroelastic (QSAE) input data. New $C_{L\alpha}^{WB}$ and ac^{WB} data were also generated by structures and performance methods, which resulted in good agreement with stability and control estimation methods. Changes in ΔC_{MO} and ΔC_{LO} were more difficult to estimate and preliminary results showed little change, so they were neglected. Changes in $\Delta \varepsilon_{\alpha}$, $\Delta \sigma_{\beta}$ were also too minor to be used. A sample of the rigid aerodynamic data changes for each wing is:

Mach	0.40	0.80
Models 768-104/-105/-106	Models 768-104/-105/-106	
$\Delta C_{L\alpha}^{WB}$	0.002/ 0.002/ 0.003	0.003/ 0.0055/ 0.0072
Δac^{WB}	0.02/ 0.01/ -0.03	0.02/ 0.01/ -0.03

Note: Data are shown for each planform based on its reference geometry.

Aeroelastic correction factors were included that reflect wing stiffness for the final design wing with selected ACT functions.

Although the depth was not as comprehensive, analysis methods and programs were the same as those used for the Initial ACT and Baseline analyses.

7.1.2 TAIL SIZING

7.1.2.1 Horizontal Tail

The horizontal tail sizing criteria for the three study wings were the same as for the Initial ACT Configuration. All three tails have the same geometry and double-hinged elevators as the Initial ACT. The tail area of the Models 768-104 and -105 is the same as the Initial ACT Configuration, but the Model 768-106 tail is 9% larger due to decreased wing-body stability. The tail-sizing chart for the Model 768-105 airplane is not shown because, with the exception of a reference mean aerodynamic chord (MAC) change, it is the same as the Model 768-104 Configuration. The tail-size charts for Models 768-104 and -106 (figs. 39 and 40) show that:

- Compared with the Initial ACT tail sizing, fore and aft cg limit requirements are nearly identical.

- The tails were sized for stall recovery at the aft limit and require an alpha limiter.

- With a single green band, mistrimmed takeoff rotation is not limiting; however, a mistrim to maximum mechanical limits would be limiting.

- Landing approach trim is not limiting.

7.1.2.2 Vertical Tail and Lateral Control

The vertical tail size requirement for the study configuration was set by either ground minimum control speed (V_{MCG}) or by the Boeing "tameness" criterion, which required that an engine failure be controlled with only lateral control input. For Models 768-105 and -106, V_{MCG} was the critical parameter and resulted in a vertical tail volume
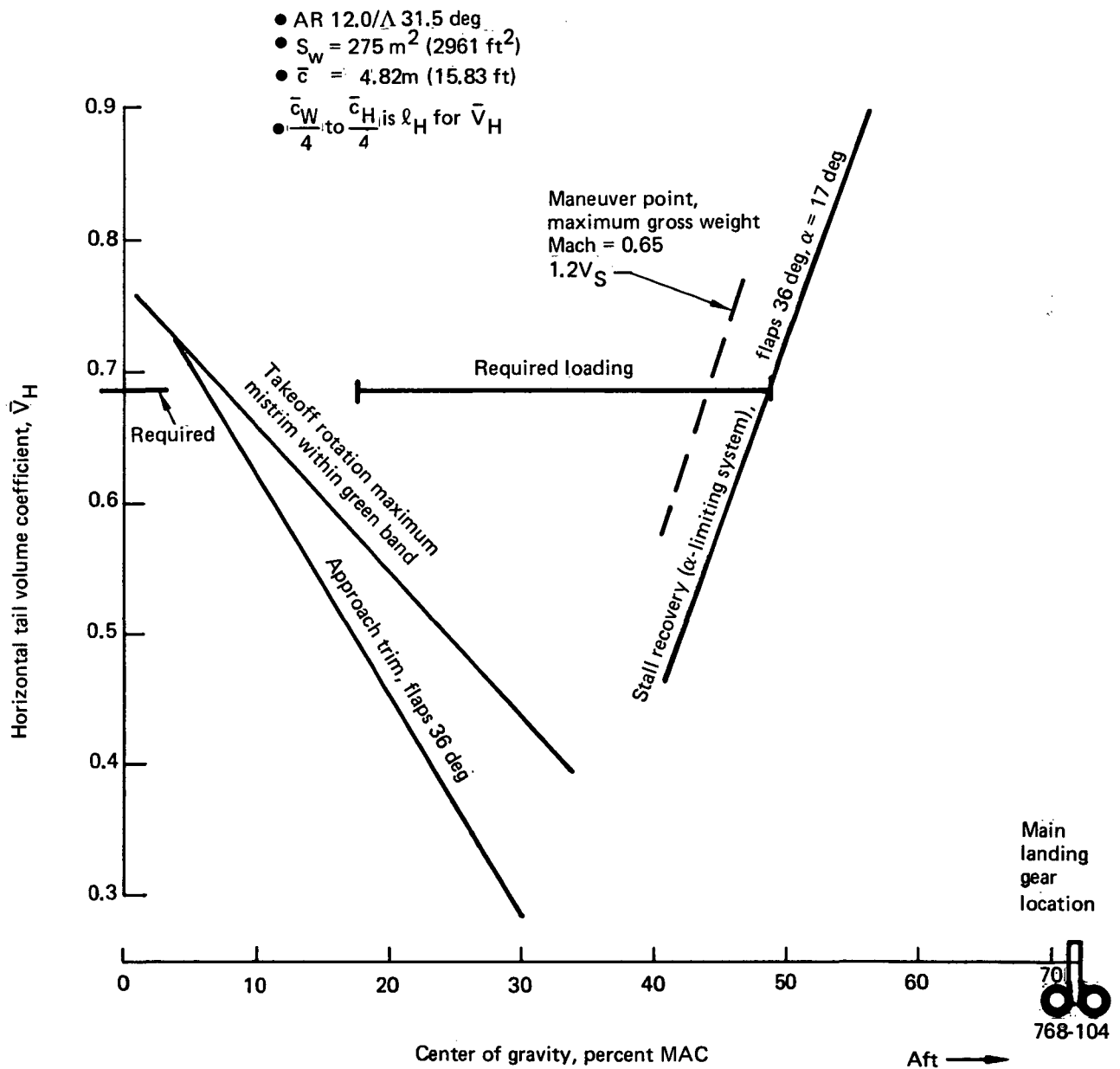
Figure 39. Horizontal Tail Size Requirements, Model 768-104
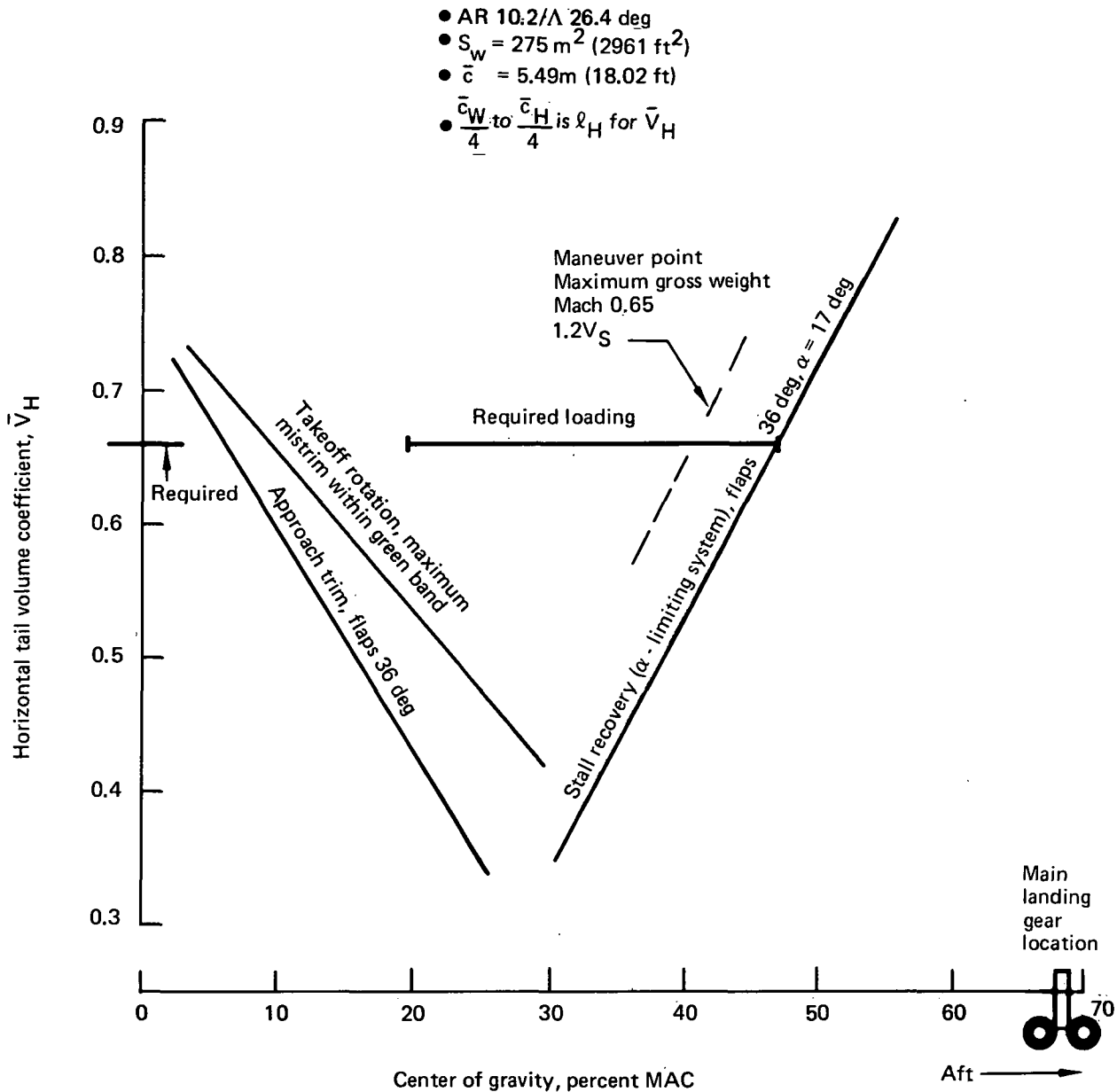
Figure 40. Horizontal Tail Size Requirements, Model 768-106

coefficient ($\bar{V}_V$) of 0.0870 for the 768-105 and 0.0878 for the 768-106. Corresponding vertical tail areas are 55.28 m^2 (595 ft^2) and 55.83 m^2 (601 ft^2), respectively. Tail size requirements for the 768-106 are shown in Figure 41.

Vertical tail size requirements for the 768-104 are shown in Figure 42. The vertical tail was initially sized by the "tameness" criterion, resulting in a $\bar{V}_V$ of 0.0849 and an area of 56.58 m^2 (609 ft^2). Subsequent to the initial layout of this configuration, analysis of the roll response, as described below and in Subsection 7.1.4, showed the

Figure 41. Vertical Tail Size Requirements, Model 768-106

- AR 12.0/Λ 31.5 deg
- S_w = 275 m^2 (2961 ft^2)
- b = 52.21m (171.3 ft)
- $\dfrac{\bar{c}_W}{4}$ to $\dfrac{\bar{c}_V}{4}$ is ℓ_V for $\bar{V}_V$

0.090

0.085 — 0.0849

0.0824

0.080

0.075

0.070

0.065

0.060

Vertical tail volume coefficient, $\bar{V}_{V_{0.25}}$

Required loading

Required loading

Tameness without inboard section of outboard aileron and extended spoiler span

V_{MCG}

V_{MCA}

Tameness with full outboard aileron and extended spoiler span

Forward cg

Aft cg

0   10   20   30   40   50   60

Center of gravity, percent MAC
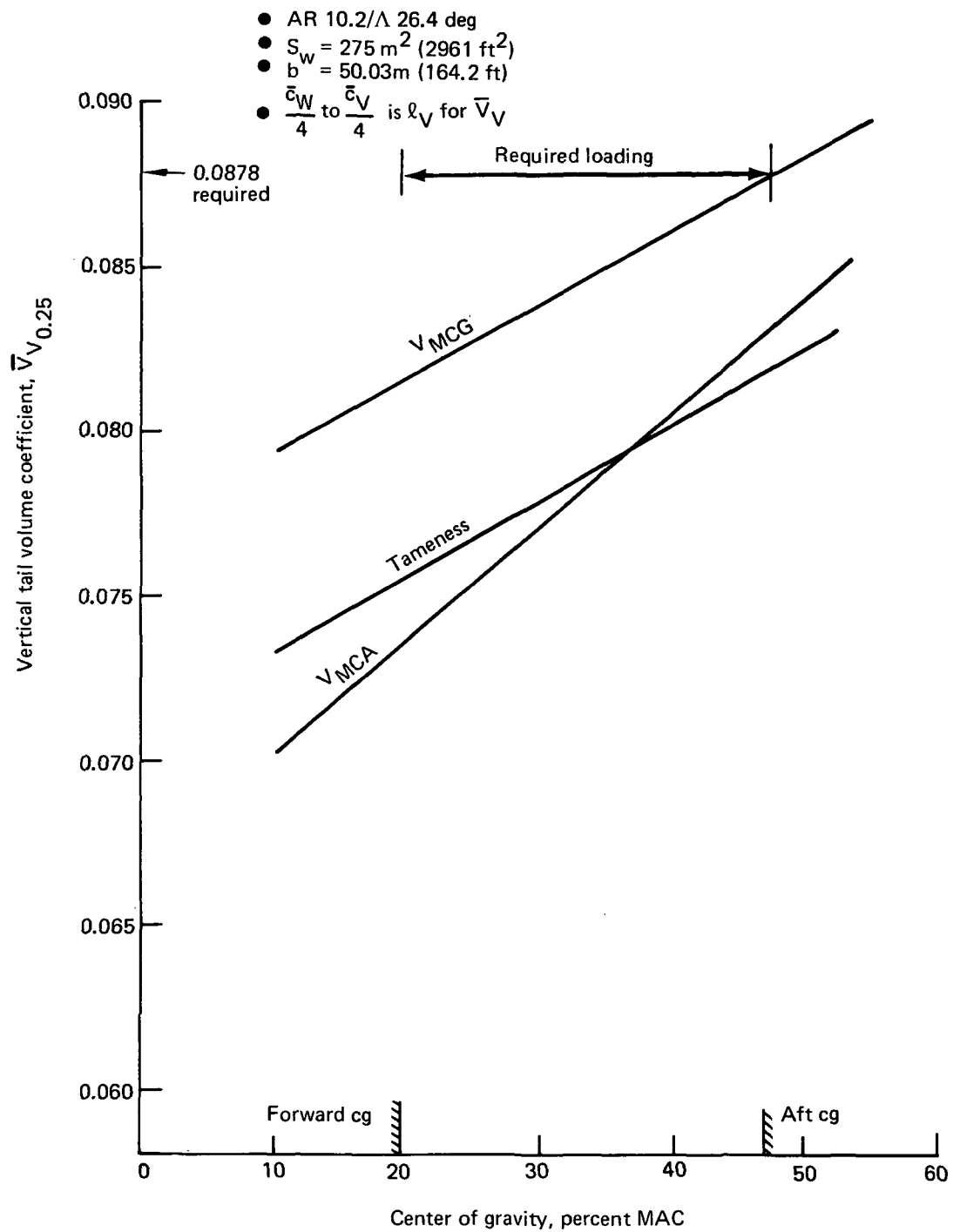
Figure 42. Vertical Tail Size Requirements, Model 768-104

requirement for additional roll control power. With additional roll control, the tameness criterion was no longer critical for the vertical tail. If the vertical tail had been resized for V_{MCG}, the $\bar{V}_V$ could have been reduced to 0.0824, corresponding to an area reduction to 54.9 m^2 (591 ft^2). However, the configuration was not changed, thus the vertical tail remains about 3% oversized.

The tail size leads to low Dutch roll damping similar to the Boeing Model 727. All three configurations required a yaw damper, as did the Baseline and Initial ACT Configurations. A conventional yaw damper was suitable and is discussed in Subsection 7.1.5. None of the configurations required lateral (roll) stability augmentation.

The lateral controls were sized to meet the roll rate requirements. The increased wing span on all three configurations resulted in increased roll damping that required greater lateral control power, which was obtained by using the entire outboard aileron for lateral control (on the Initial ACT Configuration the outboard aileron was split and the inboard section was dedicated to active controls functions) and by extending the outboard spoiler span to the maximum that was physically possible. The most outboard spoiler surface was then divided into three panels, resulting in six flight spoilers per side.

7.1.3 TRIM

The longitudinal and lateral/directional trim characteristics are presented in this subsection. Longitudinal trim is described in terms of angle of attack and stabilizer position, and lateral/directional trim is represented by wheel and rudder required for engine-out and sideslip trim.

Normal and abnormal trim requirements were the same as those for the Initial ACT Configuration. Trim angle of attack and stabilizer deflections for the study configurations were not significantly different from the Initial ACT values detailed in the Initial ACT document (ref 3). Trim angles are not shown because they were not of primary importance to flying-quality or flight-control preliminary design. Trim, as it relates to control authority, is discussed in the following subsection.

91

Rudder and lateral control wheel deflections required trim for flight with an engine failure are shown in Figure 43. Both rudder and lateral control are required for straight equilibrium flight with small bank and sideslip angles, although the lateral control required is seen to be very small for all cruise configuration flight conditions.

Figure 44 illustrates full rudder sideslip trim capability and the corresponding lateral trim required. Forward cg resulted in the smallest sideslip capability, but aft cg required the largest wheel for trim. Less than two-thirds lateral control was required to trim full rudder sideslip throughout the operational flight envelope. Landing in a 15.4 m/s (30 kn) crosswind at normal approach speed corresponds to 13.8 deg of sideslip, which must be trimmed by the rudder. However, because 4 deg crab is allowed, the rudder was required to produce only 9.8 deg of sideslip. This requires 16.9 deg of rudder and 30 deg of lateral control at aft cg. Maximum rudder capability with one hydraulic system failed provided trim to 14.7 deg sideslip.

7.1.4 CONTROL

The longitudinal and lateral/directional control characteristics are described in this subsection. Control capability and requirements are shown for takeoff, landing, landing stall recovery, roll response, and longitudinal maneuvering. Also discussed in this subsection are the control requirements that result in vertical tail and lateral control sizing.

Figure 45 shows takeoff control capability with loss of one critical hydraulic system. Takeoff control with trim set for climb provides for rotation at speeds well below the performance rotation speed. However, at the forward end of the cg range, takeoff control capability is inadequate with a full mechanical mistrim (δ_H = +4.5 deg). A single green band will be necessary to limit the amount of takeoff stabilizer mistrim.

Stall recovery is critical at landing approach, at flaps 36 deg, and at aft cg. As with the Initial ACT Configuration, these airplanes are generally unstable and pitch up severely in poststall regions. Due to nonlinearity of the pitching-moment curve at and above stall, obtaining meaningful differences in the pitching moment at high alphas would require a wind tunnel test. In sizing the horizontal tails, linear aerodynamic

Wheel Required

- Aft center of gravity
- All hydraulic systems operating
  - ☐ End cruise
  - —— Takeoff weight

Control wheel deflection, δ_W, left, deg

-80 — Maximum wheel

-60

-40 — Takeoff △ 1.2V$_S$

-20 — ○ Landing 1.3V$_S$

↕ Ailerons only — 1.2 V$_S$ — Climb — V$_D$ — M$_D$

0 — 0.3   0.4   0.5   0.6   0.7   0.8   0.9

Mach number

Rudder required

Control rudder deflection, δ_R, left, deg

20

○ Landing 1.3V$_S$

25-deg maximum rudder at Mach = 0.21

- Right engine out
- Maximum-rated thrust
- $\beta \approx -3$ deg flaps down
- $\beta = 0$ deg flaps up
- $\phi = 5$ deg flaps down
- $\phi = 0.5$ deg flaps up

15 — △ Takeoff 1.2V$_S$

10 — Rudder available at ratio changer limit for sea level

5

Climb — 1.2V$_S$ — V$_D$ — M$_D$

0 — 0.3   0.4   0.5   0.6   0.7   0.8   0.9

Mach number

Figure 43. Engine-Out Trim, Model 768-104

93

**Wheel Required
for Trim of Maximum
Rudder Sideslip**

- Aft center of gravity
- Includes blowdown
- Open symbols are normal hydraulics
- Shaded symbols are one system out

○ ● Landing $1.3V_S$
◊ ◆ Landing in 15.43 m/s (30 kn) cross wind with 4-deg crab
□ ■ End cruise
—— Normal hydraulics ⎫ Takeoff
— — One system out ⎭ weight

////// Maximum wheel

Lateral control wheel deflection, δ_W, deg

80
60
40
20
0

Landing

Ailerons only

Stall warning

Maximum altitude

$1.2 V_S$

Climb

Sea level

V_{MO} M_{MO} V_D M_D

0.3   0.4   0.5   0.6   0.7   0.8   0.9
Mach number

**Sideslip Capability
With Maximum Rudder**

Sideslip angle, β, deg

15
10
5
0

Landing
● ⊙

Crosswind requirement $\delta_R = 16.9$

Stall warning

Maximum altitude

$1.2V_S$

Climb

Sea level

V_{MO} M_{MO} V_D M_D

0.3   0.4   0.5   0.6   0.7   0.8   0.9
Mach number

Figure 44.   Sideslip Trim Capability, Model 768-104
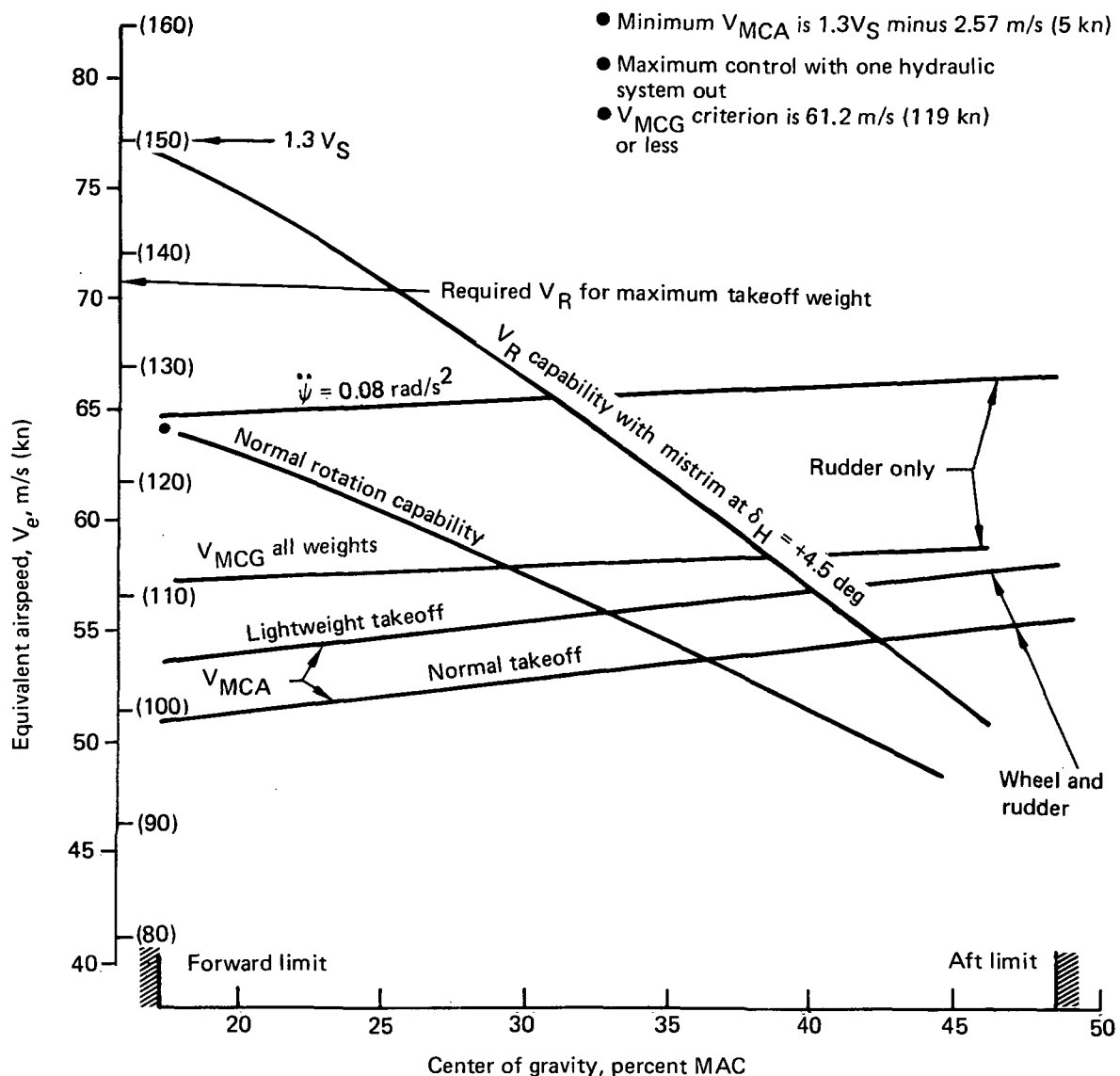
Figure 45. Takeoff Control, Model 768-104

corrections for planform differences, as discussed in Subsection 7.1.1, were applied up to and including stall. The horizontal tail was sized to meet the same pitchover acceleration ($\ddot{\theta}$ = -0.08$\frac{rad}{sec^2}$) as the Initial ACT. An alpha limiter will prevent the airplane from entering the deep-stall region, and pitch-augmented stability (PAS) will provide stable gradients up to stall identification angle of attack.

Figure 46 shows control at landing approach with one hydraulic system failed. Pitch accelerations at approach with normal stabilizer trim and with stabilizer jammed in
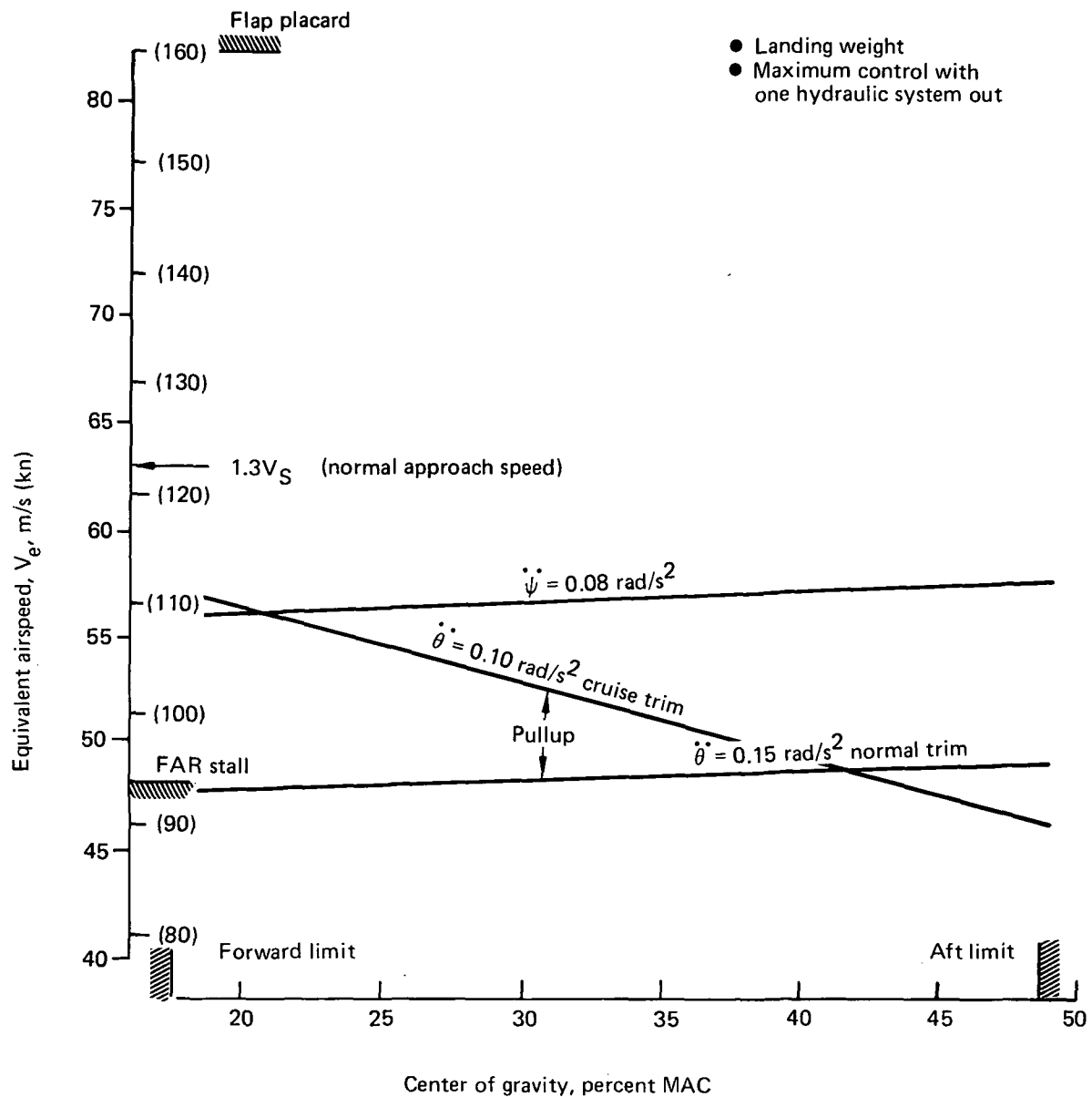
Figure 46. Landing Control, Model 768-104

the worst-cruise position was satisfactory at speeds well below normal approach speeds.

The Boeing tameness criterion was met by all three configurations with lateral control power increased to meet roll-rate requirements (see figs. 41 and 42 for Models 768-104 and -106).

The lateral controls were resized because it became evident that lateral control was not adequate to meet low-speed roll-rate requirements. This resulted in using the total outboard aileron for lateral control, whereas on the Initial ACT Configuration the inboard segment of the outboard aileron was dedicated to ACT functions. In addition, the spoilers were extended to the maximum span that was physically allowable. These changes allowed the low-speed roll-rate requirement to be met.

Figure 47 shows the roll-rate capability for takeoff and en route flight. The data are for a loading condition of maximum roll inertia and full control wheel input as a 0.5 sec ramp. Data are shown for all hydraulic systems operating and for two systems failed, which are the critical conditions for DRO specified Level 1 and Level 3 flying qualities, respectively. Criteria were satisfied at all speeds for the en route configuration. The most critical point was when the outboard aileron was locked out at 128.6 m/s (250 kn) calibrated airspeed and the roll response capability approached the Level 1 criterion, which allows 4 sec to bank 60 deg. For takeoff configuration, the Level 1 criterion of 2.5 sec to bank 30 deg was achieved down to a speed of $1.2V_S$, and with two hydraulic systems failed, the Level 3 requirement of 4.5 sec to bank 30 deg was also achieved down to $1.2V_S$. The landing configuration is not shown because lateral control power increases with flap deflection and roll inertia decreases at landing weight, making it noncritical.

The planform study configurations required an increase in lateral control power over that of the Initial ACT Configuration, mainly because of the increased roll damping due to larger wing spans.

Engine-out control on the ground (V_{MCG}) was the critical condition that determined vertical tail size. The tail on the Model 768-104 is oversized by 1.67 m^2 (18 ft^2) due to a tameness demand that became obsolete when lateral controls were resized, as described earlier. The vertical tail would be 54.90 m^2 (591 ft^2) if correctly sized by V_{MCG}. For Models 768-105 and -106, the vertical tails are 55.28 m^2 (595 ft^2) and 55.83 m^2 (601 ft^2), respectively.

The engine-out control in free air (V_{MCA}) criterion requires control of engine failure at $1.3V_S$ minus 2.57 m/s (5 kn) with one hydraulic system failed. The critical condition was lightweight takeoff, and the criterion was met by all configurations (fig. 45).

97
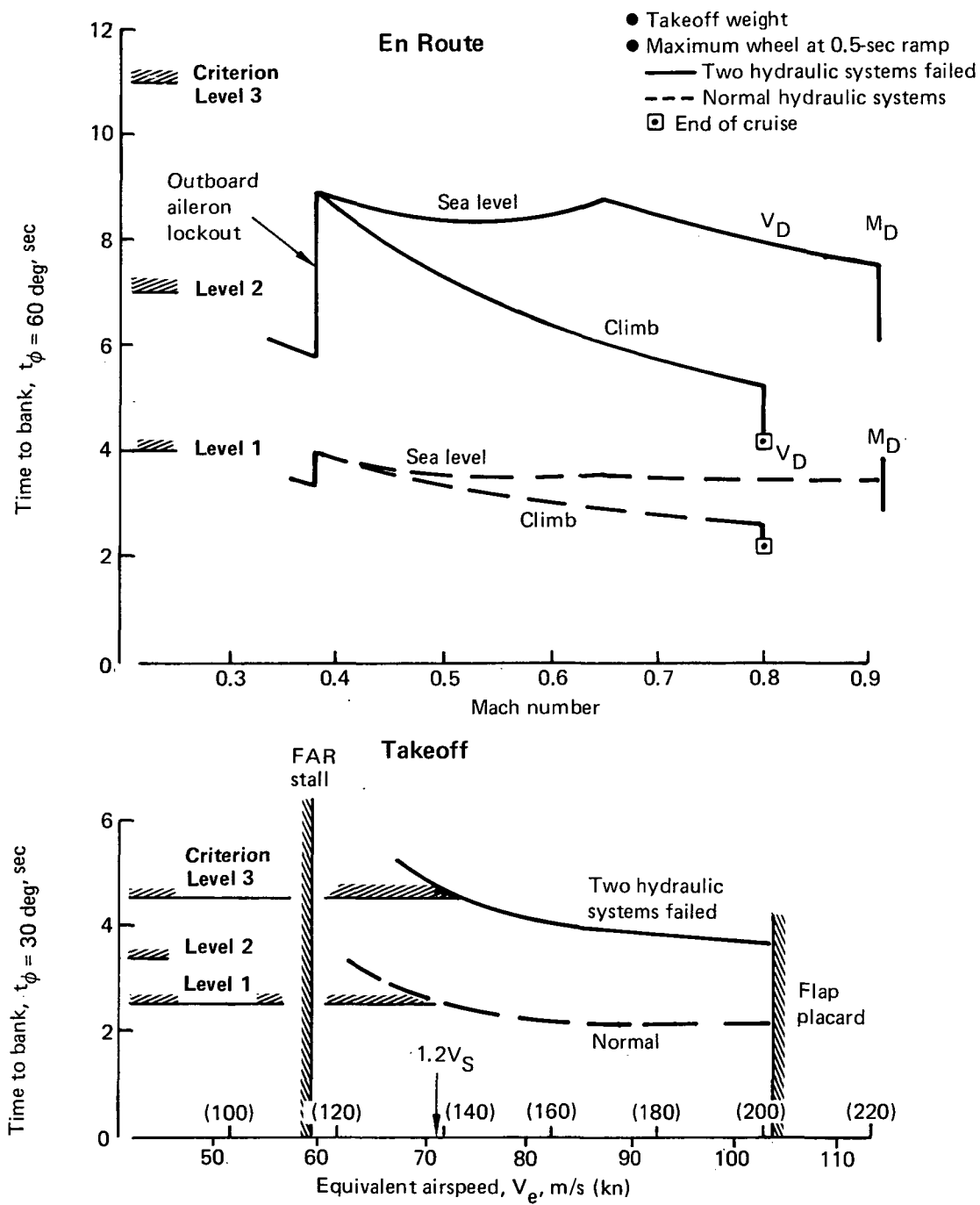
Figure 47. Roll Response Capability, Model 768-104

Rudder power capable of producing yaw acceleration of 0.08 rad/s^2 (figs. 45 and 46) is available to speeds well below normal takeoff and approach.

Unaugmented elevator angle per g (δ_E/g), Figure 48, illustrates the basic longitudinal maneuver capability and is related to short-period stability. PAS was required because δ_E/g is more positive than -2 deg per g (minimum requirements) for flaps up, aft cg.

Unaugmented elevator deflection per airspeed (δ_E/V), Figure 49, illustrates the basic airplane speed stabilty. Negative values are speed-unstable conditions and must be augmented with a feel system or PAS.

The maneuvering elevator angle per g and trim elevator deflection gradient with airspeed characteristics were similar to the Initial ACT Configuration. The critical condition, near stall at M = 0.63, was the same as for the Initial ACT Configuration.

7.1.5 STABILITY

This subsection discusses airplane static and dynamic stability. Static margin shown in Figure 50 reflects airplane pitch static stability at the aft cg. Negative static margins, which exist throughout most of the flight envelope, indicate trim reversal. As with the Initial ACT Configuration, the data reflect pitchup at M = 0.63 stall. Note that high alpha data were estimated adding low alpha linear aerodynamic increments to the Initial ACT Configuration and, therefore, reflect essentially the same pitching tendencies as the Initial ACT Configuration.

Unaugmented maneuver margin (fig. 51) shows characteristics similar to the static margin and elevator angle per g. The maneuver margin is shown for the aft cg, where stability is smallest, and indicates that maneuver stability exists for most of the flight envelope and airplane cg locations. Short-period frequency and acceleration sensitivity ($\frac{\omega n^2}{n/\alpha}$), which is directly related to the maneuver margin and airplane mass characteristics, is used for short-period handling characteristics criteria. Figure 52 illustrates cruise and landing conditions.

Figures 53 and 54 show unaugmented airplane dynamic stability in terms of characteristic root locations. These graphs can be used to compare unaugmented roots
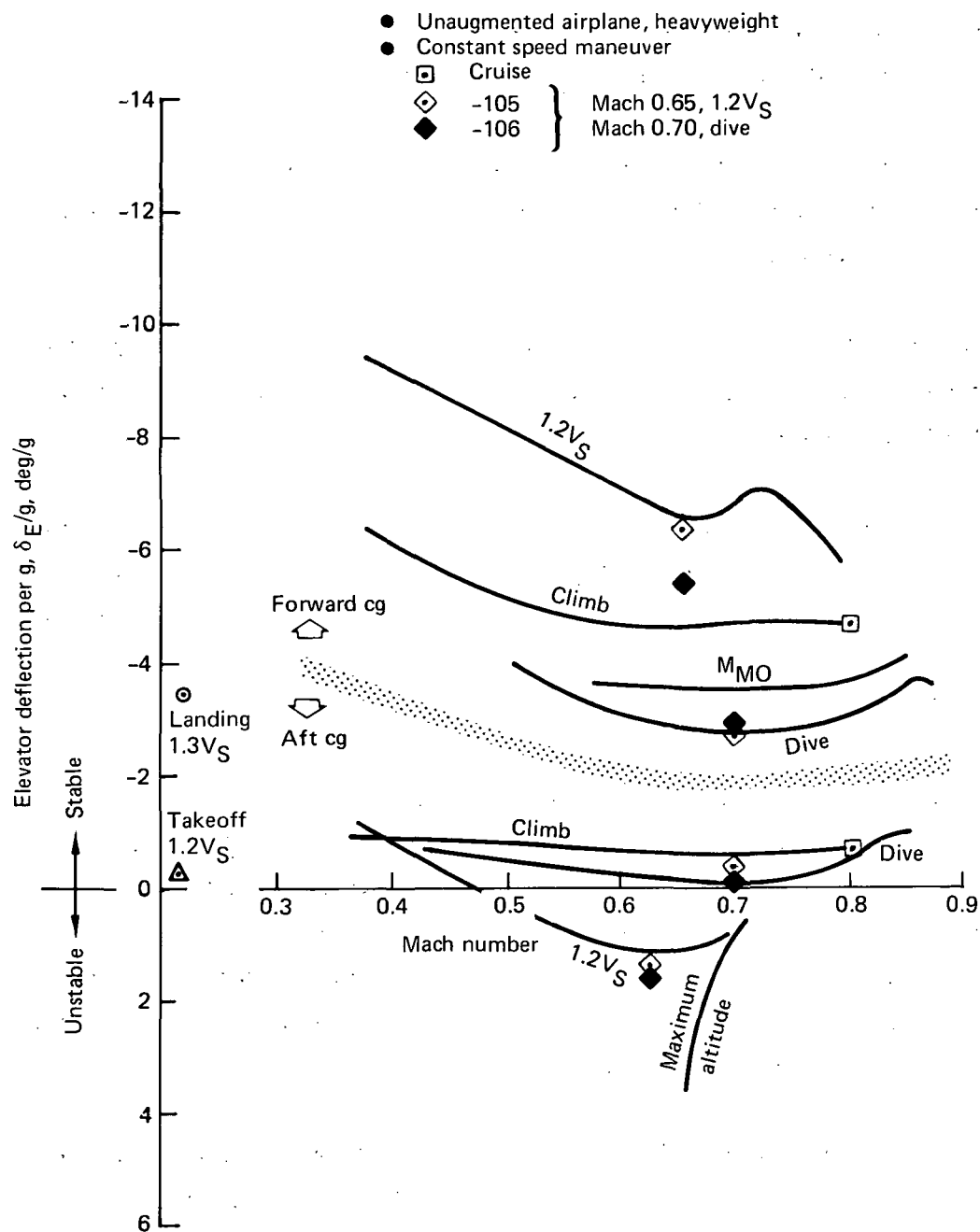
Figure 48. Elevator Angle Per g, Models 768-104, -105, and -106

100

Unaugmented airplane

Elevator required to trim speed increase

——— Aft center of gravity

— — — Forward center of gravity } Heavyweight, flaps up

⊡ Cruise

◈ -105 } Mach 0.65, 1.2V$_S$

◆ -106 } Mach 0.70, dive

Elevator deflection per airspeed, $\delta E/V$, deg/m/s (deg/kn)

0.10

(0.15)

0.05

(0I10)

Stable

Landing
1.3V$_S$

Takeoff
1.2V$_S$

(0.05)

1.2V$_S$

Climb

Dive

0

Unstable

0.4   0.5   0.6   1.2V$_S$ 0.7   0.8   0.9

Mach number

(-0.05)

(-0.05)

Stall warning

-0.05

(-0.10)

(-0.15)

-0.10

(-0.20)

-0.15

Figure 49. Elevator Angle Per Airspeed, Models 768-104, -105, and -106

101
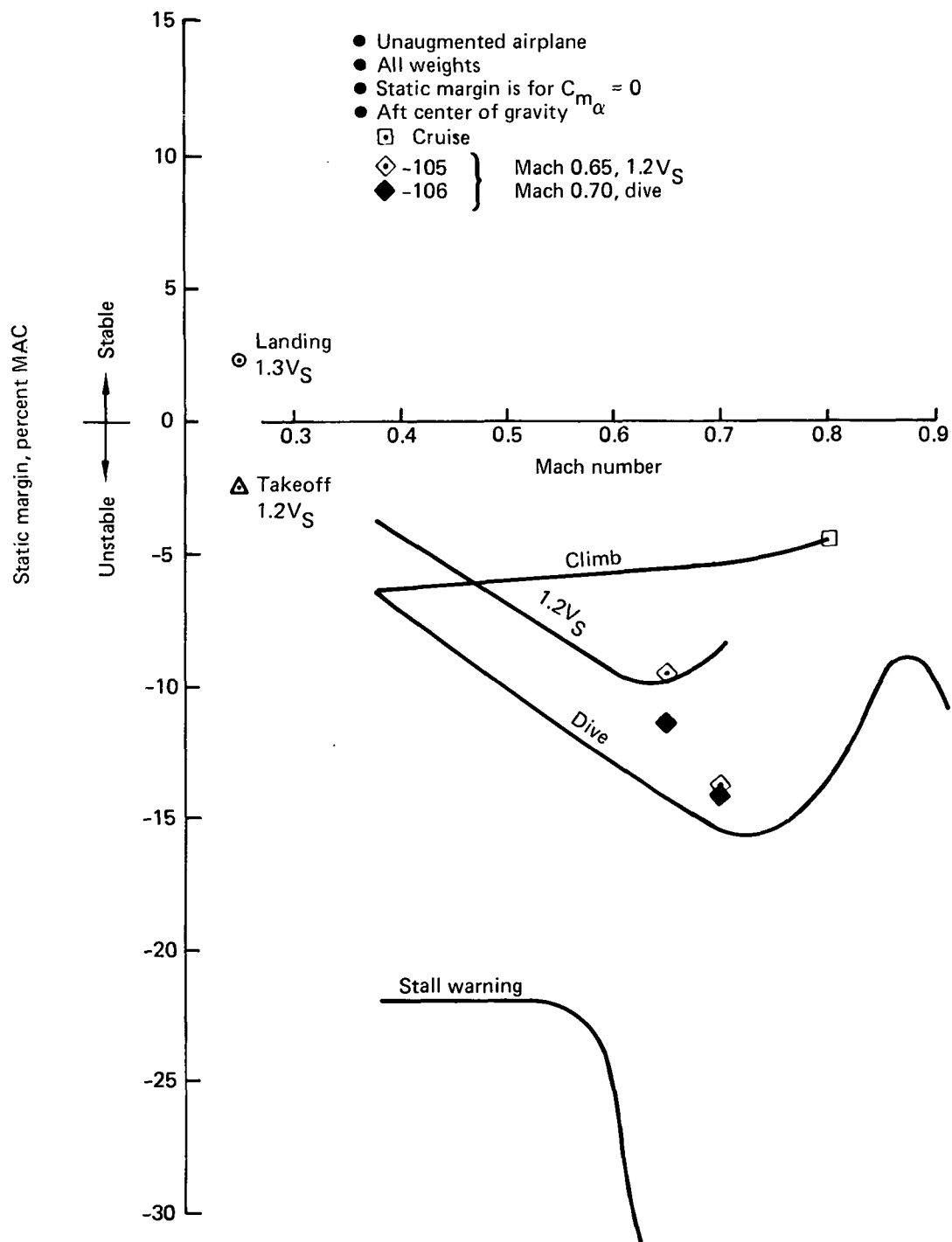
Figure 50.   Static Margin at Aft Center of Gravity, Models 768-104, -105, and -106
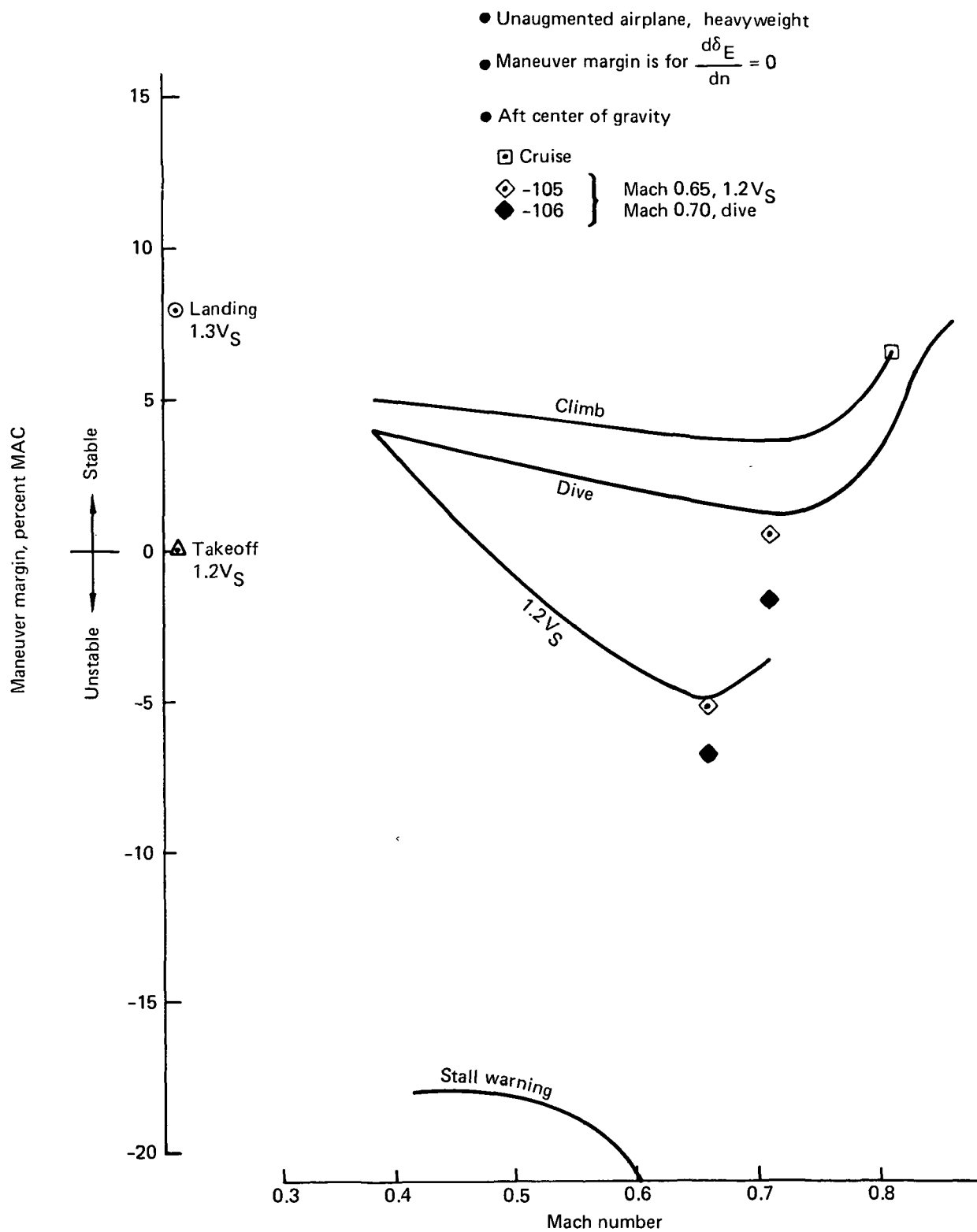
Figure 51. Maneuver Margin at Aft Center of Gravity, Models 768-104, -105, and -106
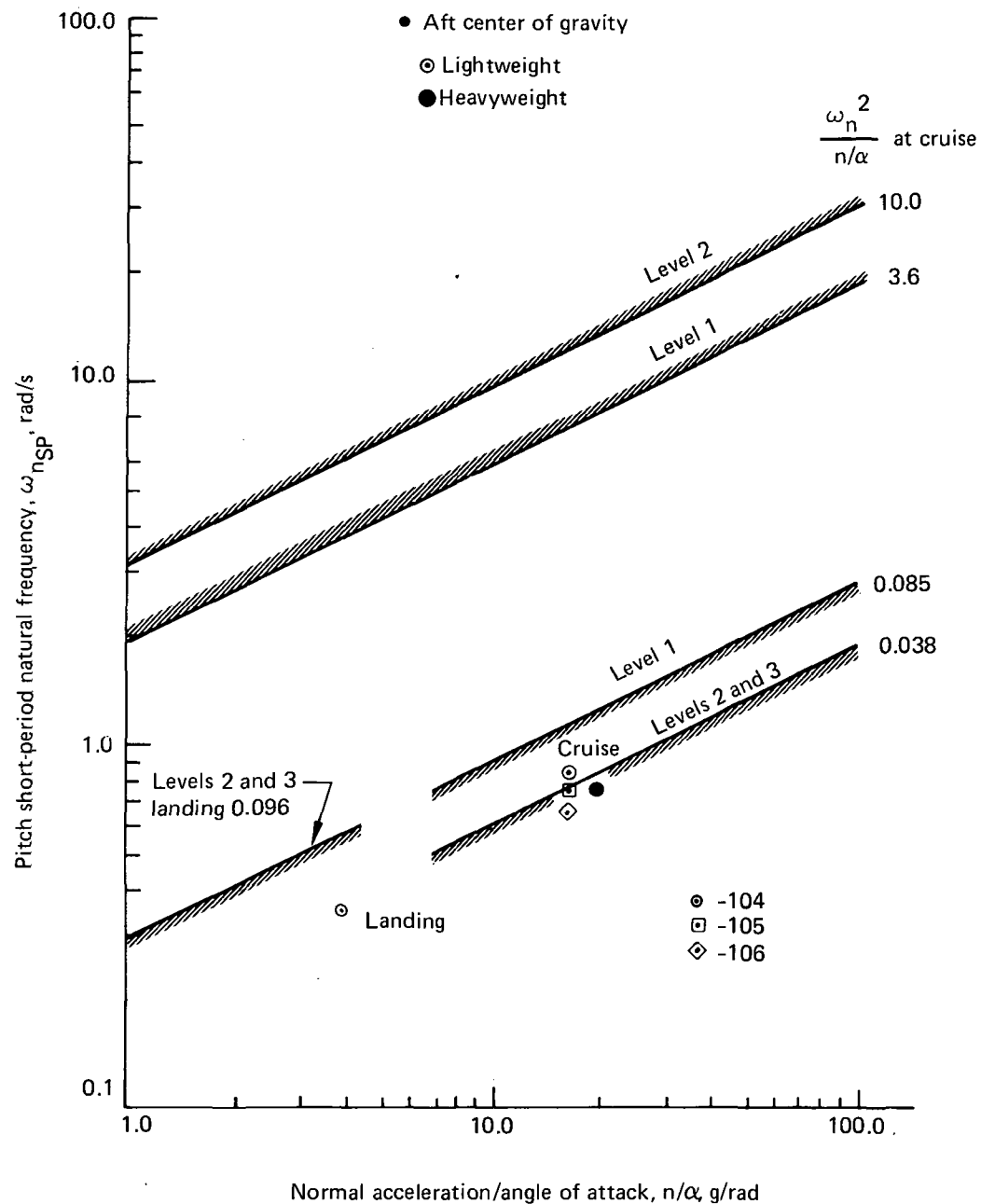
Figure 52. Unaugmented Short-Period Stability, Models 768-104, -105, and -106

● Unaugmented airplane

Flight condition*	Models -104, -105, -106		
17	▲	△	
36	●	○	
58	■	□	◰
61	◆	◇	
67	◤	▽	
107	◗	D	◗
108	★	☆	
97	X		

*From table 5
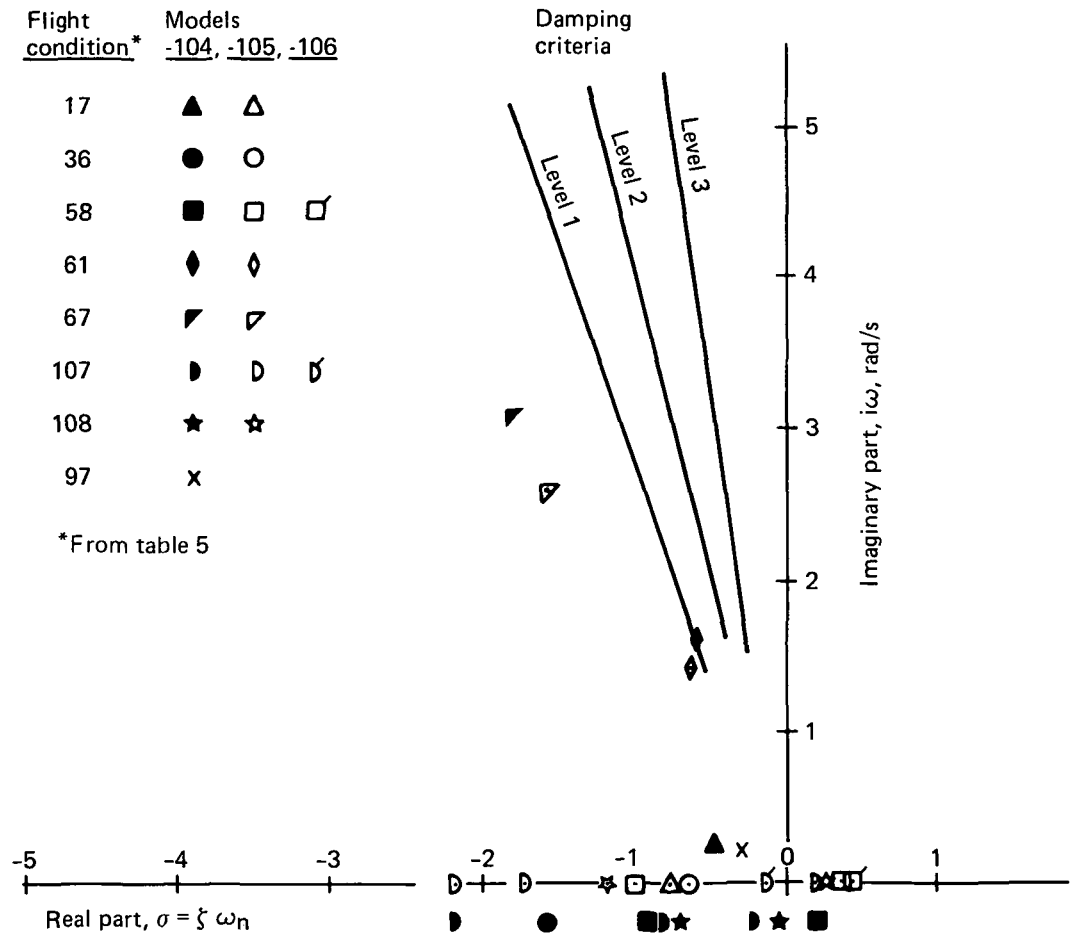
Figure 53. Short-Period Characteristics Roots, Models 768-104, -105, and -106
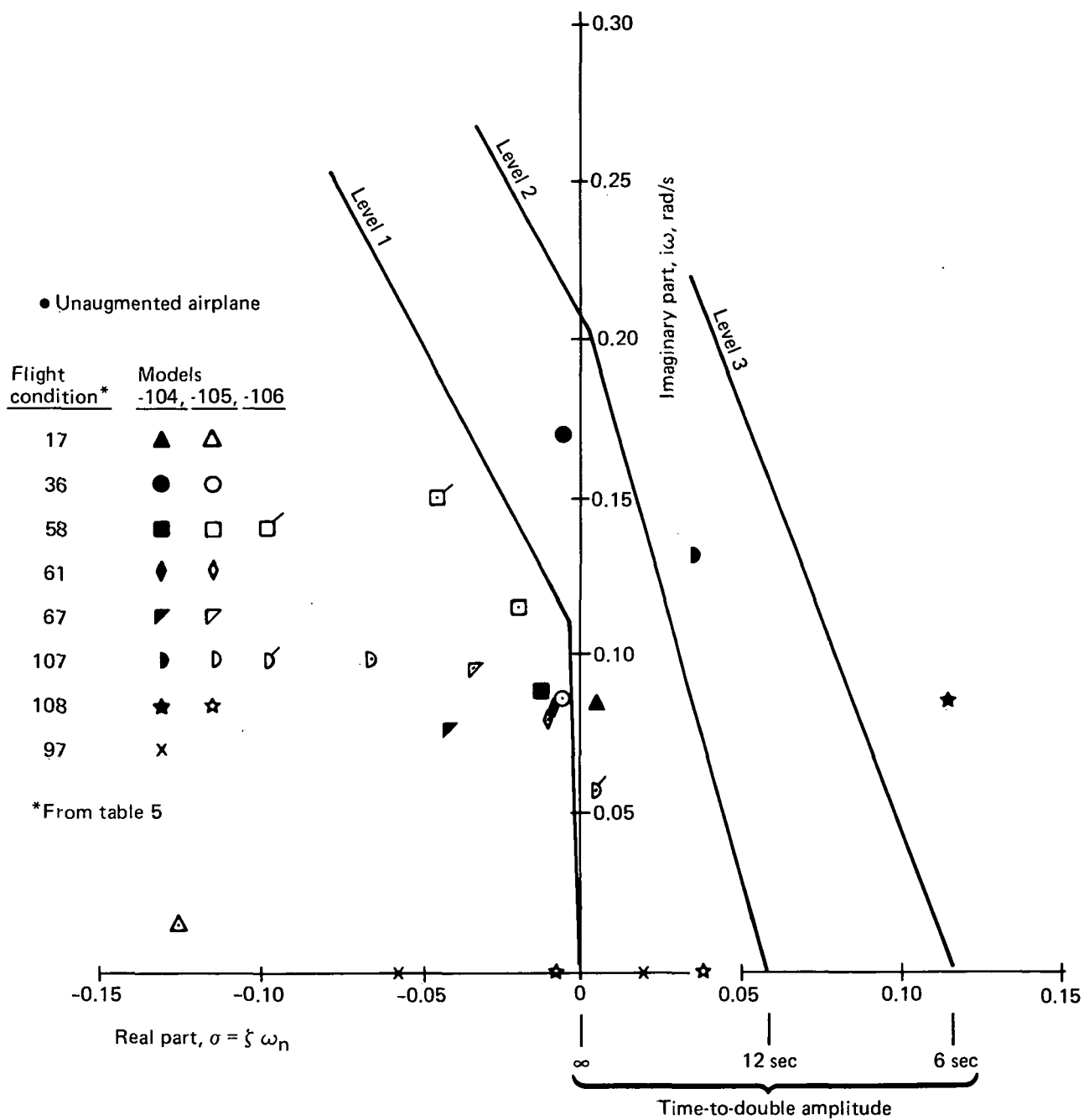
Figure 54. Phugoid Characteristics Roots, Models 768-104, -105, and -106

106

of the Wing Planform Study and the Initial ACT Configurations (ref 3) at specific flight conditions that were chosen as extreme ends of the static stability spectrum (table 5). The differences between the short-period root locations of the planform study wings are relatively small, and in most cases the Model 768-104 wing is the most stable. Comparison of the short-period roots with the Initial ACT Configuration (ref 3) shows minor differences, and the Model 768-104 wing is usually more stable.

Table 5. Design Conditions for Pitch Stability Augmentation

Flight condition	Mach No.	Speed	Weight	Center of gravity	Required criteria level
89	0.65	Maximum altitude	Heavy	Aft	3
58	0.65	$1.2V_S$	Heavy	Aft	1 or 2
17	0.65	$1.53V_S$	Heavy	Aft	1
108	0.70	$1.2V_S$	Heavy	Aft	1 or 2
61	0.80	Maximum altitude	Light	Fwd	1 or 2
107	0.70	V_D	Heavy	Aft	3
36	0.82	V_D	Heavy	Aft	3
67	0.86	V_D	Light	Fwd	3
69	0.91	V_D	Light	Fwd	3
99	Takeoff	$1.3V_S$	Heavy	Aft	1
97	Landing	$1.3V_S$	Light	Aft	1

768-104, 105, 106

The phugoid roots of the planform study wings show more diversity. As with the short-period roots, the unstable phugoid roots show improved stability over the Initial ACT Configuration.

As a result of these comparisons, the PAS design for the planform study configuration is not expected to be more difficult than for the Initial ACT Configuration.

Lateral/directional static stability, summarized in Figure 55, illustrates positive stability throughout the flight envelope for the critical heavy gross weight, aft cg condition. These characteristics ensure conventional control deflection for trim and maneuver, but the level of stability requires a yaw damper to improve Dutch roll damping. The characteristics are similar to the Initial ACT Configuration.

107

Lateral Stability
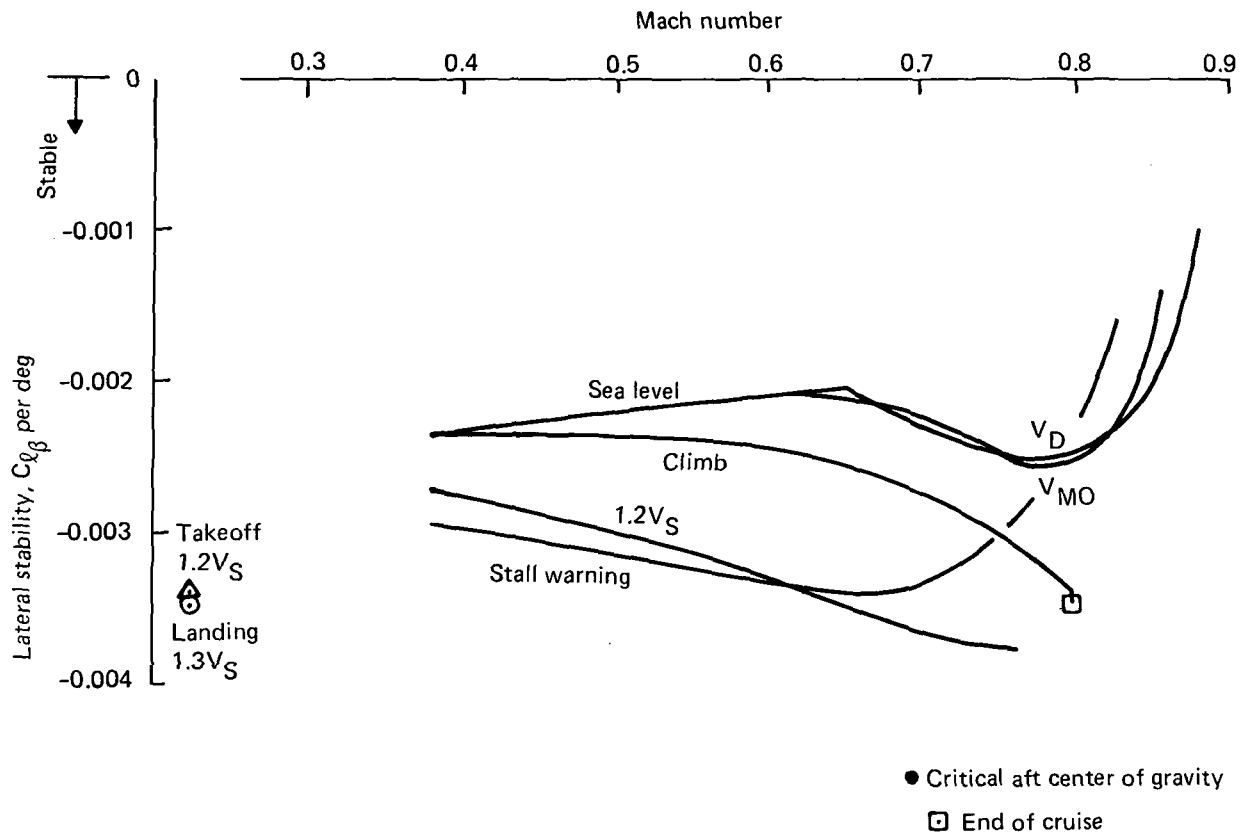
Directional Stability
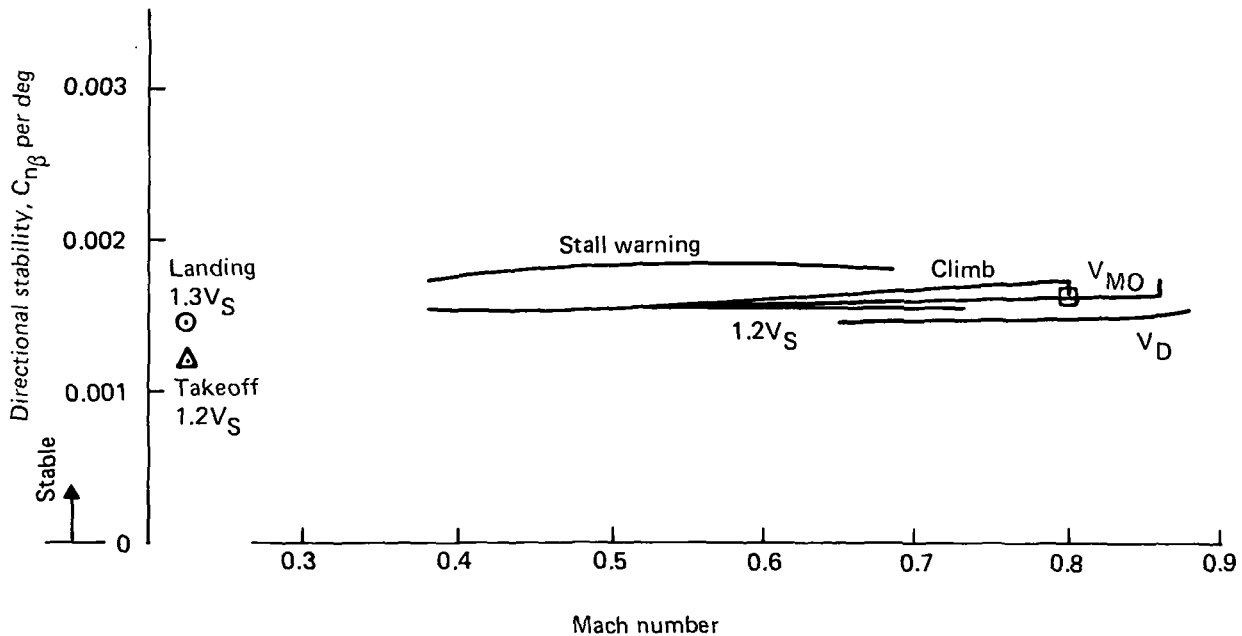
Figure 55. Lateral/Directional Static Stability, Model 768-104

108

Figure 56 shows the unaugmented Dutch roll damping and the criteria that must be met. The unaugmented airplane exhibits poor damping throughout the design envelope. The Level 3 criterion, which represents the minimum safe flying quality, is violated by stall-warning conditions and is closely approached by the end-of-cruise condition, which is within the operational flight envelope.
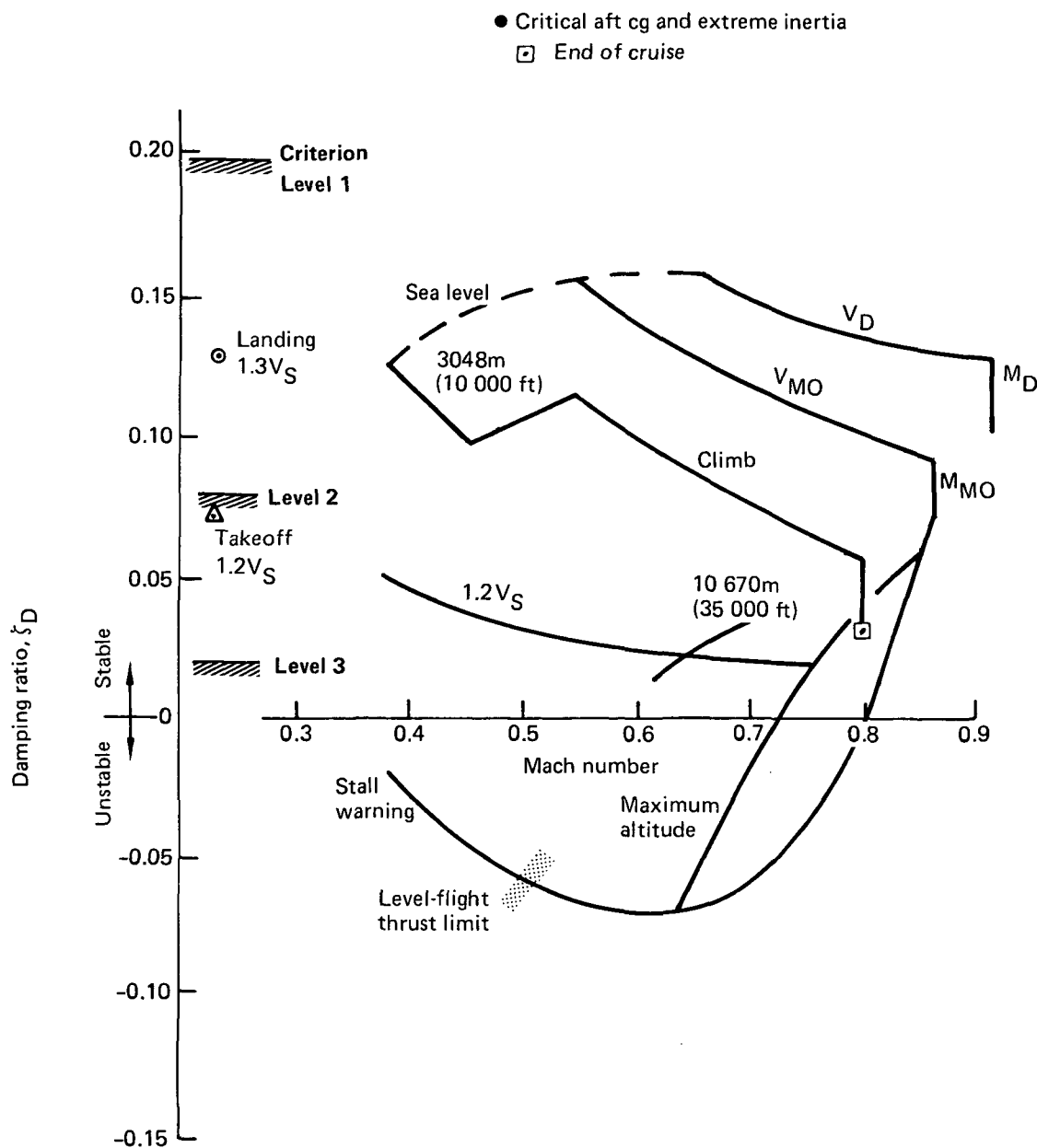
Figure 56. Dutch Roll Damping (Unaugmented), Model 768-104

A conventional yaw damper has been designed to demonstrate the feasibility of stabilizing the Dutch roll damping to satisfactory levels. Figure 57 shows a block diagram of the system. Damping can be stabilized to a Level 1 damping ratio of 0.2 throughout the operational envelope, and stall warning can be improved to satisfactory levels well above minimum safe. Table 6 shows the damping ratio for several conditions and the gain of the yaw rate gyro that is required to achieve these values. The Dutch roll damping of the three configurations is very similar, and therefore the yaw damper design of the three will be nearly the same with some variations in values of gain scheduling. Values that were developed for the Baseline Configuration are included for comparison in Table 6. This yaw damper design is not optimal, but it shows the ability to stabilize the airplane with a conventional system.

Spiral and roll-mode characteristics (figs. 58 and 59) illustrate that Level 1 flying qualities are exhibited throughout the operational flight envelope. Lateral augmentation is not required.
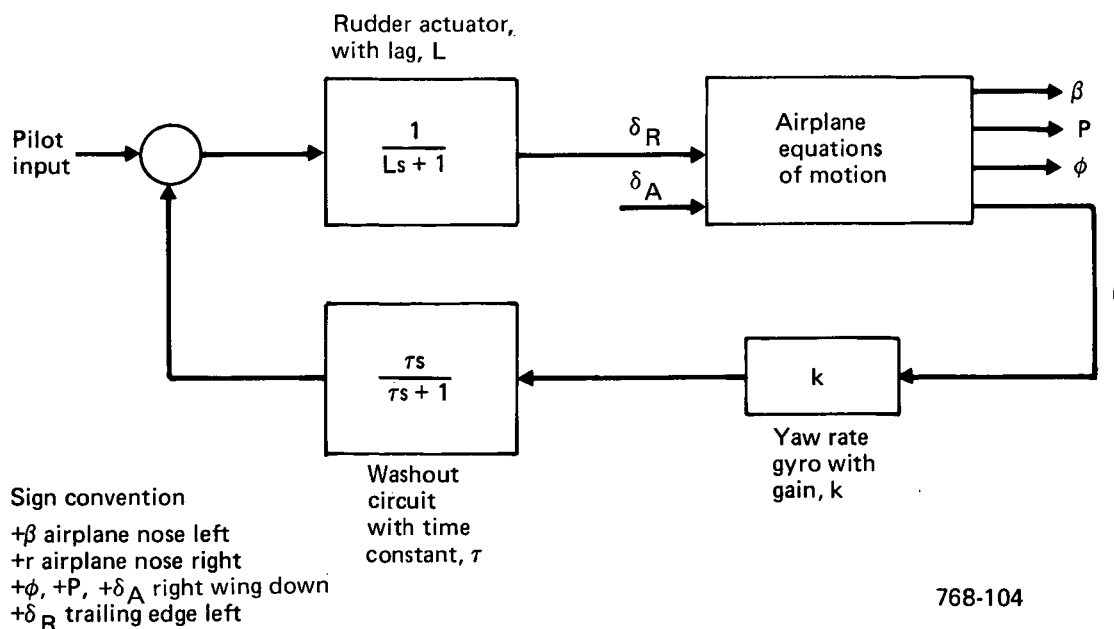
Figure 57. Block Diagram of Yaw Damper

110

Table 6.   Yaw Damper Gain Requirements

Condition	V_e, m/s (kn)	Airplane	ζ	K, rad/(rad/s)
Stall warning, Mach 0.38	89.5 (174)	Baseline	0.05 (max)	3.1
		768-104	0.10	2.36
1.2V_S, Mach 0.7	105.5 (205)	Baseline	0.20	1.31
		768-104		0.94
End cruise, Mach 0.8	112.7 (219)	Baseline		0.80
		768-104		0.58
V_D, Mach 0.91	209.4 (407)	Baseline		0.148
		768-104		0.117
Flaps 11 deg 1.2V_S	71.5 (139)	Baseline		2.87
		768-104	0.20	1.52

768-102, -104
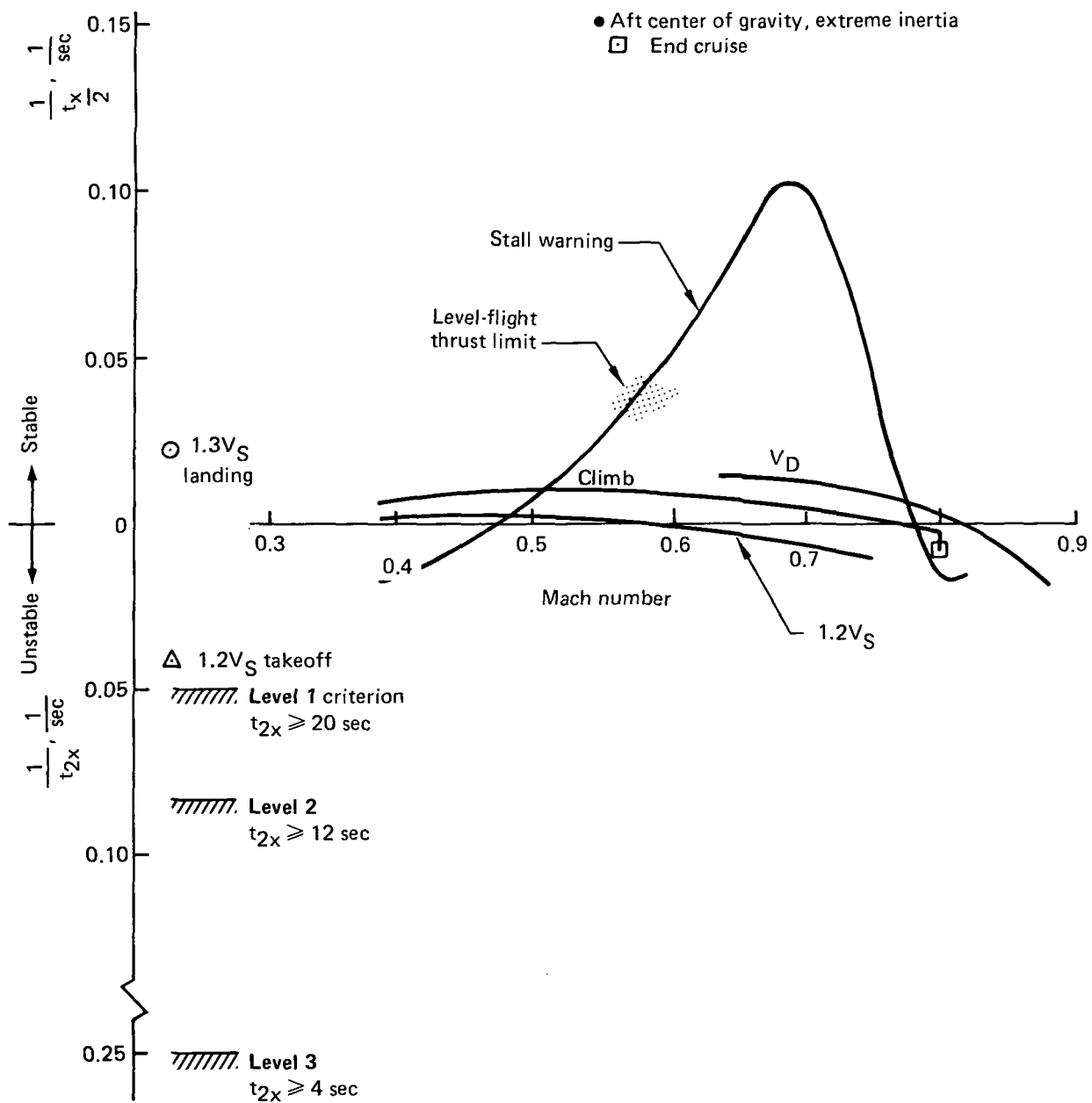
Figure 58. Spiral Mode (Unaugmented), Model 768-104

112
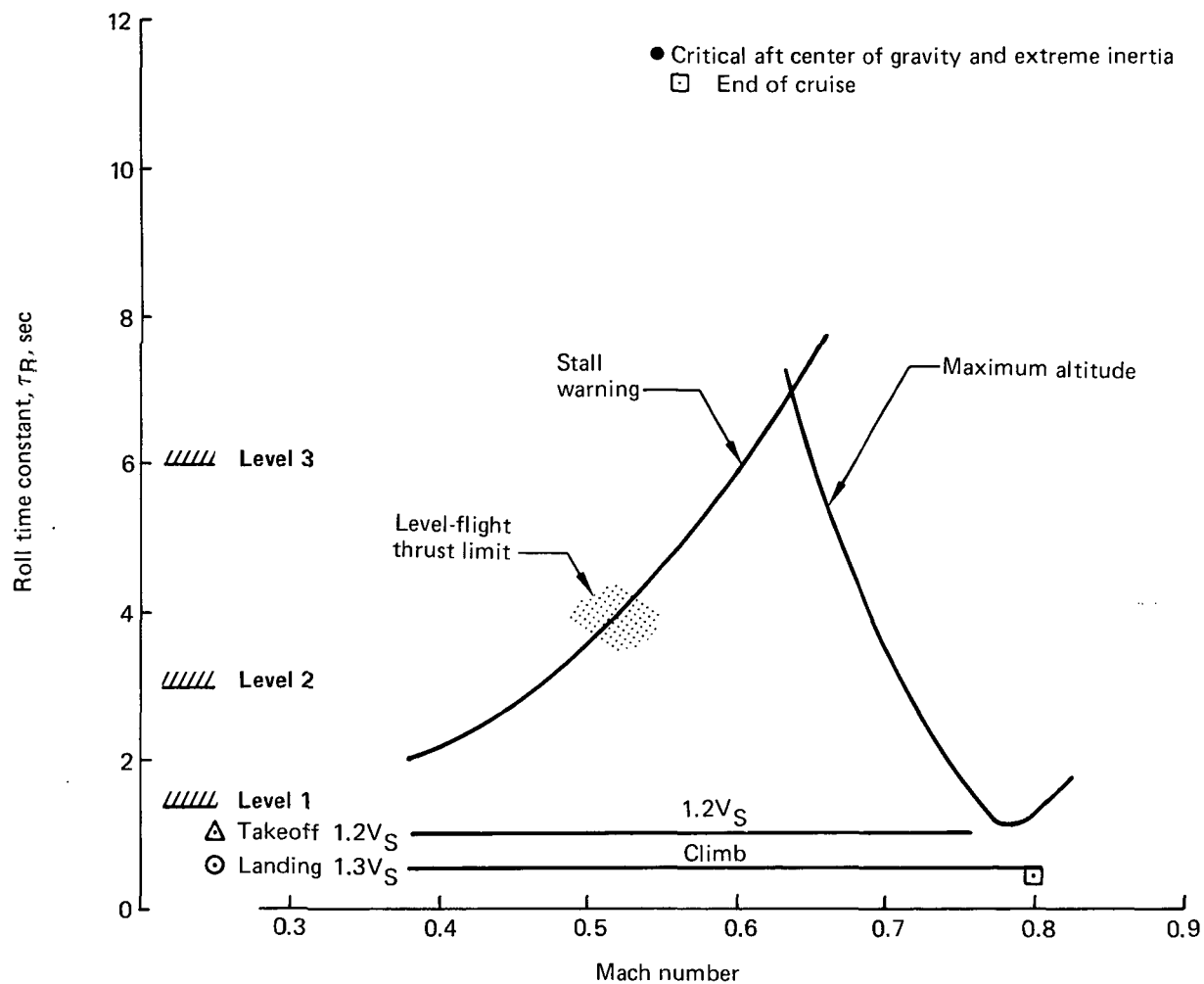
Figure 59. Roll Mode Time Constant (Unaugmented), Model 768-104

7.2 STRUCTURAL ANALYSES

7.2 STRUCTURAL ANALYSES

The structural analysis results for the IAAC Planform Study are presented in this section.

The speed-altitude envelope (fig. 60) and maximum taxi weight (MTW) for the planform study configurations are the same as for the Baseline and Initial ACT Configurations (refs 2 and 3). These configurations are defined in Figure 61 and are included as a foldout inside the back cover. The wing planforms are compared in Figure 62.

The data base, methods, and criteria used for the analysis were consistent with those used for the Baseline and Initial ACT Configurations except for modifications required to account for variations in wing planforms. The major portion of the analysis involved establishing wing-box structural requirements. Horizontal tail and aft body loads were also computed to provide a data base for weight assessment.
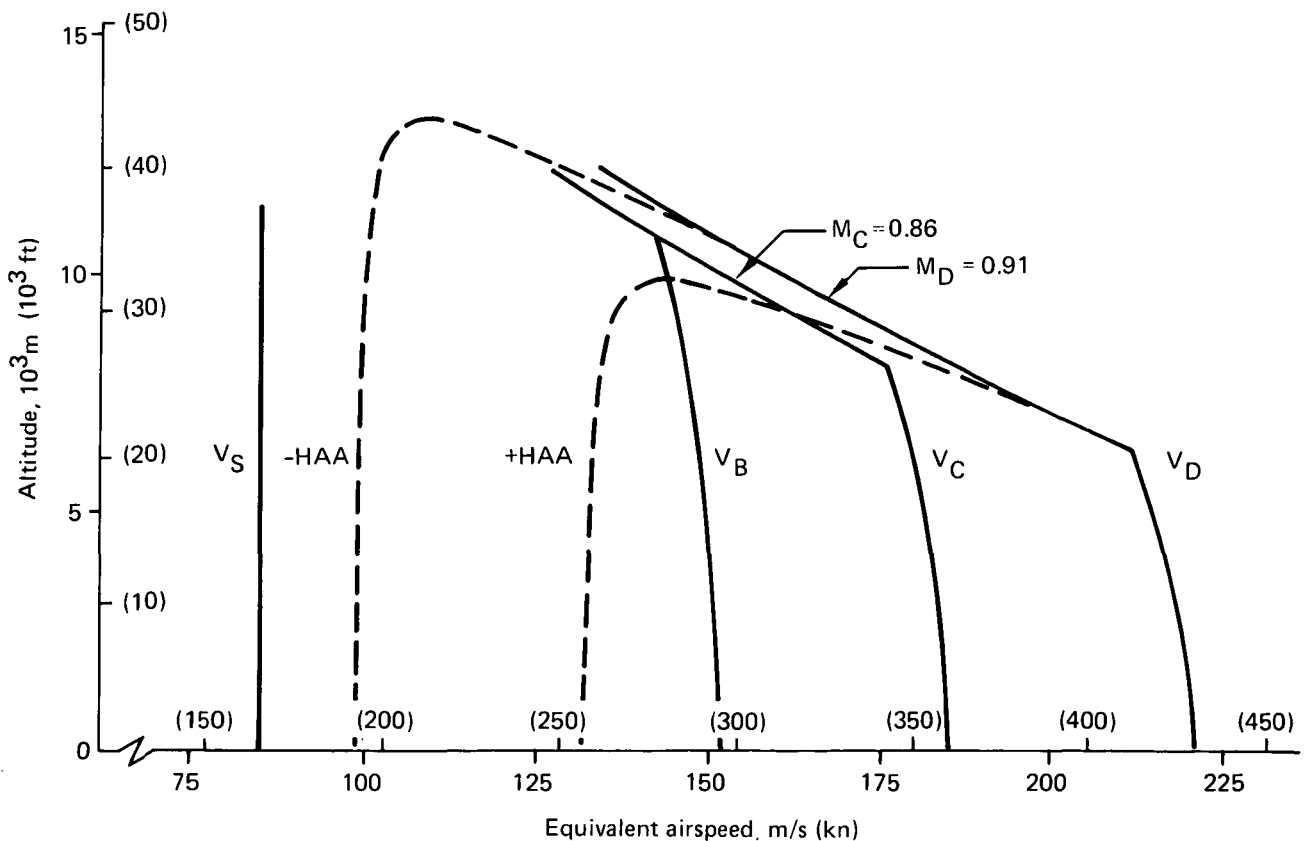
768-102, -103, -104, -105, -106

Figure 60. Speed-Altitude Envelope

115

Baseline · Initial ACT · Wing Planform Study · Final ACT

MLG 56.0% · 10.0% · 38.0% · cg · $\bar{c}_W$ = 6.031m (237.47 in)

MLG 68.0% · 21.0% · 46.0% · cg · $\bar{c}_W$ = 6.031m (237.47 in)

MLG 68.6% · 19.3% · 47.3% · cg · $\bar{c}_W$ = 5.380m (211.79 in)

MLG 67.9% · 18.1% · 47.1% · cg · $\bar{c}_W$ = 5.494m (216.28 in)

MLG 72.4% · 17.5% · 48.8% · cg · $\bar{c}_W$ = 4.827m (190.05 in)

MLG 72.4% · 17.8% · 48.8% · cg · $\bar{c}_W$ = 4.827m (190.05 in)

Model number	768-102	768-103	768-105	768-106	768-104	768-107
Sweep at $\bar{c}/4$, deg	31.5		31.5	26.4	31.5	
Aspect ratio, ref	8.1		9.0	9.1	9.9	
Aspect ratio, TRAP	8.71		10.30	10.15	12.03	
Taper ratio, ref	0.225		0.198	0.212	0.177	
Taper ratio, TRAP	0.267	Same	0.266	0.262	0.267	Same
t/c SOB, percent	15.1		15.1	13.1	15.1	
t/c tip, percent	10.3		10.3	8.3	10.3	
Span, m (ft)	47.24 (155)		49.90 (163.7)	50.03 (164.2)	52.22 (171.3)	
Area ref, m^2 (ft^2)	275.1 (2961)		275.5 (2966)	275.1 (2961)	275.8 (2969)	
Area trap, m^2 (ft^2)	256.3 (2759)		241.4 (2598)	246.7 (2656)	226.8 (2441)	

768-102, -103, -104, -105, -106, -107

Figure 61.   IAAC Wing Geometry

116
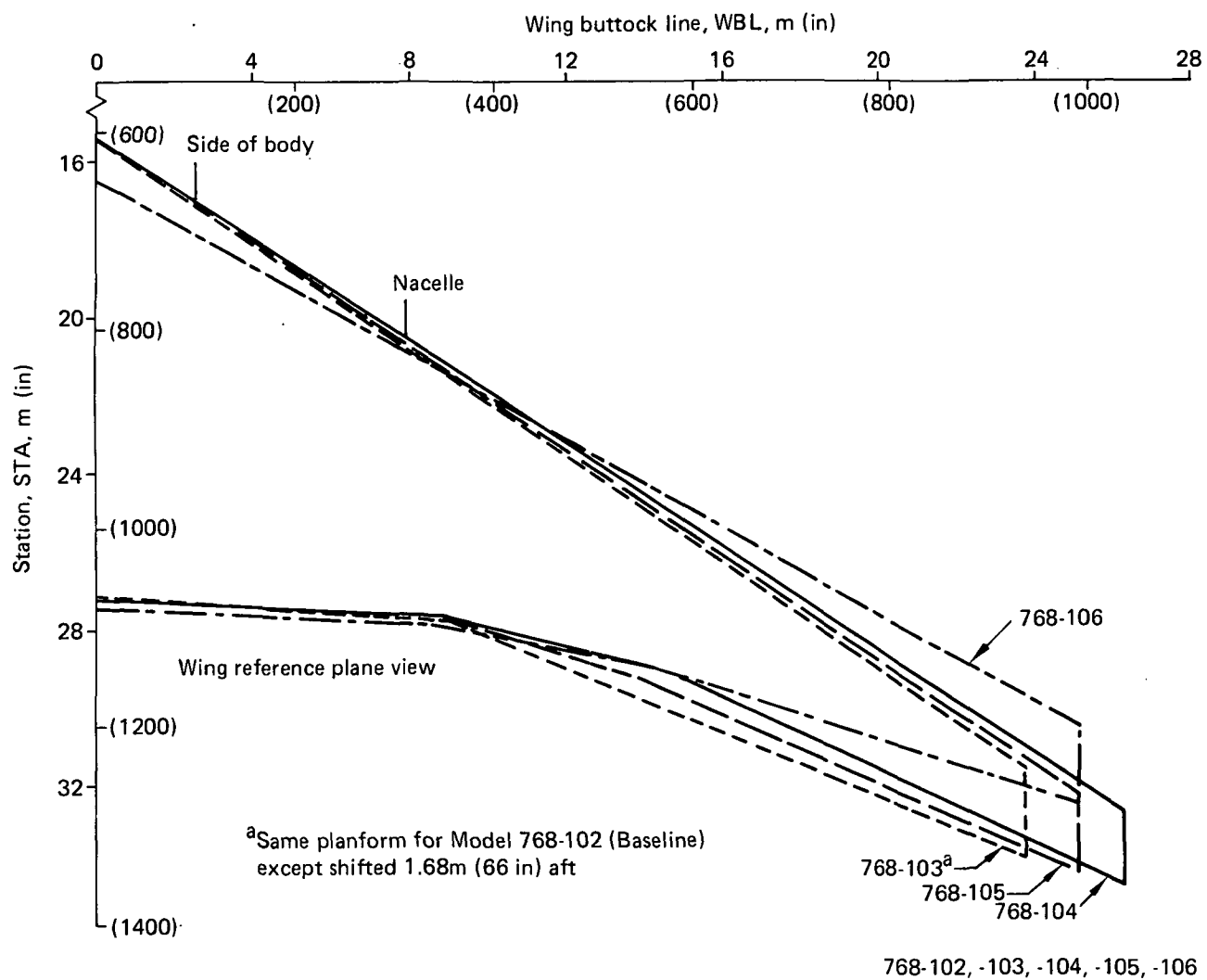
Figure 62. Wing Planforms for IAAC Configurations

A preliminary structural analysis was first performed for all the planform study wings to establish a design base (subsec 7.2.1) for performance analysis followed by a final structural analysis of the Model 768-104 Configuration. A summary of the preliminary wing-box structural sizing requirements for all planform study wings is presented in Subsection 7.2.1. The final structural sizing requirements for the 768-104 Configuration are presented in Subsection 7.2.2.

7.2.1 PRELIMINARY WING ANALYSIS

The preliminary structural analyses of the planform study wings are presented in this section. Analysis results were used to establish structural weight requirements for the planform study configurations (sec 5.4).

Figures 63 through 65 summarize the initial structural material requirements for strength. Figures 66 and 67 show the associated bending moment envelopes, which follow expected trends with sweep and aspect ratio.

Results shown in these figures are from a survey of static maneuver, FAR gust formula, and ground conditions. These conditions were selected from previous analyses of the Baseline and Initial ACT Configurations as potential design conditions in the operating speed-altitude envelope shown in Figure 60.

7.2.1.1 Maneuver and Gust Formula Loads Analysis

Maneuver and gust formula loads, wing sizing, wing stiffness, and jig twist were computed in an iterative cycle using the Boeing developed ORACLE Program. The loads solution method incorporated in the ORACLE Program was developed by Gray and Schenk (ref 6) for aeroelastic analysis of high aspect ratio wings. This method incorporates wing aerodynamics based on lifting line theory including empirical corrections derived from wind tunnel data and wing structural modeling based on beam theory.

The design airloads were obtained by dividing the wing into 12 streamwise aero-dynamic panels, conveniently grouped to provide a good representation of regions where control surfaces are located. The stress analysis of the wing box was performed for the midpanel stations (fig. 68) on sections perpendicular to the load reference axis.
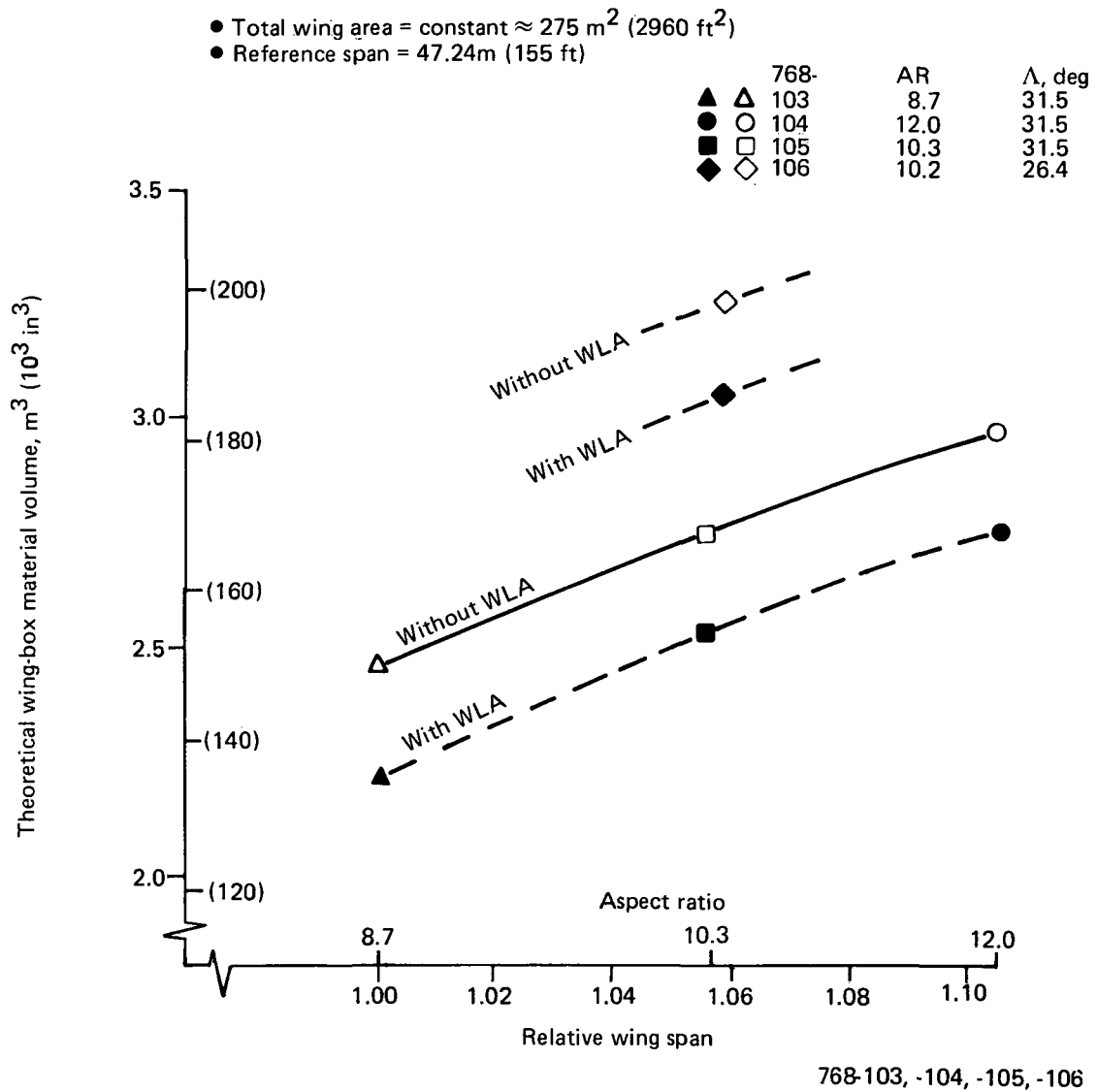
Figure 63. Theoretical Wing-Box Material Volume, Initial Strength Sizing

Surfaces Plus Spars
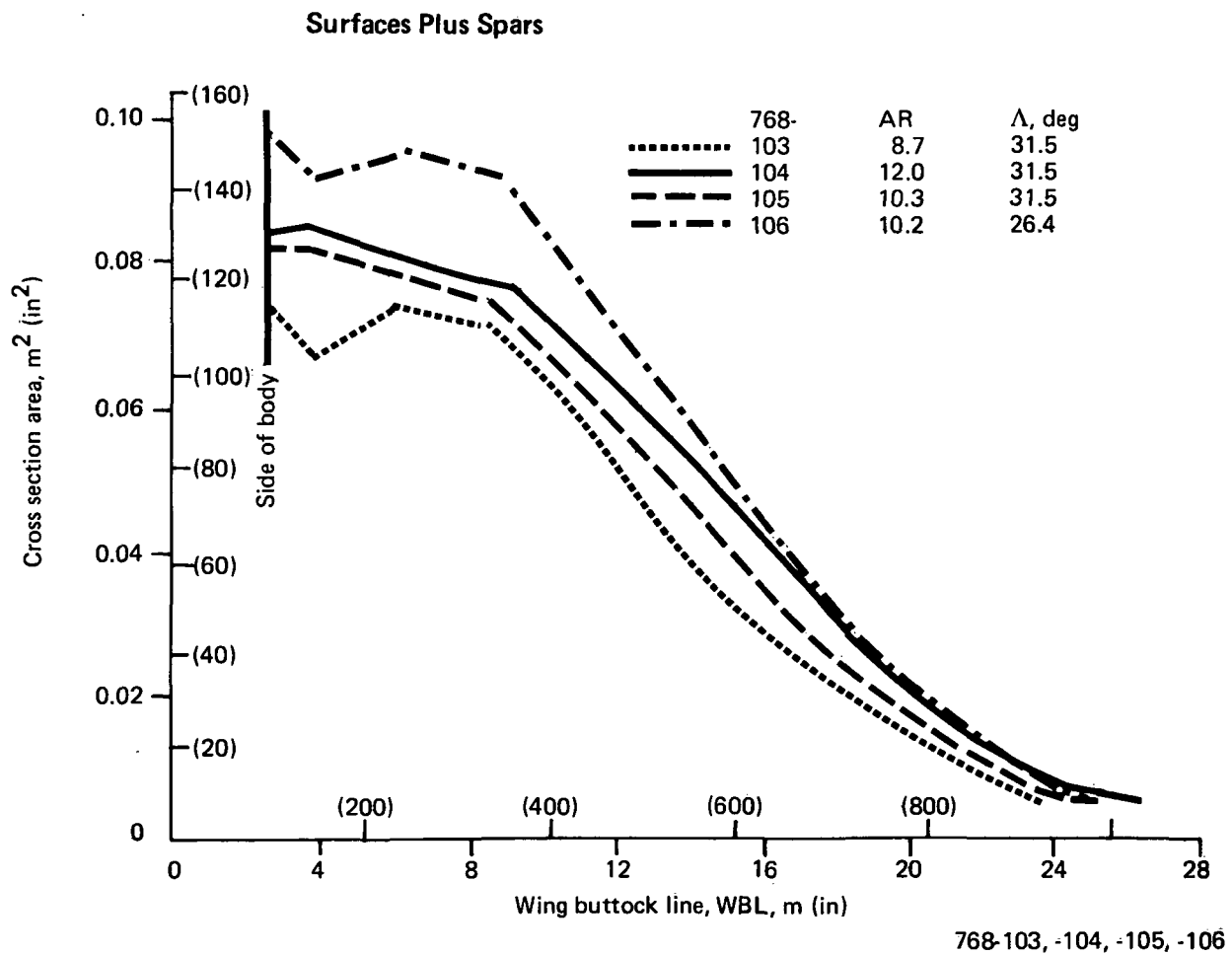
Figure 64. Theoretical Wing-Box Material Requirement, Initial Strength Sizing Without Wing-Load Alleviation

768-103, -104, -105, -106

120
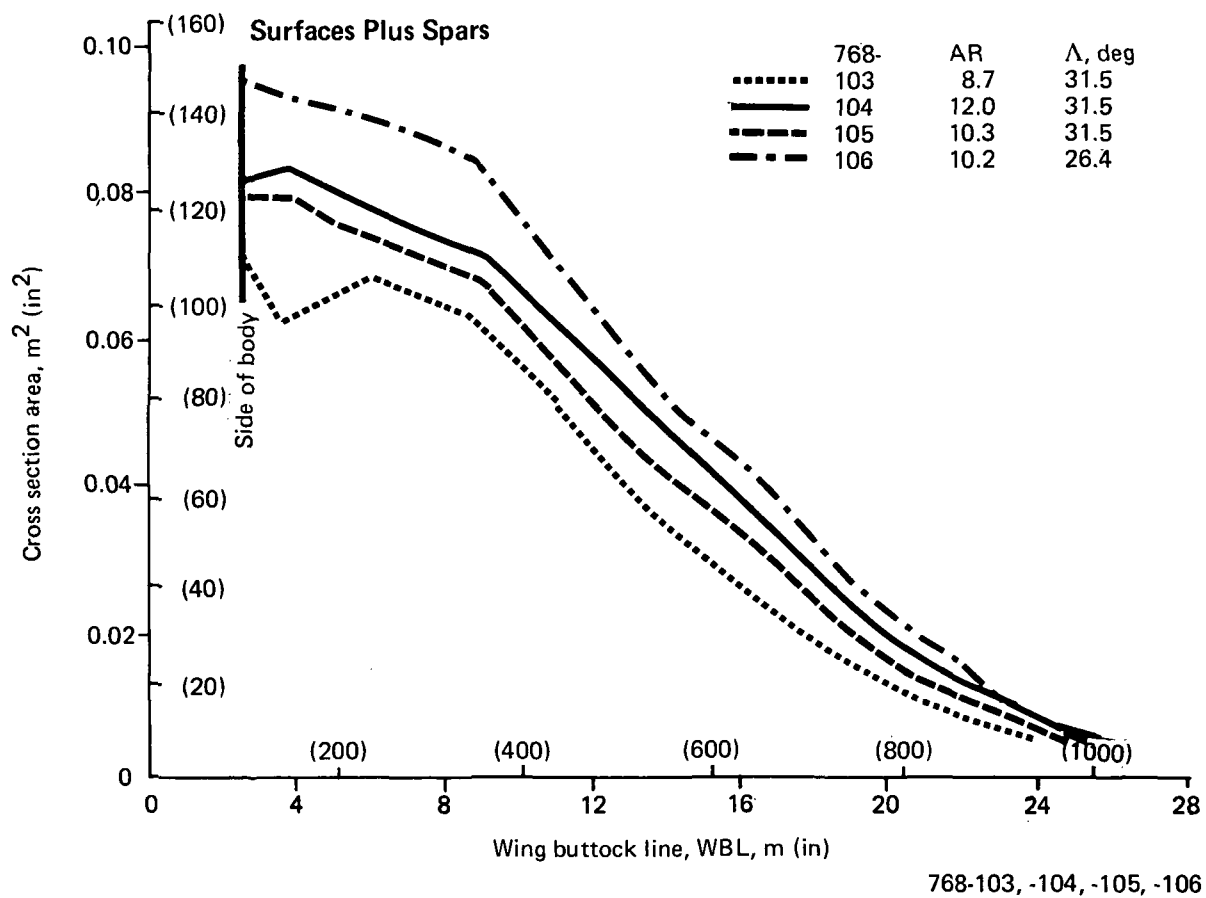
Figure 65. *Theoretical Wing-Box Material Requirement, Initial Strength Sizing With Wing-Load Alleviation*
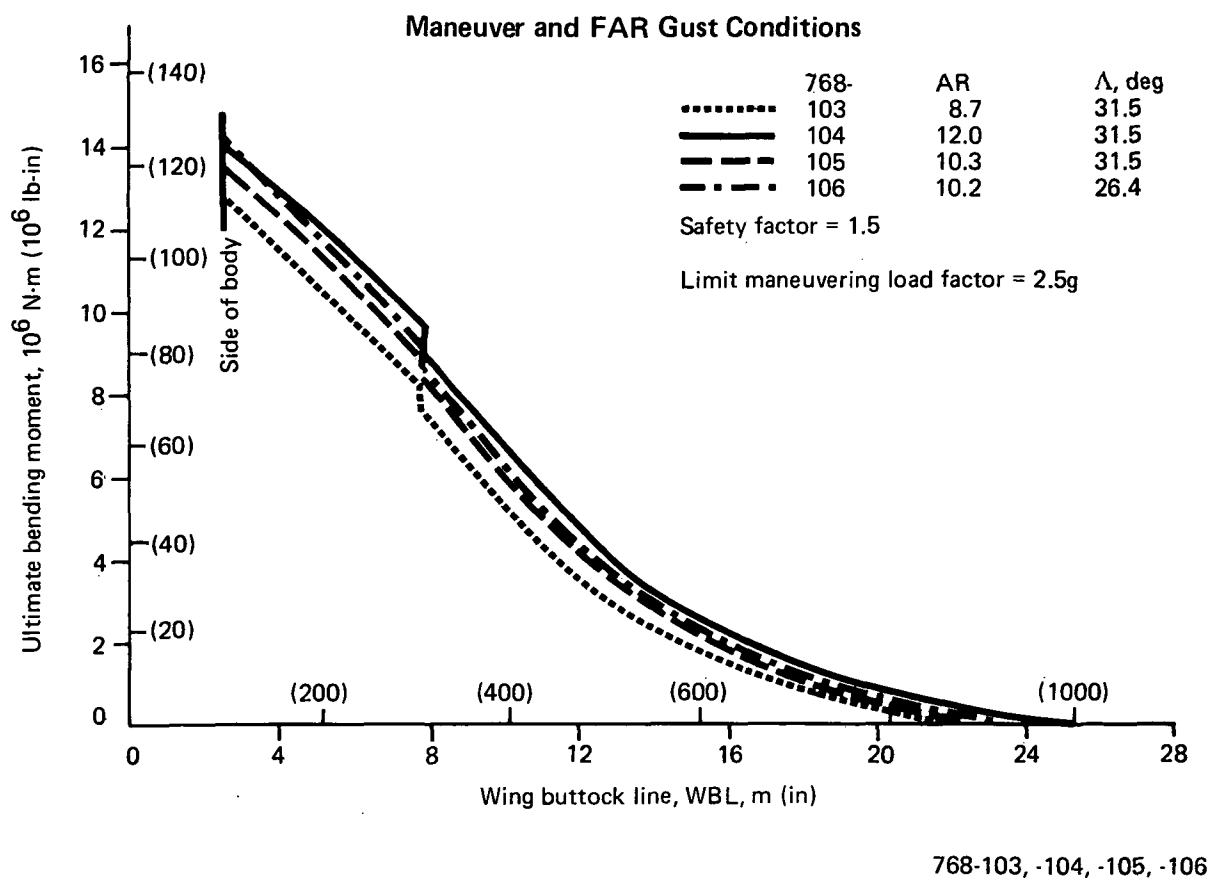
Figure 66. *Wing Design Bending Moment, Initial Strength Sizing Without Wing-Load Alleviation*

122

Maneuver and FAR Gust Conditions

768	AR	Λ, deg
103	8.7	31.5
104	12.0	31.5
105	10.3	31.5
106	10.2	26.4

Safety factor = 1.5

Limit maneuver load factor = 2.5g

768-103, -104, -105, -106
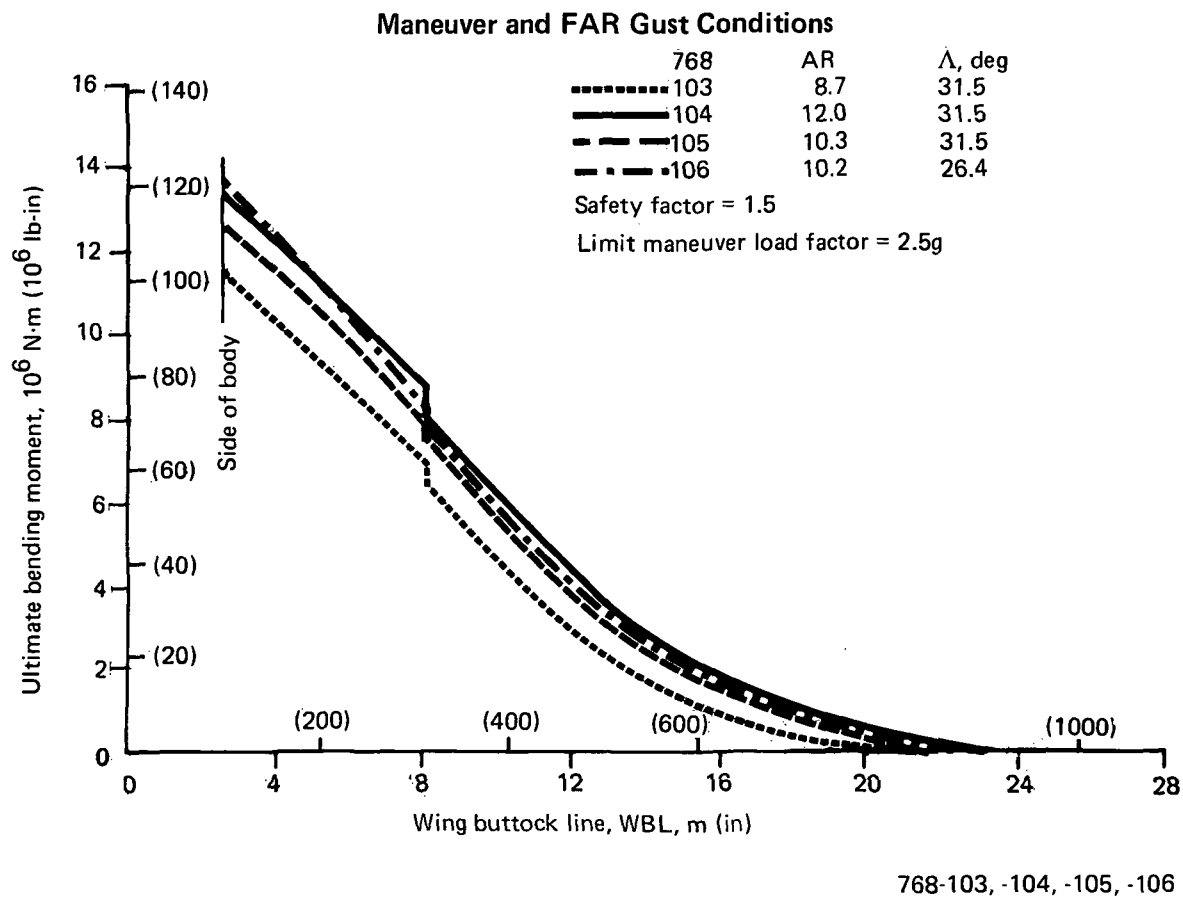
Figure 67. Wing Design Bending Moment, Initial Strength Sizing With Wing-Load Alleviation

123
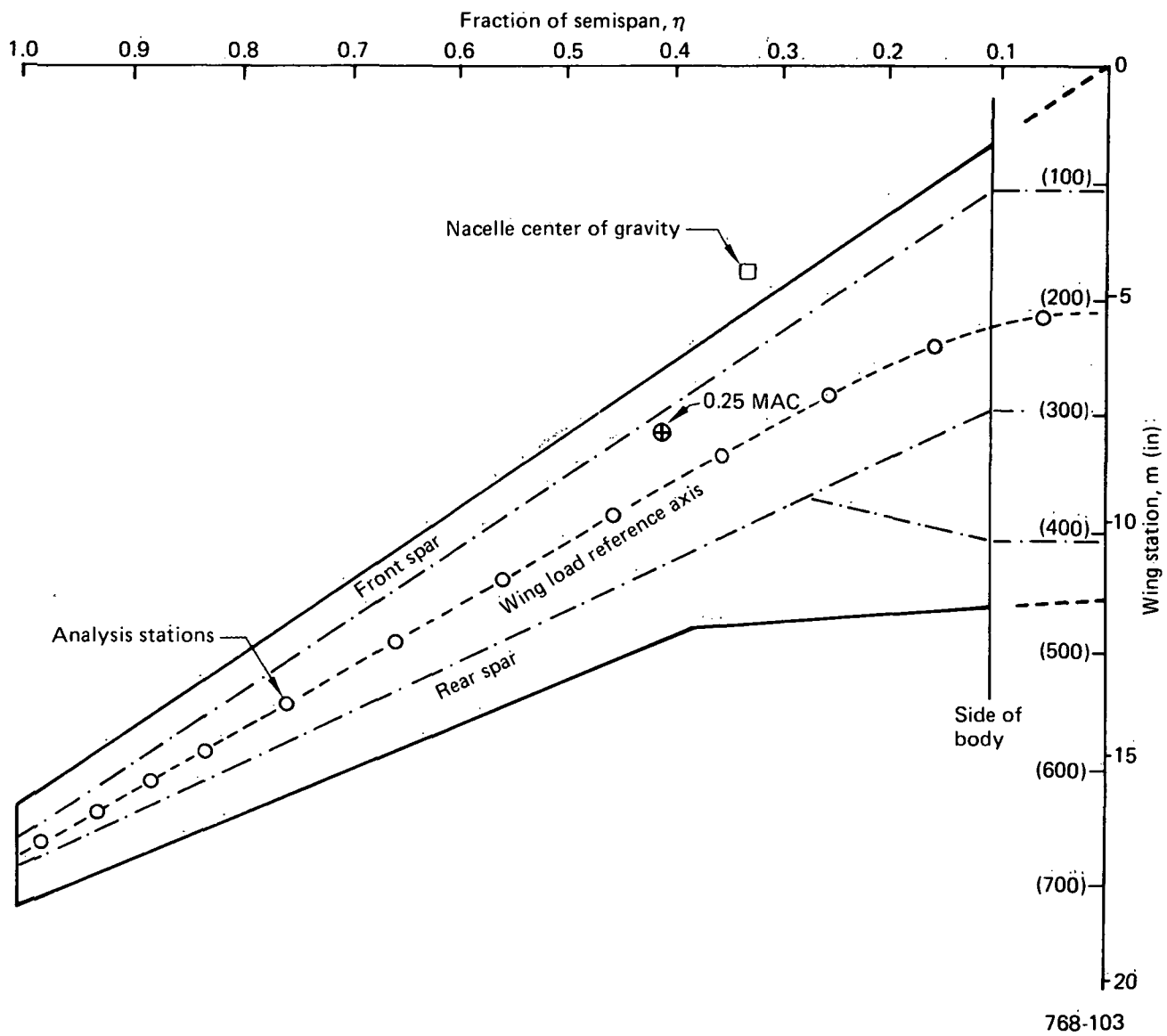
Figure 68. Wing Diagram for Structural Loads Analysis

768-103

124

Wing section normal force and pitching moment slopes for the planform study wings were ratioed from Baseline Configuration data using theoretical results from a lifting surface analysis program, which was developed by Boeing based on the Küchemann method (ref 7). Representative section lift-curve slope and section aerodynamic center location results are compared in Figure 69, and additional data are included in Appendix A for reference.
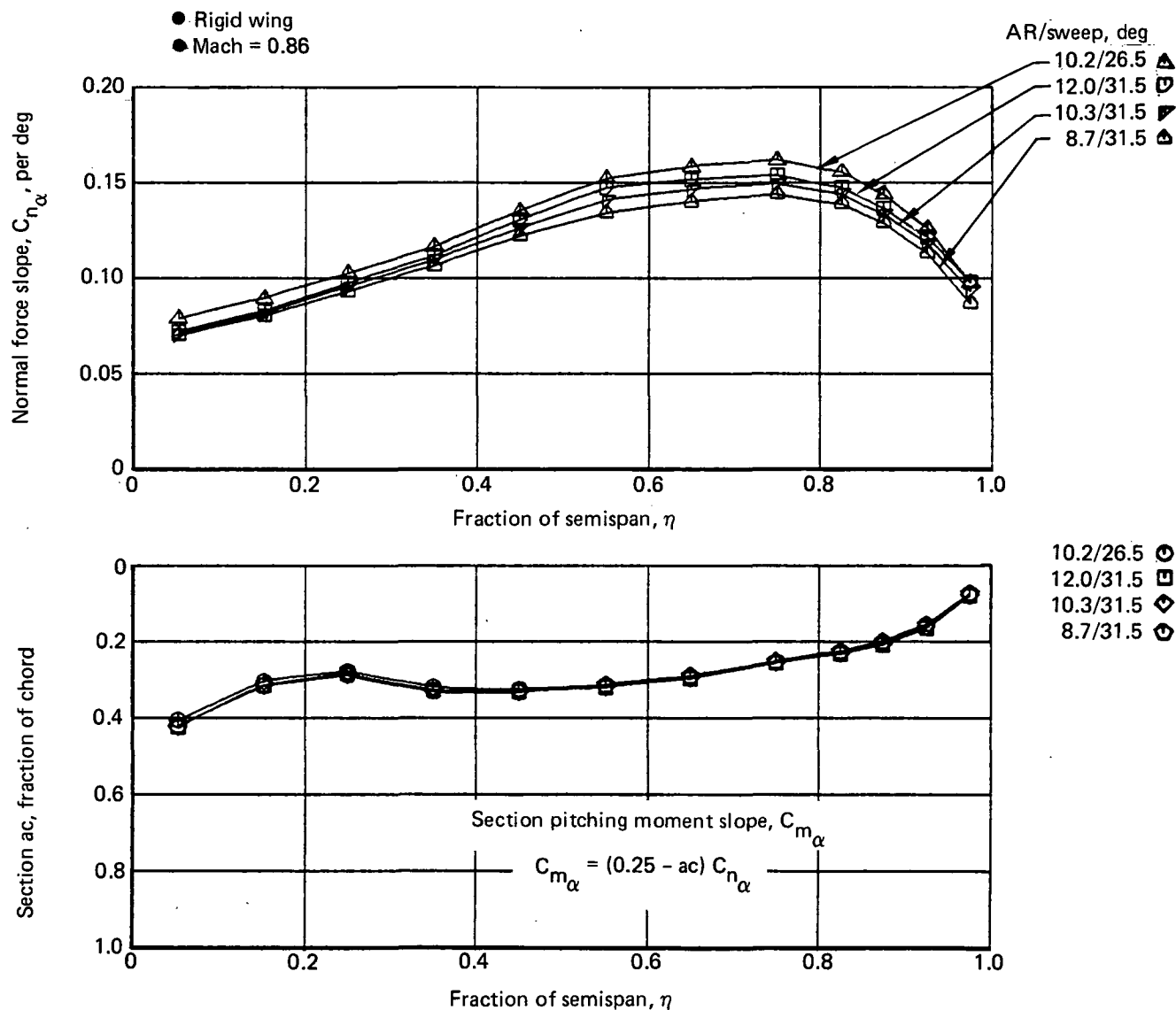
Figure 69. Sample Wing Section Aerodynamic Parameters for Planform Study Wings

Section normal force and pitching moment values for zero wing angle of attack (intercept values) were held equal to Baseline Configuration wing values (app A) for all wings with twist removed.

The above approach maintained the credibility of the Baseline aerodynamic data, which were derived from wind tunnel pressure test results. This method was considered satisfactory because only modest changes (fig. 62) were made to the Baseline wing, and the theoretical results showed reasonable agreement with the Baseline data, as illustrated, for example, in Figure 70.
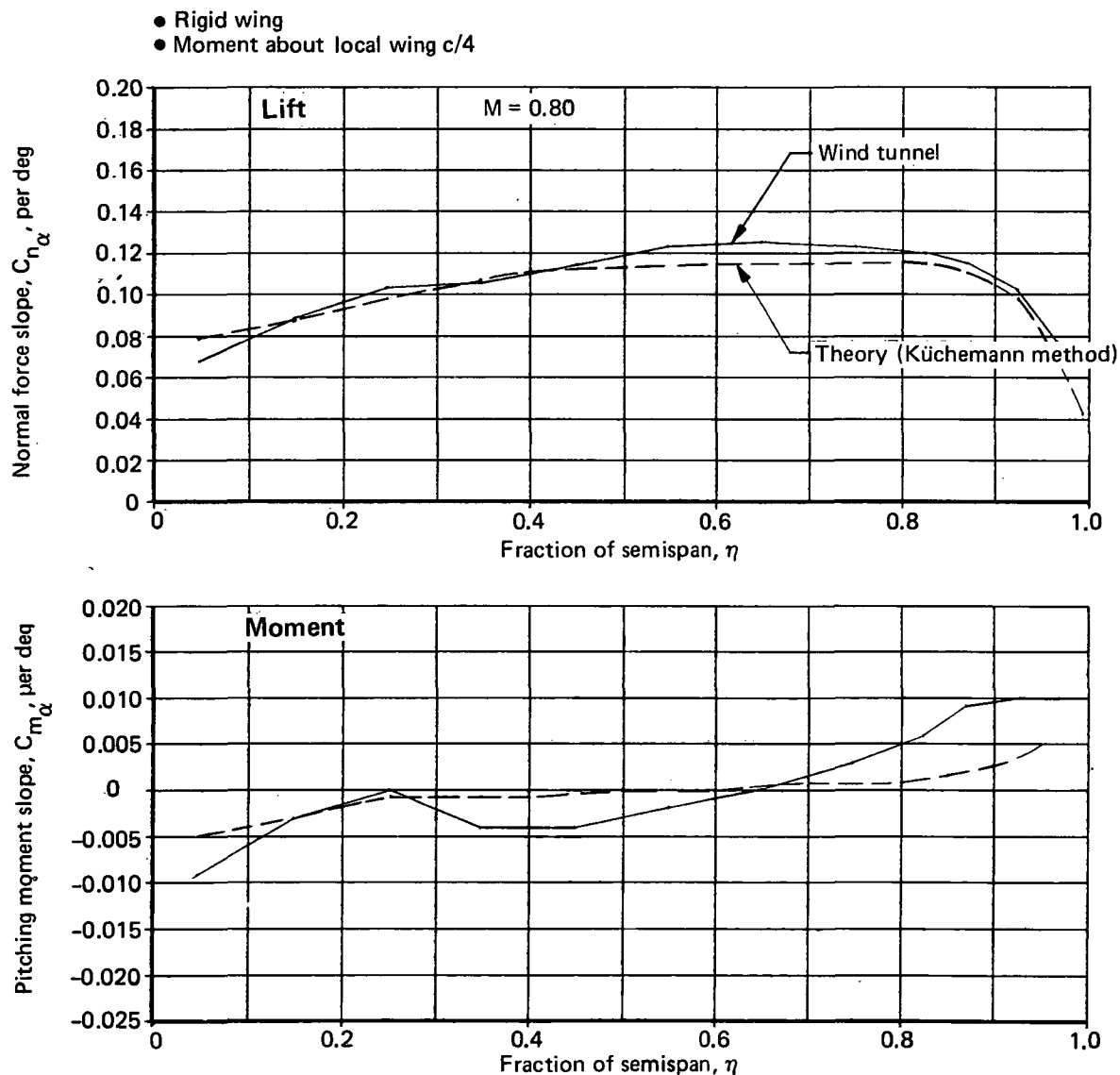
Figure 70. Wing Section Aerodynamic Data—Wind Tunnel Versus Theory,
Model 768-102

Baseline body and nacelle aerodynamic data were adjusted for differences in reference wing area and chord and quarter MAC location. Wing section aerodynamic data for the outboard ailerons were derived from wind tunnel pressure test results for the Baseline Configuration. These data are included in Appendix A for reference.

The fraction of surface material contained in the wing skins is indicated in Figure 71. This distribution is based on past experience with configurations of similar construction and provides a satisfactory balance between fail-safe design practice and high-strength allowables.

Cross Section of Wing Surface
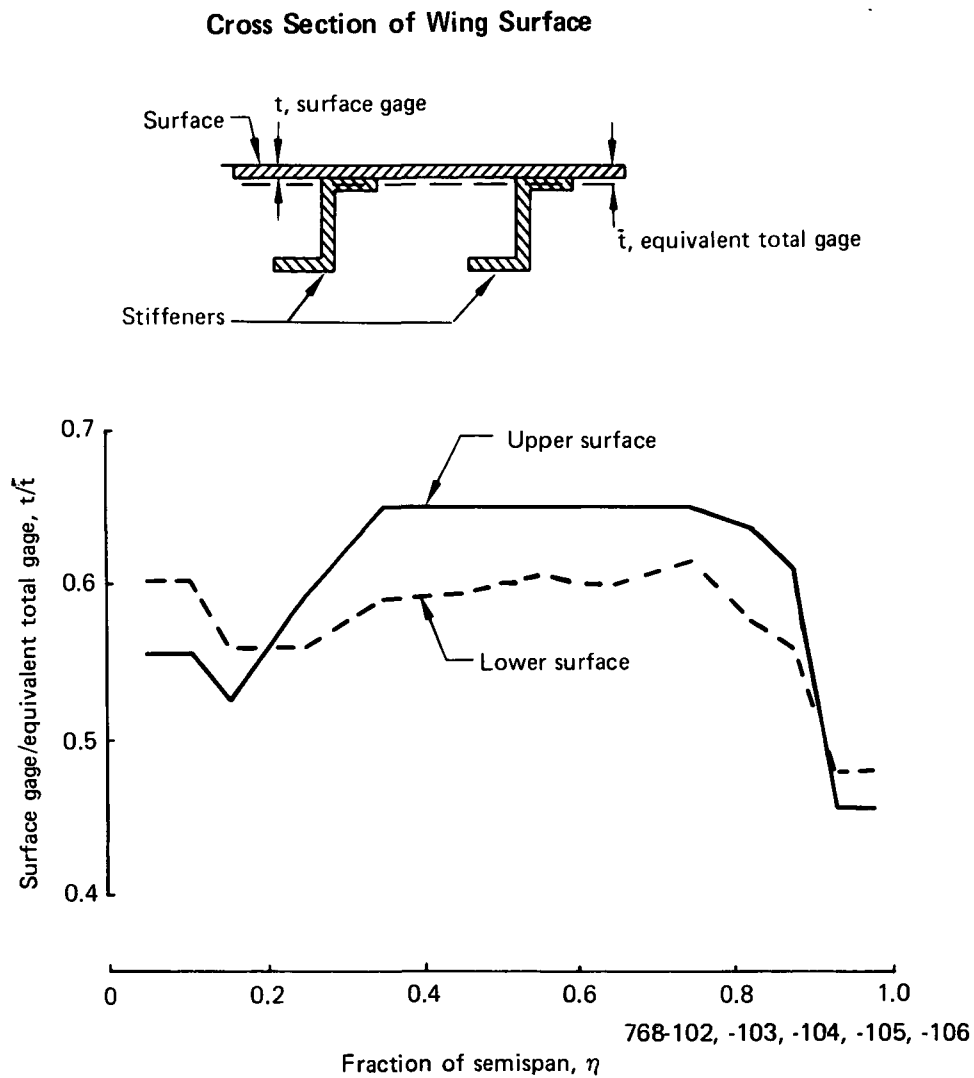
Figure 71. Wing-Box Surface $t/\bar{t}$ Ratios

The material properties used for structural sizing are presented in Figures 72 through 74. The upper surface skin and stringer properties are for 7150-T65 material; the lower surface skin properties are for 2024-T3 material with stringers of 2224-T3 material. The spar properties are for 7075-T6 material.

FAR gust formula conditions were critical for design for all configurations, including the Baseline and Initial ACT. These conditions included an allowance for power spectral density (PSD) gust and structural dynamic effects based on a load dynamic magnification factor (DMF) envelope. To account for anticipated increased dynamic effects due to added span or reduced stiffness, the DMF envelope for the Baseline wing was assumed to increase with wing-lift curve slope for the planform study configurations, as shown in Figure 75. With this assumption, the resulting DMF levels were considered reasonable for initial strength sizing based on past design practice.

7.2.1.2 Wing-Load Alleviation Modeling for Preliminary Wing Analysis

The wing sizing was performed both with and without the beneficial effects of active controls for wing-load alleviation. The wing-load alleviation was obtained by deflecting the outboard ailerons as a function of cg load factor and flight speed (fig. 76). The gain of the control surface deflection was selected to provide maximum deflection of the ailerons at or a little above the design steady-state load factors and flight speeds for the critical maneuver and FAR gust formula conditions. At higher speeds, the control surface deflection was limited to avoid excessive wing torsional loading and design hinge-moment requirements.

7.2.1.3 Model 768-104 Configuration Selection

Results from the initial strength-sizing analysis were used for weight input to determine performance characteristics of the planform study wings and to predict initial stiffness values for dynamic and fatigue analyses. The Model 768-104 was selected for detailed structural analysis to establish structural requirements for flutter, fatigue, and dynamic gust and to estimate horizontal tail and body loads.

The wing planform for the Model 768-104 is compared with the Baseline (and Initial ACT) wing in Figure 77. In this figure the planforms are aligned at the 35% MAC

128
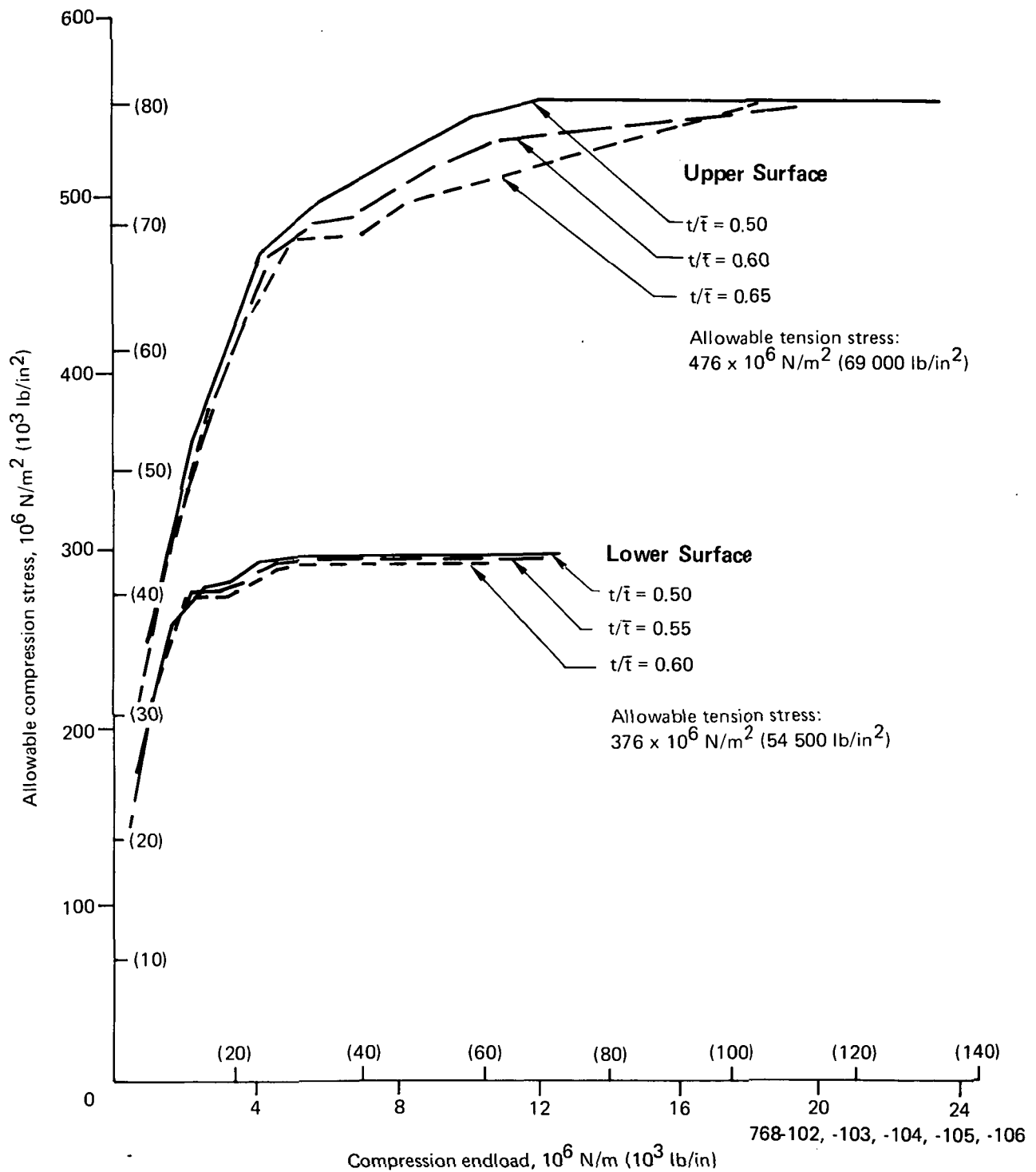
Figure 72. Allowable Compression and Tension Stress for Wing Surfaces
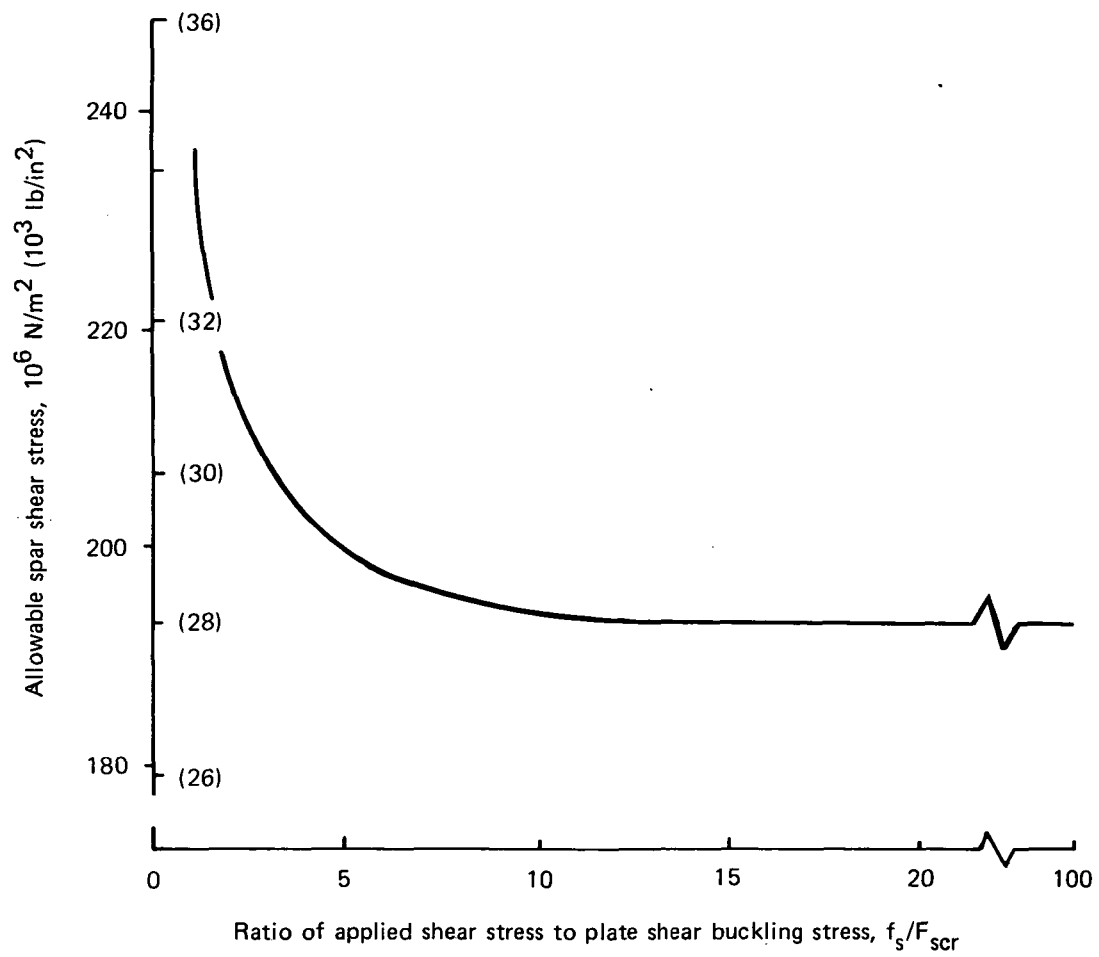
Figure 73. Allowable Shear Stress for Spars

768-102, -103, -104, -105, -106

130

300

(40)

Allowable shear stress, 10^6 N/m^2 (10^3 lb/in^2)

Upper surface

250

(35)

Lower surface

(30)

200

(25)

150

(20)

(0.1)   (0.2)   (0.3)   (0.9)   (1.0)

0   2   4   6   22   24

Surface skin gage, mm (in)   768-102, -103, -104, -105, -106
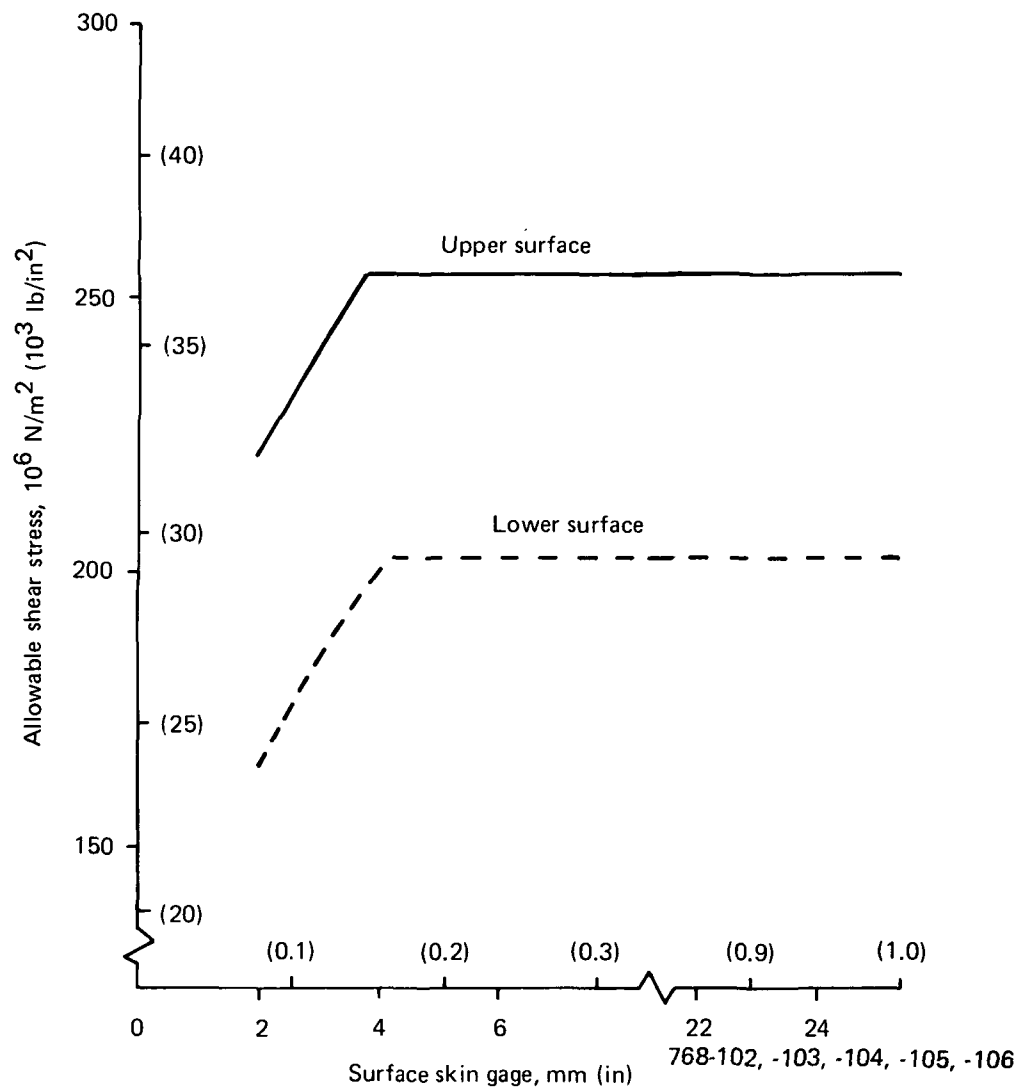
Figure 74. Allowable Shear Stress for Wing Surfaces

131

Upper chart labels:
- Mach = 0.86
- Tail off
- Rigid wing
- Airplane normal force slope, C_{N_α}, per deg
- 0.14
- $\Lambda = 26.4$ deg
- $\Lambda = 31.5$ deg
- 0.12
- $C_{N_{\alpha_{base}}}$
- 0.10
- Aspect ratio
- 8.7 10.3 12.0
- 1.00 1.04 1.08 1.12
- Relative wing span
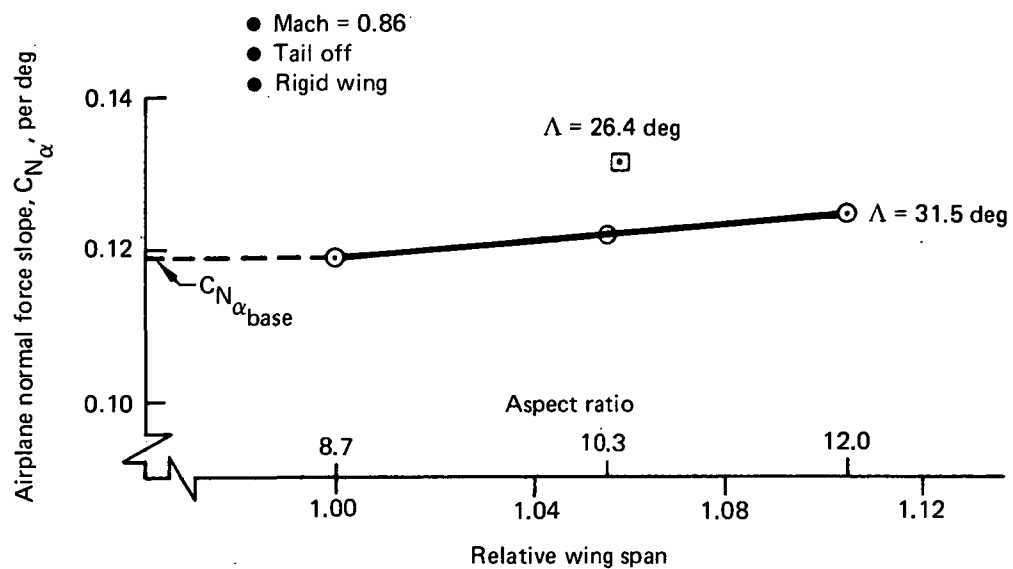
$$DMF = DMF_{base} \times Factor \qquad Factor = \frac{C_{N_\alpha}}{C_{N_{\alpha_{base}}}}$$

Lower chart:
- Dynamic magnification factor, DMF_{base}
- 3
- 2
- 1
- 0

Wing	Factor
768-103	1.00
768-104	1.05
768-105	1.02
768-106	1.10
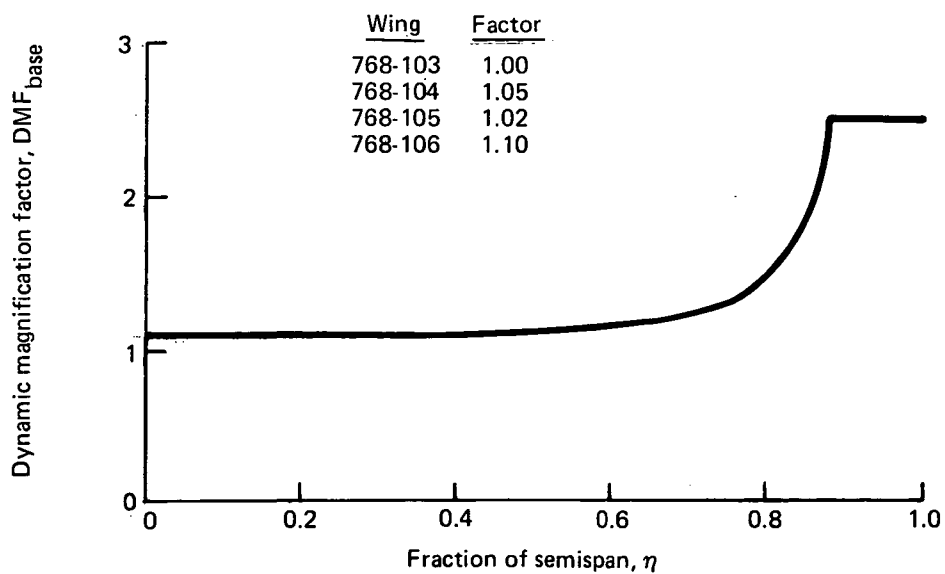
- 0 0.2 0.4 0.6 0.8 1.0
- Fraction of semispan, η
- 768-103, -104, -105, -106

Figure 75. Dynamic Magnification Factors for Initial Strength Sizing
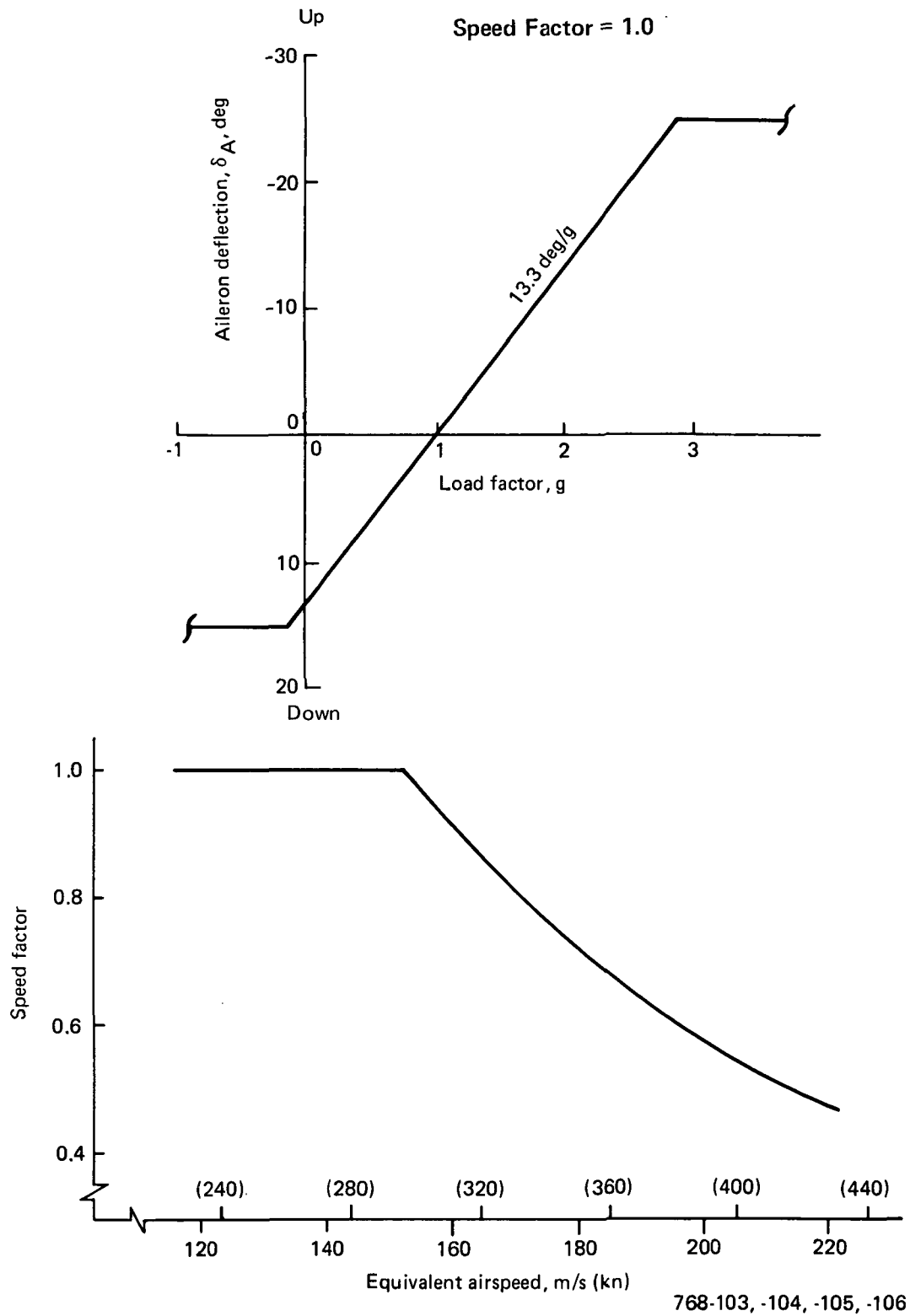
Figure 76. Outboard Aileron Wing-Load Alleviation Gain Schedule

133
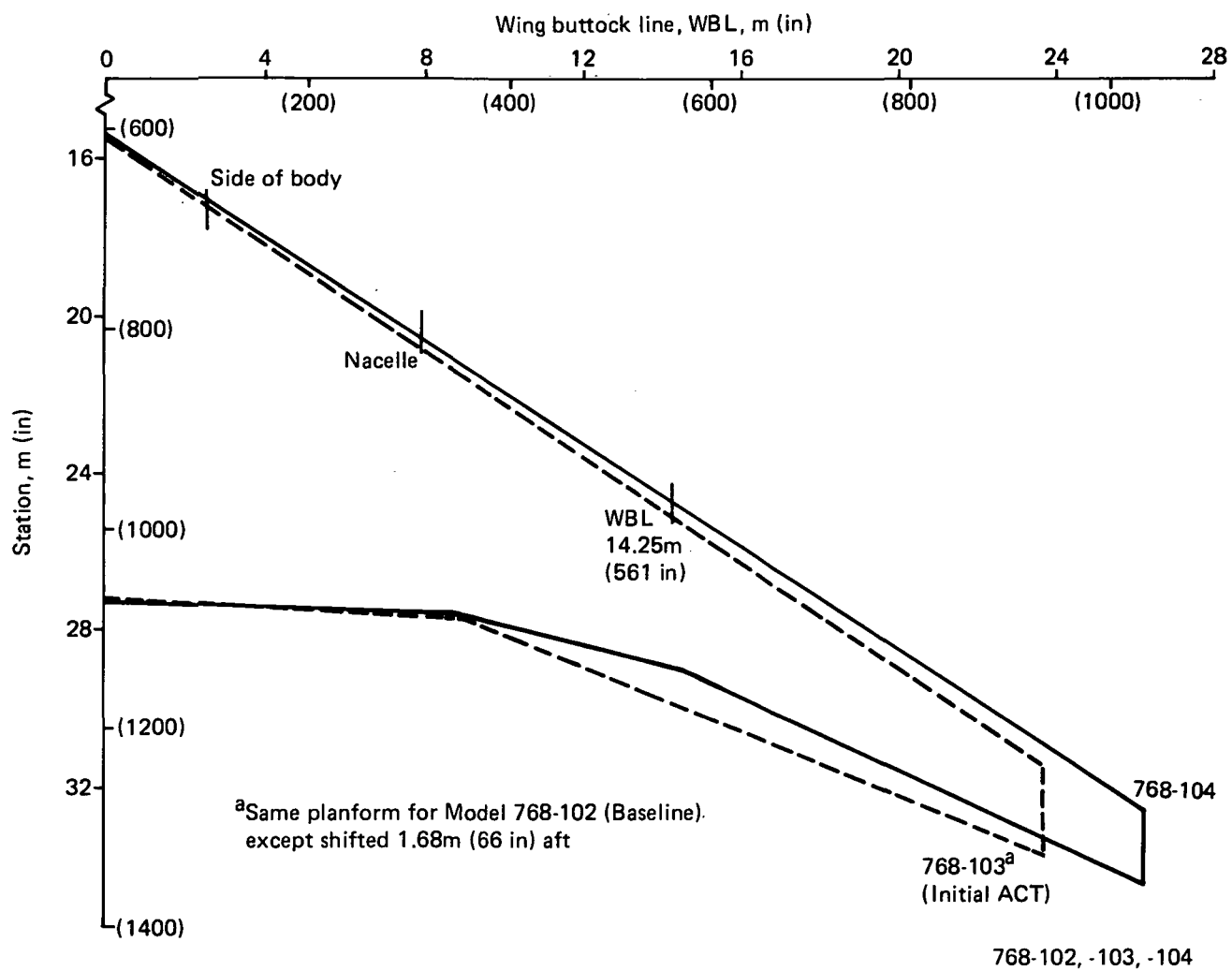
Figure 77. Wing Planform Comparison, Model 768-104 Versus Conventional Baseline
and Initial ACT

134

station for comparison. The increased aspect ratio for this configuration was achieved by increasing the span and taper of the Baseline wing while holding the wing area, root chord, and thickness ratio distribution (t/c) essentially constant. The resulting wing-box geometry and maximum box depths (figs. 78 and 79) are similar in the inboard wing, where design loads are highest, but are reduced in the outboard wing.
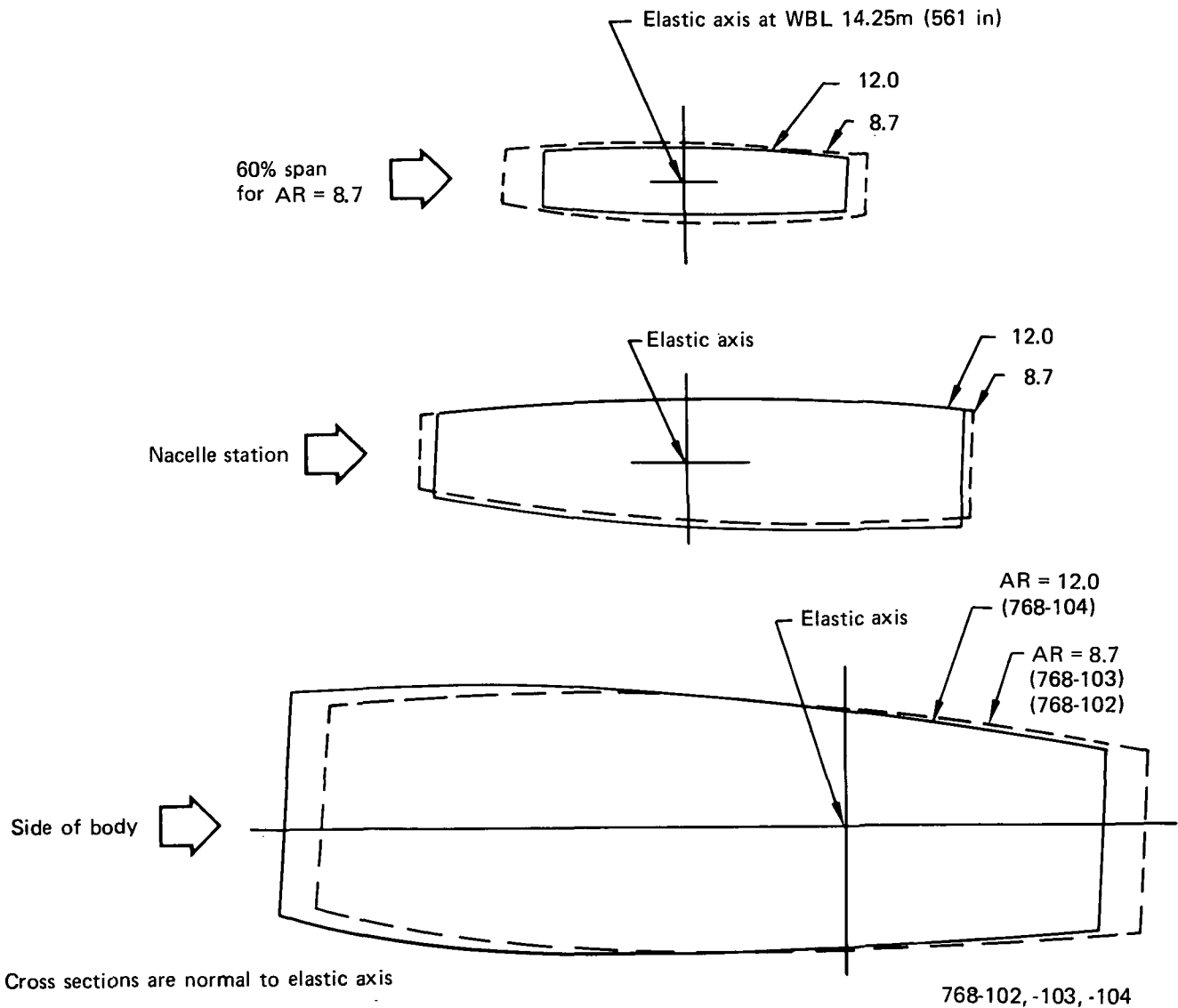
Figure 78. Wing-Box Cross-Section Comparison, Model 768-104 Versus Conventional Baseline and Initial ACT

135
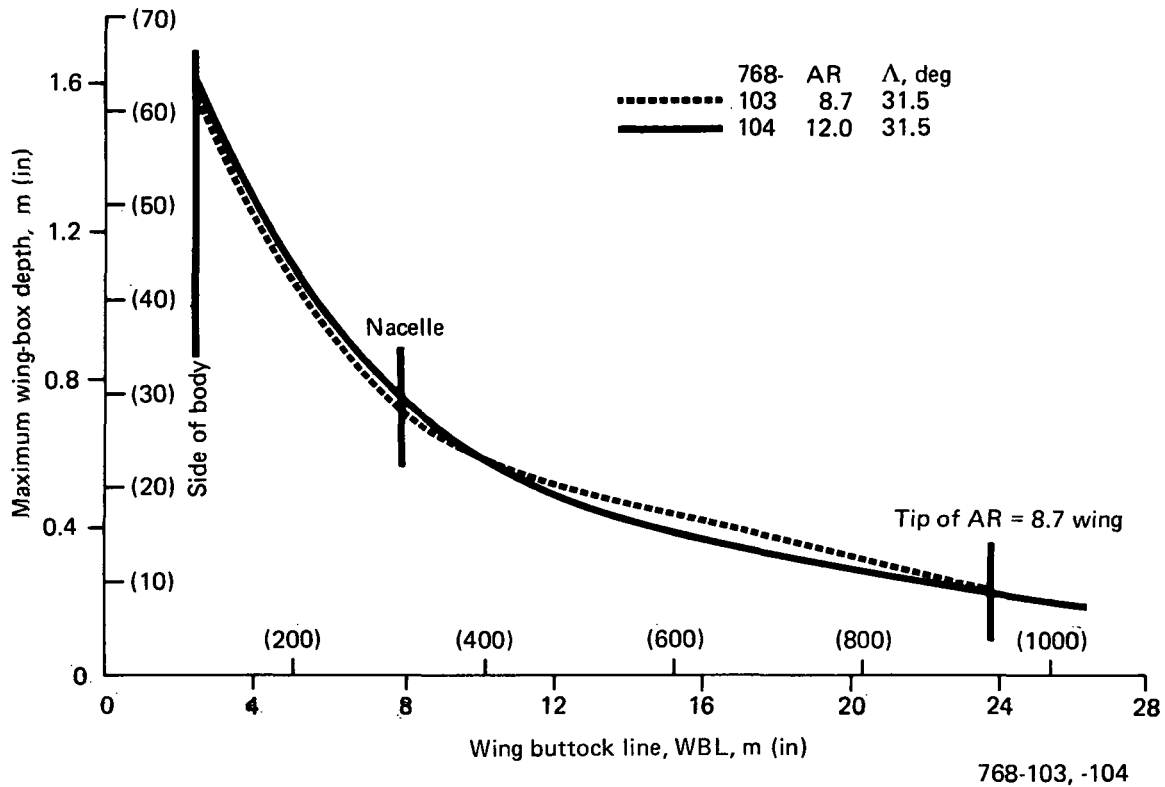
Figure 79.   Maximum Wing-Box Depths

This configuration is structurally more efficient than a configuration with the same aspect ratio and wing area but with reduced root chord and taper. Outboard wing stiffness is lower (figs. 80 and 81) due to the reduction in wing-box size, which results in increased wing-tip washout. Thus, the spanwise lift distribution for design airloads is shifted further inboard with respect to the wing tip (fig. 82). Less nose-down jig twist is required to maintain the same span loading at cruise (figs. 83 and 84) due to the shorter outboard·wing chords and associated increased wing-tip washout.

7.2.1.4 Aileron Effectiveness for Wing-Load Alleviation/Structural Material Reduction

Aileron effectiveness for wing-load alleviation is reduced for the Model 768-104 relative to the Initial Act Configuration (fig. 85) due to the lower outboard wing stiffness. The reduction in total wing structural material, however, is about constant (figs. 63 and 85). Less material is removed inboard, but more material is removed outboard (fig. 85) where the effect of load reduction is greater due to the reduction in wing-box depth.

136
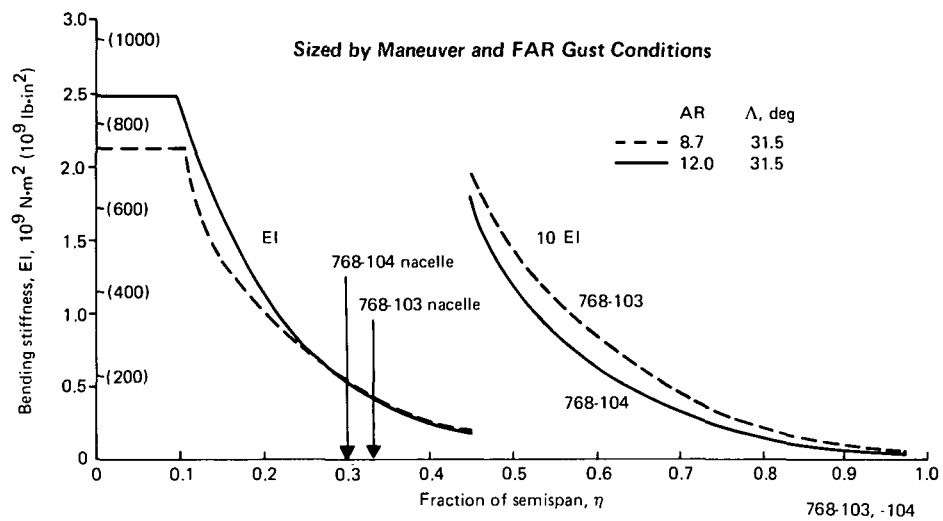
Figure 80. Wing Bending Stiffenss Comparison, Model 768-104 Versus Initial ACT

Figure 81. Wing Torsional Stiffness Comparison, Model 768-104 Versus Initial ACT

137

Flexible Wings Without WLA

- M = 0.85
- h = 9140m (30 000 ft)
- GW = 120 610 kg (265 900 lb)
- n = 2.5g

768-103 (AR = 8.7)

768-104 (AR = 12.0)

Nondimensional loading, $\ell/(L/b)$

Fraction of semispan, η

Flexible Wings With WLA

768-103

768-104

Nondimensional loading, $\ell/(L/b)$

Fraction of semispan, η
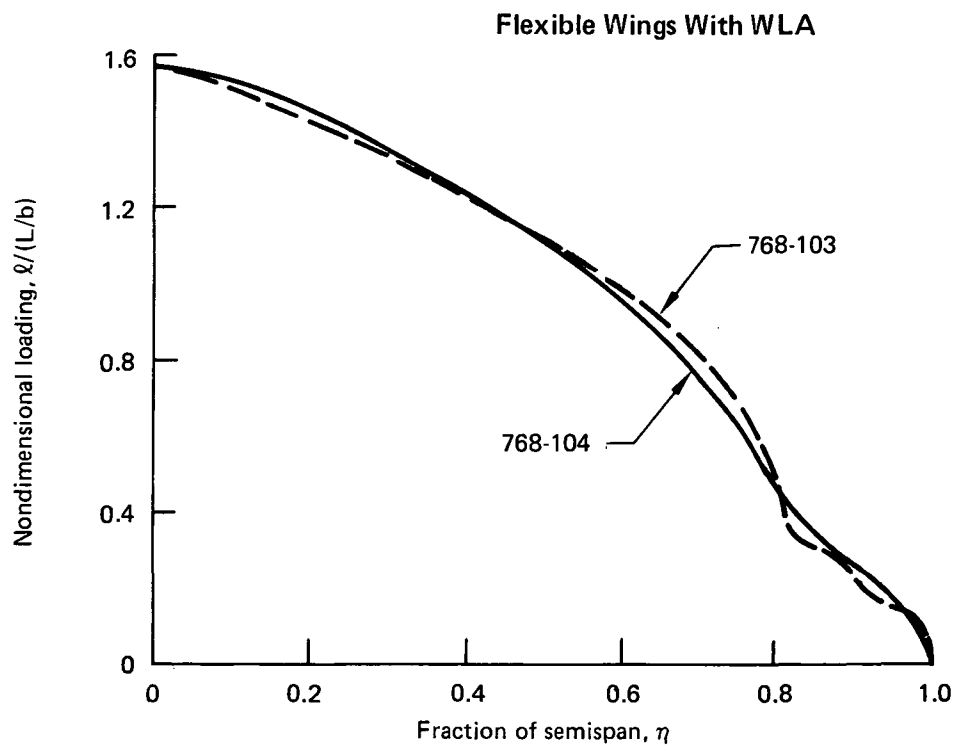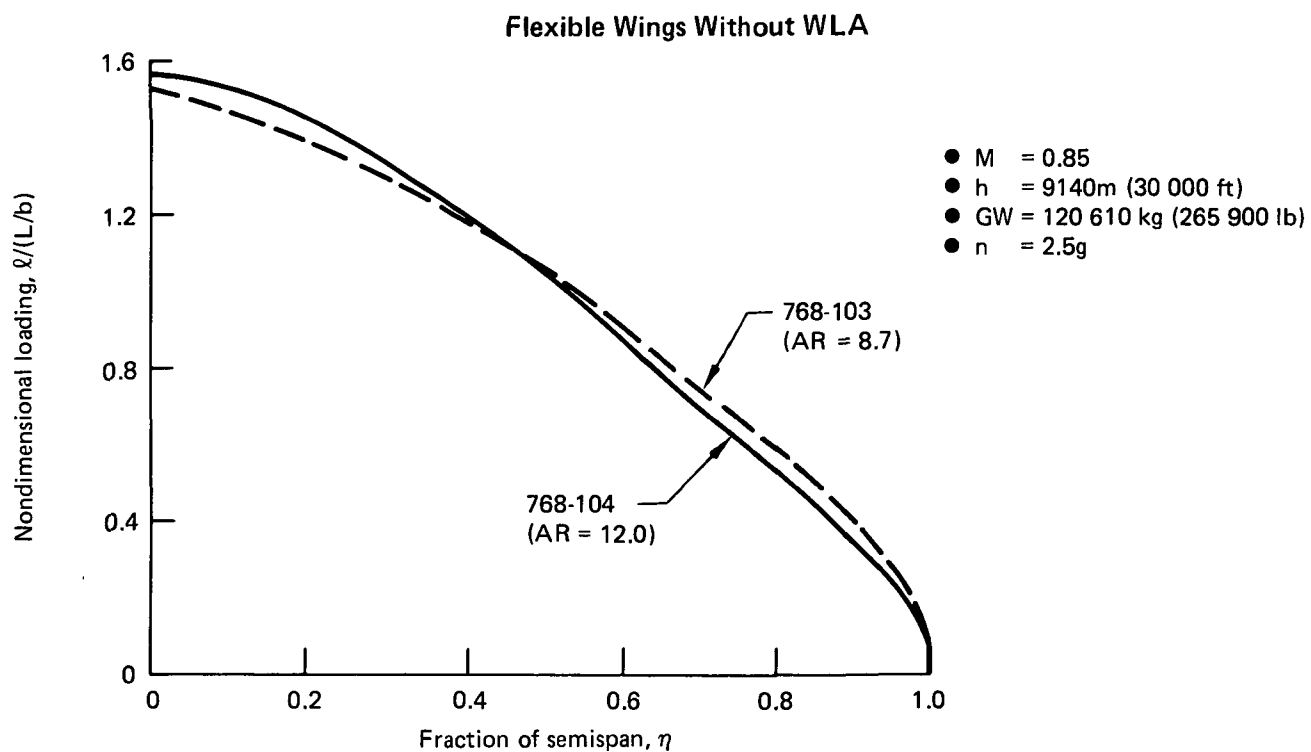
768-103, -104

Figure 82. Spanwise Lift Distribution for 2.5g Maneuver, Model 768-104 Versus Initial ACT

138
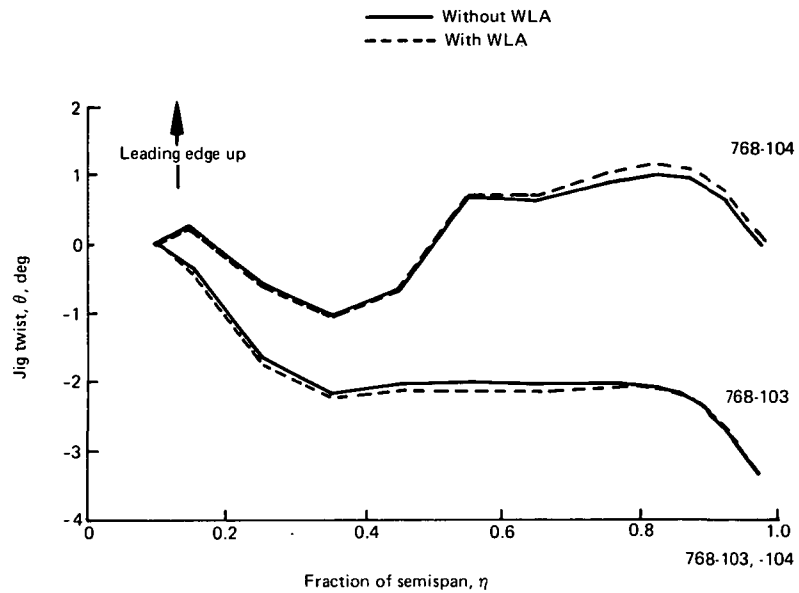
Figure 83. *Wing Jig Twist*
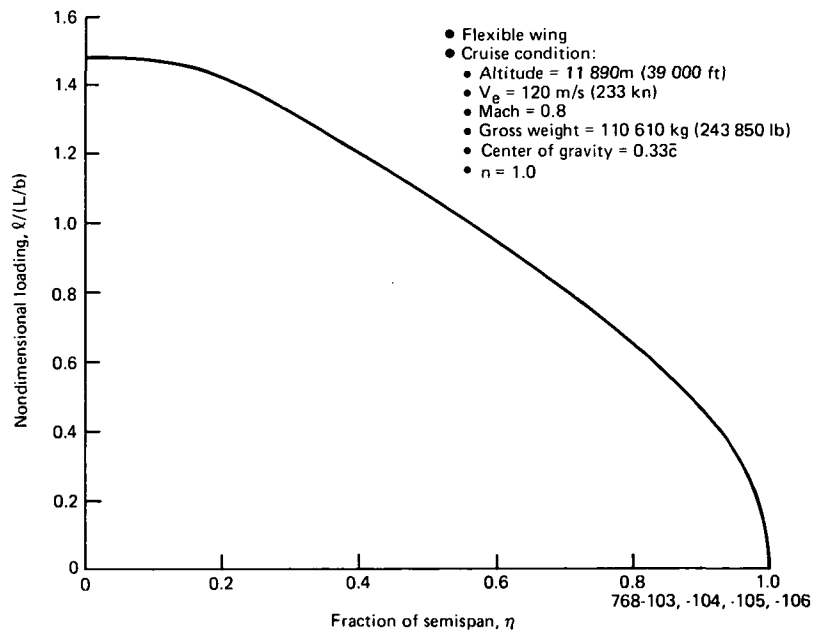
Figure 84. *Spanwise Lift Distribution Specified for Cruise Condition*

139
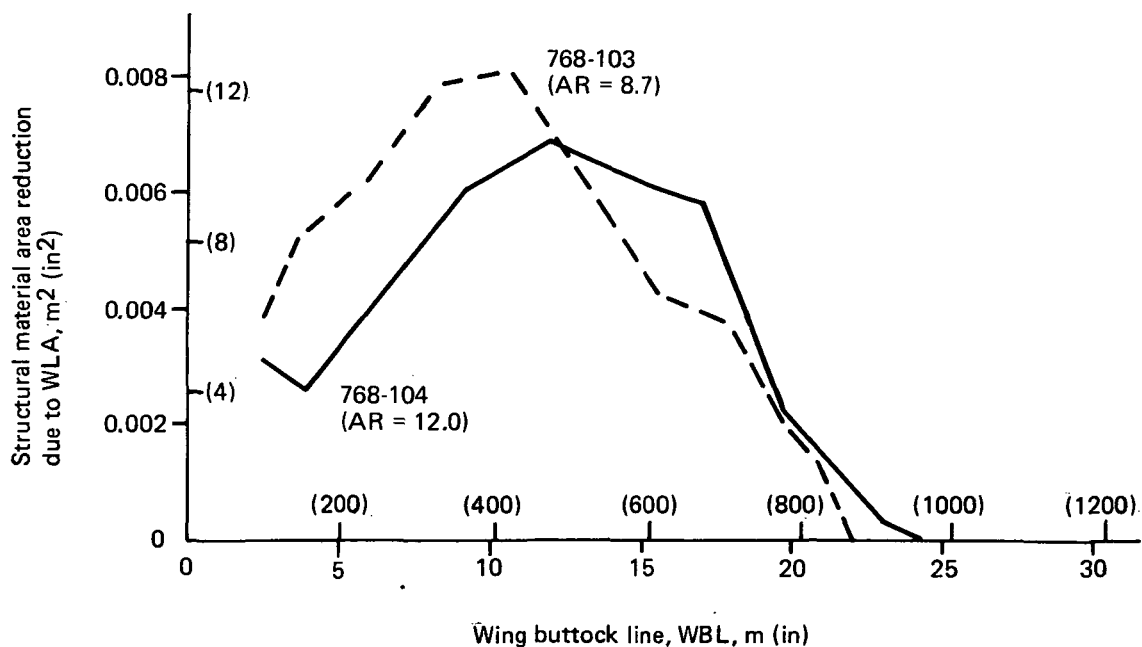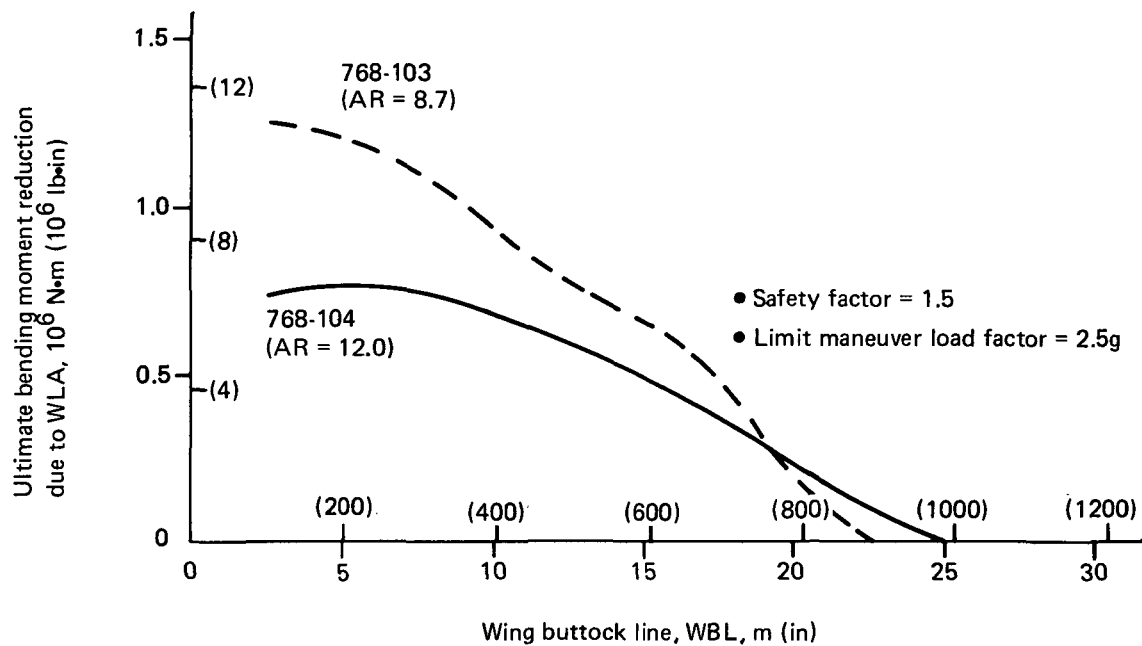
768-103, -104

Figure 85. Outboard Aileron Effectiveness for Wing-Load Alleviation and Structural Material Reduction, Model 768-104 Versus Initial ACT

The data in Figure 85 were derived from the load and structural material envelopes shown in Figures 64 through 67 and thus reflect the net benefit of wing-load alleviation. This includes a component of load reduction due to increased wing washout when the wing is resized to lower loads. This point is further illustrated in Figure 86, which shows aileron effectiveness for bending moment reduction at a critical V_B gust condition. The curves in Figure 86a were derived assuming the wing was not resized to benefit from reduced loads, while the curves in Figure 86b include the effect of wing resizing. The latter curves show the combined effects of aileron deflection and the increase in wing washout, which occurs with the resized (i.e., softer) wing.

7.2.1.5 Aileron Effectiveness at Constant C_N Versus Constant α

Effectiveness data are shown in Figure 86 at both constant C_N and constant α. The constant C_N data reflect the WLA effectiveness for maneuver load relief, which includes a component of load reduction due to reduced wing angle of attack for trim.

The change in wing angle of attack for trim accounts for the capability of outboard ailerons to reduce inboard wing loads in steady maneuvers even at speeds greater than their roll reversal speed (ref 8).

The reduction in wing angle of attack is required to maintain constant load factor when the ailerons are deflected. The reduction in wing angle of attack compensates for:

- Increased wing lift (due to wing "wash-in") when the ailerons are deflected trailing edge up at speeds above their lift reversal speed

- Reduced balancing tail load caused by nose-up pitching moment from the ailerons

7.2.2 FINAL WING STRUCTURAL SIZING RESULTS—MODEL 768-104

Figures 87 and 88 show the final wing structural sizing requirements for the Model 768-104 Configuration. These results include the beneficial effects of the selected

141

V_B condition: M = 0.86, V_e = 142 m/s (276 KEAS)

———————   constant C_N

— — — —   constant α

(a) Stiffness Based on Strength-Sized Wing Without WLA Benefit (i.e., No Wing Resizing Effects Included)

768-103 (AR = 8.7)

768-104 (AR = 12.0)

Bending moment change due to aileron, M/δ_A, 10^6 N·m/deg (10^6 lb·in/deg), limit

Fraction of semispan, η

(b) Includes Beneficial Effect of Increased Wing Washout Due to Resized Wing
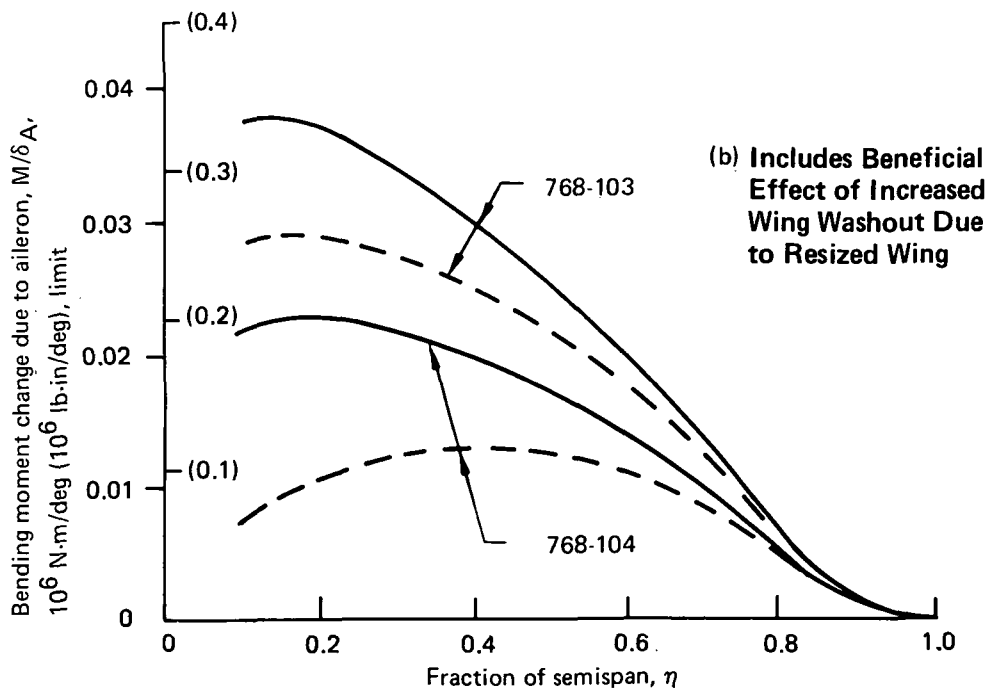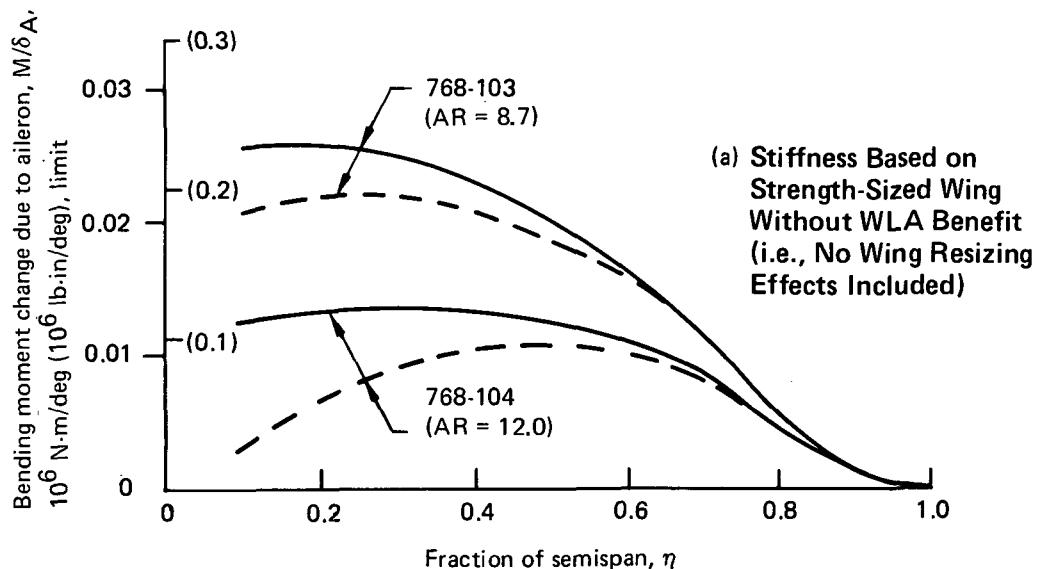
768-103

768-104

768-103, -104

Figure 86.   Outboard Aileron Wing-Load Alleviation Unit Solutions, Model 768-104 Versus Initial ACT

142
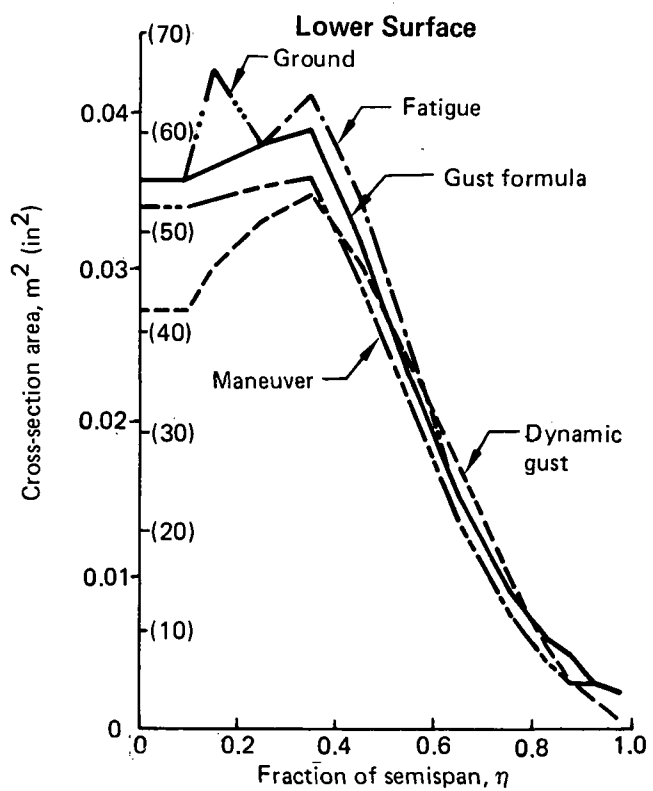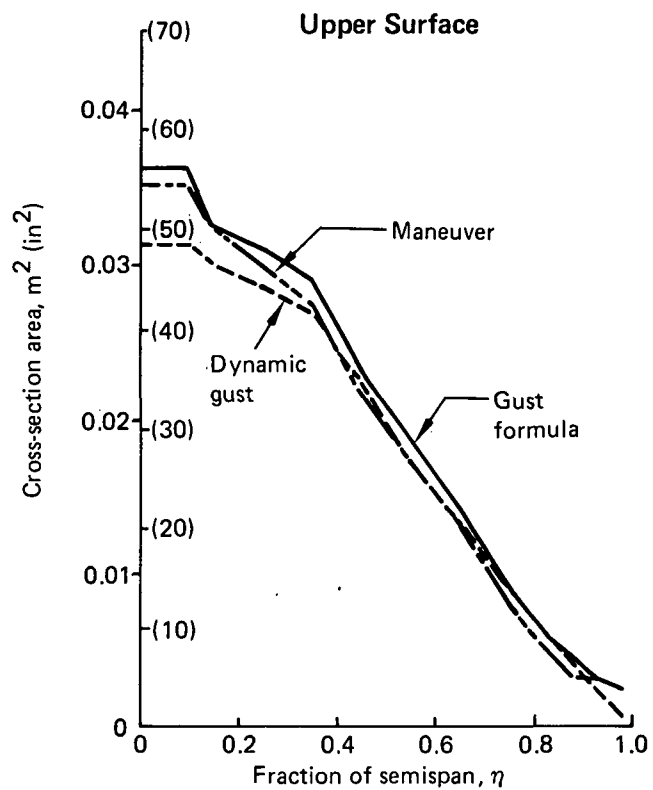
Figure 87. Final Structural Material Requirements,
Model 768-104, Surfaces

Front Spar

Rear Spar
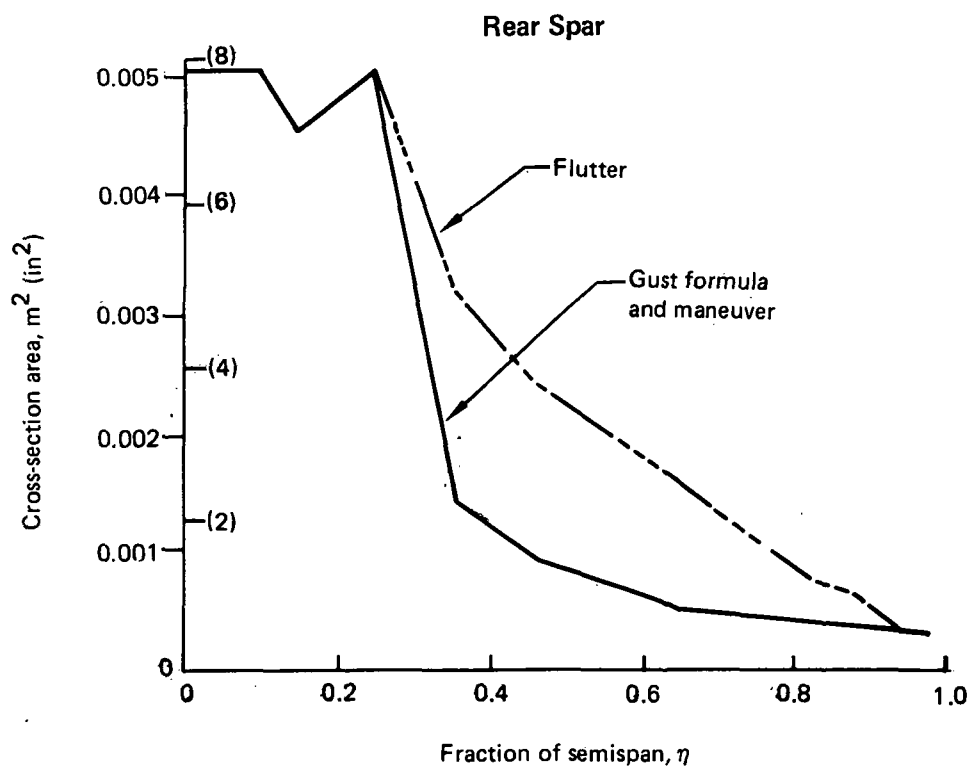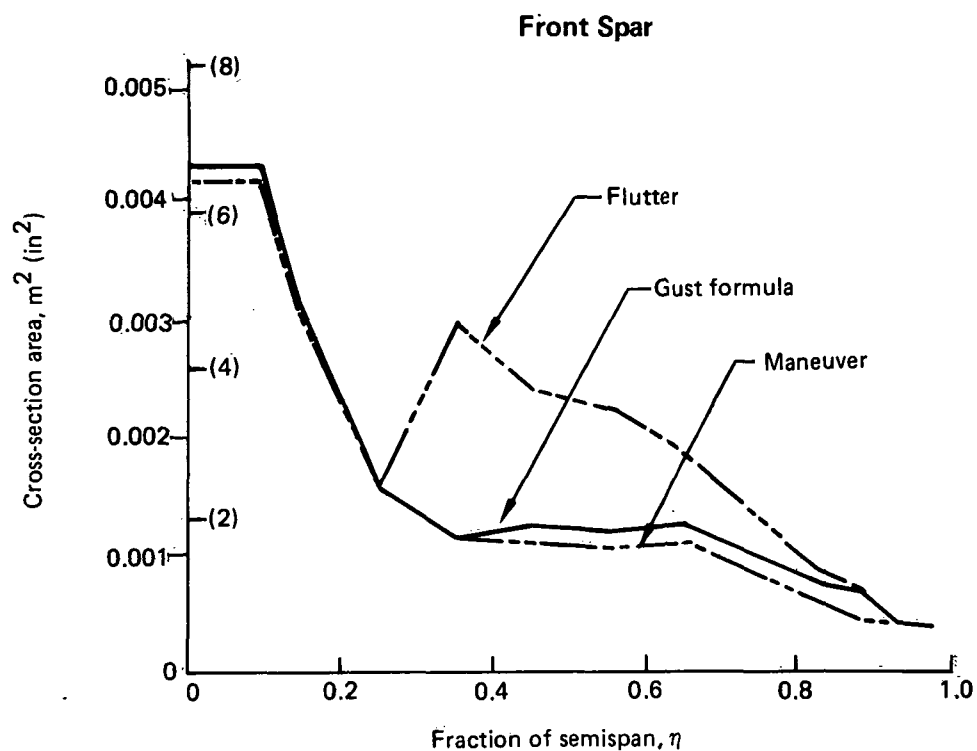
Figure 88. Final Structural Material Requirements, Model 768-104, Spars

144

ACT functions that include only maneuver load control (MLC) and PAS. These control functions use active elevators and outboard ailerons to increase the frequency and damping of pitch response and reduce maneuver and gust loads.

Small amounts of additional structural material were required for dynamic gust (subsec 7.2.2.1), flutter (subsec 7.2.2.2), and fatigue (subsec 7.2.2.3) relative to the initial strength-sizing base. Flutter-mode control (FMC) and gust-load alleviation (GLA) functions were synthesized to reduce these small penalties but were predicted to require very high control surface response rates in severe turbulence and were not retained in the final structural design.

Results from the final wing structural sizing analysis were used, together with results from the horizontal tail and fuselage loads analysis, (subsec 7.2.2.4), for weight input to the performance analysis of the Model 768-104.

7.2.2.1 Dynamic Gust Analysis for Model 768-104

The dynamic vertical gust loads on Model 768-104 were computed by a design envelope PSD procedure. The analysis was done for the structural cruise speed (V_C) at 7833m (25700 ft) altitude and for the gust penetration speed (V_B) at 10 668m (35 000 ft) altitude, as shown in Table 7. Choice of these conditions was established during the Initial ACT Configuration study (ref 3).

Figures 89 and 90 compare the ultimate wing bending moment load results from the dynamic gust analysis with similar results from the maneuver and FAR gust formula analyses. Excess structural margins were available for dynamic gust and maneuver in the inboard wing as a result of the FAR gust formula condition used for initial strength sizing (figs. 87, 89, and 90); however, additional structural material was required for dynamic gust in the outboard wing. Structural dynamic response in this portion of the wing was significantly higher than for the Baseline Configuration due to the lower outboard wing stiffness of the Model 768-104 wing. This effect was not adequately accounted for by the assumed lift-curve slope adjustment that was made to the Baseline DMF envelope for the initial strength-sizing analysis (subsec 7.2.1.1).

Table 7. Dynamic Vertical Gust Analysis Conditions

Condition	V_C	V_B
Mach number	0.86	0.86
Altitude, m (ft)	7 833 (25 700)	10 668 (35 000)
Equivalent airspeed, m/s (kn)	175.5 (341)	142.1 (276)
Stiffness base	Initial strength design	Same as V_C
Weights, kg (lb)	120 220 (265 050)[a]	Same as V_C
Center-of-gravity position	17.5% MAC	Same as V_C

[a]Maximum weight allowed at 7833m (25 700 ft) altitude
(MZFW with maximum pitch inertia +45.5% fuel)

768-104
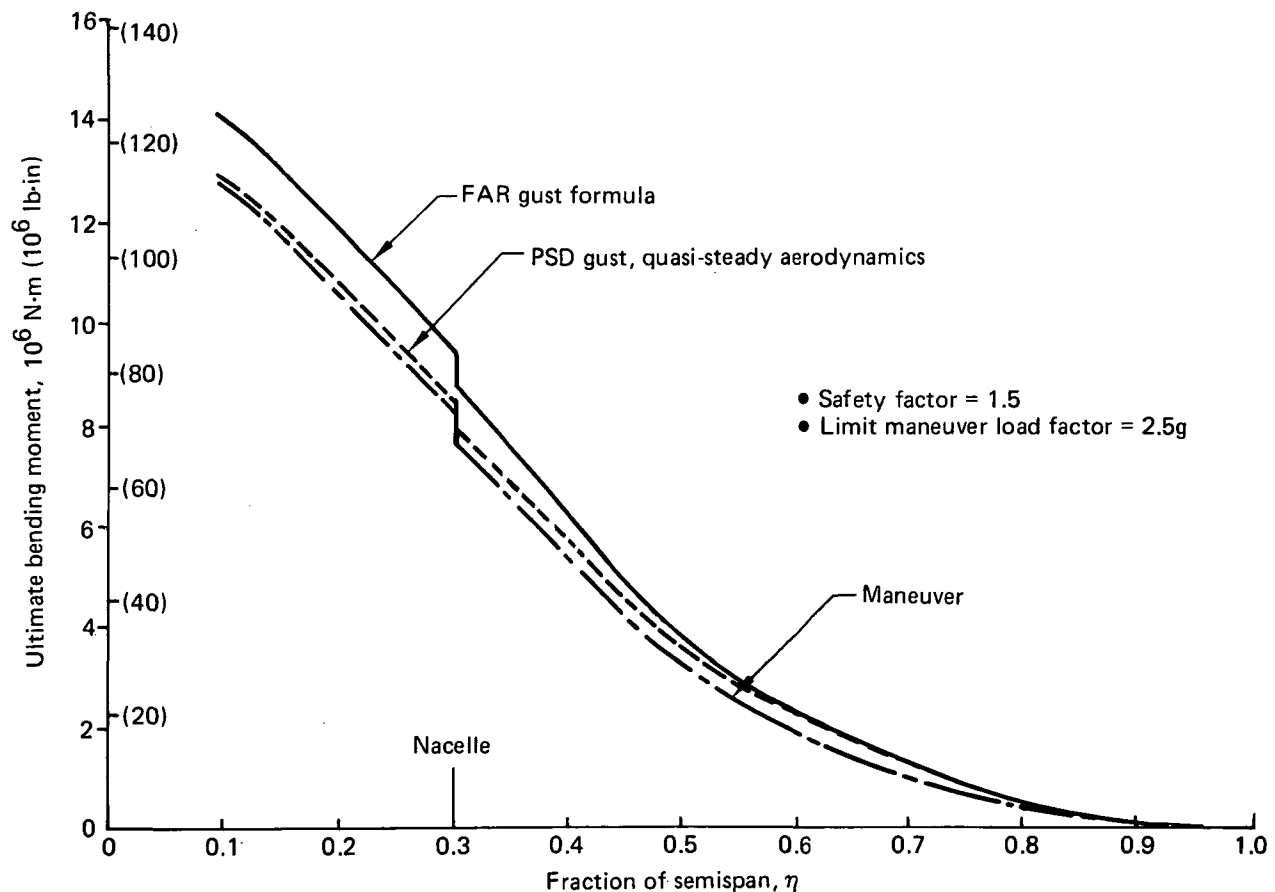
Figure 89. Bending Moment Envelopes, Maneuver, FAR Gust, and Dynamic Gust (Quasi-Steady Formulation), Model 768-104 Without Wing-Load Alleviation
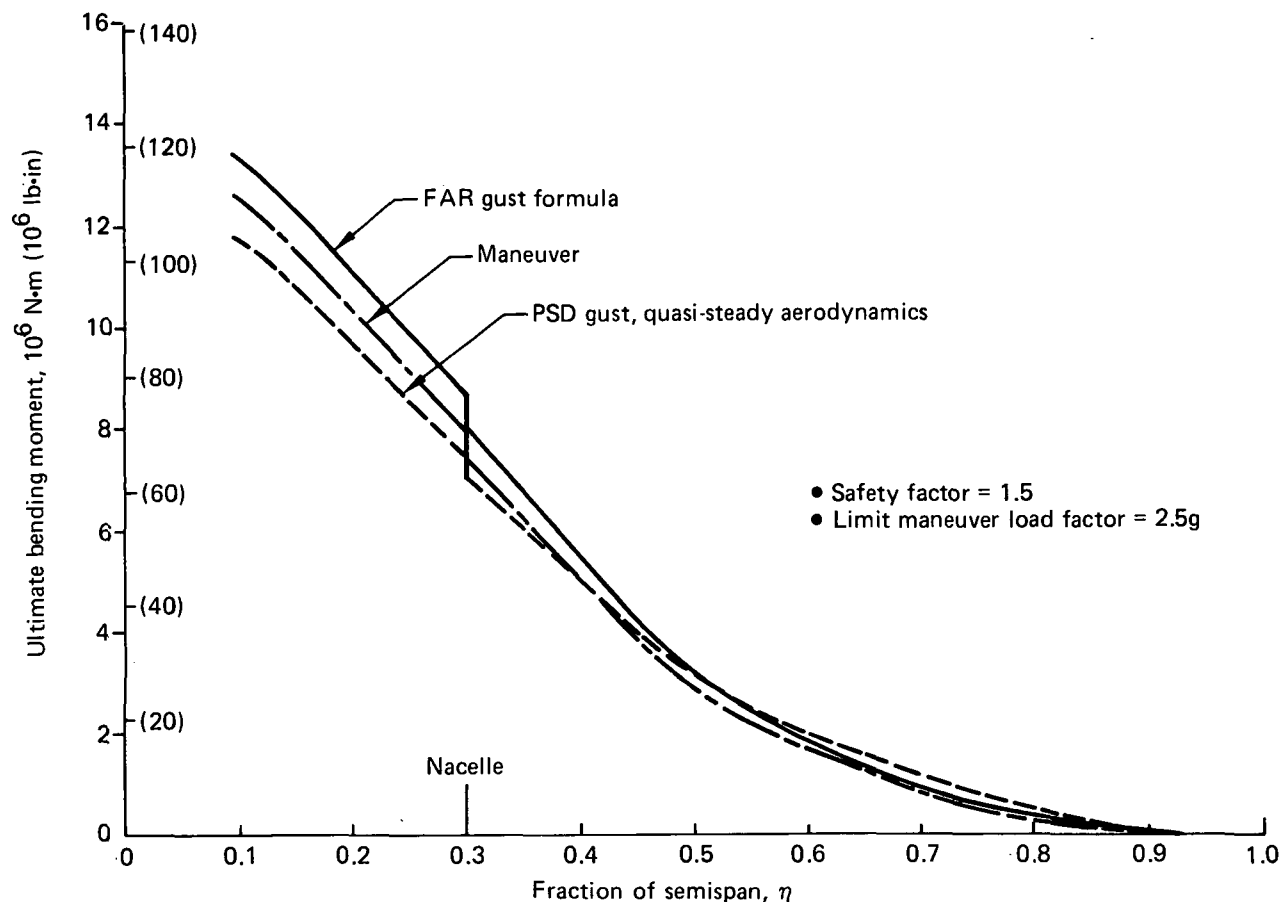
Figure 90. Bending Moment Envelopes, Maneuver, FAR Gust, and Dynamic Gust (Quasi-Steady Formulation), Model 768-104 With Wing-Load Alleviation

An additional 54 kg (120 lb) per airplane theoretical wing-box weight was needed for the dynamic gust design of the Model 768-104 relative to the initial strength-sizing base.

Dynamic Model for Gust Analysis—The dynamic gust analysis was performed using the Boeing-developed ATLAS 4.1 and DYLOFLEX (ref 9) Program systems. The conventional beam-lumped mass structural idealization for high aspect ratio wings was used. The airplane was modeled as an assembly of cantilevered branches using the main surface elastic axes and control surface hinge lines as reference axes. The wing and control surface idealization, panel inertia reference points, and control surface hinge lines are shown in Figure 91. Also shown in this figure are the load reference stations where gust loads (in terms of shear, moment, and torsion) were calculated. Wing stiffness and weight data were derived from the initial wing strength-sizing analysis presented in Subsection 7.2.1. The wing vertical bending and torsional stiffness that were used in the analysis are shown in Figures 80 and 81.

147
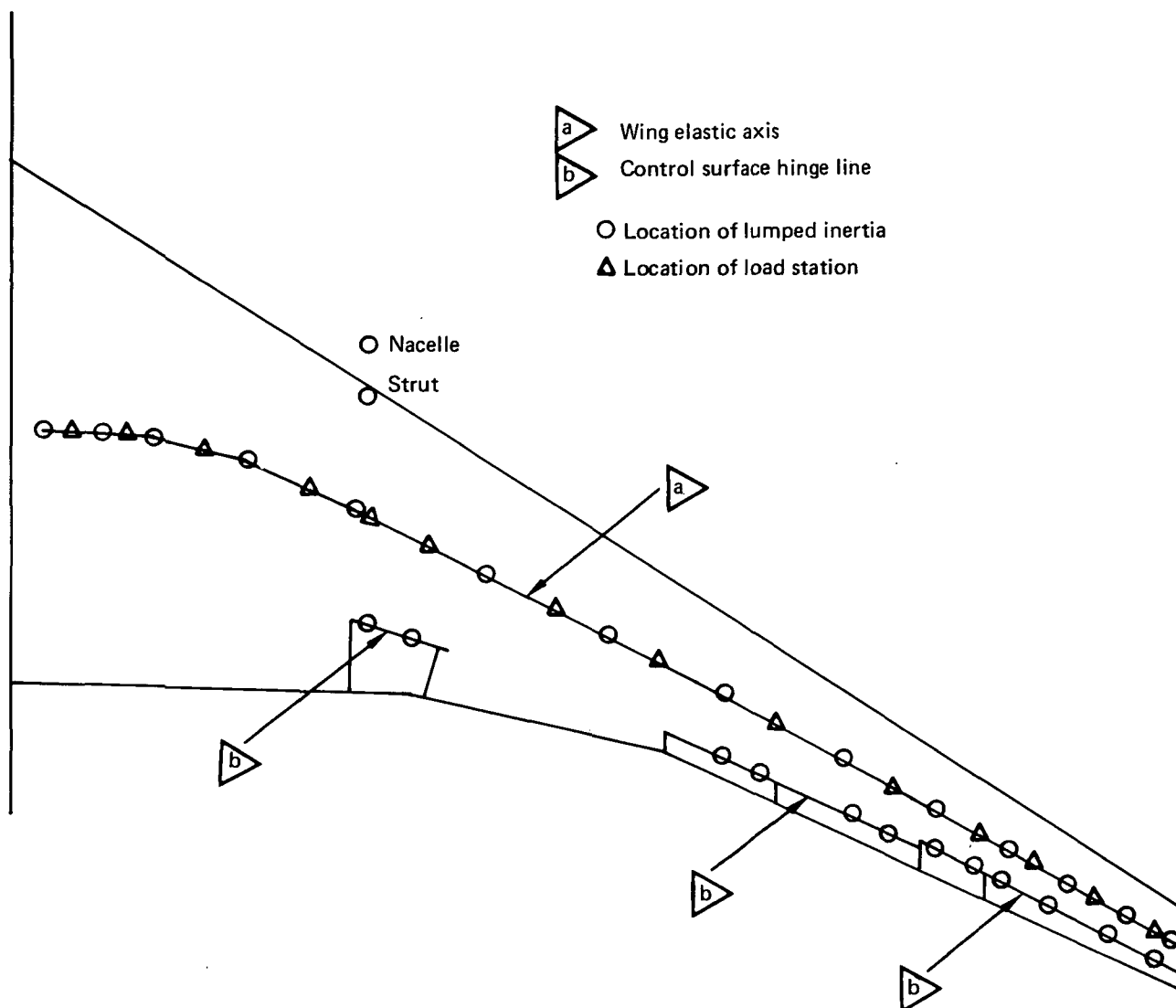
Figure 91. Wing Structural Idealization

768-104

Coupled bending-torsion branch modes were calculated based on cantilever beam theory and used as generalized coordinates in the formulation of equations of motion. The modal descriptions of the generalized coordinates are listed in Table 8. The branch modes were selected, on the basis of experience, to adequately model the flexible response of the structure to vertical gust excitation and control surface deflection. Structural damping was conservatively estimated to be 0.02g.

Doublet-lattice lifting surface theory was used for calculation of aerodynamic forces due to structural response and gust excitation, using the quasi-steady formulation provided by DYLOFLEX. Wagner and Küssner indicial lift-growth functions were used to account for unsteady aerodynamic effects. An equivalent analysis also was

148

Table 8. Generalized Coordinates for Dynamic Vertical Gust Analysis, Model 768-104 Strength-Designed Wing With Wing-Load Alleviation (Selected Branch Modes and Rigid Body Freedoms)

Branch	Frequency, Hz	Dominant mode shape
Airplane	0 0 0	Rigid airplane fore/aft Rigid airplane plunge Rigid airplane pitch
Forebody	3.86 19.78[a]	First vertical bending Second vertical bending
Aftbody (rigid empennage)	2.18 8.13 23.81[a]	First vertical bending Second vertical bending Third vertical bending
Vertical tail (rigid horizontal tail)	5.60 28.98[a]	First chordwise bending Second chordwise bending
Horizontal tail	5.91 18.71 23.94	First vertical bending Second vertical bending First torsion
Wing (45.5% fuel) (rigid nacelle pylon)	1.33 3.54 3.61 4.78 7.02 8.49 11.41 12.22 16.50 19.98	First vertical bending Second vertical bending First fore/aft bending First torsion Third vertical bending Second fore/aft bending Fourth vertical bending Second torsion Fifth vertical bending Third torsion
Nacelle	2.60 4.63 5.76	Side bending Vertical bending Roll/side bending
Control surfaces	30.0 30.0 30.0[a] 30.0[a] 30.0[a] 30.0 30.0	Inboard elevator rotation Outboard elevator rotation Inboard aileron rotation Inboard of outboard flaperon rotation Outboard of outboard flaperon rotation Inboard of outboard aileron rotation Outboard of outboard aileron rotation

[a]Formulated but not used in gust loads calculations.
For analysis with active controls system, 15 additional generalized coordinates were added for sensor and control law equations.

768-104

performed using doublet-lattice oscillatory aerodynamics, but the results were less critical; and, based on past design practice, the more conservative quasi-steady results were retained for structural design.

Doublet-lattice lifting panels were used in aerodynamic modeling of the fuselage, wing (including outboard and inboard ailerons and outboard flaperons), and horizontal tail with double-hinged elevators. The nacelles were represented by cruciform lifting panels. The wing and nacelle aerodynamic paneling are shown in Figure 92.

149
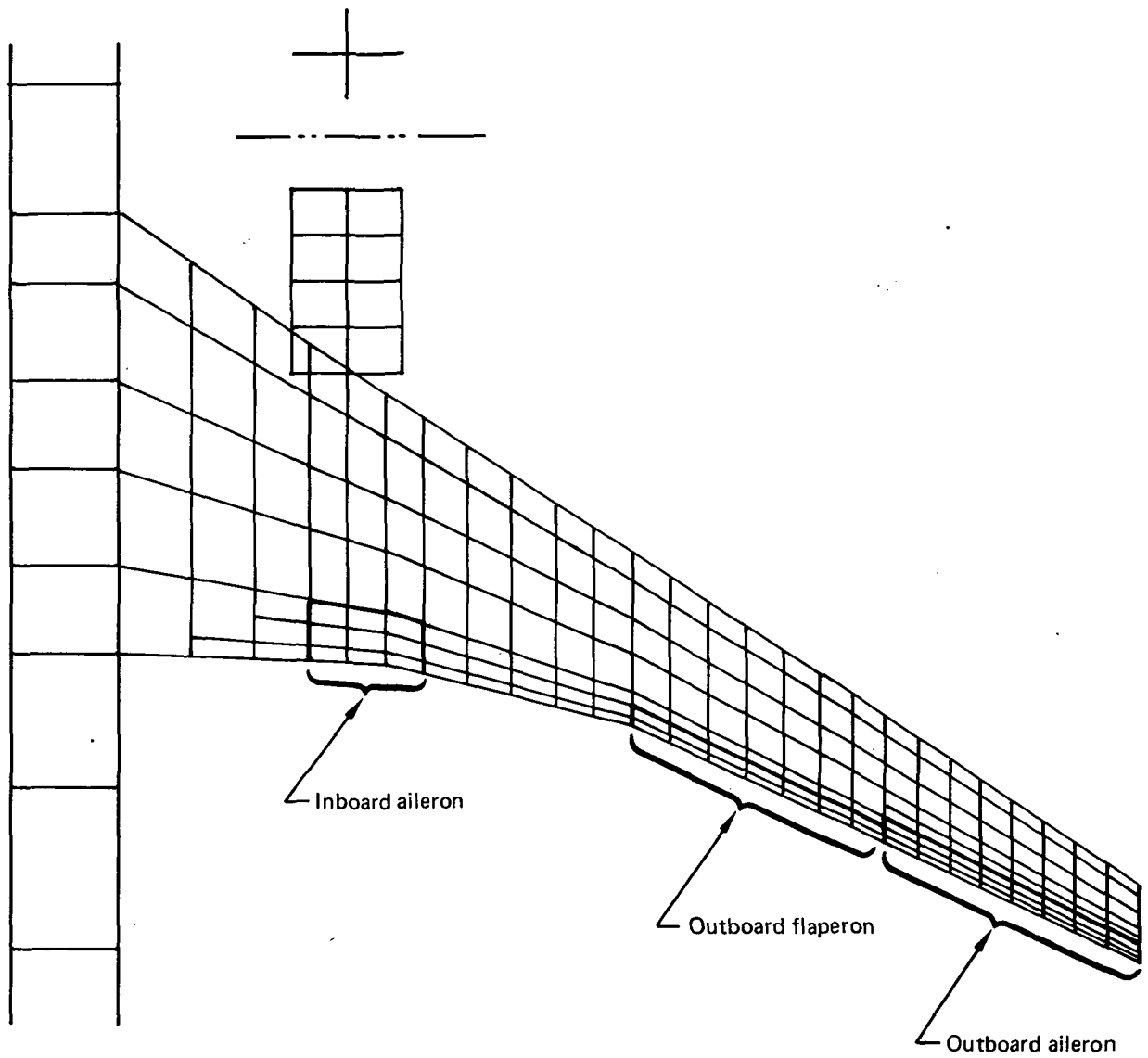
Figure 92. Doublet-Lattice Aerodynamic Paneling for Wing and Nacelle

768-104

150

In calculating the aerodynamic forces, the pressures at aerodynamic boxes were scaled to match wind tunnel static aerodynamic data at Mach 0.86, as presented in Appendix A, using scale factors that vary linearly in the chordwise direction. In the absence of experimental oscillatory aerodynamic data, the pressure scale factors from the rigid airplane static data also were used for the unsteady motion of the elastic airplane. Pressure scale factors used on the wing boxes for all the generalized coordinates except control surface rotation degrees of freedom were determined to match the experimental wing spanwise lift and moment distributions due to angle of attack. For the outboard aileron rotational freedoms, the pressure scale factors were determined to match wing spanwise lift and moment distributions due to outboard aileron rotation. Nacelle aerodynamic box pressures were not scaled. A single pressure scale factor was determined and applied on all the horizontal tail boxes to match the tail load caused by airplane pitch, including wing downwash effects as determined from available wind tunnel data. Pressure scale factors on the fuselage boxes were determined to match total airplane lift and moment curve slopes. The generalized forces due to elevator deflection were scaled to match airplane lift and pitching moment values due to elevator rotation.

Dynamic vertical gust loads were computed using the load summation method for two previously established critical flight conditions; namely, at the structural cruise speed, V_C, and at the gust penetration speed, V_B, with Mach number 0.86 for both cases. A single weight condition was used, which was the maximum allowable weight at 7833m (25 700 ft). To arrive at this weight, 45.5% fuel was added to the maximum design zero fuel weight (MZFW) with payload distributed mainly in the foward and aft sections of the fuselage, resulting in a forward cg position at 17.50% MAC and a maximum possible airplane pitching inertia. The gust conditions analyzed are summarized in Table 7.

Incremental PSD gust loads were calculated using a random harmonic analysis technique for continuous turbulence excitation. The von Karman gust spectrum with turbulence scalar constant of 762m (2500 ft) was used. Gradual gust penetration effects were not included.

Modeling of Active Controls Functions—An active controls system, which provided PAS, MLC, and GLA was analyzed. Figure 93 shows the control law functional block

[Wing]
Sensor[a] 432 $-\ddot{Z}$

$\dfrac{m/s^2}{}$ (ft/s²)

$\dfrac{1}{(S/20 + 1)}$ KGW

GLA

Outboard aileron actuators

$\dfrac{1}{(S/20 + 1)(S/40 + 1)}$ δ_{OA} (deg)

[cg]
Sensor[a] 1202 $-\ddot{Z}$

$\dfrac{m/s^2}{}$ (ft/s²)

$\dfrac{S}{(S + 9)(S/30 + 1)}$ KGCG

$\dfrac{1}{S/10 + 1}$ KMN **MLC**

KE

Elevator actuators

$\dfrac{1}{(S/20 + 1)(S/40 + 1)}$ δ_E (deg)

δ_{COL} (deg)

$\dfrac{S}{S + 0.8}$ KP **PAS**

[cg]
Sensor[a] 1202 $\dot{\theta}$
(deg/s)

$\dfrac{1}{S/10 + 1}$ KQ

[a]See Figure 109 for sensor location.

Speed - u
$\dfrac{m/s}{}$ (ft/s)

$\dfrac{25S + 1}{5S + 1}$ KU
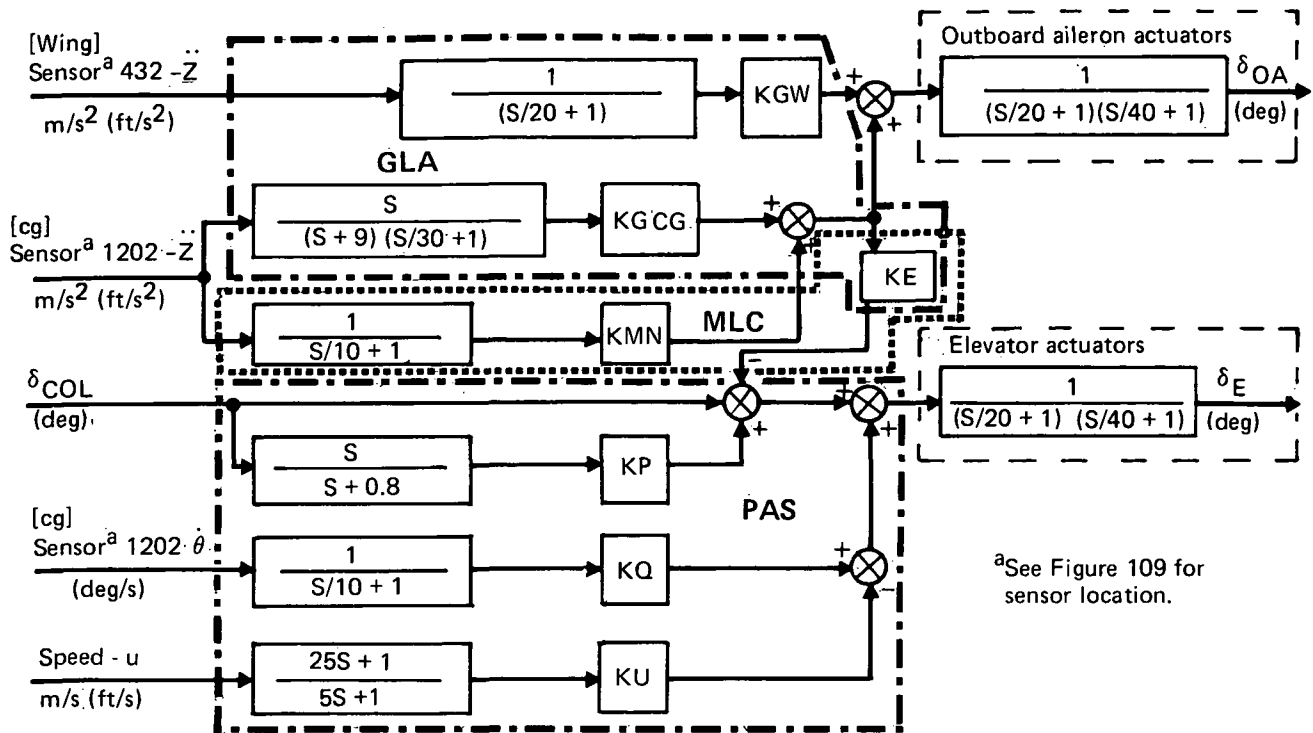
Gain values	Flight condition	
	V_B	V_{MO}
KQ	1.5	1.5
KU	0	0
KMN	1.230 (0.375)	0.886 (0.270)
KE	0.170	0.236
KGCG[b]	1.230 (0.375)	0.886 (0.270)
KGW[b]	0.1353 (0.04125)	0.0902 (0.0275)
KP	0	0

[b] Set to zero for exclusion of GLA functions as used for structural design.

Dimensions are in meters (feet), seconds, and degrees

$\dot{\theta}$

Y Right

X Forward

Control surface deflection positive down

Z Down $\ddot{Z}$
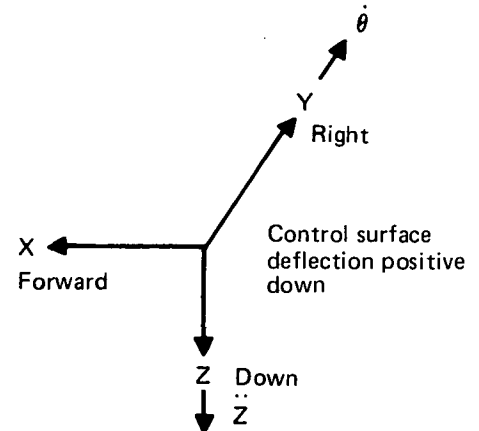
Figure 93. *Control System Functional Block Diagram and Gain Values Used for Dynamic Gust Analysis*

diagram and the gain values assigned. The outboard ailerons were activated by airplane cg acceleration for MLC, and by airplane cg acceleration and outboard wing acceleration for GLA; the elevators were activated by airplane cg pitch rate for PAS. The elevators reacted to outboard aileron motion caused by MLC and GLA commands to compensate for aileron-induced pitching moments. The actuators for the elevators and outboard ailerons were represented by two first-order lag functions as shown in Figure 93. These functions were assumed to adequately model the dynamic response of the control surfaces due to actuator commands including the flexibility effects of the actuator and backup structure and control surface aerodynamic and inertia hinge moments.

The PAS and MLC systems were found to be most effective in reducing wing gust loads. With the GLA control law included, the outboard aileron rate was found to be excessive (greater than 150 deg/s at design gust intensity). Consequently, although the GLA function could produce a small benefit in terms of additional outboard wing load relief, it was not included in the final wing design.

The control laws described above (with GLA function deleted) were used for structural design of the Model 768-104 Configuration and the load results reported in this section reflect these control laws. Subsequent to the structural design analysis, these control laws were revised to obtain improved performance as discussed in Subsection 7.3.1.3.

Dynamic Gust Analysis Results—The analysis results indicated that higher wing incremental gust loads were obtained for the V_B condition. The effect of active controls on PSD gust loads for the critical V_B gust condition is shown in Figures 94 and 95 at the wing 0.25 and 0.75 semispan stations. From these figures, it is observed that: 1) the reduction of gust loads due to the PAS and MLC functions is mainly caused by an increase in the frequency and damping of the short-period mode when the active controls system is applied; this is evidenced by the sharp reduction of the short-period spike in the bending moment spectra, 2) the contribution to the wing incremental gust loads from the 4 Hz wing bending mode becomes evident in the outboard wing, 3) the frequency responses beyond 4 Hz have negligible effects on PSD gust loads, and 4) similar spanwise wing incremental gust loads were obtained for both unsteady and quasi-steady aerodynamic formulations except that the loads from the unsteady formulation were lower and did not contribute to the wing structural sizing.

153
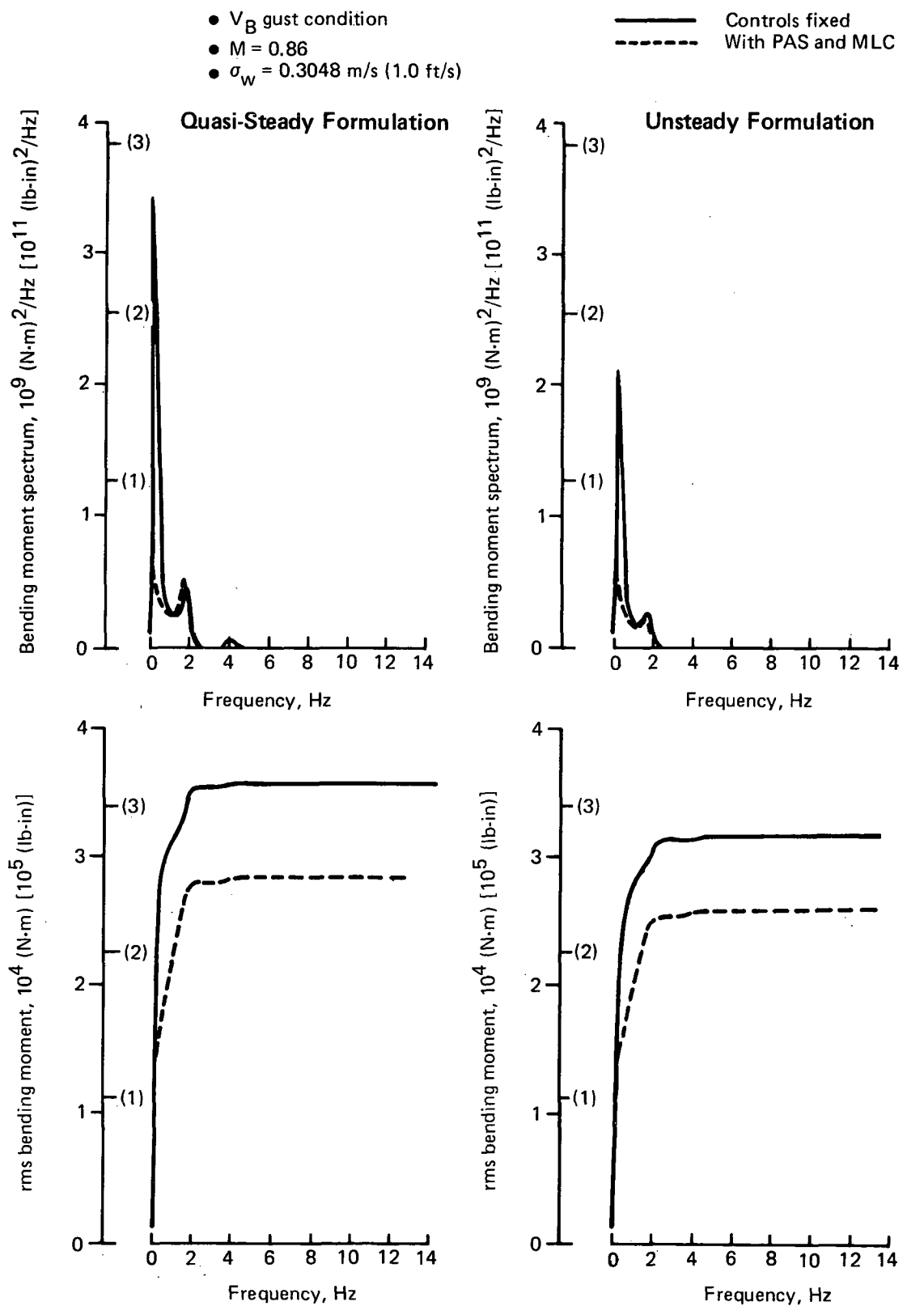
Figure 94. *Effect of Active Controls on PSD Gust Loads at $\eta = 0.25$,*
Quasi-Steady Versus Unsteady Formulation

154

- V_B gust condition
- $M = 0.86$
- $\sigma_w = 0.3048$ m/s (1.0 ft/s)

━━━ Controls fixed
▬▬▬ With PAS and MLC

Quasi-Steady Formulation

Unsteady Formulation

Bending moment spectrum, 10^6 $(N \cdot m)^2/Hz$ $[10^8$ $(lb \cdot in)^2/Hz]$

Frequency, Hz

rms bending moment, 10^3 $(N \cdot m)$ $[10^4$ $(lb \cdot in)]$

Frequency, Hz
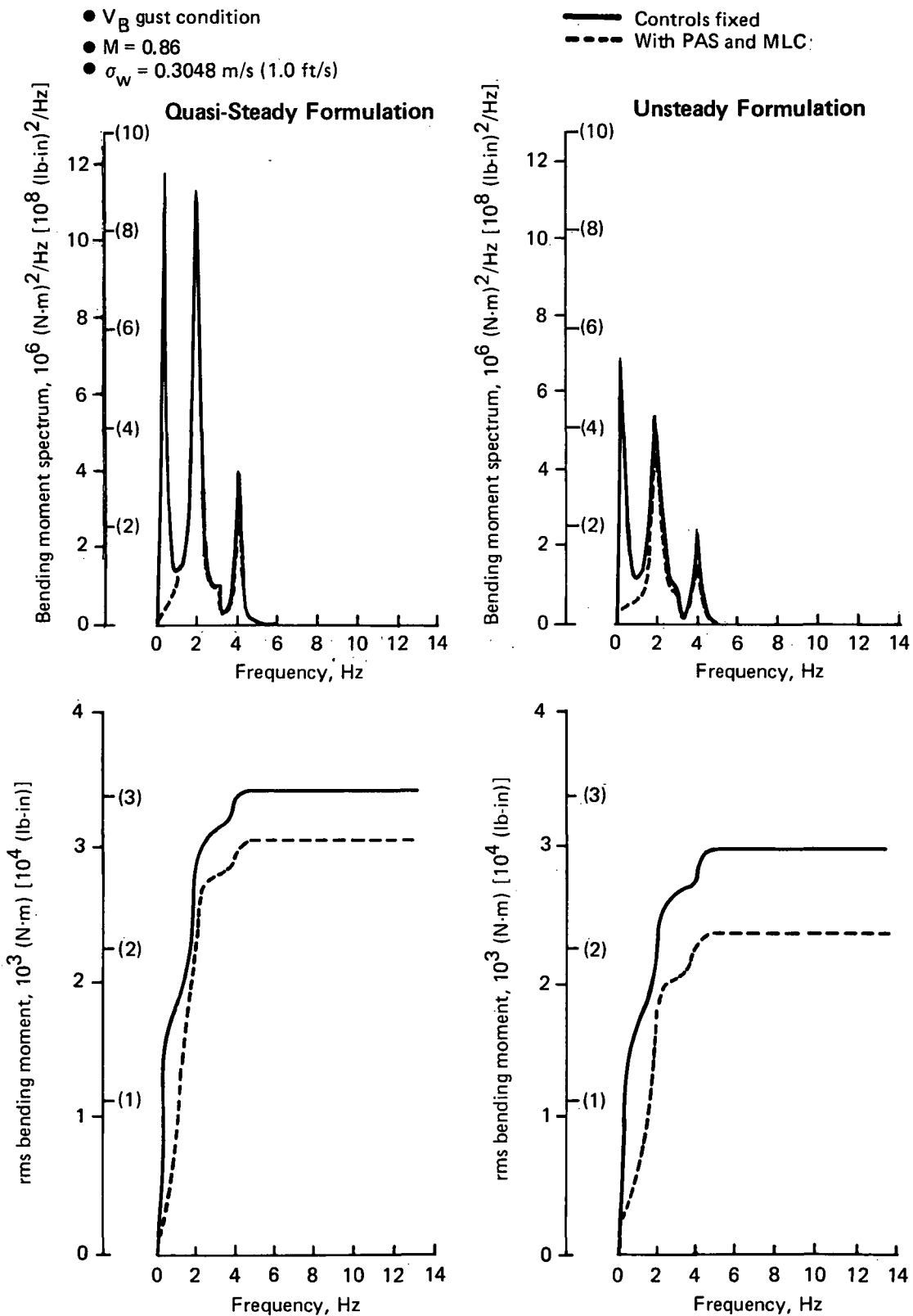
768-104

*Figure 95.   Effect of Active Controls on PSD Gust Loads at $\eta = 0.75$,
Quasi-Steady Versus Unsteady Formulation*

155

The power spectra of outboard aileron and elevator activities are shown in Figures 96 and 97. The significant contribution of the high frequency (4 Hz) wing bending mode to outboard aileron rate response is evident in Figure 96.

A major portion of the reduction in incremental gust loads, especially in the inboard wing, was due to the effects of the PAS on the airplane short-period longitudinal response. In Figure 98, the reductions in wing bending moment from PAS and from the combined PAS and MLC are compared.

The incremental wing bending moments and the correlated shears and torsions from the critical V_B gust condition using quasi-steady aerodynamics with the PAS and MLC active controls were combined with the steady level flight (1g) loads for the wing-box structural design. An additional 54 kg (120 lb) per airplane theoretical wing-box weight was needed for the dynamic gust design of the Model 768-104 relative to the initial strength-sizing base.

7.2.2.2 Flutter Analysis For Model 768-104

A flutter weight penalty was required in the outboard wing spars relative to the initial strength-sizing base (fig. 88) for increased torsional stiffness to control an explosive 7 Hz symmetric outboard wing flutter mode. This mode could not be stabilized satisfactorily with a feasible FMC system due to the control surface rate saturation effects that were predicted to occur in moderate turbulence. The required torsional stiffness increase was efficiently achieved by increasing the spar web gages to match the minimum level of the upper or lower surface gage at each analysis station. The total added weight required, including nonoptimum factors, was 263 kg (580 lb) .

No additional material was required to control inboard wing flutter for this configuration, which benefited from increased torsional stiffness in the inboard wing relative to the Baseline and Initial ACT Configurations. The torsional stiffness increased in the inboard wing because the wing-box chord and thickness ratio at side of body were held constant while structural material required for strength was increased due to higher inboard wing loads.

It was originally anticipated that an FMC system would be required to achieve higher aspect ratio and improved aerodynamic performance and that this function would

156

- V_B gust condition
- M = 0.86
- σ_w = 0.3048 m/s (1.0 ft/s)
- Quasi-steady formulation

Displacement

$\bar{A}$ = 0.417 deg/(m/s)
 [0.127 deg/(ft/s)]

Rate

$\bar{A}$ = 2.165 (deg/s)/(m/s)
 [0.660 (deg/s)/(ft/s)]

Displacement spectrum, 10^{-3} (deg)^2/Hz

Rate spectrum, 10^{-2} (deg/s)^2/Hz

Frequency, Hz

Frequency, Hz
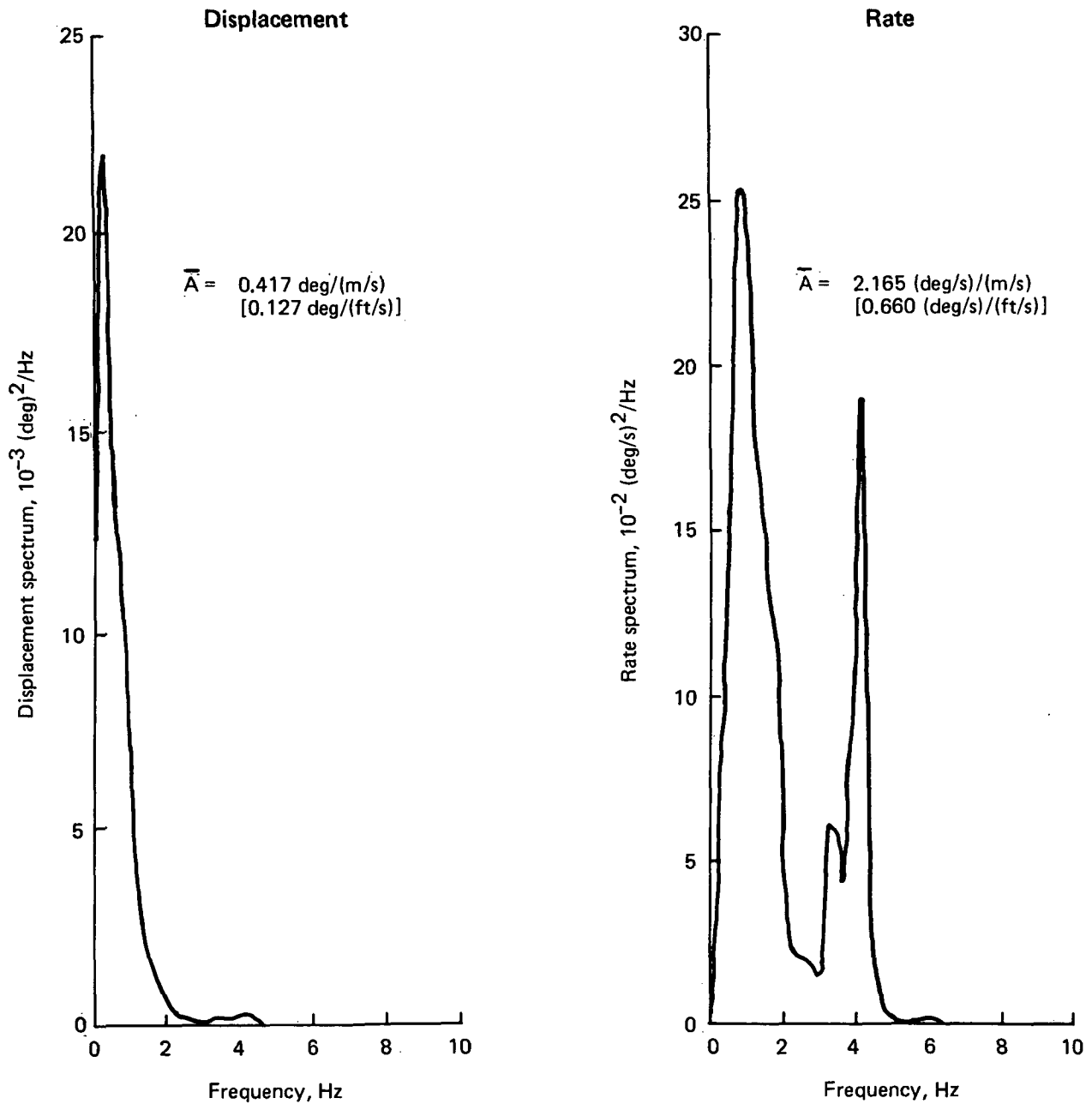
768-104

Figure 96. Outboard Aileron Activities Due to Pitch-Augmented Stability and Maneuver-Load Control

157

- V_B gust condition
- M = 0.86
- σ_w = 0.3048 m/s (1.0 ft/s)
- Quasi-steady formulation

Displacement

$\overline{A}$ = 0.164 deg/(m/s)
  [0.050 deg/(ft/s)]

Displacement spectrum, 10^{-4} (deg)^2/Hz

Frequency, Hz

Rate

$\overline{A}$ = 0.820 (deg/s)/(m/s)
  [0.250 (deg/s)/(ft/s)]

Rate spectrum, 10^{-2} (deg/s)^2/Hz

Frequency, Hz
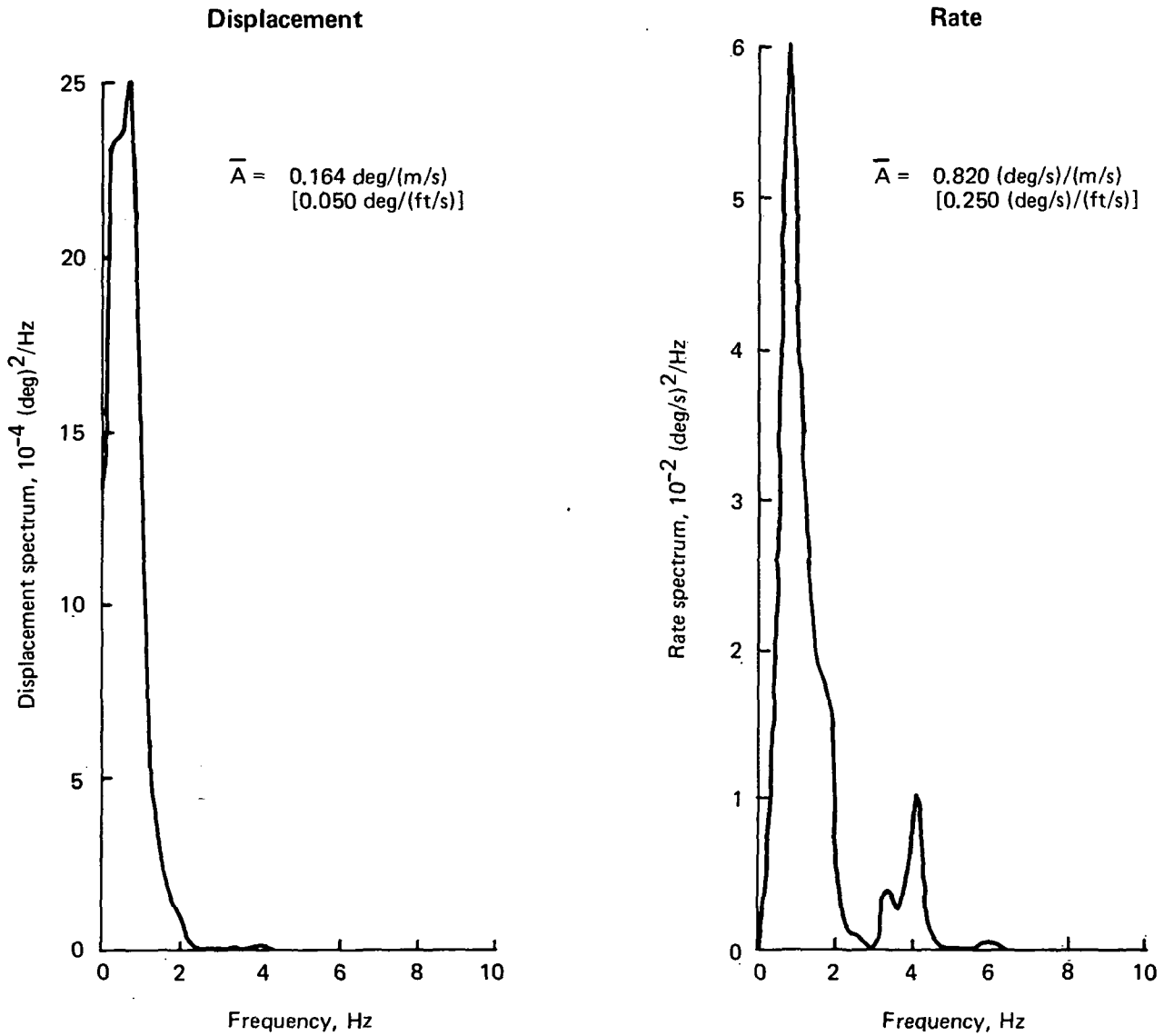
768-104

Figure 97. Elevator Activities Due to Pitch-Augmented Stability and
Maneuver-Load Control

158
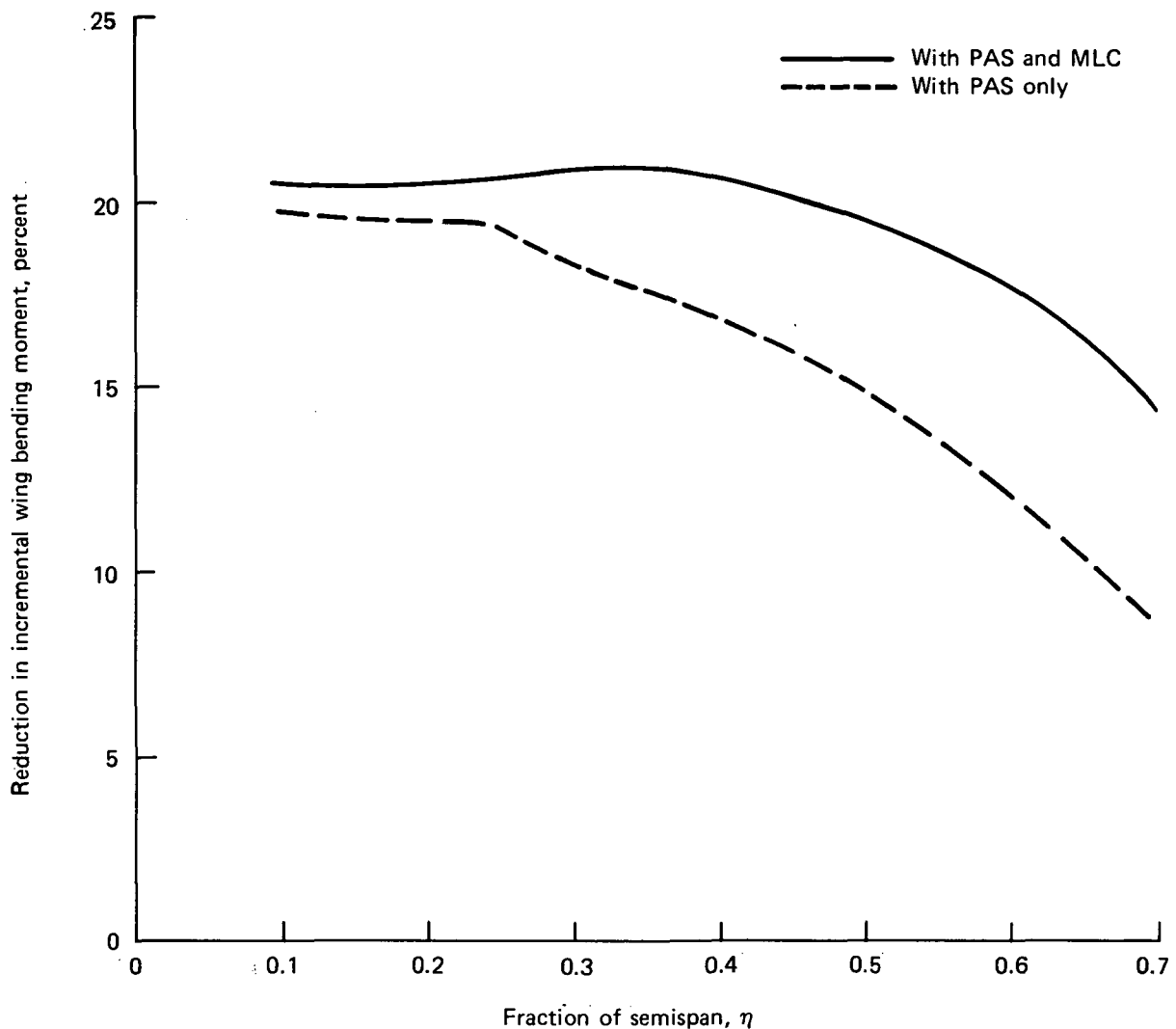
Figure 98. Effect of Pitch-Augmented Stability and Maneuver-Load Control on PSD Gust Loads, Model 768-104

provide weight advantage for a design with active controls. The anticipated flutter problem was not severe for this configuration due to the large inboard wing trailing-edge extension that was required to accommodate the wing-mounted landing gear, which was located farther aft on the wing for this configuration relative to the Baseline. The resulting inboard wing-box geometry and higher inboard wing design loads for the Model 768-104 provided sufficient torsional stiffness to preclude an inboard wing flutter penalty.

Dynamic Model for Flutter Analysis—The structural and aerodynamic paneling used for the flutter analysis was identical to that used in the gust analysis. The generalized

coordinates for the symmetric and antisymmetric analyses are listed in Table 9 and Table 10. Doublet-lattice oscillatory aerodynamics at Mach = 0.0 were used with box pressures scaled to match wind tunnel static aerodynamic data as in the dynamic gust analysis (subsec 7.2.2.1). Flutter analyses were first performed using M = 0.4 section aerodynamic data for pressure scaling and then repeated using M = 0.86 section aerodynamic data for pressure scaling. The section aerodynamic data used are reported in Appendix A.

The conventional V-g solution technique was used to determine flutter stability. The criterion used for structural damping allowance was taken from the IAAC design requirements and objectives (DRO). This criterion, which is based on past experience with configurations of similar construction, requires that the V-g plot obtained by

Table 9. Generalized Coordinates for Symmetric Flutter Analysis, Model 768-104, Strength-Designed Wing With Wing-Load Alleviation (Selected Branch Modes and Rigid Body Freedoms)

Branch	Frequency, Hz	Dominant mode shape
Airplane	0 0 0	Rigid airplane fore/aft translation Rigid airplane plunge Rigid airplane pitch
Forebody	3.98 23.38	First vertical bending Second vertical bending
Aftbody (rigid empennage)	2.07 7.17 22.59	First vertical bending Second vertical bending Third vertical bending
Vertical tail (rigid horizontal tail)	5.60 29.00	First fore/aft bending (in plane) Second fore/aft bending (in plane)
Horizontal tail	5.91 18.71 23.94	First vertical bending Second vertical bending First torsion bending (coupled)
Wing (100% fuel) (rigid nacelle pylon)	1.24 2.80 3.20 4.64 6.10 7.09 9.75 11.52	First vertical bending First fore/aft bending (in plane) Second vertical bending First torsion Third vertical bending Second fore/aft bending (in plane) Fourth vertical bending Second torsion
Nacelle	2.60 4.63 5.76	Side bending Vertical bending Roll/side bending

160

Table 10. *Generalized Coordinates for Antisymmetric Flutter Analysis, Model 768-104, Strength-Designed Wing With Wing-Load Alleviation (Selected Branch Modes and Rigid Body Freedoms)*

Branch	Frequency, Hz	Dominant mode shape
Airplane	0 0 0	Rigid airplane lateral translation Rigid airplane roll Rigid airplane yaw
Forebody	4.16 15.35	First lateral bending Second lateral bending
Aftbody (rigid empennage)	1.97 5.38 12.76 18.96	First lateral bending First torsion Second lateral bending—torsion Second torsion
Vertical tail (rigid horizontal tail)	2.57 5.99 12.39	First lateral bending First torsion Second lateral bending—torsion
Horizontal tail	5.86 19.32 23.14	First vertical bending Second vertical bending First torsion bending (coupled)
Wing (100% fuel) (rigid nacelle pylon)	1.24 2.80 3.20 4.64 6.10 7.09 9.75 11.52	First vertical bending First fore/aft bending (in plane) Second vertical bending First torsion Third vertical bending Second fore/aft bending (in plane) Fourth vertical bending Second torsion
Nacelle	2.60 4.63 5.76	Side bending Vertical bending Roll/side bending

analysis with no allowance for structural damping must not intersect the unacceptable stability region, as illustrated in Figure 99. For example, at V_D the allowance for structural damping must not exceed 0.0g, and at $1.2V_D$ must not exceed +0.03g.

The fuselage and horizontal tail stiffness used was the same as for the Initial ACT Configuration, which was conservative for flutter analysis of the Model 768-104.

Flutter Analysis Results—Flutter speed boundaries for the inboard wing flutter mode (fig. 100) were most critical based on the M = 0.4 section data. Flutter speeds for the outboard wing flutter mode were most critical based on the M = 0.86 section data, and resulted in the indicated flutter boundary and structural penalty (figs. 100 and 88). The final wing torsional stiffness that satisfied flutter stability requirements is presented in Figure 101. The inboard wing flutter mode was much more critical on the
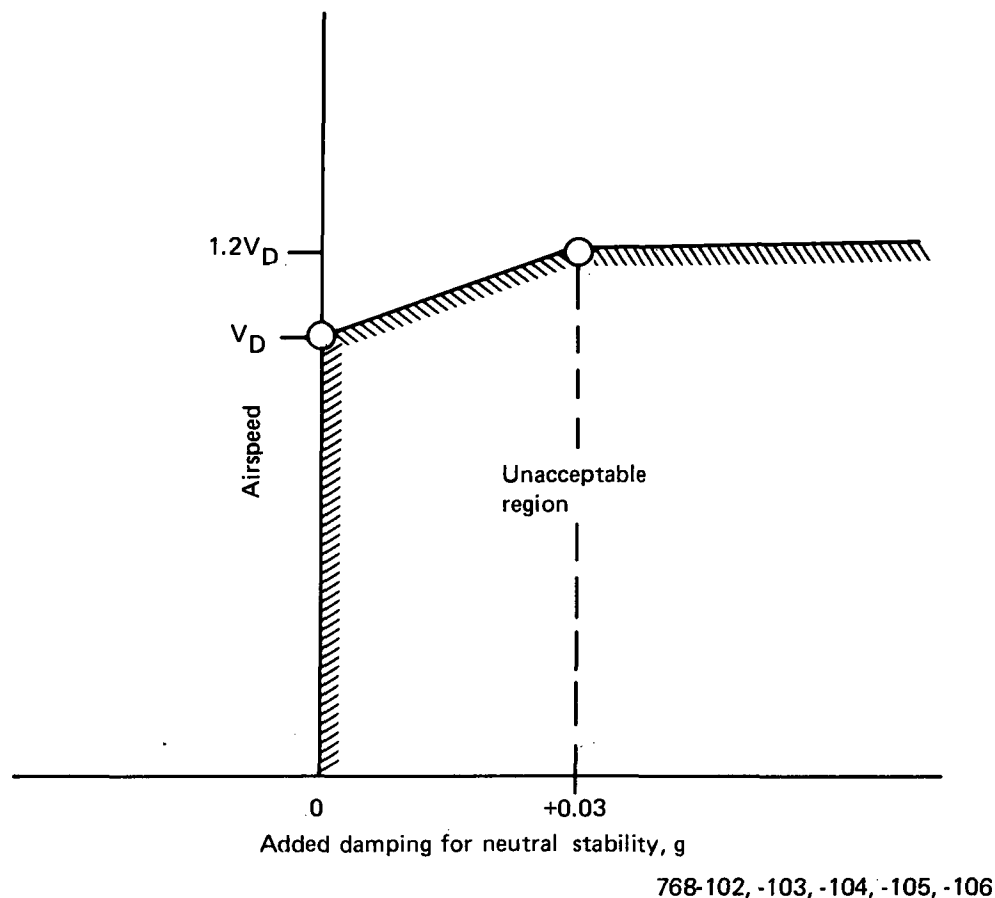
Figure 99. Flutter Criterion for Structural Damping

Initial ACT Configuration, which required added stiffness, a reserve fuel tank, and an FMC system for satisfactory flutter clearance (fig. 102).

The indicated flutter boundaries were established from V-g solutions at four altitudes. A factor, C_c, based on the variation of wing lift-curve slope with Mach number (fig. 103) was used to adjust the flutter speeds from the V-g solutions to account for variations in Mach number. A typical V-g solution is shown in Figure 104 and illustrates the "hump" character of the soft 3 Hz inboard wing symmetric flutter mode and the "explosive" character of the hard 7 Hz outboard wing symmetric flutter mode.

Five wing fuel distributions were analyzed for symmetric flutter (0, 20, 50, 80, and 100% full) and three distributions for antisymmetric flutter (0, 80, and 100% full). The variation of flutter speed with fuel distribution for the critical 3 and 7 Hz symmetric flutter modes is illustrated in Figure 105.

162
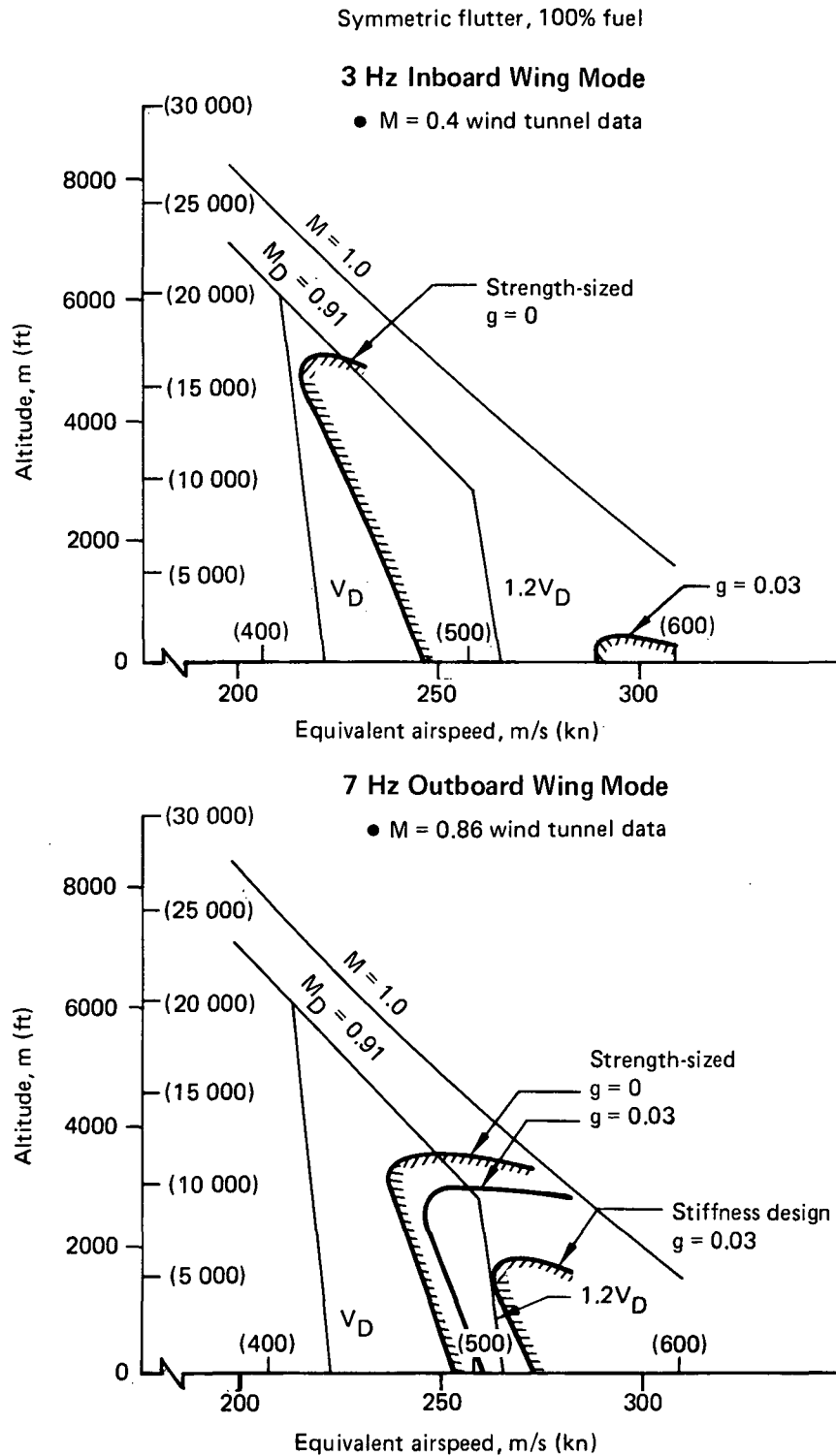
Figure 100. Flutter Boundaries for Model 768-104

163
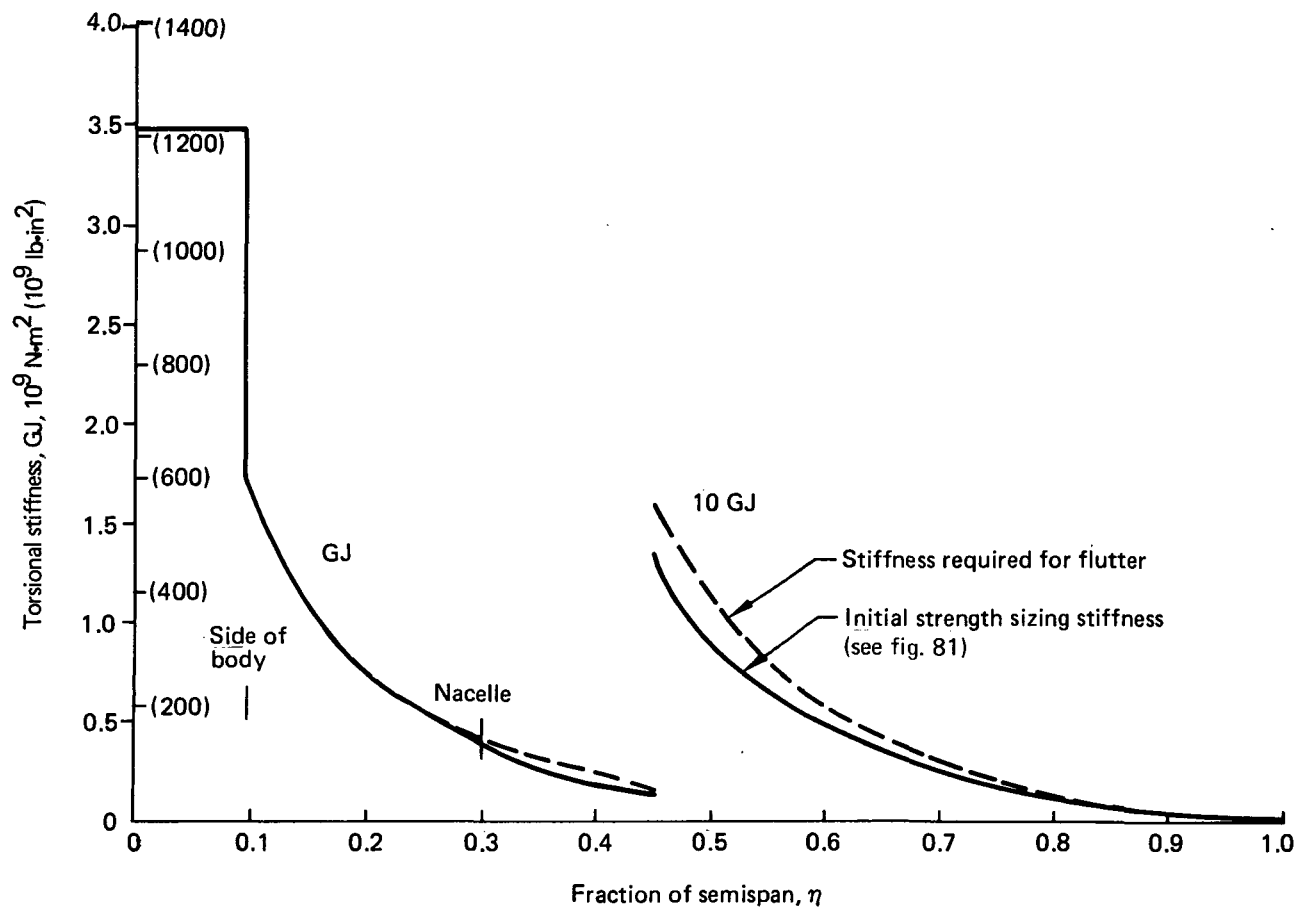
Figure 101. Wing Torsional Stiffness Required for Flutter, Model 768-104
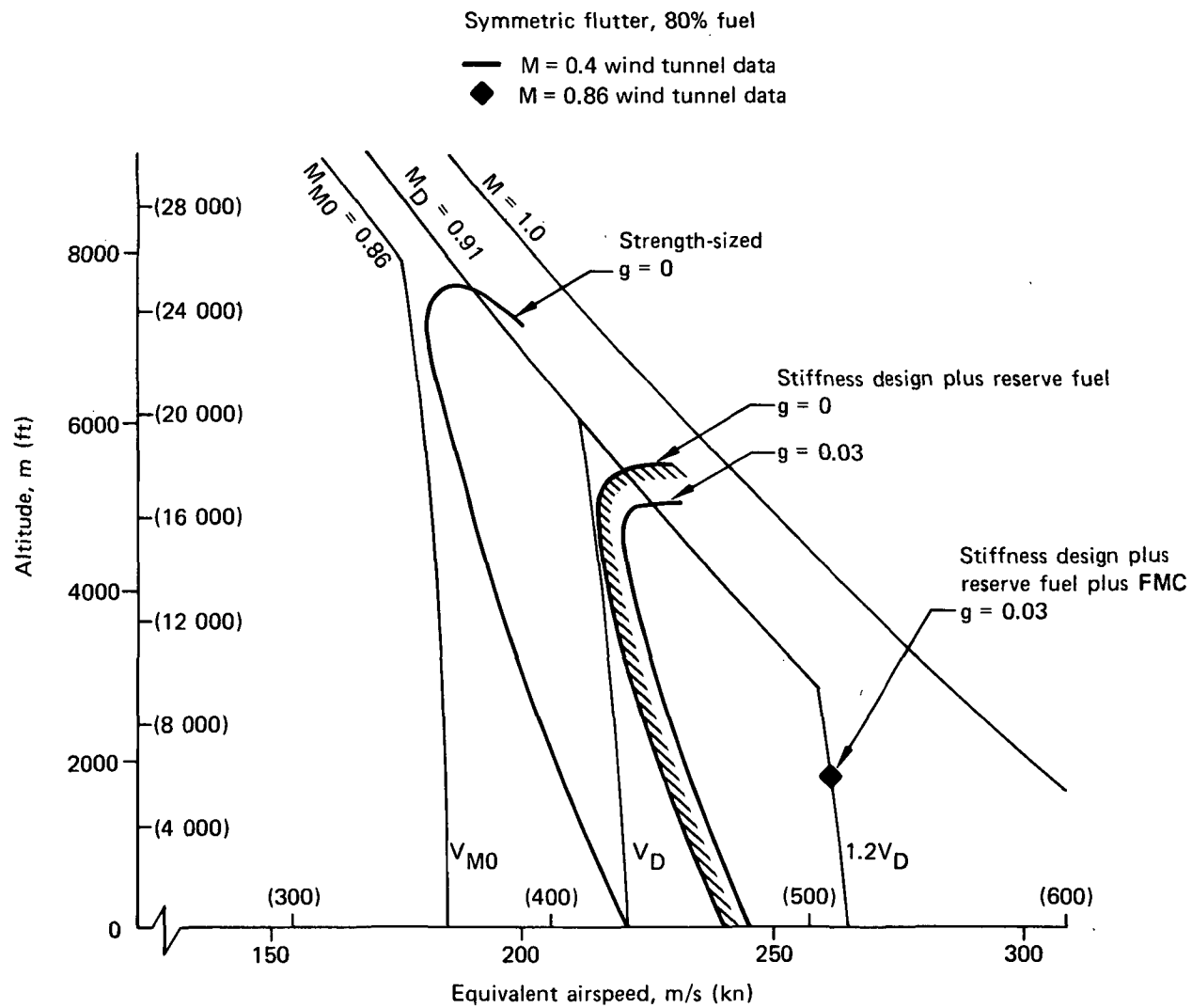
Figure 102. Flutter Boundaries for Initial ACT

768-103

165

Flutter speed, $V = C_c V_{INC}$

where V_{INC} = incompressible flutter speed

$$C_c = \left(\frac{C_{L_{\alpha_{M = 0.4}}}}{C_{L_{\alpha_M}}} \right)^{\frac{1}{2}}$$

Rigid wing + nacelle	
M	C_{L_α} per deg
0.4	0.0810
0.5	0.0828
0.6	0.0880
0.65	0.0930
0.7	0.0990
0.75	0.1062
0.775	0.1105
0.8	0.1150
0.86	0.1236
0.91	0.1125
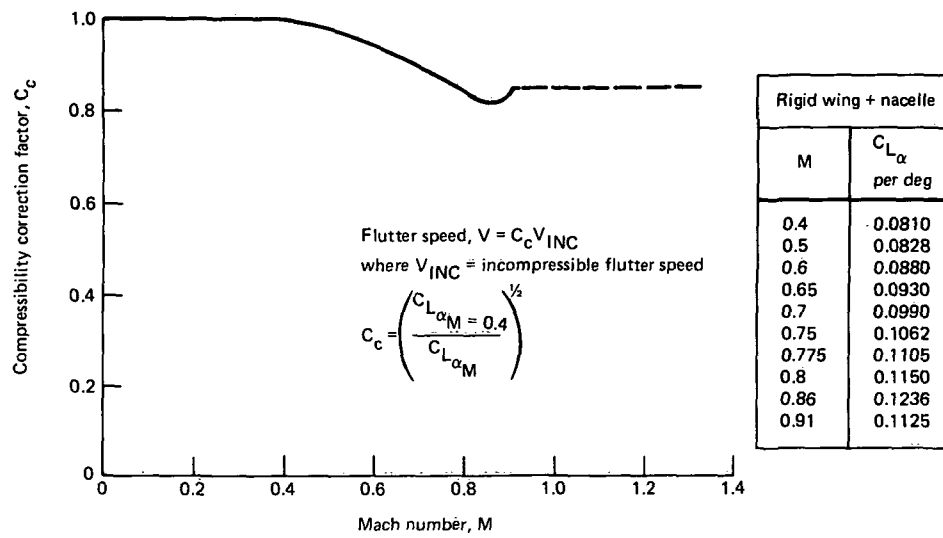
Figure 103. Compressibility Corrections for Incompressible Flutter Speeds, Model 768-104

Conditions:
- Full fuel
- Symmetric flutter
- Sea level
- Strength design
- M = 0.4 wind tunnel aerodynamic data

——— 3 Hz inboard wing mode

- - - - - 7 Hz outboard wing mode
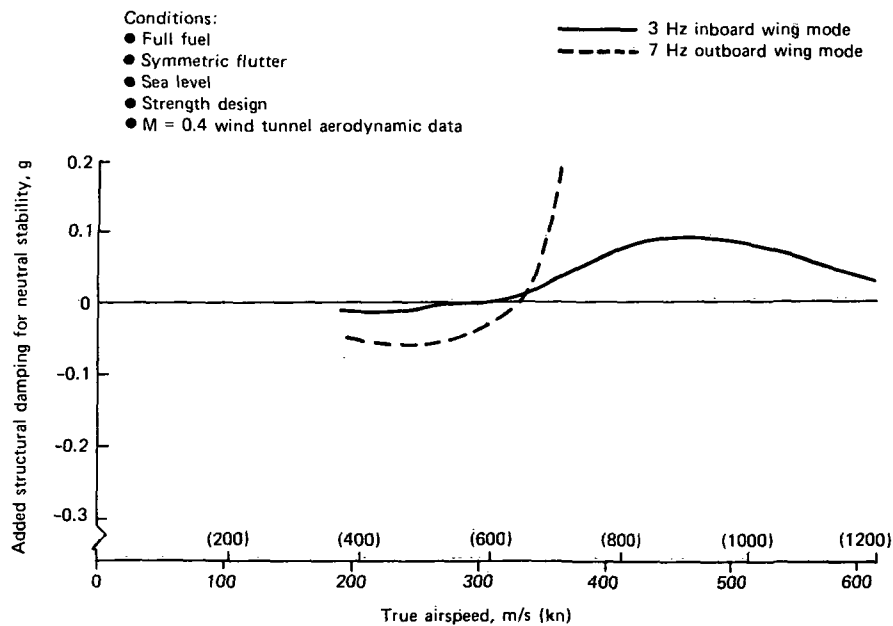
Figure 104. Typical Flutter V-g Solution, Model 768-104
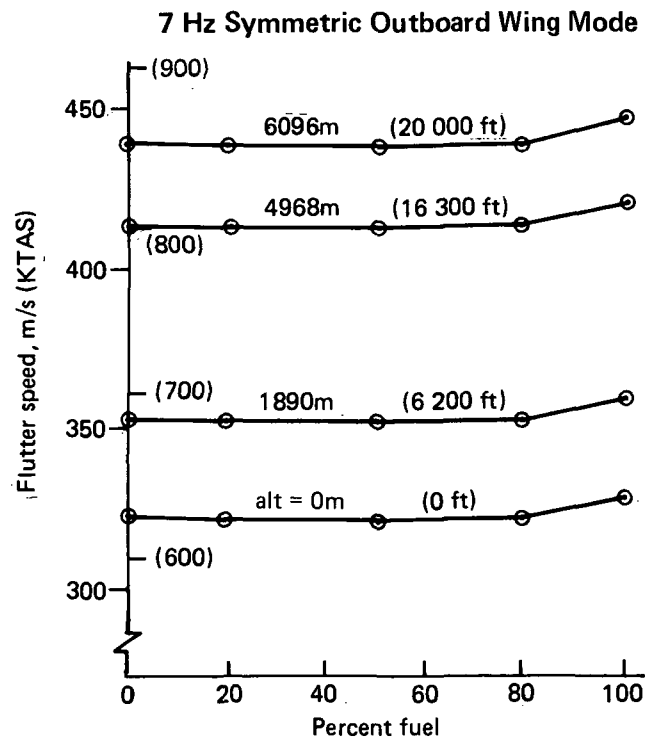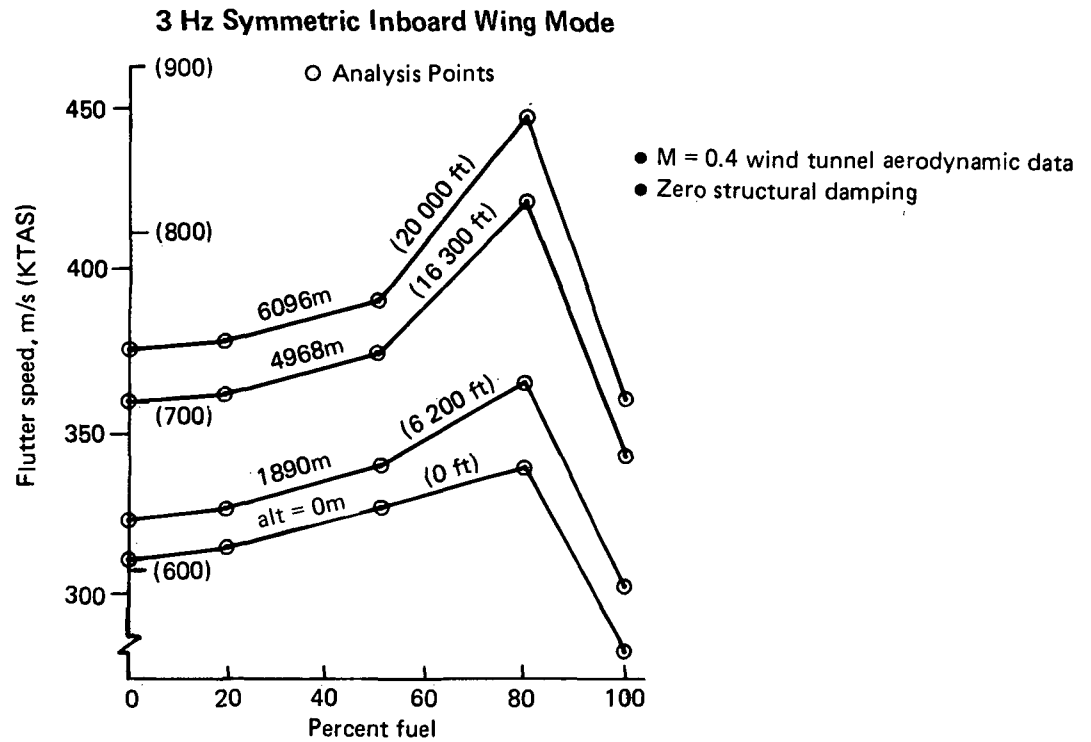
Figure 105. Variation of Flutter Speed With Wing Fuel

167

7.2.2.3 Fatigue Results–Model 768-104

A detailed wing fatigue analysis was done for the critical short-range mission, 567 km (306 nmi), based on the requirements of the IAAC DRO. Benefit was taken for reduction in the alternating stresses in the fatigue stress profile due to action of the selected ACT functions; however, an additional 125 kg (275 lb) of theoretical wing-box structural material was required in the wing lower surface (fig. 87) relative to the initial strength sizing to satisfy life-goal requirements. The flight profile and load condition spectrum (fig. 106) used in the fatigue analysis were the same as those used for the Baseline and Initial ACT Configurations. The simplified profile, applied cycles, and load increments are listed in Table 11.

7.2.2.4 Horizontal Tail and Fuselage Loads–Model 768-104

The horizontal tail and fuselage design load envelopes estimated for the Model 768-104 are compared with the design load envelopes for the Initial ACT and Baseline Configurations in Figures 107 and 108. These results are for estimating weight increments for the Model 768-104, in lieu of a more complete structural analysis, using detailed data available for the Baseline Configuration.

The horizontal tail load envelopes include critical steady-state, abrupt, and check maneuver conditions. For the Model 768-104 Configuration, the conditions with pitch acceleration were based on time-history analysis of airplane response to selected elevator inputs based on available elevator blowdown limits and by FAR maximum pitch-acceleration criteria. The reduction in tail pitching moment indicated for the Model 768-103 and -104 Configurations, relative to the Baseline Configuration (fig. 107), is due to a reduction in tail chord for these configurations. Although the design airload for the Model 768-103 and -104 was estimated to be a little less than for the Baseline Configuration, the load per unit area increased due to a 45% reduction in tail area from 57.6 m^2 (620 ft^2) for the Baseline to 31.96 m^2 (344 ft^2) for the Model 768-103 and -104.

The aft-body bending moment envelope for the Model 768-104 increased relative to the Model 768-103 envelope due to an increase in balancing tail load for the critical

- TOGW = 107 955 kg (238 000 lb)
- Fuel = 12 066 kg (26 600 lb)
- cg location = 21.4% MAC
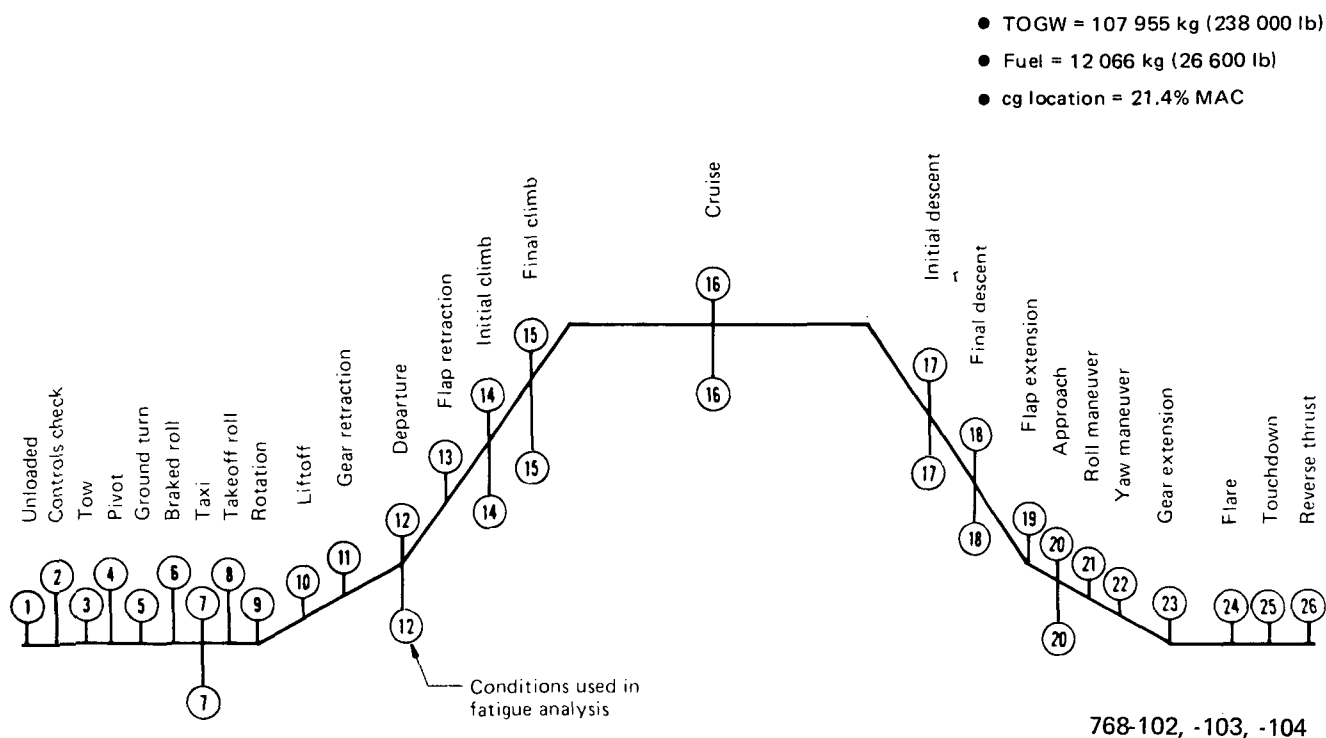
Figure 106. Flight Profile for Fatigue Analysis

Conditions used in fatigue analysis

Table 11. Fatigue Segment Distribution, Short-Flight 567 km (306 nmi) Mission, Summary Calculation

Condition number	Segment	Length		Cycles/ flight	g or gust velocity
		km	(nmi)		
7	Taxi	0	0	8	1 ± 0.3g
12	Depart	0	0	2	1 ± 0.3g
14	Initial climb	15	(8)	2	± 3.05 m/s (± 10 ft/s)
15	Final climb	100	(54)	2	± 2.74 m/s (± 9 ft/s)
16	Cruise	331	(179)		
	Gust			3	± 3.05 m/s (± 10 ft/s)
	Maneuver			2	1 ± 0.3g
17	Initial descent	104	(56)	2	± 2.74 m/s (± 9 ft/s)
18	Final descent	17	(9)	2	± 3.05 m/s (± 10 ft/s)
20	Flaps down approach	0	0	2	1 ± 0.3g

169
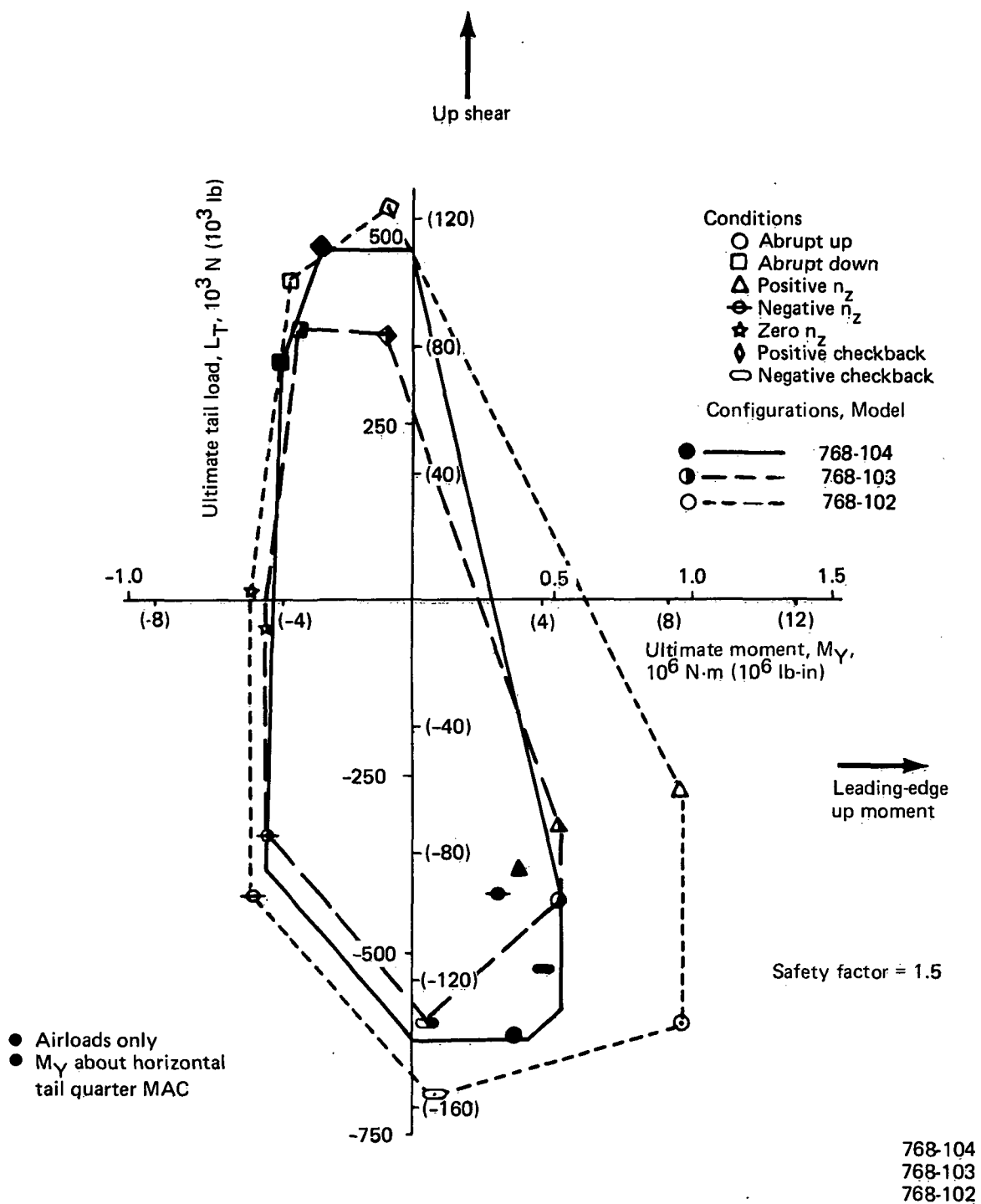
Figure 107. Comparison of Horizontal Tail Design Load Envelopes
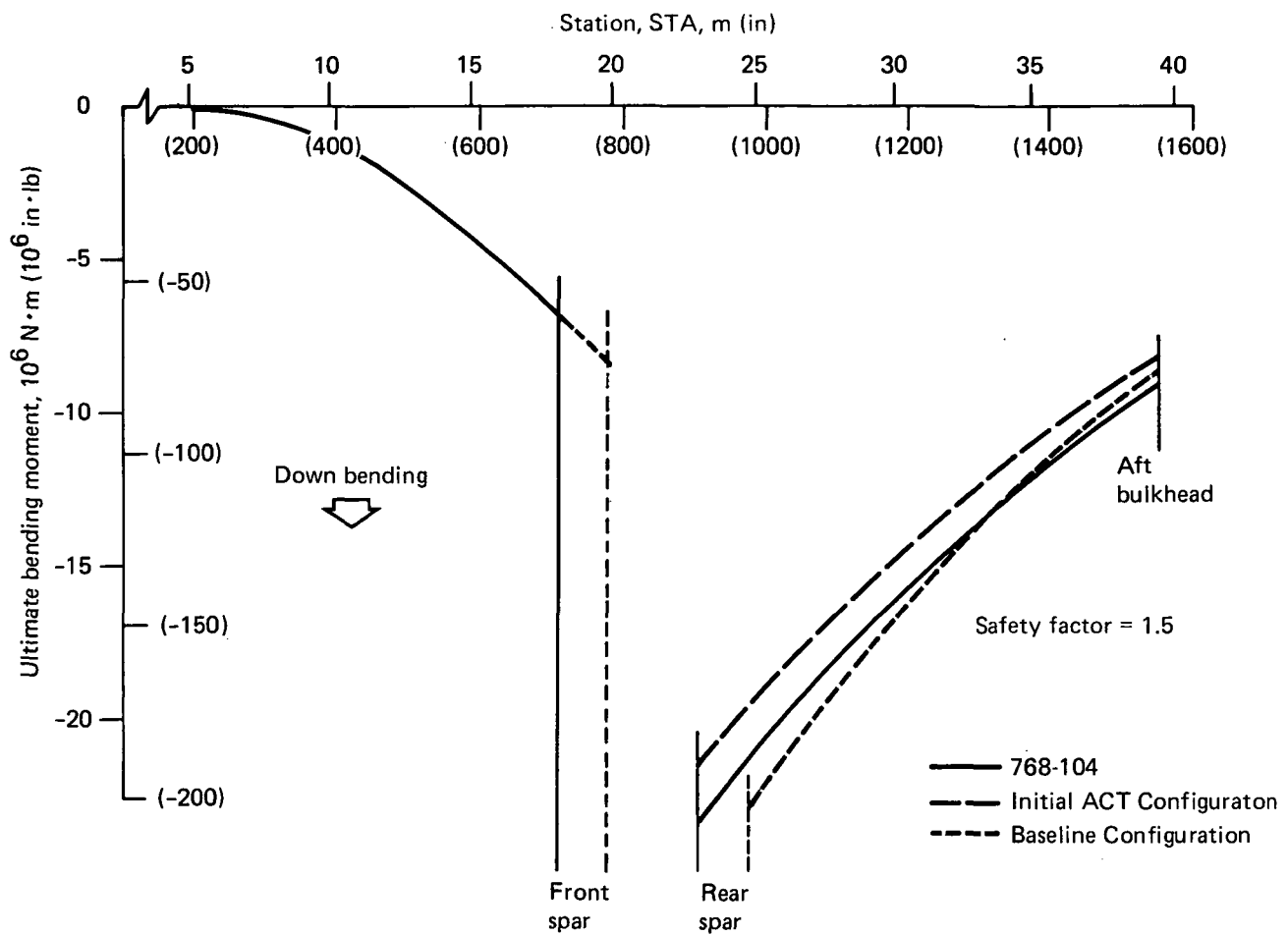
Figure 108. Fuselage Bending Moment Comparisons, Model 768-104 Versus Baseline and Initial ACT

maneuver conditions (fig. 108). The increase in balancing tail load resulted from a more nose-down wing-body aerodynamic pitching moment and a more forward cg limit for this configuration.

7.3 CONTROL SYSTEM ANALYSIS

7.3 CONTROL SYSTEM ANALYSIS

The control system analysis and synthesis conducted to support the Wing Planform Study is described in this subsection. Control system activity was concentrated on the high aspect ratio (768-104) configuration. Initial ACT Configuration control law work, which has not been previously documented, also is included. The control law synthesis is described in Subsection 7.3.1. A description of the proposed system mechanization appears in Subsection 7.3.2.

7.3.1   CONTROL LAW SYNTHESIS

Control laws were developed for four active controls functions; pitch-augmented stability (PAS) and maneuver-load control (MLC), which are low-frequency functions, and gust-load alleviation (GLA) and flutter-mode control (FMC), which are high-frequency functions. The MLC and GLA functions are combined into the wing-load alleviation (WLA) function. The flying qualities requirements described in Subsection 7.1 and the structural requirements discussed in Subsection 7.2 were used as guidelines for control law development. The control laws for the PAS system were developed using the same QSAE models discussed in Subsection 7.1. For the WLA and FMC systems, the control laws were developed using the dynamic models, described in Subsection 7.3.1.1, which are compatible with the structural models included in Subsection 7.2. The WLA and FMC systems were synthesized separately, each with a simplified PAS system.

Subsection 7.3.1.2 describes the updated PAS control laws for the Initial ACT Configuration and the PAS for the Wing Planform Study Configuration (768-104). The augmented flying quality characteristics also are included in this subsection.

In Subsection 7.2, augmented gust loads results are shown. The control laws used in that analysis contain an early version of the WLA. Because the GLA part of the system offered only modest weight benefits at the cost of high control surface rates, it was deleted from the Model 768-104 design. Subsection 7.3.1.3 contains an account of the synthesis of the final WLA control laws, which show improved performance. In both analyses, simplified PAS control laws were used.

173

Subsection 7.3.1.4 describes the updated FMC control laws and the associated gain and phase margins for the Initial ACT Configuration. The synthesis of FMC control laws to control an explosive wing-tip flutter mode on the Model 768-104 is also shown in Subsection 7.3.1.4. The control surface rates were excessive; thus, the FMC function was not included in the Model 768-104.

7.3.1.1 Dynamic Modeling

This subsection contains a description of the developments in dynamic modeling that occurred since the Initial ACT Study (ref 3) and their application to the Wing Planform Study. The development activity concentrated on the technique for providing load equations for GLA studies. Models were produced for one configuration—the Model 768-104. Appendix B of this document contains a detailed description of the theory.

Reference 3 details the features of the dynamic model chosen to provide a single mathematical model for the development of control laws for an integrated active controls system. The various features of the aeroelastic analyses used to assess flying qualities, calculate maneuver and gust loads, and predict flutter speeds are tabulated in Reference 3. Also included in the reference are the features chosen for the dynamic model on the Initial ACT Configuration.·

Table 12 shows the modeling features of the Wing Planform Study. The most significant change in these features is that gust loads in the Wing Planform Study were analyzed by using the same lifting surface aerodynamic theory (doublet-lattice) that was used for flutter analysis. Both unsteady and quasi-steady analyses (subsec 7.2) were conducted with a cantilevered structural constraint. Improvements in the computing program used to introduce empirical corrections enabled consistent lift and moment corrections to be used on all the dynamic analyses.

Figure 109 shows the wing-load stations, wing-mounted control surfaces, and sensors included in the dynamic model. The sensors are located at nodes in the structural model and are labeled with the node numbers. Symmetric/longitudinal equations were provided for two weight conditions (table 13). The first was chosen to provide a critical case for outboard wing flutter (100% fuel), with payload added to bring the cg near the aft limit. The second is critical for wing loads due to vertical

174

Table 12. Comparison of Modeling Features

Modeling features		Flying qualities	Maneuver loads	Gust loads	Flutter	Control law development[a]
Structure	Idealization		Statically determinate beam (elastic axis)			
	Mass	Contained in aeroelastic corrections from maneuver loads analysis	Lumped	Lumped	Lumped	Lumped
	Stiffness		Bending and torsion	Bending and torsion	Bending and torsion	Bending and torsion
	Constraint		Cantilevered	Cantilevered	Cantilevered	Cantilevered
	Technique			Modified theory		
Aerodynamics	Theory		Lifting line with three-dimensional induction	Lifting surface	Lifting surface	Lifting surface
	Unsteady representation	Potential flow for low-frequency damping only	Quasi-steady	Quasi-steady with lift growth Full unsteady (frequency dependent)	Full unsteady (frequency dependent)	Full unsteady with S-plane transformation
	Empirical correction technique	Direct application of rigid wind tunnel data	Lift and moment distribution by downwash	Lift and moment distribution by pressure	Lift and moment distribution by pressure	Lift and moment distribution by pressure
	Empirical data source	Wind tunnel force model	Wind tunnel force and pressure model	Wind tunnel force and pressure model	Wind tunnel pressure model	Wind tunnel force and pressure model
Motion reference axes		Body-fixed	Body-fixed	Inertia	Inertia	Body-fixed
Load coefficient technique		—	Load summation	Load summation	—	Modal displacement

[a] Dynamic model

768-104

175
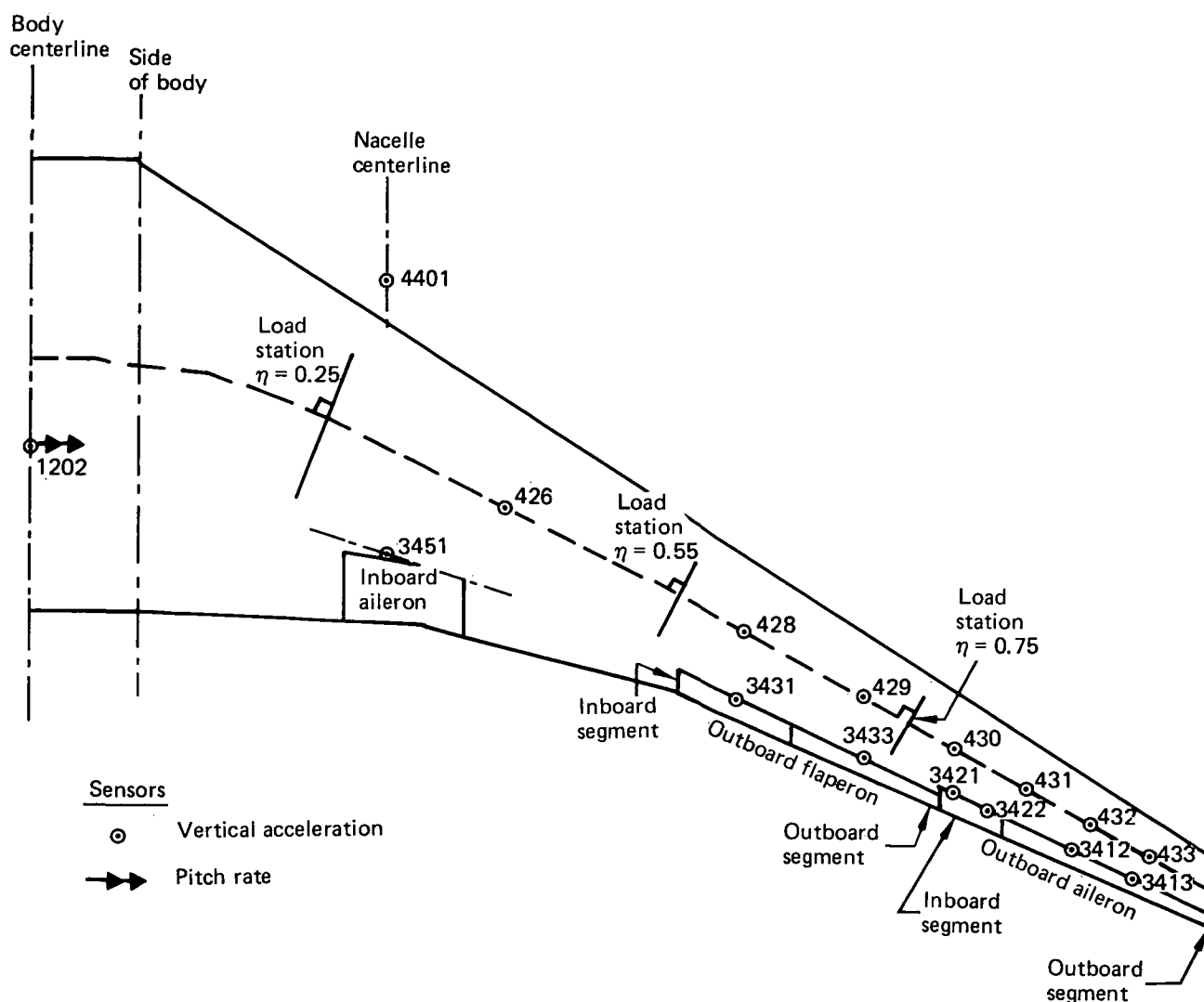
Figure 109. Modeled Wing Controls and Sensors

gust; i.e., 45.5% fuel with the cg at the forward limit. As on the Initial ACT Configuration, only one Mach number was considered. Figure 110 shows the matrix form of the equations, including the load equations.

The Initial ACT dynamic model correlates well with the handling qualities and flutter analyses, but gust load correlation is not good (ref 3). On the Wing Planform Study, the handling qualities and flutter characteristics show correlation similar to the Initial ACT Configuration. Note that for the high aspect ratio configuration, the critical flutter mode is a high-frequency explosive outboard wing mode instead of the low-frequency soft inboard wing mode exhibited by the Initial ACT Configuration. Despite

Table 13. Symmetric Conditions

Flight condition	Center of gravity, percent MAC	Mach No.	Equivalent airspeed, m/s (kn)	Altitude, m (ft)
100% fuel, V_{MO}	46	0.86	175 (341)	7 833 (25 700)
100% fuel, V_D	46	0.86	214 (416)	4 968 (16 300)
100% fuel, $1.1V_D$	46	0.86	239 (465)	2 743 (9 000)
100% fuel, $1.2V_D$	46	0.86	261 (508)	1 890 (6 200)
MZFW + 45.5% fuel, V_B	17.4	0.86	142 (276)	10 668 (35 000)
MZFW + 45.5% fuel, V_{MO}	17.4	0.86	175 (341)	7 833 (25 700)

768-104

● V_g = gust velocity

● δ_{com} = pilot command

768-104

Figure 110. Matrix Form of Equations of Motion

the high frequency (about 7 Hz), the dynamic model flutter speed is within 5.1 m/s (10 kn) equivalent airspeed of the flutter analysis result. Table 14 shows a list of branch modes included in the dynamic model for the 100% fuel case.

In Figures 111 and 112, bending moments predicted by the dynamic model (shown by the symbols) are contrasted with those calculated in the unsteady gust-loads analysis both for the unaugmented (controls fixed) case and the augmented (PAS, MLC, and GLA) case. Figure 111 shows the response to random turbulence, and Figure 112 shows the response to a FAR-25 type discrete gust consisting of one cycle of a one-minus-cosine time history. Generally, the correlation is better near the wing root than near the tip, better for random gust than for discrete, and better at low speeds than at high. The effect of closing the loop is consistent between the two analyses.

There are two areas in which the dynamic model differs from the gust loads analysis: the modal displacement technique (table 12) and the S-plane transformation.

Table 14. Modes Included in Symmetric Model 100% Wing Fuel, Aft Center of Gravity

Branch	Frequency, Hz	Dominant modal characteristic
Fore body	3.99	First vertical bending
Aft body	2.07	First vertical bending
	7.17	Second vertical bending
Vertical tail	5.60	First vertical bending (in plane)
	29.0	Second vertical bending (in plane)
Horizontal tail	5.91	First vertical bending
	18.7	Second vertical bending
	23.9	First torsion
Wing	1.24	First vertical bending
	2.80	Second vertical bending
	3.19	First fore/aft bending (in plane)
	4.64	First torsion
	6.10	Third vertical bending
	7.09	Second fore/aft bending (in plane)
	9.73	Fourth vertical bending
	11.5	Second torsion
Nacelle	2.60	Side bending
	4.63	Vertical bending
	5.76	Roll/side bending

768-104

178
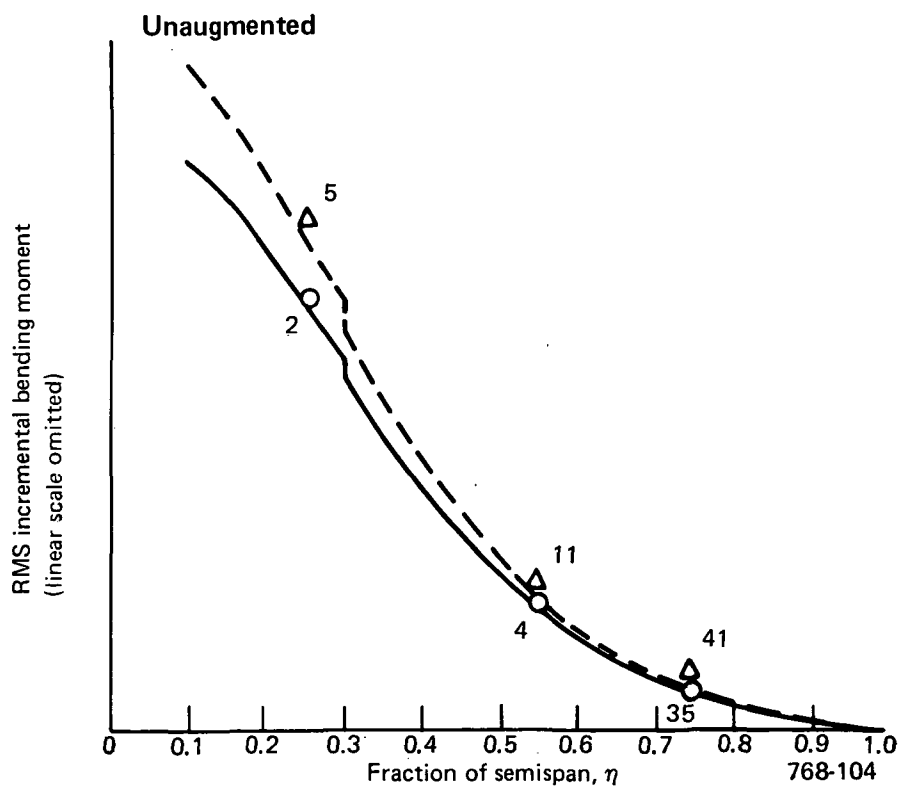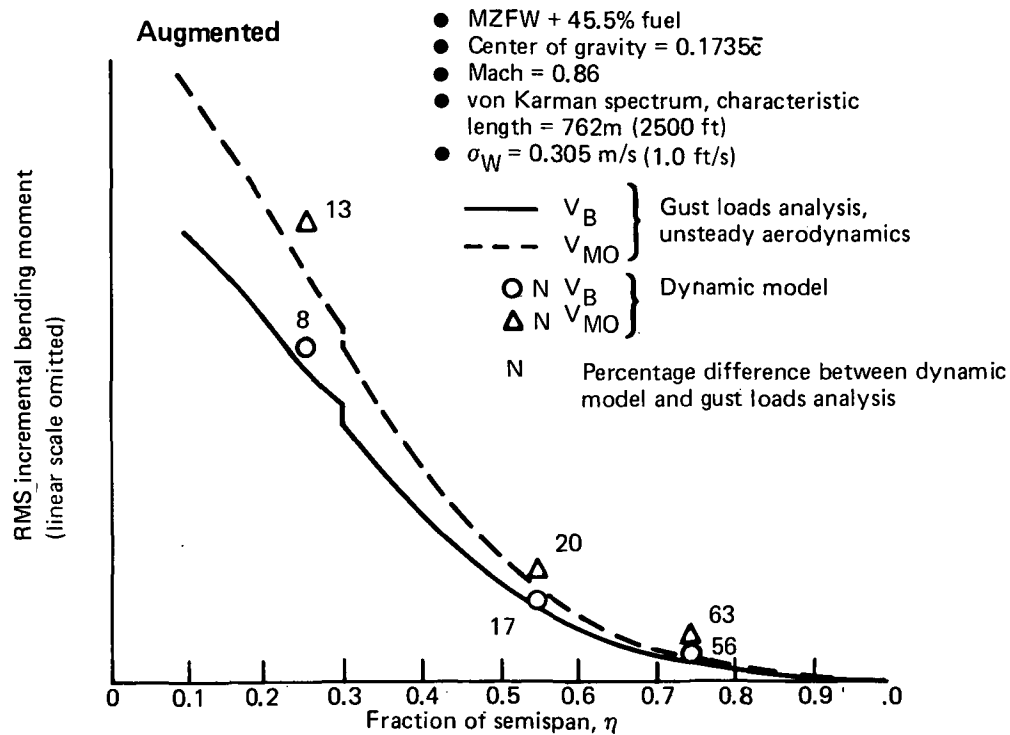
Figure 111. Wing Loads Due to Random Turbulence

768-104

179

Augmented

- MZFW + 45.5% fuel
- Center of gravity = $0.1735\bar{c}$
- Mach = 0.86
- 1-cosine (wavelength = $25\bar{c}$)
- V_B peak gust velocity 28.5 m/s (93.4 ft/s)
- V_{MO} peak gust velocity 20.8 m/s (68.4 ft/s)

—— V_B } Gust loads analysis,
—— V_{MO} } unsteady aerodynamics
⊙N V_B }
△N V_{MO} } Dynamic model

N Percentage difference between dynamic model and gust loads analysis

Unaugmented
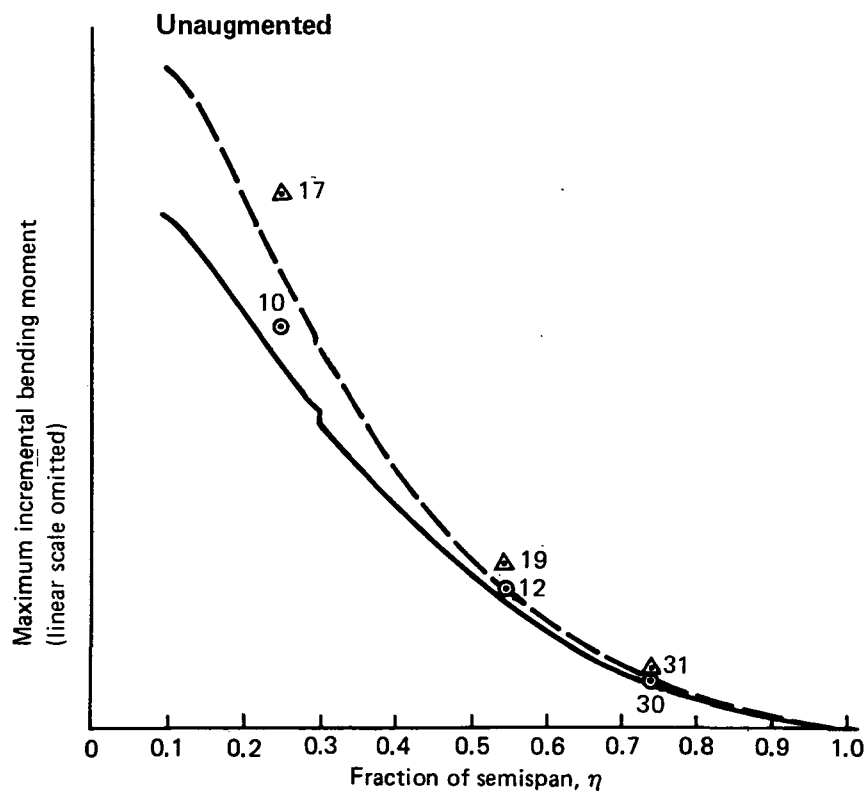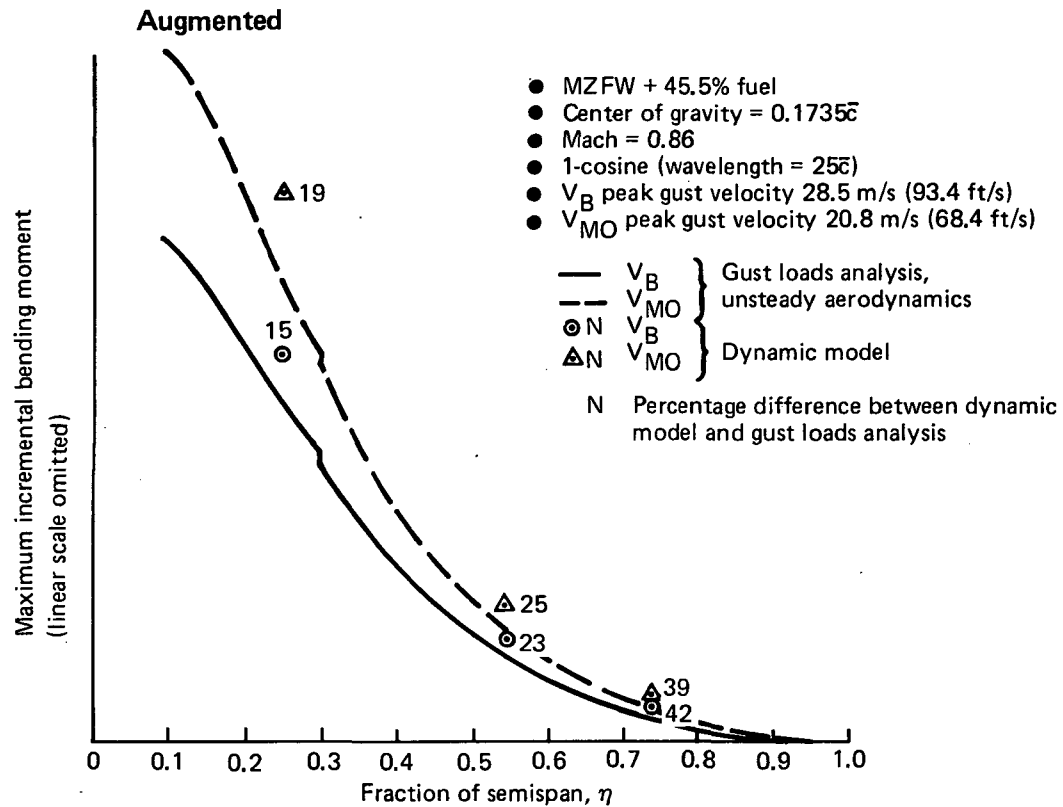
Figure 112. Wing Loads Due to Discrete Gust

768-104

180

The modal displacement method used on the IAAC Project is unique (Appendix B contains a full explanation). Briefly, it consists of finding a relationship between a preselected set of nodal forces and moments and the generalized displacements and then integrating the forces and moments to give shear, bending moments, and torsions in terms of the generalized displacements. For the bending moments in Figures 111 and 112, vertical forces at nodes 426, 428, 431, 433, and 4401 and moments in the pitch direction at nodes 429, 430, and 432 were selected (see fig. 109). The accuracy of the method can be seen in Figure 113, in which both rigid and aeroelastic load coefficients due to the three most important motion variables (angle of attack, outboard aileron deflection, and normal acceleration) are contrasted with the same data calculated in the maneuver-loads analysis. Appendix B contains a detailed account of how these data were calculated from the dynamic model. In summary, the data were calculated by neglecting forces due to elastic rates and accelerations and performing a static-elastic reduction of the whole set of equations shown in Figure 110. The reduced equations contain aeroelastic load coefficients. A rigid version is obtained by scaling the structural stiffness by a large number (in this case 10^4). Experiments were conducted using different values for this artificial scalar, and it was found that the load coefficients converged to three significant figures at a value of 10^4. Comparing the rigid load coefficients between the dynamic model and the maneuver-loads analysis suggests that the modal displacement method is fairly accurate, at least for bending moments. In the elastic case, the correlation is not as accurate. The dynamic model underestimates the losses due to aeroelasticity; this is particularly noticeable in the load due to aileron. Because poor correlation of torsion load was noted in the Initial ACT Study, in the Wing Planform Study two additional wing modes, one of which is predominantly torsion, were added to the dynamic model to improve the correlation. Despite this addition, the correlation remains poor, at least with the choice of the nodal forces and moments mentioned above.

The method used for the S-plane transformation is detailed in Appendix B. Briefly, it consisted of a least-squares fit procedure applied to the generalized aerodynamic force (GAF) matrix that calculated the coefficients in an assumed complex function of the reduced frequency (k). The function was of the form:

$$A_0 + A_1 \, (ik) + A_2 \, (ik)^2 + A_3 \, (ik)^3$$

181
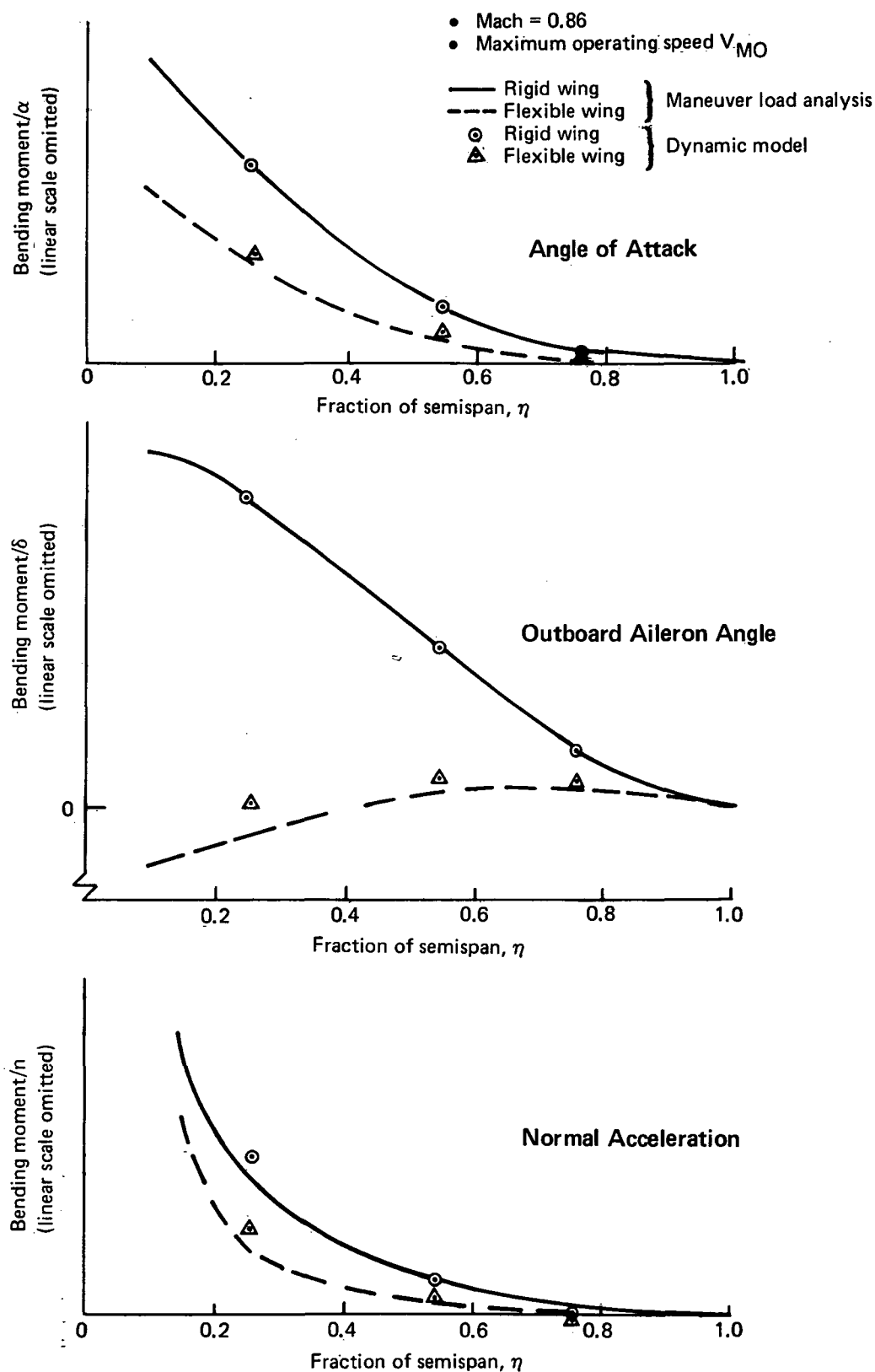
Figure 113. Wing Load Coefficients

768-104

The physically unrealizable cubic term was set to zero. Figure 114 shows a normalized plot of one element of the GAF matrix against k for the frequency-dependent case and for the polynomial approximation with and without the cubic term. The element chosen was the coefficient of first wing bending due to aileron deflection. This gives a rough indication of the change in the influence of the aileron on wing bending moment as frequency increases. The symbols are located on the three plots at the same 5 k-values, and they are labeled to indicate approximately which of the airplane modes dominate. Up to about 7 Hz, the amplitude predicted by the polynomial approximation is within 10% of the frequency-dependent amplitude and the phase error is small. The loss of accuracy from neglecting the cubic term also is small. The graph (fig. 114) suggests that inboard wing-load responses, which are dominated by the short-period

- Mach = 0.86
- Wing bending due to outboard aileron (inboard segment)

—△— Frequency dependent
—⊙— Polynominal approximation, $A_0 + A_1 (ik) + A_2 (ik)^2 + A_3 (ik)^3$
—✗— Polynominal approximation, $A_0 + A_1 (ik) + A_2 (ik)^2$
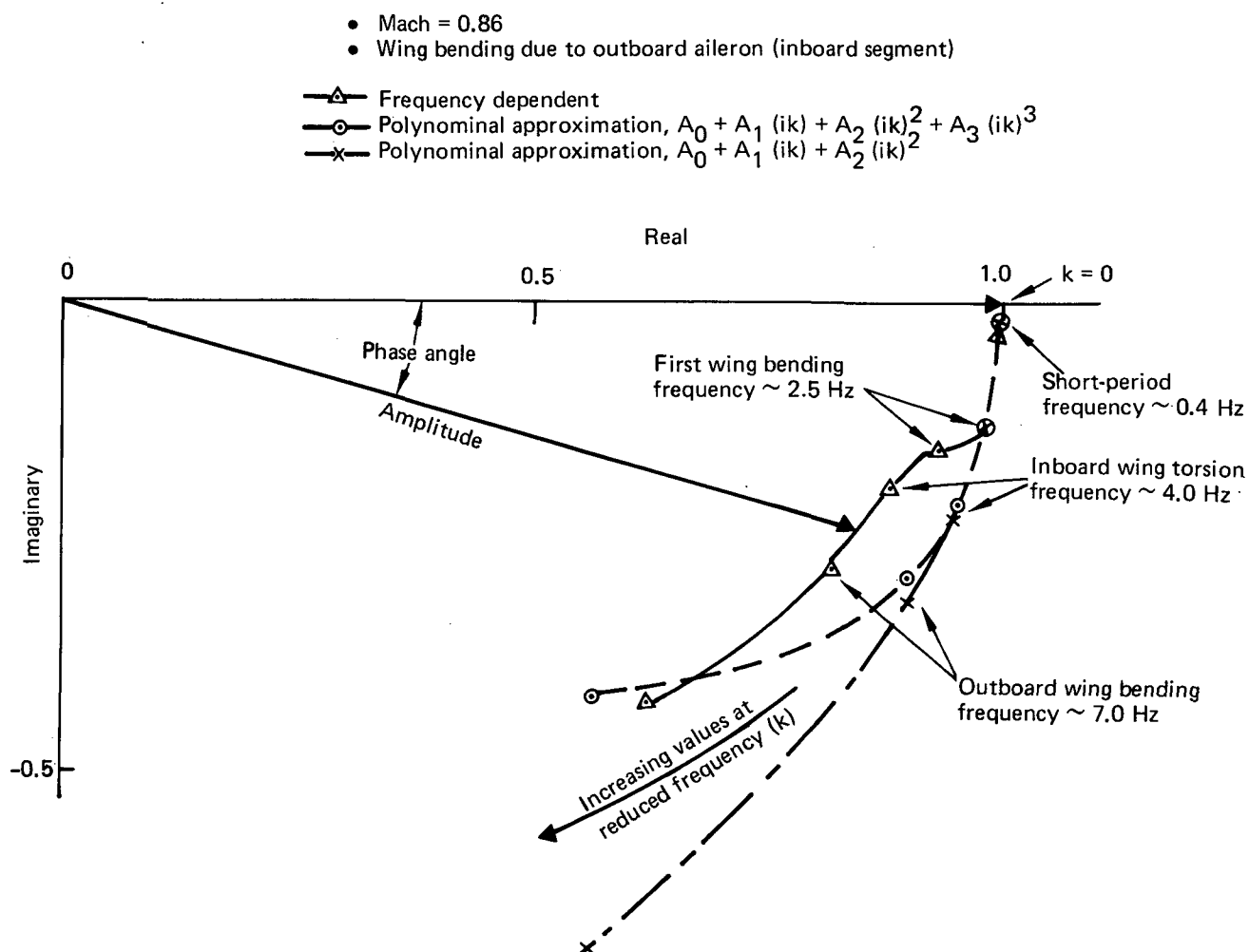
Figure 114. S-Plane Transformation

768-104

183

and first-bending modes, would be fairly accurately represented but the correlation would deteriorate near the wing tip, which is consistent with Figures 111 and 112.

The dynamic model meets the basic objectives. The approximation to the other models listed in Table 12 is accurate enough that the control laws developed using it (see subsec 7.3.1.1-3 and 7.3.1.1-4) performed as expected in the handling-qualities, loads, and flutter analyses. If needed, the accuracy could be improved by using a more elaborate S-plane transformation and by further developing the modal displacement technique.

7.3.1.2 PAS Design

Two PAS control law designs and their performance are discussed in this subsection. The first PAS was designed for the Initial ACT Configuration but was not finished in time to be reported in the Initial ACT Document (ref 3) and is included herein. The second PAS was specifically designed for the Model 768-104 Configuration and incorporates changes based on experience with the Initial ACT control synthesis.

The PAS control loops augment the basic airplane dynamics so that its pitch-rate/column response and its stability and short-period frequency are in compliance with the requirement levels for Level 1 flying qualities. Concurrently, the requirements for control-loop gain and phase margin are satisfied.

Both PAS designs use lagged pitch-rate feedback to the elevator for pitch damping. Pitch-rate feedback alone provides the minimum acceptable augmented flying qualities required of the flight-crucial PAS. The unaugmented airplane is statically unstable at some flight conditions; therefore, the set of free airplane poles contains a positive pole on the real axis. Because of the zero at the origin in the pitch-rate/elevator transfer function, the right-half plane pole cannot be driven to the left-half plane by pitch-rate feedback alone; an additional feedback signal is needed to attain absolute stability. For the Initial ACT PAS, incremental airspeed was the second feedback signal to the elevator. For Model 768-104 PAS, incremental pitch attitude was used as the second feedback signal.

Using speed feedback on the Initial ACT PAS yields an augmented airplane with a pitch-rate to step-column response that meets the DRO handling quality requirements.

184

However, shortly after its initial rise to the peak value, the pitch rate falls off toward zero at a rate that is higher than seems to be desirable.

By making the PAS an attitude-command system and by using the integral of column position as the PAS input command, the early fall-off of pitch rate is eliminated. This scheme was implemented in Model 768-104.

7.3.1.2.1 Initial ACT PAS

Figure 115 shows the PAS block diagram. The PAS synthesis used a QSAE mathematical modeling of the airplane at 11 flight conditions. The flight conditions and associated data (table 15) are plotted on the airplane's flight envelope in Figure 116.

Synthesis Method—As in earlier work, the root locus and system time response were the basic tools used for the design process. The root locus determined system stability, and time response plots were used to evaluate the flying qualities of the augmented airplane.

768-103.
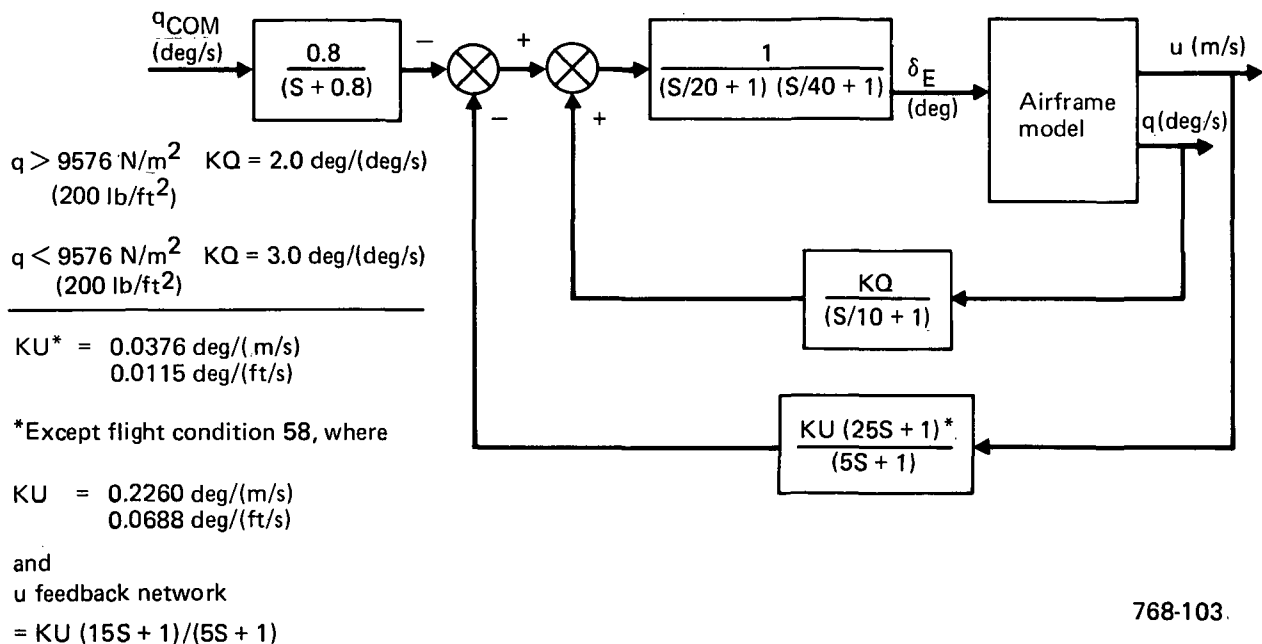
Figure 115. Initial ACT Pitch-Augmented Stability System

185

Table 15. Initial ACT Pitch-Augmented Stability Performance Data

Flight condition	q N/m^2 (lb/ft^2)	Mach	Altitude, m (ft)	cg, percent	Weight, kg (lb)	ω_P	ζ_P	ω_H	ζ_H	σ_1	σ_2	$\frac{q_{max}}{q_{10}}$
99	3 706 (77.4)	0.54	Takeoff	46	122 470 (270 000)	0.097	0.80	4.74	0.80	-0.304	-0.021	1.09
57	4 659 (97.3)	0.38	6 096 (20 000)	21	90 719 (200 000)	0.069	0.29	5.20	0.67	-0.748	-0.169	1.28
59	6 177 (129.0)	0.38	3 962 (13 000)	46	122 470 (270 000)	0.089	0.97	5.51	0.63	-0.466	-0.031	1.14
97	2 384 (49.8)	0.38	Landing	46	90 719 (200 000)	0.129	0.81	4.17	0.98	-0.358	-0.003	1.07
17	8 906 (186.0)	0.65	9 144 (30 000)	46	122 470 (270 000)	0.053	0.59	6.37	0.46	-0.536	-0.135	1.19
8	10 150 (212.0)	0.38	0	46	122 470 (270 000)	0.075	0.78	5.85	0.60	-0.85	-0.087	1.28
75	12 353 (258.0)	0.86	10 668 (35 000)	21	122 470 (270 000)	0.080	0.59	6.92	0.39	-1.10	-0.18	1.70
13	13 789 (288.0)	0.65	6 096 (20 000)	46	122 470 (270 000)	0.082	0.66	6.30	0.50	-0.742	-0.087	1.31
65	18 865 (394.0)	0.86	7 833 (25 700)	46	122 470 (270 000)	0.10	0.60	7.39	0.37	-0.961	-0.136	1.56
79	19 391 (405.0)	0.84	7 315 (24 000)	46	122 470 (270 000)	0.056	0.62	7.67	0.33	-1.46	-0.161	1.26
58	6 607 (138.0)	0.65	11 125 (36 500)	46	122 470 (270 000)	0.171	0.24	5.53	0.62	-0.362	-0.041	1.84

q_{10} = pitch rate value at t = 10 sec

768-103

Verification of Stability and Flying Qualities–The stability requirements for the augmented airplane are shown in Figure 117. With pitch-rate feedback only, the airplane exhibits Level 2 stability at all flight conditions shown in Table 15 except Conditions 17 and 58. Conditions 17 and 58 exhibit a Level 3 real-root divergence with times-to-double amplitude of 9.8 sec and 8.6 sec, respectively. Closing the speed to elevator-feedback loop with a speed gain (KU) = 0.0115 deg/ft/s through the $(25s+1)/(5s+1)$ lead network yields an augmented airplane that meets Level 1 requirements in frequency, stability, and pitch-rate/column-step response characteristics at all flight conditions except 58. At Flight Condition 58, a $1.2V_S$ high-altitude, heavy-weight case, the unaugmented airplane has a strong pitch-up instability. Increased airspeed gain (KU = 0.0688 deg/ft/s) and a $(15s+1)/(5s+1)$ network was required to stabilize the airplane to Level 1 with adequate gain and phase margin.

186

Figure 116. Speed and Altitude Flight Envelopes

Note: Points correspond to flight conditions of Table 15.
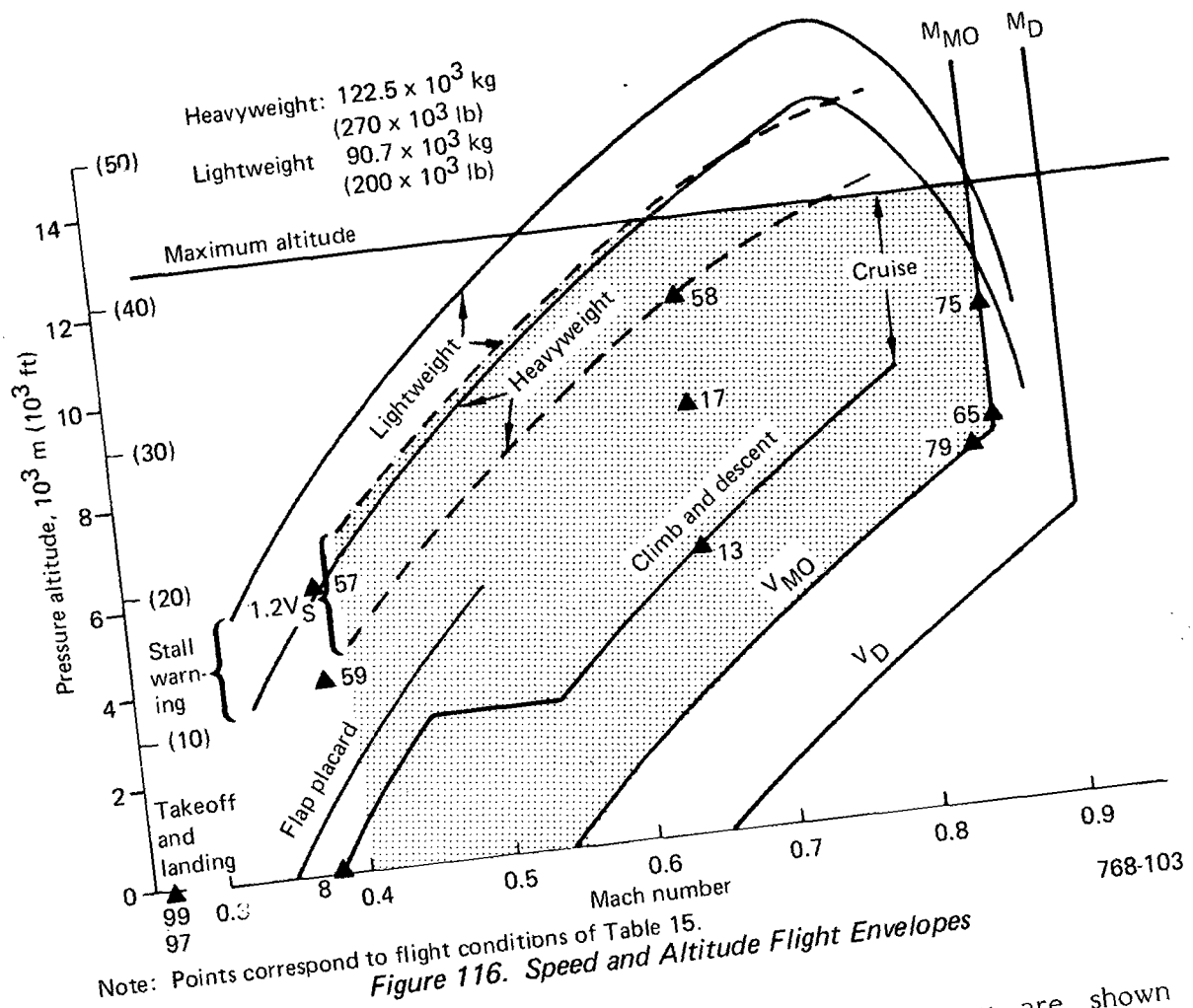
The design requirements on longitudinal short-period frequency are shown in Figure 118. In addition, the ratio of maximum to steady-state pitch rate must be less than:

En route phase

Flying Quality	q_{max}/q_{ss}
Level 1	2.5
Level 2	3.5
Level 3	(not a requirement)

Terminal phase

Level 1	2.0
Level 2	3.0

187
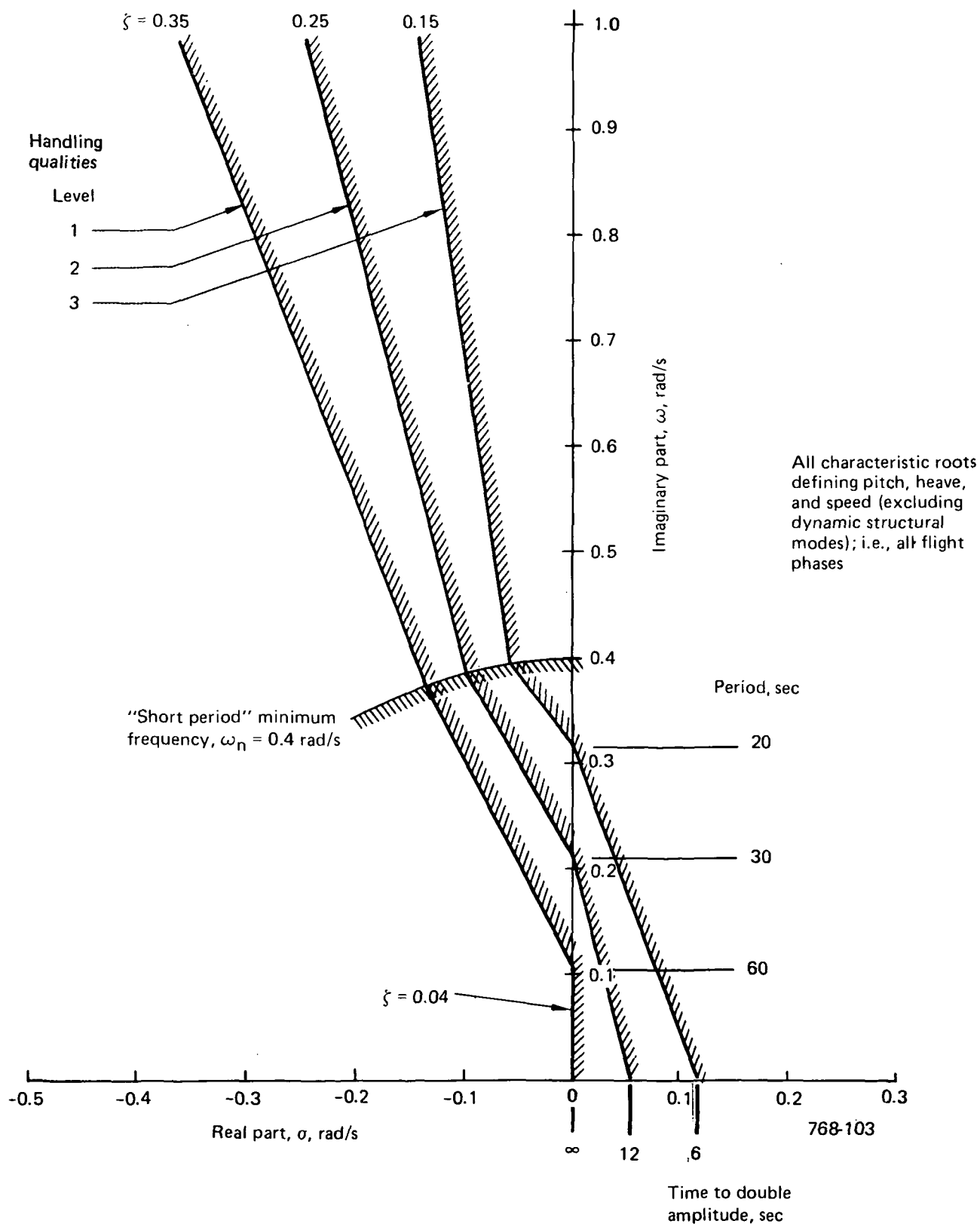
Figure 117. Minimum Damping Requirements—Longitudinal Roots

Figure 118. Flying Qualities Short-Period Requirements

Figure 119 shows the pitch-rate response of the augmented airplane to a 0.5 deg/s column-step command at four flight conditions. It is apparent in this figure that the classical short period cannot be discerned in the responses. By deleting the speed degree of freedom, the short-term response of the airplane is characterized by a cubic $(S+\sigma)$ $(S^2 + 2\zeta_H\omega_H S + \omega^2_H)$. To obtain a frequency value for the ω_{SP} versus n/α plot, each cubic time response was approximated by an appropriate quadratic $(S^2 + 2\zeta_{EQV}\omega_{EQV}S + \omega^2_{EQV})$. The results of this process are the ω_{EQV} data points shown in Figure 118. All the ω_{EQV} are Level 1.

For each pitch-rate time response of the fully augmented airplane, q_{max}/q_{10} was determined where q_{10} is the pitch-rate value at t equal to 10 sec. This ratio was chosen rather than q_{max}/q_{ss} because representative q_{ss} cannot be determined for the type of response considered here. If a small step of pitch-rate command is maintained, the airplane will undergo a modest change in pitch attitude and q will go to zero in 100 to 150 sec. Ten seconds was assumed to be a reasonable maneuver interval. If this assumption is accepted, the q_{max}/q_{10} is Level 1 for all flight conditions. Table 15 lists the values.

Gain and Phase Margin Requirements—Throughout the normal operating envelope for modes greater than 0.5 rad/s, but less than the first flexible mode frequency, the gain margin will be at least ±6 dB, and at nominal gain the phase margin will be at least ±45 deg. For modes with a frequency less than 0.5 rad/s, the gain and phase margins will be at least ±4 dB and ±15 deg throughout the normal operating envelope.

With one exception, all these margin requirements were met. In the speed loop of Flight Condition 97 there is a gain margin of -1.3 dB instead of -4 dB for the low frequency.

7.3.1.2.2 Model 768-104 PAS

Figure 120 shows the block diagram for Model 768-104 PAS. QSAE mathematical modeling of this airplane with the AR 12.0 31.5 deg swept wing was done for the same 11 flight conditions that were used for the Initial ACT PAS synthesis. New aft cg limit and n/α apply (table 16).
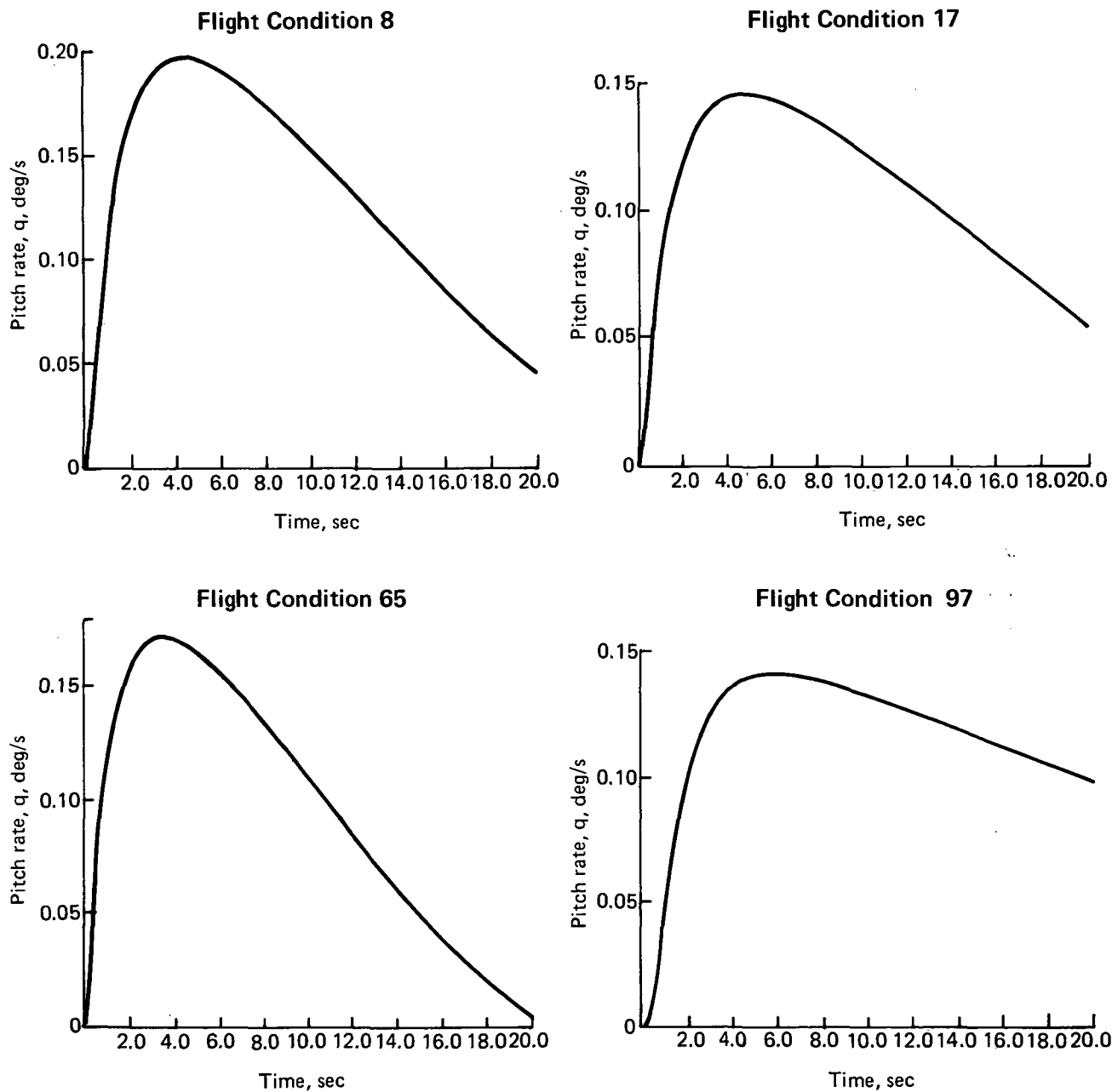
Figure 119. Pitch-Augmented Stability System Response Dynamics to a 0.5-deg/s Pitch Rate Command Step, Model 768-103

Synthesis Method—As in the preceding work, root loci were used for stability determination and time response plots for flying-qualities evaluation.

Figure 120 — Pitch-Augmented Stability System, Model 768-104

Diagram elements: q_{COM} (deg/s) → $\frac{1}{S}$ → SW1 → $\frac{S}{(S+0.6)}$; Actuator $\frac{1}{(S/40+1)(S/20+1)}$ → δE (deg) → Airframe model → θ (deg), q (deg/s); feedback $\frac{KQ}{(S/10+1)}$; $K\theta$ → SW2 → $\frac{(S+1)}{(0.357S+1)}$

Flight condition	KQ	Kθ	SW1	SW2
99	1.0	1.0	Open	Down
57				Up
59				Up
97		1.5		Down
17		1.0		Up
8				
75			Closed	
13			Open	
65			Open	
79			Closed	
58		1.25	Open	Down
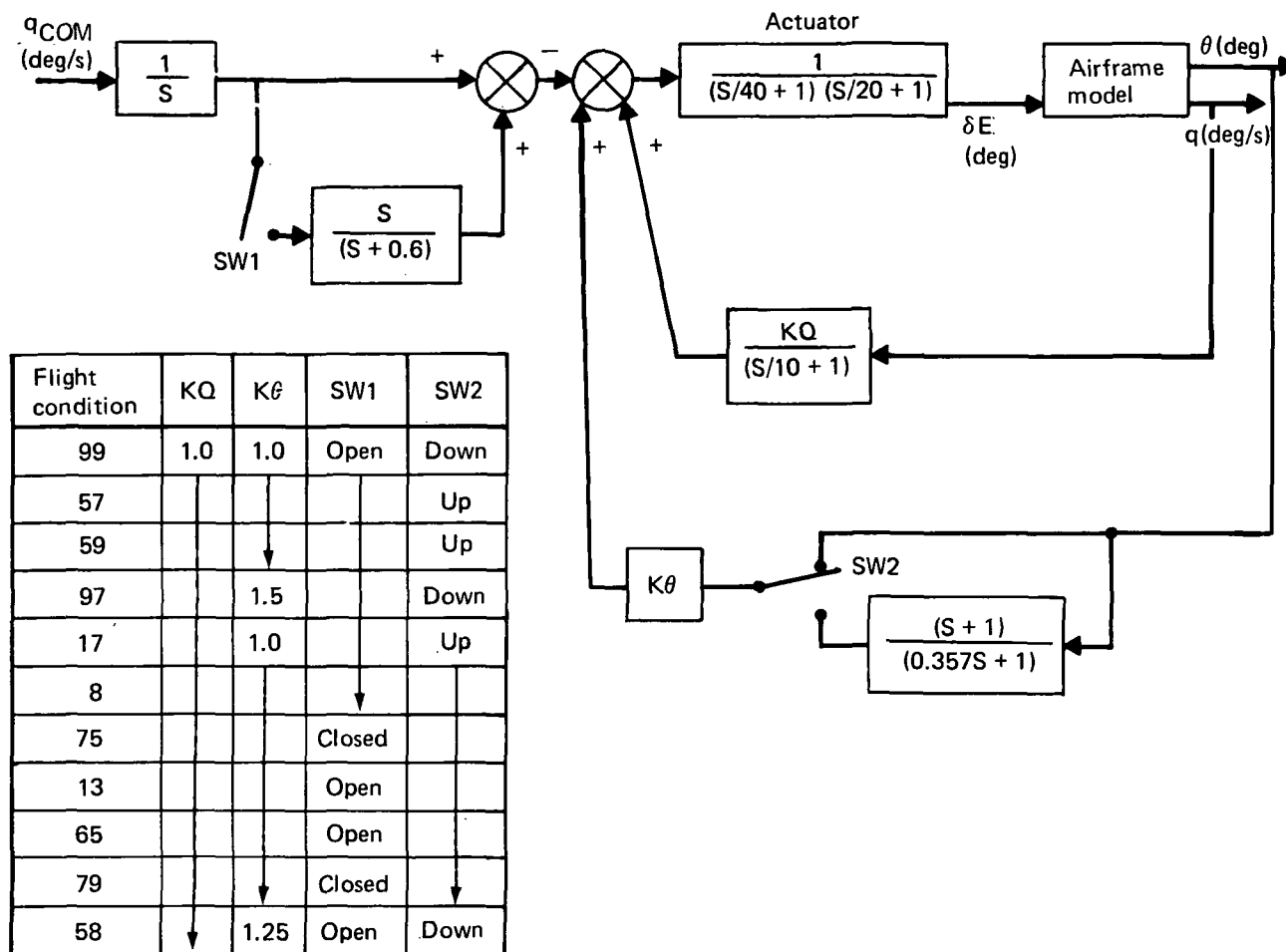
Figure 120. Pitch-Augmented Stability System, Model 768-104

Verification of Stability and Flying Qualities—The stability requirements for the augmented airplane are given in Figure 117. With only pitch-rate feedback, Level 2 stability is obtained at all the flight conditions. The use of pitch-attitude feedback yields Level 1 stability at all conditions and Level 1 flying qualities response characteristics except Flight Conditions 75 and 79. Prefilter tuning improves the apparent frequency response for these conditions to Level 1 requirements. Table 16 lists the augmented airplane poles.

Figure 121 shows the augmented airplane pitch-rate response to a step command of 0.5 deg/s at six flight conditions. The improved response form is evident in a comparison with the Initial ACT PAS responses. The values of ω_{EQV} were estimated from these responses by an approximate fitting of an appropriate second-order system step response. As stated above, the ω_{EQV} values obtained are all Level 1 (fig. 122).

Flight condition	Mach	Altitude m (ft)	cg percent	Weight, kg (lb)	q, N/m² (lb/ft²)	Velocity, m/s (ft/s)	n/α
99	Takeoff	0	48.8	122 470 (270 000)	3 706.0 (77.4)	160.3 (526.0)	5.27
57	0.38	6 096 (20 000)	17.5	90 719 (200 000)	4 659.0 (97.3)	119.5 (392.0)	6.74
59	0.38	3 962 (13 000)	48.8	122 470 (270 000)	6 177.0 (129.0)	122.8 (403.0)	7.39
97	Landing	0	48.8	90 719 (200 000)	2 384.0 (49.8)	112.2 (368.0)	4.08
17	0.65	9 144 (30 000)	48.8	122 470 (270 000)	8 906.0 (186.0)	197.2 (647.0)	11.24
8	0.38	0	48.8	122 470 (270 000)	10 150.0 (212.0)	128.6 (422.0)	12.58
75	0.86	10 668 (35 000)	17.5	122 470 (270 000)	12 353.0 (258.0)	255.1 (837.0)	17.68
13	0.65	6 096 (20 000)	48.8	122 470 (270 000)	13 789.0 (288.0)	205.4 (674.0)	22.56
65	0.86	7 833 (25 700)	48.8	122 470 (270 000)	8 863.0 (394.0)	265.5 (871.0)	25.34
79	0.84	7 315 (24 000)	17.5	122 470 (270 000)	19 391.0 (405.0)	261.2 (857.0)	27.32
58	0.65	11 125 (36 500)	48.8	122 470 (270 000)	6 607.0 (138.0)	189.3 (621.0)	7.93

Flight condition	σ_1	σ_2	$\frac{\sigma_3}{\sigma_4}$	ω_3	ζ_3	ω_P	ζ_P	$\frac{q_{max}}{q_{10}}$
99	-0.024	-0.265	-0.828	1.81	0.793	–	–	1.0
57	–	–	-7.45	1.60	0.576	0.149	0.851	1.04
59	-0.0806	-0.554	-7.10	1.08	0.772	–	–	1.34
97	-0.0532	-0.303	-1.27	1.49	0.732	–	–	1.00
17	-0.0106	-0.515	-5.49	1.66	0.857	–	–	1.00
8	-0.0456	-2.81	-4.76	0.901	0.900	–	–	1.15
75	-0.0669	-0.223	-0.6 -2.95	4.59	0.561	–	–	1.00
13	-0.0108	–	–	4.14	0.817	0.940	0.989	1.01
65	-0.0629	-0.572	-1.48	5.31	0.587	–	–	1.01
79	-0.0383	-0.285	-0.6 -2.77	5.65	0.489	–	–	1.01
58	-0.0089	–	–	2.62	0.633	0.537	0.895	1.02

The q_{max}/q_{10} values also were obtained from pitch-rate responses and are all Level 1 quality. These values are listed in Table 16.

Gain and Phase Margin Requirements—The DRO requirements on gain and phase margins were met at all flight conditions for each control loop.
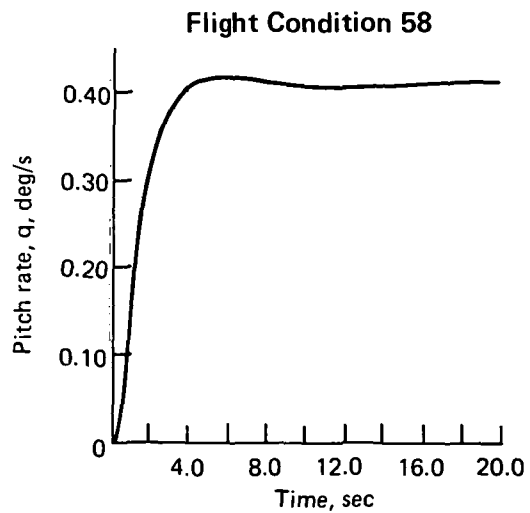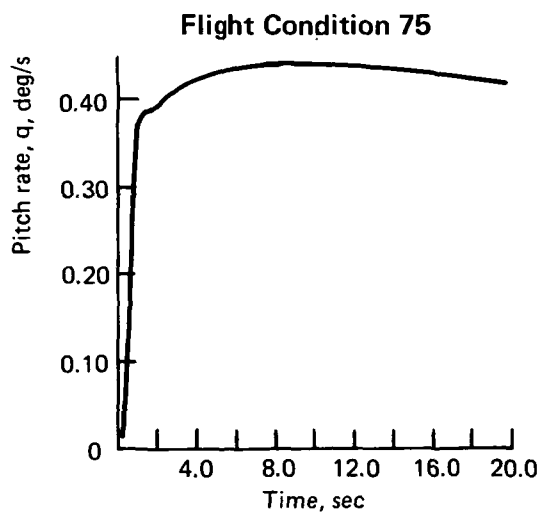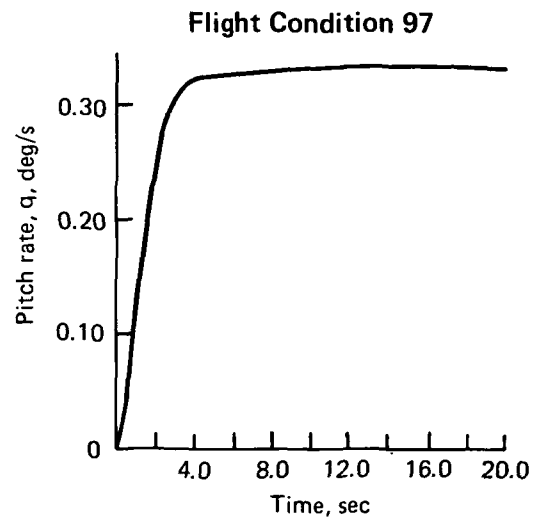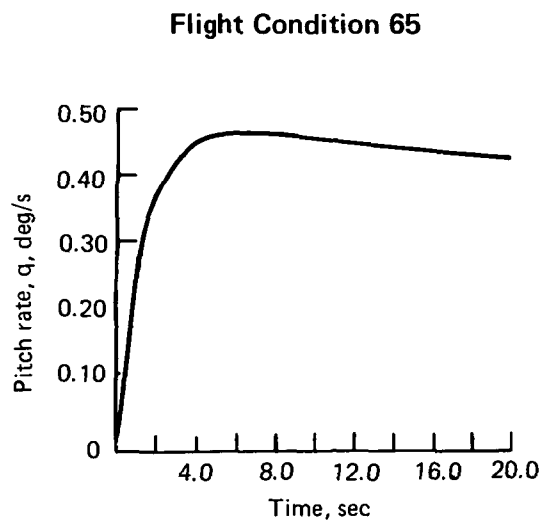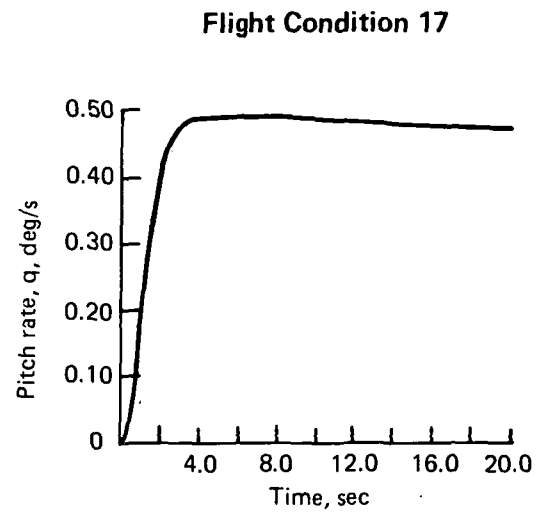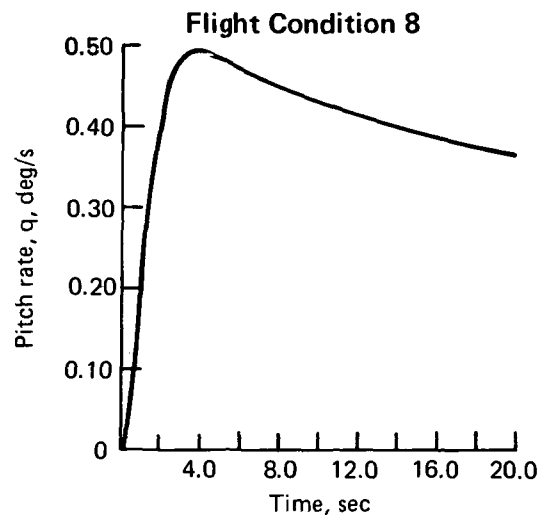
Figure 121. Pitch-Augmented Stability System Response Dynamics to a 0.5 deg/s Pitch Rate Command Step, Model 768-104

194

Pitch short-period frequency, ω_{SP}, rad/s

100.0

10.0

1.0

0.1

10.0 $\left(\dfrac{\omega^2_{SP}}{n/\alpha}\right)$

3.6

Level 2 en route and terminal

Level 1 en route and terminal

0.16

Level 1 terminal

Level 2 terminal

Level 1 terminal

65 79

13

△ 75

△ 17

△ 97

△ 99

△ 57 △ 58

△ 59

△ 8

Level 1 en route 0.085

Level 1 en route terminal 0.096

0.038

Levels 2 and 3 terminal

Levels 2 and 3 en route

Note: Conditions 97 and 99 are the only
terminal flight condition cases.

10.0

100.0

Normal acceleration/angle of attack, n/α, g/rad

768-104

Figure 122. Flying Qualities Short-Period Requirements

7.3.1.3 Wing-Load Alleviation Control System

The WLA system attenuates incremental wing-bending moments resulting from low-frequency, pilot-initiated longitudinal maneuvers and random-atmospheric turbulence. The Model 768-104's low-frequency MLC law is similar to that of the Initial ACT Configuration (ref 3). The GLA control law filter is significantly different. Besides reducing the wing loading at the fundamental wing frequency, the GLA provides low-frequency load relief, which augments the MLC function.

Figure 123 shows longitudinal-pitch control laws with WLA and the nominal loop gains. These control laws were developed for the V_B and V_{MO} (V_C) forward cg flight conditions (table 13). An FMC law is not shown because it is not feasible for the selected wing configuration (subsec 7.3.1.4). Thus the outboard aileron became a single control panel instead of a two-section configuration, as in the Initial ACT. Because the Model 768-104 PAS design was not complete at the time the -104 WLA was being synthesized, a simplified Initial ACT PAS was used. The speed loop was eliminated by setting KU = 0 (fig. 123), and the pitch-rate gain (KQ) was set at 1.5. This simplified PAS met the handling qualities and stability requirements of the DRO. The current recommended PAS for Model 768-104 is discussed in Subsection 7.3.1.2. These PAS, MLC, and GLA control laws meet the DRO handling quality and stability requirements both individually and in combination at V_B and V_{MO}.

Classical linear synthesis methods of root locus and time, frequency, and PSD response analyses were used during the WLA synthesis task. A von Karman vertical turbulence model with an integral scale of 762m (2500 ft) was used with the PSD analysis.

MLC Synthesis—The MLC law senses a change in airplane vertical acceleration (load factor) at the cg and commands symmetric deflection of the outboard ailerons. This causes an inboard shift of wing-spanwise airload distribution, which reduces the moment arms and, thus, the wing-sectional-bending moments. The MLC sensor signal also deflects the elevator to counteract the increment of pitch rate due to aileron deflections, which maintains pitch-rate characteristics similar to those of a PAS-only active response.
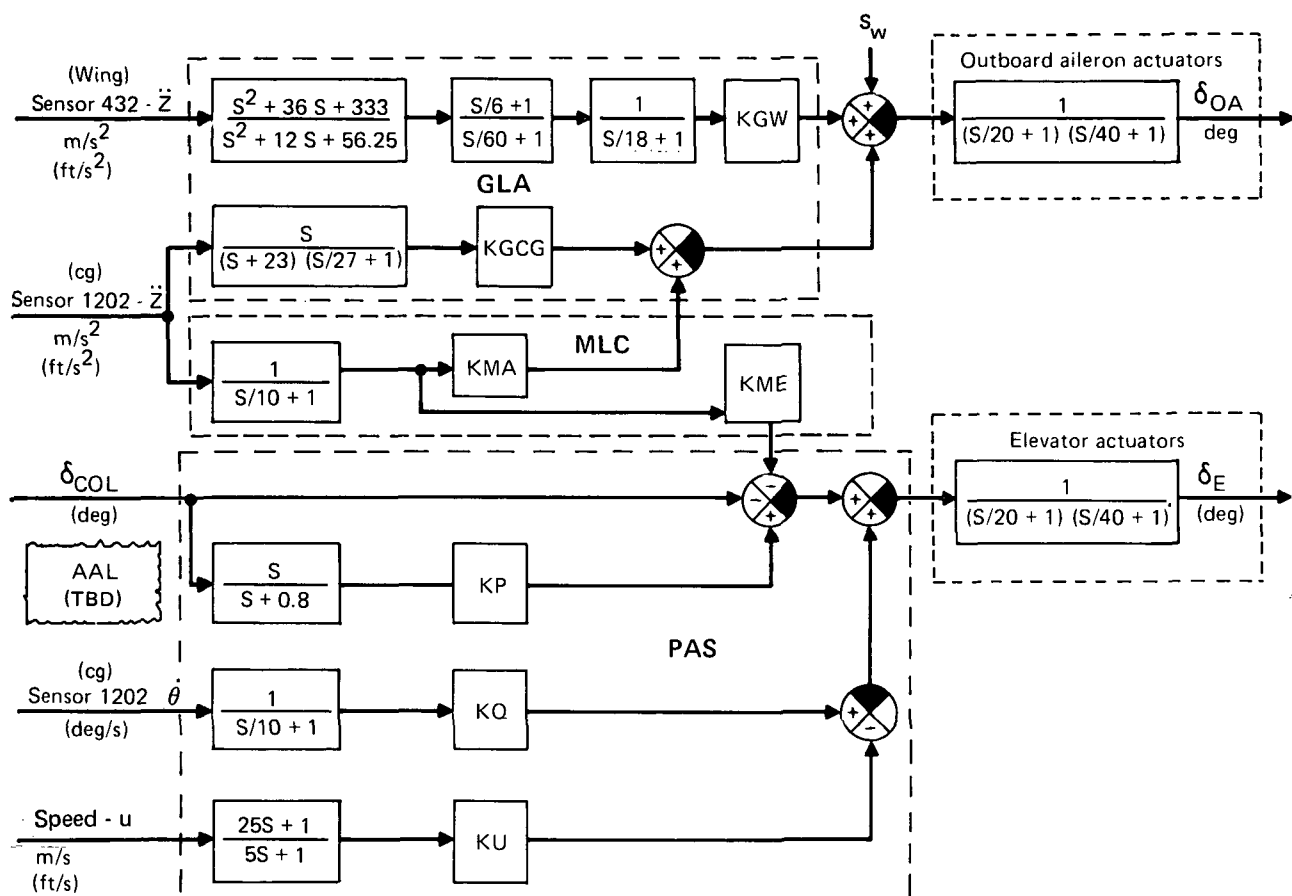
PAS, MLC, GLA Control Constants

Flight condition, C	Gains [a],[b]						
	KP	KQ	KU	KMA	KME	KGW	KGCG
V_B	1.0	1.5	0	1.2273 (0.3741)	0.1168 (0.0356)	0.00902 (0.00275)	0.8766 (0.2672)
V_{mo}	1.0	1.5	0	0.8837 (0.2694)	0.1168 (0.0356)	0.00610 (0.00186)	0.6312 (0.1924)

[a]Dimensions are in meters (feet), seconds, and degrees.

[b]For positive directions, X = forward, Y = right, and Z = down.

[c]Refer to table 16.

768-104

Figure 123. Longitudinal Pitch Stability Augmentation System With Wing-Load Alleviation

197

The redesigned GLA filter complements the MLC filter in the low-frequency region by providing additional wing-bending-moment relief, particularly on the outboard wing. At nominal gains, the GLA provides 5% incremental low-frequency load relief at wing station $\eta = 0.75$.

Root locus plots of the MLC gains, aileron gain (KMA), and elevator gain (KME), with the GLA active are presented in Figure 124 for the V_B flight condition. Neither the frequency nor the damping of the modes shown, including the higher frequency elastic modes, are significantly altered by the indicated gain variations.

Incremental 1.5g column-pulse time histories are presented in Figure 125. The pitch rate and load factor responses are relatively unchanged by the WLA control laws. The incremental wing-bending moments are decreased 9.6% at $\eta = 0.25$ and 58.1% at $\eta = 0.75$.

GLA Synthesis—The GLA control law attenuates incremental wing-bending moments induced by atmospheric turbulence. The short-period and the fundamental wing modes are the primary contributors to incremental wing loading. Both the PAS and the MLC significantly reduce the wing loads in the short-period regions; however, the MLC slightly amplifies the incremental loading at the first wing-mode frequency. The GLA effectively negates that adverse portion of the MLC response.

Wing loading at the fundamental mode can be reduced by either of two methods: (1) the damping of that mode can be increased or (2) the frequency can be increased, thereby reducing the loading due to the attenuating rolloff characteristics of the higher frequency region of the von Karman gust spectrum. The first method was chosen because atmospheric disturbances probably will not always correspond to the gust model used. The actual power rolloff could occur at significantly higher frequencies.

The recommended GLA control law primarily senses wing vertical acceleration on the elastic axis and commands the outboard ailerons. The optimum sensor location along that axis was investigated by a zero locus procedure (fig. 126). Five accelerometer locations were investigated along the outboard elastic axis of the wing (structural nodes 429, 430, 431, 432, and 433 of fig. 109). The sensor location should be chosen so that the associated transfer function has no right-half plane zeros.

Root Locus on KMA

▲ KMA 1.2273 (nominal)
■ 5.0 KMA
X Open loop poles
O Open loop zeros

Root Locus on KME

▲ KME 0.1168 (nominal
■ 5.0 KME
X Open loop poles
O Open loop zeros
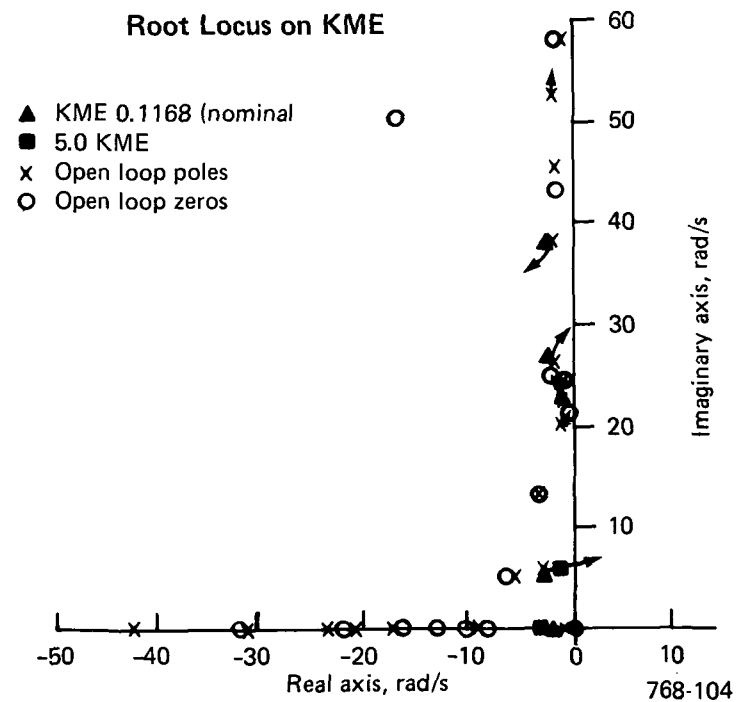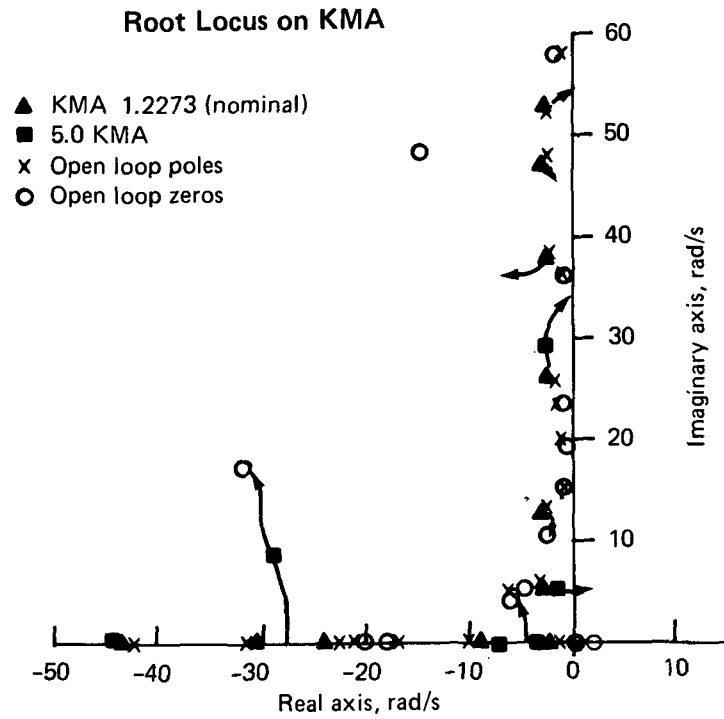
768-104

Figure 124. Wing-Load Alleviation System (KGCG = 0) (Flight Condition V_B)
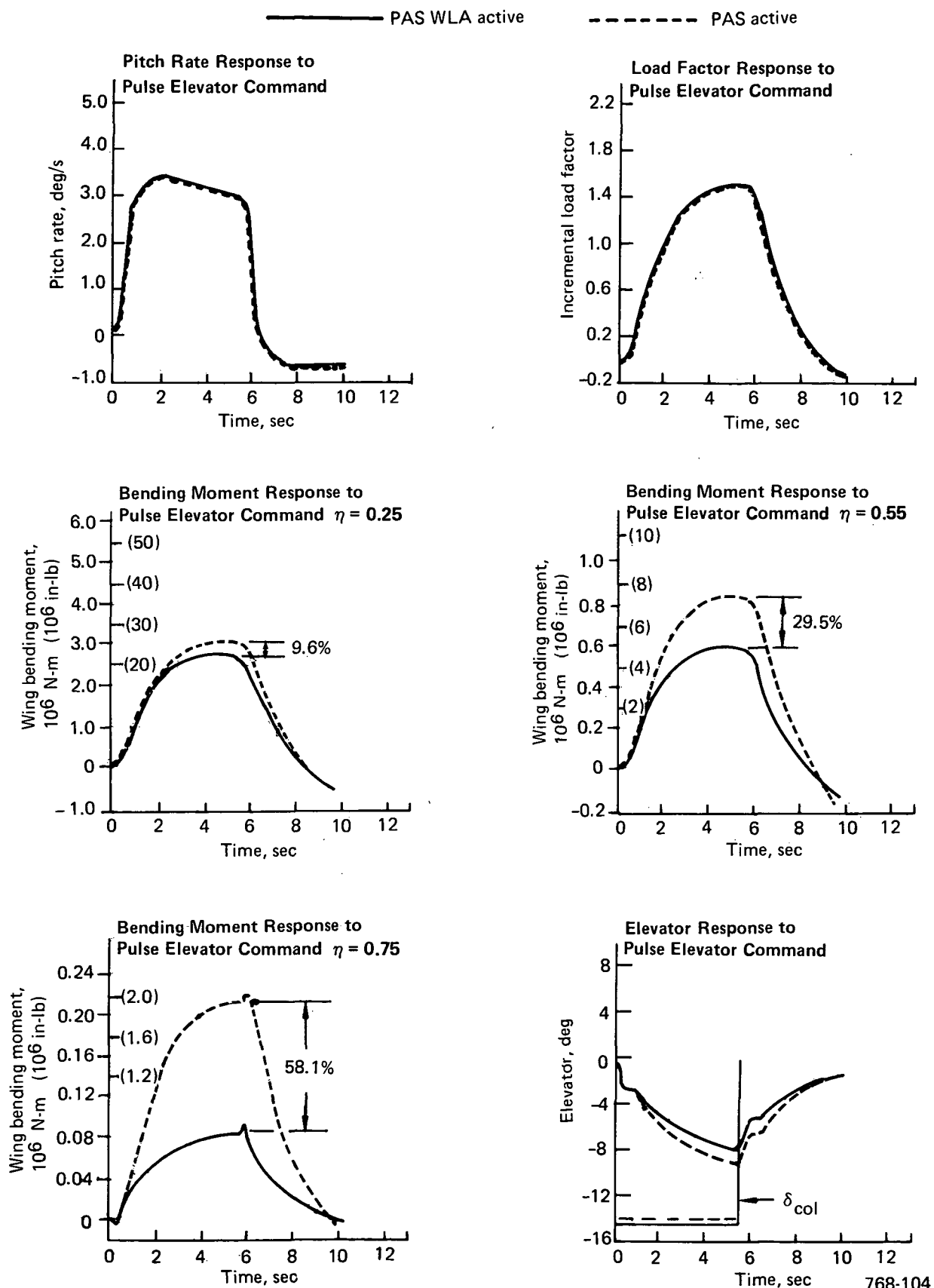
199

Figure 125. Wing-Load Alleviation System, 1.5g Incremental 5.5-sec Column Pulse Time Histories (Flight Condition V_B)

200
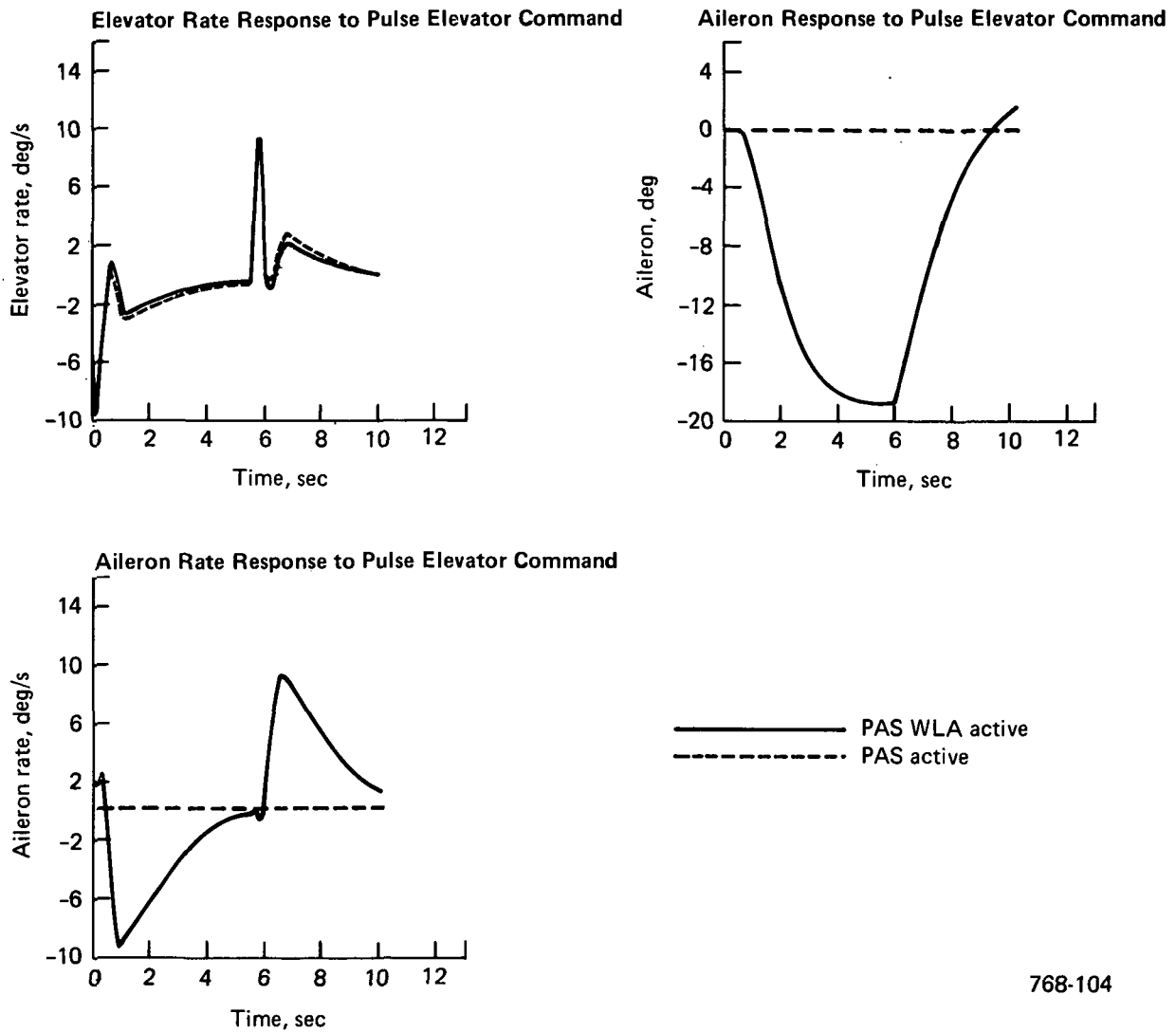
Figure 125. Wing-Load Alleviation System, 1.5g Incremental 5.5-sec Column Pulse
Time Histories (Flight Condition V_B) (Concluded)

In addition, the selected location should place the zeros relative to the mode poles to maximize the potential for increasing critical mode damping. Because a zero was not located in the vicinity of the first wing-bending mode pole, the root locus of that mode can vary depending on the filter, sensor location, and flight condition. Sensor 432, near the center of the outboard aileron, was selected for the GLA wing accelerometers.

The washout filter of the Initial ACT GLA design has been eliminated from the wing planform GLA filter. Figure 127 shows the wing planform GLA filter dynamic
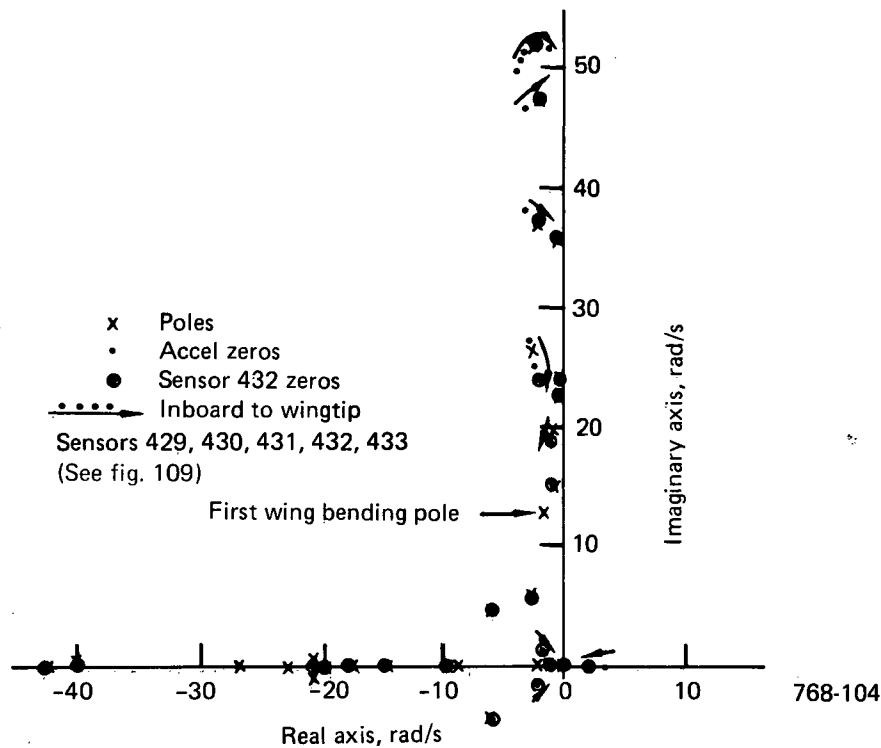
Figure 126. Wing-Load Alleviation System, Wing Accelerometer Zero Locus
(Other Gains Nominal) (Flight Condition V_B)

x   Poles
·   Accel zeros
●   Sensor 432 zeros
····▬ Inboard to wingtip
Sensors 429, 430, 431, 432, 433
(See fig. 109)

First wing bending pole ──►x

Imaginary axis, rad/s

50
40
30
20
10

-40   -30   -20   -10   0   10   768-104

Real axis, rad/s

response. A second-order pole-zero pair was added to constrain an elastic mode originating on or near the negative real axis to a highly damped region of the S-plane. At nominal gain, that mode contributed significantly to the wing-bending moments of the Initial ACT dynamic model. This filter pair tends to keep the first wing mode distinct and to increase its frequency with higher loop gains. The original GLA forced the first mode root locus toward the short-period region with increasing gain. A phase-lead filter, based on a phase-locus plot, was added to improve the damping of the basic wing mode. A lag filter was also included for optimum phasing and to prevent the GLA from amplifying the higher wing-mode responses. The lag characteristics of the surface actuators provide additional higher mode decoupling.

An outboard wing-bending mode at about 4 Hz contributes to incremental wing loading during a gust encounter. A separate control law was created to reduce the load effects of that mode. A 4 rad/s bandwidth filter centered at 25 rad/s was applied to the wing accelerometer signal and to the MLC cg signal. The wing control law

202

Wing Accelerometer Filter Response

$$\frac{(S^2 + 36S + 333)(S/6 + 1)}{(S^2 + 12S + 56.25)(S/60 + 1)(S/18 + 1)}$$

Gain magnitude, dB

Phase, deg

Magnitude

Phase

Frequency, rad/s

CG Accelerometer Filter Response

$$\frac{S}{(S + 23)(S/27 + 1)}$$

Gain magnitude, dB

Phase, deg

Magnitude

Phase

Frequency, rad/s
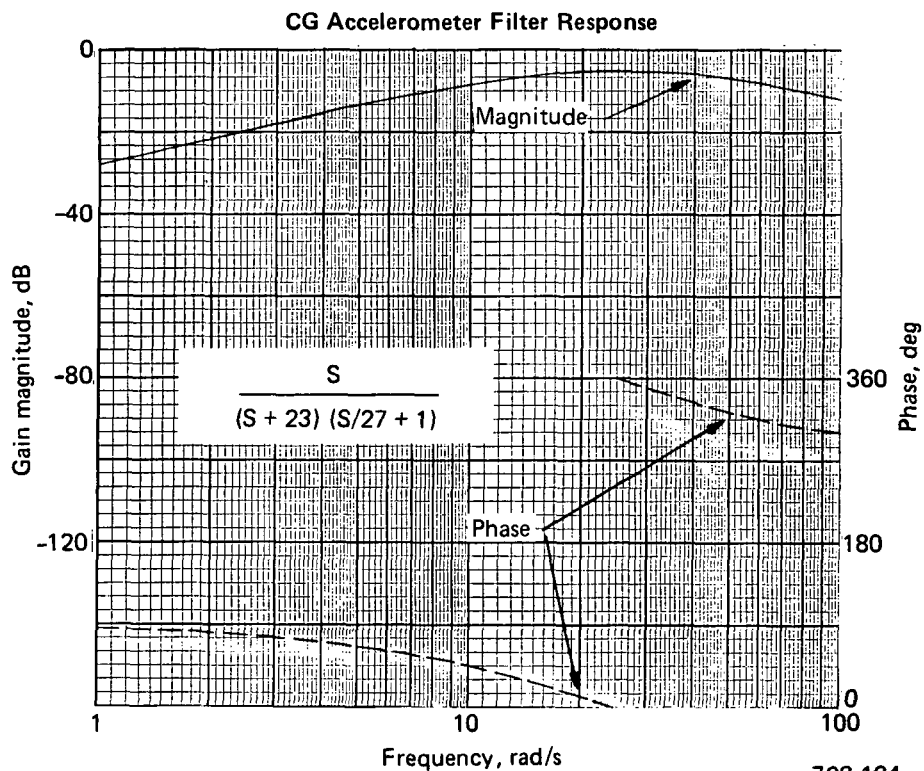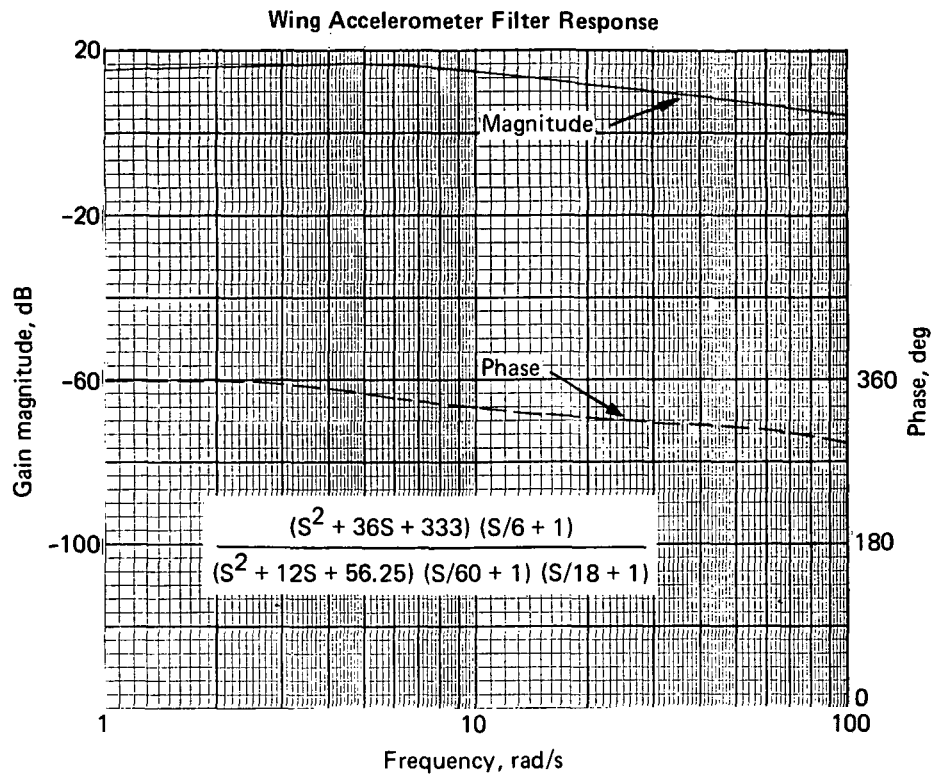
768-104

Figure 127. Gust-Load Alleviation Filter Dynamic Response

203

increased the damping of that mode, but tended to destabilize the first wing mode. The cg control law added some damping to the 4 Hz mode, but had negligible effect on the root locus of the lower modes. However, this cg filter (figs. 123 and 127) reduces gust loading at both the fundamental and 4 Hz wing modes, which probably is a result of airload redistribution inboard. The MLC low-frequency cg control law induces similar response behavior.

Root locus plots of the wing accelerometer GLA gain (KGW) with the cg GLA accelerometer gain (KGCG) loop open and of KGCG with both loops closed is shown in Figure 128. The increase in first-mode damping as the KGW is increased is very evident. A fourfold increase in gain appears to nearly maximize damping for that mode, but the damping of the two modes nearer to the real axis is decreased. The nominal value of the KGCG gain is an arbitrary value that can be changed without hindering the other control laws. Increasing that gain by a factor of 4 adds damping to the 4 Hz mode, but has very little effect on the characteristics of the other modes (fig. 128).

A summary of the PSD results for V_B showing wing-load relief and control surface activity for various control law and GLA loop-gain combinations is presented in Figure 129; the PSD responses are presented in Figures 130 and 131.

The incremental wing-load relief can be improved by increasing the KGW loop gain, or by activating the KGCG control law, or both. However, increased aileron surface activity will result. The wing filter seems to offer better load relief per unit increase in aileron rate at $\eta = 0.25$ due to increasing the KGW loop gain. Outboard on the wing at $\eta = 0.55$ and $\eta = 0.75$, the cg filter offers more relief per unit increase in surface rate.

The nominal KGW gain was selected so that significant load relief would be attained with a peak aileron rate at V_B of less than 100 deg/s. If higher surface rates were acceptable, a combination of increased KGW and an active KGCG control law would be practical, and two independent GLA filters would provide some redundancy.

Although the GLA systems studies showed that the system was feasible, the surface rates were judged to be too high for practical implementation, and the GLA system was therefore deleted.

Root Locus on KGW (KGCG = 0)

▲ KGW 0.00902 (nominal)
◆ 2.0 KGW
■ 4.0 KGW
X Open loop poles
O Open loop zeros

First wing mode ⟶

Imaginary axis, rad/s

Real axis, rad/s

Root Locus on KGCG (KGW = Nominal)

▲ KGCG 0.8766 (nominal)
◆ 2.0 KGCG
■ 4.0 KGCG
X Open loop poles
O Open loop zeros

Imaginary axis, rad/s

Real axis, rad/s

768-104
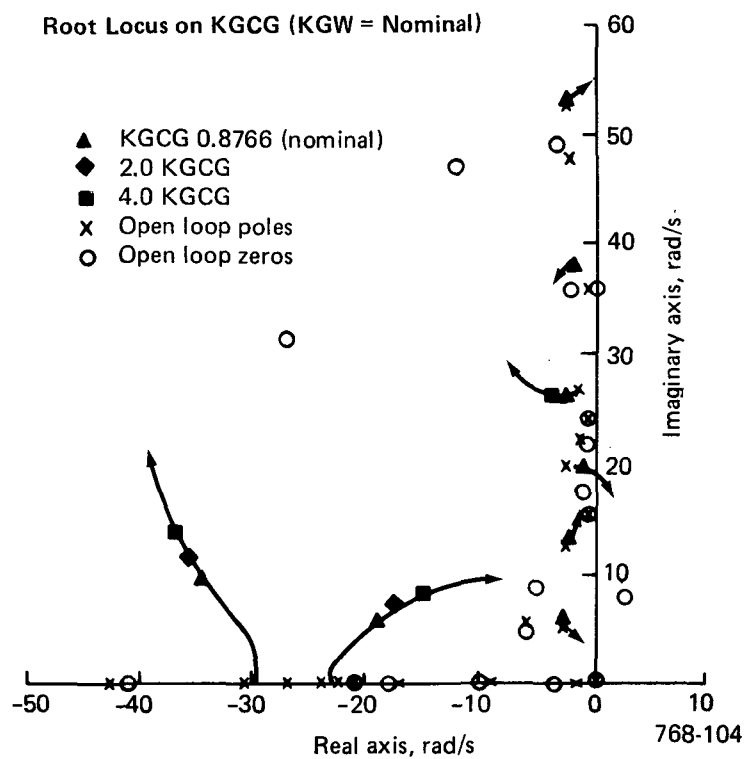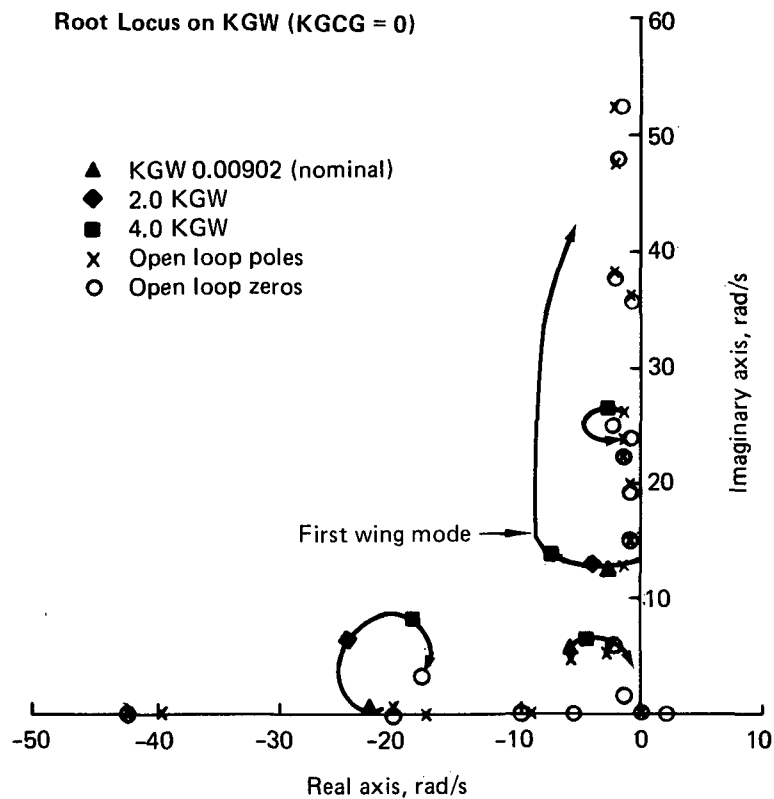
Figure 128. Wing-Load Alleviation System, Root Locus (Flight Condition V_B)

205

PAS	PAS MLC	PAS MLC GLA KGCG=0 KGW (nom)	PAS MLC GLA KGCG (nom) KGW (nom)	PAS MLC GLA KGCG=0 2 x KGW	PAS MLC GLA KGCG (nom) 2 x KGW	PAS MLC GLA KGCG=0 3 x KGW

Peak incremental control surface kinematics (absolute) — Incremental change with respect to open loop (Increase / Decrease)

Bending moment, $\eta = 0.25$ (+5 to -30): 11.5, 13.5, 16.8, 17.6, 18.7, 19.4, 19.9

Bending moment, $\eta = 0.55$ (+5 to -30): 8.9, 15.6, 23.0, 25.9, 27.7, 30.4, 31.1

Bending moment, $\eta = 0.75$ (+5 to -30): 3.9, 11.8, 19.2, 23.0, 23.3, 26.6, 25.8

Aileron, δ_A, deg (0 to 15): 9.9 (66%)*, 10.3 (69%), 10.9 (73%), 12.0 (80%), 12.7 (85%), 13.9 (93%)

*Percentage of lower authority limit 15 deg

Aileron rate, $\dot{\delta}_A$, deg/s (0 to 200): 53.4, 84.6, 105.7, 130.3, 150.9, 171.7

Elevator, δ_E, deg (0 to 4): 3.69, 3.29, 3.30, 3.27, 3.30, 3.28, 3.30

Elevator rate, $\dot{\delta}_E$, deg/s (0 to 20): 15.8, 16.3, 16.2, 16.0, 16.2, 16.0, 16.2

768-104

Figure 129. Wing-Load Alleviation System, Gust Response Summary, von Karman Vertical Gust, L = 762m (2500 ft), U_σ = 25.65 m/s (84.15 ft/s) (Flight Condition V_B)
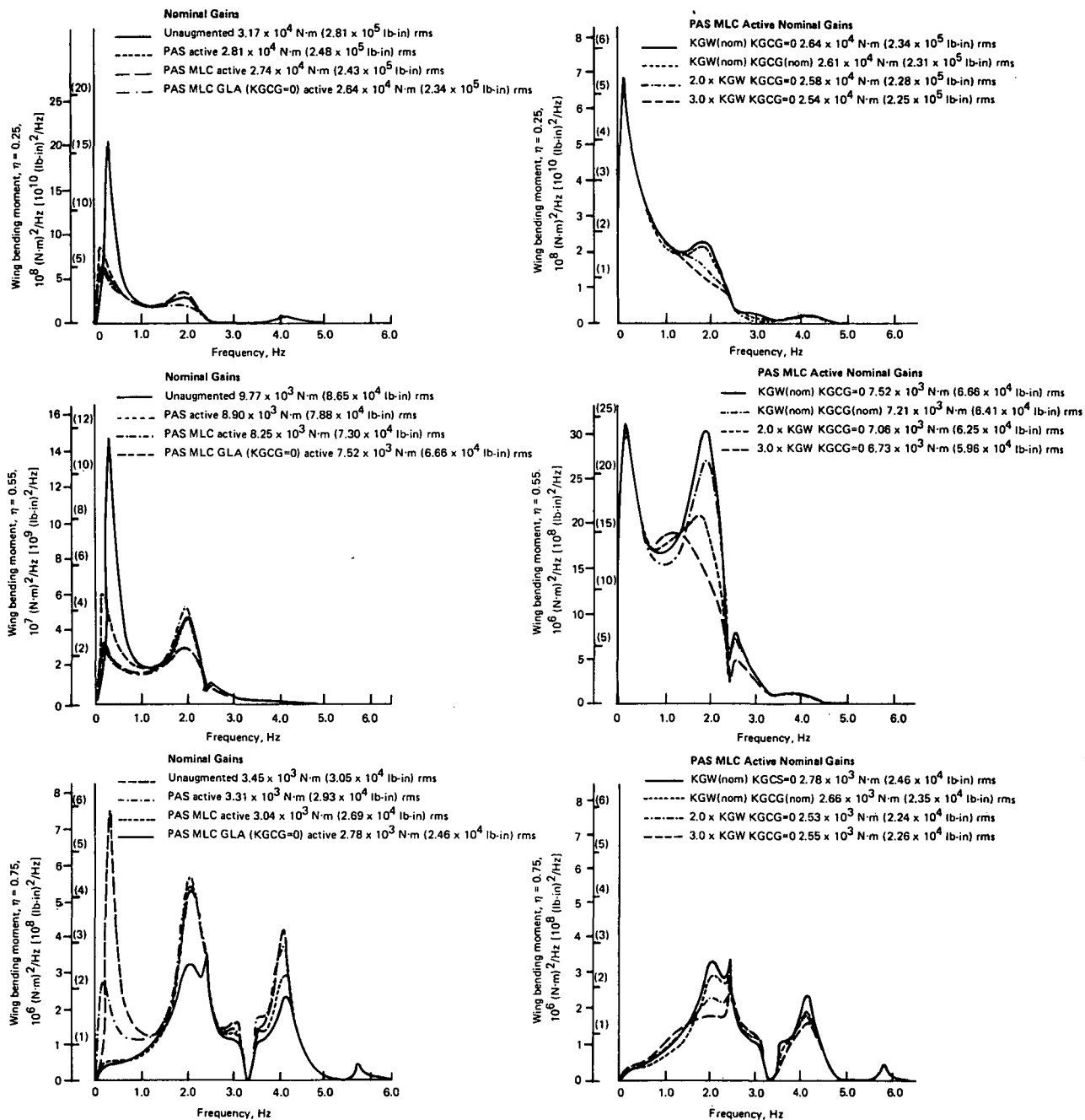
Figure 130. Wing-Load Alleviation System, Bending Moment Due to 0.305 m/s (1 ft/s) von Karman Vertical Gust, PSD (Flight Condition V_B)

207
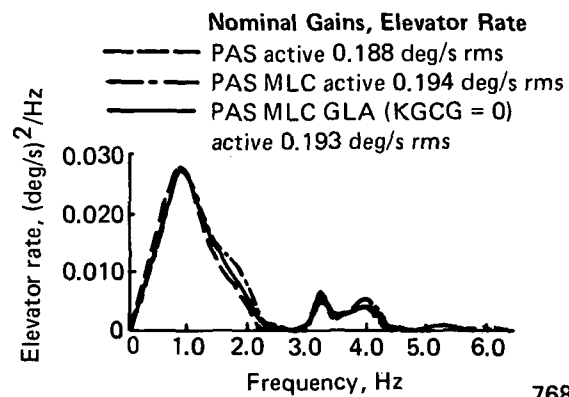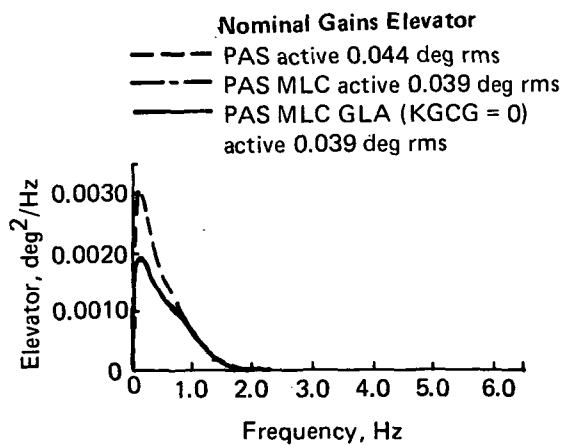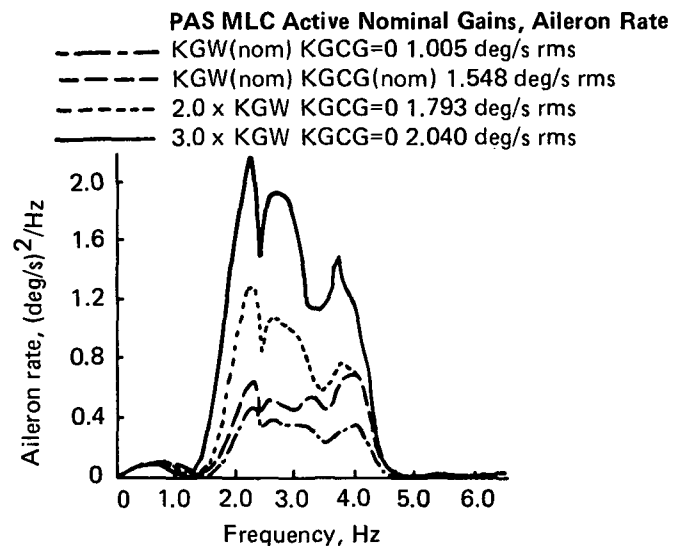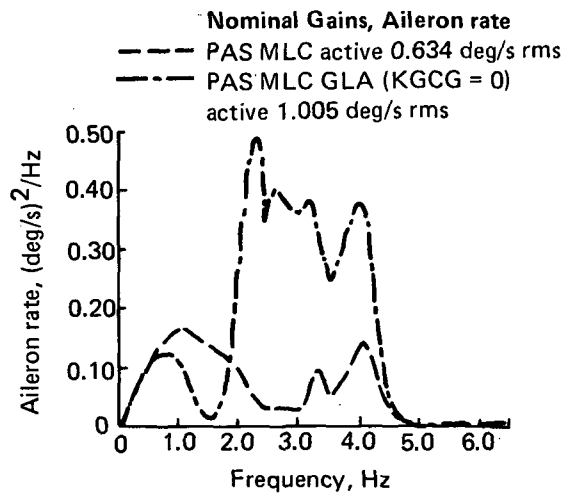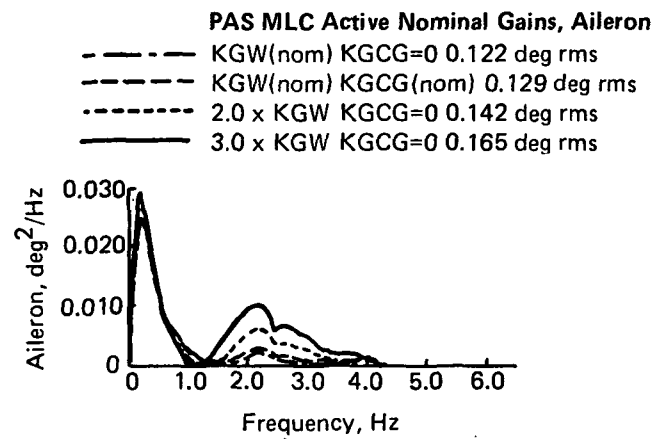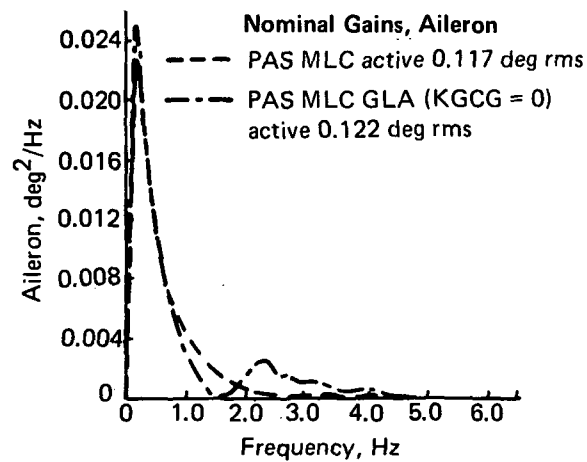
Figure 131. Wing-Load Alleviation System, Control Surface Activity Due to 0.305 m/s
(1 ft/s) von Karman Vertical Gust, PSD (Flight Condition V_B)

7.3.1.4 Flutter-Mode Control System Design

Initial ACT FMC Update—An FMC design that fulfilled the requirements on flutter-mode damping for the Initial ACT Configuration is presented in Reference 3. When reported, the gain and phase margins of this design had not been determined. Subsequent determination of these margins showed them to be deficient, and the design was reworked to correct the margin deficiencies. The rework led to a new schedule for the flutter-mode control gain (KF) and a change in the feedback filter for the $1.2V_D$ flight condition.

Figure 132 shows the FMC for the Initial ACT Configuration. As was the case with the PAS, this work was not completed in time to be reported in the Initial ACT
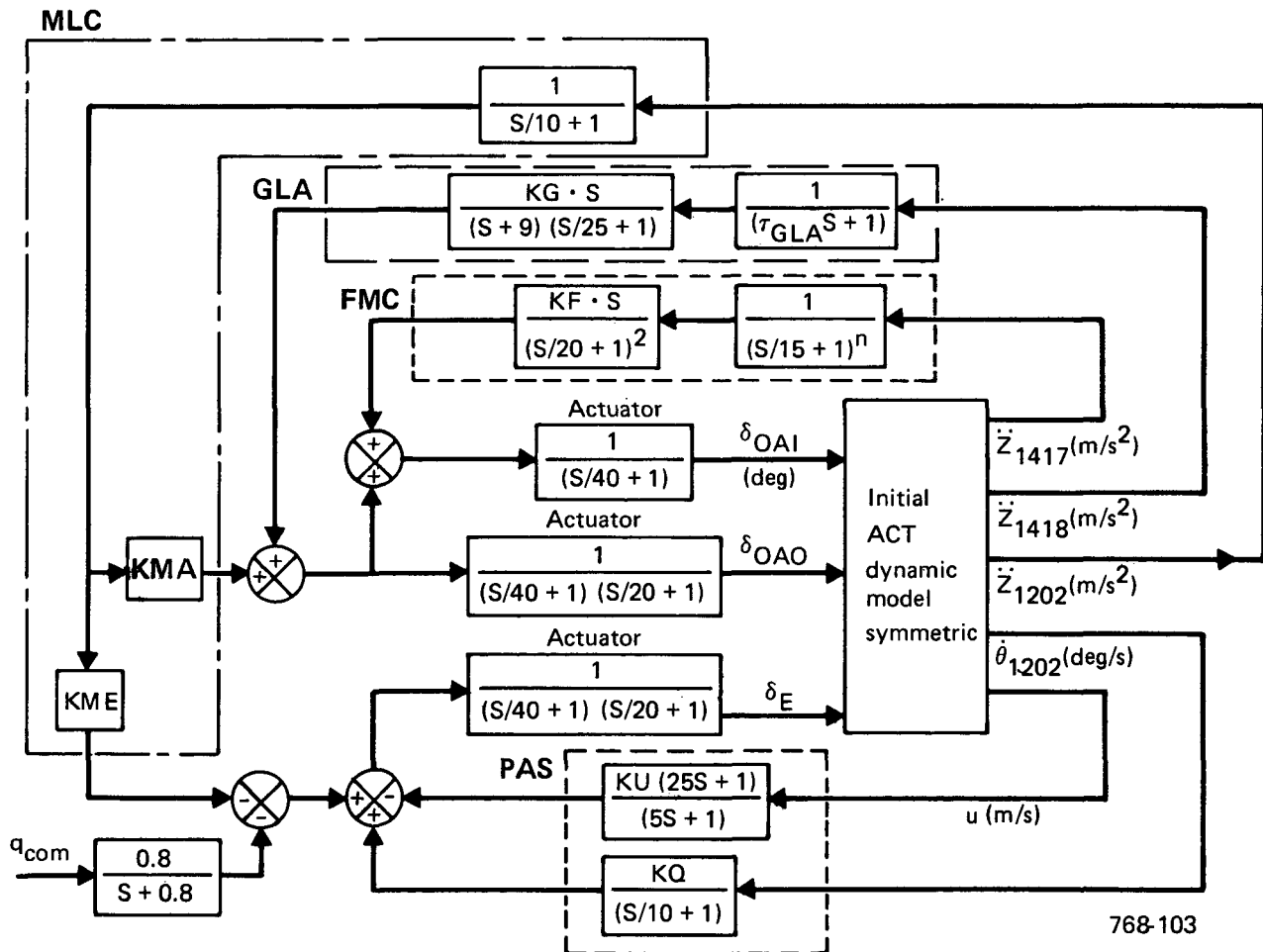
Figure 132. Active Control Systems Block Diagram

209

Document (ref 3). The FMC design was validated at four flight conditions, during which the PAS, MLC, and GLA systems were active. The flight condition data and control loop gains are given in Table 17.

Table 17. Flutter Mode Control System Validation Flight Conditions and Control Gains

Flight condition[b]	Gains[a]						FMC network exponent, n	GLA time constant, τ, sec
	KQ	KU	KMA	KME	KG	KF		
V_B	2.0	0.0376 (0.01146)	1.360 (0.4144)	0.1168 (0.0356)	0.2257 (0.0688)	0.0377 (0.0115)	1	0.16
V_{MO}	2.0	0.0376 (0.01146)	0.9807 (0.2989)	0.1168 (0.0356)	0.1129 (0.0344)	0.0377 (0.0115)	1	0.10
V_D	2.0	0.0376 (0.01146)	0.6772 (0.2064)	0.1168 (0.0356)	0.0453 (0.0138)	0.1340 (0.0409)	1	0.075
$1.2V_D$	2.0	0.0376 (0.01146)	0.4088 (0.1246)	0.1168 (0.0356)	–	0.2632 (0.0802)	2	–

[a]Dimensions are in meters (feet), seconds, and degrees

[b]For positive directions, X = forward, Y = right, and Z = down

768-103

The FMC uses the inboard section of the outboard aileron as the control surface. The feedback signal is obtained from a single vertical accelerometer placed at wing location 1417, as shown in Figure 133.

For any critical flutter mode, the FMC provides a damping ratio greater than or equal to 0.015 for all altitudes and speeds up to V_D and greater than zero for all altitudes and speeds up to $1.2V_D$. FMC performance in augmenting the critical flutter mode (third flexible mode approximately 20 rad/s) damping ratio is given in Table 18.

For the $1.2V_D$ flight condition, Figure 134 shows the Bode plot for the open-loop FMC (PAS and MLC loops closed). Table 19 gives the FMC open-loop poles (PAS and MLC loops closed); Table 20 gives the closed-loop poles.

The DRO (ref 3, app A) gives the FMC gain and phase margin requirements. As is usual in control system work, these were interpreted as giving the phase margin required with nominal gain, and the gain margin required with nominal phase; that is:
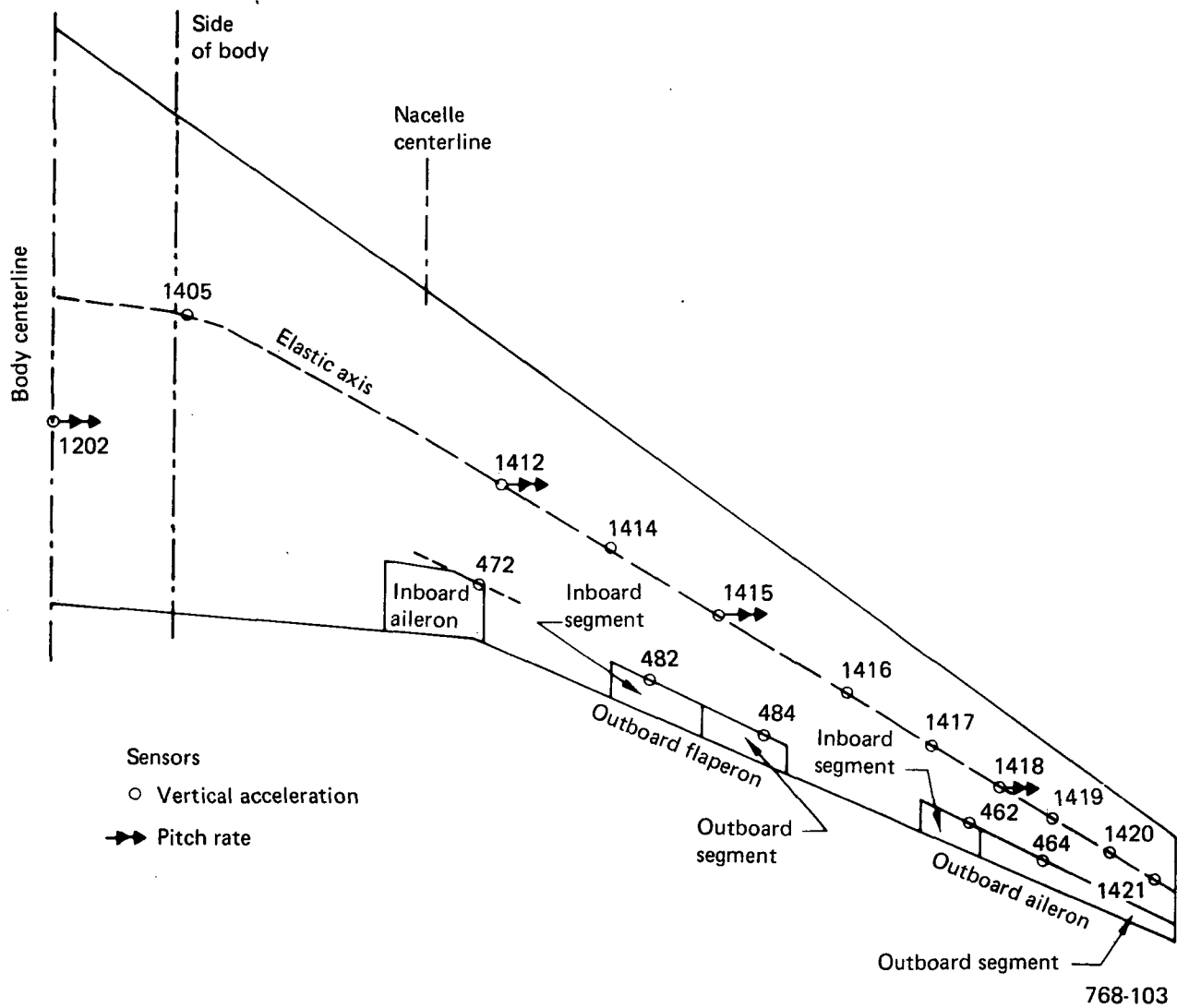
Figure 133. Modeled Wing Controls and Sensors

768-103

Table 18. Variation of Flutter Mode Damping Ratio ζ With Control Configuration Growth

Flight condition	Open loop	With/PAS	With/PAS MLC	With/PAS MLC GLA	With/PAS MLC GLA FMC
V_B	0.063	0.088	0.086	0.087	0.087
V_{MO}	0.058	0.074	0.076	0.079	0.079
V_D	-0.002	-0.004	0.000	0.005	0.034
$1.2V_D$	-0.014	-0.016	-0.012	No GLA	0.024

768-103

211
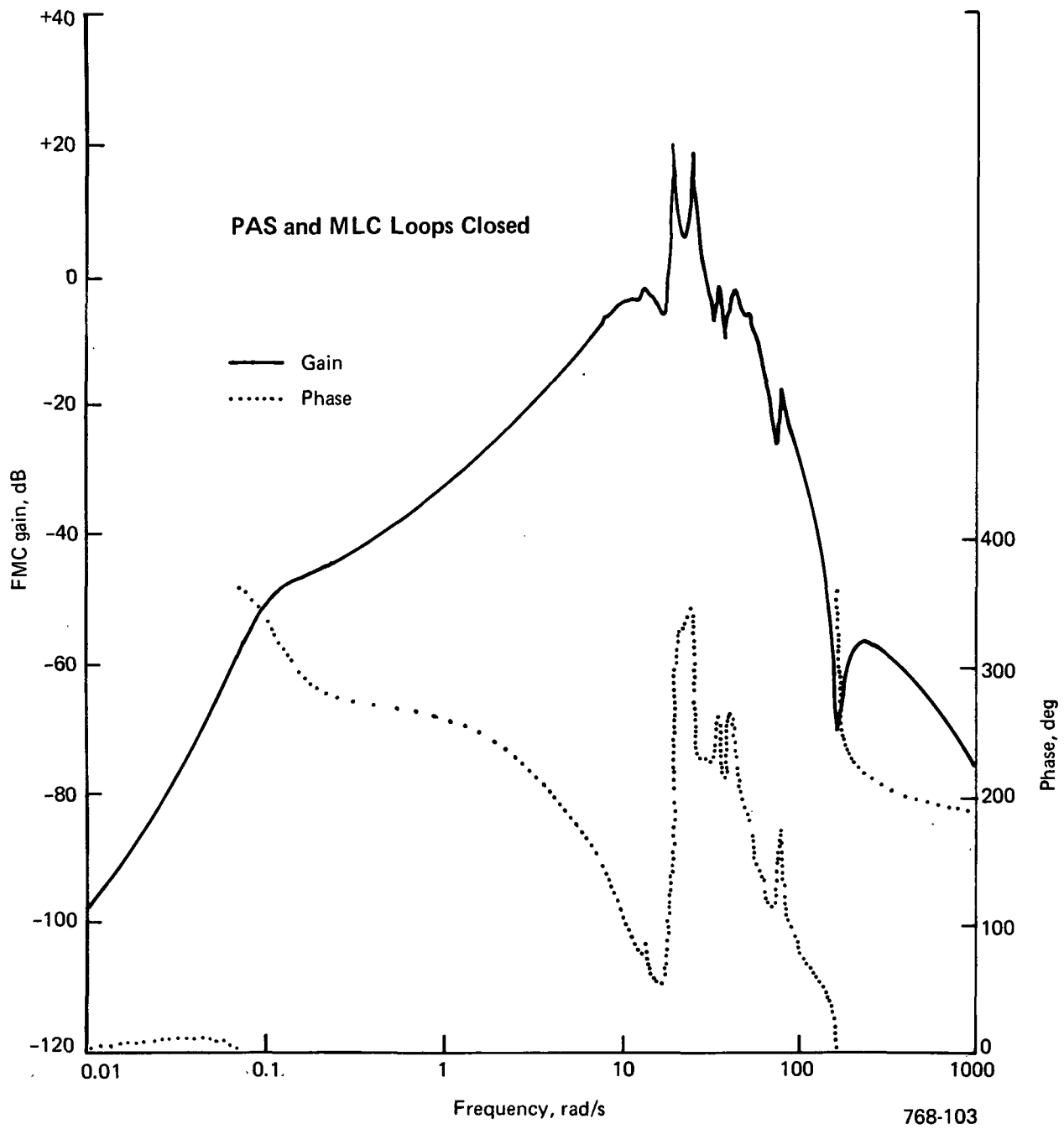
Figure 134. Flutter-Mode Control System Gain and Phase Plot at 1.2V$_D$, Pitch-Augmented Stability System and Maneuver-Load Control System Loops Closed

212

Table 19. Poles at 1.2V$_D$, Pitch-Augmented Stability and Maneuver-Load Control System Loops Closed, Flutter-Mode Control System Loop Open

Real	Imaginary	Zeta	Omega
-11.1	±300.0	0.037	300.0
-12.2	±140.0	0.086	141.0
- 7.49	±135.0	0.055	135.0
-14.7	± 97.4	0.149	98.5
- 5.78	± 89.0	0.065	89.2
- 3.13	± 82.4	0.038	82.5
- 3.50	± 64.9	0.054	65.0
-14.5	± 58.9	0.238	60.7
- 0.963	± 55.3	0.017	55.3 .
- 7.16	± 51.9	0.137	52.4
- 2.81	± 44.5	0.063	44.6
-42.3	0	1.000	42.3
-40.5	0	1.000	40.5
-40.0	0	1.000	40.0
- 3.69	± 37.3	0.099	37.5
- 1.02	± 36.4	0.028	36.5
- 0.359	± 26.6	0.014	26.6
-20.6	± 16.7	0.778	26.5
-25.0	0	1.000	25.0
-22.8	0	1.000	22.8
- 0.379	± 21.8	0.017	21.8
- 2.21	± 21.0	0.105	21.1
-20.5	0	1.000	20.5
0.237	± 20.4	-0.012	20.4
-20.0	0	1.000	20.0
-20.0	0	1.000	20.0
-15.0	0	1.000	15.0
-15.0	0	1.000	15.0
- 0.346	± 13.5	0.026	13.5
- 9.00	0	1.000	9.00
- 8.29	0	1.000	8.29
- 1.93	± 7.16	0.260	7.42
- 2.21	0	1.000	2.21
- 0.800	0	1.000	0.800
- 0.144	0	1.000	0.144
- 0.0550	± 0.102	0.475	0.116

768-103

213

Table 20. Poles at 1.2V$_D$, Pitch-Augmented Stability, Maneuver-Load Control, and Flutter-Mode Control System Loops Closed

Real	Imaginary	Zeta	Omega
-11.1	±300.0	0.037	300.0
-12.2	±140.0	0.086	141.0
- 7.49	±135.0	0.055	135.0
-14.7	± 97.4	0.149	98.5
- 5.68	± 89.0	0.064	89.2
- 2.77	± 82.3	0.034	82.3
-63.1	± 37.1	0.862	73.2
- 3.47	± 64.7	0.054	64.8
-14.5	± 58.9	0.239	60.6
- 8.798	± 55.2	0.014	55.2
- 4.77	± 52.0	0.091	52.2
- 2.39	± 46.6	0.051	46.7
-42.3	0	1.000	42.3
-40.5	0	1.000	40.5
- 0.811	± 37.2	0.022	37.2
- 5.79	± 35.9	0.159	36.4
- 4.72	± 33.1	0.141	33.5
- 2.53	± 27.3	0.092	27.5
-25.0	0	1.000	25.0
-22.8	0	1.000	22.8
- 0.404	± 21.8	0.019	21.8
- 2.07	± 21.0	0.098	21.1
-20.1	0	1.000	20.1
- 0.464	± 19.3	0.024	19.3
- 0.307	± 13.4	0.023	13.4
- 9.00	0	1.000	9.00
- 7.90	± 1.65	0.979	8.07
- 1.58	± 7.51	0.206	7.67
- 3.50	± 6.44	0.478	7.33
- 2.11	0	1.000	2.11
- 0.800	0	1.000	0.800
- 0.144	0	1.000	0.144
- 0.05514	± 0.102	0.476	0.116

768-103

1. The airplane must be free from flutter to 1.2V$_D$/M$_D$ with the FMC operating within the limits of ±6 dB gain margin at nominal phase and ±45 deg phase margin at nominal gain.

2. The airplane must be free from flutter to V$_D$/M$_D$ with the FMC operating within the limits of ±12 dB gain margin at nominal phase and ±60 deg phase margin at nominal gain.

3. A phase margin of ± 180 deg at nominal gain must be provided for frequencies twice the frequency of the highest flutter mode being actively suppressed.

The above margins were met at the V_B, V_{MO}, and V_D flight conditions. At $1.2V_D$, the plus gain margin is $+5.9$ dB instead of 6.0 dB, and the negative phase margin is -43.7 deg instead of 45.0. In Figures 135 through 137, the gain and phase root loci used to determine the margins at $1.2V_D$ are shown for the 0 to 60 rad/s frequency range. At higher frequencies, the loci activity is minimal.

Model 768-104 FMC—In contrast to the Initial ACT Configuration, where the critical flutter mode was an inboard wing mode at about 3 Hz, the Model 768-104 Configuration exhibited a "hard" 7 Hz flutter mode of the outboard wing. An FMC control law was studied for this mode.

With the flutter-mode frequency as high as 7 Hz, surface deflection and rate requirements in turbulence as well as stabilization of the mode are important FMC design factors. The requirements state that "saturation of the system must be considered by subjecting the airplane to continuous turbulence with a root mean square (rms) intensity of 14 ft/s." In this environment, at $1.2V_D$ for the control law developed in this analysis, the rms aileron displacement required is 16.66 deg, and the rms rate is 749.7 deg/s. These numbers make it impractical to use FMC to control the 7 Hz flutter mode. Satisfactory unaugmented flutter characteristics were achieved with minimal additions of stiffness material to the outboard wing. The following material describes the analyses done to reach these conclusions.

The Model 768-104 FMC is shown in the block diagram of Figure 138. The dynamic model of the airplane at the V_{MO}, V_D, $1.1V_D$, and $1.2V_D$ flight conditions were used in the FMC design work. The FMC uses the inboard section of the outboard aileron for control. Initially, a single linear displacement accelerometer was tried as the feedback sensor. It was positioned on the elastic-axis at location 430 shown in Figure 139, which is similar to the location used for the Model 768-103 Configuration. When this proved ineffective for the 7 Hz mode shape, a decision was made to sense torsional acceleration about the elastic axis and use it as the feedback signal because the 7 Hz flutter mode was primarily a torsion mode. The rotary signal was obtained by differencing the signals from accelerometers at location 430 and 3421. This feedback
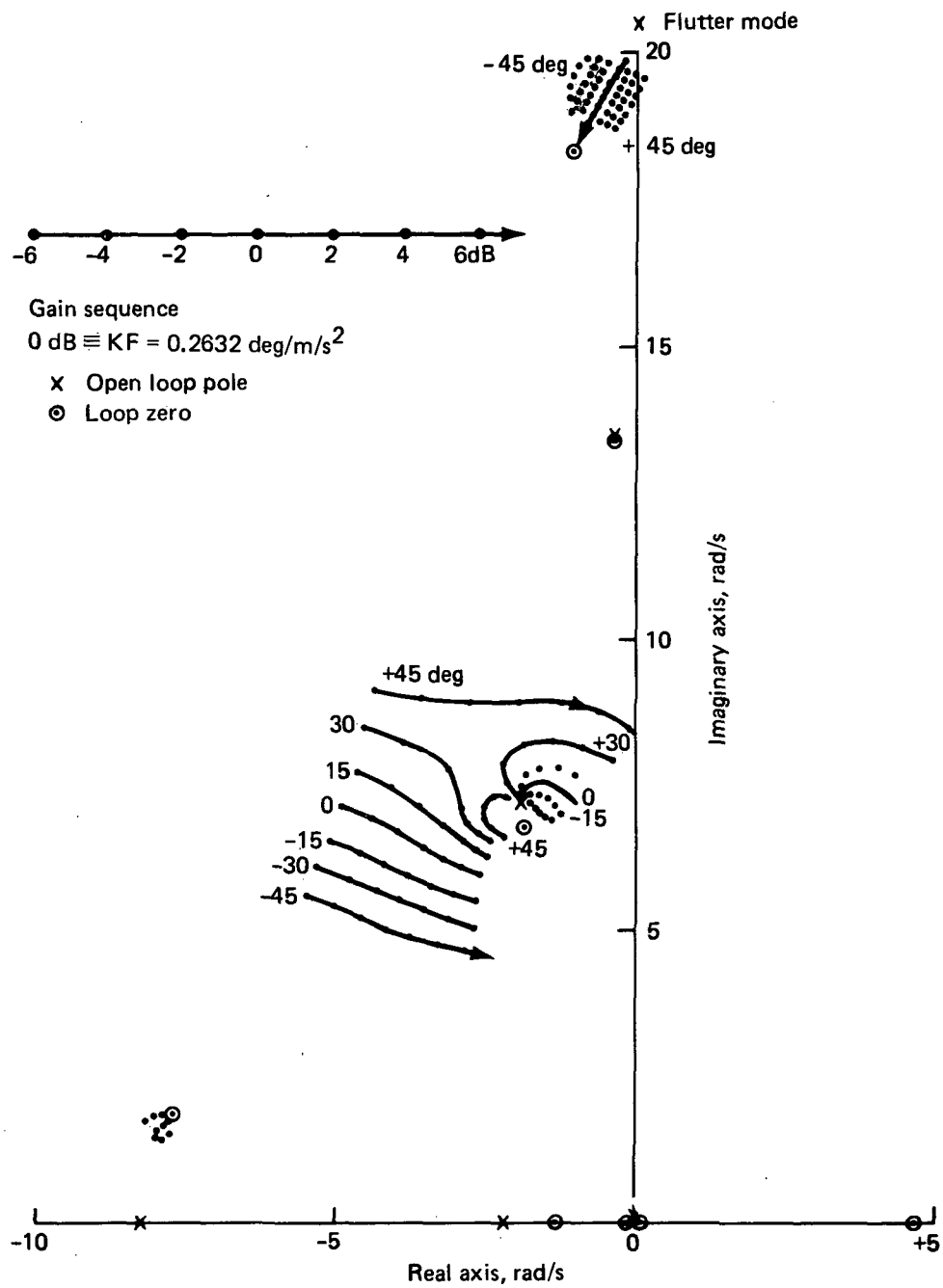
Figure 135. Flutter-Mode Control System Gain and Phase Locus at 1.2V$_D$, 0 to 20 rad/s

768-103

216
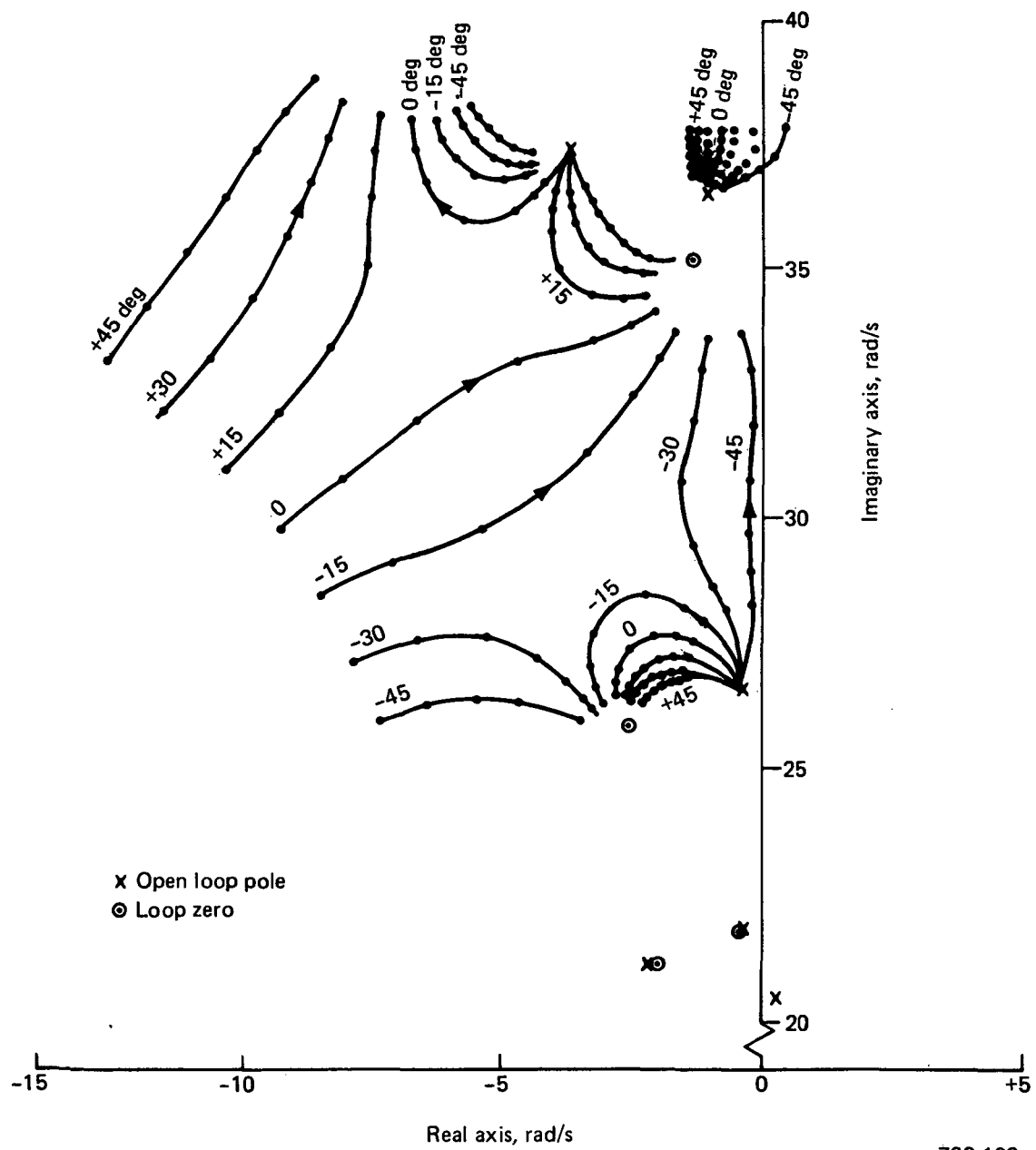
Figure 136. Flutter-Mode Control System Gain and Phase Locus at 1.2V$_D$, 20 to 40 rad/s

768-103

Figure 137. Flutter Mode Control System Gain and Phase Locus
at 1.2V_D, 40 to 60 rad/s
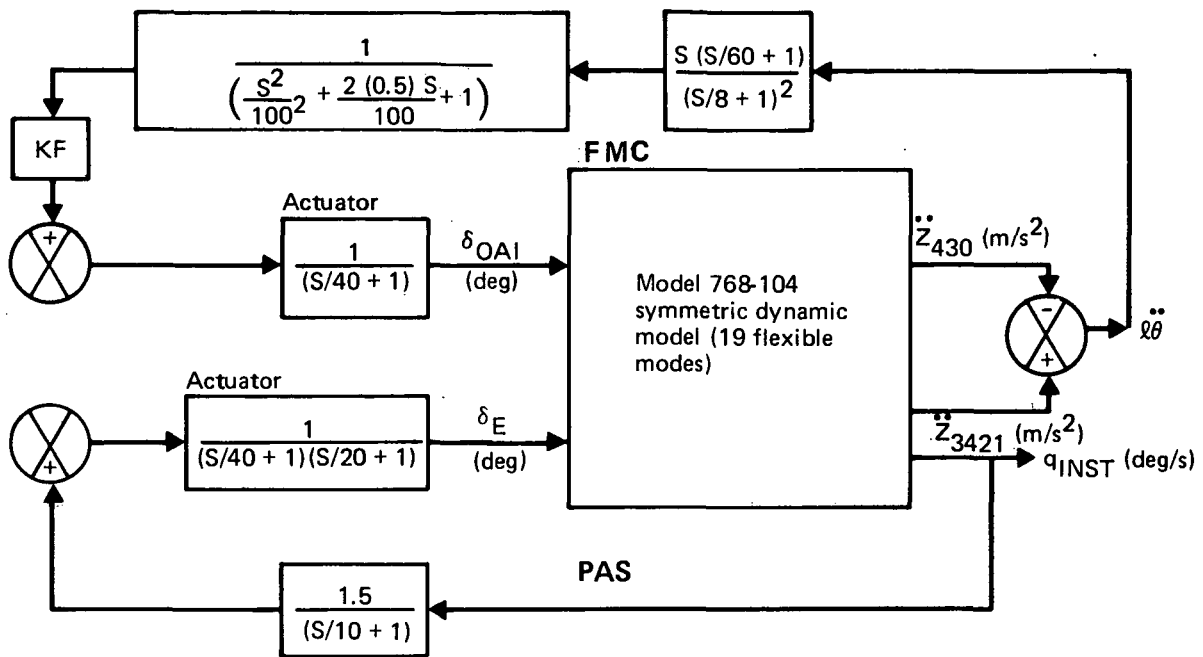
768-103

Figure 138. Flutter-Mode Control System Block Diagram, Model 768-104

signal gave rise to the FMC of Figure 138. The gain schedule for KF of the FMC as a function of V is given in Table 21. The pitch-rate gain to the elevator of the PAS loop was constant at 1.5 deg/s. This FMC meets the DRO mode-damping requirements. For ease of reference, information contained in the following figures and tables is listed:

- Table 22: Poles of Model 768-104 at $1.2V_D$

- Table 23: Poles of Model 768-104 Flutter-Mode Control System Loop (Pitch-Augmented Stability System Loop Closed)

- Figure 140: Flutter-Mode Control Loop Bode Plot at $1.2V_D$ (Pitch-Augmented Stability System Loop Closed)

- Table 24: Poles of Model 768-104 with Pitch-Augmented Stability and Flutter-Mode Control Systems Active at $1.2V_D$

- Figures 141 through 145: Root Locus at $1.2V_D$

219
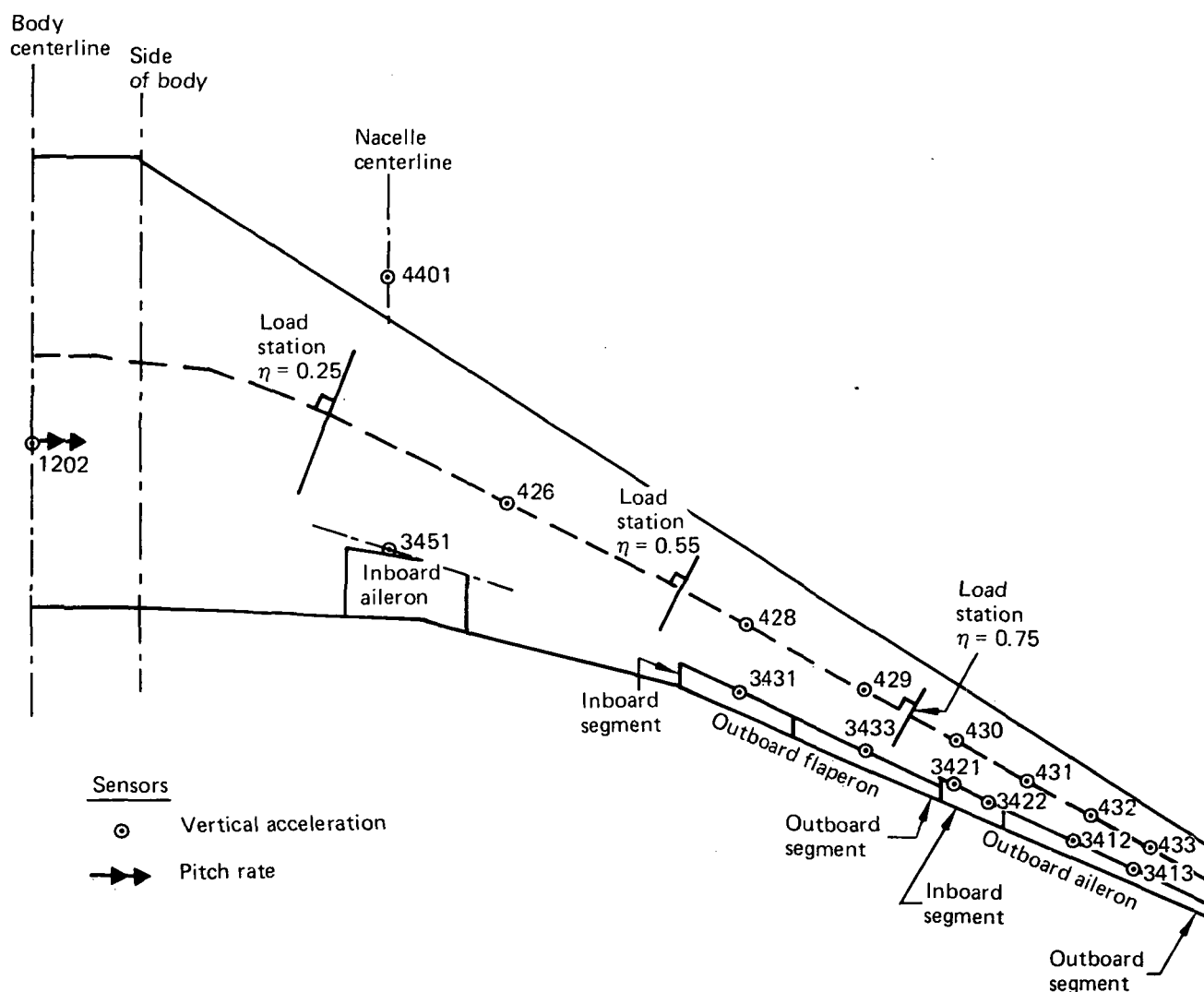
Figure 139. Modeled Wing Controls and Sensors

768-104

- Figure 146: PSD of Flutter-Mode Controlled Aileron Displacement at $1.2V_D$

- Figure 147: PSD of Flutter-Mode Controlled Aileron Rate at $1.2V_D$

An effort was made to make the FMC design meet the gain and phase margin requirements in the strong, or conjunctive, sense, as stated in the DRO. Briefly, the requirements are:

Table 21. Flutter Mode Control System KF Gain Schedule

Flight condition	Equivalent airspeed, m/s (kn)	KF, deg/(m-deg/s^2) [deg/(ft-deg/s^2)]
V_{MO}	175 (341)	0.00443 (0.00135)
V_D	214 (416)	0.00443 (0.00135)
$1.1V_D$	239 (465)	0.00886 (0.00270)
$1.2V_D$	261 (508)	0.01181 (0.00360)

768-104

Table 22. Poles of Model 768-104 at $1.2V_D$

Real	Imaginary	Zeta	Omega
- 9.00	±286.0	0.031	286.0
- 9.03	±148.0	0.061	148.0
- 9.08	±115.0	0.078	116.0
-13.4	±102.0	0.129	103.0
- 8.03	± 95.6	0.084	96.0
- 6.83	± 74.6	0.091	74.9
- 2.85	± 69.8	0.041	69.9
-15.4	± 60.4	0.247	62.4
- 0.883	± 48.3	0.018	48.3
- 3.32	± 47.3	0.070	47.4
4.88	± 38.5	-0.126	38.8
- 2.77	± 38.4	0.072	38.5
- 0.778	± 35.8	0.022	35.8
-24.3	± 19.6	0.779	31.3
- 2.20	± 23.5	0.093	23.6
- 0.398	± 22.1	0.018	22.1
- 0.534	± 21.5	0.025	21.5
- 2.17	± 19.4	0.111	19.6
- 0.336	± 13.5	0.025	13.5
- 1.58	± 0.715	0.911	1.73
- 0.02952	± 0.06414	0.418	0.0706

Table 23. Poles of Model 768-104 Flutter-Mode Control System Loop at 1.2V$_D$,
Pitch-Augmented Stability System Loop Closed

Real	Imaginary	Zeta	Omega
- 9.00	±286.0	0.031	286.0
- 9.03	±148.0	0.061	148.0
- 9.07	±115.0	0.078	116.0
-13.4	±102.0	0.130	103.0
-50.0	± 86.6	0.500	100.0
- 7.92	± 95.6	0.083	95.9
- 6.62	± 74.4	0.089	74.7
- 2.91	± 69.9	0.042	70.0
-15.4	± 60.3	0.248	62.2
- 0.881	± 48.3	0.018	48.3
- 3.47	± 47.4	0.073	47.5
-40.0	0	1.000	40.0
4.88	± 38.5	-0.126	38.8
- 2.98	± 38.5	0.077	38.6
-37.5	0	1.000	37.5
- 0.783	± 35.8	0.022	35.8
-24.3	± 19.6	0.779	31.3
-28.3	0	1.000	28.3
- 2.38	± 23.7	0.100	23.8
- 0.393	± 22.1	0.018	22.1
- 0.515	± 21.5	0.024	21.5
- 2.22	± 19.4	0.113	19.5
- 0.334	± 13.5	0.025	13.5
- 8.00	0	1.000	8.00
- 8.00	0	1.000	8.00
- 2.53	± 7.46	0.321	7.88
- 1.62	0	1.000	1.62
- 0.02849	± 0.01708	0.858	0.03321

1. The airplane must be free from flutter to 1.2V$_D$/M$_D$ with the FMC operating within the limits of ±6 dB gain margin in conjunction with ±45 deg phase margin.

2. The airplane must be free from flutter to V$_D$/M$_D$ with the FMC operating within the limits of ±12 dB gain margin in conjunction with ±60 deg phase margin.

3. A phase margin of ±180 deg must be provided for frequencies greater than twice the frequency of the highest flutter mode being actively suppressed.

4. The damping ratio for any critical flutter mode will be at least 0.015 for all altitudes and speeds up to V$_D$ for normal system operation.
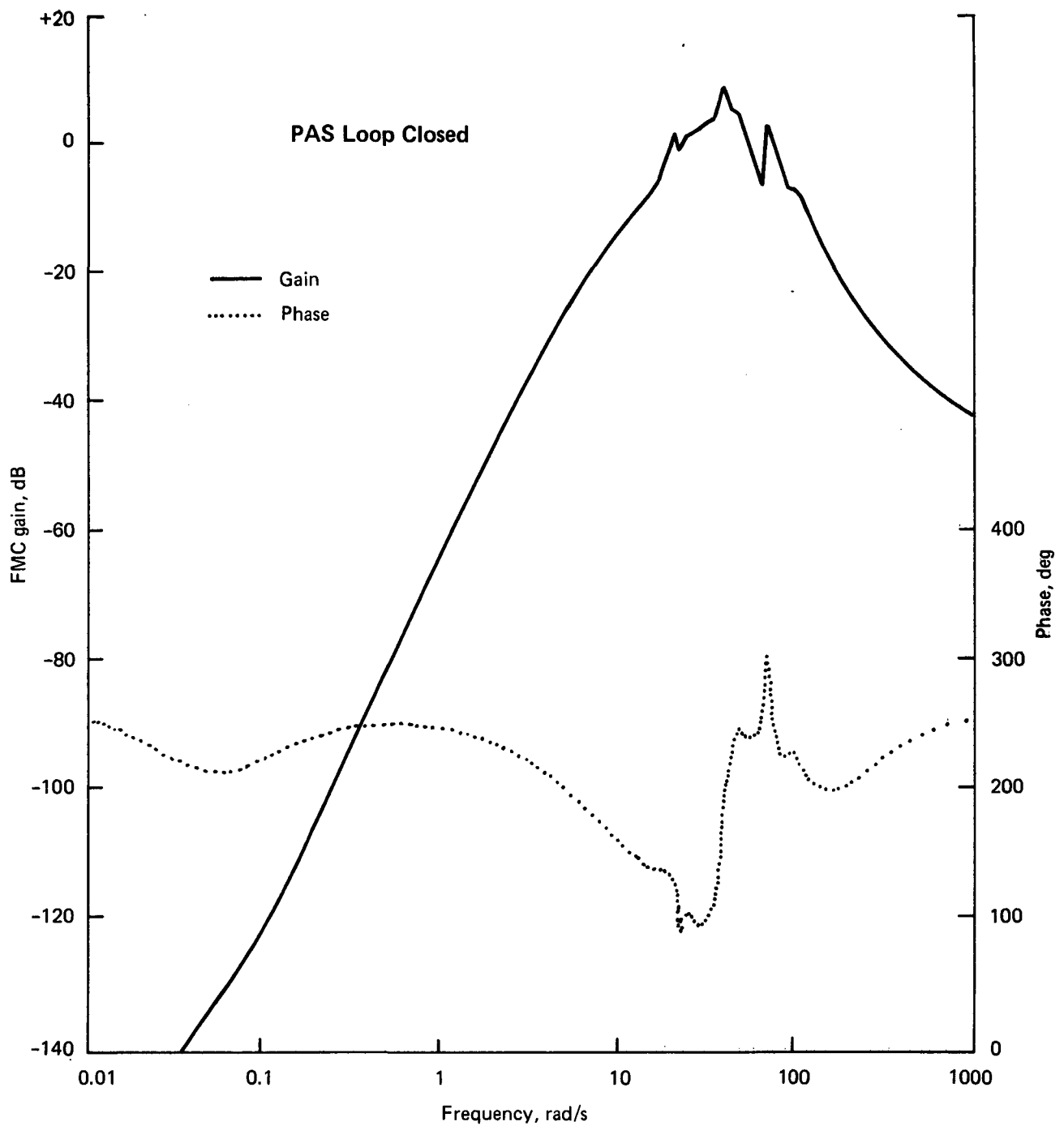
Figure 140. Flutter-Mode Control System Gain and Phase Plot at 1.2V$_D$, Pitch-Augmented Stability System Loop Closed

768-104

Table 24. Poles of Model 768-104 at 1.2V_D With Pitch-Augmented Stability and Flutter Mode Control Systems Active

Real	Imaginary	Zeta	Omega
- 9.00	±286.0	0.031	286.0
- 9.04	±148.0	0.061	148.0
- 9.19	±115.0	0.079	116.0
-12.7	±102.0	0.124	103.0
-11.6	± 94.3	0.122	95.0
-24.6	± 90.3	0.263	93.6
- 7.14	± 73.5	0.097	73.9
- 8.69	± 69.3	0.124	69.9
-15.4	± 60.2	0.247	62.1
-44.8	± 23.9	0.882	50.8
- 0.916	± 48.3	0.019	48.3
-11.8	± 44.6	0.255	46.1
- 4.64	± 45.6	0.101	45.8
-37.5	0	1.000	37.5
- 1.25	± 37.2	0.033	37.2
- 0.690	± 35.8	0.019	35.8
-28.3	0	1.000	28.3
- 2.08	± 23.2	0.090	23.3
- 0.405	± 22.1	0.018	22.1
- 0.794	± 21.6	0.037	21.6
- 1.73	± 18.7	0.092	18.8
- 9.34	± 10.6	0.660	14.2
- 0.329	± 13.5	0.024	13.5
- 2.53	± 7.47	0.320	7.88
- 5.48	0	1.000	5.48
- 1.62	0	1.000	1.62
- 0.02849	± 0.01708	0.858	0.03321
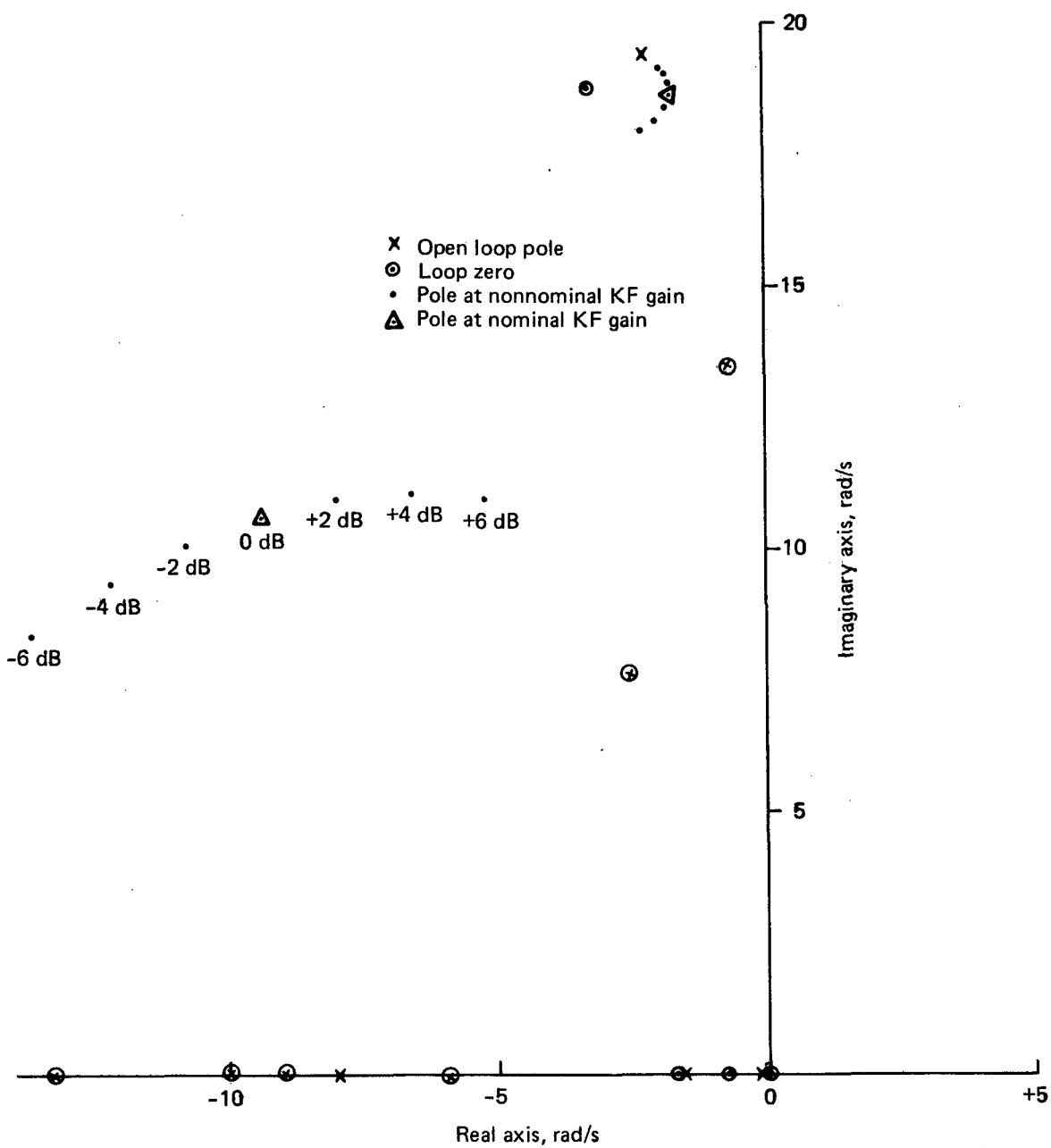
Figure 141. Flutter-Mode Control System Gain Locus at 1.2V_D, 0 to 20 rad/s

768-104

X Open loop pole
◎ Loop zero
• Pole at nonnominal KF gain
△ Pole at nominal KF gain

Imaginary axis, rad/s

Real axis, rad/s
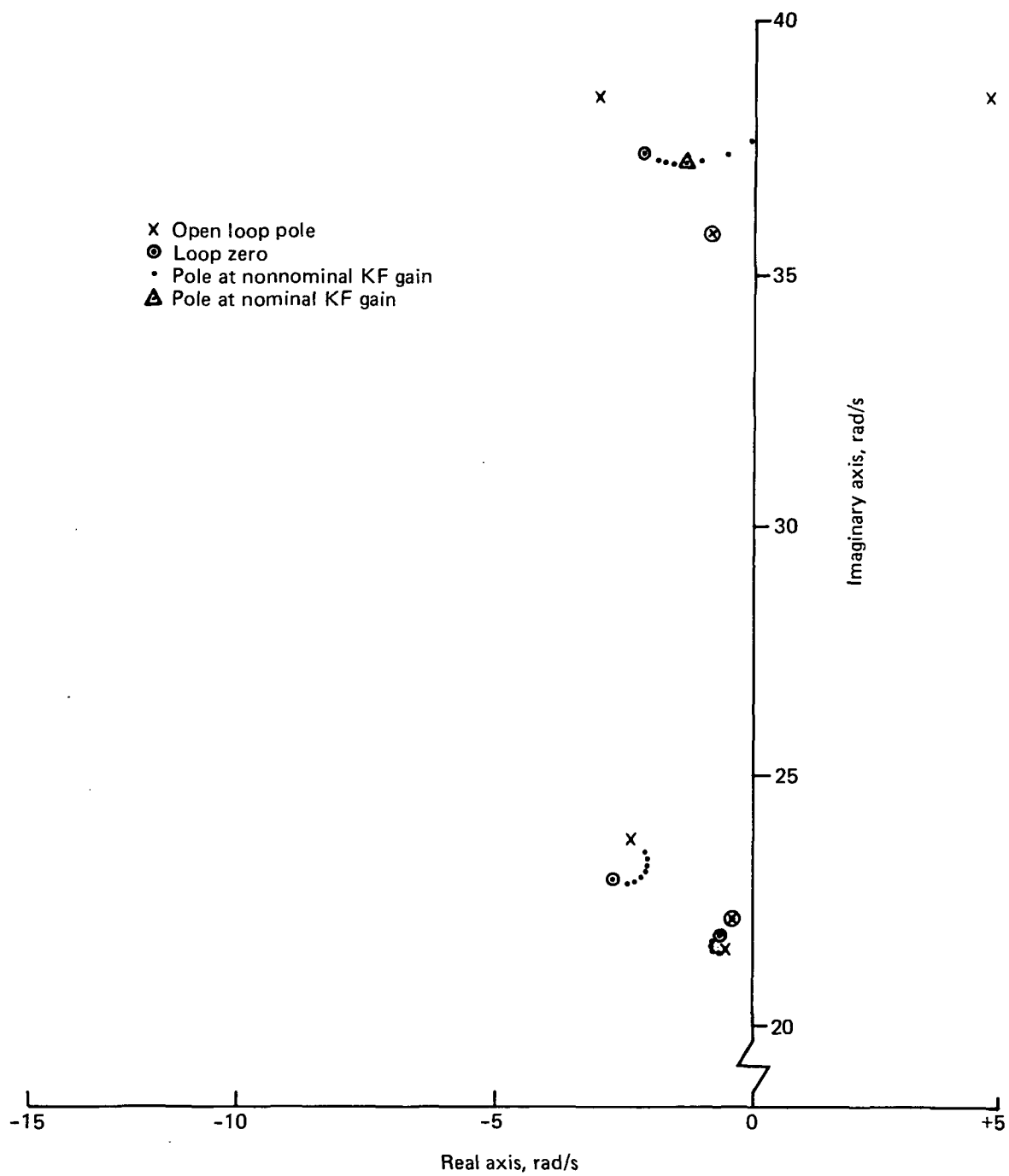
768-104

Figure 142. Flutter-Mode Control System Gain Locus at 1.2V$_D$, 20 to 40 rad/s
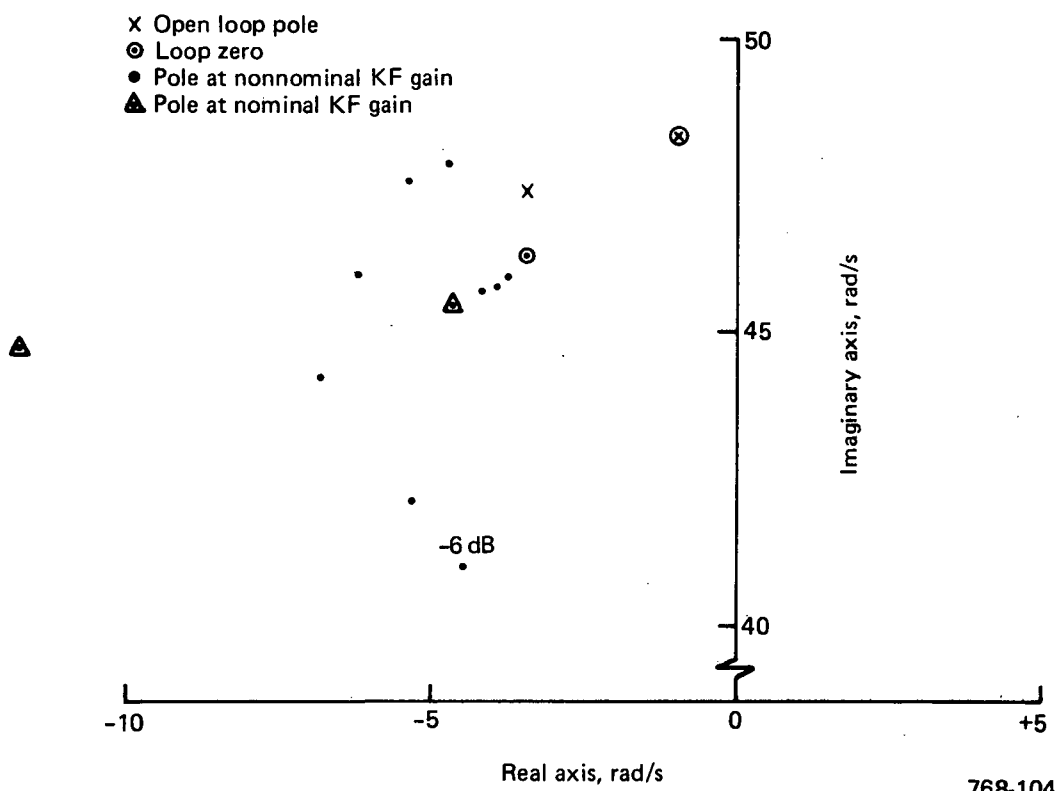
Figure 143. Flutter-Mode Control System Gain Locus at 1.2V_D, 40 to 60 rad/s

768-104

227

x Open loop pole
⊙ Loop zero
• Pole at nonnominal KF gain
△ Pole at nominal KF gain
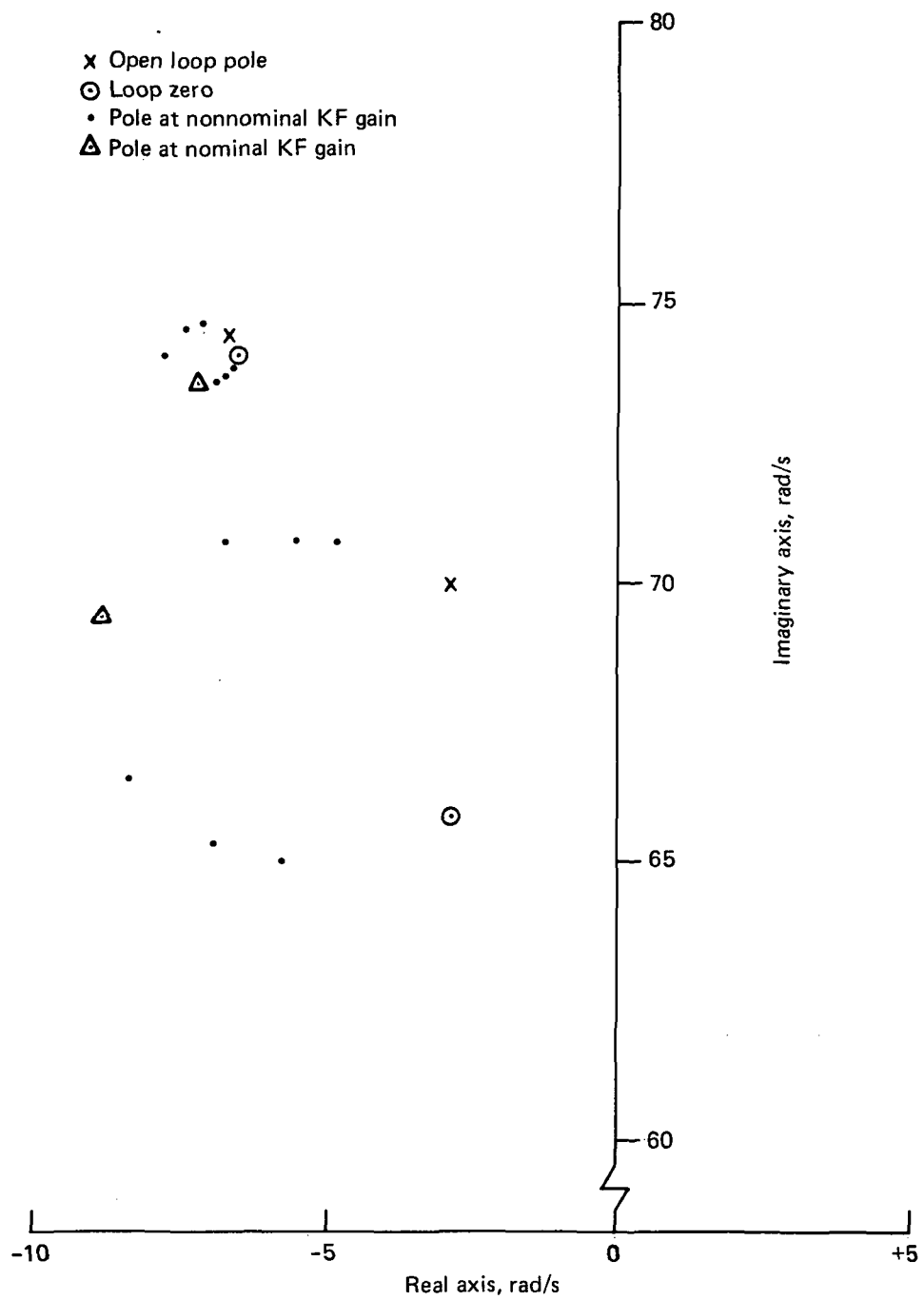
Figure 144. Flutter-Mode Control System Gain Locus at 1.2V_D, 60 to 80 rad/s
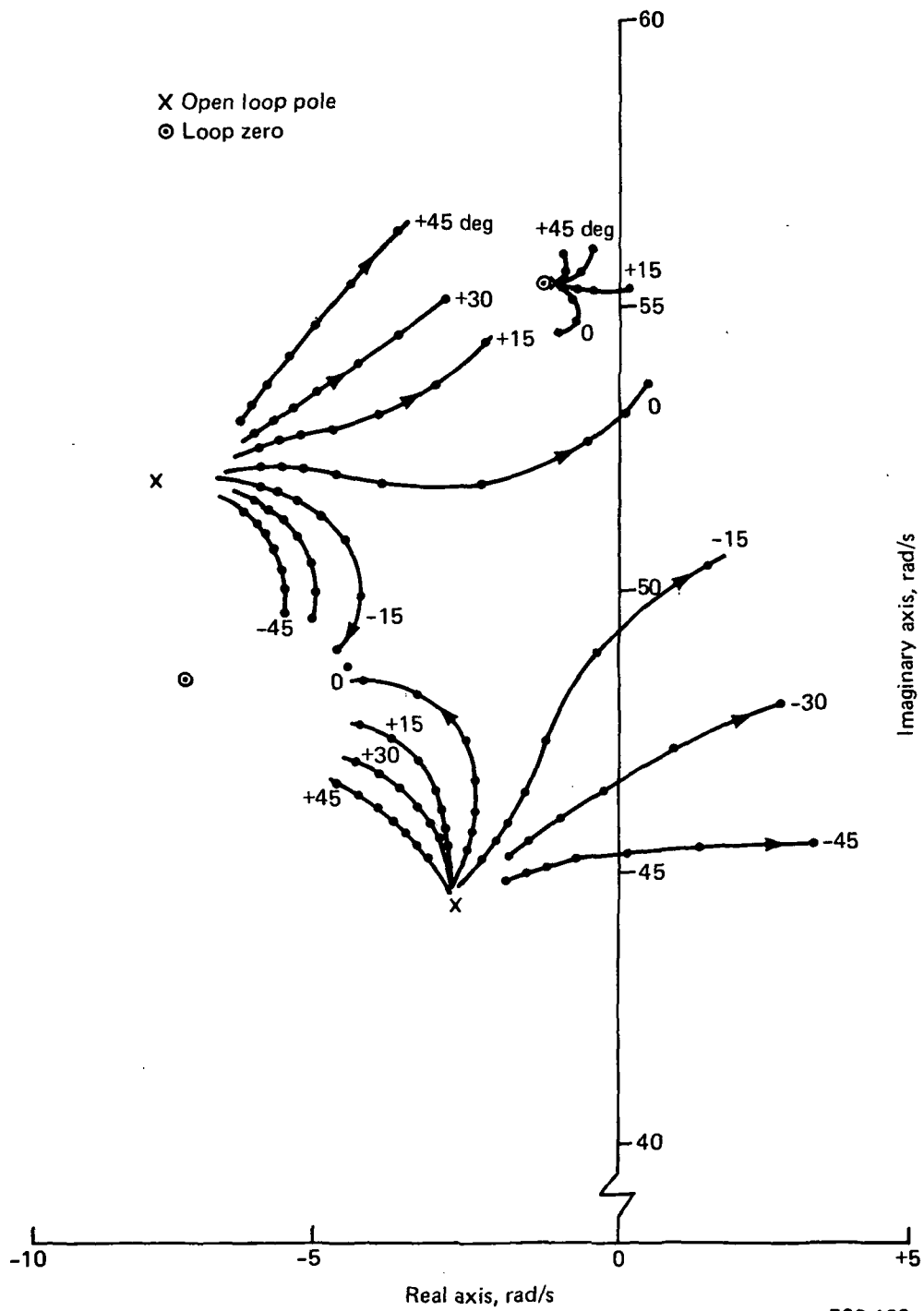
768-104

228
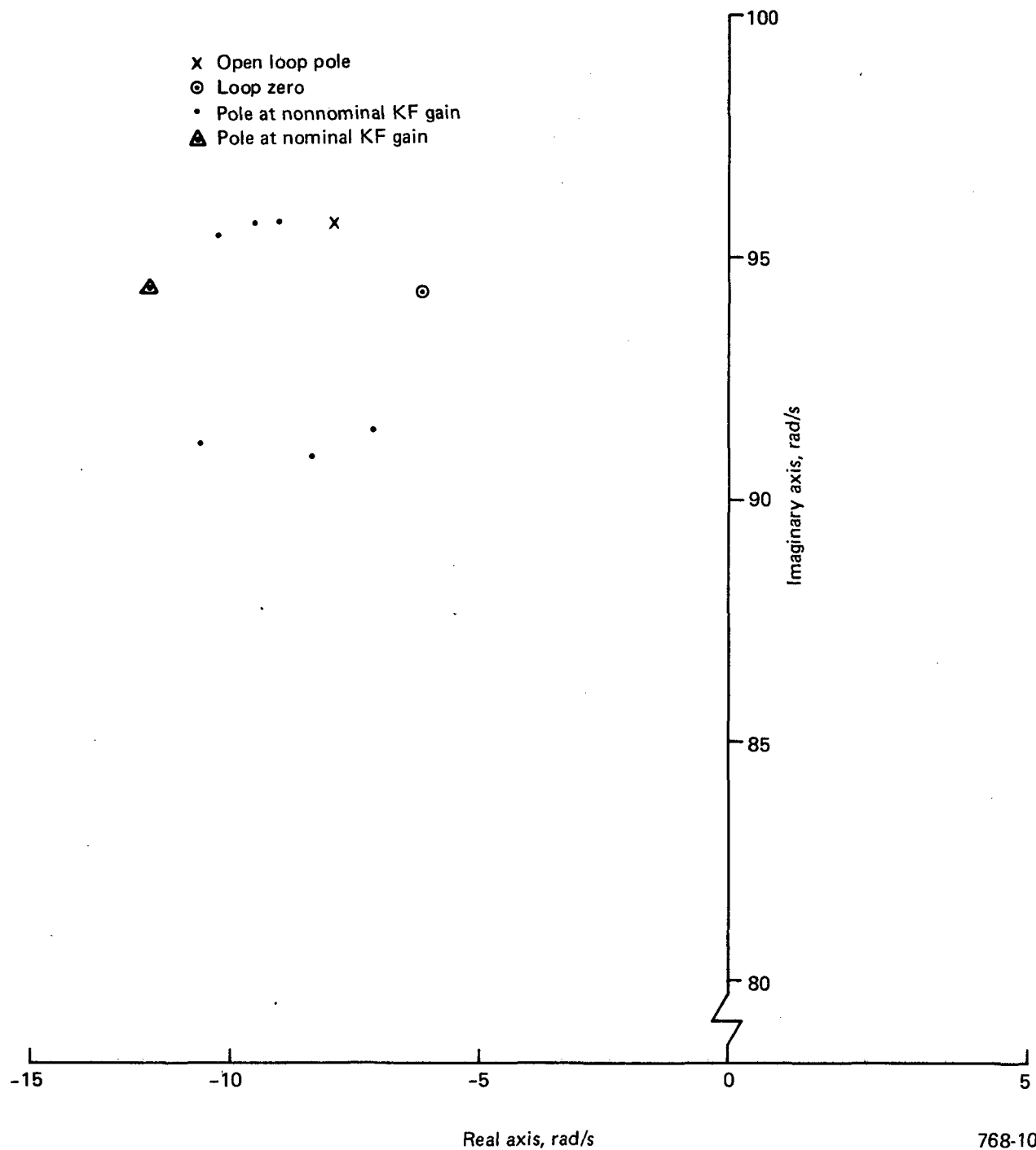
Figure 145. Flutter-Mode Control System Gain Locus at 1.2V_D, 80 to 100 rad/s

768-104
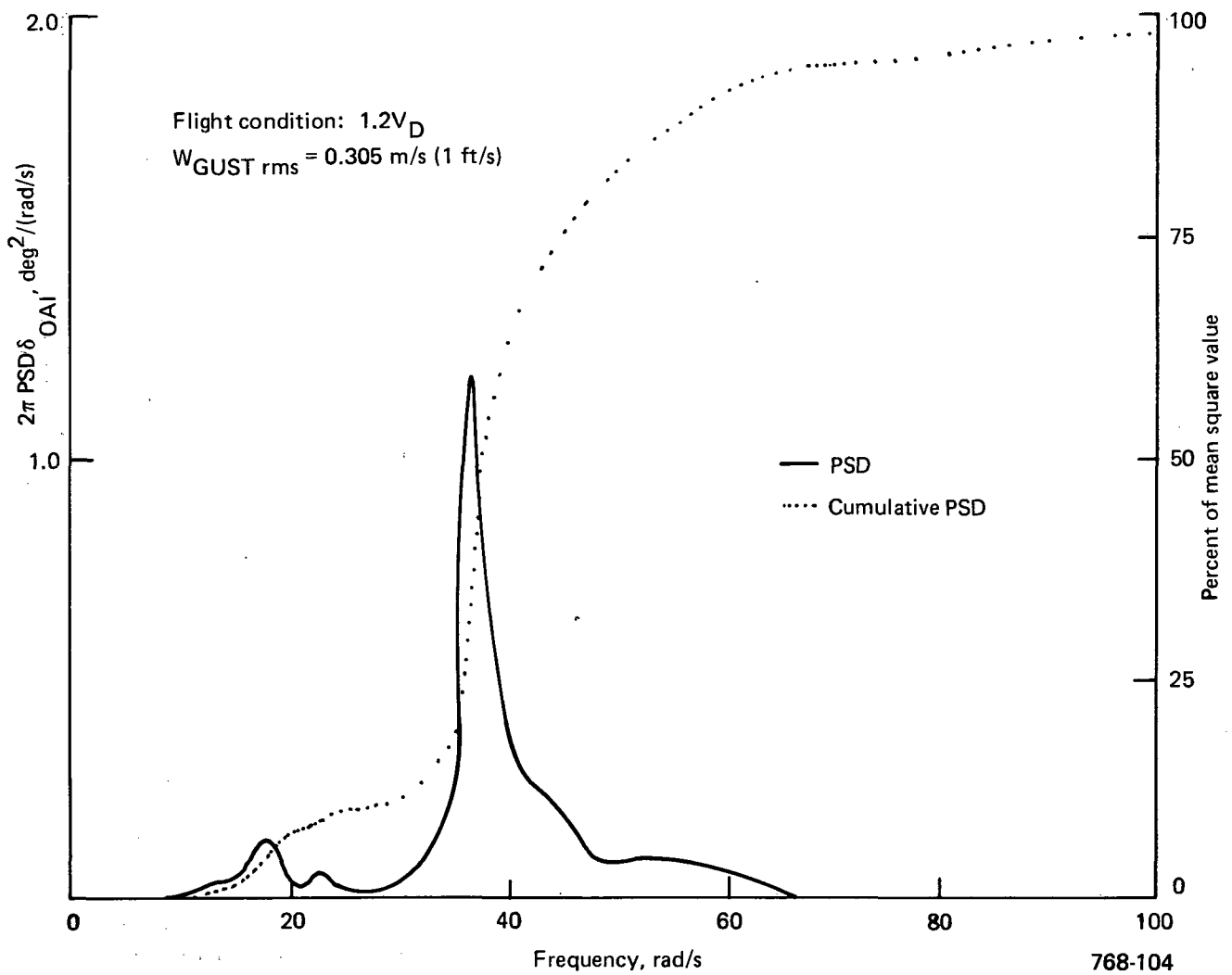
Figure 146. Flutter-Mode Control System Aileron Displacement, δ_{OAI}, Power Spectral Density Plot

768-104
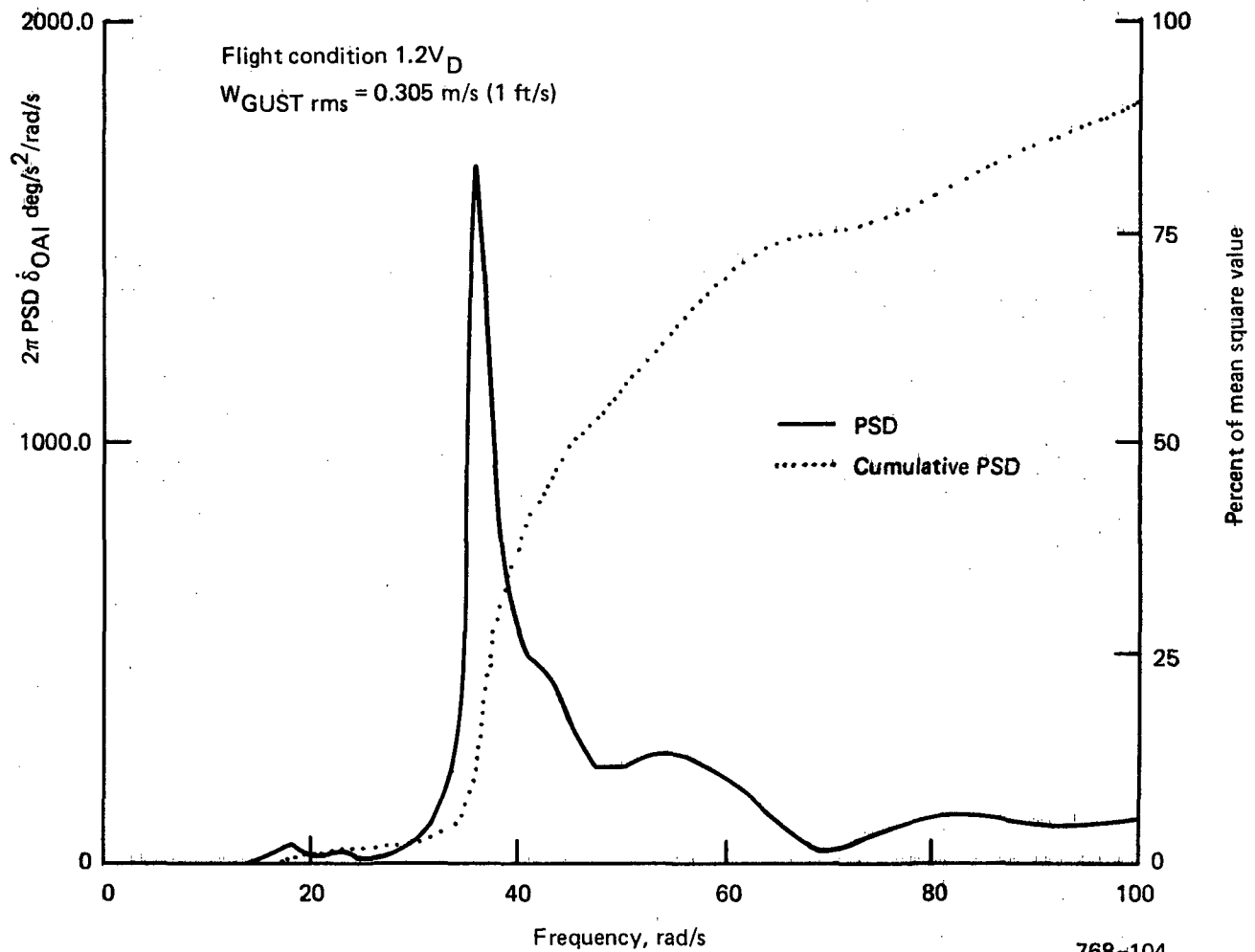
Figure 147. Flutter-Mode Control System Aileron Rate, δ_{OAI}, Power Spectral Density Plot

768-104

At the design flight conditons of V_{MO}, V_D, and $1.1V_D$, the above requirements are fully met by the FMC design shown in Figure 23. At $1.2V_D$, the conjunctive sense of item 1 of the requirements is not satisfied. At nominal-loop phase, the gain margin is ± 6 dB, and at nominal-loop gain, the phase margin is ± 45 deg.

The conjunctive gain and phase margin performance of the FMC at $1.2V_D$ is:

- For +35 deg, -4 dB, +6 dB
- For -35 deg, ± 6 dB
- For +45 deg, -5 dB, +1 dB
- For -45 deg, ± 6 dB

No attempt was made to correct these deficiencies because the high rate requirements of the FMC in turbulence preclude practical mechanization of the system.

In Figures 141 through 145, the roots for the $1.2\ V_D$ condition are shown for gains of ± 6 dB from mominal. The plots show five frequency ranges up to 100 rad/s. The 0 dB point, as identified by Δ, represents the nominal gain on all plots. These data show system stability is maintained over these gain ranges from nominal.

In most instances, the open-loop poles (X), zeros (0), and the seven intermediate roots are shown. When this is not the case, a +6 next to a locus point indicates a root for KF = 6 dB.

7.3.2 ACT SYSTEM MECHANIZATION

7.3.2.1 ACT System Architecture

The ACT system used with this Wing Planform Study is the Initial ACT integrated system (ref 3) minus the FMC function. This system is described in the following paragraphs. As discussed elsewhere in this report, analysis did not indicate any significant benefit from FMC for the 768-104 Configuration.

This ACT system mechanizes three ACT functions; PAS, WLA, and AAL. Figure 148 outlines the interface between major sensors, computers, and actuation systems. This

232
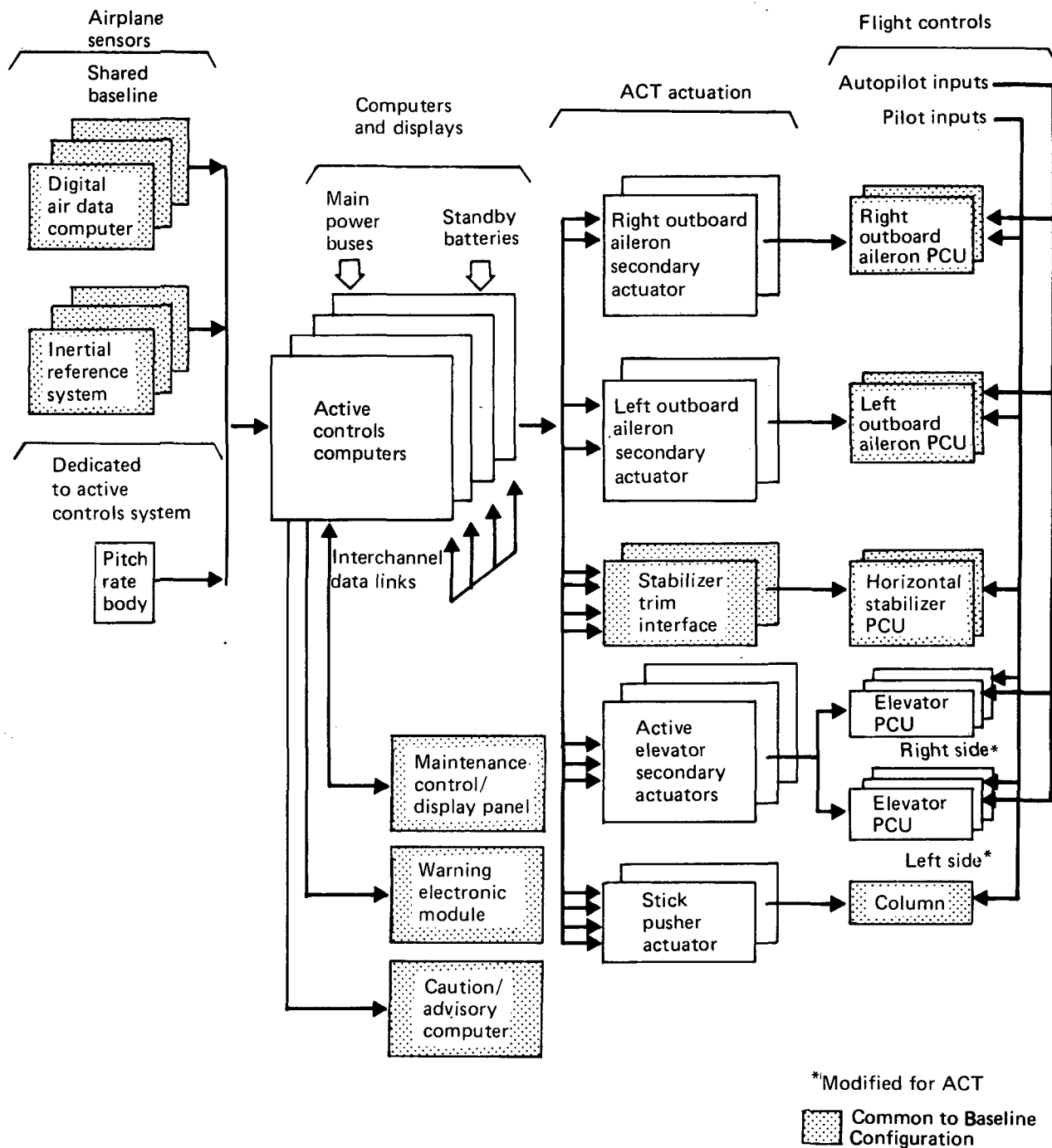
Figure 148. Planform Study ACT System Architecture

768-104, -105, -106

233

control system shares sensors with the automatic flight control and avionics functions of the Baseline Configuration. Each computer receives signals directly from the sensors in the same channel, and the data from the sensors in other channels are transferred from the other computers over cross-channel links. These are dedicated one-way high-speed digital data buses that connect transmitters and receivers in the computers. This cross-channel data communication scheme has been used in the Baseline automatic flight controls system (AFCS) and other applications. The crucial ACT function (PAS) is mechanized in quadruple redundancy, and the critical functions (WLA and AAL) are mechanized in triple redundancy. To minimize the probability of loss of all critical functions if two computers fail, the critical functions are distributed among the four computers, which have identical software for interchangeability.

Each computer consolidates all input signals (analog, digital, and discrete) in a signal selection and failure detection (SSFD) process. The SSFD process selects the most trustworthy of the redundant sensor inputs. Controlled by software, the process is necessarily varied because of differing signal character and use and differing levels of redundancy. Fundamentally, it uses midvalue selection for three input signals, average derivation for two inputs, and a substitute value where one sensor input remains. A four-sensor set is treated as three with an operating standby. The failure detection is a software-controlled logical comparison of inputs and selected signal to single out any value that is inordinately different from the others.

The SSFD provides the same sensor signal in all computers for computation of the control laws. The computers of the Initial ACT system are frame synchronized such that each simultaneously executes the same computations. Using the SSFD process and frame synchronization, the four computers transmit essentially identical command signals to the ACT actuators, reducing the need for actuator equalization, simplifying the design, and simplifying the failure detection algorithm for passive failures. The redundant ACT command signals sent to the actuators are consolidated at the actuator for use in a mechanical voting process.

A force-summed multiple-channel secondary actuation system converts the ACT electric signals into a mechanical signal that series-sums with the pilot's mechanical input.

234

ACT Functions—The PAS function includes short-period and phugoid mode control. Figure 149 shows a block diagram of the redundant PAS and the elevator off-load functions. The short-period PAS is a crucial function that is implemented by quadruple pitch-rate sensors and computers and by triple actuators. Mathematical models of the actuators are mechanized in the quadruple computers to provide
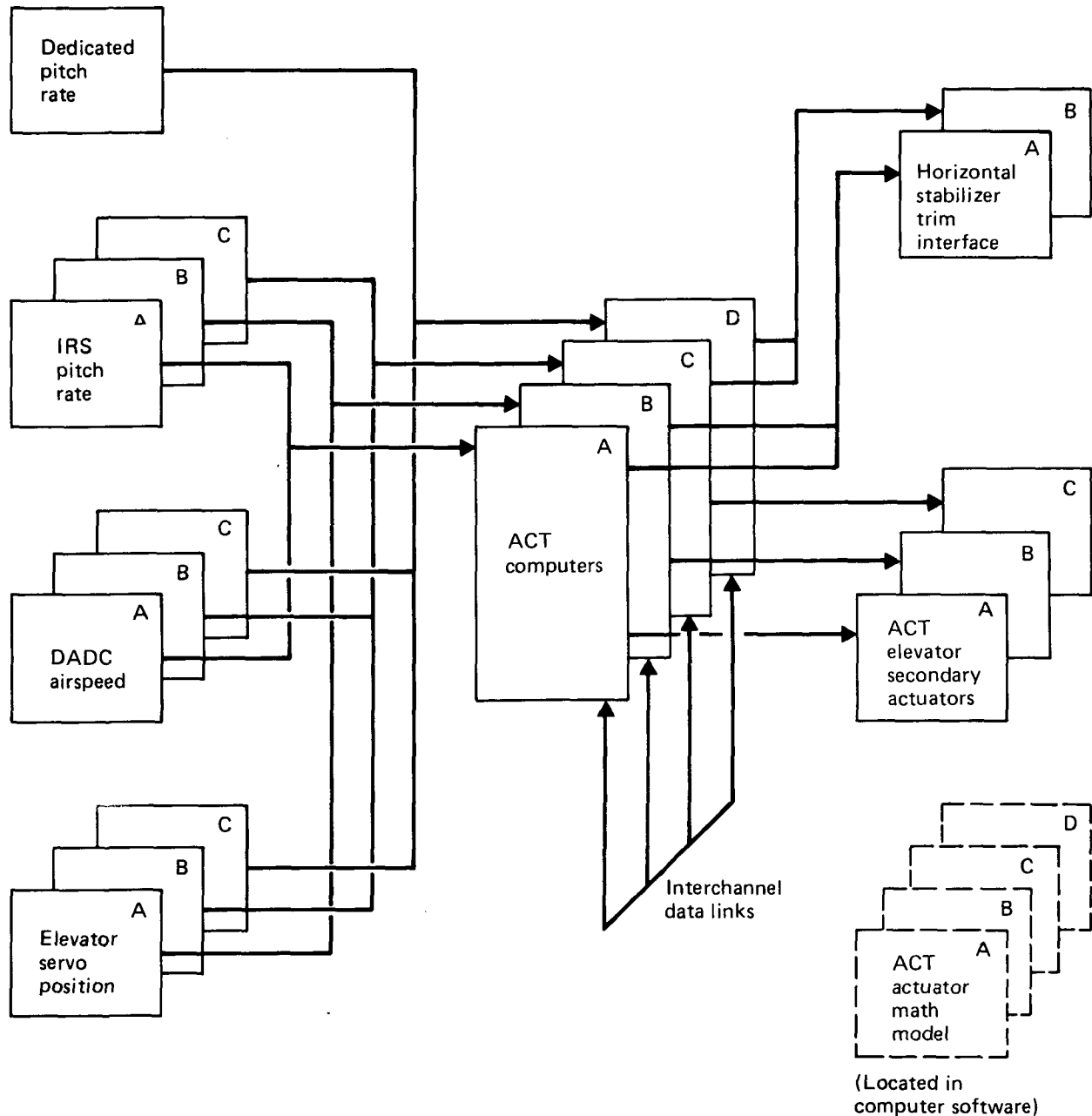
Figure 149. Pitch-Augmented Stability (PAS)

effective quadruple signal selection of actuator output. The short-period control essential PAS requires a fixed pitch-rate feedback gain, and the phugoid control full PAS requires an airspeed feedback to stabilize the airplane. The servo position signals are used to relieve a steady-state elevator trim deflection. This is achieved by trimming the horizontal stabilizer through the horizontal stabilizer trim interface (fig. 149).

Figure 150 shows a block diagram of the WLA function. WLA reduces maneuver-induced wing vertical bending moment by sensing vertical acceleration at the airplane
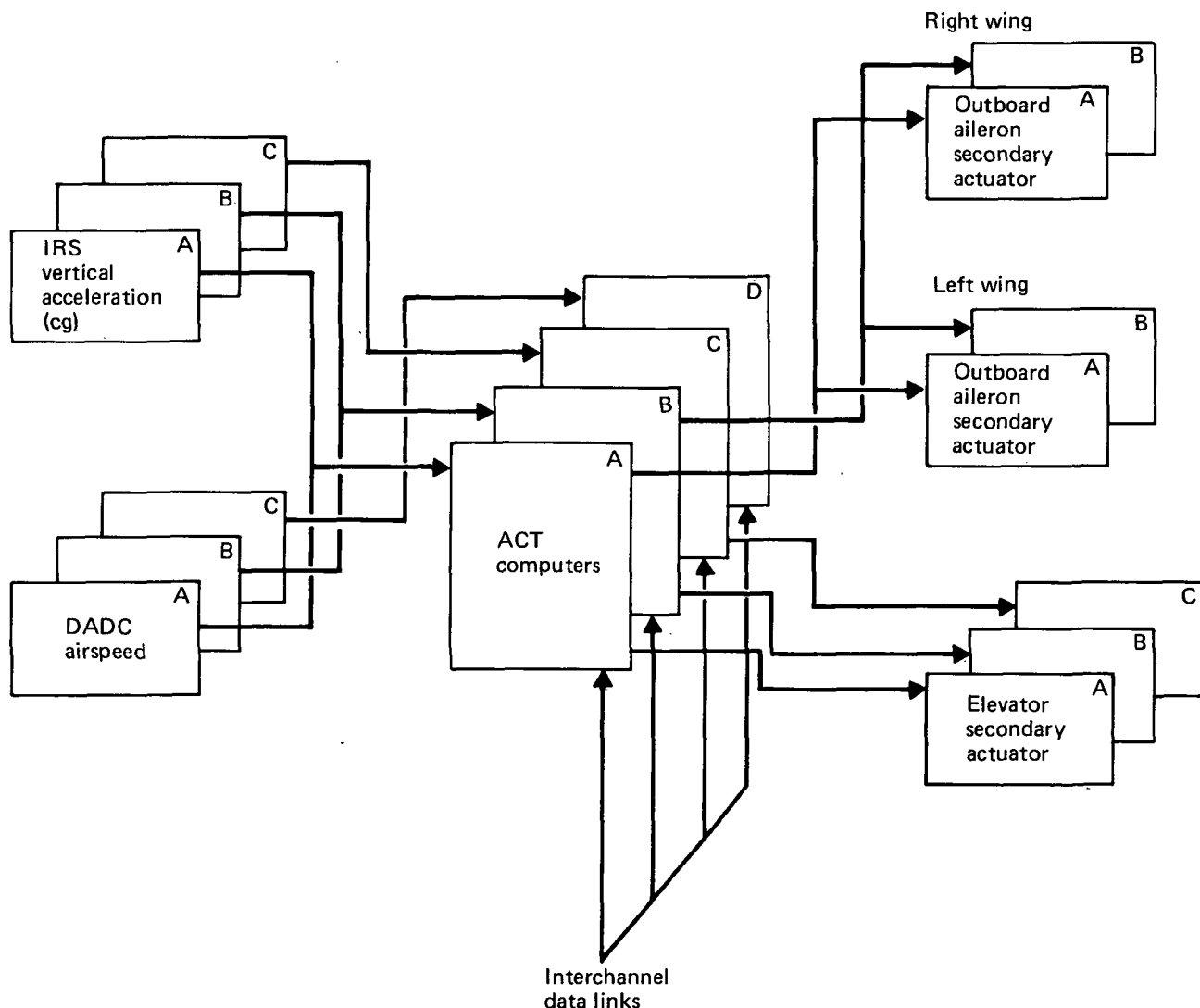
Figure 150. Wing-Load Alleviation (WLA)

768-104, -105, -106

cg and by commanding the outboard aileron. The feedback from the accelerometer at cg to the aileron destabilizes the short-period and phugoid modes, but cross-feeding the MLC command signal to the elevator compensates for the instability. For the outboard aileron, force-summed secondary actuators convert the electric WLA command to a mechanical signal.

The AAL function prevents the ACT airplane from reaching excessive angle of attack by sensing angle of attack and commanding a forward (airplane nose-down) column deflection. Figure 151 is a block diagram of the AAL function. The pitch-rate signal is used to provide anticipation in the AAL control to prevent overshoot of the limiting angle of attack in rapid maneuvering.
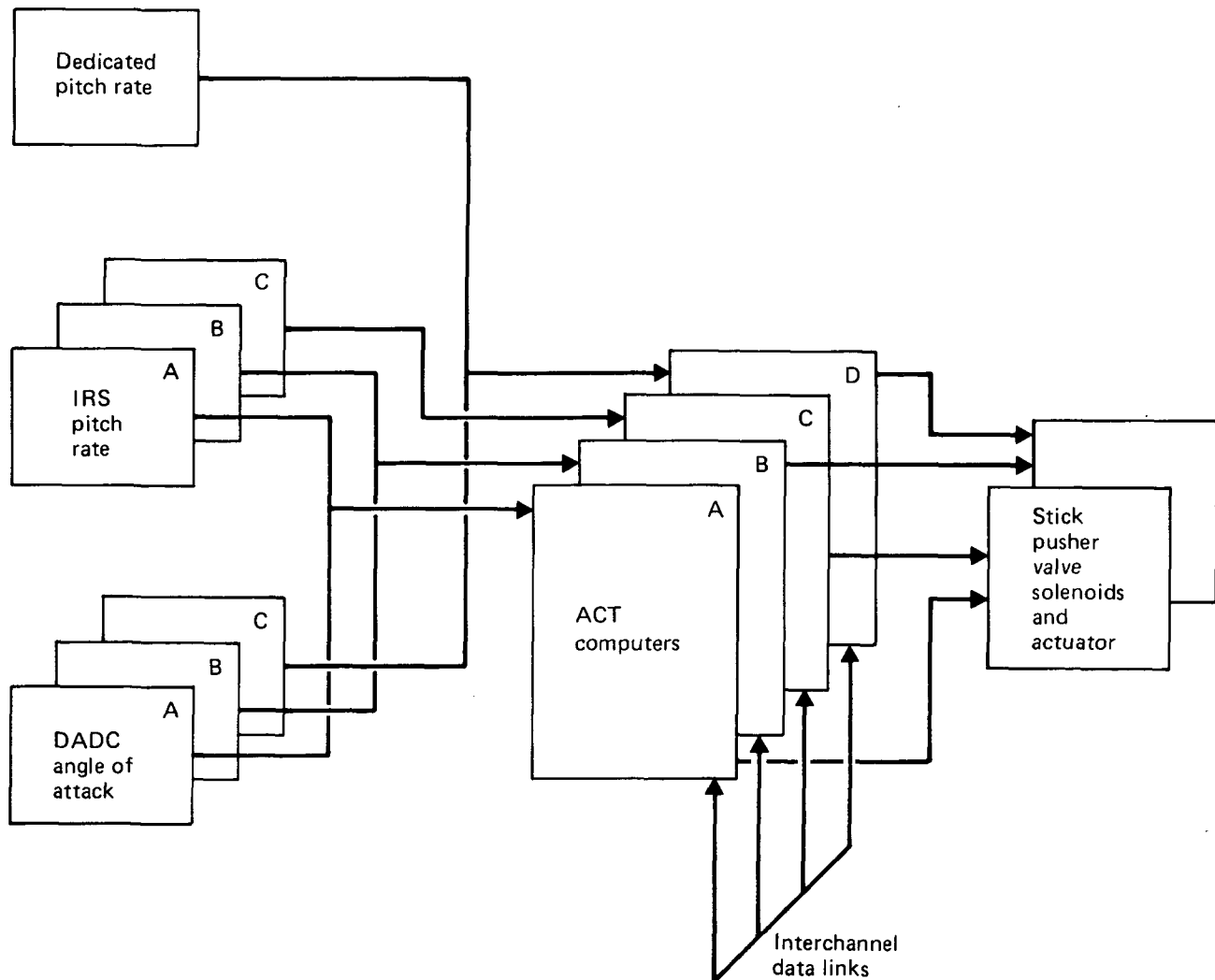
Figure 151. Angle-of-Attack Limiter (AAL)

768-104, -105, -106

237

7.3.2.2 Sensors

This ACT system uses both shared and dedicated sensors to implement the various ACT functions. Figure 152 illustrates the general locations of the ACT major sensors. Many sensed parameters required for ACT are already in the Baseline Configuration inertial reference system (IRS) and the digital air data computer (DADC), both configured in triplex. These computers provide airspeed, Mach number, angle of attack, pitch rate, and vertical acceleration at the cg.

The dedicated pitch-rate sensor, used in conjunction with the Baseline Configuration triplex IRS pitch-rate signal, serves to implement the quadruply redundant PAS
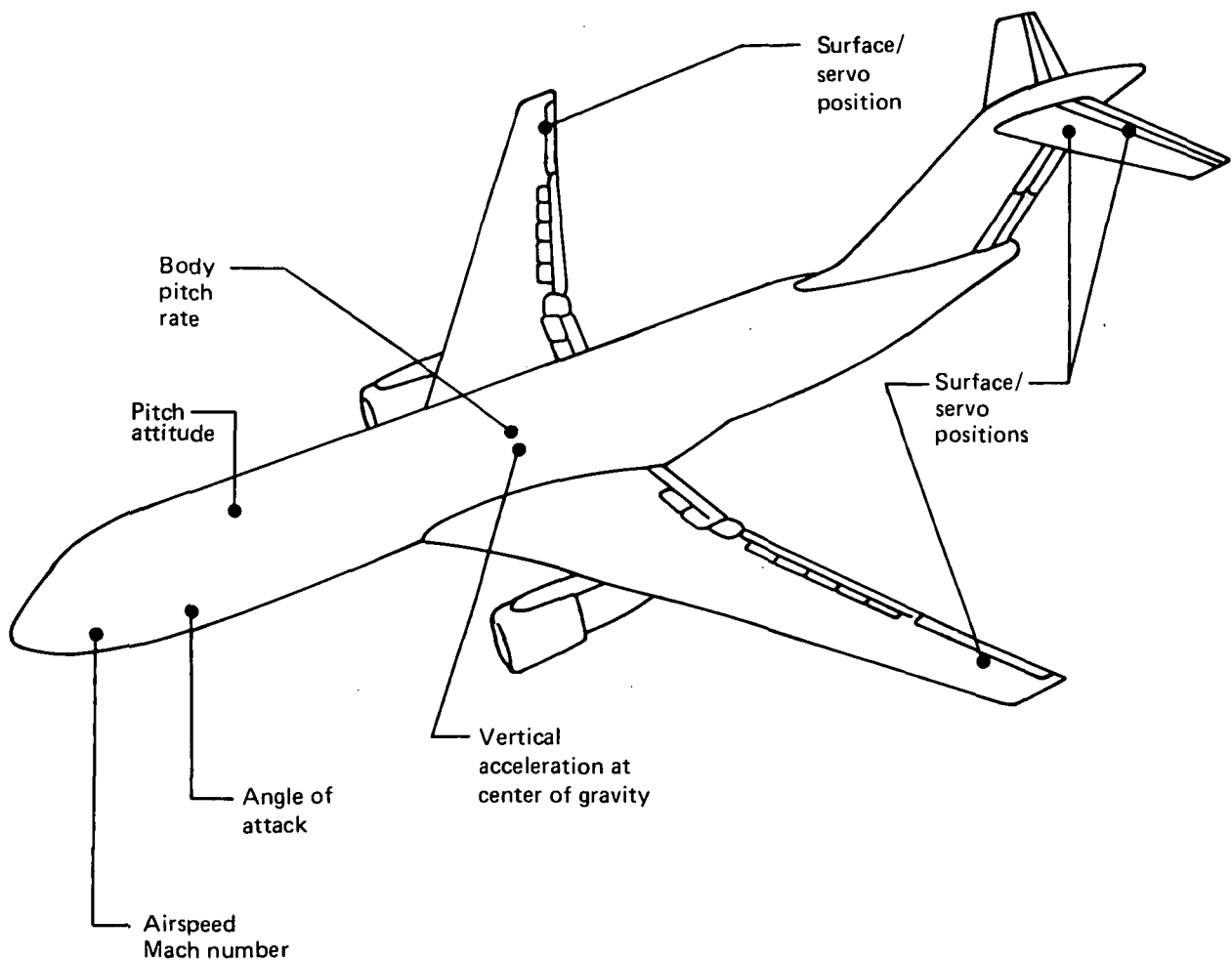
768-104, -105, -106, -107

Figure 152. ACT System Variable Sensors

function. Sensors are dedicated to their respective digital ACT computers, where data are then transmitted cross-channel to satisfy the redundancy requirements. Table 25 relates the various sensors to the respective ACT control functions.

Table 25. ACT Variable Sensors

ACT variable sensors	ACT functions			
	PAS		MLC	AAL
	Essential	Full		
Pitch rate, body	X			X
Vertical acceleration at center of gravity			X	
Mach number				X
Airspeed		X	X	X
Angle of attack				X
Elevator secondary servo position	X	X	X	
Stabilizer position		X		
Outboard aileron, secondary servo position			X	
Pitch attitude		X		

768-104, -105, -106

7.3.2.3 ACT Computer

The ACT computer is the key element in this integrated control system concept. This section presents the salient features of a candidate ACT computer that was based upon work described in the Airborne Advanced Reconfigurable Computer System (ARCS) Program (ref 10). Data estimates for the ACT computer were derived from current technology production flight control hardware.

The ACT computer may be characterized by the following design features, which are responsive to the overall system requirements:

● Digital implementation to facilitate a comprehensive and flexible design suitable for real-time control applications

239

- A computer architecture structured to handle flight safety crucial and critical ACT functions

- A highly fault-tolerant design, which implies the ability to withstand transient faults in the system and recover normal operation

- Extensive fault identification and fault storage capability, necessary to enhance maintainability of the overall system

Computer Architecture—The ACT computer (fig. 153) retains many of the ARCS architectural features, such as the bus-oriented structure, autonomous input/output (I/O) operations, and microprogrammed control processing. The basic change from the ARCS to the ACT application is in partitioning crucial and noncrucial functions; i.e., PAS is separated in both I/O and memory from noncrucial functions such as WLA. This change is essential because of the extremely high reliability required of the crucial function.

Each ACT computer in the parallel redundant system possesses identical hardware and software. Communication between computers is required to provide sensor data exchange and synchronous operation from duplex through quadruplex redundancy levels. The ACT computer consists of three major sections, central digital processing, I/O, and power supplies, communicating on a common bus structure. The central digital processing section is common to all processes and is therefore a critical element for all ACT functions. The I/O section is designed for flexibility and can be adapted to the computer application.

The digital processing section contains the central processor unit, memory, and iteration timing reference/discrete modules fundamental to the processing of all ACT functions. All intracommunication is handled by the bus structure. The modules are:

- A central processing unit microprogrammed as a general purpose parallel processor

- Two main memories partitioned into flight-crucial and not flight-crucial operations (physical memory mapping aligned to software module structure)

Digital Processing Section

Crucial memory

Noncrucial memory

Program memory (ROM)

Scratch-pad memory (RAM)

Program memory (ROM)

Scratch-pad memory (RAM)

Central processing unit

Timing reference and watchdog monitor

Discrete and maintenance memory

28V dc supply

ACT T-R bus

Standby battery

Power supplies

Short-term energy storage

—— Data
---- Control
—·—· Power

CPU bus B

CPU bus C

PAS_SHORT input/output and servo electronics

Analog input/ output and servo electronics

Discrete input/ output

Digital input/ output

Cross-channel input/ output

Ground support interface

Crucial input/output

Noncrucial input/output

Input-output section

768-104, -105, -106

Figure 153. ACT Computer Block Diagram

● A timing/discrete module for timing, monitoring, machine/system status, and nonvolatile maintenance data storage

The I/O section of each ACT computer consists of analog, digital, and discrete modules providing communication between the digital processing section and the

241

external environment. All I/O modules interface directly with the bus structure, and each contains a dedicated memory addressed by the central processing section. The I/O modules are process oriented:

● An essential PAS I/O dedicated to the flight-crucial function and containing a mixture of analog/digital processing and servo drives

● An analog I/O partitioned into analog/digital signal conditioning, conversions, and servo output drives

● A discrete I/O that services system discretes at two logic levels

● A digital I/O providing serial digital Aeronautical Radio Incorporated (ARINC) 429 Digital Information Transfer System (standard) data communication between the ACT computer and system sensors, the maintenance control/display panel, and the flight deck caution system

● A cross-channel data link for high-speed data exchange between redundant ACT computers

● A ground support interface with line and shop maintenance support equipment

The power supply section for each computer accepts ACT channel power, which draws from dual 28V dc sources (main dc bus and standby battery bus). It conditions and generates output power for internal computer operations, discrete circuit excitation, and actuator shutdown logic. Sensor excitation in the integrated system configuration is derived from the ACT power buses. The same excitation power is input to the computer for demodulation reference and power normalization. The computer power supplies contain monitor and protection circuitry for internal high/low dc-voltage tolerance monitors, short circuit, over voltage, and thermal overheat conditions. Computer power outputs can sustain a short circuit without causing failure to internal voltage supplies.

Computer Characteristics—Table 26 summarizes both functional and physical characteristics of the ACT computer. The computer timing is multirate structured to accommodate all the ACT function control law requirements. A minor time frame of 10 ms was selected to meet all the ACT control law bandwidth requirements except MLC. MLC control laws are executed at the major frame interval of 20 ms.

Table 26. ACT Computer Characteristics

General	Digital, general purpose, stored program
Arithmetic	Binary, 2s complement fixed point, 16-bit data/instructions standard
Memory (main)	32K ROM, program/data constants 2K RAM, variable program 128-word, 8-bit nonvolatile, fail vector data
Input/output	16/5 analog 40/20 discrete 3/2 serial digital (ARINC 429) 3/1 digital (cross channel) 1 GSE interface
Timing	10-ms minor frame 20-ms major frame
Interrupts	8 priority level, software maskable
Power	Dual 28V dc, 100W dissipation
Volume	0.0164 m^3 (1000 in^3) (ARINC 600—8 MCUs)
Weight	12 kg (26.5 lb)
Reliability	6800 hr MTBF (inhabited, 40°C [104°F])

768-104, -105, -106

Memory sizing was estimated based on comparable digital automatic flight control computer programs for tasks similar to those required for ACT; these were capacity sizing estimates only and include a 50% growth allowance. I/O signal capacity reflects the integrated system configuration based on control laws chosen to fulfill the Initial ACT requirements. The physical characteristics summarize the size, weight, and packaging configuration typical of the new ARINC 600 standards for digital avionic equipment. Reliability estimates are consistent with new-generation digital flight control hardware used on the Baseline Configuration.

Redundancy Management—Redundancy management is an automatic process designed into the ACT computers to provide maximum functional survivability in the presence of transient or permanent fault conditions. Redundancy management is the heart of the fault-tolerant system and is based on the following strategy:

- Information exchange between the system-redundant channels, made through the ACT computers, is largely implemented in software.

- All system elements are monitored for faults by strategically placed failure detectors in the computer hardware and software.

- Faults declared hard failures are isolated under software control to prevent detrimental effect to the good signal outputs.

- The remaining good elements are then reconfigured to allow continued operation with normal or degraded performance.

The various processes that provide redundancy management are illustrated in Figure 154 and described in the following subsections.

Synchronization—The ACT computer uses a software-controlled routine to establish and maintain major frame synchronous computations in all four channels. The synchronization concept is based on a "wait" algorithm, which requires that all computers be ready within a set time window with no detected failures before synchronization release is achieved. Lack of synchronization will not inhibit continued processing of any channel, but a fault notice will be stored for maintenance.

Signal Selection—The Integrated ACT system consolidates signals from redundant channels in two voting planes, one between the ACT sensors and the computers and another at the secondary actuators force-summed output.

Signal selection provides a point for consolidating the redundant sensor data so that all processors operate on identical data, and, therefore, perform identical processes with identical results. Such a voting plane provides additional fault tolerance to the system. A signal selection concept is chosen primarily for its ability to prevent sensor

244
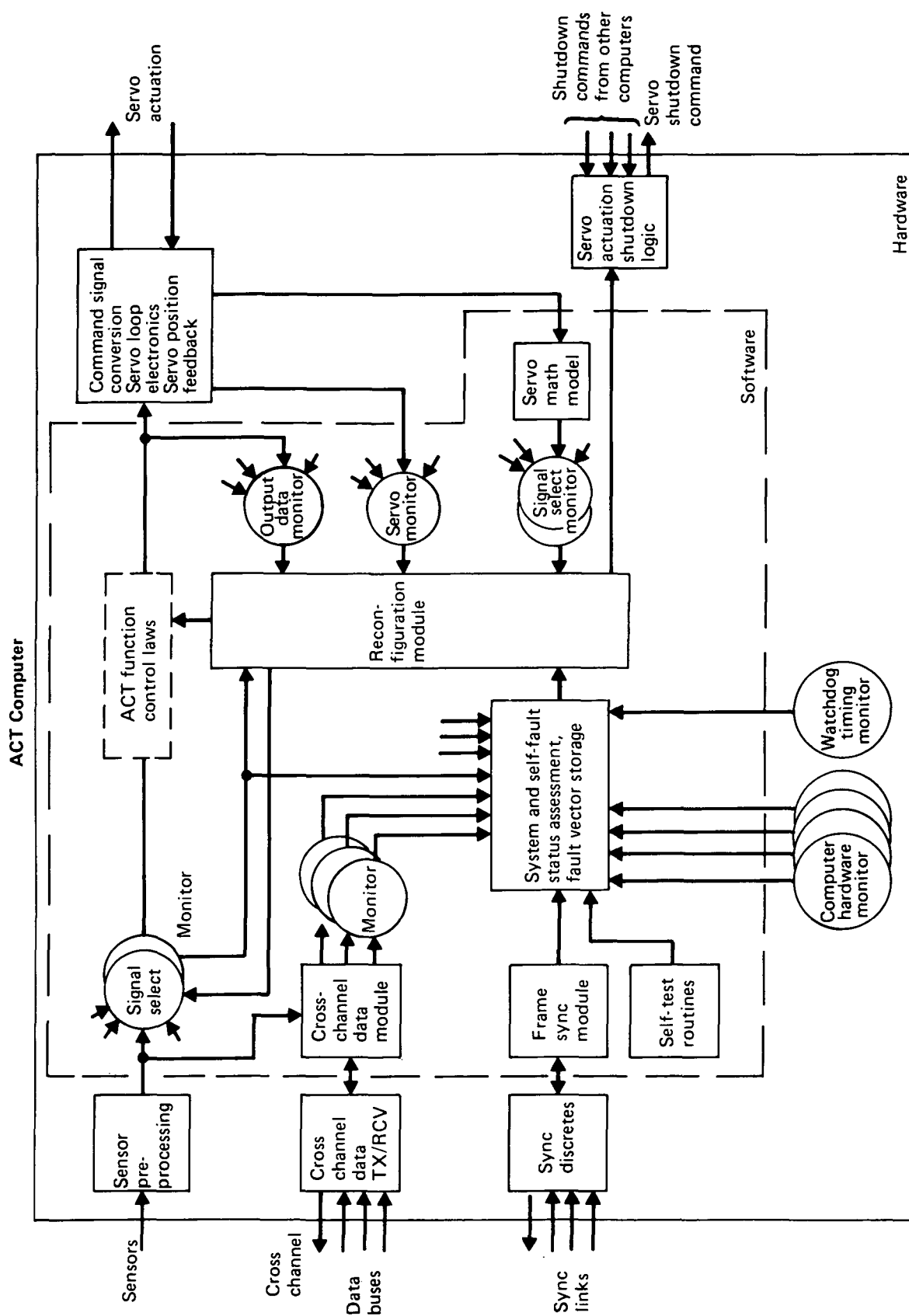
Figure 154. ACT Redundancy Management Process Overview

768-104, -105, -106

245

failures propagating into a hazardous airplane maneuver. It is anticipated that oscillatory and step modes will present the most severe conditions for ACT with regard to pitch stability and wing structural design.

The signal-selection process for the ACT system is implemented in the computer software. Sensor sets are dedicated to the computers (figs. 149 through 151), and the only interconnection between redundant channels is through the computer cross-channel data transfer link. Sensor data are, therefore, transferred between computers ahead of the signal-selection voting plane.

The concept is based upon an active-standby method for quadruple-channel operation, with three inputs designated "active"; the fourth input, on "standby," switches into "active" status when the first "active" signal fails. Triplex sensor inputs are treated as quadruple inputs with a first failure. Upstream failure monitoring inhibits the signal selector from switching to a bad standby signal at the first failure of an active input. The median is selected for both normal and first-failure operation. Signals are averaged after a second input failure, operating in dual-channel mode. A third failure switches the selector output to a default value, which may be zero, or the last averaged value, depending on the type of sensor involved. For example, a direct control variable (such as acceleration) can be made zero, but a variable (such as airspeed) that drives functions would be held to a constant value to avoid a large control transient.

Cross-Channel Data Link—Dedicated, high-speed, one-way digital data buses provide the cross-channel communication link between the redundant computers to achieve interchannel transfer of sensor data, synchronization of computations, and flow of necessary data to perform cross-channel signal monitoring and reconfiguration if failures occur. Redundant data must be transferred between channels and processed within the same minor time frame to minimize computation delays. Careful design is required to avoid propagating faults between redundant channels through the data links.

Failure Protection—Several methods of failure protection are incorporated into the ACT System to maximize survivability and minimize effects of failures on airplane performance. Figure 155 summarizes the overall failure protection design for the

246

```
                    ┌─────────────────────┐
                    │ ACT failure protection │
                    └─────────────────────┘
```

System design

- Redundant channel physical/functional isolation
- Hydromechanical voting in actuation
- Computer architecture hardware/software

Failure monitoring

System level monitors

Primary detection by cross channel comparison of:
- Sensor inputs
- *Computer command* outputs
- Servo valve spool position and current feedback

Computer self monitors

- Internal power
- Watchdog timing
- Memory partitioned sumchecks, crucial/*critical*
- Memory data parity and pattern testing
- Arithmetic overflow
- Input/output wrap-around tests on analog, discrete, serial digital hardware

Computer/system interfaces

Test/maintenance fault diagnosis by inline monitoring of:
- *Sensor validity discretes* (self test)
- Servo position feed-back LVDT
- Power supplies status
- Digital communication links *between computer and maintenance panel and between computer and flight deck caution/ warning systems*

768-104, -105, -106

Figure 155. ACT Failure Protection Summary

ACT system and illustrates the top-down structure for redundant channel operation. This is divided into failure detection by design and by monitoring. Failure detection by design includes such features as hydromechanical voting in the actuation concepts, redundant channels, physical and functional isolation, and computer architecture, hardware and software design. Failure detection by monitoring, accomplished within each ACT computer, is composed of system monitoring and computer self-monitoring.

247

System monitoring, largely a software process, uses cross-channel comparison by the computers to decide the level of redundant operations. Single-channel operation is unacceptable in the ACT design. To detect sensor faults, computer faults, and servo actuation faults, monitoring at three basic planes uses cross-comparison techniques in a continuous checking process associated with the real-time control activity.

Basic areas checked are:

● Internal power supplies

● Machine timing

● Processor capability, memory sum checks and parity, and invalid arithmetic operation

● Input/output, wraparound testing of all digital, discrete, and analog circuitry

Reconfiguration—The flight-critical nature of the ACT system dictates the need to maximize system survival through reconfiguration techniques. Because reconfiguration relies on fault detection by cross-channel monitoring, single-channel operation cannot be guaranteed. Even current inline monitoring techniques cannot totally ensure channel health.

Reconfiguration is defined as the process of attempting to recover from a fault. A detected fault may appear temporarily (transient) or become permanent. Three possible outcomes result from such fault conditions within the ACT system:

● The system recovers normal operation
● The system survives with degraded capability
● The system fails and shutdown occurs

Degradation is defined as: (1) reduced system redundancy level, or (2) operation with simpler control laws and perhaps a penalty in airplane flying qualities or restricted operation. The latter accommodates sensor faults, presuming that alternate control laws exist. For example, WLA (fig. 150) uses airspeed as a gain schedule input. If a

248

DADC fails, the system would be reduced to a two-channel operation. If a second DADC fails, a substitute control law could be activated using the flap position as an approximate airspeed indication.

Reconfiguration for ACT is divided into four areas: electric power, sensor inputs, computer functions, and servo outputs. The strategic monitoring points in the computer hardware and software (fig. 154) are basic to the reconfiguration process.

Electric Power—The ACT electric power system is organized on a per-channel basis, with airplane battery backup power available to each operating channel within 50 ms of detection of primary dc power loss. Each ACT computer would store sufficient energy to maintain the entire computer regulated power for a minimum of 50 ms, sufficient to overlap acquisition of main battery power. Therefore the computer software would not require special reconfiguration.

Sensor Inputs—The signal-selection failure monitoring algorithms handle the sensor inputs. Reconfiguration of an ACT function due to sensor faults at triplex or higher redundancy levels reduces redundancy by one level until recovery is achieved. The minimum redundancy level is duplex; no single-channel operation is permitted. The deviating signal is isolated until it recovers within the prescribed threshold detection bands and remains "good" for a prescribed time. The recovery time selection is influenced by several factors: type of sensor signal characteristics; risk of encountering a second, like failure during recovery; the concern for latent failures; and the possibility of false recoveries. In case the remaining signals disagree during recovery of the initial faulted signal, the latter is declared a permanent failure, and the recovery procedure is attempted on the second like occurrence. A total time-out period must be mechanized for the attempted recovery procedure to accommodate a hardover failure; i.e., the signal exceeding threshold and never returning.

Computer Faults—These are defined as faults generated within the software; faults generated in the digital-to-analog output hardware are handled differently. Further assumptions are:

- The basic machine executive is not faulted, and the machine does have the ability to attempt recovery.

- The cross-channel data links are not faulted, and vital information appropriate to the monitoring process is transferred between redundant machines.

- Read-only memory (ROM) is not destroyed, such that program instructions and constants remain intact.

If any of these assumptions does not apply, computer shutdown is indicated. The computer fault recovery mechanism is based upon cross-channel comparison for monitoring computed command outputs. Additionally, watchdog monitoring of individual machines indicates the local computer's ability to operate logically.

Methods proposed to reestablish the faulty processor computation through variable data exchange from other good processors include rollahead, rollback, coast, memory copy, and restart (see ref 10). A "warm restart" method was selected in which, upon detection of an output data fault, each operating computer determines the level of redundancy by checking its resident status table of permanent computer faults, then determines which computer is at fault by examining the output monitor table. When a fault occurs during three-computer redundant operations, the system attempts to recover the faulted computer. A fault occurring in duplex will result in a shutdown. The unfaulted computers will maintain normal operation, assuming that the faulted machine is operable until a permanent fail flag is set, which indicates the faulted machine's inability to recover.

Servo Outputs—Each servoactuator is directly commanded by the associated processor. Servoactuator faults are monitored and detected in the software of the associated processor. Each channel engagement is controlled by servo-shutdown logic voting on discretes from the command computer. Consent is required of the other channel computers for the local servo to remain engaged. If a failed computer does not disengage its servochannel, then disengagement is accomplished through the servo-shutdown logic.

Reconfiguration for servoactuation results from redundancy degradation upon faulting, with recovery after a prescribed number of iterations (wait time) after signals exceed the monitor threshold. The recovery delay time should be sufficient to avoid possible oscillatory actuator engage-disengage cycling. The local faulted machine first freezes

its affected servocommand outputs, then it attempts recovery. Meanwhile it still communicates with the unfaulted machines, and loss of synchronization will not cause shutdown. Recovery is not attempted if a fault occurs in duplex actuation in which the faulty actuator cannot be determined; in such case both actuator channels shut down.

The recovery mechanism, "warm restart," is a simplified power-up routine. Program variables are initiated once, and time is allowed for the command outputs to recover within the output tolerance of the operating computers. If the attempt is successful, the faulted machine will be permitted to release its affected servocommands. If the attempt is unsuccessful, the affected servos in the faulted channel will be permanently shut down, and the unfaulted computers will be reconfigured to recognize the faulted machine and reduce their respective machine status tables to reduce the monitor redundancy level.

7.3.2.4 Actuation

Two actuator configurations are used in the ACT system: ACT secondary actuation configuration and stick-pusher actuation configuration.

ACT Secondary Actuator Configuration—A side-by-side, force-summed, secondary actuation concept was chosen to implement the PAS and WLA ACT functions, which use the primary flight control surfaces of the Initial ACT Configuration (fig. 156). ACT secondary actuator output is series-summed with the pilot's mechanical control signal to form a command input to the power control unit (PCU). Both PAS and WLA actuation concepts use a multichannel, side-by-side arrangement, selected on the basis of the installation envelope. The number of channels are compatible with the respective redundancy requirements of each ACT function. For reasons of weight, cost, reliability, and compatibility with the airplane's three hydraulic systems, the quadruple-channel PAS is implemented by three actuators and one mathematical model channel. The WLA actuation uses the same principle with two active channels and one model channel.

The selection of the force-summed concept was based upon the ability of the digital computer to produce essentially identical actuator command signals. Identical channel

251
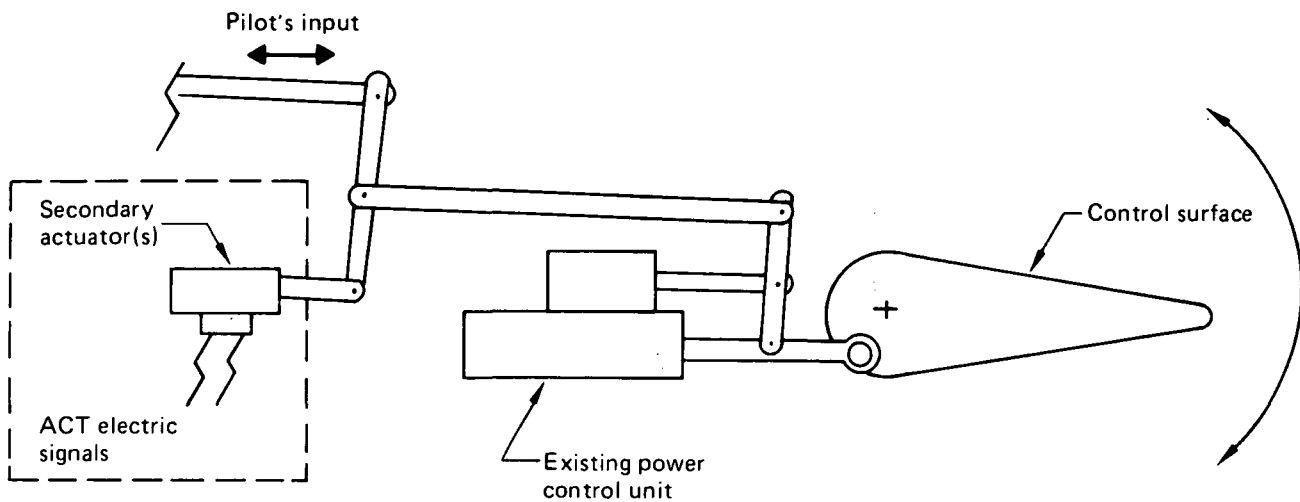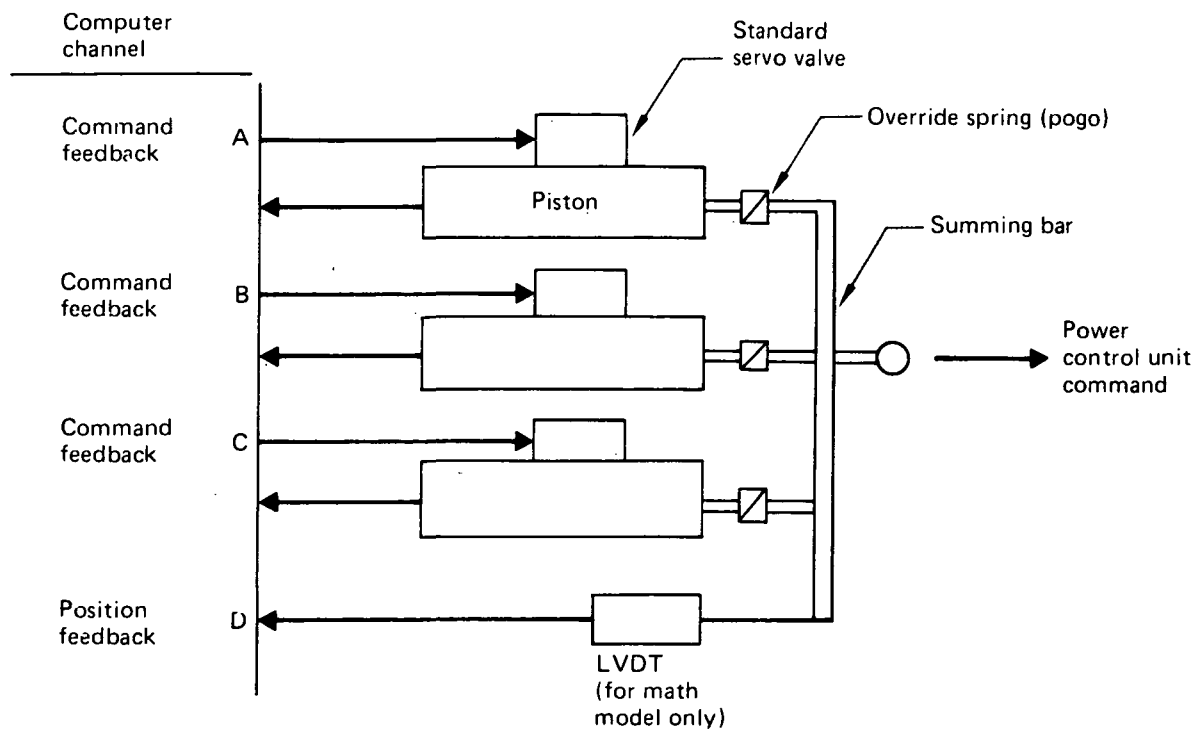
Figure 156. *ACT Secondary Actuation Configuration*

768-104, -105, -106

command signals depend on computer sensor selection and cross-channel synchronization.

Each channel of the concept has a conventional two-stage, low-pressure gain electrohydraulic servovalve operating a single ram. Valve spool and ram positions are fed back to each ACT computer for servoloop control and failure detection. The model channel in each computer receives the summed actuator ram position feedback and combines this with the command signal to compute servovalve position.

Stick-Pusher Actuator Configuration—The Baseline Configuration is equipped with a stick-shaker system that provides aural and tactile warning of an impending stall by sensing the angle of attack, computing the airplane stall margin, and operating two stick-shaker motors, one on each control column.

The Initial ACT Configuration AAL system uses a fail-operational stick-pusher actuation mechanism to follow up the stick-shaker system. It provides positive stall prevention by causing a large, rapid, forward motion of the control column at the stall recovery angle of attack if the pilots fail to act after the stall-warning system is activated.

The stick-pusher concept (fig. 157) uses three sensors, four computers, a dual-tandem floating actuator, and two pneumatic power sources. The actuator exerts the same force when pressurized by either one or both sides. The installation linkage is such that the force exerted on the control column continuously decreases as it travels forward; 356N (80 lb) exerted at the full aft position reduces to 178N (40 lb) at the full forward position. Each pneumatic power source consists of a nitrogen bottle at 13 790 kPa (2000 psi) and a regulator that reduces the pressure to the 3447 kPa (500 psi) required for actuation. Two series solenoids, each signaled by an ACT computer, must be opened before the actuator will operate.

Actuation time is approximately 0.2 sec. When either command is removed, the actuator vents to ambient through the solenoid valve. The pilot may override the pusher at any time by exerting sufficient force on the column or by operating the manual dump valve, which directly vents the actuator to ambient. Operating the dump valve also actuates two switches that deenergize the solenoid valves and provide logic information to the computers.

253

Pilot's
control
column

Aft

Stroke

Forward

Section A-A

A

Pilot's manual
override

A

Dump
valve

Dump
valve

Pilot manual
bypass

A ⟶ Valve
solenoid

Both
solenoids
open to
pressurize
actuator

ACT
computer
command
signals

B ⟶ Valve
solenoid

C ⟶ Valve
solenoid

D ⟶ Valve
solenoid

13 788 kPa
(2000 lb/in^2)

Regulator

Nitrogen
bottle

3447 kPa
(500 lb/in^2)

Regulator

Nitrogen
bottle

3447 kPa
(500 lb/in^2)

Pneumatic
power source

Figure 157.   Stick-Pusher Actuation Concept

254

7.3.2.5 Operational Status and Maintenance

The ACT system must inform the flight crew of system failure status and required procedural actions, and it must facilitate system preflight checkout and maintenance support activities. The system communicates with the flight crew through the flight deck caution and warning systems and with the ground crew through a maintenance control and display panel in the main electronics bay that also serves other flight systems. A dedicated ACT control and display panel, located at the flight engineer's station, could be considered for in-flight maintenance support. All these communication media, except the latter, are Baseline Configuration equipment. ACT digital processing offers extensive built-in test capability and decision logic necessary to implement these interface requirements.

In-flight Operation—Two levels of in-flight fault data are processed and transmitted by the ACT computers to the flight deck for appropriate crew actions. Information relevant to loss of ACT function capability is presented to the pilots through the respective warning and caution priority structure. Procedural actions normally listed in the flight operations manual (carried in the flight deck) are displayed on the caution system alphanumeric message display unit to aid pilot decision.

Information relevant to ACT equipment failures at the line replaceable unit (LRU) level, which impacts flight dispatch, is presented at the flight engineer's station to permit maintenance support "call-ahead" action. The fault vector data from monitor detection outputs and the annunciated decisions are stored in the ACT computer's nonvolatile memory and transferred to the maintenance control and display panel at touchdown for appropriate ground crew actions.

Ground Operations—Two basic ground operations are defined for the ACT system. First, preflight testing is required to establish system integrity for both flight safety and airplane dispatch. Preflight testing must be fully automated, must be conducted with flight crew concurrence, and must conclude with a recommended decision as to whether the airplane may be dispatched normally, with operational restrictions, or not at all.

Second, maintenance activities associated with ACT must be consistent with other airplane flight control systems maintenance. That is, the system must be assumed operational and available for service unless preflight test indicates a failure or a flight squawk was generated in a previous flight. Through-flight maintenance will be restricted to changing components that are dispatch required, easily removable, and readily replaced with spares made available by the call-ahead procedure. Most system maintenance will be deferred to turnaround or overnight facilities with less impact upon flight operations.

System maintenance testing is structured to be an extension of preflight checkout with the capability to diagnose equipment problems to the LRU level. The in-flight stored fault data assist the ground crew toward this goal. An important objective in structuring the maintenance testing is to preserve the separation between flight-crucial and flight-critical functions to avoid extensive testing of functions other than those repaired.

7.4   AERODYNAMIC DRAG

7.4 AERODYNAMIC DRAG

The drag estimates for the Baseline, Initial ACT, and Wing Planform Study Configurations are compared in this subsection. Initial ACT drag improvements are due to reductions in trim and skin friction drag associated with the smaller horizontal tail, farther aft cg, and longer tail arm (wing shifted forward). The planform study configurations have higher wing spans that increase cruise L/D an additional 3 to 6% and also improve takeoff and landing characteristics.

The principal geometric characteristics for the Baseline and ACT Configurations are defined in Subsection 7.2 (fig. 61). All airplanes have the same gross weight, engine size, wing area, and payload.

7.4.1 AERODYNAMIC ANALYSIS APPROACH

During the configuration phase of the Wing Planform Study, combinations of wing sweep, t/c, t/c distribution, and span were chosen to maintain constant compressibility and polar shape drag characteristics while airfoil technology and wing design C_L were fixed. The cruise drag components that were adjusted for geometry changes are shown in Figure 158. The predominant component adjusted for configuration changes was induced drag, which depends on wing span.

7.4.2 CRUISE DRAG COMPARISONS

The ACT and Baseline Configurations have many identical design components (e.g., engine and fuselage). Differences between the configurations affecting the high-speed lift and drag performance include the horizontal and vertical tail sizes, the wing location (longitudinal) on the fuselage, midcruise cg locations, and wing geometry. Similarly, values of minimum parasite drag for the body, engines, and struts are identical to those for the Baseline Configuration. The incompressible drag polar shape (M = 0.7) and the compressibility drag at Mach numbers from 0.7 to 0.84 are identical for all configurations. Because total wing area for the changes in sweep and span is nearly constant, minimum parasite drag for the wings is nearly the same. However, the higher span wings require two additional flap track fairings per wing side.

257

Cruise Drag Components
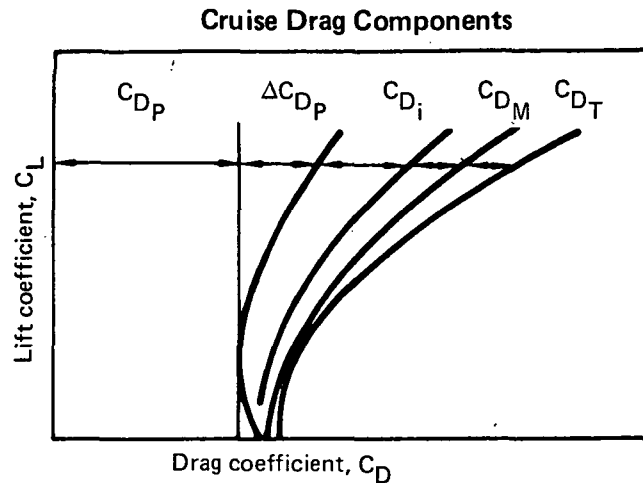
Note: On Conventional Baseline, total
predicted drag was adjusted to
wind-tunnel-based drag polar.

Drag adjustments for
configuration changes:

C_{D_p} (wetted area)

ΔC_{D_p} no change

C_{D_i} (aspect ratio)

C_{D_M} no change

C_{D_T} $(C_{m_{tail-off}}$, tail length, $S_H)$

768-102, -103, -104, -105, -106, -107

Figure 158. Cruise Aerodynamic Drag Buildup

Fundamentally, cruise L/D is a function of wing span and airplane total wetted area. As the total wetted areas are nearly the same for the Initial ACT and all the Wing Planform Study Configurations, wing span is the primary factor affecting cruise L/D. Nevertheless, differences among the configurations studied were specifically evaluated to reflect their effects in cruise efficiency results.

The use of PAS and AAL systems allowed the ACT Configurations to have reduced horizontal tail sizes and more aft cg locations relative to the Baseline. Two beneficial drag effects result: (1) less tail wetted area reduces parasite drag, and (2) the more aft cg reduces the balancing tail load at cruise, decreasing trim drag. Required tail

areas for the Wing Planform Study Configurations are presented and compared to those for the Baseline and Initial ACT in Figure 159. For the 31.5 deg swept wings, the horizontal tail areas were reduced about 44% from the Baseline. Model 768-106, with 26.4 deg sweep, required a slightly larger horizontal tail than the other ACT airplanes. The greater tail moment arms for the ACT Configurations resulted in vertical tail areas slightly smaller than for the Baseline.
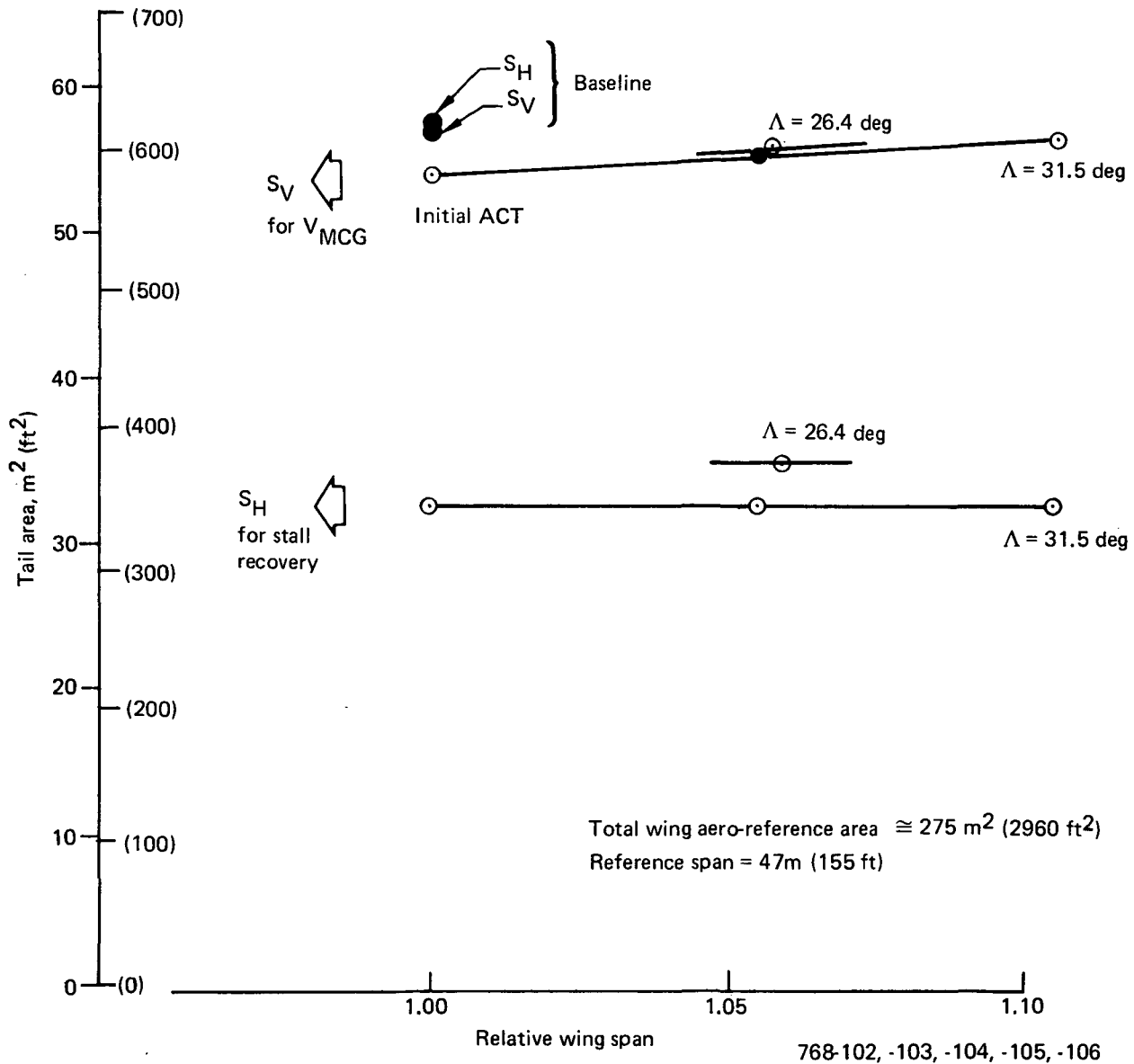
Figure 159. Horizontal and Vertical Tail Sizes

Trim drag variations with cg locations for the ACT Configurations are shown in Figure 160. At the midcruise cg locations indicated on the curves, the ACT airplane trim-drag coefficients are from 3.2 to 4.4 counts lower than for the Baseline.

The resulting cruise efficiencies, normalized to Initial ACT, are presented in Figure 161. This figure also shows that the midcruise L/Ds for the ACT Configurations are within 1% of the maximum values attainable within the respective established cg ranges. Midcruise L/D is shown as a function of wing span in Figure 162. The highest span ACT Configuration, Model 768-104, has the highest L/D; 5.8% greater than the Initial ACT Configuration. Model 768-106, with 26.4 deg wing sweep, had the least wing profile drag (because of its thinner airfoils), but this was offset by the slightly larger empennage required (fig. 162).

The comparisons presented and discussed in Subsection 5.3 showed that the Model 768-104 (AR = 12, Λ = 31.5 deg) had the best performance of all configurations studied and, consequently, was selected as the basis for developing the Final ACT Configuration. A

768-102, -103, -104, -105, -106
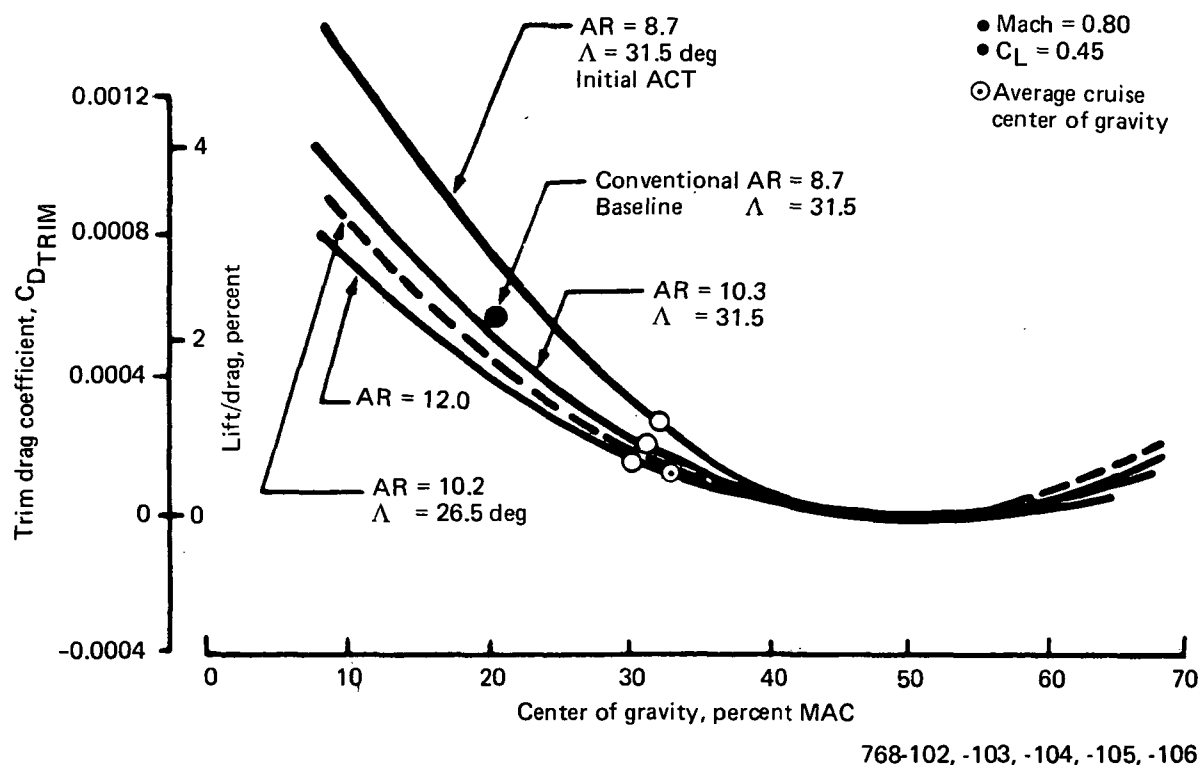
Figure 160. Effect of Center of Gravity on Trim Drag

260
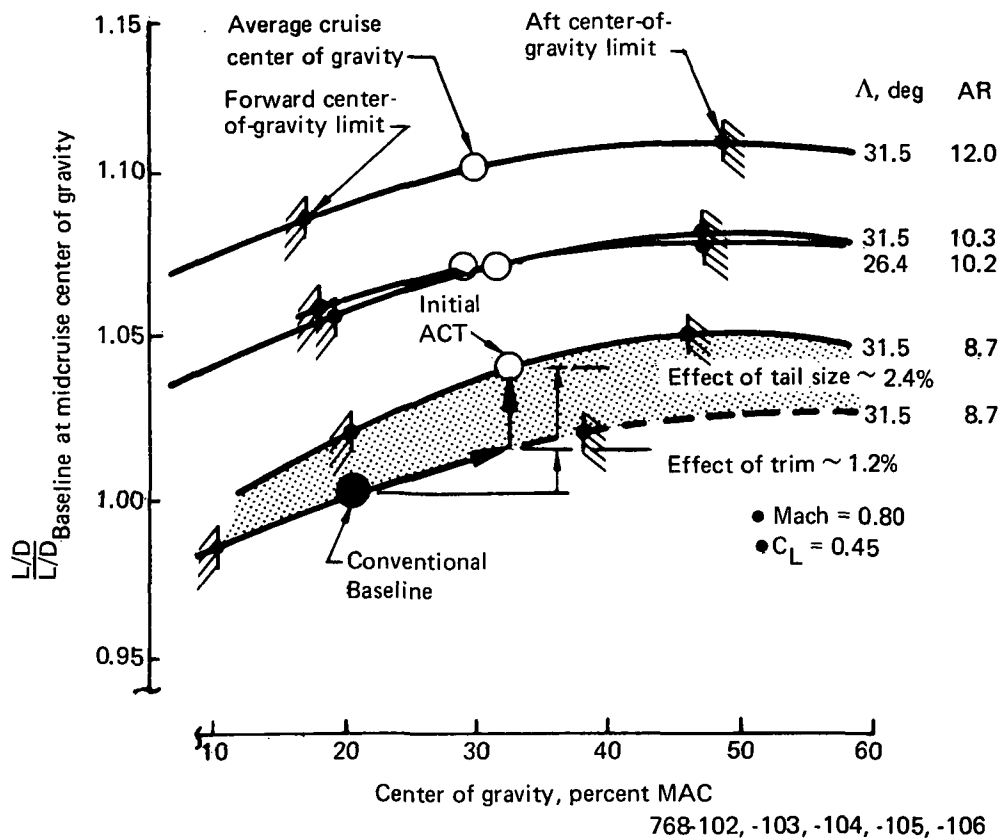
Figure 161. Relative Cruise Efficiency
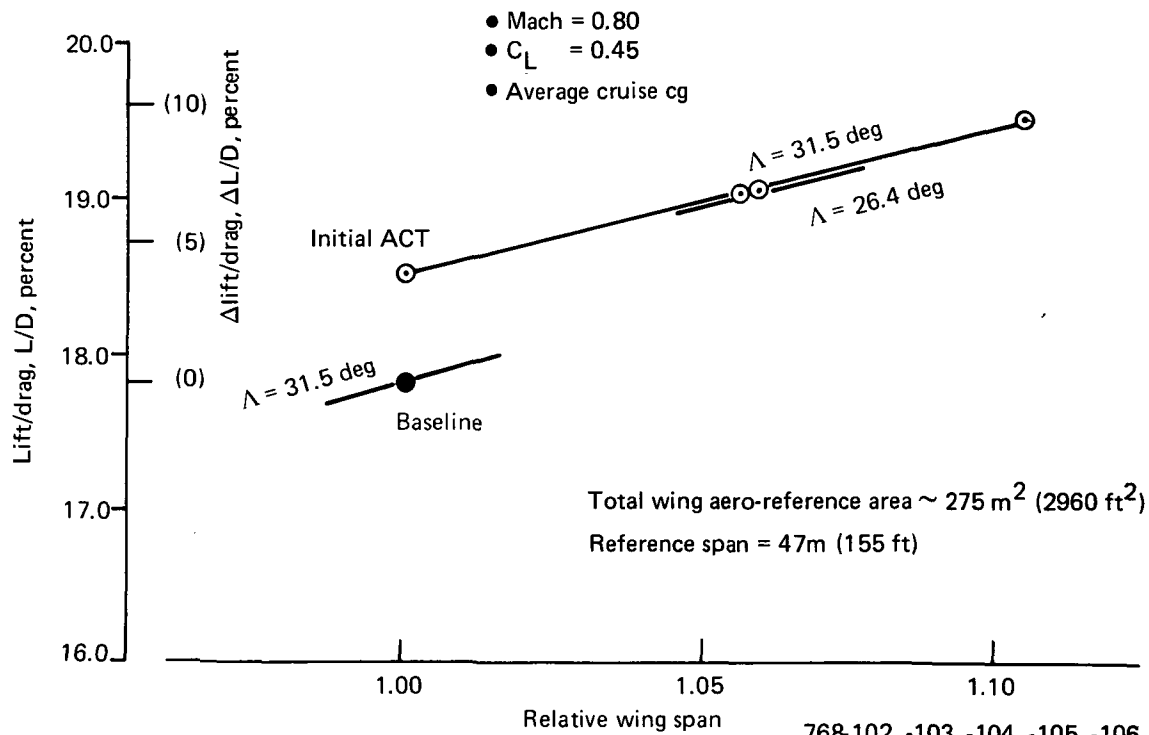
Figure 162. Effect of Wing Span on Cruise L/D

comparison of its general arrangement with the Baseline and Initial ACT is shown in Figure 163. A summary of the Model 768-104 drag differences and cruise L/D relative to the Baseline is included in Table 27.
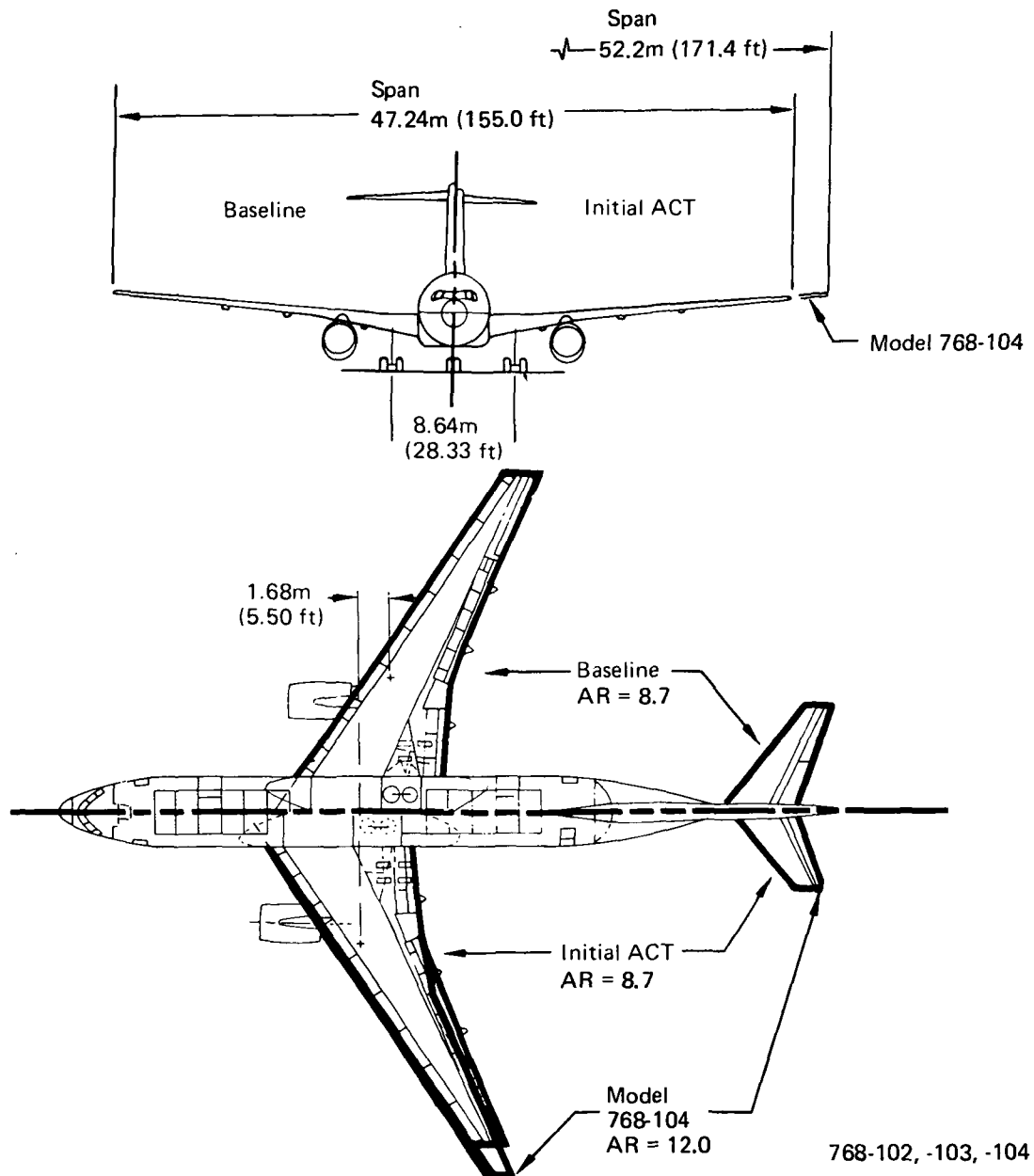
Figure 163. *Conventional Baseline, Initial ACT Configuration, and Model 768-104 Comparison*

*Table 27. Conventional Baseline Configuration and Model 768-104
Cruise Drag Summary*

Drag item	Drag difference: Model 768-104 relative to Baseline Configuration		
	ΔC_D	$\Delta C_{D_{total}}'$ percent	Total percent
Parasite drag			
Wing	+0.00007	-3	-0.3
Body	-0.00001	0.5	0
Horizontal tail	-0.00051	22.5	2.0
Vertical tail	-0.00002	1	0.2
Nacelles and struts	0.00001	0.5	0
Flap tracks and seals	+0.00012.	-5	-0.4
Excrescence	-0.00003	1.5	0.1
Drag rise and polar shape	0	0	0
Trim drag	-0.00044	19.5	1.7
Induced drag	-0.00143	63.5	5.7
Total ΔC_D	-0.00226	100%	9.0%

	C_D		L/D	
Baseline Configuration	0.02525	100%	17.8	100.0%
Model 768-104	0.02299	91.1%	19.6	109.8%
Total change	0.00226	-9.0%	1.8	9.8%

● Cruise drag, C_D at C_L = 0.45 (M = 0.80)   768-102, -104

7.4.3 TAKEOFF AND LANDING AERODYNAMICS

Estimated takeoff and landing aerodynamics for the Baseline and ACT Configurations are presented in this subsection. Improvements of 2% to 13% in takeoff L/D and 3 to 6% in landing approach C_L are indicated for the ACT Configurations. These improvements are the result of the farther aft location of the forward cg limit and increased wing span.

Figure 164 shows the effects of cg location on takeoff L/D and landing approach C_L. At their forward cg limits (approximately 20% MAC), all configurations have L/D values within 2% of maximum available at their optimum cg positions for the sea level takeoff case. However, the forward limits are nearly optimium cg locations for hot-day, high-altitude takeoff conditions sometimes encountered at airports such as Denver. On the other hand, landing approach lift coefficients for all configurations could be improved by more aft cg locations.

The effect of span at each configuration's forward cg limit is shown in Figure 165. Span has a strong influence on low-speed L/D due to reducing induced drag. Approach C_L is directly related to $C_{L_{max}}$, where trim loads and sweep are the predominant influences.

Takeoff

• Takeoff flaps = 11 deg

O Forward center-of-gravity location

Landing

• Landing flaps = 36 deg, gear down
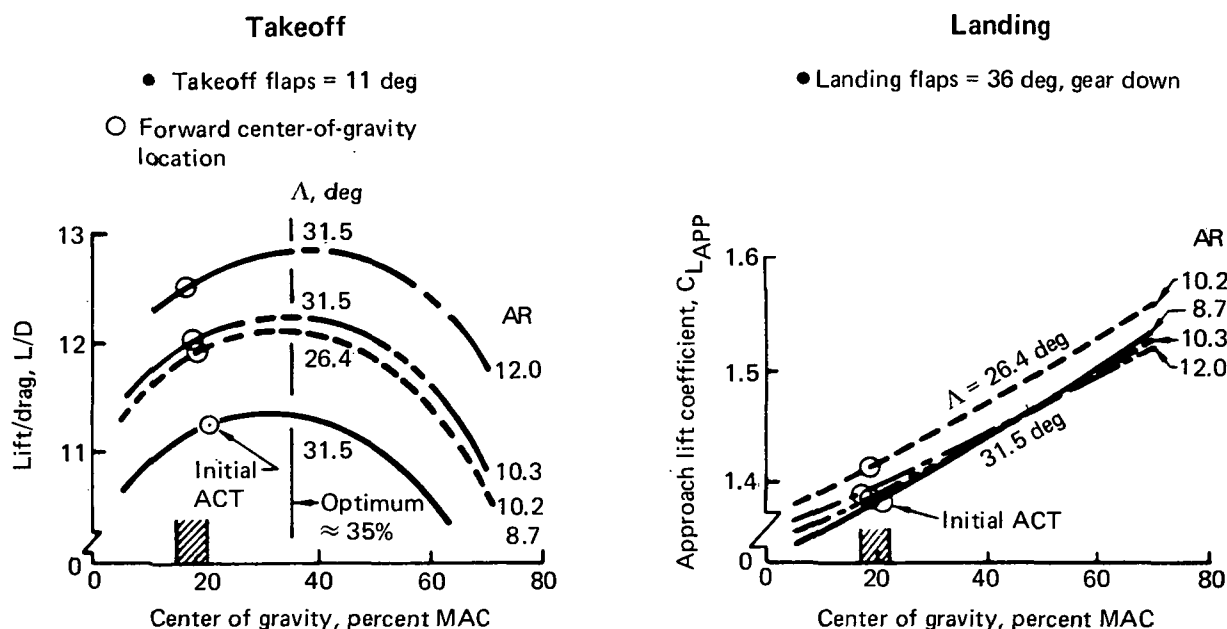
768-103, -104, -105, -106

Figure 164. Low-Speed Characteristics, Effect of Center of Gravity

264

Forward center-of-gravity limit, percent MAC				
Center of gravity	21.0	17.5	19.3	19.6
Λ, deg	31.5	31.5	31.5	26.4
AR	8.7	12.0	10.3	10.4

Takeoff

$1.2V_S, \delta_F = 11$ deg

AR 12.0

AR 10.3

AR 10.2

(Initial ACT)
AR 8.7

AR 8.7 (Baseline)

Lift/drag L/D

Landing

$1.3V_S, \delta_F = 36$ deg, gear down

AR 10.2

AR 8.7 (Initial ACT)

AR 10.3

AR 12.0

AR 8.7 (Baseline)

Approach lift coefficient, $C_{L_{APP}}$

1.00   1.05   1.10

Relative wing span
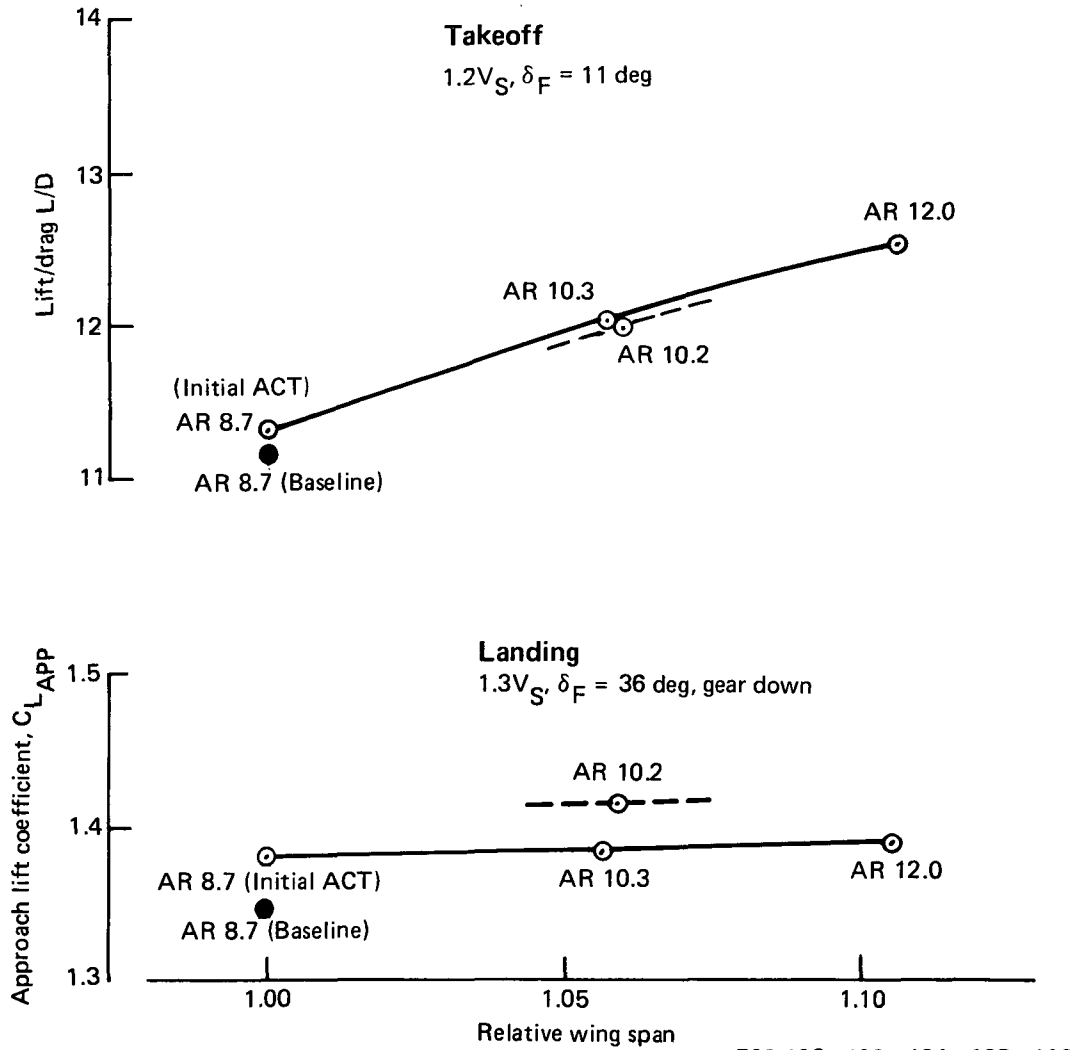
768-102, -103, -104, -105, -106

Figure 165. Low-Speed Characteristics, Effect of Wing Span

265

7.5   WEIGHT ANALYSIS

7.5 WEIGHT ANALYSIS

This section presents a weight and moment-of-inertia definition of the Wing Planform Study that is more detailed than the data provided in Subsection 5.4. Weight and balance analyses of airplane components are discussed in Subsection 7.5.1. Mass distribution and panel moments of inertia were obtained by incrementing from the Initial ACT Configuration data provided in Subsection 7.4.2 of Reference 3 (Initial ACT Document).

7.5.1 WEIGHT AND BALANCE

7.5.1.1 Weight Statement

A weight statement for Model 768-104 is shown in Table 28. Weight distribution within individual groups is consistent with aerospace industry practice (ref 11). Weight statements were not provided for Models 768-105 and -106 because they had not been analyzed to the same level of detail. Increments for wing fatigue, flutter, and dynamic gust were estimated by comparing the results of Models 768-103 and -104 analysis and by using previous experience (fig. 166).

7.5.1.2 Weight and Balance Analysis Methods

The wing box was analyzed using a computerized beam analysis (ORACLE) to size "theoretical" structure, including upper and lower skins and stringers and front and rear spar webs (refer to subsec 7.2). Additional components required for an "installed" weight were applied, based on development experience with similar commercial airplane structures. These components consist of manufacturing tolerance, feather material, pads, fasteners, spar web stiffeners, and ribs.

Wing secondary structure (leading and trailing edges) was based upon a reference airplane unit weight and adjusted for loads and geometry. Main and nose landing gear weights were derived using a computer program, "GEARS," which is sensitive to design loads and configuration geometry. Body primary structure was adjusted for differences in horizontal tail load from the Baseline Configuration. Empennage weights represent reference airplane unit weight adjusted for geometry and function.

Table 28. Weight and Balance Statement, Model 768-104

Functional group	Weight		Longitudinal cg body station	
	kg	(lb)	m	(in)
Wing	17 200	37 920	24.48	964
Horizontal tail	1 075	2 370	52.73	2076
Vertical tail	1 878	4 140	47.40	1866
Body	15 776	34 780	23.88	940
Main landing gear	6 505	14 340	24.71/25.35[a]	973/998[a]
Nose landing gear	894	1 970	6.17/6.76[a]	243/266[a]
Nacelle and strut	2 545	5 610	19.56	770
Total structure	45 873	101 130	25.27/25.37[a]	995/999[a]
Engine	7 951	17 530	19.84	781
Engine accessories	100	220	16.79	661
Engine controls	82	180	16.10	634
Starting system	77	170	18.82	741
Fuel system	599	1 320	24.46	963
Thrust reverser	1 638	3 610	19.96	786
Total propulsion system	10 447	23 030	20.07	790
Instruments	485	1 070	11.10	473
Surface controls	2 227	4 910	30.96	1219
Hydraulics	1 021	2 250	24.49	964
Pneumatics	354	780	20.02	788
Electric	1 021	2 250	13.41	528
Electronics	775	1 710	12.04	474
Flight provisions	417	920	4.90	193
Passenger accommodations	6 681	14 730	22.30	878
Cargo handling	1 229	2 710	23.39	921
Emergency equipment	422	930	19.79	779
Air conditioning	975	2 150	18.21	717
Anti-icing	186	410	20.09	791
Auxiliary power unit	676	1 490	42.80	1685
Total fixed equipment	16 469	36 310	22.38	881
Exterior paint	68	150	23.04	907
Options	907	2 000	23.95	943
Manufacturers empty weight	73 764	162 620	23.88/23.92[a]	940/942[a]
Standard and operational items	6 196	13 660	25.86	1018
Operational empty weight	79 960	176 280	24.03/24.07[a]	946/948[a]

[a]Gear up/gear down.

768-104

268

● Total wing aero-reference area ≈ 275 m² (2960 ft²)
● Reference span = 47.24 m (155 ft)

□ Fatigue, flutter, and dynamic gust increment estimates added
○ Complete structural analysis (including fatigue, flutter, and dynamic gust)
△ Strength wing analysis with WLA only
◆ Strength wing analysis without WLA

768-102, -103, -104, -105, -106
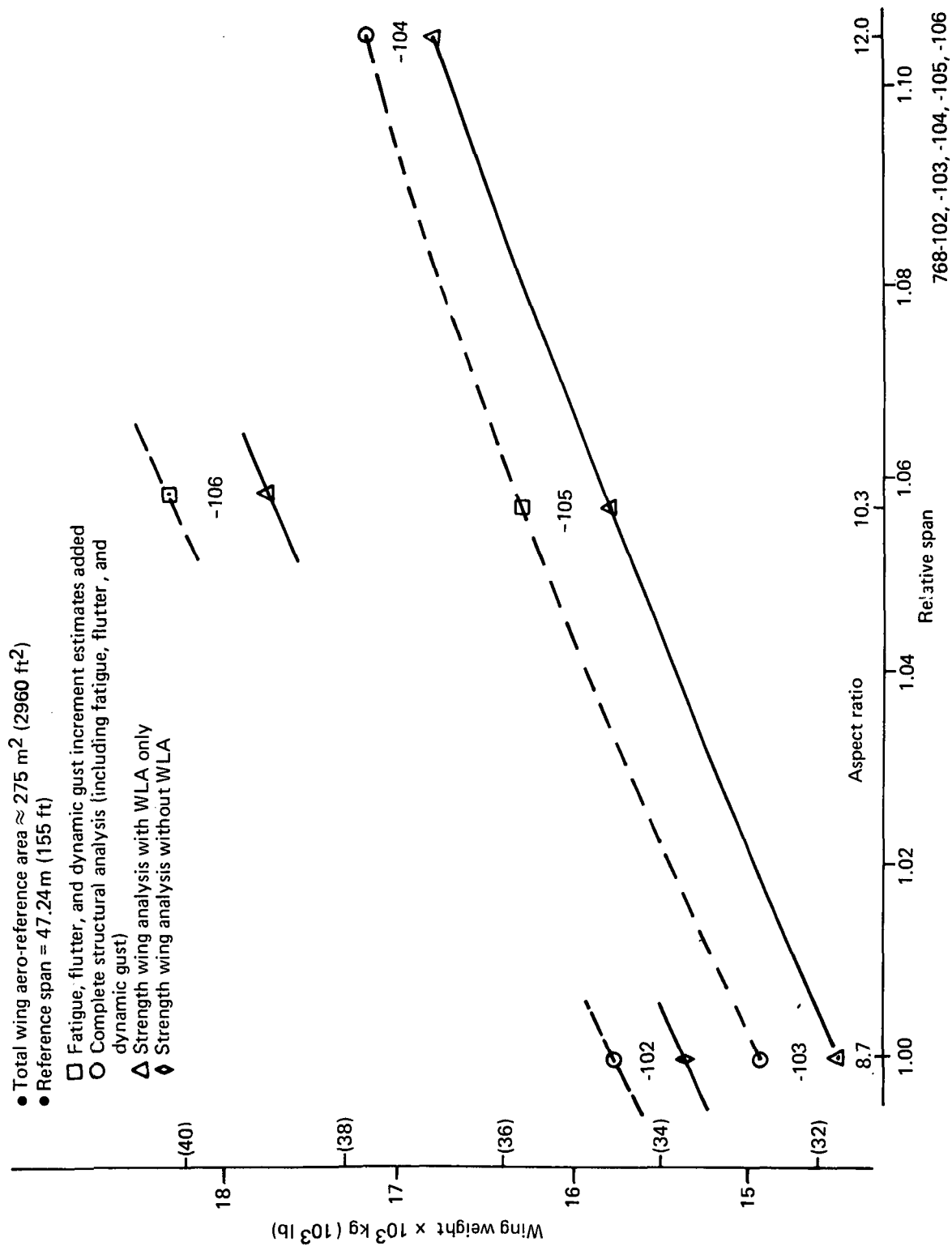
Figure 166. Wing Weight Versus Relative Span

269

Surface controls, hydraulics, electric, and electronics systems components were defined in detail. A weight was calculated for each component/subsystem, representative of the definition.

Conventional manual analysis was applied to the cg of detailed airplane components. As with the Initial ACT Configuration, much of the data were obtained by incrementing the Baseline Configuration data.

7.5.2 MASS DISTRIBUTION AND MOMENTS OF INERTIA

In support of the airplane mathematical model for structural loads analyses, mass distribution and moments of inertia of detailed components were analyzed. Detailed components were subtotaled for the entire wing, body, horizontal tail, vertical tail, landing gear, and propulsion pod. Panel geometry definition for each of the major airplane components was similar for each study wing. Calculation methods were consistent with the computerized methodology used on Boeing's commercial airplanes.

8.0 SENSITIVITY AND
TRADE STUDIES

8.0 SENSITIVITY AND TRADE STUDIES

A major objective of the Wing Planform Study was to evaluate the effects of wing planform shape on the overall performance of an airplane incorporating ACT functions. Of necessity, the planform variations that could be studied in detail were limited. However, it was recognized that some further modifications of the study wings might be beneficial or, at least, alleviate some potential problems. Accordingly, a group of short studies was conducted to evaluate the sensitivity of the main study results to several types of wing alterations. In addition, a trade study to assess configuration changes required for a flight-critical rather than flight-crucial pitch-augmented stability (PAS) was conducted. Consistent with the level of detail used in these studies, results have been rounded to the nearest 0.5%.

8.1 SENSITIVITY STUDIES

Three of the four sensitivity studies involved the largest span configuration, Model 768-104, and evaluated the effects of reducing wing taper and increasing design lift coefficient. The other study concerned the reduced-sweep airplane, Model 768-106, which had insufficient fuel volume to meet the growth objective, although it was adequate for the design mission. Figure 167 shows the four wing variations that were included in the sensitivity studies. Incremental weight data for these studies were based on strength and did not consider fatigue, flutter, and dynamic gust requirements.

8.1.1 MODEL 768-104A

The taper of the Model 768-104 wing from side of body to about 60% span was considerably greater than the Baseline and Initial ACT wing, raising the concern that buffet margins or pitchup characteristics, or both, might be degraded. This concern arises because the outboard wing sections must operate with higher pressure gradients, possibly causing premature flow separation.

The -104A wing added area at the trailing edge to decrease taper, resulting in an appreciably greater total wing area. The addition of a trailing-edge extension reduced the fuel efficiency about 3.5%. The 14% increased wing area and reduced aspect ratio of 12.5%, shown in Figure 168, had offsetting effects on lift/drag (L/D) at a fixed lift

271
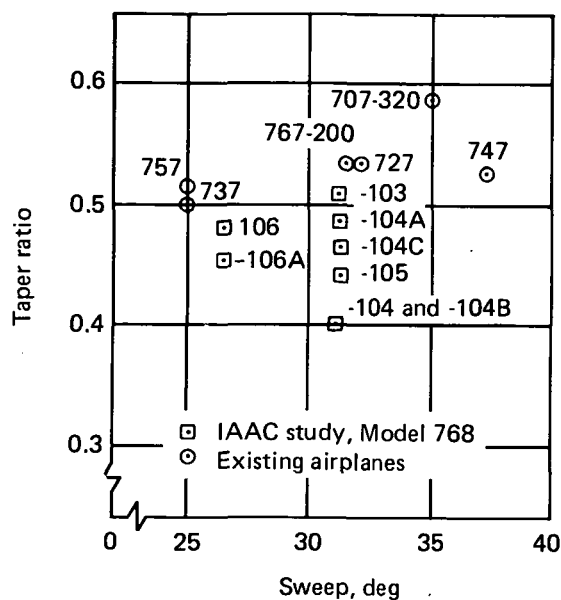
$\lambda' = \text{taper ratio} = \dfrac{\text{chord at } \eta = 0.55}{\text{chord at SOB}}$

768-104A

with TE extension
same t/c versus b/2

Λ = 31.5 deg
AR = 8.7
λ' = 0.475

S(trap) = 282.2 m^2 (3038 ft^2)
S_w = 314.6 m^2 (3386 ft^2)

768-104B

with increased design
C_L decreased t/c
versus b/2

reduced t/c 1%

31.5
9.8
0.391

226.8 m^2 (2441 ft^2)
278.0 m^2 (2992 ft^2)

768-104C

with revised c_R and
c_T, same t/c versus
b/2, wing shifted aft

31.5
9.66
0.490

266.6 m^2 (2870 ft^2)
282.2 m^2 (3038 ft^2)

768-106A

with glove,
increased
inboard t/c

glove

Same as 768-104

26.5
9.0
0.455

246.6 m^2 (2654 ft^2)
279.1 m^2 (3004 ft^2)

Figure 167. IAAC Wing Planform Study New Sensitivity Studies Geometry Definition

272

Taper Ratio
- Model 768-104A
- Chord extension

$\Delta S_w = +13\%$
$\Delta f_B = +3.5\%$

- Model 768-104C
- Gear integration
  considerations

1.68m (66 in) aft

$\Delta S_w = +2\%$
$\Delta f_B = +2\%$

Design C_L
- Model 768-104B

C_L

ΔC_L

t/c

M_c

$\Delta C_L = +0.1$
$\Delta t/c = -1\%$
$\Delta S_w = 0$
$\Delta f_B = 0\%$
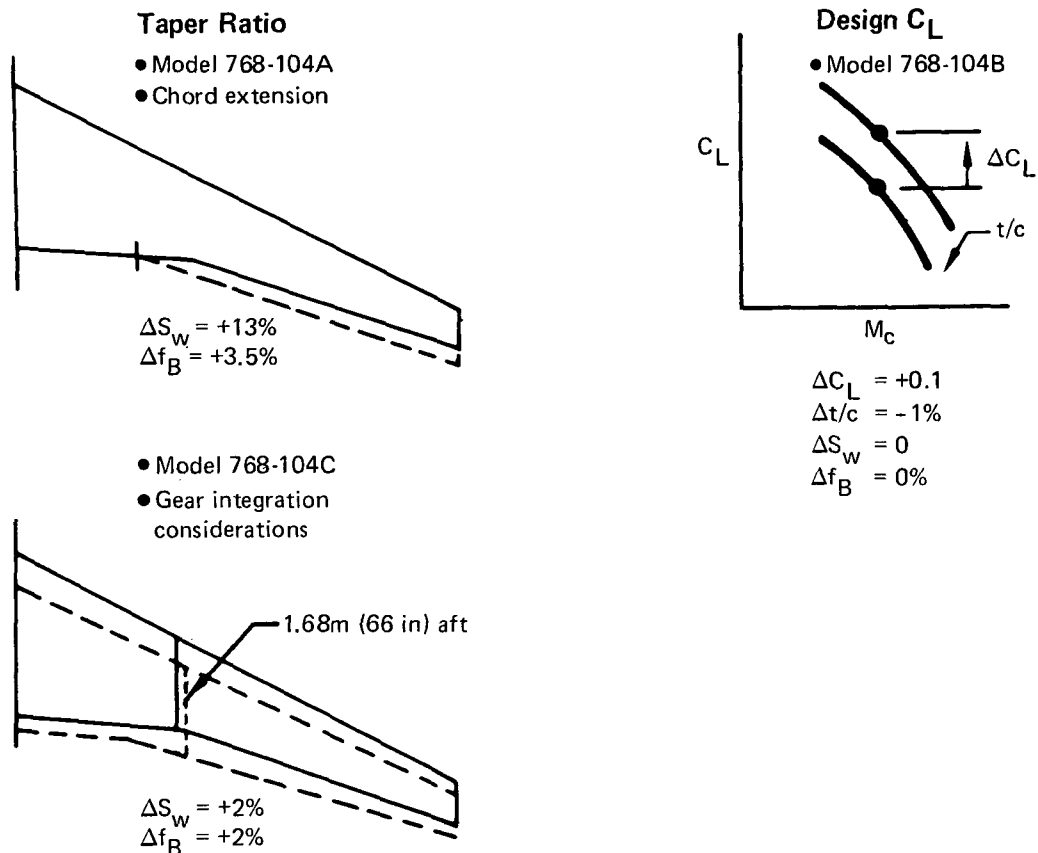
Figure 168. Taper Ratio and Design C_L Sensitivity, Model 768-104, AR = 12.0

coefficient (C_L). However, the higher wing area reduced the average cruise C_L and L/D, resulting in 3% higher cruise drag. The -104A wing with increased outboard chord weighed approximately the same as the base -104 wing because a weight saving obtained from the larger and deeper spar box was offset by the weight of the larger secondary structure area.

8.1.2 MODEL 768-104B

The -104B planform was used for a design C_L-versus-wing thickness trade study. The 768-104 configuration's higher span, relative to the Baseline and Initial ACT, reduced the induced drag and opened the subcritical polar, which resulted in a higher L/D

273

airplane. However, at cruise Mach, drag rise, polar shape, and trim drag limited the benefit of the reduced induced drag. Increasing design C_L by changing camber and thinning the outboard wing would increase the cruise maximum L/D.

Designing for a 0.1 higher design cruise C_L required thinning the wing 1% from the side of body to the tip (fig. 168) to offset the associated decrease in critical Mach number. In this study, the improved drag of higher design C_L and reduced thickness/chord ratio (t/c) was offset by the higher wing weight (approximately 1% OEW). Therefore, fuel efficiency was essentially unchanged.

8.1.3 MODEL 768-104C

The 768-104C wing, shown in Figure 168, was developed to provide reduced taper with a much smaller area increase than the -104A. This was achieved by shifting the wing aft 1.68m (66 in) so that the landing gear fairing remained about the same size.

The planform change reduced aspect ratio about 2.5% and increased the aero-reference wing area about the same amount. Reducing side-of-body chord was important to reduce wing taper while keeping aspect ratio almost constant. However, this reduced the landing gear fairing area and thickness, requiring a wing shift aft to enclose the gear. The aft wing shift of 1.68m (66 in) moved the average cruise cg forward about 10% mean aerodynamic chord (MAC). Moreover, the tail areas were larger due to the shorter tail arm. The combined effects increased OEW about 1% (0.5% for the wing with a smaller side-of-body box and additional 0.5% for tail size and body loads). The cruise drag increased nearly 2% due to higher trim drag with center of gravity (cg) 10% farther forward, larger tail size, and reduced aspect ratio. The resulting fuel efficiency is reduced 3.5% relative to the base 768-104 planform.

8.1.4 MODEL 768-106A

The reduced-sweep Model 768-106 wing was heavy, causing poor fuel efficiency, and had less than the desired fuel volume for growth. Adding an inboard leading-edge glove resulted in a lighter wing with more fuel volume. The inboard leading-edge glove provided greater effective sweep and a longer, deeper inboard structural box. The greater inboard sweep allowed corresponding t/c increase from 13.1% to 15.1%.

274

Adding the glove to the -106 planform improved the fuel efficiency slightly, approximately 0.5%, and the fuel volume 13%. Approximately 40% of the fuel efficiency improvement was due to increased L/D; reduced OEW accounted for the other 60%. The small increase in wing area reduced $C_{D_{P_{MIN}}}$ slightly more than induced drag was increased with a lower aspect ratio. Figure 169 shows the planform change for Model 768-106. Increased side-of-body wing-box structural efficiency reduced OEW. The aerodynamic drag rise was held approximately constant with the local inboard sweep offsetting the increased inboard t/c.

Root Airfoil Thickness
● Model 768-106A

Conditions:

t/c_{root} = +2%

Λ_{root} = +5 deg

⎱ Constant M_c

t_{root} = +14%

Δ fuel volume = +13%

Δ fuel efficiency = -0.5%
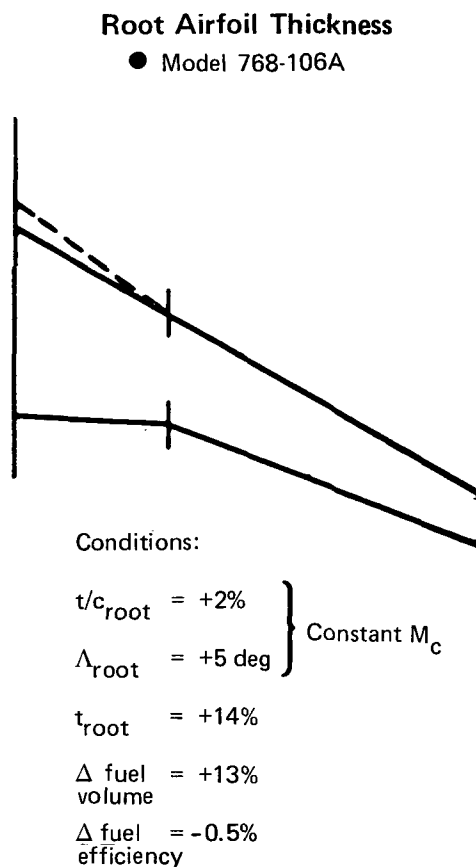
Figure 169. Fuel Volume and Wing-Box Size Sensitivity Study, Model 768-106, AR = 10.2, Λ = 26.4 deg

8.1.5 CONCLUSIONS

Table 29 summarizes the weight, drag, and performance results for the four alternate planforms studied. Either of the approaches studied for reducing the taper of the 768-104 planform would reduce fuel efficiency by about 3.5% and almost offset the 4% fuel efficiency improvement obtained with the greater span of the 768-104. Although taper reduction, in principle, would alleviate pitchup and buffet margin degradation tendencies for the higher aspect ratio wings, whether such planform modifications are required has not yet been established.

Changing design C_L for the higher aspect ratio planforms does not show any additional fuel-burned benefits.

Adding a glove and increasing the side-of-body t/c on the reduced-sweep 768-106 improved fuel efficiency 0.5% but this was not enough to make it competitive with the increased sweep 768-105.

Table 29. Wing Planform Sensitivity Study Results

Percent Δ^a	Model			
	768-104A	768-104B	768-104C	768-106A
S_w	+14	+1	+2.5	+1.5
Aspect ratio, AR^b	-12.5	-1	-2.5	-1.5
OEW^c	0	+1	+1	-0.5
L/D^a (average cruise)	-3	+1	-2	+0.5
Fuel efficiency	-3.5	0	-3.5	+0.5

^{a}Increments are relative to base planform
^{b}Based on aerodynamic reference area
^{c}Includes strength weight increments only (no gust, fatigue, or flutter)

8.2 TRADE STUDIES

All IAAC configurations used a trimmable stabilizer and elevator system for pitch control and trim. For the Initial ACT Configuration, the elevator was double hinged for additional control effectiveness. The trade between this rather mechanically complex system and a "flying tail" with simple geared elevator is discussed in the following subsection.

In the configuration development of the Initial ACT and the Wing Planform Study Configurations, the criteria for aft cg limit horizontal tail size were based on controllability margin for stall recovery; no consideration was given to minimum unaugmented longitudinal stability. The resulting Models 768-103 and 768-104 are unstable at their aft cg limits over a significant part of their flight envelopes and therefore require a flight-crucial PAS system. Most margins of instability are small, and the unstable regions occur at high altitude and intermediate Mach number. Therefore, a study was made to determine what combination of aft cg restriction, flight envelope restriction, and increased horizontal tail size would provide acceptable emergency unaugmented longitudinal handling qualities and permit the use of a flight-critical PAS.

8.2.1 FLYING TAIL VERSUS STABILIZER/ELEVATOR

The Models 768-103 and -104 currently have a trimmable stabilizer with a double-hinged elevator.

The flying tail envisioned for the two models (a column-actuated stabilizer with a mechanically geared single-hinged elevator) would have the same geometrical characteristics as the current stabilizer/elevator. The flying tail would still require a green band, but takeoff mistrims would only affect column forces, not maximum usable tail lift.

Horizontal-tail lift curves from Model 7X7 wind tunnel data were used to estimate tail lift for takeoff rotation and stall recovery. Landing approach trim and flare capability of a flying tail are approximately the same as for a conventional tail being dependent

on the maximum horizontal tail lift attainable. Figure 170 shows the Initial ACT tail-sizing chart with the flying-tail requirements added. Surface deflections of δ_H/δ_E = +12 deg/+20 deg for stall recovery and -15 deg/-25 deg for takeoff rotation are required to achieve a 10% tail-area reduction. The ability to achieve this
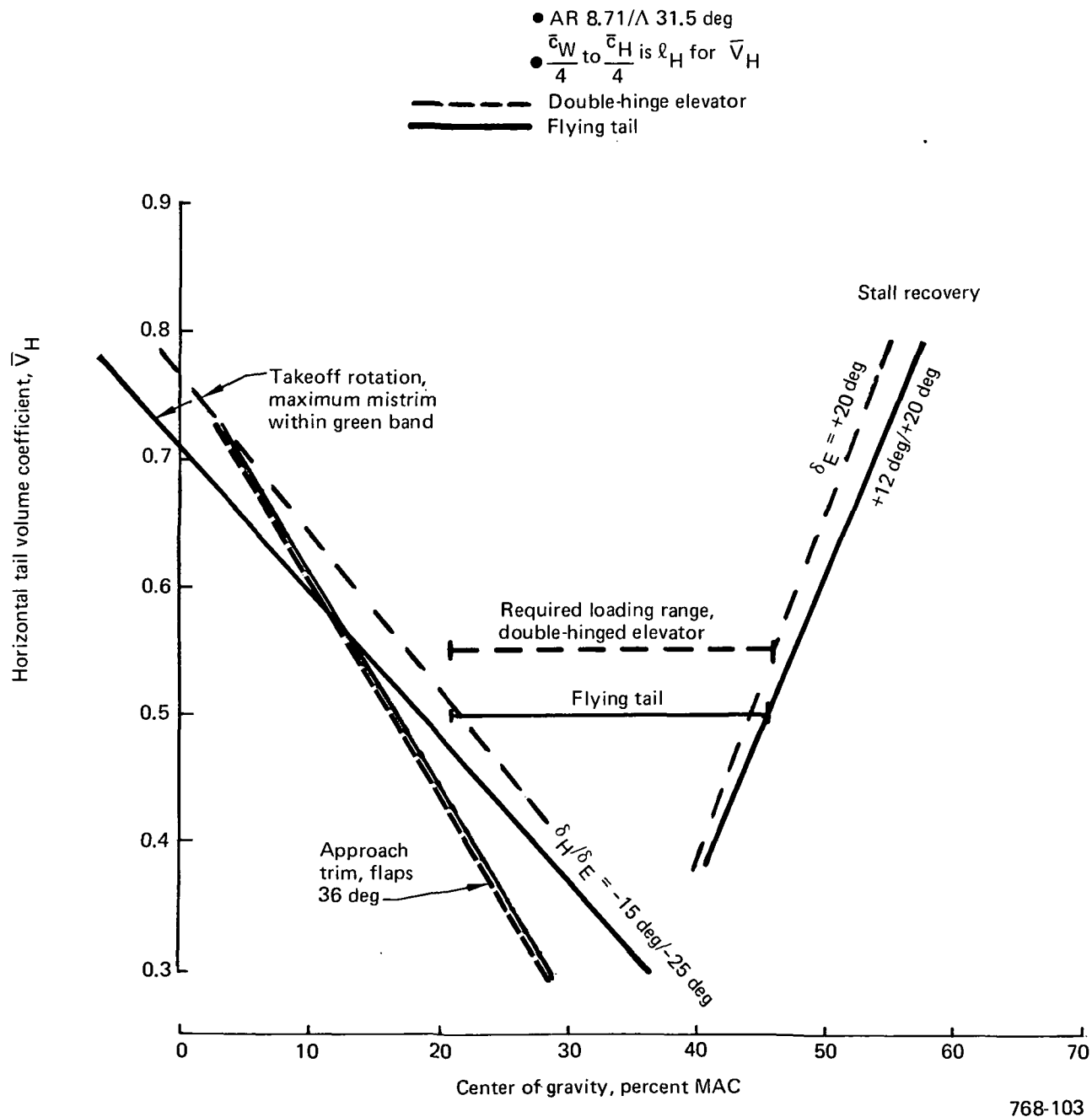
Figure 170. Flying Tail Comparison, Model 768-103

768-103

reduction is dependent on tail-sizing criteria, airplane stability, and wing-shift flexibility, as well as these tail surface deflections. Moreover, because a complete loss of hydraulic pressure would mean a loss of trim and control, an additional independent hydraulic system may be necessary for protection.

8.2.2 FLIGHT-CRUCIAL VERSUS FLIGHT-CRITICAL PAS

Models 768-103 and -104 are currently configured with a flight-crucial PAS. That is, the unaugmented airframe stability may be inadequate for completion of a flight and landing.

A flight-critical PAS, which may have significantly less complexity, would require the airplane to be safe to fly and land without the aid of a PAS. Therefore, the unaugmented airplane must meet minimum safe, Level 3, flying-quality requirements at all flight conditions within a permissible flight envelope. Level 3 criterion requires that the most unstable dynamic root will have a time to double amplitude that is greater than or equal to 6 sec. A dynamic analysis has shown that the Model 768-103 and -104 Configurations equal or better this criterion for most of the operational flight envelope with small tail size increases and/or shifts in the aft cg, as shown in the horizontal-tail-sizing charts (figs. 171 and 172). This portion of the envelope is defined in Figure 173. Because outside this "restricted" envelope the increase in tail area to meet Level 3 criteria is significantly larger, it was decided to retain the restricted flight envelope to which the airplane must retreat if one or more of the PAS channels fail. If the remaining channels fail, the airplane may be flown to a safe landing.

Performance analysis indicates that, on the average, a 0.5% loss in fuel efficiency results from the increase in tail area and aft cg restriction.

A study indicates that a cg shift forward of 1% MAC, or 0.0483m (1.9 in), would attain flight-critical PAS. A less restricted flight envelope might be accomplished by adding ballast in the nose or other detail configuration changes.

The ACT system configuration used for Models 768-103 and -104 and under development in the ACT System Technology Base Task (ref 3) uses a triplex set of primary
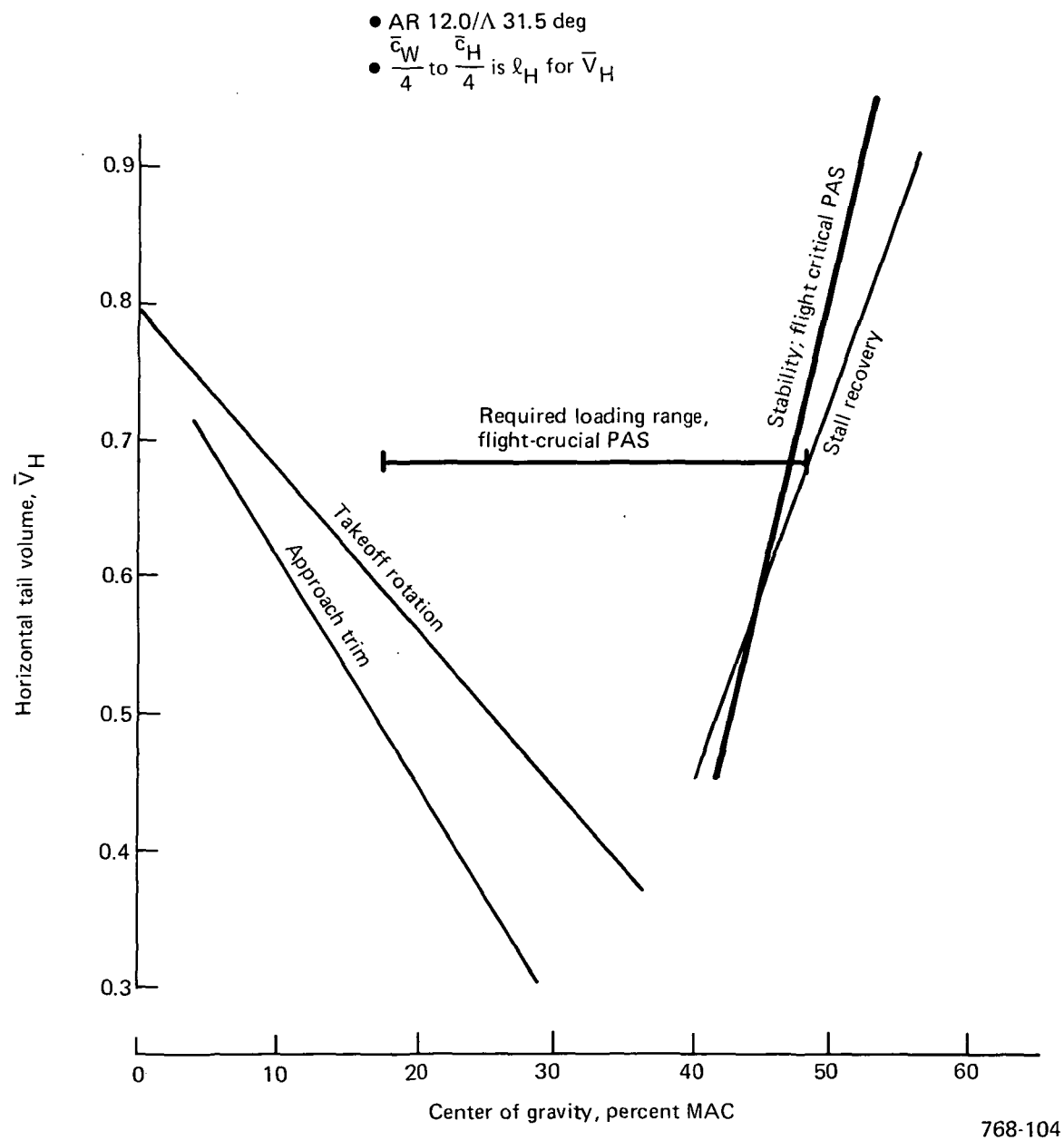
Figure 171. *Flight-Critical Pitch-Augmented Stability Requirements, Model 768-104*
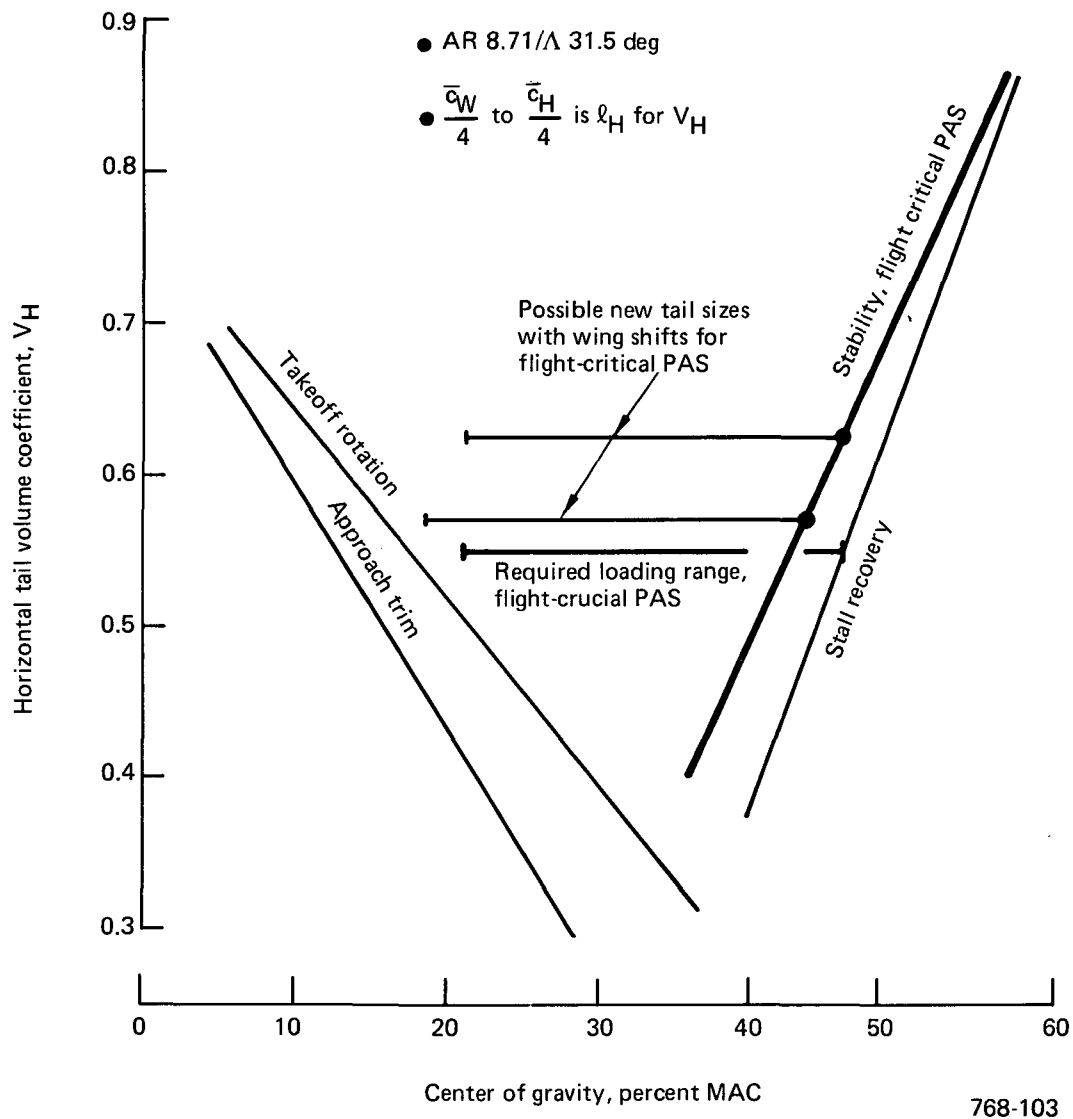
768-104

Figure 172. Flight-Critical Pitch-Augmented Stability Requirements, Model 768-103

computers to perform all ACT functions, including PAS. In addition, the flight-crucial PAS control law is mechanized in a quadruplex set of essential PAS computers that also provide the servocommands for the pitch-axis secondary actuator loop. If the flight-crucial PAS requirement is removed, as this trade suggests, the essential PAS computers would be eliminated, and the elevator servocommands would be issued by the primary computers.

These trades indicate that most of the ACT benefits can be realized with a flight-critical rather than a flight-crucial PAS.

281

Figure 173. Speed and Altitude Flight Envelope

9.0 FINAL ACT
AIRPLANE

9.0 FINAL ACT AIRPLANE

This section describes the sizing, configuration, and performance characteristics of the Final ACT Configuration (Model 768-107) and compares them to the Baseline Configuration.

9.1 FINAL ACT AIRPLANE SIZING

The Model 768-104 wing planform showed the largest improvement in fuel efficiency of the wings studied and therefore was selected for the Final ACT Configuration. This airplane was sized to the same range as the Baseline Configuration, while meeting or exceeding other performance requirements such as takeoff field length (TOFL), landing approach speed, and initial cruise altitude capability. In addition, performance at hot, high airports was determined.

Parametric wing area and engine size effects for the Model 768-104 Configuration are shown in Figures 174 through 176. Two approach-speed lines are shown, the maximum permitted by the design requirements and objectives (DRO) and the slightly lower value for Model 768-104. Parametrically, a 5% smaller wing area showed about a 1% improvement in fuel efficiency. The 768-104 engine size remained close to a minimum block fuel point for both approach speed constraints. A detailed configuration layout of 5% smaller wing was made to check landing gear integration. Reducing wing area geometrically did not allow integration of the landing gear behind the rear spar. Increasing the size of the gear fairing to do so caused a decrease in aspect ratio. When the drag was adjusted, the net fuel savings was less than 0.5% (figs. 174 and 175). Because the 768-104's 5% larger wing area results in improved performance at hot, high airports at negligible penalty in fuel efficiency, it was retained on the the Final ACT Configuration. The engine size was also retained. The changes from the Model 768-104 planform study configuration consist of a 889 kg (1960 lb) reduction in takeoff gross weight (TOGW), and 73 kg (160 lb) less operating empty weight (OEW) to reduce the range to 3589 kn (1938 nmi), which is identical to the Baseline Configuration.

The plan and front view comparisons (fig. 177) of the Baseline Configuration and Model 768-104 show the main configuration changes for the Final ACT Configuration.

- Range = 3590 km (1938 nmi)
- Payload = 197 passengers
- TOFL ≤ 2210m (7250 ft)
- $V_{APP_{MLW}}$ ≤ 70.0 m/s (136.1 KEAS)
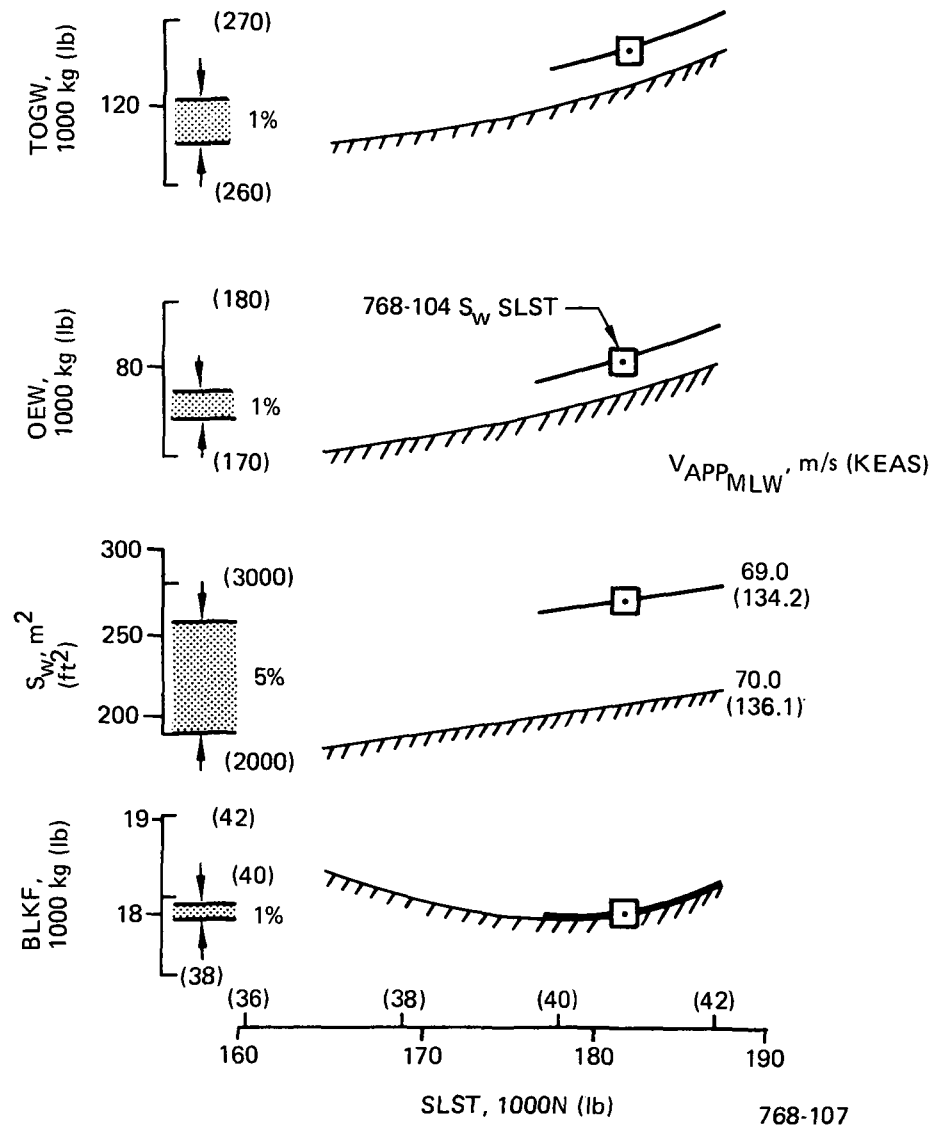
Figure 174. Final ACT Configuration Sizing, Effect of Engine Size

768-107

284

● Range = 3590 km (1938 nmi) ● SLST = 181 265N (40 750 lb)
●Payload = 197 passengers   ● TOFL ≤ 2210m (7250 ft)

$V_{APP_{MLW}}$ = 70 m/s
(136.1 KEAS)

TOGW, 1000 kg (lb)

(270)

1%

120

(260)

OEW, 1000 kg (lb)

(180)

1%

80

(170)

$V_{APP_{MLW}}$ = 70 m/s (136.1 KEAS)

V_{APP} (MLW)' m/s (in/s)

(140)

70

(130)

65

(120)

BLKF, 1000 kg (lb)

19

(42)

(40)

18

1%

(38)

(2800)   (2900)   (3000)   (3100)   (3200)

265   270   275   280   285   290   295

Wing area, m² (ft²)   768-107
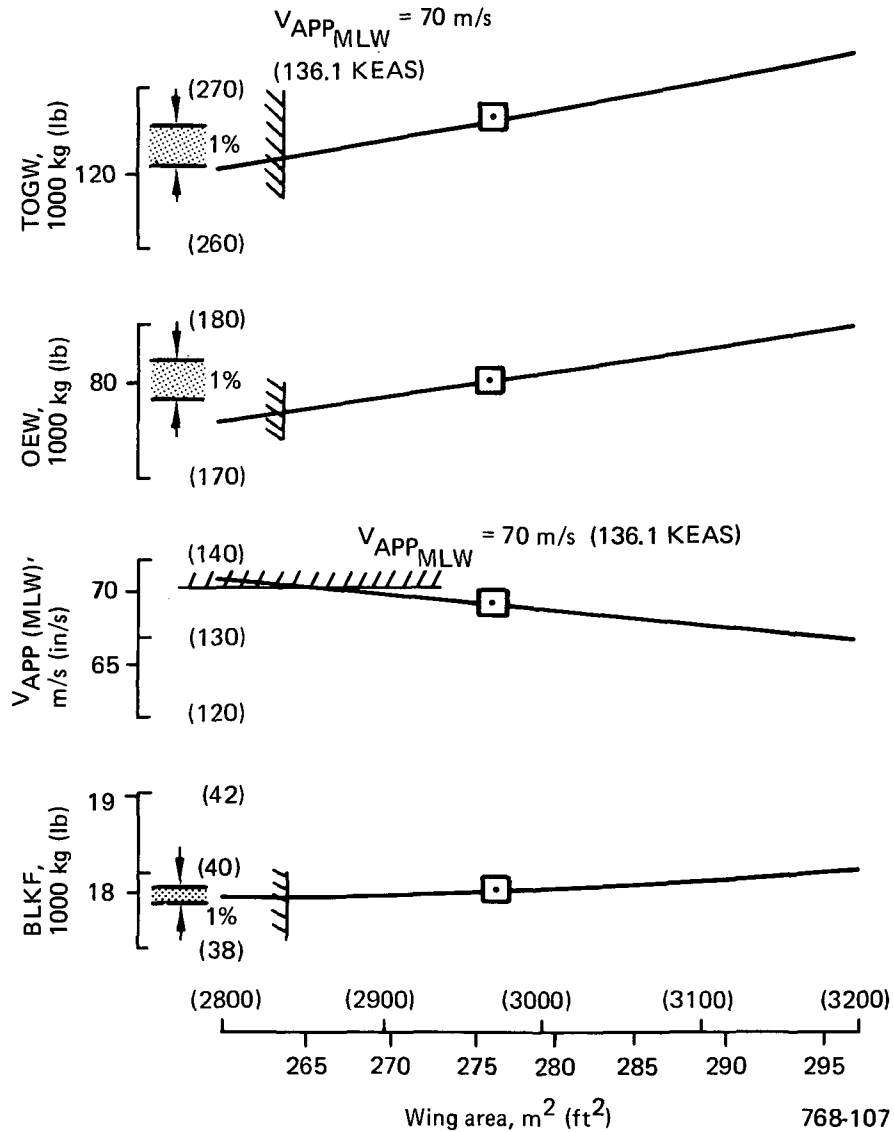
Figure 175. Final ACT Configuration Sizing, Effect of Wing Area

285

-5% Wing Area

Parametric assumption

Actual integrated wing

Model
768-104

768-104, -107
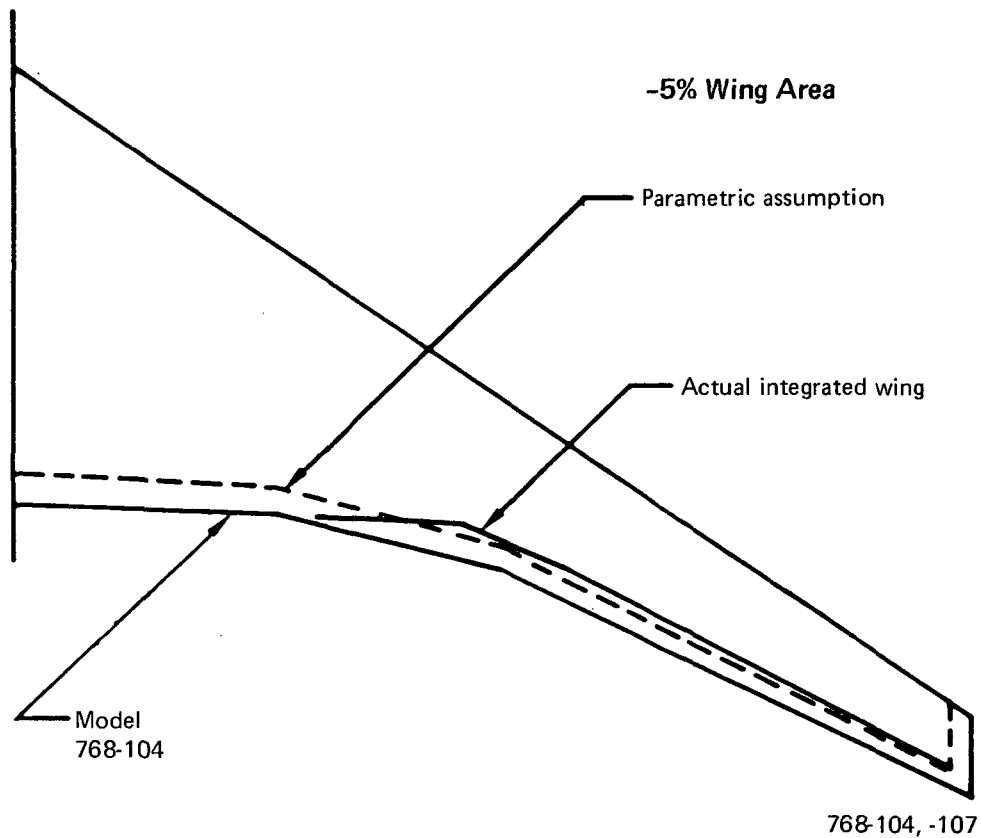
Figure 176. Final ACT Configuration Sizing, Landing Gear Integration

These changes are:

● Wing shifted forward 1.676m (66 in); center of gravity (cg) moved aft

● Smaller tail size

● Higher wing span with more taper

Changes not visible from Figure 177 include:

● Different main gear concept

● Maneuver-load alleviation (MLA); angle-of-attack limiter (AAL) and pitch-augmented stability (PAS)

Figure 178 shows a three-view of the Final ACT Configuration with tabulated configuration characteristics.

286
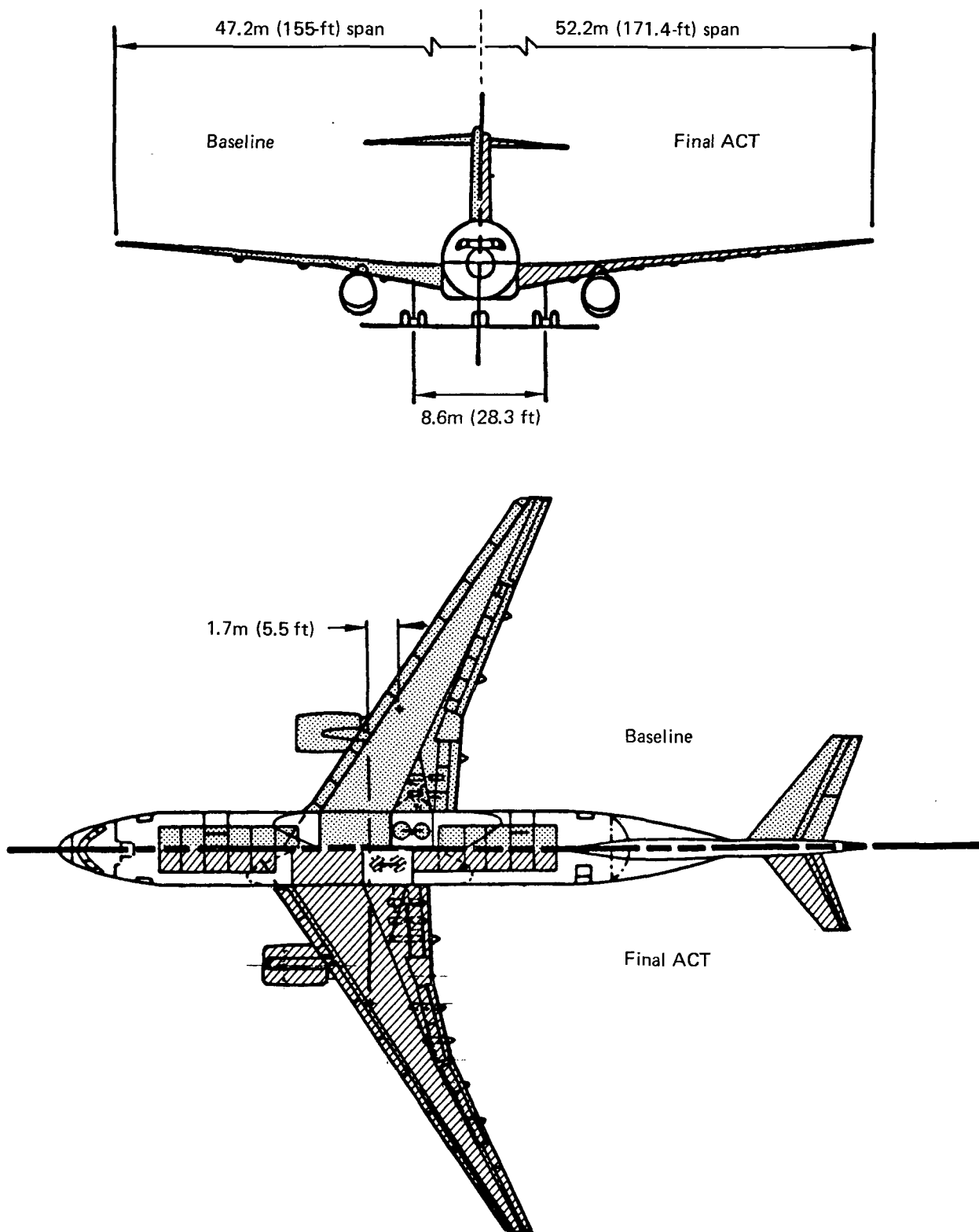
Figure 177. Conventional Baseline and Final ACT Configuration Comparison

287

Figure 178. Model 768-107 Final ACT Airplane General Arrangement

Weights, kg (lb):
TOGW: 121 580 (268 040)
OEW: 79 890 (176 120)
MLW: 114 160 (251 670)
Propulsion: Two CF6-6D2

Passenger accommodations

	Passengers	Abreast	Pitch
First class:	18	6	0.965m (38 in)
Tourist:	179	7	0.864m (34 in)

Cargo and baggage, m³ (ft³):

Containers	22 LD-2	or 11 LD-3	or 11 LD-4
Forward	33.98 (1200)	22.37 (790)	27.61 (975)
Aft	40.78 (1440)	26.85 (948)	33.13 (1170)
Bulk cargo (aft only)	11.33 (400)	11.33 (400)	11.33 (400)
Total	86.09 (3040)	60.55 (2138)	72.07 (2545)

Geometry:

Body cross section, m (in)
Shape: Vertical double lobe
Maximum width m (in): 5.029 (198.0)
Maximum height, m (in): 5.410 (213.0)

Landing gear	Nose	Main
Type	Dual	Truck
Location, m (in)	BS 6.896 (271.50)	72.4% MAC
Spacing, m (in)	0.610 (24)	1.143 x 1.422 (45 x 56)
Tire size, m (in)	0.940 x 0.330-0.406 (37 x 13-16)	1.092 x 0.394-0.508 (43 x 15.5-20)
Oleo stroke, m (in)	0.381 (15)	0.508 (20)

Aerodynamic surfaces	Wing	Vertical tail	Horizontal tail
Area, m² (ft²)	226.8 (2441)a	56.6 (609)	32.0 (344)
Aspect ratio	12.03a	0.67	4.00
Taper ratio	0.267a	0.700	0.400
Sweep at c/4, deg	31.5a	55.0	35.0
Incidence, SOB, deg	3.8a	—	—
Dihedral, deg	6.0a	—	-3.0
Root t/c, percent	15.1	12.0	11.0
Tip t/c, percent	10.3	12.0	9.0
Root chord, m (in)	6.855 (269.89)a	10.811 (425.64)	4.038 (158.98)
Tip chord, m (in)	1.830 (72.06)	7.568 (297.94)	1.615 (63.59)
MAC m(in)	4.827 (190.05)a	9.285 (365.57)	3.000 (118.10)
Span, m (in)	52.222 (2056)	6.157 (242.40)	11.291 (444.53)
Tail arm, m (in)	—	21.534 (847.78)	28.709 (1130.27)
Tail volume coefficient b	—	0.085	0.689

Engine toe-in angle = 1 deg to a BBL
Nacelle incidence = 2.625 deg to a BWL
Wing upper surface at SOB rib at BWL 4.953m (195 in)

aTrapezoid geometry, quoted: aero reference area = 275.8 m² (2969 ft²)
bBased on aero reference area

9.2 WEIGHT ANALYSIS

The Final ACT Configuration, Model 768-107, detailed weight and balance data are included in this subsection. The Final ACT is nearly identical to the Model 768-104 with only a small OEW improvement due to the maximum TOGW reduction, which was a result of sizing to the Baseline Configuration range. The sized design weights for structural loads analyses are listed in Table 30.

A weight statement for the Final ACT Configuration is shown in Table 31. The small weight increments due to changes in design conditions were not structurally analyzed: they were estimated based on past airplane growth-trend results. The cg range (loadability) is very similar to that of Model 768-104, which is described in Subsection 5.3.3.

9.3 AERODYNAMIC CHARACTERISTICS

The Final ACT Configuration (Model 768-107) external geometry is identical to the Wing Planform Study Configuration (Model 768-104). Also, average cruise cg and forward takeoff and landing cg remained unchanged for the 768-104 and Final ACT Configuration. Therefore, the Final ACT high- and low-speed lift and drag

Table 30.   Design Weights for Structural Load Analysis

Item	Weight			
	Model 768-104		Model 768-107	
	kg	(lb)	kg	(lb)
Operational empty weight (OEW)	79 960	176 280	79 890	176 120
Maximum design zero full weight (MZFW)	106 060	233 830	105 990	233 670
Maximum design landing weight (MLW)	114 230	251 830	114 160	251 670
Maximum design takeoff weight (MTOW)	122 470	270 000	121 580	268 040
Maximum design taxi weight (MTW)	122 920	271 000	122 040	269 040

768-104, -107

Table 31.   Weight and Balance Statement, Model 768-107

Functional group	Weight		Longitudinal cg body station	
	kg	(lb)	m	(in)
Wing	17 160	37 840	24.48	964
Horizontal tail	1 070	2 360	52.73	2076
Vertical tail	1 878	4 140	47.40	1866
Body	15 770	34 770	23.88	940
Main landing gear	6 480	14 280	24.71/25.35[a]	973/998[a]
Nose landing gear	894	1 970	6.17/6.76[a]	243/266[a]
Nacelle and strut	2 545	5 610	19.56	770
Total structure	45 800	100 970	25.27/25.37 [a]	995/999[a]
Engine	7 951	17 530	19.84	781
Engine accessories	100	220	16.79	661
Engine controls	82	180	16.10	634
Starting system	77	170	18.82	741
Fuel system	599	1 320	24.46	963
Thrust reverser	1 638	3 610	19.96	786
Total propulsion system	10 447	23 030	20.07	790
Instruments	485	1 070	11.10	473
Surface controls	2 227	4 910	30.96	1219
Hydraulics	1 021	2 250	24.49	964
Pneumatics	354	780	20.02	788
Electric	1 021	2 250	13.41	528
Electronics	775	1 710	12.04	474
Flight provisions	417	920	4.90	193
Passenger accommodations	6 681	14 730	22.30	878
Cargo handling	1 229	2 710	23.39	921
Emergency equipment	422	930	19.79	779
Air conditioning	975	2 150	18.21	717
Anti-icing	186	410	20.09	791
Auxiliary power unit	676	1 490	42.80	1685
Total fixed equipment	16 469	36 310	22.38	881
Exterior paint	68	150	23.04	907
Options	907	2 000	23.95	943
Manufacturers empty weight	73 690	162 460	23.88/23.92[a]	940/942[a]
Standard and operational items	6 196	13 660	25.86	1018
Operational empty weight	79 890	176 120	24.03/24.07[a]	946/948[a]

[a]Gear up/gear down.

768-107

characteristics are identical to the aspect ratio (AR) 12 planform shown in Subsection 7.4.   A comparison of low-speed drag and configuration characteristics between the Baseline and Final ACT Configurations is shown in Table 32.

290

Table 32. Low-Speed Configuration and Drag Comparison

Configuration	Baseline (Model 768-102)	Final ACT (Model 768-107)	Improvement, percent
Forward center of gravity, percent MAC	10.0	17.5	—
Horizontal tail			
ℓ_H, m (ft)	27.14 (89.03)	28.7 (94.19)	—
S_H, m^2 (ft^2)	57.60 (620)	32.0 (344.0)	
$\overline{V}_H$	0.942	0.689	
Vertical tail			
ℓ_V, m (ft)	19.97 (65.5)	21.50 (70.55)	—
S_V, m^2 (ft^2)	57.41 (618)	56.78 (611.0)	
$\overline{V}_V$	0.088	0.085	
Takeoff climbout			
$C_{L_{V_2}}$	1.35	1.35	
L/D_{V_2} (all engines operating)	11.6	12.4	6.9
Landing approach			
$C_{L_{APP}}$ (1.3V_S)	1.334	1.389	4.1
L/D_{APP}	8.11	8.81	8.6

768-102, -107

9.4 PERFORMANCE

The performance improvements achieved by the Final ACT Configuration relative to the Baseline are shown in Table 33. At the design range, block fuel was reduced 10.1%. TOFL was reduced 14% at sea level due to better climb performance resulting from trim-drag reduction and lower drag due to lift (higher span). Additional benefits are realized for high-altitude, hot-day conditions where payload is limited by takeoff performance. For example, at Denver 33.3°C (92°F), the climb-limited takeoff performance improvement allows a 7260 kg (16 000 lb) gross weight increase, which is sufficient to give full payload-range capability from Denver. This could increase the airplane's profitability for some operators on some routes.

Table 33. Conventional Baseline and Final ACT Performance Comparison

	Baseline (Model 768-102)	Final Act (Model 768-107)	Δ	Δ percent
MTW, kg (lb)	122 920 (271 000)	122 040 (269 040)	-890 (-1960)	-0.7
MTOW, kg (lb)	122 470 (270 000)	121 580 (268 040)	-890 (-1960)	-0.7
MZFW, kg (lb)	104 400 (230 160)	105 990 (233 670)	+1590 (+3510)	1.5
MLW, kg (lb)	112 570 (248 160)	114 160 (251 670)	+1590 (+3510)	1.4
OEW, kg (lb)	78 300 (172 610)	79 890 (176 120)	+1590 (+3510)	2.0
Forward center of gravity, percent MAC	10.0	17.5	+7.5	—
Average cruise center of gravity, percent MAC	20.5	30.6	+10.1	—
Cruise L/D, (M = 0.8, C_L = 0.45)	17.82	19.57	+1.75	9.8
SAR, km (nmi)	3 589 (1 938)	3 589 (1 938)	—— ——	0
TOFL, SL 29°C (84°F) m (ft)	2 210 (7 250)	1 890 (6 200)	-320 (-1050)	-14.5
V_{APP} at maximum landing weight, m/s (kn)	70.0 (136.1)	69.0 (134.2)	-1.0 (-1.9)	-1.4
Landing field length, sea level, dry, at maximum landing weight, m (ft)	1 443 (4 735)	1 411 (4 630)	-32 (-105)	-2.2
Block fuel, kg (lb)	19 930 (43 930)	17 920 (39 500)	-2010 (-4430)	-10.1
Denver performance				
SAR (1625m [5334 ft] 33.33°C [92°F]), m (nmi)	2 370 (1 280)	3 590 (1 938)	+1220 (+658)	51

768-102, -107

Landing approach speed is about 1.03 m/s (2 kn) lower at maximum landing weight. The maximum flap approach stall C_L is higher for the Final ACT Configuration due to the more aft forward cg limit.

Figure 179 shows block fuel and time versus range for the Final ACT and Baseline. Block time is the same for both configurations because climb, cruise, and descent speed schedules are identical. Figure 180 shows incremental block fuel savings. Fuel savings for the Final ACT Configuration vary from about 4% at short ranges to about

292
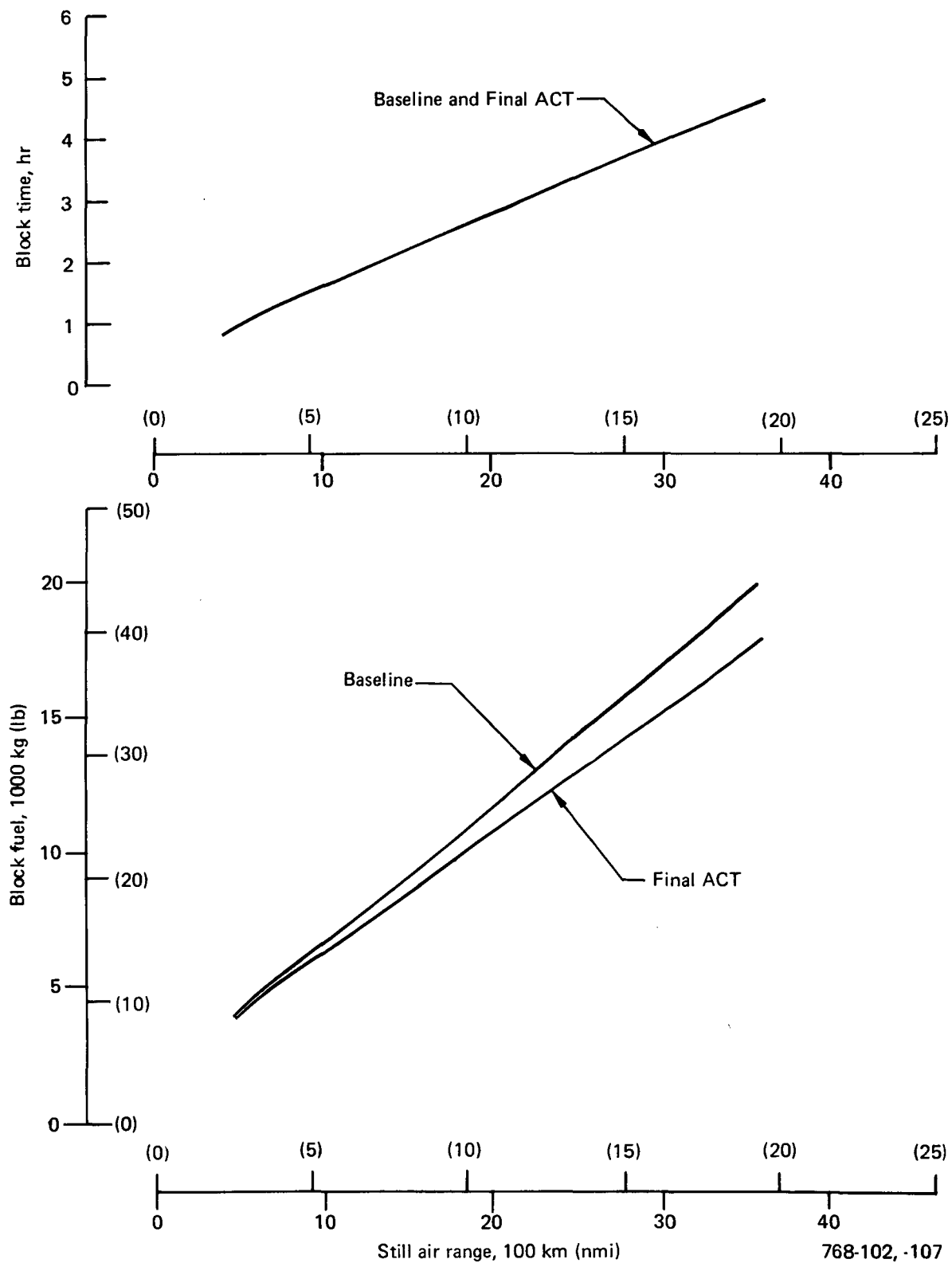
*Figure 179. Block Fuel and Block Time Data for Conventional
Baseline and Final ACT*
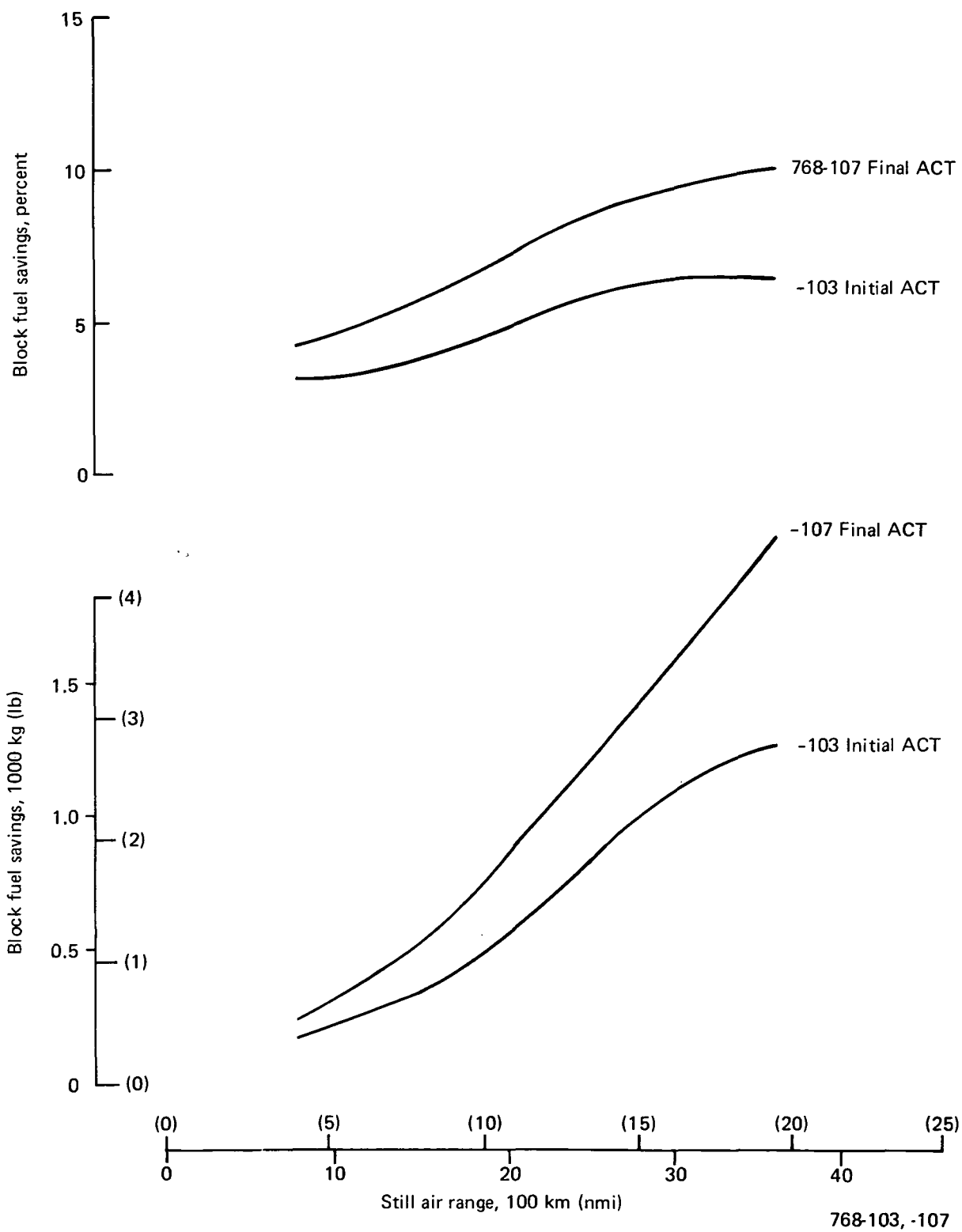
Figure 180. Block Fuel Savings of Final ACT and Initial ACT Relative to Conventional Baseline Configuration

10% at maximum range relative to the Baseline. The effect of span on fuel savings is shown by comparison with the Initial ACT Configuration. The 10.5% span increase for the Final ACT Configuration improved fuel efficiency by 1% (short range) to 3.5% (design range).

Figure 181 shows the benefit of ACT systems and wing geometry to fuel efficiency. The majority of fuel savings was due to PAS. Wing-load alleviation (WLA) had a net benefit of 0.5%. Planform improvements included 3.5% for increasing wing span while keeping wing reference area constant. This incremental improvement would tend to be the same for non-ACT airplanes with the same wing planform; i.e., landing gear fairing providing a large side-of-body structural wing box.

- SAR = 3589 km (1938 nmi)
- Payload = 197 passengers
- Cruise Mach = 0.80
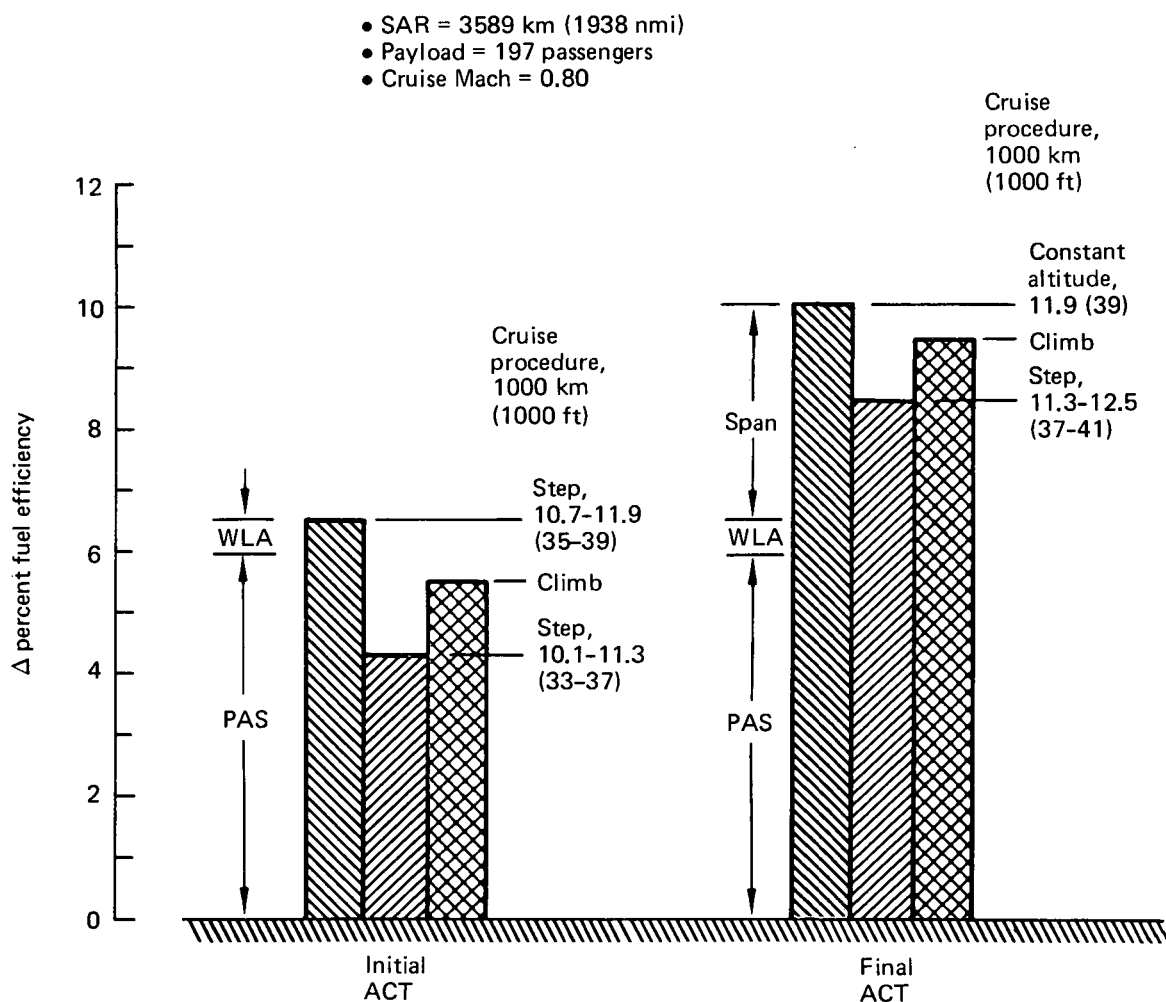
Figure 181. Fuel Efficiency Relative to Baseline Configuration

Also, depending on flight direction (east versus west), assigned altitudes for traffic separation will alter total relative fuel savings for the ACT Configurations. Flying from west to east reduces cruise altitude significantly below best-cruise altitude for the ACT Configurations and reduces the relative fuel efficiency by 1.5 to 2%. However, allowing both airplanes to cruise-climb at best-cruise altitude shows the fundamental benefit of ACT without current constant altitude Federal Aviation Administration flight-level assignments masking the results. Cruise-climb results show the fuel savings for Initial and Final ACT Configurations at 5.5 and 9.5%, respectively.

10.0 CONCLUDING REMARKS AND RECOMMENDATIONS

The principal objective of the IAAC Project is to assess the effects of the integrated application of ACT to a medium-range subsonic transport airplane. After establishing a Conventional Baseline Configuration, the Initial ACT Configuration was developed and showed a 6% improvement in fuel efficiency at design range. The next two stages, covered by this document, were the evaluation of several different wing planforms and the selection and definition of a Final ACT Configuration.

10.1 CONCLUDING REMARKS

The Wing Planform Study evaluated three active controls airplanes that had different wing geometries. Two of these retained the 31.5 deg sweep of the Baseline and Initial ACT Configurations but had higher wing spans. The third configuration used a wing with 5 deg less sweep and an intermediate wing span. Study results clearly showed the configuration with the highest wing span had the best fuel efficiency. Some of the key study results are shown in Table 34.

The most beneficial ACT functions were the pitch-augmented stability (PAS) and angle-of-attack limiter (AAL) systems. Over 90% of the fuel savings due to active controls were directly related to these functions; the remainder were due to maneuver-load control (MLC) and lateral/directional-augmented stability (LAS). The WLA system, although not showing large benefits for the design configurations, may

Table 34. Percent Change Relative to Baseline Configuration

Configuration	Model 768-103 Initial ACT	Model 768-105	Model 768-104	Model 768-106
● Wing geometry				
● Aero-reference area	0	0.2	0.3	0
● Sweep at c/4, deg	31.5	31.5	31.5	26.4
● Span	0	5.6	10.5	5.9
● Cruise L/D	3.7	7.2	9.8	7.2
● OEW	-1.2	0.7	2.1	3.5
● Range (MTOW = 122 470 kg (270 000 lb))	13.1	7.8	4.8	-6.3
● Fuel efficiency	6.3	8.1	10.3	6.4

297

produce greater benefits for growth airplanes with, for example, increases in design takeoff gross weight or wing-tip extensions.

Designing the ACT airplanes for flight-critical rather than flight-crucial PAS may be a beneficial cost-performance trade. The flight-critical PAS would be a simpler, less expensive system.

Large side-of-body wing chords, required for gear integration with aft centers of gravity, improve wing-box structural efficiency, allowing higher spans for less weight increase.

Performance studies revealed possible wing-size reduction for the Final ACT Configuration. Design studies showed that reductions in the Model 768-104 wing size would increase the relative trailing-edge extension for the landing gear and thus reduce wing aspect ratio, taper ratio, and effective sweep. Therefore, the selected Final ACT Configuration is identical in shape to the Model 768-104. Cycling to the Baseline Configuration design mission range allowed structure and fuel weight to be reduced a small amount. Performance levels of the Final ACT and Model 768-104 Configurations are nearly identical.

Weight, drag, and fuel efficiency relative to the Conventional Baseline are:

- Cruise lift/drag (L/D)   +9.8%

- Operating empty weight (OEW)   +2.0%

- Takeoff gross weight (TOGW)
  at still air range = 3589 km (1938 nmi)   -0.7%

- Fuel efficiency at design range   +10.0%

According to current certification rules and procedures, there are no serious technical obstacles to achieving the above results, with the exception of software reliability validation to the high levels required. However, considerable control system work remains to be done. The software reliability problem is currently being addressed in

other ongoing research programs. Control system development (including acquisition, laboratory test, and, potentially, flight test) of critical ACT system elements must also proceed for ACT to become an integral part of future commercial transports.

Reliability and maintainability required for commercial operation were considered throughout. Criteria postulated for reliability and degree of dependence upon ACT functions may appear conservative; however, they represent an engineering judgment of what would be acceptable to the authority certifying airworthiness and to the airline customer.

Designing an airplane to use ACT results in many complex interactions such as loadability, center-of-gravity range, stability and controllability requirements, and landing gear geometry. With the removal or modification of minimum longitudinal stability requirements, high angle-of-attack controllability limits will define minimum longitudinal control power and horizontal tail size. Hydraulic and electric power systems must have reliability and redundancy compatible with the control system requirements. An assessment of ACT without consideration of a fully integrated design could result in misleading or invalid conclusions.

The results shown in this document pertain to a class of airplanes described in Appendix A of the Initial ACT document (ref 3). Airplanes with other mission requirements and configuration characteristics may show significantly different results due to the integration of ACT. However, although the magnitude of these results are not universal they do indicate that significant benefits due to ACT should be available in typical air transport applications.

10.2 RECOMMENDATIONS

ACT study development should be continued according to the IAAC Project Plan (ref 1). Final ACT Configuration evaluation and control system development should proceed as described. These activities should address concerns with hardware and software implementation of the ACT functions and flying qualities characteristics with normal and failed ACT systems under various weather conditions.

Because the fuel efficiency penalty for using flight-critical PAS rather than flight-crucial (PAS) appears to be small for the IAAC configurations, consideration of changing to the less complex system should be made in any future ACT airplane design.

Finally, current reliability analysis methods need to be extended to adequately treat redundant digital systems.

11.0 REFERENCES

1   Integrated Application of Active Controls (IAAC) Technology to an Advanced Subsonic Transport—Project Plan. NASA CR-3305, Boeing Commercial Airplane Company, February 1981.

2   Integrated Application of Active Controls (IAAC) Technology to an Advanced Subsonic Transport Project—Conventional Baseline Configuration Study. NASA CR-159248, Boeing Commercial Airplane Company, June 1980.

3   Integrated Application of Active Controls (IAAC) Technology to an Advanced Subsonic Transport Project—Initial ACT Configuration Design Study. NASA CR-159249, Boeing Commercial Airplane Company, July 1980.

4   Integrated Application of Active Controls (IAAC) Technology to an Advanced Subsonic Transport Project—Current and Advanced ACT Control System Definition Study—Volume I; Appendices—Volume II. NASA CR-165631, Boeing Commercial Airplane Company, 1981.

5   USAF, Stability and Control DATCOM, Flight Control Division, Air Force Flight Dynamics Laboratory, Wright-Patterson Air Force Base, Ohio, April 1978.

6   Gray, W. L., and K. M. Schenk. A Method for Calculating the Subsonic Steady-State Loading on an Airplane with a Wing of Arbitrary Planform and Stiffness. NACA TN 3030, December 1953.

7   Küchemann, D. A Simple Method for Calculating the Span and Chordwise Loading on Straight and Swept Wings of Any Given Aspect Ratio at Subsonic Speeds. Aeronautical Research Council, Reports and Memoranda No. 2935, August 1952.

8   Selected Advanced Aeronautics and Active Controls Technology Concept Development on a Derivative B-747 Aircraft. Final Report, NASA CR-3164, Boeing Commercial Airplane Company, February 1980.

9   Miller, R. D., R. I. Kroll, and R. E. Clemmons. Dynamic Loads Analysis System (DYLOFLEX) Summary. NASA CR-2846, 1979.

10   Bjurman, B. E., G. M. Jenkins, C. J. Maereliez, K. L. McClellan, and J. E. Templeman. Airborne Advanced Reconfigurable Computer System. NASA CR-145024, 1976.

11   Weight and Balance Data Reporting Forms for Aircraft. MIL-STD-1374, Part 1, March 31, 1972.

APPENDIX A

AERODYNAMIC DATA FOR STRUCTURAL ANALYSIS

The aerodynamic data used in the wing loads analysis of the planform study wings were derived from wind tunnel test results for the Baseline Configuration as discussed in Subsection 7.2.1.

Wing section normal force and pitching moment slopes are shown in Figures A-1 through A-4. Note that the data in Figure A-1 apply to both the Baseline and Initial ACT Configurations because they have identical wing planforms.

Wing section normal force and pitching moment at zero angle of attack are shown in Figure A-5.

Wing section normal force and pitching moment due to outboard ailerons are shown in Figure A-6 for the Initial ACT wing and in Figure A-7 for the planform study wings. The data in Figure A-6 were derived from wind tunnel test results that were available at the beginning of the IAAC Project. The data in Figure A-7 are from wind tunnel test results for the Baseline Configuration, which became available and were incorporated during the Wing Planform Study.

Body lift and moment data for the Model 768-103 Configuration are shown in Figure A-8. Nacelle lift and moment data are shown in Figure A-9. These data were adjusted for other configurations to account for differences in reference wing area and chord and quarter MAC location.

Figure A-1. Wing Section Normal Force and Moment Due to Angle of Attack, Models 768-102 and -103

- Rigid wing
- Moment about local wing c/4
- Symbols represent values derived for analysis

Mach No.

0.40	☉
0.70	⊞
0.85	◇
0.86	⬠
0.91	△

Lift

Normal force slope, C_{n_α}, per deg vs Fraction of semispan, η

Mach No.

0.40	☉
0.70	⊞
0.85	◇
0.86	⬠
0.91	△

Moment

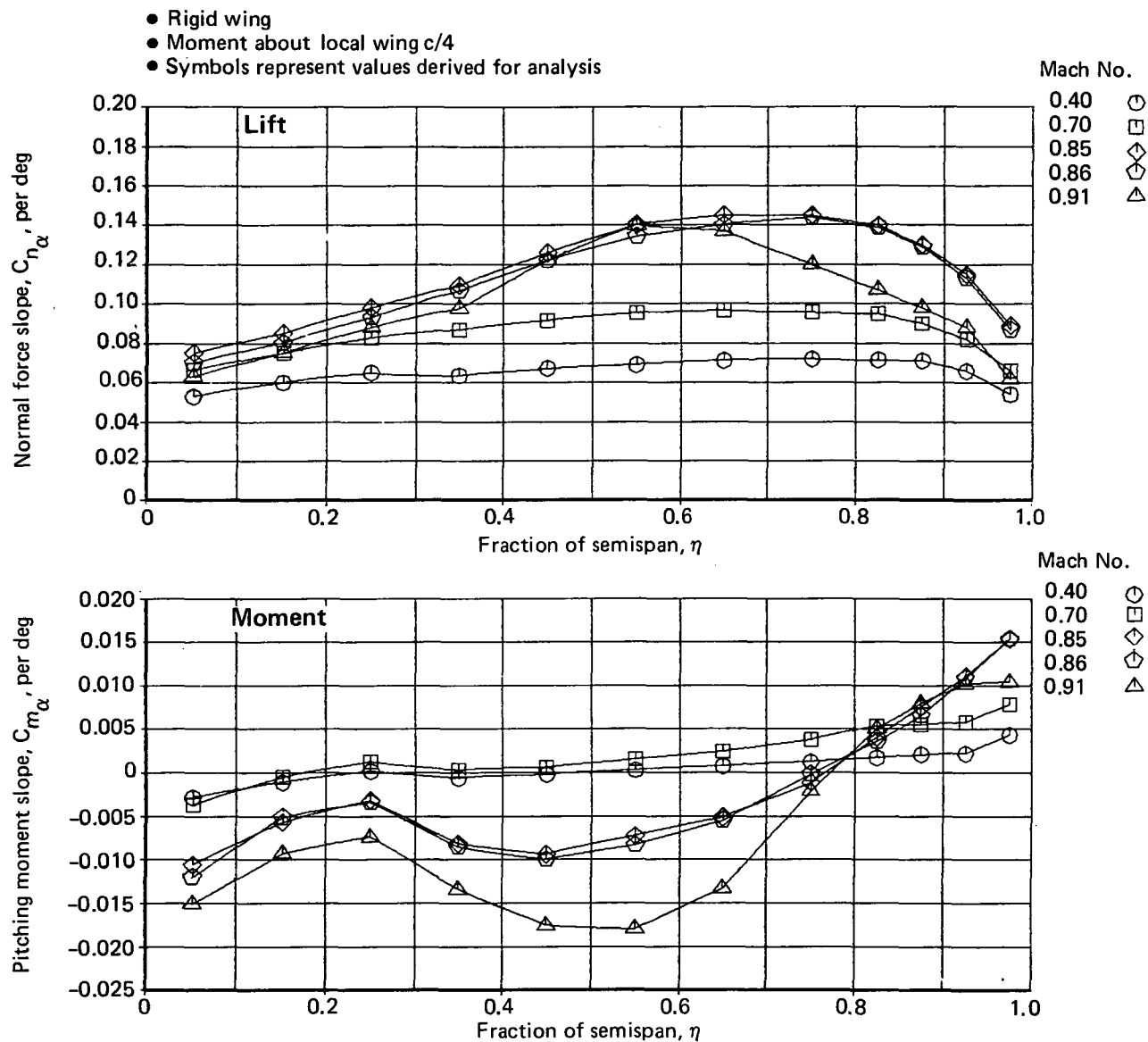Pitching moment slope, C_{m_α}, per deg vs Fraction of semispan, η
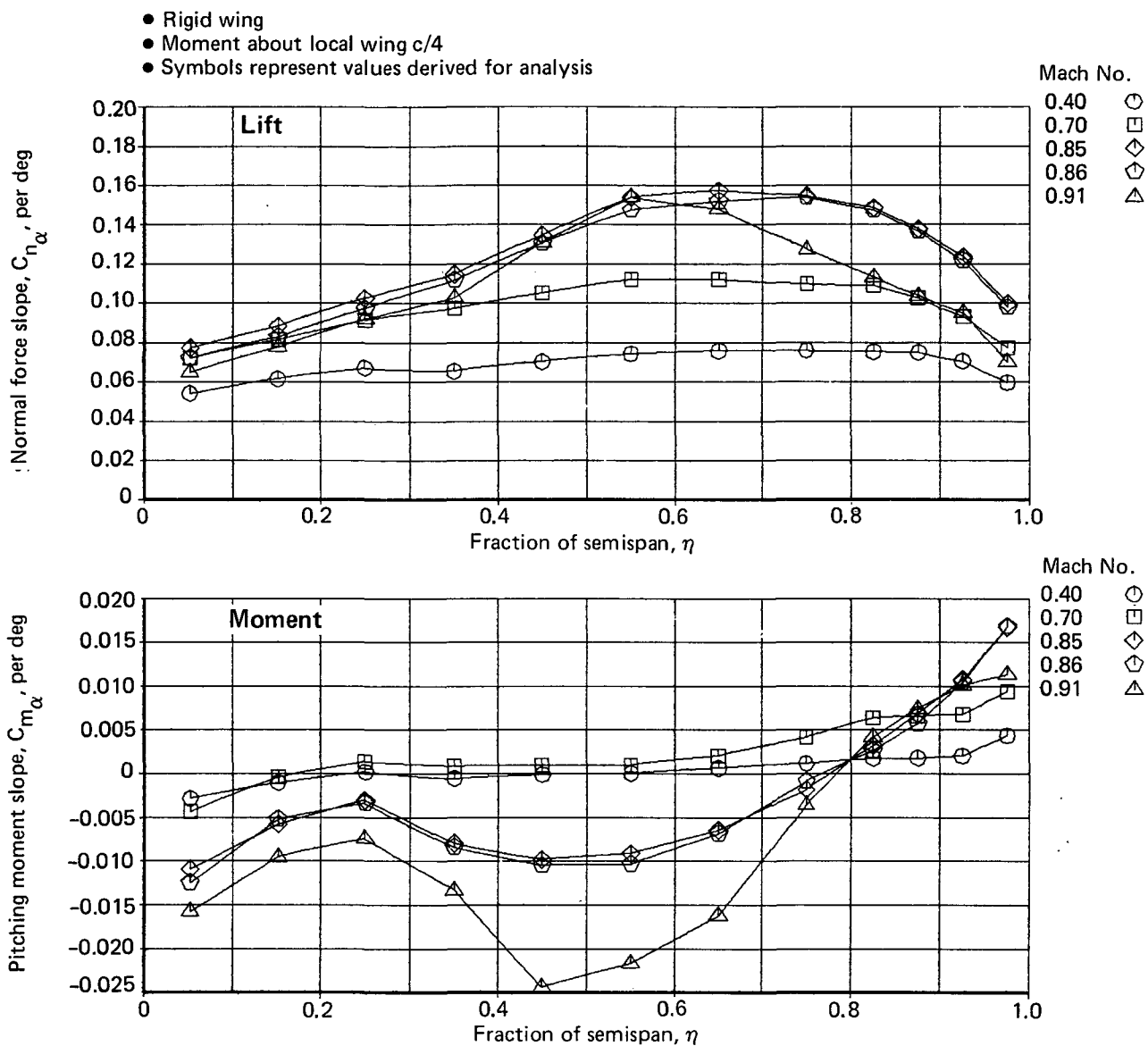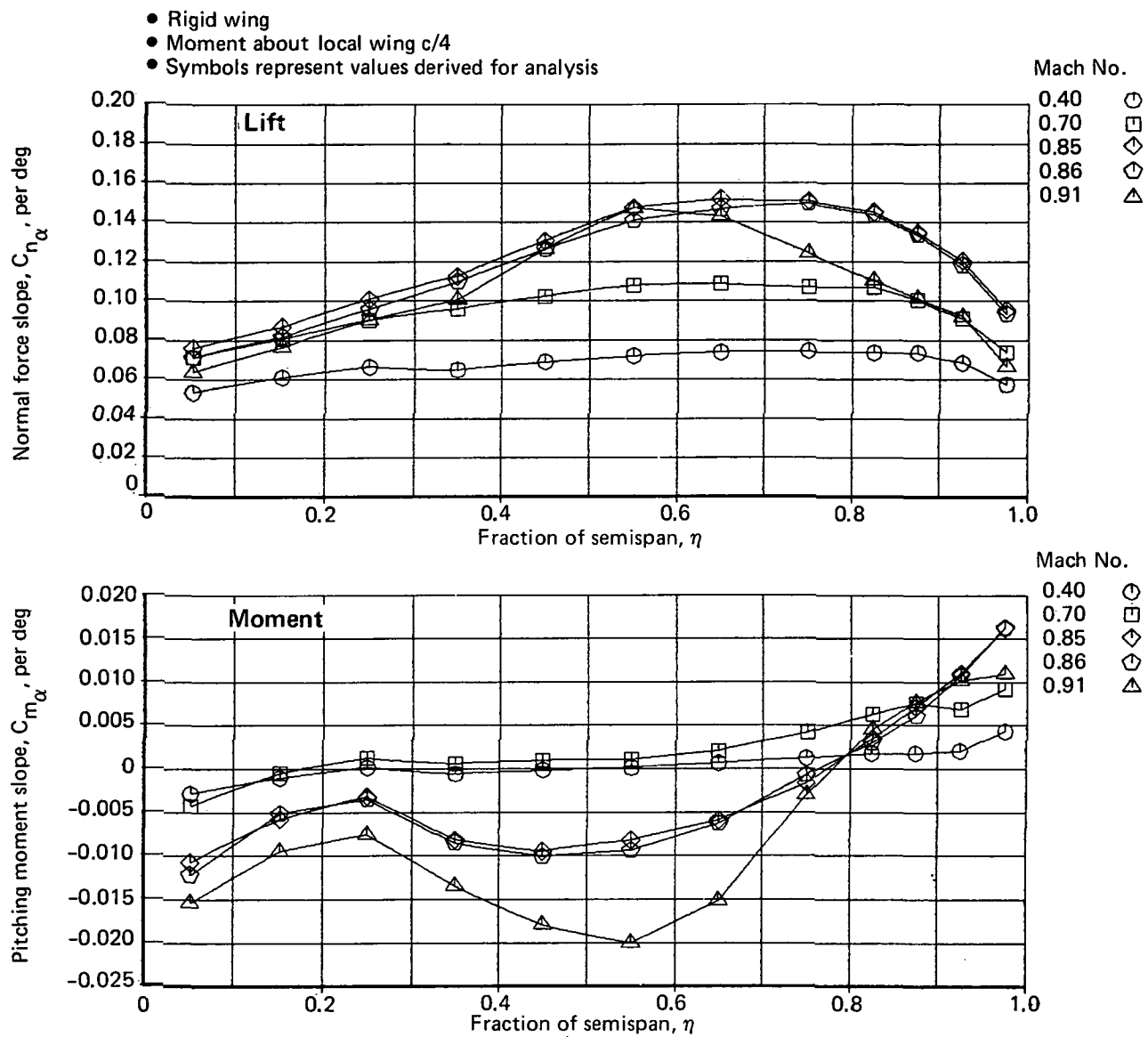
Figure A-2. Wing Section Normal Force and Moment Due to Angle of Attack, Model 768-104

Figure A-3. Wing Section Normal Force and Moment Due to Angle of Attack, Model 768-105

- Rigid wing
- Moment about local wing c/4
- Symbols represent values derived for analysis
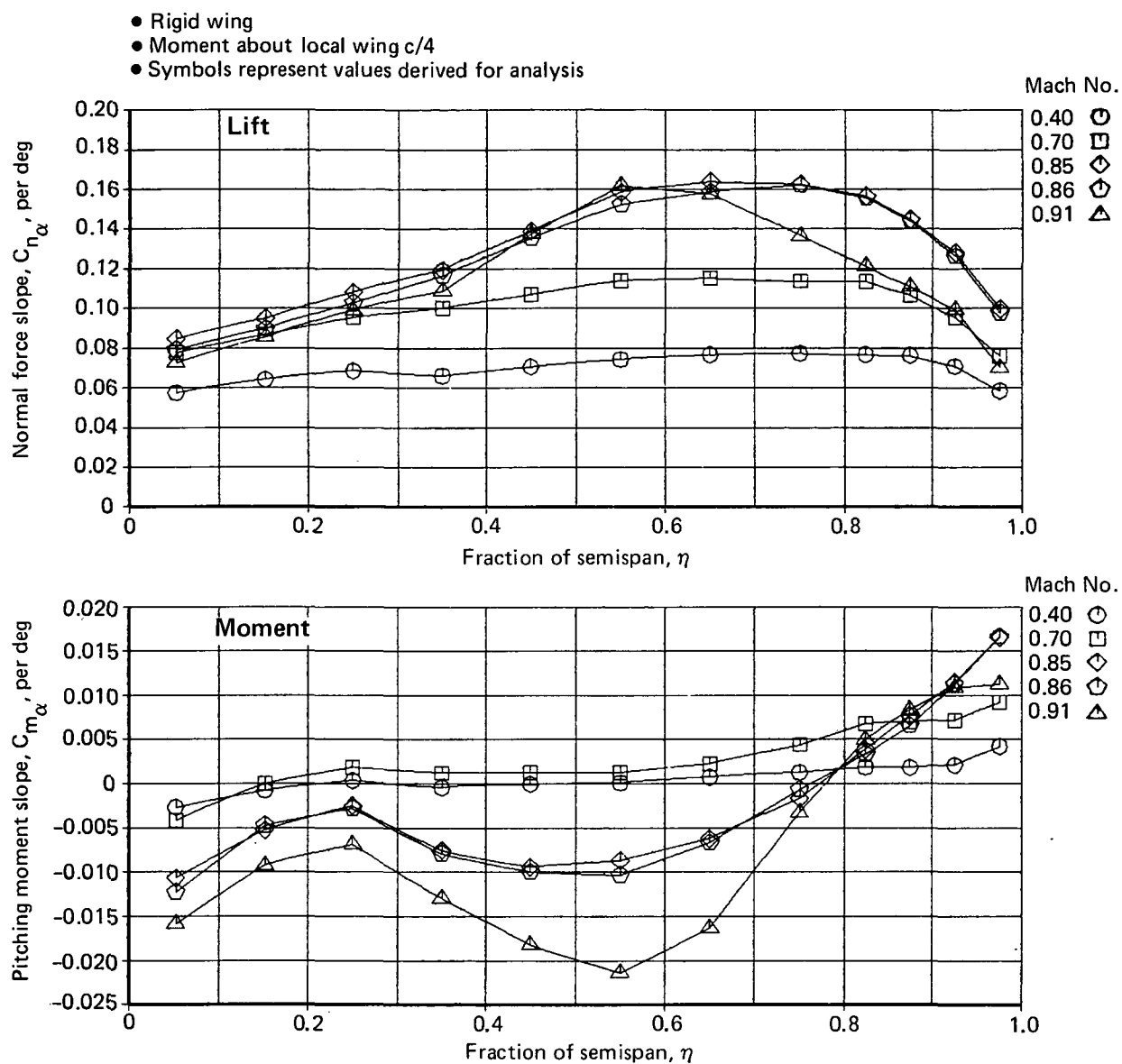
Figure A-4. Wing Section Normal Force and Moment Due to Angle of Attack,
Model 768-106

307

- Flat rigid wing at $\alpha_W = 0$
- Moment about local wing c/4
- Symbols represent values derived for analysis

Lift

Normal force coefficient, C_n

Fraction of semispan, η

Mach No.
0.40 ⊙
0.70 ⊟
0.85 ◇
0.86
0.91 △

Moment

Pitching moment coefficient, C_m

Fraction of semispan, η

Mach No.
0.40 ⊙
0.70 ⊟
0.85 ◇
0.86 ⊙
0.91 △
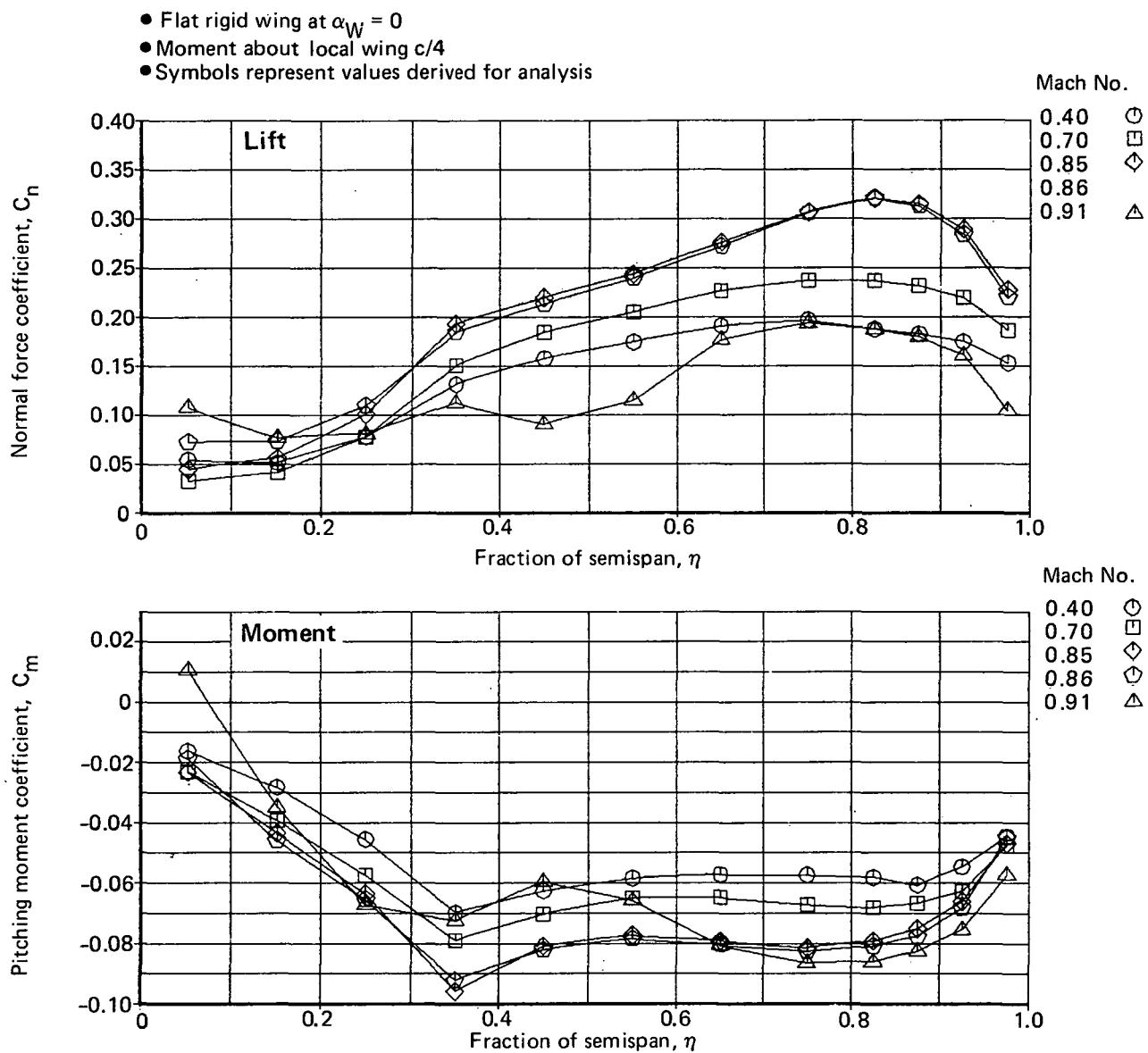
768-102, -103, -104, -105, -106

Figure A-5. Wing Section Normal Force and Moment at Zero Angle of Attack, All Models

308

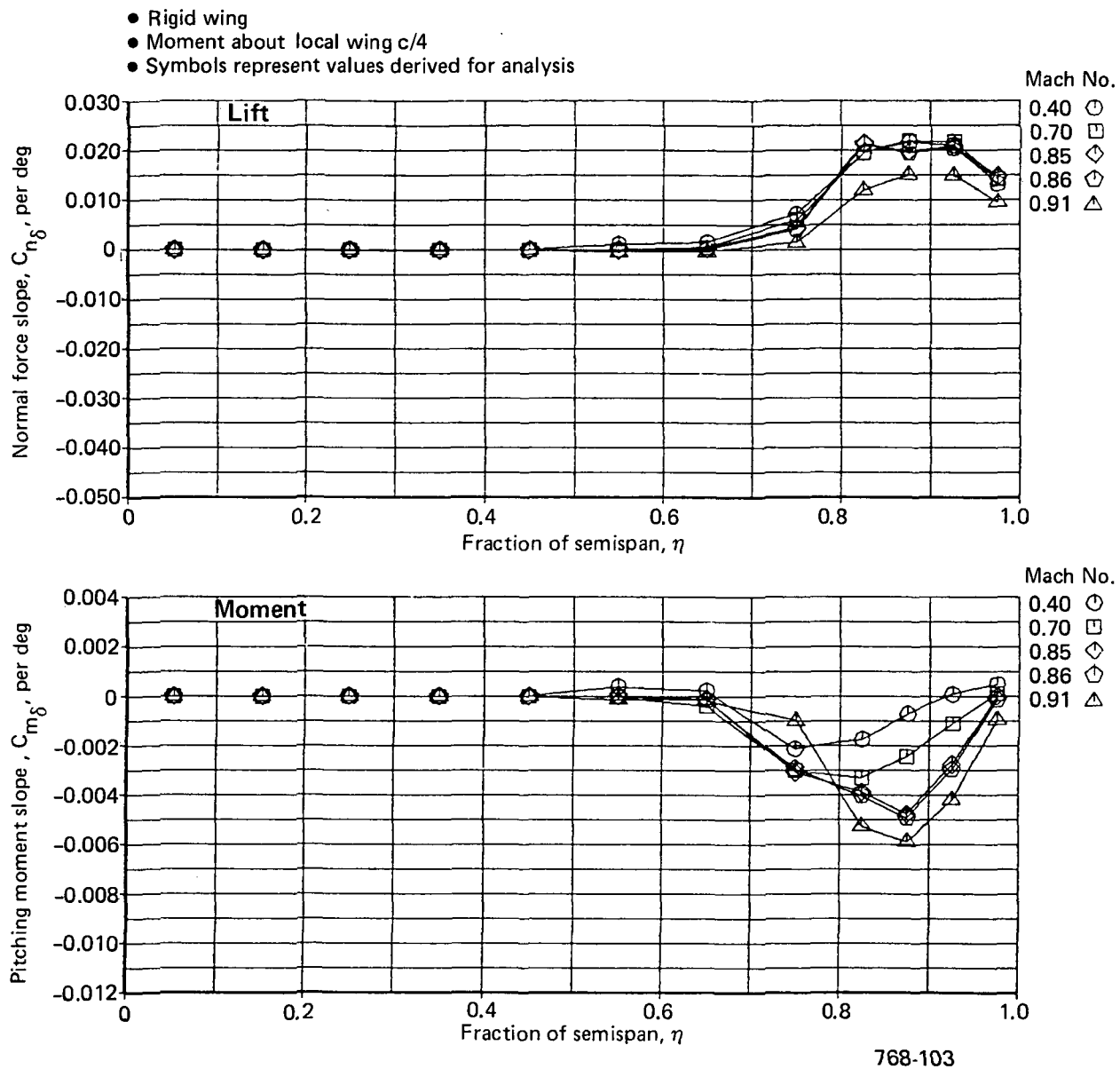*Figure A-6. Section Normal Force and Moment Due to Outboard Ailerons, Model 768-103*

768-103

- Rigid wing
- Moment about local wing c/4
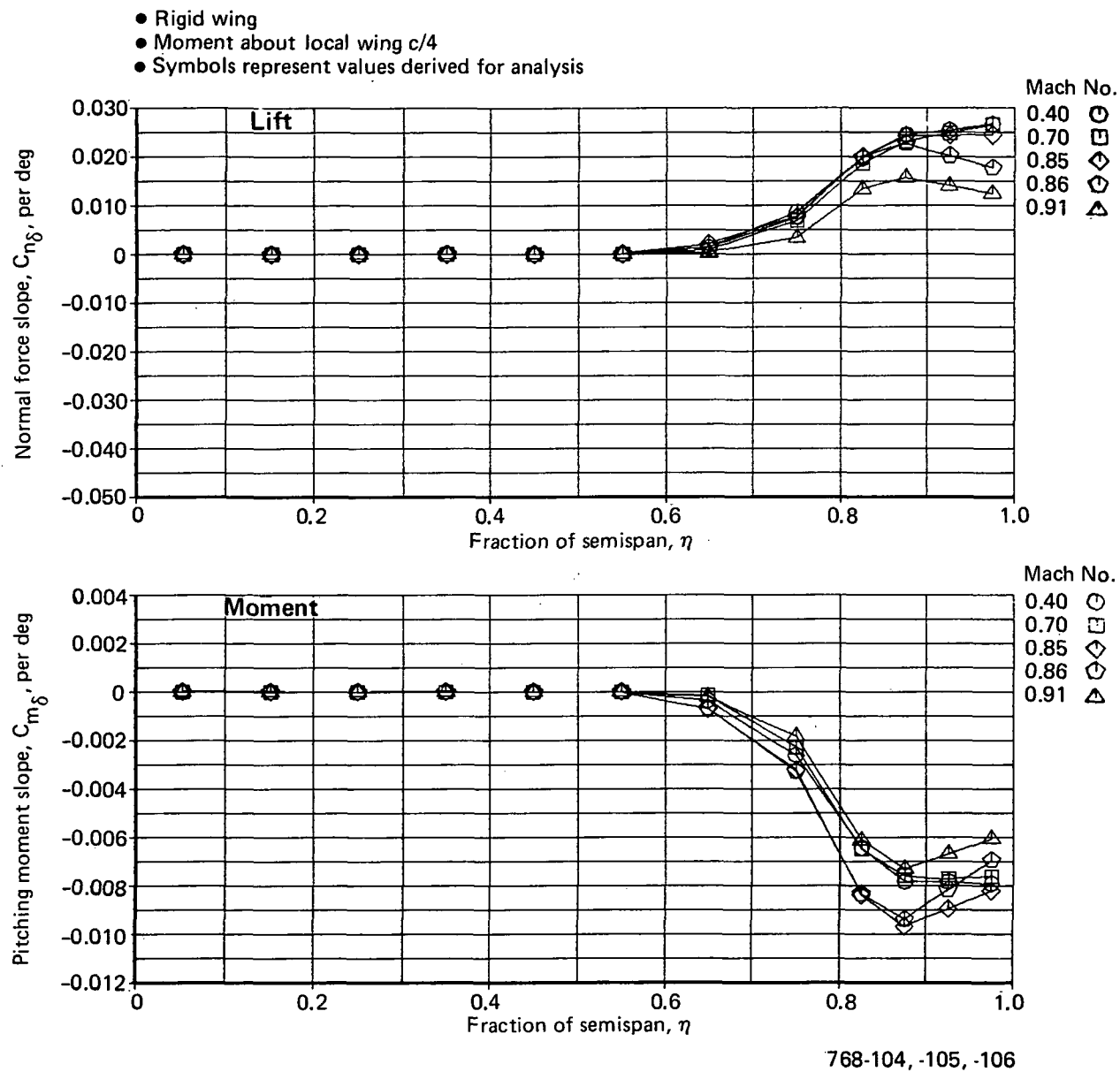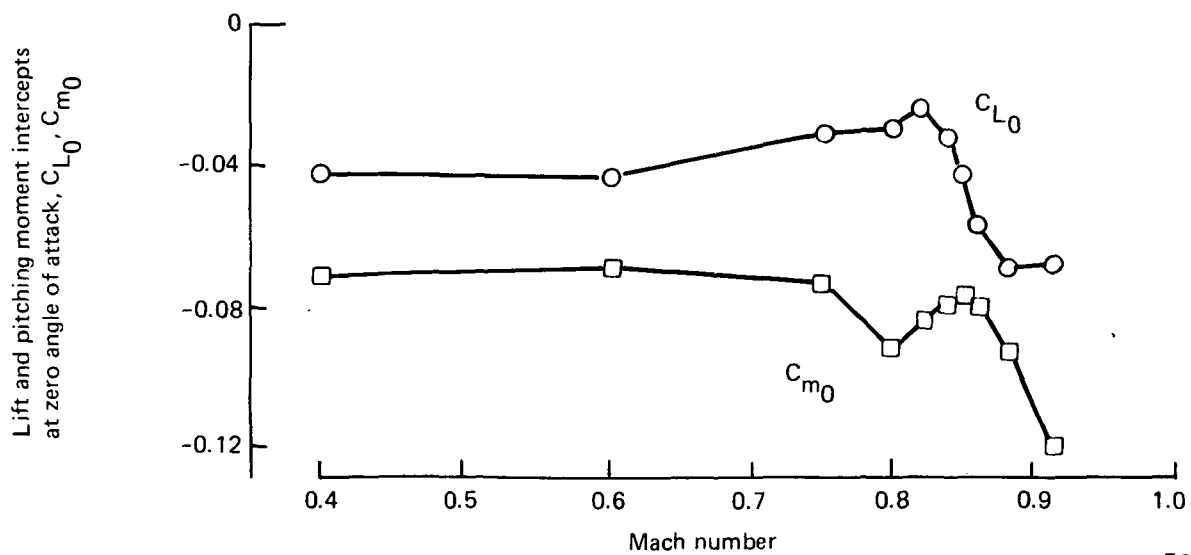- Symbols represent values derived for analysis

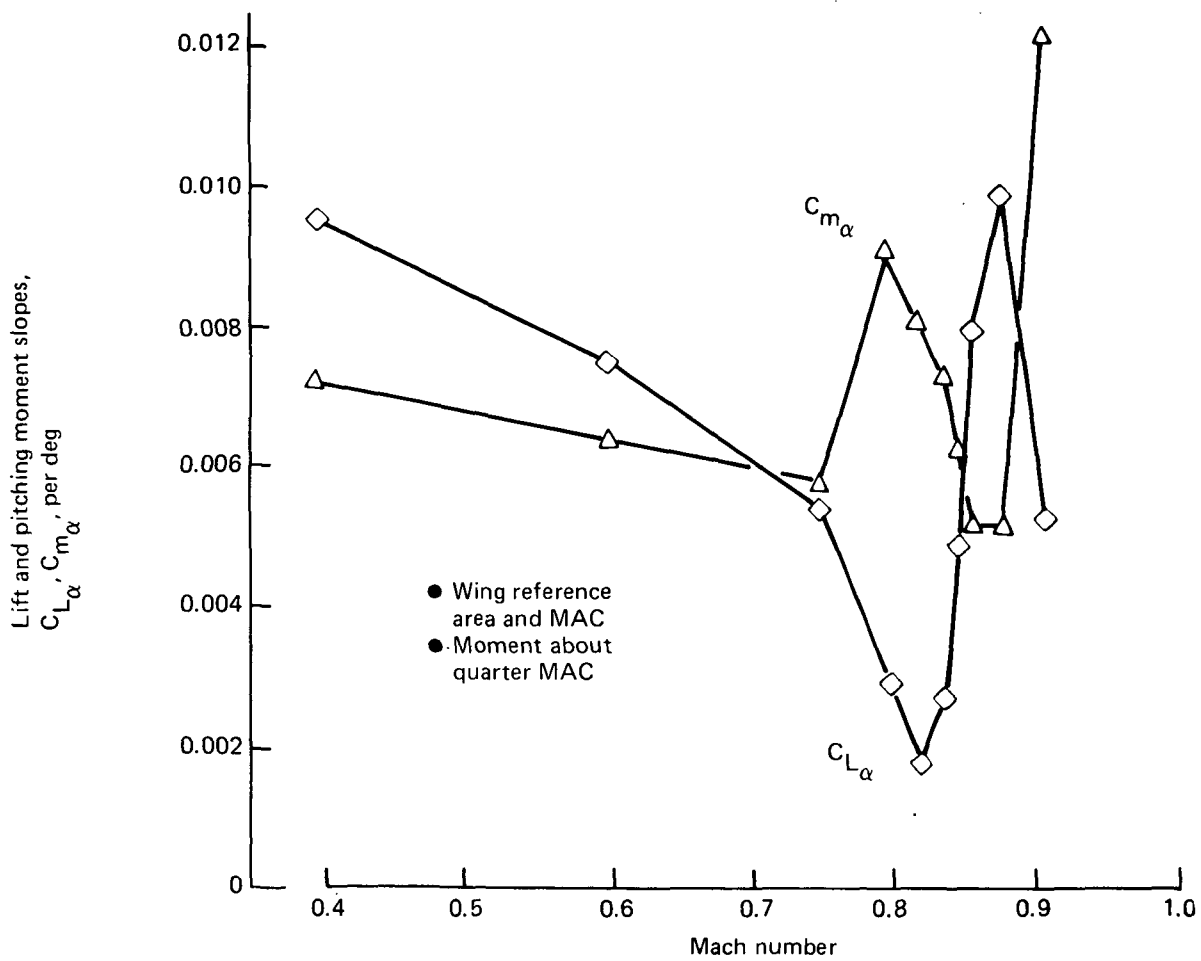Figure A-7. Section Normal Force and Moment Due to Outboard Ailerons, Planform Study Wings
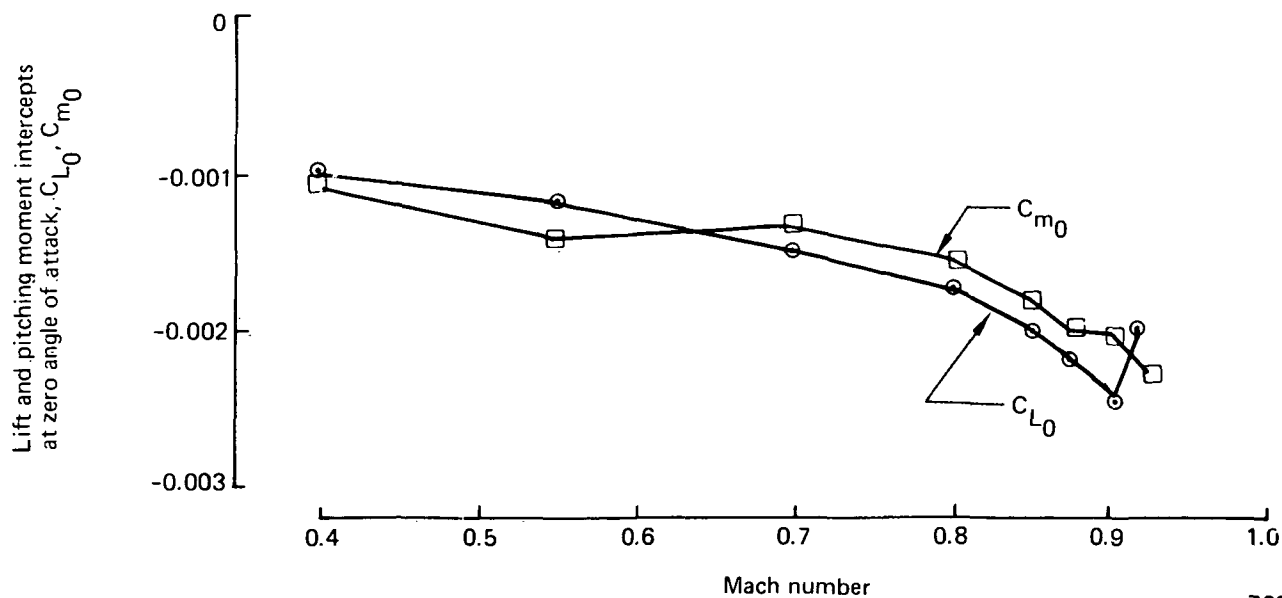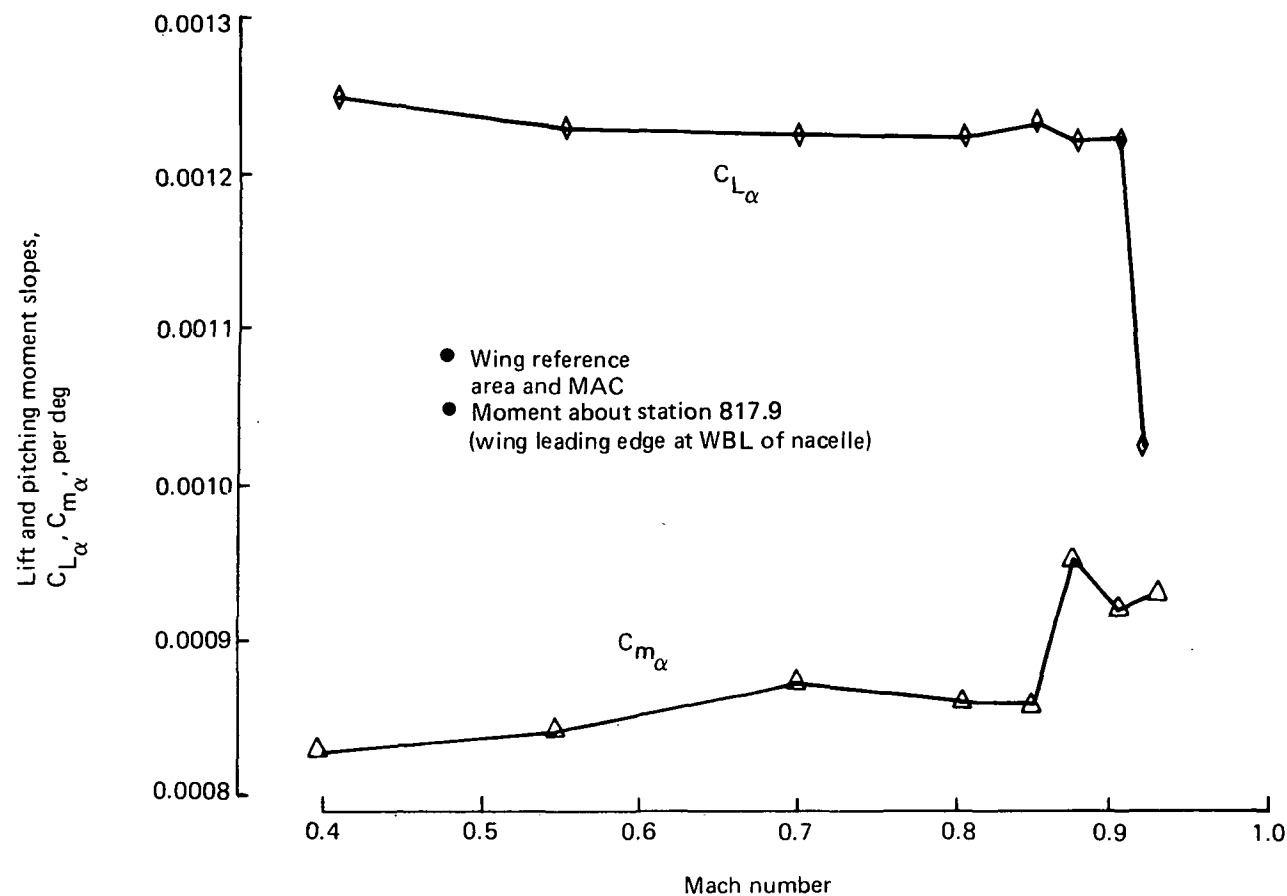
768-104, -105, -106

310

Figure A-8. Body Lift and Moment

768-103

311

Figure A-9. Nacelle Lift and Moment

768-103

312

APPENDIX B

DYNAMIC MODELING THEORY

This section contains the new theoretical developments made on the IAAC Project. Specifically, it describes the S-plane transformation, gives the rationale for writing the equations in body axes, explains the modal displacement technique for load prediction, and gives the method of obtaining aeroelastic load coefficients.

S-PLANE TRANSFORMATION

The form of the frequency dependent (k value) equation is:

$$\left[\omega^2[M] - (1 + ig)\,[K] + \tfrac{1}{2}\rho V^2[Q(M, k) + iQ'(M,k)]\right]\{q\} = 0 \tag{1}$$

where

[M]	=	Generalized mass
[K]	=	Generalized stiffness
[Q+iQ']	=	Generalized airforces (function of Mach number and reduced frequency $k = \frac{\omega b_R}{V}$)
$\{q\}$	=	Generalized coordinates
g	=	Structural damping coefficient
b_R	=	A reference length

Because the configuration is symmetrical, equations are written for one side of the airplane. Two sets of equations are generated, one for symmetric (SYM) and one for antisymmetric (ASYM) motions.

The coordinates $\{q\}$ are:

$$\{q\}_{SYM} = \begin{Bmatrix} x \\ z \\ \theta \\ \xi_S \\ \delta_{c_S} \end{Bmatrix} \qquad \{q\}_{ASYM} = \begin{Bmatrix} y \\ \phi \\ \psi \\ \xi_A \\ \delta_{c_A} \end{Bmatrix}$$

313

where

$x, z, \theta, y, \phi, \psi$ =   Rigid body motions at center of gravity (cg)

$\{\xi_S\} \cdot \{\xi_A\}$ =   Elastic coordinates

$\{\delta_{c_S}\} \cdot \{\delta_{c_A}\}$ =   Control surface deflections

To make the equations suitable for control law development either by conventional or modern control theory, the generalized airforce coefficients (GAF), which are functions of complex reduced frequency (ik) must be approximated by a physically realizable function of ik. Thus the Laplace transform is easily derived; $i\omega$ is replaced by s. There are three fundamental properties of the aerodynamic forces that must be preserved in the approximating process:

Condition 1.   The imaginary part of the forces are zero at k = 0.

$$[Q'(o)] = 0$$

Condition 2.   The real parts of the forces due to rigid body linear displacements are zero at k = 0.

$$\{Q_x(o)\} = \{Q_y(o)\} = \{Q_z(o)\} = 0 \; *$$

Condition 3.   The forces due to pitch angle and vertical velocity are related as k → 0. Both types of motion give rise to a uniform angle of attack.

$$\{Q_\theta(o)\} = {}^b R \left\{ \frac{\partial Q'_z}{\partial k}(o) \right\}$$

---

* Throughout Appendix B the symbol $\{\ \}$ is used to denote the column of coefficients of the subscript variable.

314

These can be seen by considering the expression for the GAF:

$$[Q + iQ'] = [\hat{H}_1]^T \ulcorner PSF \lrcorner \ulcorner S \lrcorner [A + iA'] \, [\hat{H}_2 + i\frac{k}{b_R} \hat{H}_3]$$

(2)

where

$[\hat{H}_1]$ =   Aerodynamic box modal displacements

$\ulcorner PSF \lrcorner$ =   Aerodynamic box pressure scale factors

$\ulcorner S \lrcorner$ =   Aerodynamic box areas

$[A + iA']$ =   Aerodynamic box influence coefficients

$[\hat{H}_2]$ =   Aerodynamic box modal slopes

$[\hat{H}_3]$ =   Aerodynamic box modal displacements

writing

$$[\hat{H}_1]^T \ulcorner PSF \lrcorner \ulcorner S \lrcorner = [H]^T$$

$$[Q] = [H]^T [A] [\hat{H}_2] - [H]^T [A'] \frac{k}{b_R} [\hat{H}_3]$$

$$[Q'] = [H]^T [A'] [\hat{H}_2] + [H]^T [A] \frac{k}{b_R} [\hat{H}_3]$$

as $k \to o$ $[A'] \to [o]$

$$\therefore [Q]_{k \to o} = [H]^T [A] [\hat{H}_2]$$

$$[Q']_{k \to o} = [H]^T [A] \frac{k}{b_R} [\hat{H}_3] = [o]$$

in particular, the columns of forces due to rigid pitch and translation are

315

$$\left\{Q_z(o)\right\} = [H]^T [A] \left\{\hat{H}_{2_z}\right\}$$

$$\left\{Q_\theta(o)\right\} = [H]^T [A] \left\{\hat{H}_{2_\theta}\right\}$$

now $\dot{z} = i\omega z$

then $i\left\{Q'_z\right\} z = \left\{\dfrac{Q'_z}{\omega}\right\}\dot{z}$

and $\left\{\dfrac{Q'_z}{\omega}\right\}_{k \to o} = [H]^T [A] \dfrac{k}{\omega b_R}\left\{\hat{H}_{3_z}\right\} = [H]^T [A] \dfrac{1}{V}\left\{\hat{H}_{3_z}\right\}$

now $\left\{\hat{H}_{2_z}\right\} = 0$

and $\left\{\hat{H}_{2_\theta}\right\} = \left\{\hat{H}_{3_z}\right\}$

and $k = \dfrac{\omega b_R}{V}$

$\therefore \left\{Q_z(o)\right\} = 0$

and $\left\{\dfrac{Q'_z}{\omega}\right\}_{k \to o} = \dfrac{1}{V}\left\{Q_\theta(o)\right\}$

or $b_R\left\{\dfrac{Q'_z}{k}\right\}_{k \to o} = \left\{Q_\theta(o)\right\}$

or $b_R\left\{\dfrac{\partial Q'_z}{\partial k}(o)\right\} = \left\{Q_\theta(o)\right\}$

Similarly in the antisymmetric case

$$b_R\left\{\dfrac{\partial Q'_y}{\partial k}(o)\right\} = \left\{Q_\psi(o)\right\}$$

and $\left\{Q_\phi(o)\right\} = 0$

316

It is usual to assume a function of the form

$$[Q + iQ'] = [A_0] + ik [A_1] + (ik)^2 [A_2] + \frac{ik [B_1]}{ik + a} + \frac{ik [B_2]}{ik + b} + \text{etc.} \tag{3}$$

where the coefficients are determined by an approximating procedure (e.g., ref B-1). Obviously, Condition 1 is satisfied by the form of the function, and Condition 2 can be satisfied by constraining the function at k = 0; i.e.,

$$[A_0] = [Q(o)]$$

For most purposes, this constraint is necessary to ensure that the static aeroelastic and control surface airforces, which are contained in [Q(o)] , are exactly reproduced in the approximating function.

Condition 3 may be satisfied by constraining the first derivative with respect to k of the imaginary part of the translation terms as k → 0; e.g.,

$$\left\{ A_{1_z} \right\} + \frac{1}{a} \left\{ B_{1_z} \right\} + \frac{1}{b} \left\{ B_{2_z} \right\} + \text{etc.} = \left\{ \frac{\partial Q'_z}{\partial k}(0) \right\}$$

In most applications, it is also necessary to ensure that the airforces due to steady pitch, roll, and yaw rate are reproduced exactly, and this requires that the first derivative of the imaginary part of the rotation terms be constrained; e.g.,

$$\left\{ A_{1_\theta} \right\} + \frac{1}{a} \left\{ B_{1_\theta} \right\} + \frac{1}{b} \left\{ B_{2_\theta} \right\} + \text{etc.} = \left\{ \frac{\partial Q'_\theta}{\partial k}(0) \right\}$$

The general form of these two conditions is

$$\left[A_{1_R} \right] + \frac{1}{a} \left[B_{1_R} \right] + \frac{1}{b} \left[B_{2_R} \right] + \text{etc.} = \left[\frac{\partial Q'_R}{\partial k}(0) \right] \tag{4}$$

Where the subscript R denotes the partition containing the rigid body columns. Note that if the function is simplified to a quadratic, equation (4) simplifies to a constraint of $\begin{bmatrix} A_1_R \end{bmatrix}$.

The effect of these constraints is illustrated in Figures B-1 and B-2, which show the equations of motion for a rigid airplane, free to translate vertically and to pitch. The GAF were calculated using an unsteady lifting surface theory (doublet lattice) for 12 k-values. The equations shown in Figure B-1 are for two k-values (zero and a value chosen to match the short-period frequency). The equations have been solved and the roots are shown. Conditions 1, 2, and 3 are satisfied at k = 0, and two of the four roots are exactly zero. The two zero roots are valid because k is matched. At the other k-value, a valid (matched k) pair of roots representing the short-period mode, and an invalid pair of nonzero roots, appear. Figure B-2 shows the equations transformed into the S-plane using the polynomial part of equation (3) and the roots of the equations. The coefficients were calculated using a least-squares fit of all 12 k-values. The equations are shown with $[A_0]$ constrained and with both $[A_0]$ and $[A_1]$ constrained. The first case does not satisfy Condition 3, and an unrealistic root (unstable in this case) appears. In the second case, the unrealistic root has a very small value that is the result of round-off error. The form of the equations built up from the conventional stability derivatives is also shown in Figure B-2. The α terms appear in two places, which means that Condition 3 is satisfied. Note that with $[A_0]$ and $[A_1]$ constrained, the short-period damping is significantly different from the original k-dependent version. In the derivative form, the unsteady $\dot{\alpha}$ damping terms appear in two places, which suggests that to ensure an accurate approximation it would be necessary to constrain $[A_2]$. An equivalent derivative form for the k-dependent case is shown in Figure B-1.

Constraining only $[A_0]$ is unsatisfactory for most purposes because it gives unrealistic responses at low frequencies. One way of incorporating both constraints is to approximate the elements of $[A + iA']$ with an appropriate function and then find $[Q + iQ']$ by multiplying by the exact expression for $[\hat{H}_2 + i\dfrac{k}{b_R} \hat{H}_3]$. See equation (2). This is essentially the method described in Reference B-2, which yields an expression of the same form as equation (3). A simpler technique is to reduce the order of the k-dependent equations by rewriting them in terms of body-fixed variables using the relationships

- z + down
- θ + noseup

k = 0

$$\omega^2 \begin{bmatrix} 3.4 \times 10^2 & 0 \\ 0 & 7.7 \times 10^7 \end{bmatrix} + \begin{bmatrix} 0 & -4.44 \times 10^6 \\ 0 & -3.95 \times 10^8 \end{bmatrix} + i \begin{bmatrix} 0 & 0 \\ 0 & 0 \end{bmatrix} \begin{Bmatrix} z \\ \theta \end{Bmatrix} = 0$$

Solution: $i\omega = 0,\ 0,\ 0 \pm i2.26$

$$k = \frac{2.5\ b_R}{V}$$

$$\omega^2 \begin{bmatrix} 3.4 \times 10^2 & 0 \\ 0 & 7.7 \times 10^7 \end{bmatrix} + \begin{bmatrix} -31.7 & -4.40 \times 10^6 \\ +7.47 \times 10^3 & -3.93 \times 10^8 \end{bmatrix} + i \begin{bmatrix} -1.01 \times 10^3 & -2.4 \times 10^5 \\ -9.21 \times 10^4 & -1.60 \times 10^8 \end{bmatrix} \begin{Bmatrix} z \\ \theta \end{Bmatrix} = 0$$

Solution: $i\omega = 0.055 \pm i\ 0.532,\ -1.05 \pm i2.20$

Derivative form for small k

$$\omega^2 \begin{bmatrix} M & 0 \\ 0 & I \end{bmatrix} + \begin{bmatrix} qS_w \dfrac{\bar{c}}{2V} \dfrac{V^2 k^2}{b_R^2} \dfrac{C_{L\hat{\alpha}}}{V} & -qS_w C_{L\alpha} \\ -qS_w \bar{c} \dfrac{\bar{c}}{2V} \dfrac{V^2 k^2}{b_R^2} \dfrac{C_{m\hat{\alpha}}}{V} & qS_w \bar{c} C_{m\alpha} \end{bmatrix} + i \begin{bmatrix} -qS_w \dfrac{kV}{b_R} \dfrac{C_{L\alpha}}{V} & -qS_w \dfrac{\bar{c}}{2V} \dfrac{kV}{b_R}\left(C_{L\hat{q}} + C_{L\hat{\alpha}}\right) \\ +qS_w \bar{c} \dfrac{kV}{b_R} \dfrac{C_{m\alpha}}{V} & qS_w \dfrac{\bar{c}}{2V} \dfrac{kV}{b_R}\left(C_{m\hat{q}} + C_{m\hat{\alpha}}\right) \end{bmatrix} \begin{Bmatrix} z \\ \theta \end{Bmatrix} = 0$$

$M,\ I,\ S_w$ — half airplane mass, pitch inertia, wing reference area

Figure B-1. k-Dependent Rigid Equations of Motion

● s^2 polynomial approximation
● z + down
● θ + noseup

[A_0] Constrained

$$s^2 \begin{bmatrix} 3.48 \times 10^2 & 5.86 \times 10^2 \\ -6.51 \times 10^2 & 7.86 \times 10^7 \end{bmatrix} + s \begin{bmatrix} 0 & +4.44 \times 10^6 \\ 0 & 3.95 \times 10^8 \end{bmatrix} + \begin{bmatrix} 3.04 \times 10^2 & +1.62 \times 10^5 \\ +5.25 \times 10^4 & 4.35 \times 10^7 \end{bmatrix} \left\{ \begin{array}{c} \mathcal{L}[z] \\ \mathcal{L}[\theta] \end{array} \right\} = 0$$

Solution: $s = 0,\ 0.627,\ -1.03 \pm i2.35$

[A_0] and [A_1] Constrained

$$s^2 \begin{bmatrix} 3.48 \times 10^2 & 5.86 \times 10^2 \\ -6.51 \times 10^2 & 7.86 \times 10^7 \end{bmatrix} + s \begin{bmatrix} 0 & +4.44 \times 10^6 \\ 0 & 3.95 \times 10^8 \end{bmatrix} + \begin{bmatrix} 4.09 \times 10^2 & +1.53 \times 10^5 \\ +3.64 \times 10^4 & 5.09 \times 10^7 \end{bmatrix} \left\{ \begin{array}{c} \mathcal{L}[z] \\ \mathcal{L}[\theta] \end{array} \right\} = 0$$

Solution: $s = 0,\ -1.7 \times 10^{-6},\ -0.914 \pm i2.20$

Derivative Form

$$s^2 \begin{bmatrix} M & O \\ O & I \end{bmatrix} + s \begin{bmatrix} +qS_w \dfrac{C_{L_{\hat{\alpha}}}}{V} & +qS_w C_{L_\alpha} \\ -qS_w \bar{c} \dfrac{C_{m_{\hat{\alpha}}}}{V} & -qS_w \bar{c} C_{m_\alpha} \end{bmatrix}$$

$$s^2 \begin{bmatrix} 0 \\ 0 \end{bmatrix} + s \begin{bmatrix} qS_w \dfrac{\bar{c}}{2V} \dfrac{C_{L_{\hat{\alpha}}}}{V} & +qS_w \dfrac{\bar{c}}{2V} \left(C_{L_{\hat{q}}} + C_{L_{\hat{\alpha}}} \right) \\ -qS_w \bar{c} \dfrac{\bar{c}}{2V} \dfrac{C_{m_{\hat{\alpha}}}}{V} & -qS_w \bar{c} \dfrac{\bar{c}}{2V} \left(C_{m_{\hat{q}}} + C_{m_{\hat{\alpha}}} \right) \end{bmatrix} + $$

$$\begin{bmatrix} qS_w \dfrac{C_{L_\alpha}}{V} \\ -qS_w \bar{c} \dfrac{C_{m_\alpha}}{V} \end{bmatrix} \left\{ \begin{array}{c} \mathcal{L}[z] \\ \mathcal{L}[\theta] \end{array} \right\} = 0$$

Figure B-2. S-Plane Rigid Equations of Motion

320

$$u = \dot{x} \qquad\qquad v = \dot{y} - V\psi$$
$$w = \dot{z} + V\theta \qquad\qquad p = \dot{\phi} \qquad\qquad (5)$$
$$q = \dot{\theta} \qquad\qquad r = \dot{\psi}$$

This "body axis transformation" is valid for small perturbations, as shown in Reference B-3. The transformation has the effect of moving the steady forces due to rigid body motion from the imaginary to the real part of the GAF. This imaginary to real force conversion effect can be seen by considering the symmetric airforces for a rigid airplane.

$$[Q + iQ'] \begin{Bmatrix} z \\ \theta \end{Bmatrix} = \{Q_z\} z + \{Q_\theta\} \theta + \{Q'_z\} iz + \{Q'_\theta\} i\theta$$

from equation (5)

$$w = i\omega z + V\theta$$

and $q = i\omega\theta$

$$k = \frac{\omega{}^bR}{V}$$

$$\therefore [Q + iQ'] \begin{Bmatrix} z \\ \theta \end{Bmatrix} = \frac{{}^bR}{Vk} \{Q'_z\} w + \frac{{}^bR}{Vk} \{-Q_z\} iw + \left\{ \frac{{}^bR}{Vk} Q'_\theta + \frac{{}^bR{}^2}{Vk^2} Q_z \right\} q + \left\{ \frac{-{}^bR}{Vk} Q_\theta + \frac{{}^bR{}^2}{Vk^2} Q'_z \right\} iq$$

as $k \to 0$ this reduces to

$$[Q + iQ'] \begin{Bmatrix} z \\ \theta \end{Bmatrix} = \frac{{}^bR}{V} \left\{ \frac{Q'_z}{k} \right\}_{k \to o} w + \frac{{}^bR}{V} \left\{ \frac{Q'_\theta}{K} \right\}_{k \to o} q$$

or

$$\frac{1}{V} \{Q_\theta(o)\} w + \frac{{}^bR}{V} \left\{ \frac{Q'_\theta}{k} \right\}_{k \to o} q$$

The partition $\left\{\dfrac{Q'_\theta}{k}\right\}_{k\to o}$ can be found at a very small k-value.

Writing the GAF in body axes as

$[\overline{Q} + i\overline{Q}']$

then

$$\left\{\overline{Q}_w(o)\right\} = \frac{{}^b R}{V}\left\{\frac{Q'_z}{k}(o)\right\}_{k\to o}$$

and

$$\left\{\overline{Q}_q(o)\right\} = \frac{{}^b R}{V}\left\{\frac{Q'_\theta}{k}(o)\right\}_{k\to o}$$

Because the rigid body variables are rates, it is no longer physically realistic to use a second-order polynomial to approximate the rigid body aerodynamic forces because the second-order term would represent forces proportional to the rate of change of acceleration. Using body axes the form of the function is:

$$[\overline{Q} + i\overline{Q}'] = [\overline{Q}(o)] + ik\,[\overline{A}_1] + (ik)^2[o\,\,|\overline{A}_2] + \frac{ik[\overline{B}_1]}{ik + a} + \frac{ik[\overline{B}_2]}{ik + b} + etc. \qquad (6)$$

$\llcorner$RIGID BODY
COLUMNS

Condition 3 is satisfied without imposing a constraint of the type given by equation (4).

Figure B-3 shows the equations of motion in body axes for the same example as used in Figure B-1 and for the same k-values. Conditions 1, 2, and 3 are automatically satisfied because steady forces due to $\overset{\cdot}{z}$ and θ have been combined. The forces due to steady pitch rate are now in the real part of the GAF, and the unsteady forces are concentrated in the imaginary part. Figure B-3 also shows a derivative form. Figure B-4 shows the S-plane equations of motion with $[A_0]$ constrained and with both $[A_0]$ and $[A_1]$ constrained. The solution of the latter case is a close approximation to the k-dependent short period.

• w + down
• q + noseup

k = 0

$$\left[-i\omega \begin{bmatrix} 3.4\times10^2 & 0 \\ 0 & 7.7\times10^7 \end{bmatrix} + \begin{bmatrix} 0 & -3.72\times10^6 \\ 0 & 0 \end{bmatrix} + \begin{bmatrix} 4.09\times10^2 & 1.53\times10^5 \\ 3.64\times10^4 & 5.09\times10^7 \end{bmatrix} + \begin{bmatrix} 0 & 0 \\ 0 & 0 \end{bmatrix} \right] \begin{Bmatrix} w \\ q \end{Bmatrix} = 0$$

Solution: $i\omega = -0.928 \pm i2.22$

k = $\dfrac{2.5\,b_R}{V}$

$$\left[-i\omega \begin{bmatrix} 3.4\times10^2 & 0 \\ 0 & 7.7\times10^7 \end{bmatrix} + \begin{bmatrix} 0 & -3.72\times10^6 \\ 0 & 0 \end{bmatrix} + \begin{bmatrix} 4.03\times10^2 & 1.51\times10^5 \\ 3.69\times10^4 & 5.10\times10^7 \end{bmatrix} + \begin{bmatrix} -13.2 & -9.84\times10^3 \\ 3.106 & 1.281\times10^6 \end{bmatrix} \right] \begin{Bmatrix} w \\ q \end{Bmatrix} = 0$$

Solution: $i\omega = -1.05 \pm i2.20$

Derivative Form for Small k

$$\left[-i\omega \begin{bmatrix} M & 0 \\ 0 & 1 \end{bmatrix} + \begin{bmatrix} -VM & 0 \\ 0 & 0 \end{bmatrix} + \begin{bmatrix} qS_w\dfrac{C_{L\alpha}}{V} & qS_w\dfrac{\bar{c}}{2V}C_{L\hat{q}} \\ -qS_w\bar{c}\dfrac{C_{m\alpha}}{V} & -qS_w\bar{c}\dfrac{\bar{c}}{2V}C_{m\hat{q}} \end{bmatrix} + \begin{bmatrix} qS_w\dfrac{\bar{c}}{2V}\dfrac{kV}{b_R}C_{L\hat\alpha} & 0 \\ -qS_w\bar{c}\dfrac{\bar{c}}{2V}\dfrac{kV}{b_R}C_{m\hat\alpha} & 0 \end{bmatrix} \right] \begin{Bmatrix} w \\ q \end{Bmatrix} = 0$$

Figure B-3. k-Dependent Body Axis Equations of Motion

323

[A₀] Constrained

$$s \begin{bmatrix} 3.4 \times 10^2 & 0 \\ 0 & 7.7 \times 10^7 \end{bmatrix} + \begin{bmatrix} -3.72 \times 10^6 & 0 \\ 0 & 0 \end{bmatrix} + \begin{bmatrix} 4.09 \times 10^2 & 1.53 \times 10^5 \\ 3.64 \times 10^4 & 5.09 \times 10^7 \end{bmatrix} + s \begin{bmatrix} 3.39 & -1.83 \times 10^3 \\ -7.15 \times 10^2 & 1.06 \times 10^6 \end{bmatrix} \left\{ \begin{array}{c} \mathcal{L}[w] \\ \mathcal{L}[q] \end{array} \right\} = 0$$

Solution: s = − 0.872 ± i2.22

[A₀] and [A₁] Constrained

$$s \begin{bmatrix} 3.4 \times 10^2 & 0 \\ 0 & 7.7 \times 10^7 \end{bmatrix} + \begin{bmatrix} -3.72 \times 10^6 & 0 \\ 0 & 0 \end{bmatrix} + \begin{bmatrix} 4.09 \times 10^2 & 1.53 \times 10^5 \\ 3.64 \times 10^4 & 5.09 \times 10^7 \end{bmatrix} + s \begin{bmatrix} -5.27 & -3.94 \times 10^3 \\ 1.24 \times 10^3 & 1.28 \times 10^6 \end{bmatrix} \left\{ \begin{array}{c} \mathcal{L}[w] \\ \mathcal{L}[q] \end{array} \right\} = 0$$

Solution: s = − 1.05 ± i2.19

Derivative Form

$$s \begin{bmatrix} M & 0 \\ 0 & \cdots \end{bmatrix} + \begin{bmatrix} 0 & -VM \\ 0 & 0 \end{bmatrix} + \begin{bmatrix} qS_w \dfrac{C_{L_\alpha}}{V} & qS_w \dfrac{\bar{c}}{2V} C_{L_{\hat{q}}} \\ -qS_w \bar{c} \dfrac{C_{m_\alpha}}{V} & -qS_w \bar{c} \dfrac{\bar{c}}{2V} C_{m_{\hat{q}}} \end{bmatrix} + s \begin{bmatrix} qS_w \dfrac{\bar{c}}{2V} C_{L_{\hat{\alpha}}} & 0 \\ -qS_w \bar{c} \dfrac{\bar{c}}{2V} C_{m_{\hat{\alpha}}} & 0 \end{bmatrix} \left\{ \begin{array}{c} \mathcal{L}[w] \\ \mathcal{L}[q] \end{array} \right\} = 0$$

- s polynomial
- w + down
- q + noseup

Figure B-4. S-Plane Body Axis Equations of Motion

324

In the IAAC Project, a sufficiently accurate flutter solution was obtained by using only the polynomial part of equation (6). Note that the airforces due to elastic and control surface motions are not affected by the body axis transformation and that they are constrained only in $[A_0]$. Sensor equations written in the original inertia axis variables were also transformed to body axes. The imaginary structural damping term of equation (1) was replaced by an equivalent viscous damping using the relationship:

$$-ig[K] \{\xi\} \doteq -g\lceil \omega_n \rfloor^{-1} [K] \{\dot{\xi}\}$$

where

$\lceil \omega_n \rfloor$ modal frequencies

Gust-forcing terms were added to the right-hand side of the equations.

MODAL DISPLACEMENT METHOD

For a number of forces and moments $\{F\}$ applied at the structural nodes, the shear (V), bending moments (M), and torsion (T) are given by

$$\begin{Bmatrix} V \\ M \\ T \end{Bmatrix} = [\Sigma] \{F\}$$

where $[\Sigma]$ is a summing matrix that is dependent upon the geometry of the structural model.

By the conventional method of modal displacement, $\{F\}$ may be approximated by

$$\{F\} \doteq [k] [\phi] \{\xi\}$$

where

$[k]$ =   Structural stiffness matrix relating forces and moments at the structural nodes to the displacements at the structural nodes

$[\phi]$ =   A modal matrix relating the nodal displacements to the generalized elastic coordinates

$\{\xi\}$ =   Elastic coordinates

325

The load can then be related to the elastic coordinates by the equation:

$$\begin{Bmatrix} V \\ M \\ T \end{Bmatrix} = [\Sigma] \, [k] \, [\phi] \, \{\xi\}$$

In the IAAC Project, a simple technique for estimating $\{F\}$ has been devised that does not require the nodal stiffness matrix.

The elastic coordinates may be found from $\{F\}$ by the relationship

$$[K_\xi] \, \{\xi\} = [\phi]^T \{F\}$$

where

$[K_\xi] =$ Generalized stiffness matrix

In general, $\{F\}$ cannot be found from $\{\xi\}$ because $[\phi]^T$ is singular. However, $\{F\}$ may be approximated by a small number of forces and moments chosen so that $[\phi]^T$ is nonsingular.

For instance, in the planform study dynamic model, eight wing forces and moments (subsec 7.3.1.1) were used and related to eight of the 10 wing modes. The two modes omitted were predominantly fore and aft bending. $\{F\}$ can be approximated:

$$\{F\} \doteq [\phi^T]^{-1} \, [K_\xi] \, \{\xi\}$$

$$\therefore \begin{Bmatrix} V \\ M \\ T \end{Bmatrix} \doteq [\Sigma] \, \{F\}$$

$$\doteq [\Sigma] \, [\phi^T]^{-1} \, [K_\xi] \, \{\xi\} = [\overline{M}_1] \, \{\xi\}$$

The accuracy of this method can be influenced by the choice of $\{F\}$, and a different choice can be used for each load.

STATIC-ELASTIC LOAD COEFFICIENTS

Figure 110 (subsec 7.3.1.1) shows the final equations of motion. To illustrate the mechanism by which static-elastic load coefficients are found, equations of the following form may be extracted:

$$\left[\begin{bmatrix} S_o \\ R,R \end{bmatrix} \begin{matrix} S_o \\ R,\xi \end{matrix} \\ \begin{matrix} S_o \\ \xi,R \end{matrix} \begin{matrix} S_o \\ \xi,\xi \end{matrix} \end{bmatrix} + \begin{bmatrix} \begin{matrix} S_1 \\ R,R \end{matrix} \begin{matrix} S_1 \\ R,\xi \end{matrix} \\ \begin{matrix} S_1 \\ \xi,R \end{matrix} \begin{matrix} S_1 \\ \xi,\xi \end{matrix} \end{bmatrix} s + \begin{bmatrix} \begin{matrix} S_2 \\ R,R \end{matrix} \begin{matrix} S_2 \\ R,\xi \end{matrix} \\ \begin{matrix} S_2 \\ \xi,R \end{matrix} \begin{matrix} S_2 \\ \xi,\xi \end{matrix} \end{bmatrix} s^2 \right] \begin{Bmatrix} R \\ \xi \end{Bmatrix} = 0 \qquad (7)$$

where

$\{R\}$ =   The Laplace transform of the body and control surface variables

$\{\xi\}$ =   The Laplace transform of the elastic variables

and

$$[\bar{M}_1]\{\xi\} - \{L\} = 0 \qquad (8)$$

where

$[\bar{M}_1]$ =   Modal displacement load coefficients

$\{L\}$ =   The Laplace transform of the loads

Neglecting the following terms

$$[S_1 \ ]_{R,\xi} s\{\xi\}, [S_2 \ ]_{R,\xi} s^2\{\xi\}$$

and

$$[S_1 \ ]_{\xi,\xi} s\{\xi\}, \text{ and } [S_2 \ ]_{\xi,\xi} s^2\{\xi\}$$

equation (7) yields

$$\{\xi\} = [S_{o}]^{-1}_{\xi,\xi} [S_{o}]_{\xi,R} \{R\} + [S_{o}]^{-1}_{\xi,\xi} [S_1]_{\xi,R} s\{R\} + [S_{o}]^{-1}_{\xi,\xi} [S_2]_{\xi,R} s^2\{R\}$$

Substituting in equation (8)

$$\{L\} = [\bar{M}_1] [S_{o}]^{-1}_{\xi,\xi} [S_{o}]_{\xi,R} \{R\}$$

$$+ [\bar{M}_1] [S_{o}]^{-1}_{\xi,\xi} [S_1]_{\xi,R} s\{R\}$$

$$+ [\bar{M}_1] [S_{o}]^{-1}_{\xi,\xi} [S_2]_{\xi,R} s^2\{R\}$$

The above equations relate the loads to $\{R\}$, the body and control surface motions. Aeroelastic load coefficients can be deduced using the following relationships:

$$\alpha = \frac{w}{V}$$

$$n = -\frac{\dot{w} - V_q}{g}$$

328

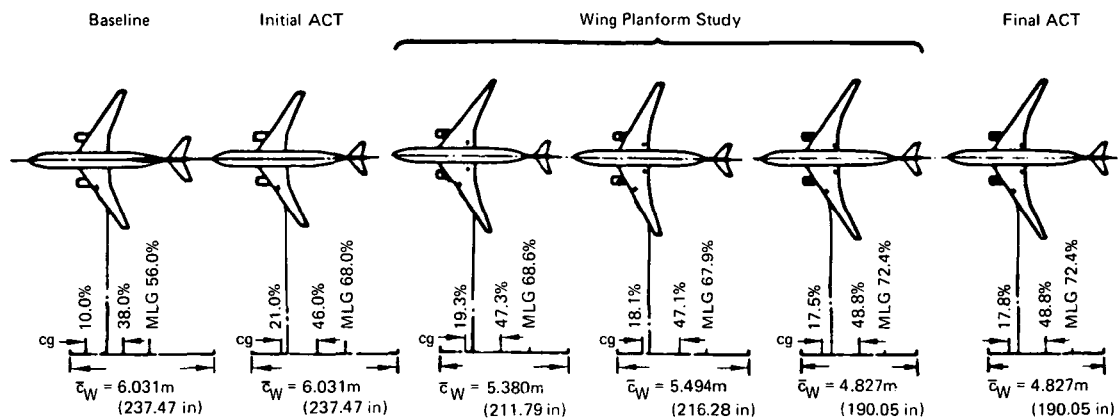# REFERENCES

B-1 Karpel, Mordechay. "Design for Active Flutter Suppression and Gust Alleviation Using State-Space Aeroelastic Modeling." AIAA-21st Structures, Structural Dynamics and Materials Conference, May 1980.

B-2 Roger, K. L. "Airplane Math Modeling Methods for Active Control Design." AGARD-CP-228, August 1977.

B-3 Equation Modifying Program, L219 (EQMOD). NASA CR-2846, May 1978.

1. Report No. NASA CR-165630	2. Government Accession No.	3. Recipient's Catalog No.
4. Title and Subtitle Integrated Application of Active Controls (IAAC) Technology to an Advanced Subsonic Transport Project —Wing Planform Study and Final Configuration Selection, Final Report		5. Report Date June 1981
		6. Performing Organization Code
7. Author(s) Boeing Commercial Airplane Company Preliminary Design Department		8. Performing Organization Report No. D6-48676
		10. Work Unit No.
9. Performing Organization Name and Address Boeing Commercial Airplane Company P. O. Box 3707 Seattle, Washington 98124		
		11. Contract or Grant No. NAS1-15325
12. Sponsoring Agency Name and Address National Aeronautics and Space Administration Washington, D. C. 20546		13. Type of Report and Period Covered Contractor Report June 1979 to Oct. 1980
		14. Sponsoring Agency Code

15. Supplementary Notes

Technical Monitors: D. B. Middleton and R. V. Hood
NASA Langley Research Center

16. Abstract

This report documents the Wing Planform Study and Final Configuration Selection Task of the Integrated Application of Active Controls (IAAC) Technology Project within the Energy Efficient Transport Program. Application of Active Controls Technology (ACT) in combination with increased wing span resulted in significant improvements over the Conventional Baseline Configuration (Baseline) and the Initial ACT Configuration previously established. The configurations use the same levels of technology, takeoff gross weight, and payload as the Baseline. The Final ACT Configuration (Model 768-107) incorporates pitch-augmented stability (which enabled an approximately 10% aft shift in cruise center of gravity and a 44% reduction in horizontal tail size), lateral/directional-augmented stability, an angle-of-attack limiter, and wing-load alleviation. Flutter-mode control was not beneficial for this configuration. This resulted in an 890 kg (1960 lb) reduction in airplane takeoff gross weight and a 9.8% improvement in cruise lift/drag. At the Baseline mission range (3589 km 1938 nmi), this amounts to 10% block-fuel reduction. Results of this task strongly indicate that the IAAC Project should proceed with the Final ACT evaluation, and begin the required control system development and test.

17. Key Words (Suggested by Author(s)) Energy Efficient Transport Program, Active Controls Technology, Augmented Stability, Wing-Load Alleviation, Flutter-Mode Control, Angle-of-Attack Limiter, Airplane Design	18. Distribution Statement FEDD Distribution	
19. Security Classif. (of this report) Unclassified	20. Security Classif. (of this page) Unclassified	21. No. of Pages 329	22. Price

N-305   Available: NASA's Industrial Applications Centers

D R O

AR = 12.0
Λ   = 31.5 deg

AR = 8.7
Λ   = 31.5 deg

CR-159248

AR = 8.7
Λ   = 31.5 deg

CR-3304
CR-159249

AR = 10.3
Λ   = 31.5 deg

AR = 10.2
Λ   = 26.4 deg

AR = 12.0
Λ   = 31.5 deg

Evaluation

ΔFuel
ΔDOC
ΔROI

Baseline
Configuration
Model 768-102

Initial ACT
Configuration
Model 768-103

Wing Planform
Studies—Models
768-104, -105, -106
(top to bottom)

Final ACT
Configuration
Model 768-107

Final ACT
Evaluation

ACT Configuration Evolution

Baseline   Initial ACT   Wing Planform Study   Final ACT

| | cg 10.0% 38.0% MLG 56.0% | cg 21.0% 46.0% MLG 68.0% | cg 19.3% 47.3% MLG 68.6% | cg 18.1% 47.1% MLG 67.9% | cg 17.5% 48.8% MLG 72.4% | 17.8% 48.8% MLG 72.4% |

$\bar{c}_W$ = 6.031m (237.47 in)　$\bar{c}_W$ = 6.031m (237.47 in)　$\bar{c}_W$ = 5.380m (211.79 in)　$\bar{c}_W$ = 5.494m (216.28 in)　$\bar{c}_W$ = 4.827m (190.05 in)　$\bar{c}_W$ = 4.827m (190.05 in)

Model number	768-102	768-103	768-105	768-106	768-104	768-107
Sweep at $\bar{c}/4$, deg	31.5		31.5	26.4	31.5	
Aspect ratio, ref	8.1		9.0	9.1	9.9	
Aspect ratio, TRAP	8.71		10.30	10.15	12.03	
Taper ratio, ref	0.225		0.198	0.212	0.177	
Taper ratio, TRAP	0.267	Same	0.266	0.262	0.267	Same
t/c SOB, percent	15.1		15.1	13.1	15.1	
t/c tip, percent	10.3		10.3	8.3	10.3	
Span, m (ft)	47.24 (155)		49.90 (163.7)	50.03 (164.2)	52.22 (171.3)	
Area ref, m^2 (ft^2)	275.1 (2961)		275.5 (2966)	275.1 (2961)	275.8 (2969)	
Area trap, m^2 (ft^2)	256.3 (2759)		241.4 (2598)	246.7 (2656)	226.8 (2441)	

768-102, -103, -104, -105, -106, -107

IAAC Wing Geometry